Studies on morpho-physiological adaptations in microalgae from different marine habitats

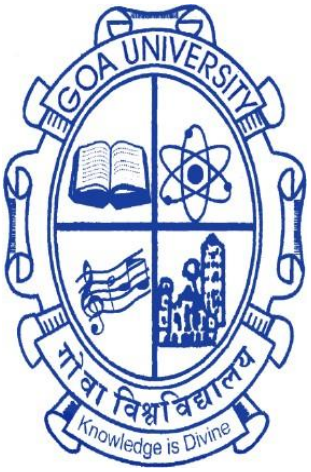
A Thesis submitted in partial fulfillment for the Degree of

DOCTOR OF PHILOSOPHY

in

The School of Earth, Ocean, and Atmospheric Sciences
(Marine Sciences)

Goa University



By

Pranoy Paul

Biological Oceanography Division

CSIR-National Institute of Oceanography,
Dona Paula, Goa 403004, India

Registration No.: **201812728**

January 2026

Studies on morpho-physiological adaptations in microalgae from different marine habitats

A Thesis submitted to

Goa University
For the award of the degree of Doctor of Philosophy
In

The School of Earth, Ocean, and Atmospheric Sciences
(Marine Sciences)

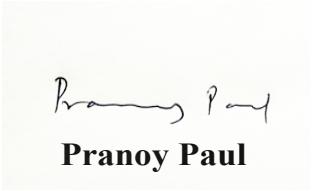
By
Pranoy Paul
CSIR-National Institute of Oceanography

Under the Guidance of
Dr. Jagadish S Patil
Senior Principal Scientist,
Biological Oceanography Division
CSIR-National Institute of Oceanography
Dona Paula, Goa-403004, India

2026

DECLARATION

I, **Mr. Pranoy Paul**, hereby declare that this thesis titled "Studies on morpho-physiological adaptations in microalgae from different marine habitats" represents work that has been carried out by me and that it has not been submitted, either in part or full, to any other University or Institution for the award of any research degree.



Place: Dona Paula, Goa
Date:07-01-2026

Pranoy Paul
(Ph.D. candidate)

CERTIFICATE

I hereby certify that the above declaration of the candidate, **Mr. Pranoy Paul**, is true and the work was carried out under my supervision.



Dr. Jagadish S Patil
Senior Principal Scientist,
Biological Oceanography Division
CSIR-National Institute of Oceanography
Dona Paula, Goa-403004, India

Acknowledgment

My PhD journey would not have been possible without thanking all the people who played a significant role in helping me immensely during my journey to achieve this monumental task.

First and foremost, I would like to express my deepest gratitude to my PhD supervisor, Dr. Jagadish S Patil, for allowing me to work with him. His constant support, guidance, and encouragement have been invaluable throughout my PhD journey. Since I joined him in the project, registering PhD and till the final submission of my thesis, his unwavering presence, wisdom, and knowledge have been instrumental in shaping my academic growth. Whatever little I have learned about phytoplankton ecology is all through his teaching. Above all, the scientific fervor he instilled in me will keep me pushing forward.

I sincerely thank Dr. A. C. Anil, Chief Scientist and Head (retired) of the Bio-fouling and Bio-invasion Division, for allowing me to work in the lab and providing all the necessary facilities. I am greatly indebted to him for his support, constructive criticism, and valuable suggestions throughout the journey.

I am also grateful to all my Doctoral Research Committee members, Senior Professor Dr. C. U. Rivonker and Dr. Smita Mitbavkar, for assessing my research progress regularly and improving my PhD work by giving valuable advice and suggestions. Their sincere efforts, patience, and valuable time are greatly acknowledged.

I would like to thank Professor Dr. Sunil Kumar Singh, Director, Council of Scientific and Industrial Research-National Institute of Oceanography (CSIR-NIO), for allowing me to carry out the research work at the institute. I thank the Head of the Department of Biological Oceanography Division (BOD), Dr. Manguesh U Gauns, for his help and valuable suggestions during PhD proposal and SRF assessment. I also wish to acknowledge the library, administrative, security, and HRM staff of NIO and the administrative staff of the School of Earth, Ocean, and Atmospheric Sciences, Goa University, for their timely help during my PhD tenure.

I acknowledge UGC for providing Junior and Senior research fellowships, which helped me financially during my PhD tenure. I am gratefully indebted to Dr. Samir Damare, who gave me immense support and numerous opportunities to participate in scientific cruises. I will cherish those cruise memories forever. I thank all the crew

members and ship cell participants for their invaluable help during the extensive samplings. I also acknowledge the TraceBioMe and Poly Metallic Nodule (PMN) projects and their respective project leaders for funding those cruise trips.

I sincerely thank all the BBD scientists and technical officers Dr. S.S. Sawant, Mr. K. Venkat, Dr. Dattesh Desai, Dr. Lidita Khandeparker, Dr. Temjensangba Imchen, and Mr. Kaushal Mapari for their support and guidance. My special thanks to Dr. V.V.S.S. Sarma for his constant moral support and for providing me with a few cruise experiences. I have learned much about oceanography from his insightful discussions and presentations during those cruises.

I am obliged to my supportive seniors, Dr. Roy Rodrigues, who taught me about dino cysts, and Dr. Satish K, who taught me about phytoplankton pigment analysis and CHEMTAX analysis. I appreciate Ms. Ashwini Sawant's unconditional help in the pre-processing of various samples and for helping me with various daily lab chores. I also appreciate my other super seniors, colleagues, and friends from the BBD department Dr. Dhiraj, Dr. Rajath, Dr. Rajaneesh, Dr. Lalita, Dr. Suchandan, Dr. Gobardhan, Dr. Atchutan, Dr. Laxman, Dr. Noyel, Dr. Deodatta, Dr. Sangeeta, Dr. Nishanth, Dr. Ranjith, Dr. Niyati, Dr. Sailesh, Mr. Aseem, Mr. Wasim, Dr. Dipesh, Mr. Siddesh, Mr. Rafi, Ms. Vedangi, Ms. Alisha, Mr. Rinaldo, Mr. Sushant, Mr. Sumit, Mr. Roshan, and Mr. Nitin for their enormous help and support.

I would like to thank my NIO friends, Dr. Shrikant, Dr. Vineet, Mr. Santhos, Mr. Murali, Dr. Reshma, Mr. Rahul, Mr. Arpita, Dr. Liju, Dr. Afreen, Dr. Seyie, Dr. Jacky, Dr. Debosmita, Dr. Diksha, and Dr. Aziz for making life at NIO colony happening and fun.

I would also like to thank all the cruise buddies, Ms. Natasha, Ms. Vruti, Ms. Shruti, Ms. Komal, Ms. Shalini, Ms. Devyani, Mr. Dawood, Dr. Venkatesh, Dr. Damodararao, Dr. Kuldeep, Dr. Mandar, Dr. Sambhaji, Ms. Abantika, Dr. Nirmalya, Ms. Chhaya, Dr. Arvind, Mr. Mahesh, Mr. Akshay, Mr. Conroy, Dr. Muruganandam, Dr. Naman, Dr. Shrinivash, Dr. Krushna, Dr. Subha Anand, Dr. Sabyasachi, Mr. Abhimanyu, Mr. Jayesh, Mr. Santosh, Mr. Rahul, Mr. Anthony, Mr. Milind, Mr. Kuldeep, and Mr. Kalathian for making sailing smooth and memorable.

I am sincerely grateful and lucky to have very understanding, supportive, cooperative, and helpful lab mates and juniors like Ms. Aparna Mol T.A., Mr. Sarun T.P., Mr. Ankur Sharma, Mr. Akash P., Ms. Rosmin Joseph, Ms. Garima Chaudhari, Ms. Ankita Praharaj, Ms. Geetanjali Thakur, and Ms. Sanah Khan. My PhD journey

would have been monotonous and boring without my lab mates.

This acknowledgment would be incomplete without mentioning the unconditional love and support I have received from Ms. Safia Khan. I greatly appreciate Mr. Barkat Ali Khan, Mrs. Farida Khan, Ms. Aafreen Khan, and Ms. Bahaar Khan for being my family in Goa and showing me love, care, and compassion.

This journey would not have been possible, and no amount of appreciation can justify the sacrifices my parents have made for me. My loving Maa (Mrs. Chitra Paul) and Baba (Mr. Pradip Paul) have always been there through all my thick and thin, ups and downs. They have been my constant cheerleaders, support pillars, and inspiration. It's all their teachings, love, and faith that push me to become a better person every day. This PhD journey is not merely a degree but a beacon of hope and a testament to resilience, which was instilled by my parents.

I honestly thank all those who helped me directly or indirectly to complete this thesis. Above all, I thank God Almighty!

Prancy Paul

Dubito, ergo cogito, ergo sum

"I doubt, therefore I think, therefore I am"

-René Descartes

Abbreviations

19′BF: 19′-butanoyloxyfucoxanthin

19′HF: 19′-hexanoyloxyfucoxanthin

2C: 2 Cones

ABW: Antarctic Bottom Water

Allo: Alloxanthin

AS: Arabian Sea

AST1: Arabian Sea Transect 1

AST2: Arabian Sea Transect 2

B: Box

B2Cyl: Box + 2 Cylinders

BElliP: Box + Elliptic prism

BoB: Bay of Bengal

C:P: Centri to pennate ratio

Car: β carotene

C-AS: Coastal Arabian Sea

Chl-a: Chlorophyll a

Chl-b: Chlorophyll b

Chl-c: Chlorophyll c

CHs: Cone + Half sphere

Cyl: Cylinder

Cyl2Hs: Cylinder + 2 Half sphere

Cym: Cymbelloid

d: Diameter or body size

d: Species richness

DCA: Detrended correspondence analysis

DD: Diadinoxanthin

Df: Dinoflagellates

Dt(C): Centric diatoms

Dt(M): Both pennate and centric diatoms

Dt(P): Pennate diatoms

DT: Diatoxanthin

DTF: Dias tidal flat

DW: Distilled water

EF: East front

EICC: East Indian Coastal Current

EIO: Equatorial Indian Ocean

Elli: Ellipsoid

Elli2CCyl: Ellipsoid + 2 Cones + Cylinder

Elli2CoCyl: Ellipsoid + 2 Cones + Cylinder

ElliP: Elliptic prism

ElliP4C: Elliptic prism + 4 Cones

F (Fa and Fb): Flushed or flushing period

F: Frontal region

F_0: Initial fluorescence

F_m: Maximum fluorescence

FRRF: Fast repetition rate fluorometer

Fuco: fucoxanthin

F_v/F_m: Photosynthetic efficiency

F_v: Variable fluorescence

GALD: Greatest axial linear dimension

Gam: Gamphonemoid

H': Species diversity

HAB: Harmful algal bloom

HPLC: High-performance liquid chromatography

HT: High tide

IDW: Indian Deep Water

IO: Indian Ocean

ITF: Indonesian Through Flow

J': Species evenness

LT: Low tide

Lut: Lutein

MF: Main front

MLD: Mixed layer depth

MPB: Microphytobenthos

MPN: Most probable number

MT: Mid tide

MTF: Miramar tidal flat

N: Total number of cysts

NEAS: North-eastern Arabian Sea

NEAS-C: North-eastern Arabian Sea Coastal

NEAS-O: North-eastern Arabian Sea Open Ocean

NEIO: North Equatorial Indian Ocean

Neo: Neoxanthin

NF: Non-flushed or non-flushing period

NF: Non-frontal region

NFE: Non front east

NFW: Non front west

NIO: North Indian Ocean

NPQ: Non-photochemical quenching

O-AS: Oligotrophic Arabian Sea

OMZ: Oxygen minimal zone

PAR: Photosynthetically active radiation

Per: Peridinin

PFZ: Potential fisheries zone

PGS: Phytoplankton geometric shapes

PGW: Persian Gulf Water

PL: Process length

POC: Particulate organic carbon

PoP: Prism on parallelogram

PoT: Prism on triangle

PPC: Photoprotective carotenoids

Pras: Prasinoxanthin

ProS: Prolate spheroid

ProS2Cyl: Prolate spheroid + 2 Cylinders

PSC: Photosynthetic carotenoids

PSII: Photosystem II

RDA: Redundancy analysis

RP: Rock pool

RSW: Red Sea Water

S: Species count

S:V: surface-to-volume ratio

SCML: Sub-surface chlorophyll maximum layer

SEAS: South-eastern Arabian Sea

SEAS-O: South-eastern Arabian Sea Open Ocean

SEIO: South Equatorial Indian Ocean

SIO: South Indian Ocean

SLA: Sea level anomaly

SM: Summer monsoon

SST: Sea Surface Temperature

STIO: South Tropical Indian Ocean

SW: Surf water

UVR: UV radiation

Viola: Violaxanthin

W: Wet sediment weight

WC: Water content

WF: West front

WM: Winter monsoon

WS: Wet sediment

Zea: Zeaxanthin

σ_{PSII}**:** Functional absorption cross section

Dedicated to

My beautiful mother
a lady known for her candor, patience, and love

&

My beloved father
a gentleman known for his kindness, hard work, and empathy

Contents

Declaration
Acknowledgment
Abbreviations
List of Tables
List of Figures

1. General Introduction **1-7**

2. Materials and Methods **8-37**
2.1. The Intertidal Ecosystem **8**
2.1.1. Tidal flat Ecosystem **8-17**
2.1.2. The Rockpool Ecosystem **18-20**
2.2. The Pelagic Ecosystem **21**
2.2.1. Water column **21-28**
2.2.2. Sediment **28-34**
2.2.3. Experimental setup to assess the photo-physiological adaptation of microalgae **35-37**

3. Diversity and distribution of planktonic and benthic microalgae **38-107**
3.1. The Intertidal Ecosystem **38-79**
3.1.1. Introduction **38-40**
3.1.2. Methodology **40**
3.1.3. Results **40-69**
3.1.3.1. Environmental variables at Dias and Miramar tidal flat **40-45**
3.1.3.2. The phytoplankton and microphytobenthos assemblage of Dias and Miramar tidal flat **46-64**
3.1.3.3. Influence of surf water on MPB assemblage **65-69**
3.1.4. Discussion **70-78**
3.1.4.1. Inter-annual variations **71-75**
3.1.4.2. Inter-seasonal variations **75-77**
3.1.4.3. Decadal variations at DTF **77-78**

3.1.5. Conclusion **78-79**
3.2. The Pelagic Ecosystem **80-107**
3.2.1. Introduction **80-82**
3.2.2. Methodology **82**
3.2.3. Results **82-99**
3.2.3.1. Dinoflagellate cyst diversity and distribution **82-90**
3.2.3.2. Comparison with previous studies **90-95**
3.2.3.3. Morphometric variability in the cosmopolitan species **95-97**
3.2.3.4. Plankton drift simulations to track the origin of dinoflagellate cysts **97-99**
3.2.4. Discussion **100-106**
3.2.4.1. Dinoflagellate cyst diversity and distribution **100-102**
3.2.4.2. Transport scenarios for dinoflagellate cyst in the IO **102-103**
3.2.4.3. Comparison of dinoflagellate cyst assemblages with previous studies in the IO **103-105**
3.2.4.4. Morphometric variabilities in cosmopolitan dinoflagellate cysts and potential proxy **105-106**
3.2.5. Conclusion **106-107**

4. Delineating the phytoplankton distribution patterns based on taxonomic and functional classification **108-202**
4.1 The Intertidal Ecosystem **108-131**
4.1.1. Rockpools and tidal flats **108-131**
4.1.1.1. Introduction **108-110**
4.1.1.2. Methodology **111**
4.1.1.3. Results **111-125**
4.1.1.3a. Distribution of microalgae based on taxonomic nomenclature in rockpool **111-112**
4.1.1.3b. Microalgal composition and distribution based on geometric shape as a trait in the rockpool **112-120**

4.1.1.3c. The phytoplankton shape variability in the surf water of tidal flats **121**

4.1.1.3d. MPB shape variability in the tidal flats **122-123**

4.1.1.3e. Effect of *A. carterae* cell-free filtrate on other rockpool microalgae **124-125**

4.1.1.4. Discussion 126-130

4.1.1.4a. Influence of location on the microalgal community based on taxonomic nomenclature **126-127**

4.1.1.4b. Microalgal community based on geometric shapes at different tidal zones in the intertidal regions **127-129**

4.1.1.4c. Allelopathy of bloom-forming dinoflagellate *Amphidinium* against other microalgae **129-130**

4.1.1.5. Conclusion 131

4.2 The Pelagic Ecosystems 132-202

4.2.1. Different oceanographic settings 132-166

4.2.1.1. Introduction 132-136

4.2.1.2. Methodology 137

4.2.1.3. Results 137-160

4.2.1.3a. Taxonomic and shape diversity of the north-eastern Arabian Sea (NEAS) **137-152**

4.2.1.3b. Taxonomic and shape diversity of the south-eastern Arabian Sea (SEAS) **152-156**

4.2.1.3c. Taxonomic and shape diversity comparison between NEAS-O and SEAS-O **157-160**

4.2.1.4. Discussion 160-166

4.2.1.4a. Variability between coastal and open ocean ecosystems **161-162**

4.2.1.4b. Variability in contrasting oceanographic settings **162-164**

4.2.1.4c. Variability in frontal and non-frontal regions **164-166**

4.2.1.5. Conclusion **166**

4.2.2. The sea surface and sub-surface chlorophyll maximum layers in different bioregions **167-202**

4.2.2.1. Introduction **167-169**

4.2.2.2. Methodology **169-174**

4.2.2.3. Results **175-192**

4.2.2.3a. Hydrographic condition of the Indian Ocean **175-177**

4.2.2.3b. Relationship between PGS, morphological traits, and environmental variables **177**

4.2.2.3c. PGS diversity of surface waters **177-183**

4.2.2.3d. PGSs in varying depths of SCML **183-186**

4.2.2.3e. S:V and GALD of PGSs in varying depths of SCML **187**

4.2.2.3f. Comparative results between the sea surface and SCML **187-192**

4.2.2.4. Discussion **192-201**

4.2.2.4a. Variability of diversity and morphological traits of PGS in sea surface **193-195**

4.2.2.4b. Variability of diversity and morphological traits of PGS in varying depths of SCML **195-199**

4.2.2.4c. Sea surface vs SCML **199-201**

4.2.2.5. Conclusion **202**

5. Photo-physiological adaptation of microalgae from different bioregions **203-219**

5.1. Introduction **203-205**

5.2. Methodology **205**

5.3. Results **205-213**

5.3.1. Phytoplankton community **205-206**

5.3.2. Effect of solar radiation on PSII parameters **206-211**

5.3.3. Effect of solar radiation on photoprotective pigments **211-213**

5.4. Discussion **213-218**

5.4.1. Effect of solar radiation on PSII parameters and photoprotective pigments **213-216**

5.4.2. Comparison of photoprotection mechanism from habitats receiving extremely high light **216-218**

5.5. Conclusion **218-219**

6. Summary **220-225**

Bibliography **226-278**

Publications

List of Figures

Figure 1.1. Figure showing typology of phytoplankton functional traits. (Illustration from Litchman & klausmeier, 2008).

Figure 1.2. Figure showing studies conducted worldwide on (a) microphytobenthos topics, (b) country-wise number of publications, and (c) dinoflagellate cyst. (Illustration (a) & (b) from Park et al., 2014; (c) from Marret et al., 2020).

Figure 1.3. Figure showing studies conducted based on phytoplankton traits worldwide from different habitats and research perspectives. (Illustration from Weithoff & Beisner, 2019.

Figure 2.1. Map showing the location of the tidal flat sampling stations at a) Miramar Beach and b) Dias Beach.

Figure 2.2. Map showing the location of the Rockpools.

Figure 2.3. Map showing the location of the water column sampling site in a) the northeastern and southeastern Arabian Sea and b) the Indian Ocean.

Figure 2.4. Map showing the location of the sediment sampling stations in the Indian Ocean.

Figure 2.5. Map showing the location of the experimental study site in different bioregions of the Arabian Sea and South tropical Indian Ocean.

Figure 3.1. Plot showing sediment grain size in low, mid, and high-tide zones at a) Dias tidal flat and b) Miramar tidal flat during the study period.

Figure 3.2. Plots showing environmental variables during the study period: a-b) Temperature, c-d) Salinity, e-f) Chlorophyll *a*, and g) Rainfall at both DTF (a-c) and MTF (d-f). Shaded regions represent the monsoon seasons.

Figure 3.3. Plots showing inter-annual variability in diatoms and dinoflagellates, centric

and pennate diatoms, and abundance of epipelic and episammasic diatoms in a) surf water, b) low-tide, c) mid-tide, and d) high-tide zones during the study period at DTF. Shaded regions represent the monsoon seasons.

Figure 3.4. Plots showing cluster analysis of the dominant phytoplankton species in the surf water of a) DTF and b) MTF.

Figure 3.5. Plots showing inter-annual variability in diatoms and dinoflagellates, centric and pennate diatoms, and abundance of epipelic and episammasic diatoms in a) surf water, b) low-tide, c) mid-tide, and d) high-tide zones during the study period at MTF. Shaded regions represent the monsoon seasons.

Figure 3.6. Plots showing diversity indices of surf water (SW), low-tide (LT), mid-tide (MT), and high-tide (HT) zones during the study period at Dias tidal flat (a-d) and Miramar tidal flat (e-h).

Figure 3.7. Plots showing cluster analysis of the dominant MPB species in a) low-tide, b) mid-tide, and c) high-tide zone of DTF.

Figure 3.8. Plots showing cluster analysis of the dominant MPB species in a) low-tide, b) mid-tide, and c) high-tide zone of MTF.

Figure 3.9. Plots showing seasonal variability of phytoplankton in a) surf water and in microphytobenthos in b) low-tide, c) mid-tide, and d) high-tide zones during pre-monsoon, monsoon, and post-monsoon season at DTF. Data presented here is the months' average in the respective seasons and years.

Figure 3.10. Plots showing seasonal variability of phytoplankton in a) surf water and in microphytobenthos in b) low-tide, c) mid-tide, and d) high-tide zones during pre-monsoon, monsoon, and post-monsoon season at MTF. Data presented here is the months' average in the respective seasons and years.

Figure 3.11. Plots showing seasonal diversity indices of surf water, low-tide, mid-tide, and high-tide zones in pre-monsoon, monsoon, and post-monsoon seasons at Dias tidal flat.

Figure 3.12. Plots showing seasonal diversity indices of surf water, low-tide, mid-tide,

and high-tide zones in pre-monsoon, monsoon, and post-monsoon seasons at Miramar tidal flat.

Figure 3.13. Regression plot showing correlation between a) microphytobenthos and SW-phytoplankton, b) MPB-centric and SW-centric diatoms, and c) MPB-pennate and SW-pennate diatoms in low-tide (red diamond shape), mid-tide (black circle shape), and high-tide (blue triangle) zones of Dias and Miramar tidal flat.

Figure 3.14. The schematic shows tidal zone, seasonal, and comparative inter-annual variations between the Dias tidal flat (DTF) and Miramar tidal flat (MTF). The darker, slightly light, and light color shades represent the highest, comparatively low, and lowest values of different parameters. The pennate diatom SEM image indicates the MPB community, the wave symbol indicates wave intensity, the meter symbol indicates salinity, the thermometer indicates temperature, and the droplet indicates nutrients.

Figure 3.15. The schematic shows pre-monsoon, monsoon, and post-monsoon inter-seasonal variations between the Dias tidal flat (DTF) and the Miramar tidal flat (MTF). The darker, slightly light, and light color shades represent the highest, comparatively low, and lowest values of different parameters.

Figure 3.16. Micrograph of dinoflagellate cysts **A) Autotrophic:** 1) Cyst of *Alexandrium* sp., 2) *Bitectatodinium spongium,* 3) *Impagidinium aculeatum,* 4) *Impagidinum paradoxum,* 5) *Impagidinum patulum,* 6) *Impagidinum strialatum* 7) *Nematosphaeropsis labyrinthus*, 8) *Operculodinium centrocarpum,* 9) *Operculodinium janduchenei*, 10) Cyst of *Pentapharsodinium dalei,* 11) *Polysphaeridium zoharyi,* 12) *Spiniferites bentorii,* 13) *Spiniferites hyperacanthus,* 14) *Spiniferites mirabilis,* 15) *Spiniferites ramosus*, 16) *Tuberculodinium vancampoae*, **B) Heterotrophic:** 17) *Brigantedinium simplex,*18) *Brigantedinium sp., 19*) Cyst of *Cladopyxis sp.*, 20) Cyst of *Polykrikos kofoidii,* 21) Cyst of *Polykrikos schwartzii,* 22) Cyst of *Protoperidinium denticulatum,* 23) Cyst of *Protoperidinium latissimum,* 24) Cyst of *Protoperidinium monospinum,* 25) Cyst of *Diplopelta* sp., 26) *Echinidinium* sp., 27) *Lejeunecysta sabrina,* 28) *Quinquecuspis pentagonum,*

29) *Selenopemphix nephroides*, 30) *Selenopemphix quanta*, 31) *Stelladinium abei*, 32) *Stelladinium bifurcatum*, 33) *Stelladinium reidii*, 34) *Stelladinium stellatum*, 35) *Trinovantedinium applanatum*, 36) *Votadinium calvum*, **C) Mixotrophic:** 37) Cyst of *Polykrikos hartmannii*, 38) *Lingulodinium machaerophorum*, 39) *Ligulodinium* sp. (all scale bar 20 micron).

Figure 3.17. Variations in dinoflagellate cyst a) abundance, b) Autotrophic, heterotrophic, and mixotrophic forms, c) species count, d) species evenness, e) species richness, and f) species diversity in the Indian Ocean. C-AS: coastal Arabian Sea, O-AS: oligotrophic Arabian Sea, OMZ-AS: oxygen minimum zone Arabian Sea, BoB: Bay of Bengal, EIO: the equatorial Indian Ocean, and STIO: south tropical Indian Ocean.

Figure 3.18. Bar plots showing a) HAB cyst concentration and species count and b) percentage contribution in different bioregions of the Indian Ocean. C-AS: coastal Arabian Sea, O-AS: oligotrophic Arabian Sea, OMZ-AS: oxygen minimum zone Arabian Sea, BoB: Bay of Bengal, EIO: equatorial Indian Ocean, and STIO: south-tropical Indian Ocean.

Figure 3.19. Plots showing comparative data for dinoflagellate cysts in the Indian Ocean a) dinoflagellate cyst concentration (cysts g^{-1}) and b) Species count. Present study locations are represented using numbers, and unnumbered dots represent previous studies. Data for species count and concentration for comparison are taken from Zonneveld et al., 2013; D'Silva et al., 2011; Narale et al., 2015; Dcosta et al., 2008 and Rodrigues et al., 2022.

Figure 3.20. The plot shows morphometric measurements of dinoflagellate cyst body size (L=length, W=width, and D=diameter) and process length (PL) in the Indian Ocean. **i)** *Operculodinium centrocarpum* a) body size (diameter) and b) process length, and **ii)** *Nematosphaeropsis labyrinthus* c) body size (length and width) and d) process length. C-AS: coastal Arabian Sea, O-AS: oligotrophic Arabian Sea, OMZ-AS: oxygen minimum zone Arabian Sea, BoB: Bay of Bengal, EIO: the equatorial Indian Ocean, and STIO: south tropical Indian Ocean.

Figure 3.21. The map shows the possible surface origin locations of the sinking

particles by the ocean currents for a sinking speed of 11 m/day. The data points are generated from the planktondrift.science.uu.nl website and plotted in the ODV using a surface plot.

Figure 4.1. Bubble plot of the temporal (2014 & 2015) and spatial (among low-tide (LT), mid-tide (MT), and high-tide (HT) rock pools) variation of the total rock pool phytoplankton abundance. The maximum symbol diameter corresponds to 70 x 10^3 cells L^{-1}. Fa: flushing during the first five days, NF: non-flushing, and Fb: flushing during the last five days of the 15-day sampling. Species highlighted in red are known to be toxic or harmful species.

Figure 4.2. Taxonomy-wise diversity indices of RP microalgae. S: species count, d: species richness, J': evenness, H': Shannon–Weiner's index, Fa, and Fb: flushing period, NF: non-flushing period, LT: low-tide, MT: mid-tide and HT: high-tide.

Figure 4.3. Bubble plot showing the temporal (2014 and 2015) and spatial (among low-tide (LT), mid-tide (MT), and high-tide (HT) rock pools) variation of the total rock pool phytoplankton abundance based on shapes. The maximum symbol diameter corresponds up to 809x10^3 cells L^{-1}. Fa: flushing during the first five days, NF: non-flushing, and Fb: flushing during the last five days of the 15-day sampling. Df: dinoflagellates; Dt(P): pennate diatoms; Dt(C): centric diatoms; Dt(M): both pennate and centric diatoms.

Figure 4.4. Diversity indices of RP microalgae based on shapes. S: species count, d: species richness, J': evenness, H': Shannon–Weiner's index, Fa, and Fb: flushing period, NF: non-flushing period, LT: low-tide, MT: mid-tide and HT: high-tide.

Figure 4.5. Cluster dendrogram based on geometric shapes for the years 2014 (a) and 2015 (b) using the Bray–Curtis similarity coefficient and group average method: grouping done at 50% similarity (data is log transformed; LT: low-tide, MT: mid-tide, HT: high-tide, Fa, and Fb: flushing period and NF: non-flushing period).

Figure 4.6. Cluster dendrogram based on geometric shapes with respect to flushing (Fa and Fb) and non-flushing (NF) period for the year (a) 2014 and (b) 2015 using the Bray–Curtis similarity co-efficient and group average method: grouping done at 50% similarity. Data is log-transformed: LT: low-tide, MT: mid-tide, HT: high-tide.

Figure 4.7. Plots showing percentage contribution of phytoplankton geometric shapes in pre-monsoon, monsoon, and post-monsoon seasons in a & e) surf water, b & f) low-tide, c & g) mid-tide, and d & h) high-tide zones of DTF (a-d) and MTF (e-h). The data presented here is the month's average for the respective seasons and years.

Figure 4.8. Effect of *A. carterae* cell-free filtrate on the growth of (a) *Skeletonema costatum*, (b) *Dunaliella tertiolecta*, and (c) *Bysmatrum gregarium* in different filtrate concentrations.

Figure 4.9. Groupwise distribution of phytoplankton in the water column of NEAS and SEAS. NEAS-O: North-eastern Arabian Sea open ocean; NEAS-C: North-eastern Arabian Sea coastal region and SEAS-O: South-eastern Arabian Sea open ocean.

Figure 4.10. Univariate measures of phytoplankton (both taxonomy and shape-wise) from NEAS (both coastal and open ocean) and SEAS (open ocean). Station data are pooled and presented here.

Figure 4.11. Relationship between GALD and S:V for the 8 dominant shapes recorded in North-eastern (NEAS-O and NEAS-C) and South-eastern Arabian Sea during the study period. a) NEAS-O: North-eastern Arabian Sea open-ocean, b) NEAS-C: North-eastern Arabian Sea coastal waters, and c) SEAS-O: South-eastern Arabian Sea open ocean; Cyl: Cylinder; ElliP: Elliptic prism; Cyl2Hs: Cylinder + 2 Half sphere; PoP: Prism on parallelogram.

Figure 4.12. Map showing Sea level anomaly (SLA) plot with SST frontal and non-frontal regions in coastal region of NEAS. The blue line is showing the location of the fronts, the black rectangle and white oval shapes showing the frontal and non-frontal part sampled in the present study.

Figure 4.13. Univariate measures of phytoplankton (both taxonomy and shape-wise) from frontal and non-frontal in the coastal region of NEAS. EF: East front; WF: West front; MF: Main front and NF: Non-front. Station data from the frontal and non-frontal regions are pooled and presented here.

Figure 4.14. Shape-wise cluster plot of micro-phytoplankton community of frontal and non-frontal coastal NEAS. WF: West front, EF: East front, MF: Main front and NF: Non-front.

Figure 4.15. Univariate measures of phytoplankton (both taxonomy and shape-wise) from transects T1 and T2 of SEAS (open ocean). Station data are pooled and presented here.

Figure 4.16. Univariate measures of phytoplankton (both taxonomy and shape-wise) from frontal and non-frontal in the oceanic region of SEAS. NFW: Non-front West; F: Frontal region and NFE: Non-front East. Station data from the frontal and non-frontal regions are pooled and presented here.

Figure 4.17. Taxonomy wise Cluster plot of open ocean frontal and non-frontal region micro-phytoplankton community of SEAS. NFW: Non-front West, F: Frontal region and NFE: Non-front East.

Figure 4.18. Distribution of dominant phytoplankton shape in the frontal and non-frontal water column of NEAS and SEAS. NEAS-C: Coastal North-eastern Arabian Sea; SEAS-O: Open Ocean South-eastern Arabian Sea; NF: Non-front; MF: Main front; WF: West front; EF: East front; NEF: Non-front East and NFW: Non-front West.

Figure 4.19. Taxonomy-wise cluster plot of micro-phytoplankton community of NEAS and SEAS. NEAS-O: North-eastern Arabian Sea open ocean, NEAS-C: North-eastern Arabian Sea coastal region, and SEAS-O: South-eastern Arabian Sea open ocean.

Figure 4.20. Distribution of dominant phytoplankton shape in the water column of NEAS and SEAS. NEAS-O: North-eastern Arabian Sea open ocean; NEAS-C: North-eastern Arabian Sea coastal region and SEAS-O: South-eastern Arabian Sea open ocean.

Figure 4.21. RDA results show the relationship between environmental variables and dominant PGS and morphometric traits (S:V and GALD) in a) shallow surface and SCML, b) intermediate surface and SCML, and c) deep surface and SCML. PGS: phytoplankton geometric shape, S:V: surface-to-volume ratio, and GALD: greatest axial linear dimension.

Figure 4.22. Dendrogram based on PGS of the micro-phytoplankton community of a) surface and b) SCML waters among the different regions of the Indian Ocean (IO). AST1: Arabian Sea transect 1, AST2: Arabian Sea transect 2, BoB: Bay of Bengal, NEIO: North equatorial Indian Ocean, SEIO: South equatorial Indian Ocean, STIO: South tropical Indian Ocean.

Figure 4.23. Box plot based on taxonomy and PGS from the Sea surface and SCML waters of different regions in the Indian Ocean. a,d,g,j) Margalef's species richness, b,e,h,k) Shannon-Wiener diversity, c,f,i,l) number of species. AST1: Arabian Sea transect 1, AST2: Arabian Sea transect 2, BoB: Bay of Bengal, NEIO: North equatorial Indian Ocean, SEIO: South equatorial Indian Ocean, STIO: South tropical Indian Ocean and SCML: sub-surface chlorophyll maximum layer.

Figure 4.24. Non-linear regression of dominant PGS in surface waters of the IO. AST1: Arabian Sea transect 1, AST2: Arabian Sea transect 2, BoB: Bay of Bengal, NEIO: North equatorial Indian Ocean, SEIO: South equatorial Indian Ocean, STIO: South tropical Indian Ocean, S:V: surface-to-volume ratio and GALD: greatest-axial-linear-dimension. ElliP: elliptic prism, Cyl: cylinder, and PoP: prism on parallelogram.

Figure 4.25. Non-linear regression of dominant PGS in varying depths of SCML in the IO. S:V: surface-to-volume ratio, GALD: greatest-axial-linear-dimension, ElliP: elliptic prism, Cyl: cylinder, and PoP: prism on parallelogram.

Figure 4.26. Non-linear regression of dominant PGS in surface waters of the IO. AST1: Arabian Sea transect 1, AST2: Arabian Sea transect 2, BoB: Bay of Bengal, NEIO: North equatorial Indian Ocean, SEIO: South equatorial Indian Ocean, STIO: South tropical Indian Ocean, S:V: surface-to-volume ratio, GALD: greatest-axial-linear-dimension, ElliP: elliptic prism, Cyl: cylinder and PoP:

prism on parallelogram.

Figure 4.27. Violin plot of morphological attributes (S:V and GALD) in dominant PGS from varying SCML depths. S:V: surface-to-volume ratio, GALD: greatest-axial-linear-dimension, SCML: sub-surface chlorophyll maximum layer, Cyl: cylinder, ElliP: elliptic prism, and PoP: prism on parallelogram.

Figure 4.28. Violin plot of morphological attributes (S:V and GALD) in dominant PGS from sea surface and SCML waters. S:V: surface-to-volume ratio, GALD: greatest-axial-linear-dimension, SCML: sub-surface chlorophyll maximum layer, Cyl: cylinder, ElliP: elliptic prism, and PoP: prism on parallelogram.

Figure 4.29. Violin plot of morphological attributes (S:V and GALD) in dominant PGSs from the sea surface and SCML of different regions in the Indian Ocean. AST1: Arabian Sea transect 1, AST2: Arabian Sea transect 2, BoB: Bay of Bengal, NEIO: North equatorial Indian Ocean, SEIO: South equatorial Indian Ocean, STIO: South tropical Indian Ocean, S:V: surface-to-volume ratio, GALD: greatest-axial-linear-dimension, Cyl: cylinder, ElliP: elliptic prism, and PoP: prism on parallelogram.

Figure 5.1. Plots showing a) pennate and centric percentage contribution, b) dial variation in solar radiation, and c-f) percentage contribution of pico-, nano-, and micro-phytoplankton based on marker pigment in PAR and PAR+UVR treatment during the incubation period in the Arabian Sea.

Figure 5.2. Plots showing a) diatom and dinoflagellate percentage contribution, b) dial variation in solar radiation, and c-h) percentage contribution of pico-, nano-, and micro-phytoplankton based on marker pigment in PAR and PAR+UVR treatment during the incubation period in the South-tropical Indian Ocean.

Figure 5.3. PSII parameters during the three days incubation in the Arabian Sea.

Figure 5.4. PSII parameters during the three days incubation in the South-tropical Indian Ocean.

Figure 5.5. Plot showing values of a) photoprotective carotenoids (PPC) to photosynthetic carotenoids (PSC), b) photoprotective pigment ratios, i.e., DD + DT/Chlorophyll-*a*, and c) de-epoxidation of the xanthophyll cycle pigment DD, i.e., DT/DD + DT during the incubation period in the Arabian Sea. DT: Diatoxanthin, DD: Diadinoxanthin; M: Morning, and E: Evening.

Figure 5.6. Plot showing values of a) photoprotective carotenoids (PPC) to photosynthetic carotenoids (PSC), b) photoprotective pigment ratios, i.e., DD + DT/Chlorophyll-*a*, and c) de-epoxidation of the xanthophyll cycle pigment DD, i.e., DT/DD + DT during the incubation period in the South-tropical Indian Ocean. DT: Diatoxanthin, DD: Diadinoxanthin; M: Morning, and E: Evening.

List of Tables

Table 2.1. Most probable number (MPN) in 10 ml of sample, based on the presence and absence of growth in well-plates from three subsequent steps of a dilution-culture series: 5 well-plates with 1.0 ml inoculum each, 5 well-plates with 0.1 ml, and 5 well-plates with 0.0l ml (Taken from Throndsen, 1978).

Table 2.2. Table showing all the phytoplankton geometric shapes and their respective formulae used for calculation of volume and surface area during this study from different marine habitats (taken from Hillebrand et al., 1999; Sun & Liu, 2003). V: volume; A: surface area; a: length; b: width; c: height.

Table 2.3. Station details with regions and geographic positions.

Table 2.4. Details of the sampling locations, water depth, species count, and dinoflagellate cyst count per sample. C-AS: coastal Arabian Sea, O-AS: oligotrophic Arabian Sea, OMZ-AS: oxygen minimum zone Arabian Sea, BoB: Bay of Bengal, EIO: equatorial Indian Ocean, STIO: south-tropical Indian Ocean.

Table 3.1. Table showing phytoplankton and microphytobenthos taxa recorded in surf water (SW), low-tide (LT), mid-tide (MT), and high-tide (HT) zones during the study period and also indicates percentage contribution at both DTF and MTF.

Table 3.2. Dinoflagellate cysts concentration (cysts g^{-1} dry weight) in the Arabian Sea (AS), Bay of Bengal (BoB), Equatorial Indian Ocean (EIO), and South tropical Indian Ocean (STIO) A: autotrophic, H: heterotrophic, M: mixotrophic, C: coastal, O: oligotrophic, OMZ: oxygen minimum zone, NIO: North Indian Ocean and SIO: South Indian Ocean. (*): Indicates potential HAB species. The motile affinity is based on Li et al., 2023; Marret et al., 2020; Ramírez-Valencia et al., 2021; Rigel et al., 2022.

Table 3.3. The table shows dinoflagellate cysts abundance (cysts g^{-1} dry weight) in transects 1 and 2 of the Arabian Sea. A: Autotrophs; M: Mixotrophs; H: Heterotrophs; EAS: eastern Arabian Sea; WAS: western Arabian Sea. Trophic

status is given following Marret et al., 2020. The motile affinity is based on Li et al., 2023; Marret et al., 2020; Ramírez-Valencia et al., 2021; Rigel et al., 2022. Indet: indeterminate, + means previously reported.

Table 4.1. Phytoplankton abundance (cells L-1) in low (LT), mid (MT), and high (HT) tide rock pools during non–flushing (NF) and flushing (Fa – before NF; and Fb– after NF) periods in the summer months of both years (2014 and 2015).

Table 4.2. Hydrography and nutrient concentration at surface and sub-surface in NEAS-O, NEAS-C, and SEAS-O in winter monsoon. The mean value is calculated for temperature, salinity, and oxygen concentration. The median value is used for nutrient concentration. The numbers in parenthesis indicate the parameter's range values, and the * indicates the chlorophyll concentration value.

Table 4.3. Hydrography and nutrient concentration at surface and sub-surface frontal and non-frontal regions of NEAS-C and SEAS-O in winter monsoon. The mean value is calculated for temperature, salinity, and oxygen concentration. The median value is used for nutrient concentration. The numbers in parentheses indicate the range values of the parameter.

Table 4.4. Micro-phytoplankton abundance (depth-averaged cells L^{-1}) and the corresponding shape in the open ocean and coastal region of North-eastern Arabian Sea (NEAS-O and NEAS-C) and open ocean of South-eastern Arabian Sea (SEAS-O). Species in bold font indicate diatoms and normal font indicates dinoflagellates; numbers in parenthesis are numbers of shapes recorded.

Table 4.5. Station details with regions, geographic positions, mixed layer depth, and nitracline depth.

Table 4.6. Stations are grouped according to varying depths of SCML.

Table 4.7. The environmental parameters and nutrient concentration at the sea surface and SCML of different regions of the Indian Ocean. The values of environmental parameters are mean, and nutrients are median. The range values are given in parentheses.

Table 4.8. The environmental parameters and nutrient concentration at varying depths of SCML of the Indian Ocean. The values of environmental parameters are mean, and for nutrients, it is median along with standard error.

Table 4.9. The table shows the percentage contribution of PGSs and dominant taxa in the sea surface and SCML of the Indian Ocean bioregions.

Table 4.10. The table shows the percentage contribution of PGSs and dominant taxa in different depths of SCML.

Chapter 1
Introduction

Chapter 1: General Introduction

Microalgae are microscopic photosynthetic organisms, ubiquitous in all the waterbodies (freshwater and marine). They are a very diverse group that includes green algae, phytoplankton (diatoms and dinoflagellates), and coccolithophores with an unknown number of species (De Clerck et al., 2013; Guiry, 2012). Microalgae are abundant in the sunlit zone of the water column (rivers, lakes, reservoirs, and oceans) and the upper layer of sediment (e.g., shallow water and intertidal regions). Microalgae in water columns and sediment are called phytoplankton and phytobenthos, respectively. Their capability to thrive in such contrasting habitats shows that they have a variety of adaptive strategies. Morphological and physiological (hereafter Morpho-physiological) adaptation is the only alternative for these primary producers to sustain in their respective habitats, dependent on constantly changing physicochemical forces. For example, the species belonging to pennate (having the ability to attach) and centric diatoms (ability to float) are mostly dominant in the benthic and pelagic systems. Further, the abiotic (e.g., light, nutrients, hydrodynamics) and biotic (e.g., grazers) factors construct the ultimate fate of microalgae in their respective habitat. The complete dependence on nutrient uptake, light availability, and a limited capacity to evade grazers significantly shape their morphology and physiology. Thus, morphology (size, shape, presence of flagella, presence of mucilage, colony formation, and resting stages) and physiology (photosynthetic efficiency, photo-adaptations/protection, nutrient uptake, mixotrophic ability, and buoyancy regulation) of these primary producers are the major descriptors of their surrounding ecological conditions (Figure 1.1). Different microalgal groups dominate different habitats of the marine ecosystem. For instance, in the shallow neritic regions, diatoms dominate both the planktonic (mostly centric diatoms) and benthic communities (mostly pennate diatoms), whereas, in the oceanic regions, diatoms, dinoflagellate, chlorophytes, and cyanobacteria are prominent in the water column and frustules and resting stages (e.g., dinoflagellate cysts, spores) in the underlying sediments. The microalgae in the intertidal and shallow subtidal sediments are known as microphytobenthos (MPB) (Underwood & Kromkamp, 1999).

The MPB assemblages, though mostly dominated by diatoms, can also include dinoflagellates, cyanobacteria, and euglenoids (MacIntyre et al., 1996). The MPB is one of the major primary producers in the intertidal system (Underwood & Kromkamp, 1999) and plays key ecological roles by serving as food sources for meiofauna, macrofauna, and

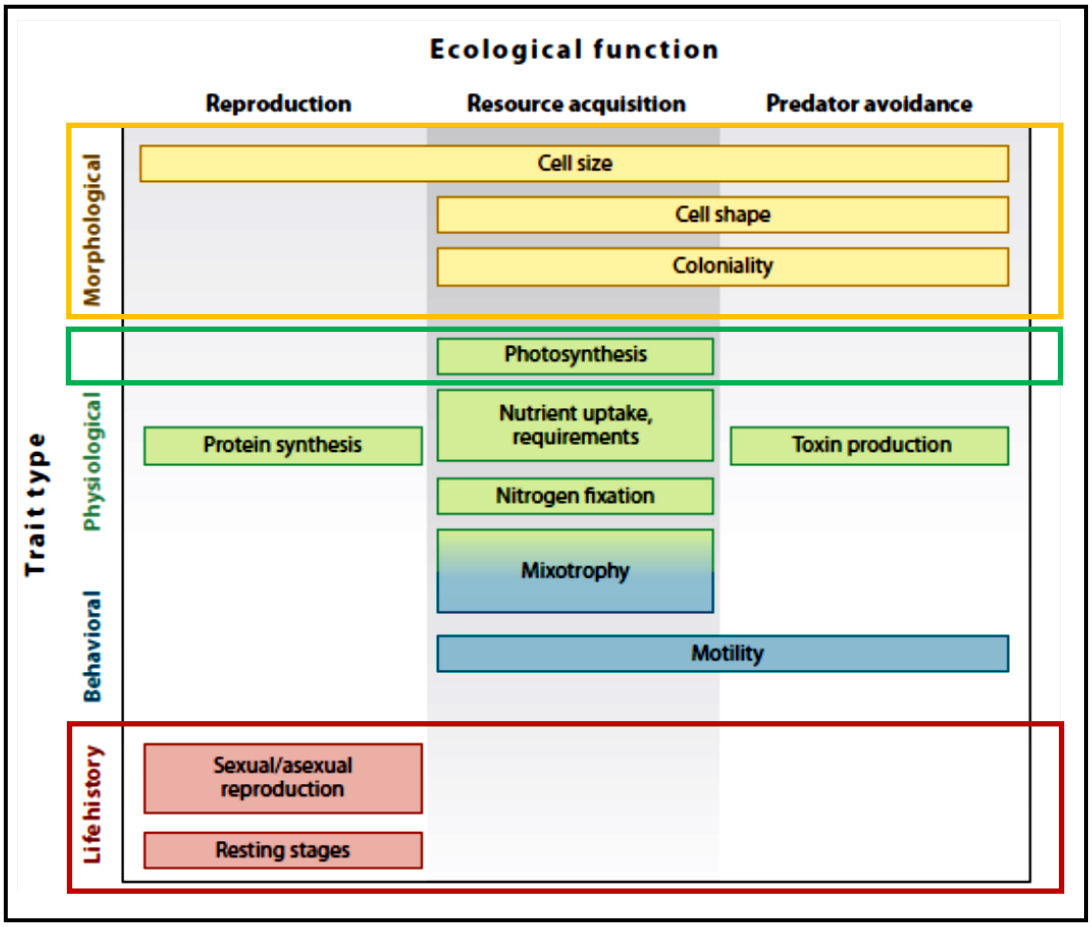


Figure 1.1. Figure showing typology of phytoplankton functional traits. (Illustration from Litchman & klausmeier, 2008).

other deposit-feeders, which in turn support the upper levels of the trophic food web, like birds and fish (Kang et al., 2015). However, when MPB are resuspended in the adjacent water column, they also serve as a food source for suspension feeders (Lefebvre et al., 2009; Ubertini et al., 2012; Herman et al., 2001; Oakes et al., 2016). MPB colonizes large areas of intertidal sediment in estuaries and coastal areas, facilitates vital ecosystem services (Hope et al., 2020), and can even extend to the edge of the continental shelf (Cahoon, 1999; Pinckney, 2018). The phytoplankton community has been extensively studied in Indian waters, but the focus has always been on the planktonic forms (Chitari & Anil, 2017; Bharathi et al., 2018; Jagadeesan et al., 2017; Arunpandi et al., 2017; Kusum et al., 2017; Hardikar et al., 2017; Ahmed et al., 2016). The microphytobenthos (MPB) community, compared to elsewhere in the world (Park et al., 2014 and the references therein), has received very limited attention from India (Mitbavkar and Anil,

2002, 2004, 2006; Anil et al., 2007; Patil et al., 2017; Benny et al., 2021; Mandal et al., 2021; Jeslin et al., 2021; Amal et al., 2024) (Figure 1.2a-b).

Similarly, dinoflagellates (only 12-13%) are known to produce organic-walled and calcareous cysts as part of their life cycles (Head, 1996), but in some cases, adverse environmental conditions (like changes in temperature, salinity, and nutrient flux), can also induce cyst production. Many of these resting organic-walled cysts resist physical, chemical, and biological degradation (Dale, 1996) and settle at the bottom of the ocean floor. These cysts help dinoflagellates to form seed banks for blooms (including harmful algal blooms), produce toxins (e.g., *Alexandrium* Halldal & Dale, 1971 and *Gymnodinium* Ehrenberg, 1834 species), and help in unwanted marine bio-invasion as they remain viable for many years (Matsuoka & Fukuyo, 2000; Lundholm et al., 2011; Delebecq et al., 2020). Generally, the morphology of dinoflagellate cysts is species-specific, but their variability, particularly in cyst size and process length, due to environmental factors (temperature and salinity), makes them potential proxies for such factors (Rodrigues & Patil, 2021). Dinoflagellate cyst morphology and their variability is well documented from both laboratory and field studies (e.g., Ellegaard et al., 2002; Mertens et al., 2009a, 2009b, 2010 and 2012; Rodrigues & Patil, 2021). So far, most of the work on dinoflagellate cysts are from the shallow coastal regions and port areas of the eastern Arabian Sea (Godhe et al., 2000; D'costa et al., 2008; Dsilva et al., 2011, 2012; Narale et al., 2015; Rodrigues et al., 2019, 2022) and from the productive coastal regions of the western Arabian Sea (Zonneveld et al., 1997, 2003, 2013; Marret & Zonneveld, 2003), but studies from the pelagic regions are none (Figure 1.2c).

Traditionally, morphology was used for phylogenetic classification as a main feature, but it reveals nothing about the ecological functions (Salmaso & Padisak, 2007). Though the recent use of genetic and molecular techniques has refined the taxonomic and phylogenetic classification, they do not always reflect the perceived ecological functions of the organism and are of little use to ecologists (Solbrig, 1993). The ecological value of morphological descriptors in phytoplankton in relation to the uptake of light and nutrients was first deciphered by Lewis (1976). Later on, Margalef (1978) suggested that phytoplankton life forms, when used as determinants of seasonal succession, show that morphological variability has an adaptive value directed toward the best fitting of the environmental template. Much later, Reynolds (1997, 2006, and literature therein) elaborated on how differences in phytoplankton morphology are related to adopting diverse ecological strategies.

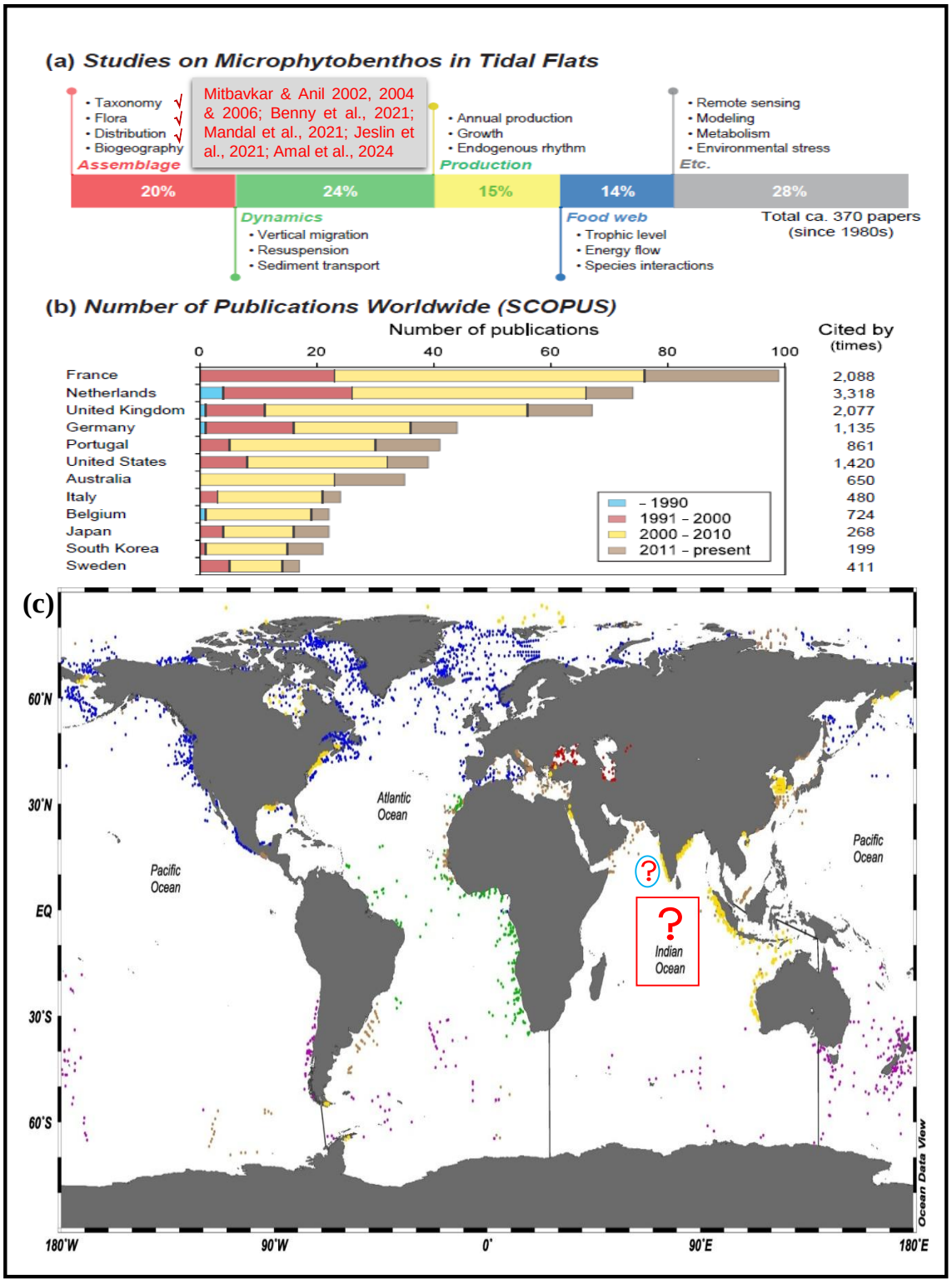
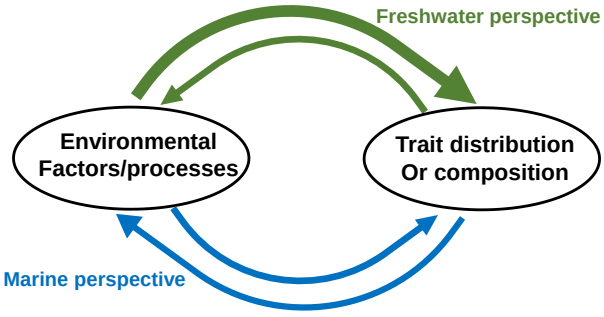


Figure 1.2. Figure showing studies conducted worldwide on (a) microphytobenthos topics, (b) country-wise number of publications, and (c) dinoflagellate cyst. (Illustration (a) & (b) from Park et al., 2014; (c) from Marret et al., 2020).

Phytoplankton assemblages under variable environmental conditions can perhaps be shaped by size and form selection in natural environments (Morabito et al., 2007; Naselli-Flores & Padisak, 2024). A large diversity of different sizes and shapes of species can be supported by the dynamic aquatic environments, either present in the assemblages or as propagules ready to develop when the environmental template turns favorable (Padisak, 1992). The size and shape of phytoplankton expressed by greatest axial linear dimension (GALD) and surface-to-volume ratio (S:V) reflect their ability to obtain nutrients, light, resist sinking, and reduce grazing pressure (Lewis, 1976; Naselli-Flores et al., 2007). In the past few decades, the use of these morphometric traits to explain and understand phytoplankton community distribution is well explored in various ecosystems: freshwater ecosystem (Margalef, 1978; Reynolds, 1988; Weithoff, 2003; Salmaso & Padisak, 2007; Litchman & Klausmeier, 2008; Kruk et al., 2010; Naselli-Flores & Barone, 2011; Martini et al., 2021; Laraib et al., 2023; Naselli-Flores & Padisak, 2024; Welbara et al., 2024) estuarine ecosystem (O'Farrell et al., 2007; Kruk et al., 2015) and marine ecosystems (Stanca et al., 2013; Barton et al., 2013; Litchman et al., 2007, 2015; Finkel et al., 2010; Mao et al., 2024). However, to our knowledge, this approach has not been used in Indian waters. Therefore, it will be interesting to study the shape and size variability and their related attributes from various contrasting marine habitats (e.g., intertidal, coastal, and pelagic) (Figure 1.3).



Research perspective	Marine	Freshwater	Marine/freshwater	Estuaries
Effects of the environment on trait assembly or dynamics	8	29	1	3
Trait interactions on community structure or dynamics	7	6	3	0
Traits on ecosystem function or its biogeography	8	3	2	0
Other topics	1	1	1	0
Total	24	39	7	3

Figure 1.3. Figure showing studies conducted based on phytoplankton traits worldwide from different habitats and research perspectives. (Illustration from Weithoff & Beisner, 2019.

Other than the morphological adaptations, physiological adaptations also play a significant role in the life strategies of phytoplankton. When it comes to physiological adaptations, nutrients, and light are the main factors that determine the survival conditions for microalgae. Their limited ability to avoid any nutrient or light constraint by evading it leaves them with the only option to adapt to any given condition by modifying their physiological setups. Photo adaptation is a strategy that allows microalgae to survive in any given light environment. Three main groups of pigments participate in light harvesting for photosynthesis: chlorophylls, carotenoids, and phycobilins. Chl-*a*, Chl-*b*, and Chl-*c* are the most common chlorophylls. Carotenoids include carotenes and a subgroup called xanthophylls, which are oxygenated derivatives of carotenes (Jeffrey et al., 2011; Jin et al., 2003). Some xanthophylls act as protective pigments in high light intensities (Koyama et al., 1996; Faraloni & Torzillo, 2017; Aardema et al., 2024). The excess light can be regulated by dynamic photoinhibition, non-photochemical quenching of the reaction center, and by producing photoprotective pigments (Raven, 2011). Conversion of Xanthophylls in phytoplankton is a very fast (seconds to minutes) process (Moisan et al., 1998; Demers et al., 1991; Meyer et al., 2000; Michelberger et al., 2024); therefore, it can cope with the rapidly changing light environment. Strzepek and Harrison (2004) studied the two different species of diatom *Thalassiosira*, one oceanic and another coastal, and found differences in their photosynthetic architecture and iron requirements. Phytoplankton cells can even respond to large changes in PAR (Photo-synthetically Active Radiation) levels by short-term physiological adaptations through photo-acclimation and chlorophyll reorganization (Joythibabu et al., 2018). A contrasting habitat like intertidal and oceanic ecosystems, where light varies greatly, will pose different challenges for the microalgae community to cope with high and low light conditions (Patil et al., 2017). In response to the light fluctuations, microalgal communities might differ in their photo-adaptation strategies, which have yet to be understood spatially and temporally along the Indian coast.

Hence, it becomes a pressing question in the present scenario that the morpho-physiological adaptive strategies of microalgae have a more significant role in better understanding the nature of habitat functioning. Moreover, the present study will not only initiate a new way of looking at the microalgae ecology but also might present the key factors deciding their fate in the ecosystem. Phytoplankton morphology-based studies have gained pace recently, and studies done so far show promising results that could help to simplify the understanding of ecosystem functioning and species succession without

going into the taxonomical details. The various life strategies, like cyst formations, can better elucidate the benthic-pelagic coupling and give a better understanding of seasonal bloom formation. A better understanding of photo-adaptation in microalgae from intertidal and oceanic habitats will have implications in the studies related to ecological surveillance and primary productivity, in particular. Therefore, the proposed study not only points out a new take i.e., morpho-physiological approach (which has not been attempted) in addition to the regular taxonomic approach, but will also aid in a better understanding of microalgae ecology holistically. Nevertheless, to the best of our knowledge, a morpho-physiological approach toward understanding the population dynamics of microalgae in the respective habitat has not been attempted and is proposed in this study. The study focuses on understanding the variability in the morphological (e.g., cyst, shape, and size) and physiological (photo-adaptation/protection) adaptations under different environmental settings. Therefore, in light of the above, the following three objectives are addressed:

1. ***Diversity and distribution of planktonic and benthic microalgae.***
2. ***Delineating the phytoplankton distribution patterns based on taxonomic and functional classification.***
3. ***Photo-physiological adaptation of microalgae from different bioregions.***

Chapter 2

Methodology

Chapter 2: Materials and Methods

The present chapter describes the study area and the methods for addressing all three objectives. Objectives one (i.e., Diversity and distribution of planktonic and benthic microalgae in chapters 3) and two (i.e., Delineating the phytoplankton distribution patterns based on taxonomic and functional classification in chapters 4) are based on field observations, whereas objective three (i.e., Photo-physiological adaptation of microalgae from different bioregions in chapter 5) is addressed based on field sampling followed by onboard experiments.

2.1. The intertidal ecosystem

For the study, two intertidal ecosystems, rockpools and beaches (also referred to as tidal flats), were selected to address objectives 1 and 2. The findings from objectives 1 and 2 are dealt with in chapters 3 and 4. The sampling details of the planktonic and benthic microalgae from both ecosystems are described in the subsequent section.

2.1.1. Tidal flat ecosystem

2.1.1a. Study area

The microphytobenthos (MPB) were studied from two tidal flats (for objective 1a), Dias tidal flat (DTF;15^{o}27’12.2” N; 73^{o}48’05.2” E) and Miramar tidal flat (MTF;15^{o}28’57” N; 73^{o}48’24.7” E), former located at Dona Paula Bay near Zuari estuary and latter adjacent to Mandovi estuary near Panaji (Figure 2.1a & b). The DTF, protected by rocky cliffs on both sides, is ~200 m long, whereas the MTF, a tourist-influenced famous beach around Panaji city, is 3 km long. Both the tidal flats are influenced by semi-diurnal tides, with average spring tide reaching up to 2 m and neap tide up to 0.7 m. The DTF is sheltered (Mitbavkar & Anil, 2002), whereas the MTF is dissipative tidal flat (Seelam et al., 2014). These tidal flats receive a fair amount of precipitation annually during the southwest monsoon (June-September), adding fresh water to the adjacent sea and drastically reducing the salinity (10±5.5 PSU).

DTF is a sheltered beach near the Zuari estuary, influenced by the southwest monsoons. The tidal range of this tidal flat is restricted by a sea wall at the high-tide zone, making the environmental conditions at the high-tide zone similar to the mid-tide zone. This tidal flat is moderately influenced by tourism and fishing activities, making it less prone to anthropogenic pressure, unlike other famous beaches in Goa. Although the MPB studies were conducted over two decades ago in the same area, the shape variability concerning inter-annual and seasonal changes were not addressed.

The Mandovi estuary is formed when the Mandovi River (77 km long), which originates from the sub-Ghats region at an elevation of 888 m, meets the Arabian Sea. This estuary is known for moored casinos and tourist boats and has heavy traffic of commercial barges and mechanized fishing boats (Loveson et al., 2014). The left bank of the estuary has a well-developed stretch of sandy beaches (Miramar and Caranzalem), whereas, on the right bank, beaches are either absent or poorly developed (Murty et al., 1976). The Miramar beach (referred to as Miramar tidal flat hereafter, MTF) has gone through extraordinary biotic and abiotic changes majorly caused by the iron ore mining activities and is well-documented in various studies (Nigam et al., 2002 and 2005; Loveson et al., 2014; Mascarenhas & Ingole, 2009; Ansari & Ingole, 2002, Ingole, 2003 & 2004). Rekadwad and Khobragade (2015) have shown in their study that MTF is affected by oil spills and tar-ball pollution. Earlier studies have extensively focused on foraminiferal, macro, and meiobenthic diversity (Nigam et al., 2002, 2005; Ingole, 2002, 2003, 2004); however, the MPB received no attention. Various studies have shown the potential of MPB as an indicator of anthropogenic impacts (Du et al., 2017; Barinova et al., 2019; Dalu et al., 2020) and the assemblage change caused by anthropogenic activities can severely impair the ecosystem functioning (Bere et al., 2014).

2.1.1b. Sampling strategy and Microphytobenthos enumeration

The sampling was conducted monthly for 4 months in 2019 (April-August) and 16 months in 2022-23 (July 2022 to October 2023) during the spring tide. Sediment samples were collected in triplicates from the low-tide (LT), mid-tide (MT), and high-tide (HT) zones using a PVC core (length:15 cm and diameter: 4.5 cm) and transferred to the lab immediately. Further, each core was sectioned, and the top 2 cm were used for the MPB analysis. The extinction dilution method (most-probable-number method; MPN) (Throndsen, 1978; Imai et al., 1984, 1990; Yamochi, 1989; Ishikawa & Tamaguchi, 1994; Itakura et al., 1997) with slight modification was used for the quantification of the MPB.

In this method, the wet weight of one gram of sediment was diluted to 10 mL with f/2 medium (Guillard & Ryther, 1962) and sonicated for 15 seconds. This stock was further used to start the dilution series. Firstly, 1.8 mL of f/2 medium was transferred into a 24-well plate, and 0.2 mL hand-mixed stock was inoculated into the first six wells for a 10^{-1} dilution. The sixth well from the first row was again mixed well, and 0.2 mL inoculum was further added to the second row of the six wells for a 10^{-2} dilution, leaving very little quantity in the sixth well of the first row; therefore, it was not considered for the enumeration, leaving only five wells for each dilution. This was repeated for 10^{-3} and

10^{-4} dilutions. This entire procedure (i.e., five wells, four dilutions) was repeated in triplicate for each tide zone using a new 1g of sediment. These 24-well plates were further incubated using white light (100 µmol photon m^{-2} s^{-1}) under a 12 light:12 dark cycle at a controlled temperature of 26ºC for 8-10 days. The 24-well plates were enumerated using an inverted microscope (IX73; Olympus made). In this method, the wells where growth was observed were given a positive score. The MPN for each species in the sediment sample was then calculated according to a statistical table (Table 2.1; Throndsen, 1978). This table includes a range of five dilution steps, and three dilutions have to be chosen out of the five cultured to get the MPN number. The taxonomic identification of phytoplankton and MPB was based on standard identification keys (Taylor, 1976; Tomas, 1997). Further, the MPB is classified based on geometric shapes (Hillebrand et al., 1999; Sun & Liu, 2003) and life forms (i.e., epipelic and episammasic based on Meleder et al., 2007). A total of 12 shapes were identified, with nine simple (Box-B, Cylinder-Cyl, Cymbelloid-Cym, Ellipsoid-Elli, Elliptic prism-ElliP, Gamphonemoid-Gam, Prism on parallelogram-PoP, Prolate Spheroid-ProS, and Prism on triangle-PoT) and three combined shapes (2 Cones-2C, Cylinder + 2 Half spheres-Cyl2Hs, and Prolate spheroid + 2 Cylinders-ProS2Cyl) (Table 2.2).

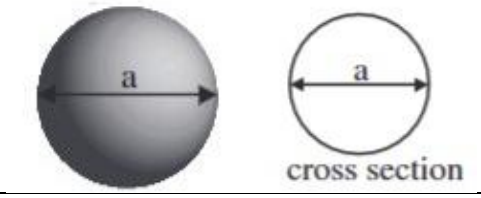
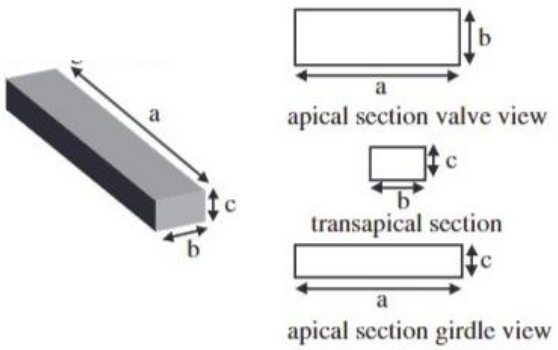
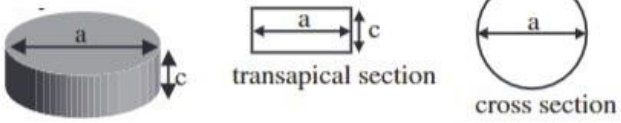
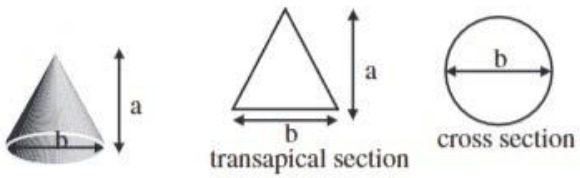
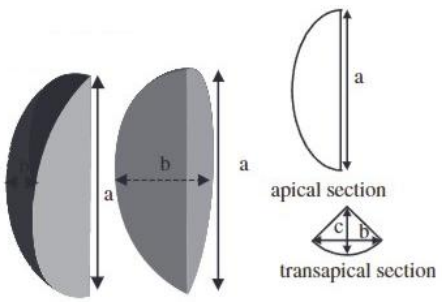
Further, interstitial water samples were collected at MT and HT wherever possible by digging (up to 15 cm) the sediment with a shovel each month. The adjacent surf water (SW) was collected at about 2-3 m from the LT zone to analyze the phytoplankton community, marker pigments, and nutrients. The temperature of the SW, interstitial water, and surface sediment was recorded at the study site, whereas other environmental variables, like salinity and dissolved inorganic nutrients, were estimated in the lab. Seawater samples for dissolved inorganic nutrient analysis were collected in 4.5mL cryo-vials in 4 replicates and frozen at -20ºC until analysis. Samples were thawed to room temperature before the analysis, and nutrients (nitrate, nitrite, phosphate, and silicate) were measured using an auto-analyzer (Model: Skalar Analytical San^{++}, the Netherlands) following standard colorimetric methods (Grasshoff et al., 1983). Separately, a known amount of surface sediment was collected at all the tidal zones to analyze chlorophyll-*a* (Parsons et al., 1984) and extracted in 90% acetone for 24 hours. The extracted chlorophyll-*a* was measured using a fluorometer (Model: Trilogy Turner designs). The sediment grain size (sand, >63µm; silt, 4-63µm; and clay, <4µm) was measured by dry sieving and pipette analysis (Folk et al., 1970; Folk, 1974).

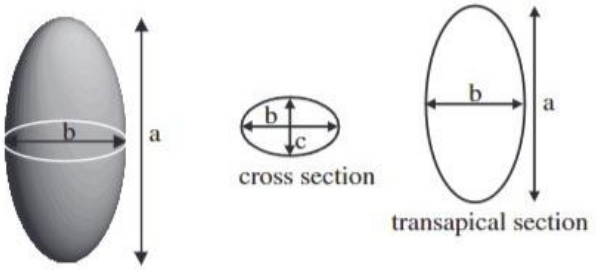
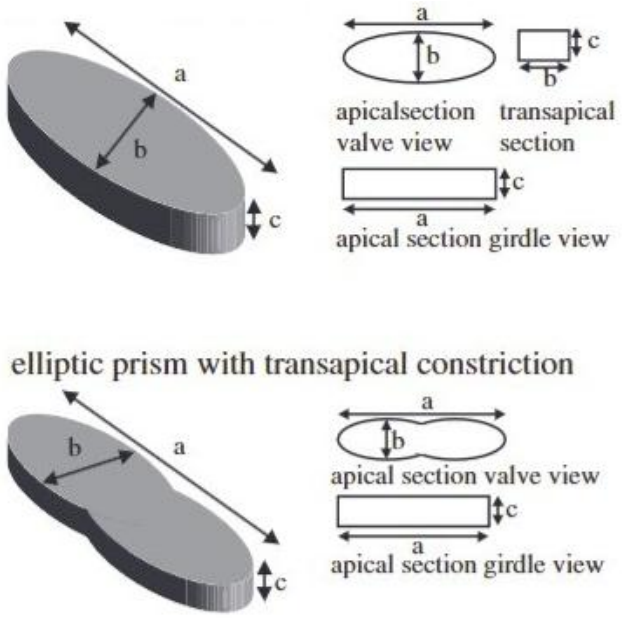
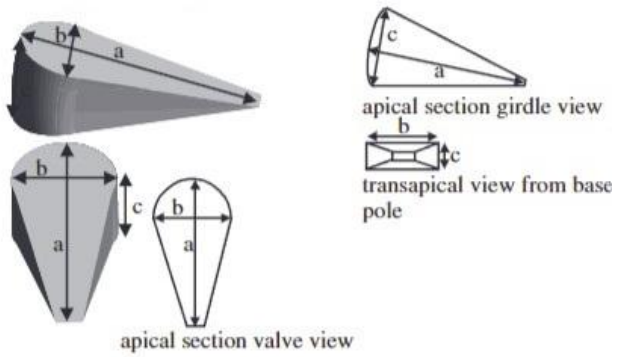
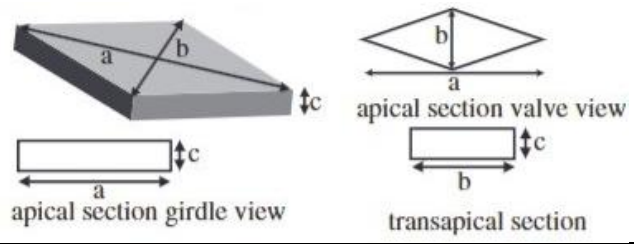
Table 2.1. Most probable number (MPN) in 10 ml of sample, based on the presence and absence of growth in well-plates from three subsequent steps of a dilution-culture series: 5 well-plates with 1.0 ml inoculum each, 5 well-plates with 0.1 ml, and 5 well-plates with 0.0l ml (Taken from Throndsen, 1978)

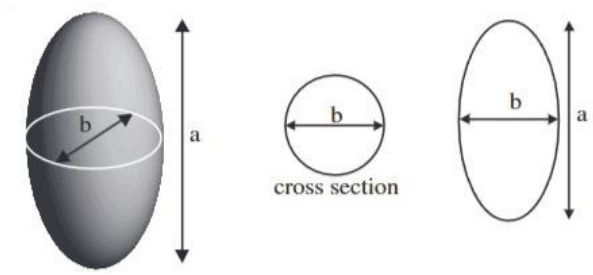
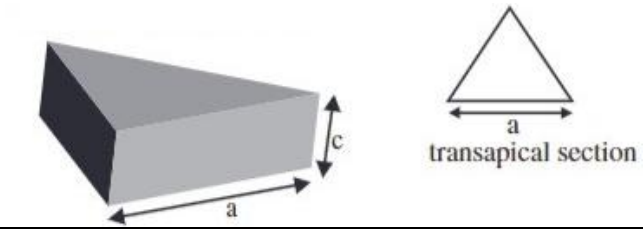
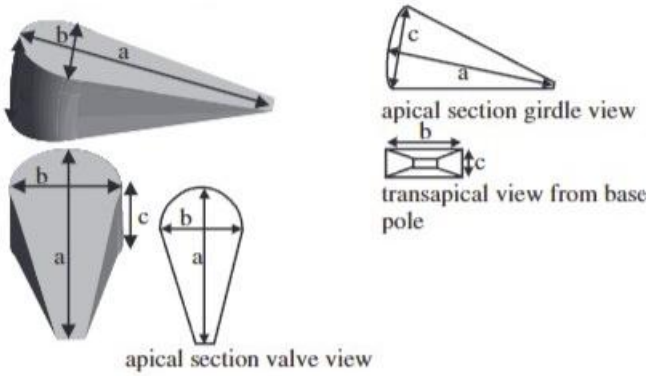
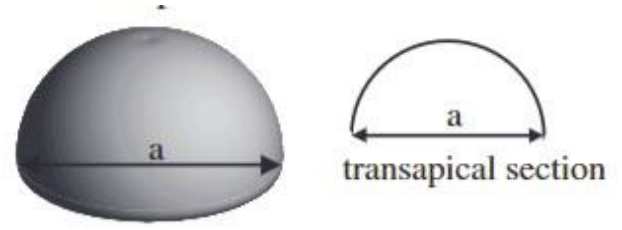
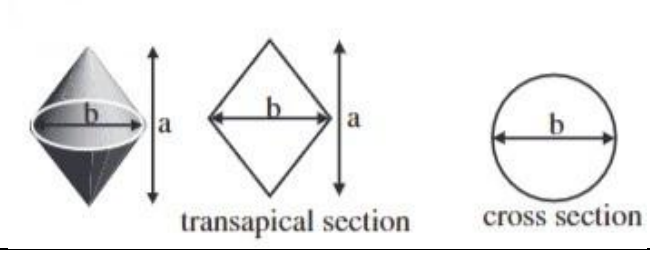
Growth in			MPN	Growth in			MPN	Growth in			MPN
1.0	**0.1**	**0.01 ml**		**1.0**	**0.1**	**0.01 ml**		**1.0**	**0.1**	**0.01 ml**	
0	0	0	**0**	1	0	0	**2**	2	0	0	**4.5**
0	0	1	**1.8**	1	0	1	**4**	2	0	1	**6.8**
0	0	2	**3.6**	1	0	2	**6**	2	0	2	**9.1**
0	0	3	**5.4**	1	0	3	**8**	2	0	3	**12**
0	0	4	**7.2**	1	0	4	**10**	2	0	4	**14**
0	0	5	**9**	1	0	5	**12**	2	0	5	**16**
0	1	0	**1.8**	1	1	0	**4**	2	1	0	**6.8**
0	1	1	**3.6**	1	1	1	**6.1**	2	1	1	**9.2**
0	1	2	**5.5**	1	1	2	**8.1**	2	1	2	**12**
0	1	3	**7.3**	1	1	3	**10**	2	1	3	**14**
0	1	4	**9.1**	1	1	4	**12**	2	1	4	**17**
0	1	5	**11**	1	1	5	**14**	2	1	5	**19**
0	2	0	**3.7**	1	2	0	**6.1**	2	2	0	**9.3**
0	2	1	**5.5**	1	2	1	**8.2**	2	2	1	**12**
0	2	2	**7.4**	1	2	2	**10**	2	2	2	**14**
0	2	3	**9.2**	1	2	3	**12**	2	2	3	**17**
0	2	4	**11**	1	2	4	**15**	2	2	4	**19**
0	2	5	**13**	1	2	5	**17**	2	2	5	**22**
0	3	0	**5.6**	1	3	0	**8.3**	2	3	0	**12**
0	3	1	**7.4**	1	3	1	**10**	2	3	1	**14**
0	3	2	**9.3**	1	3	2	**13**	2	3	2	**17**
0	3	3	**11**	1	3	3	**15**	2	3	3	**20**
0	3	4	**13**	1	3	4	**17**	2	3	4	**22**
0	3	5	**15**	1	3	5	**19**	2	3	5	**25**
0	4	0	**7.5**	1	4	0	**11**	2	4	0	**15**
0	4	1	**9.4**	1	4	1	**13**	2	4	1	**17**
0	4	2	**11**	1	4	2	**15**	2	4	2	**20**
0	4	3	**13**	1	4	3	**17**	2	4	3	**23**
0	4	4	**15**	1	4	4	**19**	2	4	4	**25**
0	4	5	**17**	1	4	5	**22**	2	4	5	**28**
0	5	0	**9.4**	1	5	0	**13**	2	5	0	**17**
0	5	1	**11**	1	5	1	**15**	2	5	1	**20**
0	5	2	**13**	1	5	2	**17**	2	5	2	**23**
0	5	3	**15**	1	5	3	**19**	2	5	3	**26**
0	5	4	**17**	1	5	4	**22**	2	5	4	**29**
0	5	5	**19**	1	5	5	**24**	2	5	5	**32**

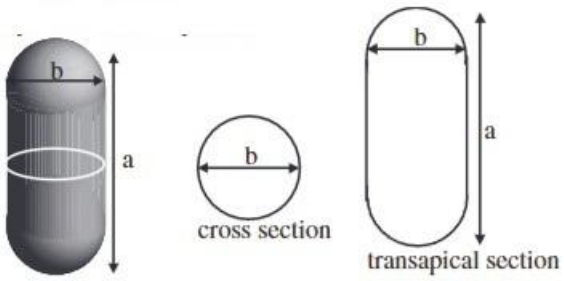
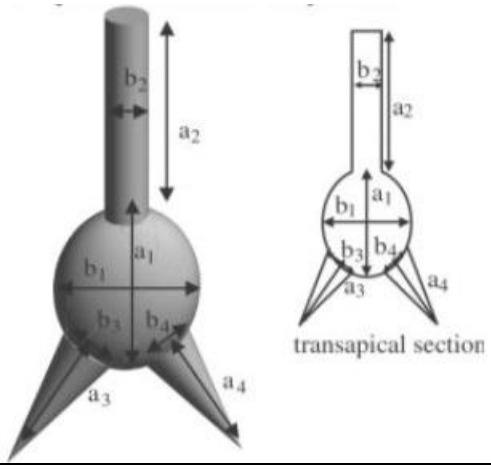
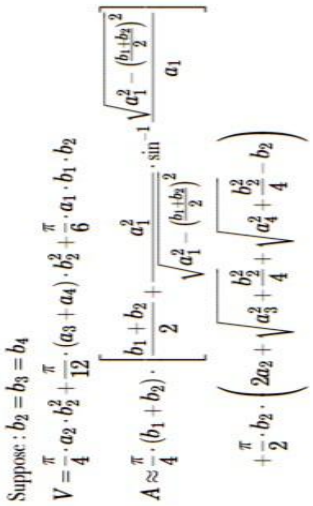
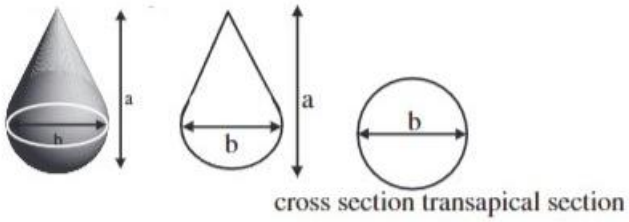
Growth in			MPN	Growth in			MPN	Growth in			MPN
1.0	**0.1**	**0.01 ml**		**1.0**	**0.1**	**0.01 ml**		**1.0**	**0.1**	**0.01 ml**	
3	0	0	**7.8**	4	0	0	**13**	5	0	0	**23**
3	0	1	**11**	4	0	1	**17**	5	0	1	**31**
3	0	2	**13**	4	0	2	**21**	5	0	2	**43**
3	0	3	**16**	4	0	3	**25**	5	0	3	**58**
3	0	4	**20**	4	0	4	**30**	5	0	4	**76**
3	0	5	**23**	4	0	5	**36**	5	0	5	**95**
3	1	0	**11**	4	1	0	**17**	5	1	0	**33**
3	1	1	**14**	4	1	1	**21**	5	1	1	**46**
3	1	2	**17**	4	1	2	**26**	5	1	2	**64**
3	1	3	**20**	4	1	3	**31**	5	1	3	**84**
3	1	4	**23**	4	1	4	**36**	5	1	4	**110**
3	1	5	**27**	4	1	5	**42**	5	1	5	**130**
3	2	0	**14**	4	2	0	**22**	5	2	0	**49**
3	2	1	**17**	4	2	1	**26**	5	2	1	**70**
3	2	2	**20**	4	2	2	**32**	5	2	2	**95**
3	2	3	**24**	4	2	3	**38**	5	2	3	**120**
3	2	4	**27**	4	2	4	**44**	5	2	4	**150**
3	2	5	**31**	4	2	5	**50**	5	2	5	**180**
3	3	0	**17**	4	3	0	**27**	5	3	0	**79**
3	3	1	**21**	4	3	1	**33**	5	3	1	**110**
3	3	2	**24**	4	3	2	**39**	5	3	2	**140**
3	3	3	**28**	4	3	3	**45**	5	3	3	**180**
3	3	4	**31**	4	3	4	**52**	5	3	4	**210**
3	3	5	**35**	4	3	5	**59**	5	3	5	**250**
3	4	0	**21**	4	4	0	**34**	5	4	0	**130**
3	4	1	**24**	4	4	1	**40**	5	4	1	**170**
3	4	2	**28**	4	4	2	**47**	5	4	2	**220**
3	4	3	**32**	4	4	3	**54**	5	4	3	**280**
3	4	4	**36**	4	4	4	**62**	5	4	4	**350**
3	4	5	**40**	4	4	5	**69**	5	4	5	**430**
3	5	0	**25**	4	5	0	**41**	5	5	0	**240**
3	5	1	**29**	4	5	1	**48**	5	5	1	**350**
3	5	2	**32**	4	5	2	**56**	5	5	2	**540**
3	5	3	**37**	4	5	3	**64**	5	5	3	**920**
3	5	4	**41**	4	5	4	**72**	5	5	4	**1600**
3	5	5	**45**	4	5	5	**81**	5	5	5	**2400+**

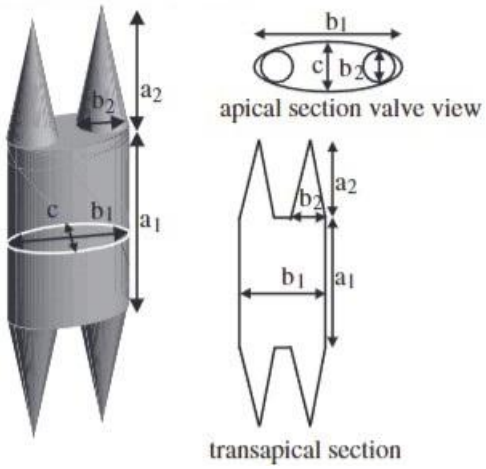
Table 2.2. Table showing all the phytoplankton geometric shapes and their respective formulae used for calculation of volume and surface area during this study from different marine habitats (taken from Hillebrand et al., 1999; Sun & Liu, 2003). V: volume; A: surface area; a: length; b: width; c: height.

Sl. No.	Shape type	Phytoplankton Geometric Shapes (PGS)	Volume and surface area formula
1	Simple shapes	Sphere (**S**) 	$V = \frac{\pi}{6} \cdot a^3$ $A = \pi \cdot a^2$
2		Box (**B**) 	$V = a \cdot b \cdot c$ $A = 2 \cdot a \cdot b + 2 \cdot b \cdot c + 2 \cdot a \cdot c$
3		Cylinder (**Cyl**) 	$V = \frac{\pi}{4} \cdot a^2 \cdot c$ $A = \pi \cdot a \cdot \left(\frac{a}{2} + c\right)$
4		Cone (**C**) 	$V = \frac{\pi}{12} \cdot a \cdot b^2$ $A = \frac{\pi}{4} \cdot b \cdot \left(b + \sqrt{4a^2 + b^2}\right)$
5		Cymbelloid (**Cym**) 	$V = \frac{2}{3} \cdot a \cdot c^2 \cdot \text{asin}\left(\frac{b}{2c}\right)$ $A = \frac{\pi}{2} \cdot a \cdot c + b \cdot \left[c + \frac{a^2}{2\sqrt{a^2 - 4c^2}} \cdot \sin^{-1}\left(\frac{\sqrt{a^2 - 4c^2}}{a}\right)\right]$

6		Ellipsoid (**Elli**) 	$V=\frac{\pi}{6}\cdot a\cdot b\cdot c$ $A\approx\frac{\pi}{4}\cdot(b+c)\cdot\left[\left(\frac{b+c}{2}\right)+\frac{2a^2}{\sqrt{4a^2-(b+c)^2}}\sin^{-1}\frac{\sqrt{4a^2-(b+c)^2}}{2a}\right]$
7		Elliptic prism (**ElliP**)  elliptic prism with transapical constriction 	$V=\frac{\pi}{4}\cdot a\cdot b\cdot c$ $A=\frac{\pi}{2}\cdot(a\cdot b+b\cdot c+a\cdot c)$
8		Gamphonemoid (**Gam**) 	$V\approx\frac{a\cdot b}{4}\cdot\left[a+\left(\frac{\pi}{4}-1\right)\cdot b\right]\cdot\text{asin}\left(\frac{c}{2a}\right)$ $A\approx\frac{b}{2}\cdot\left(2a+\pi\cdot a\cdot\text{asin}\left(\frac{c}{2a}\right)+\left(\frac{\pi}{2}-2\right)\cdot b\right)$
9		Prism on parallelogram (**PoP**) 	$V=\frac{1}{2}\cdot a\cdot b\cdot c$ $A=a\cdot b+\frac{\sqrt{a^2+b^2}}{4}\cdot c$

10		Prolate Spheroid (**ProS**) 	$V = \frac{\pi}{6} \cdot b^2 \cdot a$ $A = \frac{\pi \cdot b}{2}\left(b + \frac{a^2}{\sqrt{a^2 - b^2}} \sin^{-1} \frac{\sqrt{a^2 - b^2}}{a}\right)$
11		Prism on triangle (**PoT**) 	$V = \frac{\sqrt{3}}{4} \cdot c \cdot a^2$ $A = 3a \cdot c + \frac{\sqrt{3}}{2} \cdot a^2$
12		Gamphonemoid (**Gam**) 	$V \approx \frac{a \cdot b}{4} \cdot \left[a + \left(\frac{\pi}{4} - 1\right) \cdot b\right] \cdot \operatorname{asin}\left(\frac{c}{2a}\right)$ $A \approx \frac{b}{2} \cdot \left(2a + \pi \cdot a \cdot \operatorname{asin}\left(\frac{c}{2a}\right) + \left(\frac{\pi}{2} - 2\right) \cdot b\right)$
13		Half sphere (**Hs**) 	$V = \frac{\pi}{12} \cdot a^3$ $A = \frac{3\pi}{4} \cdot a^2$
14	**Complex or combined shapes**	2 Cones (**2C**) 	$V = \frac{\pi}{12} \cdot a \cdot b^2$ $A = \frac{\pi}{2} \cdot b \cdot \sqrt{a^2 + b^2}$

15		Cylinder + 2 Half spheres (**Cyl2Hs**) 	$V = \pi \cdot b^2 \cdot \left(\frac{a}{4} - \frac{b}{12}\right)$ $A = \pi \cdot a \cdot b$
16		Prolate spheroid + 2 Cylinders (**ProS2Cyl**)	Calculation is combination of Prolate spheroid and 2 cylinders
17		Ellipsoid + 2 cones + cylinder (**Elli2CCyl**) 	
18		Box+2 Cylinders (**B2Cyl**)	Calculation is combination of Box and 2 cylinders
19		Box+Elliptic prism (**BElliP**)	Calculation is combination of Box and elliptic prism
20		Cone+Half sphere (**CHs**) 	$V = \frac{\pi}{4} \cdot a \cdot b^2$ $A = \frac{\pi}{2} \cdot b^2 \cdot \left(b + \sqrt{\frac{2a^2 - ab + b^2}{2}}\right)$

21		Elliptic prism+4 Cones (**ElliP4C**) 	$V = \frac{\pi}{4} \cdot a_1 \cdot b_1 \cdot c_1 + \frac{\pi}{3} \cdot a_2 \cdot b_2^2$ $A = \frac{\pi}{2} \cdot a_1 \cdot b_1 + \frac{\pi}{2} \cdot b_1 \cdot c_1 + \frac{\pi}{2} \cdot a_1 \cdot c_1 + \pi \cdot b_2 \cdot \left(\sqrt{4a_2^2 + b_2^2} - b_2 \right)$

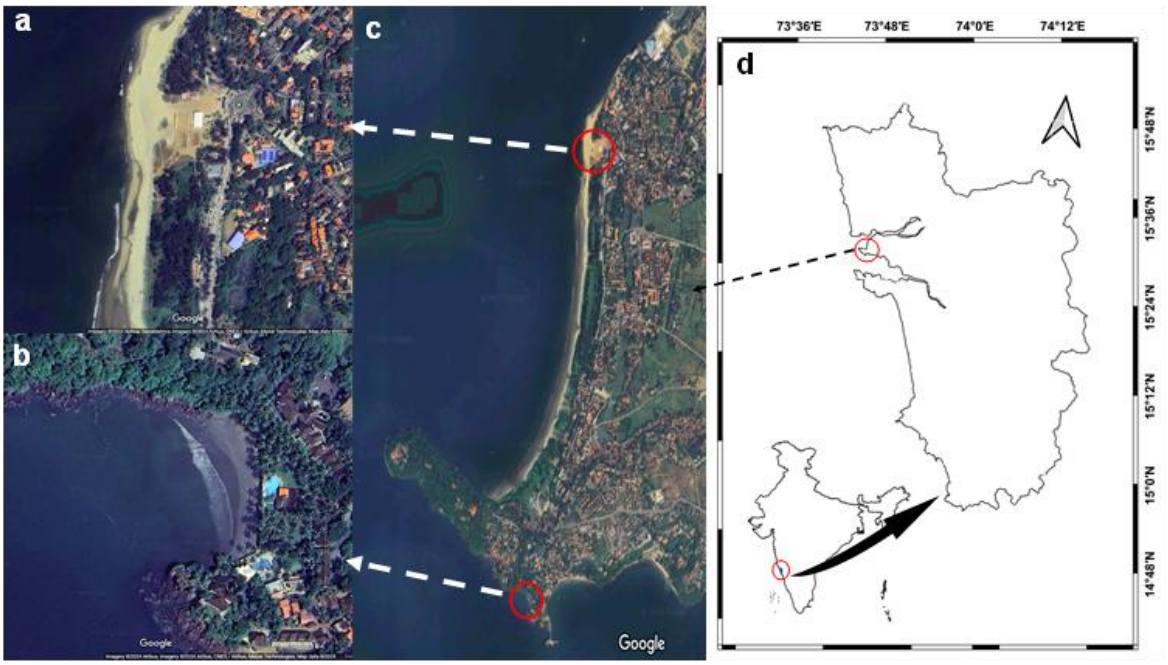


Figure 2.1. Map showing the location of the tidal flat sampling stations at a) Miramar Beach and b) Dias Beach.

2.1.2. Rockpool ecosystem

2.1.2a. Study area and sample collection

The taxonomic and functional classification of phytoplankton was analyzed from the rockpool of the intertidal region (objective 2a). The sampling was conducted at the rocky shores of Anjuna, Goa (15º34'34.986" N; 73º44'23.895" E; Figure 2.2), known for various-sized rock pools located on the western coast of India. A total of nine RPs located at various tidal levels (three at each low tide (LT), mid-tide (MT), and high tide (HT)) were selected for water sampling. The sampling was conducted in the summer season of two different years (May 2014 and April 2015) during the LT every day for 15 days. The rationale for sampling during the summer season is as follows: (i) RPs experience maximum solar radiation resulting in increased water temperature, light penetration, and salinity (due to evaporation), (ii) Two summer seasons to confirm consistency in trends, (iii) Feasibility for sampling keeping in mind the semi-diurnal nature of the tide in the region. The sampling days were designed in such a way so that the variation in both 'Flushed (F)' (when the adjacent water replaces the RP water with tidal action) and 'Non-flushed (NF)' (when the RP water is not replaced for several days, particularly for HT-RPs) scenario can be apprehended. In the first and last five days of the sampling, the tidal amplitude of the highest high tide was >1.8, and all the RPs got flushed, whereas when the high tide amplitude was <1.8, only LT and MT-RPs got flushed except the HT-RP. The small quantity of undisturbed HT-RP water during the NF time was exposed to direct sunlight, making the environmental extremes inevitable. Environmental parameters (like temperature and salinity) were collected from the selected RPs of different tidal levels. During the sampling period, water temperature and salinity in HT-RPs ranged between 27–37°C and 28–49.5 PSU, respectively, whereas water temperature and salinity in LT and MT-RPs ranged between 26–37°C and 35–38 PSU, respectively (Patil et al., 2017). The lowering of salinity during the 2014 sampling was due to precipitation (up to 2.6 mm; MICD, NIO) during the latter half of sampling. Even a small amount of precipitation is sufficient to lower salinity in RPs harboring smaller volumes of water. However, no precipitation occurred during the 2015 sampling.

2.1.2b. Sample analysis

A known volume (1 L) of the water samples collected from all the RPs were preserved with 4% Lugol's iodine at the site and then transported immediately (within 2h) to the laboratory in dark condition for the analysis of microalgal composition and abundance (in triplicates) using an inverted microscope (IX-73 Olympus Make). The identification

of microalgae was carried out manually based on the standard identification guides (Tomas, 1997). Further, all the recorded species were assigned to their known geometric shapes as described in Hillebrand et al. (1999) and Sun and Liu (2003) to find out if shapes can be used as a functional trait. A total of 12 shapes were identified, among which eight shapes were simple (Box (B), Cylinder (Cyl), Cymbelloid (Cym), Ellipsoid (Elli), Elliptic prism (ElliP), Gamphonemoid (Gam), Prism on parallelogram (PoP) and Prism on triangle (PoT)) and 4 were combined (Cylinder + 2 half spheres (Cyl2Hs), Ellipsoid + 2 cones + cylinder (Elli2CCyl), Prolate spheroid + 2 cylinders (ProS2Cyl) and 2 cones (2C)) (Table 2.2).

2.1.2c. Experimental design to elucidate allelopathic effect of A. carterae on other microalgae

The observation of unpreserved samples during the sampling period from the HT-RP waters under the microscope revealed a very high abundance of dinoflagellates, which prompted us to further isolate the microalgae and culture for detailed identification and experiments. The dinoflagellates were identified as *Amphidinium carterae* sensu stricto (potential harmful dinoflagellate) and *Bysmatrum gregarium*, formerly known as *B. caponii* and maintained in f/2 media (Guillard and Ryther 1962). The abundance data suggested their high number in HT-RPs whereas, other microalgae were less abundant and literature also advocated some of the *A. carterae* strain to be toxic (Murray et al. 2015). Given this, an experiment was designed to confirm the allelopathic effect of *A. carterae* on the various microalgae found in either the same HT-RP or adjacent waters. A diatom (*Skeletonema costatum*), green algae (*Dunaliella tertiolecta*), and a dinoflagellate (*Bysmatrum gregarium*) were selected as test organisms for the allelopathic effect of *A. carterae* cell-free filtrate. The culture of *A. carterae, S. costatum, D. tertiolecta* and *B. gregarium* were maintained at 27 ± 1°C under a light photocycle of 12:12 h light: dark in their exponential growth phase by weekly re-inoculation of fresh culture media.

2.1.2d. Amphidinium carterae culturing for cell-free filtrate and allelopathy evaluation

In order to obtain large quantities of cell-free filtrate during stationary phase, *A. carterae* was cultured in four one litre sterile flasks containing 800 ml of f/2 media at 35 PSU salinity. The culture conditions are the same as mentioned above. The growth of *A. carterae* was monitored every day by cell counts (using haemocytometer and upright microscope (Olympus; 10x objective) until the culture reached its stationary phase so that it can be harvested to obtain a cell-free filtrate. The culture of *A. carterae* was harvested

on 10th day to obtain cell-free filtrate and it was carried out by first passing through 10-l mesh followed by filtering on 0.22-l Millipore filter paper under very low pressure. The obtained cell-filtrate (designated as 100% strength) was then used for allelopathic experiments.

For the experiments, the different strength of cell free filtrate (100%, 75%, 50%, 25%, 10%) was evaluated for allelopathic effect against *S. costatum*, *D. tertiolecta*, and *B. gregarium*. Additionally, all the cultures were grown in f/2 media and are treated as control (0%). The different strength of the cell-free filtrate was prepared using sterile 0.22 µm filtered seawater. The experiments were performed in triplicates in 150 ml polycarbonate bottles (Nalgene make) containing different strength cell-free filtrates enriched with f/2 media. A known number of the cell of *S. costatum* (1068 cells mL^{-1}), *D. tertiolecta* (2437 cells mL^{-1}) and *B. gregarium* (10 cells mL^{-1}) were inoculated in triplicates and incubated for 4 days at 27 ± 1°C under a light photocycle of 12:12 h light: dark. To evaluate the effect of allelopathy, counting and morphological changes were observed every day for the period of 4 days. Counting was performed in the same way as mentioned above for *A. carterae* using hemocytometer and upright microscope (Olympus; 10x objective) and the abundance was expressed as cells/ml.

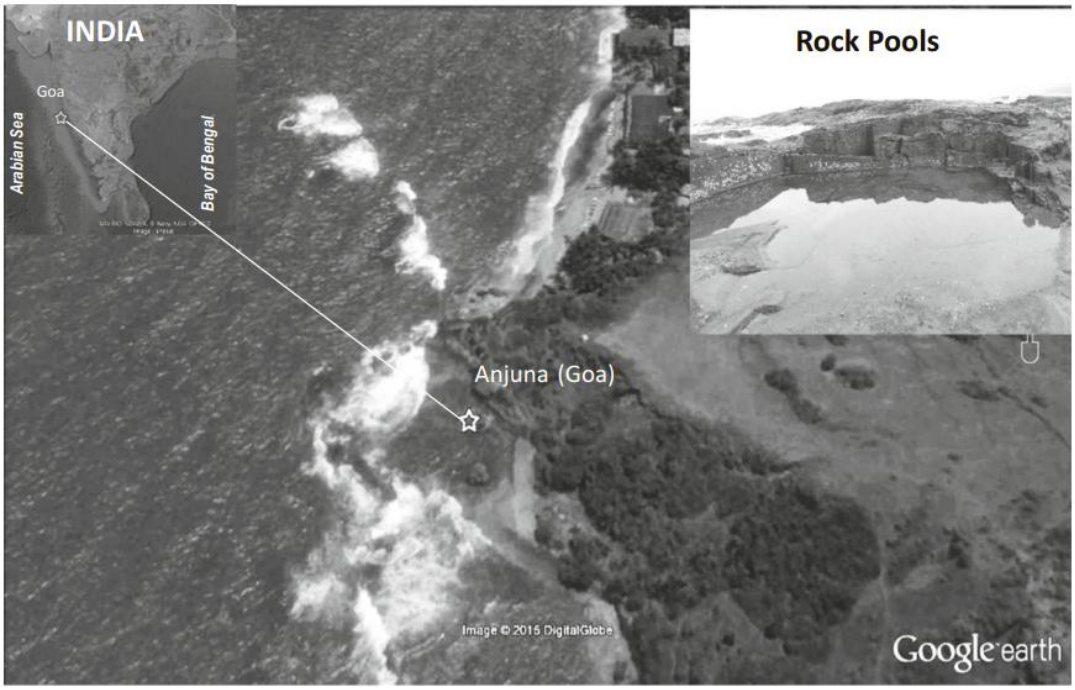


Figure 2.2. Map showing the location of the Rockpools.

2.2. The pelagic ecosystem

In the present objective, the dominant planktonic forms (i.e., diatoms and dinoflagellates) from the photic zone of the water column and the dominant benthic phytoplankton forms from the open ocean sediments (i.e., dinoflagellate cysts) were sampled and studied. The planktonic forms were studied based on taxa, shapes, and morphometry, whereas the dinoflagellate cysts were studied only based on taxa and morphometry. The resting diatom spores also contribute minimally to the benthic microalgae in the open ocean. However, it is difficult to identify them as the numbers are considerably lower, and thus, they have not been studied. The details of the sampling methods for the sediment and planktonic forms of microalgae from the oceanic regions are described in the subsequent section.

2.2.1. Water column

2.2.1a. Study area and sample collection

To study the taxonomic and functional classification of phytoplankton in the open ocean ecosystem (objectives 2b and c), data from five cruises, R/V *Sindhu Sankalp* (SSK077; 11-22 February 2015) and R/V *Sindhu Sadhana* (SSD029; 18 November - 2 December 2016), took place during late winter monsoon and winter monsoon, respectively, in the north-eastern Arabian Sea (NEAS), R/V *Sindhu Sadhana* (SSD028; 6 – 17 November 2016) in winter monsoon in the south-eastern Arabian Sea (SEAS), and SSD069 (2020) in the oligotrophic and oxygen minimum zone (OMZ) part of the Arabian Sea (SSD069; 12 January – 11 February 2020) and a three-month long cruise (SSD079; 14 March - 5 June 2021) encompassing Bay of Bengal (BoB) and North and South Equatorial Indian Ocean up to 30ºS (NEIO, SEIO, and STIO) (Figure 2.3a and b; Table 2.3) were utilized for data analysis (taxonomic and shape diversity) and interpretation. The study in the NEAS and SEAS was conducted using the integrated water column depths from surface to 200 m, whereas, for the oligotrophic, OMZ, BoB, NEIO, SEIO, and STIO, only sea surface and sub-surface chlorophyll maximum layer (SCML) water was studied. The water samples were collected at 127 stations (NEAS-Open ocean-20 stations, NEAS-Coastal-38 stations, SEAS-Open ocean-31 stations, AS-14 stations, BoB-4 stations, NEIO-3 stations, SEIO-6 stations, and STIO-11 stations) at discrete depths (surface to 100 m) for NEAS-SEAS (2015-16 cruises, hereafter termed as AS-cruises) and from the sea surface and sub-surface chlorophyll maximum layers (SCML) from different bioregions of the Indian Ocean (IO 2020-21 cruises, hereafter termed as IO-cruises) with

10 L Niskin bottles attached to 32 Carousel Water Sampler (Sea-bird Electronics Inc.; SBE), which is operated with SBE 911 plus CTD equipped with sensors such as temperature (SBE 3 plus SN5552; ±0.001 °C), conductivity (SBE 4 SN4088; ±0.0003 S m^{-1}), dissolved oxygen (SBE 43SN2288; ±2% of saturation), transmissometer (WET Labs C-star), fluorometer (Seapoint Sensors; 0.02 µg L^{-1}) and surface PAR (LI-COR Biospherical; µmol photons $m^{-2}s^{-1}$) for real-time data acquisition.

2.2.1b. Sample analysis

A fixed volume (1L) of the water sample for AS-cruises and 5L water samples from the sea surface and SCML were passed through a 20µm mesh, concentrated to 100 ml for IO-cruises, and preserved with 4% acidic Lugol's iodine for further analysis. A known aliquot (2-5 ml) of sample volume was analyzed in duplicates using an inverted microscope (IX73 Olympus Make) at 200-400x to assess micro-phytoplankton composition and abundance. Microalgaal identification was performed using standard identification keys (Tomas, 1997; Taylor, 1976). was preserved with 4% Lugol's iodine and used for further analysis.

The morphological measurements (length, width, breadth, area, volume, and maximum linear dimension) for each phytoplankton cell or colony were performed using a factory-calibrated FlowCAM (Fluid Imaging Technologies) at 4x magnification (flowcell 300 µm) and a microscope digital camera adapter system (QimagingMicroPublisher 5.0 RTV) attached to the inverted microscope at 200–600x magnification (Olympus IX73), respectively. These measurements were then used for the calculation of volume (V; μm^3) and surface area (S; μm^2) following Hillebrand et al. (1999) and Sun and Liu (2003). In algal ecology and physiology, shape and size variability play a key role (Capblancq & Catalan, 1994) wherein the surface/volume ratios of a biomass unit need to be maintained within physiologically necessary bounds in a given environment (Lewis, 1976). Given this, the surface-to-volume ratio (S:V) of the phytoplankton was calculated according to Lewis (1976) and Aubry et al. (2017). Each cell in the chain was considered for chain-forming cells like *Chaetoceros* and *Skeletonema*, and the morphological measurements were taken in higher magnifications (400x or 600x). The greatest axial linear dimension (GALD; µm) or maximum linear dimension (Weithoff & Beisner, 2019) is measured directly from the linear dimensions like diameter, height, total length, and apical axis length of a given cell based on the geometric approximation given by Hillebrand et al. (1999) and Sun and Liu (2003). Here, in this study, the GALD of a cell is measured according to its cell geometry, as described

by Ryabov et al. (2021). For instance, in the simple shapes, the maximum cell linear dimension (e.g., diameter in the sphere, height in ellipsoid and cylinder, apical axis length in prism on parallelogram) was considered GALD, whereas for combined shapes (Box + 2 Cylinders, Cylinder + 2 Half spheres, Ellipsoid + 2 Cones + Cylinder, etc.,) consisting of few segments measured separately (e.g., cylinder with 2 half spheres), the sum of the linear dimensions of these parts or the total height or length was considered.

Overall, a total of 22 shapes were identified, among which 11 shapes were simple (Box-B, Cone-C, Cylinder-Cyl, Cymbelloid-Cym, Ellipsoid-Elli, Elliptic prism-ElliP, Half sphere-Hs, Prism on parallelogram-PoP and Prism on triangle-PoT, Prolate spheroid-ProS, and Sphere-S) and 8 were combined (Box+2 Cylinders-B2Cyl, Box+Elliptic prism-BElliP, Cone+Half sphere-CHs, Cylinder+2 Half spheres-Cyl2Hs, Ellipsoid+2 Cones+Cylinder-Elli2CCyl, Elliptic prism+4 Cones-ElliP4C, Prolate spheroid+2 Cylinders-ProS2Cyl, and 2 Cones-2C) (Table 2.2).

2.2.1c. Environmental variables

Seawater samples for dissolved inorganic nutrient analysis were collected in 4.5mL cryo-vials in 4 replicates and frozen at -20^{o}C until analysis. Samples were thawed to room temperature before analysis, and nutrients (nitrate, nitrite, phosphate, and silicate) were measured using an auto-analyzer (Model: Skalar Analytical San++, Netherlands) following standard colorimetric methods (Grasshoff et al., 1983). Other environmental parameters (temperature, salinity, oxygen, and PAR) were obtained from the onboard-operated CTD profiler. The SCML depth was determined using fluorescence downward profiles generated by a fluorometer (Seapoint Sensors; 0.02 μg L^{-1}) attached to the CTD profiler. The mixed layer depth (MLD) was calculated using a 0.03 kg m^{-3} density difference from the surface (de Boyer Montegut et al., 2004), and nitracline depth was taken where the nitrate concentration reached 1 μM L^{-1} (Zhuang et al., 2020).

Table 2.3. Station details with regions and geographic positions.

Regions	Cruises	Stations	Latitude (ºN)	Longitude (ºE)
NEAS-O	SSK077	1	20.17444	68.78389
	SSK077	2	20.00778	68.99361
	SSK077	3	19.76917	69.23667
	SSK077	4	19.55583	69.45778
	SSK077	5	19.36917	69.52028
	SSK077	6	19.78472	68.86139
	SSK077	7	20.10083	68.80028
	SSK077	8	20.21028	68.75028
	SSK077	9	20.30028	68.70278
	SSK077	10	20.40944	68.65083
	SSK077	11	20.50806	68.6025
	SSK077	12	20.60444	68.50194
	SSK077	13	20.80972	68.30111
	SSK077	14	20.99139	68.28583
	SSK077	15	21.30167	68.89333
	SSK077	16	21.51556	68.20056
	SSK077	17	20.59944	68.33417
	SSK077	18	20.25306	68.70556
	SSK077	19	19.70639	68.02361
	SSK077	20	18.99861	69.26972
NEAS-C	SSD029	21	20.326	70.986
	SSD029	22	20.324	70.983
	SSD029	23	20.433	70.53
	SSD029	24	20.326	70.502
	SSD029	25	20.427	70.571
	SSD029	26	20.433	70.562
	SSD029	27	20.359	70.546
	SSD029	28	20.391	70.748
	SSD029	29	20.436	70.554
	SSD029	30	20.495	70.312

	SSD029	31	20.359	70.546
	SSD029	32	20.338	70.545
	SSD029	33	20.484	70.527
	SSD029	34	20.467	70.732
	SSD029	35	20.508	70.51
	SSD029	36	20.534	70.274
	SSD029	37	20.299	70.544
	SSD029	38	20.542	70.512
	SSD029	39	20.409	70.723
	SSD029	40	20.543	70.488
	SSD029	41	20.653	70.163
	SSD029	42	20.301	70.645
	SSD029	43	20.544	70.503
	SSD029	44	20.548	70.467
	SSD029	45	20.447	70.64
	SSD029	46	20.548	70.453
	SSD029	47	20.627	70.211
	SSD029	48	20.3	70.54
	SSD029	49	20.513	70.491
	SSD029	50	20.357	70.715
	SSD029	51	20.384	70.77
	SSD029	52	20.449	70.567
	SSD029	53	20.55	70.298
	SSD029	54	20.301	70.543
	SSD029	55	20.6	70.49
	SSD029	56	20.5	70.5
	SSD029	57	20.409	70.72
	SSD029	58	20.546	70.5
SEAS-O	SSD028	59	9.499367	72.49785
	SSD028	60	9.477233	72.7005
	SSD028	61	9.496768	72.76771
	SSD028	62	9.448483	72.87425
	SSD028	63	9.414667	73.10517

	SSD028	64	9.38998	73.29144
	SSD028	65	9.357667	73.526
	SSD028	66	9.350932	73.56317
	SSD028	67	9.343947	73.61814
	SSD028	68	9.332058	73.70162
	SSD028	69	9.319833	73.78467
	SSD028	70	9.3	73.8685
	SSD028	71	9.277033	74.10019
	SSD028	72	9.242792	74.33305
	SSD028	73	9.300177	74.53414
	SSD028	74	9.1881	74.73323
	SSD028	75	9.165667	74.92533
	SSD028	76	9.131157	75.14098
	SSD028	77	9.104667	75.34167
	SSD028	78	7.396667	74.16667
	SSD028	79	7.545833	74.27667
	SSD028	80	7.6812	74.38007
	SSD028	81	7.82	74.48167
	SSD028	82	7.8835	74.53917
	SSD028	83	7.965167	74.59367
	SSD028	84	8.104467	74.69837
	SSD028	85	8.235	74.795
	SSD028	86	8.373333	74.90067
	SSD028	87	8.42	74.93
	SSD028	88	8.644833	75.10583
	SSD028	89	8.865	75.275
Oligotrophic-AS	SSD069	90	9.0011	75.5022
	SSD069	91	9.0011	74.0167
	SSD069	92	9	72.5
	SSD069	93	9	69.5
	SSD069	94	9	68
	SSD069	95	9	66.5
	SSD069	96	9	65

	SSD069	97	9	63.5108
	SSD069	98	9	62
	SSD069	99	9	60
OMZ-AS	SSD069	100	11	62.5711
	SSD069	101	14.5022	65.5769
	SSD069	102	17.3883	67.9583
	SSD069	103	16.7513	69.0008
BoB	SSD079	104	20.22196	88.04142
	SSD079	105	17.00005	89.85014
	SSD079	106	10.40959	92.64739
	SSD079	107	7.999984	92.38994
NEIO	SSD079	108	5.196757	92.81323
	SSD079	109	2.912549	92.15678
	SSD079	110	7.000241	75.58351
SEIO	SSD079	111	-1.9849	90.4707
	SSD079	112	-4.00001	90.46665
	SSD079	113	-7.7639	90.02884
	SSD079	114	-9.99986	89.6332
	SSD079	115	-7.32432	75.98251
	SSD079	116	-2.03855	75.56623
STIO	SSD079	117	-16.0541	88.29497
	SSD079	118	-20.9998	85.00018
	SSD079	119	-25.5001	82.53329
	SSD079	120	-30.0002	80.00053
	SSD079	121	-30.0002	75.00016
	SSD079	122	-30	69.9996
	SSD079	123	-18.2747	61.25387
	SSD079	124	-16.3667	67.27418
	SSD079	125	-12.9358	74.67573
	SSD079	126	-13.5574	75.55698
	SSD079	127	-12.0574	75.55744

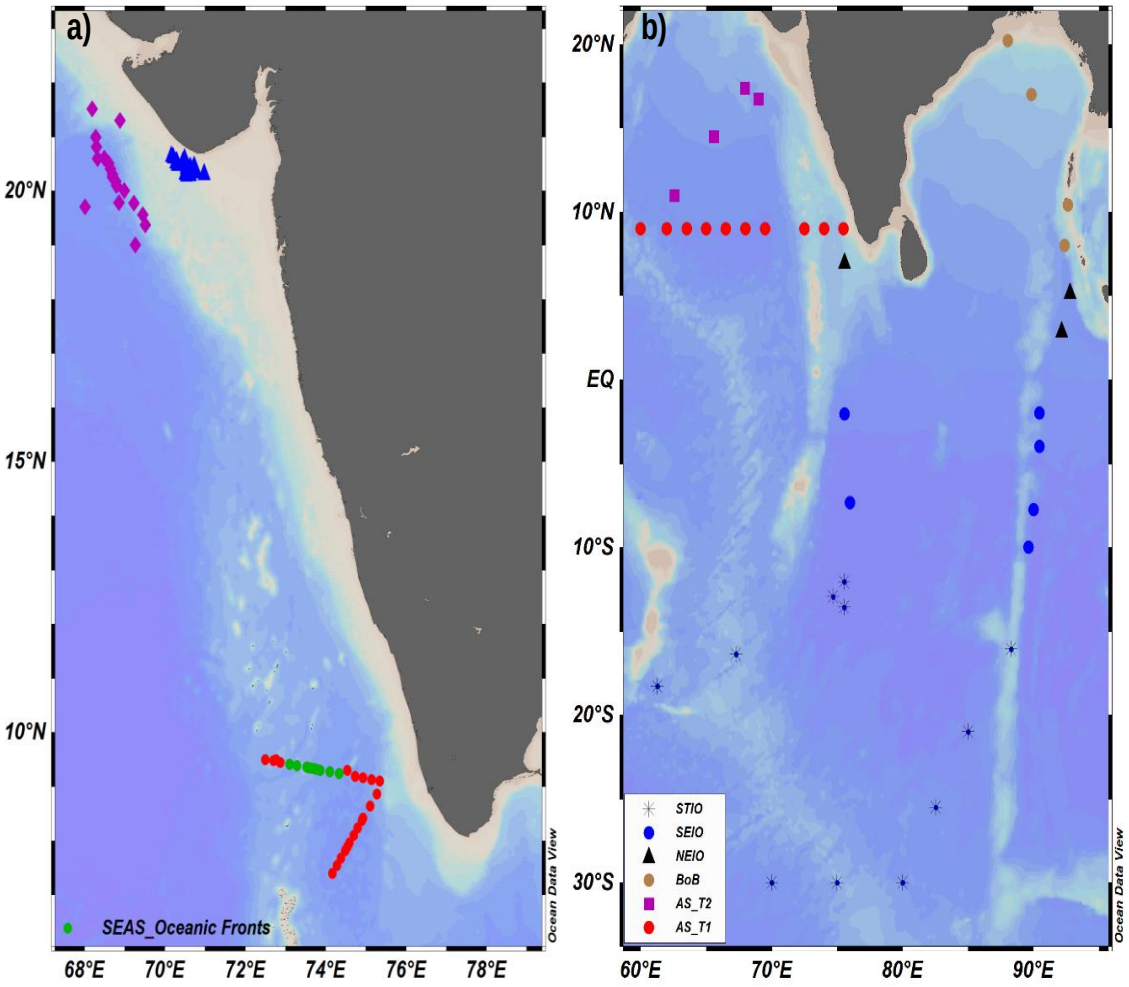


Figure 2.3. Map showing location of the water column sampling site in a) northeastern and southeastern Arabian Sea, and b) Indian Ocean.

2.2.2. Sediment

2.2.2a. Study area and sampling strategies

To study the dinoflagellate cysts, observations were made during two cruises onboard R/V *Sindhu Sadhana (SSD),* one in the Southeastern and oxygen minimum zone (OMZ) part of the AS (SSD069; 12 Jan-11 February 2020) and another in OMZ part of BoB, EIO, and STIO up to 30^{o}S in a three-month long cruise (SSD079; 14 March-5 June 2021). Overall, the surface sediment samples (0-2cm) were collected at 24 stations (Figure 2.4; Table 2.4), which includes 8 stations from AS (5 and 3 from oligotrophic and OMZ, respectively), 4 from BoB, 3 from EIO, and 9 from STIO at water column depths ranging from 113-5396m using a maxi multiple corer (60cm length x 100mm diameter; Ocean Scientific International Ltd.). The sediment grain size (sand, >63µm; silt, 4-63µm; and clay, <4µm) was measured by dry sieving and pipette analysis (Folk et al., 1970; Folk, 1974). The stations were grouped into six regions based on geographical locations to study the biogeographic variations. Stations in the AS are grouped in three groups: the coastal station as coastal-AS (C-AS), stations in the oligotrophic East to West directions are grouped as oligotrophic AS (O-AS), and stations in the Oxygen minimum zone (OMZ) are grouped as OMZ-AS, stations from the BoB and the Andaman Sea are grouped as BoB, stations 5^{o}N to 5^{o}S are grouped as EIO, and 10^{o}S to 30^{o}S as STIO (Table 2.4). Further, the AS and BoB are grouped as the North IO (NIO), whereas the EIO and STIO are grouped as the South IO (SIO).

2.2.2b. Sediment processing

The surface sediment (0-2 cm) samples were processed following the palynological method (Matsuoka & Fukuyo, 2000) with slight modifications (Matsuoka et al., 2003). Approximately (5-15g of wet sediment was gently sonicated for 30s with distilled water (DW) and sieved through 100 and 10 µm mesh repeatedly. The residue retained on 10 µm mesh was treated with 10% hydrochloric acid for 24h to remove calcium carbonate and later washed thoroughly with DW and then with 30% hydrofluoric acid to dissolve silicate materials. All the acid-treated samples were washed thoroughly with DW (4-5 times) to remove any trace of acid. The acid-free residue was sieved again through 10 µm mesh and re-suspended carefully to 10 mL DW in a vial.

The entire 10 mL was analyzed using an inverted microscope (Olympus IX73) (Cho & Matsuoka, 2001; Matsuoka et al., 2003; Wang et al., 2004; Baula et al., 2011) equipped with a digital camera (Qimaging MicroPublisher 5.0 RTV) at 100-400x magnification for identification and quantification of dinoflagellate cysts. Various published literature was

used for the identification of dinoflagellate cysts (Wall & Dale, 1968; Sonneman & Hill, 1997; Matsuoka & Fukuyo, 2000; Liu et al., 2012; Radi et al., 2013; Rigel et al., 2022; Li et al., 2020; online version: https://www.marum.de/en/Modern_dinoflagellate_cyst_determination_key.html) and categorized into autotrophic, mixotrophic, and heterotrophic (Marret et al. (2020). Cysts with clear morphologies were identified at their species level; however, a few cysts are represented as genus "spp."

A minimum of ~100-300 cysts were counted per sample from the productive regions of the NIO, and 50 cysts were counted from the oligotrophic regions of the SIO, where counts were very low. However, a low count (<100 dinoflagellate cysts) might underestimate the diversity and statistical analysis; 50 dinoflagellate cyst cut-offs, as suggested by Marret et al. (2001), have proved to represent the dinoflagellate cyst species in the areas with low dinoflagellate cyst concentrations. Stations from BoB (station 3), EIO (stations 5 and 15), and STIO (stations 6 and 12-14) with <50 dinoflagellate cyst counts were excluded from the statistical analysis. In this study, dinoflagellate cyst abundances are represented by cyst concentrations and were calculated as the number of cysts per gram of dry sediment [cysts g^{-1}] using the formula N/(W*(1-WC)), where N: total number of cysts; W: wet sediment weight taken for analysis and WC: Water content (Matsuoka et al., 2003; Cho & Matsuoka, 2001). To estimate the water content, a known weight (0.5-1 g) of the wet sediment sample was oven-dried at 70◦C for 24 h (Matsuoka et al., 2003; Cho & Matsuoka, 2001). Additionally, the hydrochloric and hydrofluoric acids used for cyst processing might destroy the calcareous cysts (e.g., *Scrippsiella*) and the cysts lacking distinctive cyst wall ornamentation (e.g., *Alexandrium*); therefore, additionally, 5-10g of sediment was sieved without the acid treatment and scanned under the microscope for the calcareous cysts. Various dinoflagellate cysts' morphometric measurements (body size and process length) are recorded and presented.

The method used in this study for dinoflagellate cyst enumeration and identification is microscopy-based. However, a few recent methods, like the use of Lycopodium spores (Price et al., 2016) and metabarcoding sequencing (Gao et al., 2017; Liu et al., 2023; Bolch, 2022; Gu et al., 2024), are being readily used. Based on tracer experiments, Price et al. (2016) documented loss (average 8.2 %) of Lycopodium spores during processing, with the greatest loss occurring through the fine sieve and resulting in only a 4.8% overestimation of the cyst concentration. Since the loss in cyst is mainly during the sieving process, and we have analyzed the entire residue sample (i.e., 5-15g except for

coastal stations) rather than just a portion, the loss in cyst concentration might not affect our results significantly. Moreover, metabarcoding sequencing applications, which can even be used for a single cyst sample (Gao et al., 2017), can reveal many novel dinoflagellate cysts from oligotrophic regions with low cyst concentrations. Unfortunately, in this study, the metabarcoding sequencing approach is not used; therefore, it can be assumed that the actual species count might be underestimated. However, in the present study, a high volume of sediment samples was analyzed entirely to overcome underestimation.

2.2.2c. Planktondrift simulation

Further, the dinoflagellate cyst data were subjected to planktondrift simulation using an online particle trace simulation tool (planktondrift.science.uu.nl; henceforth referred to as planktondrift) to reconstruct the surface origin of sedimentary particles and its lateral transport in a specific location (Nooteboom et al., 2019, 2020). Planktondrift simulation is applied to trace the potential dinoflagellate cyst sources. Planktondrift (https:// planktondrift.science.uu.nl) is an online particle trace simulation tool developed to simulate the trajectories and dispersal patterns of virtual particles representing plankton in the ocean (Nooteboom et al. 2019, 2020). The planktondrift simulation utilizes climate models like the Ocean General Circulation Model for the Earth Simulator (OFES), Nucleus for European Modelling of the Ocean (NEMO), or the Parallel Ocean Program (POP). These climate models provide a 3D flow field of the ocean currents in which particles are released every 3 days for 6 years at the bottom of the ocean and tracked back in time along the flow field. These sinking particles are assumed to be heavier than water; therefore, a vertical sinking velocity is added to the velocity along the transport. This study used the OFES model of the planktondrift simulation tool to trace the possible surface origin locations for all sampling stations, which incorporates more sinking scenarios than other models for locations falling below 75° North and South (https://planktondr ift.science.uu.nl). The typical sinking speed for dinoflagellate cysts is 11 m/day (Anderson et al. 1985), and the same was selected to run the simulations.

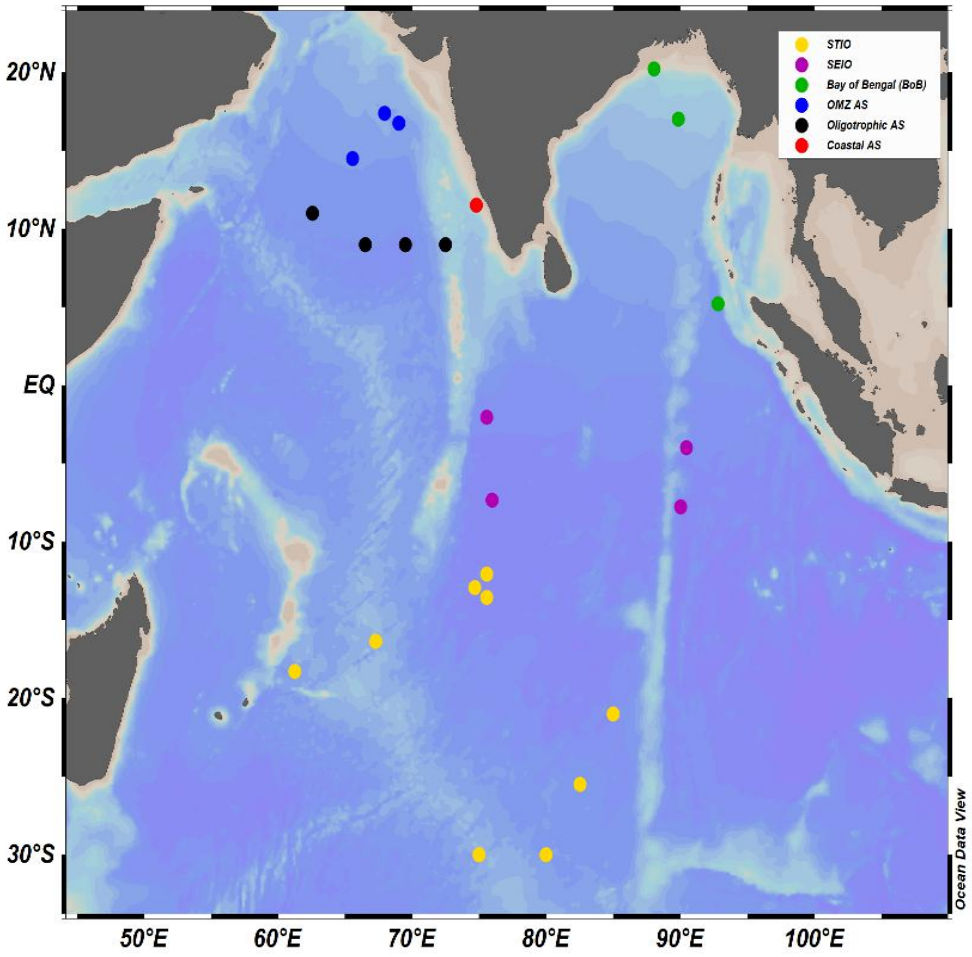


Figure 2.4. Map showing the location of the sediment sampling stations in the Indian Ocean.

Table 2.4. Details of the sampling locations, water depth, species count, and dinoflagellate cyst count per sample. C-AS: coastal Arabian Sea, O-AS: oligotrophic Arabian Sea, OMZ-AS: oxygen minimum zone Arabian Sea, BoB: Bay of Bengal, EIO: equatorial Indian Ocean, STIO: south-tropical Indian Ocean.

Stations	**Regions of the Indian Ocean**		**Longitude (ºE)**	**Latitude (ºN/S)**	**Water Depth (m)**	**Sediment type**
1	**North Indian Ocean (NIO)**	C-AS	74.7	11.5	113	Sandy
2		O-AS	72.5	9	2105	Silty clay
3			69.5	9	4607	Silty
4			66.5	9	4520	Silty
5			62.5	11	4368	Silty
6		OMZ-AS	65.5	14.5	3911	Silty
7			67.9	17.3	3505	Silty clay
8			69.0	16.7	3643	Silty
9		BoB	88.0	20.2	200	Sandy
10			89.8	17.0	2300	Silty clay
11			92.8	5.1	4300	silty
12	**South Indian Ocean (SIO)**	EIO	90.4	-4.0	4238	Silty clay
13			90.0	-7.7	5396	Silty clay
14			75.9	-7.3	5300	Silty clay
15			75.5	-2.0	4000	Clayey silt
16		STIO	85.0	-20.9	2700	Sandy
17			82.5	-25.5	4400	Silty clay
18			80.0	-30.0	3600	Silty
19			75.0	-30.0	3600	Silty
20			61.2	-18.2	4200	Clayey silt
21			67.2	-16.3	2500	Silty

22			74.6	-12.9	5100	Silty clay
23			75.5	-13.5	5200	Clayey silt
24			75.5	-12.05	5200	Clayey silt

2.2.3. Experimental setup to assess the photo-physiological adaptation of microalgae

2.2.3a. Study region

To study the photo-physiology of phytoplankton (objective 3), an investigation was conducted in the Arabian Sea (AS) and South-tropical Indian Ocean (STIO) during two different cruises on board RV *Sindhu Sadhana* (SSD069 and SSD079) (Figure 2.5). Four onboard microcosm experiments were performed with only sea surface water in the AS and using sea surface and sub-surface chlorophyll maximum layer (SCML) water in STIO. The sea surface and SCML water was sampled with 10 L Niskin bottles attached to 32 Carousel Water Sampler (Sea-bird Electronics Inc.; SBE), which is operated with the SBE 911 plus CTD equipped with various sensors (e.g., temperature, conductivity, dissolved oxygen sensor, and fluorometer) for real-time data acquisition. Photosynthetic Active Radiation (PAR; $mWcm^{-2}$) and ultraviolet radiation-A+B (UVR; $mWcm^{-2}$) were measured using a hand-held dual-input radiometer equipped with a PAR and UVA+B sensor (Make: Solar light Co. model: PAM2100).

The sea surface temperature, dissolved oxygen, and salinity at the experimental in the AS stations were 25.1-26.0 ^{o}C, 3.6-3.7 mg/L, and 36.3-36.4 PSU. In STIO experimental stations, the sea surface temperature, dissolved oxygen, and salinity ranges were 25.3-27.3 ^{o}C, 4.2-4.5 mg/L, and 34.7-35.3 PSU, respectively, whereas SCML temperature, dissolved oxygen, and salinity ranges were 20.0-22.4 ^{o}C, 3.6-4.3 mg/L, and 35.1-35.7 PSU.

2.2.3b. Experimental setup

To evaluate the effect of solar radiation on the photo-physiology of phytoplankton, two treatments were designed: one phytoplankton community was incubated in 2L Nalgene bottles in triplicates, which allows only PAR exposure, and the other in 1.6L in Whirlpack Bags in five replicates, which allows both PAR+UVR exposure. The water samples were passed through 200 µm nylon mesh to separate zooplankton and detritus. They were enriched with f/2 macro-nutrients (nitrate + phosphate + silicate) and incubated in a water-circulating incubator simulating *in-situ* conditions to maintain the *in-situ* temperature under natural light onboard the research vessel. The experiments containing only sea surface water were incubated directly under natural sunlight. In contrast, in experiments with SCML water, density screens were used to reduce the sunlight by 60% to simulate the *in-situ* SCML light conditions. The incubation lasted for 72 hours, and the measurements for (i) physiological parameters were made every three hours from sunrise to sunset, (ii) diagnostic pigments twice a day, one in the morning and one in the evening,

and (iii) for phytoplankton community, initial and final samples were collected. The physiological parameters were measured using a benchtop fast-repetition-rate-fluorometer (FRRF; Fast Act system, Chelsea Company Ltd) and high-performance liquid chromatography (HPLC; Agilent Technology; Series 1200). The physiological status of the photosynthesizing organisms was assessed using initial (F_0), maximum (F_m), and variable (F_v) components of photosystem II (PSII) fluorescence, photosynthetic efficiency (F_v/F_m), functional absorption cross section (σ_{PSII}), and the production of photo-protective pigments. Samples were dark adapted for 30 minutes under ambient temperature before FRRF reading. A known volume of water sample (500 mL to 1 L) was filtered using Whatman GF/f filter paper in dim light conditions and stored at -80^o C till analysis.

2.2.3c. Sample analysis

For the phytoplankton community analysis, a known volume (100 mL) of water sample from each experimental setup was collected, preserved (4% Lugol's iodine at the site), and analyzed using an inverted microscope (IX-73 Olympus make). The initial and final phytoplankton composition and abundance were estimated by analyzing 2 mL of sample in duplicates, and identification was carried out based on standard identification keys (Tomas, 1997; Taylor, 1976).

Phytoplankton marker pigments were extracted in 3 mL of 100% HPLC grade acetone. The samples were ultrasonicated in cold conditions for 1 min and stored overnight at -20^{o}C for extraction. Before injection, the unwanted debris was separated from the extracts using disposable syringe filters (pore 0.2 μm). All the extraction and injection procedures were performed under subdued light to prevent photolysis. The phytoplankton diagnostic pigments were analyzed following the standard method (Van Heukelem, 2002; Roy et al., 2015). The pigments were quantified against DHI (Denmark) standards: chlorophylls (a, b, and c family) and carotenoids (diagnostic pigments: fucoxanthin-Fuco, peridinin-Per, 19′-hexanoyloxyfucoxanthin-19′HF, 19′-butanoyloxyfucoxanthin-19′BF, alloxanthin-Allo, zeaxanthin-Zea; photoprotective carotenoids: diadinoxanthin-DD, diatoxanthin-DT, β carotene-Car, lutein-Lut; other carotenoids: violaxanthin-Viola, neoxanthin-Neo, and prasinoxanthin-Pras). In this study, photosynthetic carotenoids (PSC) include 19'HF, 19'BF, fuco, and per, whereas photoprotective carotenoids (PPC) include allo, car, DD, DT, lut, zea, and viola. Further, the experiment's pigment data were used to calculate different phytoplankton size fractions (pico-phytoplankton, nano-phytoplankton, and micro-phytoplankton),

taxonomic groups (diatoms, dinoflagellates, and prokaryotes), and various pigment ratios (DT/DT+DD, DT+DD/Chl-*a*, and PPC/PSC) following Brewin et al. (2015) and Barlow et al. (2007). The fractions of pico-, nano-, and microplankton were computed from the weighted diagnostic pigments. (see Brewin et al. 2015 for details).

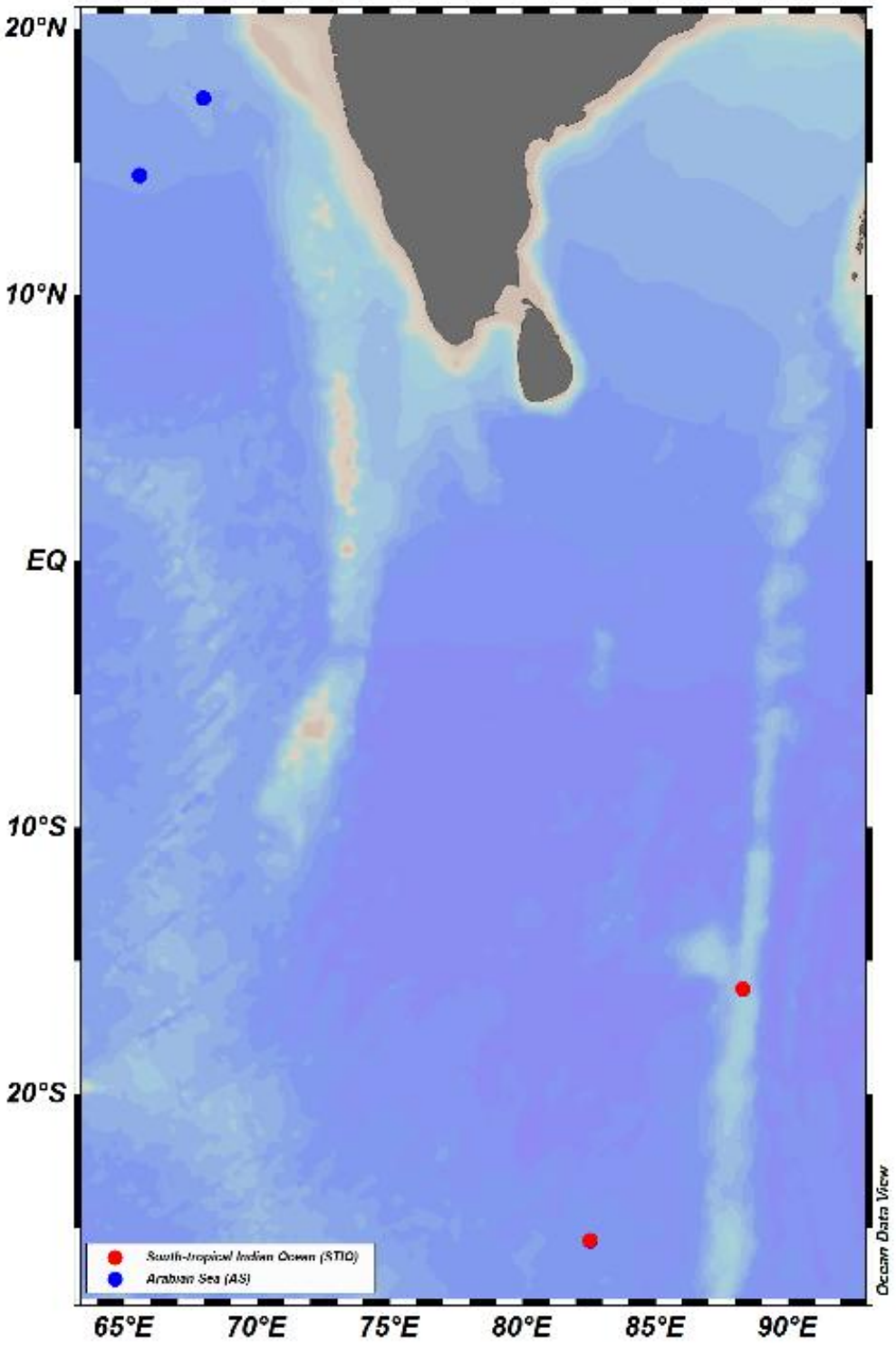


Figure 2.5. Map showing location of the experimental study site in different bioregions of the Arabian Sea and South tropical Indian Ocean.

Chapter 3

Diversity and distribution of planktonic and benthic microalgae

Chapter 3: Diversity and distribution of planktonic and benthic microalgae

Various taxa belonging to different microalgal groups dominate different parts of the intertidal and pelagic ecosystems. For instance, in the shallow intertidal ecosystem, diatoms dominate both the planktonic (mostly centric diatoms) and benthic (microphytobenthos; MPB) communities (mostly pennate diatoms), whereas, in the pelagic ecosystems, diatoms dominate in the upper photic zone of the water column and diatom frustules and dinoflagellate cysts in the underlying sediments. The MPB are the major primary producers in the intertidal system (Underwood & Kromkamp, 1999) and play key ecological roles. Similarly, dinoflagellates (only 12-13%) are known to produce organic-walled and calcareous cysts that help dinoflagellates to form seed banks for blooms (including harmful algal blooms), produce toxins (e.g., *Alexandrium* and *Gymnodinium* species), and help in unwanted marine bio-invasion as they remain viable for many years (Matsuoka & Fukuyo, 2000; Lundholm et al., 2011; Delebecq et al., 2020). The phytoplankton community has been extensively studied in Indian waters, but the focus has always been on the planktonic forms (Ahmed et al., 2016; Chitari & Anil, 2017; Jagadeesan et al., 2017; Arunpandi et al., 2017; Kusum et al., 2017; Hardikar et al., 2017; Bharathi et al., 2018) than the benthic forms (e.g., MPB and dinoflagellate cysts).

Therefore, in this chapter, the planktonic (in the surf water) and benthic (MPB) microalgae from the intertidal ecosystem and the planktonic (in the photic zone of the water column) and dominant benthic (dinoflagellate cysts) microalgae from the pelagic ecosystems were studied. The findings of the intertidal and pelagic ecosystems are presented in two sub-chapters, 3.1 and 3.2, respectively.

3.1. The intertidal ecosystem

3.1.1. Introduction

The autotrophic and heterotrophic microalgae in the intertidal and shallow subtidal sediments are known as microphytobenthos (MPB) (Underwood & Kromkamp, 1999). The MPB assemblages, though mostly dominated by diatoms, can also include dinoflagellates, cyanobacteria, and euglenoids (MacIntyre et al., 1996). The MPB are one of the major primary producers in the intertidal ecosystem (Underwood & Kromkamp, 1999) and play key ecological roles by serving as food sources for meiofauna, macrofauna, and other deposit-feeders which in turn supports the upper levels of trophic food web like birds and fish (Kang et al., 2015). However, when MPB are resuspended in the adjacent water column, they also serve as a food source for suspension feeders

(Herman et al., 2001; Lefebvre et al., 2009; Ubertini et al., 2012; Oakes et al., 2016). MPB colonizes large areas of intertidal sediment in estuaries and coastal areas, facilitates vital ecosystem services (Hope et al., 2020), and can even extend to the edge of the continental shelf (Cahoon, 1999; Pinckney, 2018). The presence of MPB, when in extremely high numbers, can appear as light brown or green shading on the surface sediments or can also be invisible to the naked eye (Hope et al., 2020). The hydrodynamic conditions on a tidal flat fluctuate regularly; however, the MPB are well adapted to such harsh conditions where temperature, light, salinity, nutrients, and tides change rapidly. These rapidly changing abiotic factors tightly regulate the MPB productivity (Kromkamp et al., 1995; Perkins et al., 2001), but they adapt efficiently to the prevailing abiotic conditions (Falkowski & Raven, 2013; Hopes & Mock, 2015). The diatoms and cyanobacteria, one of the significant contributors in the MPB community, are also known to regulate small and large-scale processes (Chapman et al., 2010) like influencing biogeochemical gradients in the sediment (MacIntyer et al., 1996), influencing sediment stability (Fagherazzi et al., 2014) and trapping particles from overlying water (Kornman & de Deckere, 1998). Hope et al. (2020) have pointed out the importance of MPB in sediment ecology and their contribution to various ecosystem services like carbon and nitrogen cycling, improving water quality by regulating the benthic-pelagic coupling of nutrients, sediments, and pollutants, etc. However, the existence and functioning of MPBs are highly dependent on their habitats (i.e., tidal flats, sand flats, mud flats, etc.). Murray et al. (2019) estimated that the global area of tidal flats is 127,921 km^2, of which around 44% is in Asia, 15.5% in North America, and 11% in South America. Among these continents, 49.2% of tidal flats are concentrated in eight countries: Indonesia, China, Australia, the United States, Canada, India, Brazil, and Myanmar. India has a total of 5788 km^2 of tidal flat area. The tidal flats are vulnerable ecosystems and are under intense pressure due to coastal developments (Arkema et la., 2013), sea-level rise (Galbraith et al., 2002; Kirwan & Megonigal, 2013; Passeri et al., 2015; Lovelock et al., 2017), coastal erosion (Parry, 2007), sediment fluxes from rivers (Syvitski et al., 2005; Blum & Roberts, 2009), and subsidence and compaction of coastal sediments (Blum & Roberts, 2009; Syvitski et al., 2009). These tidal flats are also regularly claimed for commercial and residential use (Goodwin et al., 2001) and have already lost over 50% of their original area in many regions of the world (Gibson et al., 2007).

MPB has been extensively studied by European countries (see Park et al., 2014 for more details), mainly from the tidal flats, and the topics are related to assemblages,

dynamics, production, food web, and remote sensing. However, in the Asian continents, only Japan, South Korea, and China have done some pioneering work, whereas in India, only a few representative works have been done (Mitbavkar and Anil, 2002, 2004 & 2006). Despite having a large tidal flat area, the studies on MPB from tidal flats are scarce.

Therefore, the present study aims to address the following: (i) inter-annual variability of MPB from DTF and MTF, (ii) seasonal variability of MPB in contrasting Indian summer monsoon from DTF and MTF, (iii) comparison with the previous study to assess the decadal shift in MPB assemblage at the DTF, and (iv) impact of anthropogenic activities on the MPB assemblage at the MTF. Thus, the present study will delineate the resilience or vulnerability of the MPB on the intertidal flats, which will help for better coastal management and sustainable use of coastal ecosystem services.

3.1.2. Methodology

The details of the sampling site, sample collection, and analysis from the tidal flats situated at both Zuari Estuary (Dias tidal flat; DTF) and Mandovi Estuary (Miramar tidal flat; MTF) are presented in Chapter 2 sub-section 2.1.1.

Data analysis

Univariate measures such as species count (S), Shannon–Wiener's diversity (H'), species richness (d), and evenness (J') were performed on MPB abundance data. The two-way analysis of variance (ANOVA) was performed on log-transformed data to evaluate the variations between tidal zones and tidal flats. Univariate calculation and clustering analysis were performed using statistical software PRIMER 6 and ANOVA using Statistica software (release 8).

3.1.3. Results

3.1.3.1. Environmental variables at Dias and Miramar tidal flat

Intra-annual variations

The temperature range recorded in the SW showed slightly higher values in DTF than in MTF, whereas the salinity values showed no significant variations between the tidal flats. The average temperature and salinity values in the tidal zones (interstitial water) of MTF and DTF showed no significant differences. The sediment of HT was very dry in MTF, whereas HT sediment was relatively wet in DTF. The average nitrate (NO_3) and nitrite (NO_2) values in the SW and the interstitial water were higher in MTF than in DTF. The average phosphate (PO_4) and silicate (SiO_2) values in the SW were higher in MTF than

DTF, whereas in the interstitial water, it was higher in DTF than in MTF. The sediment texture was mostly sandy throughout the study period in all the tidal zones at both tidal flats. However, in DTF, the silty sediment proportion marginally increased in both pre-monsoon and post-monsoon seasons in LT and MT (Figure 3.1a and b).

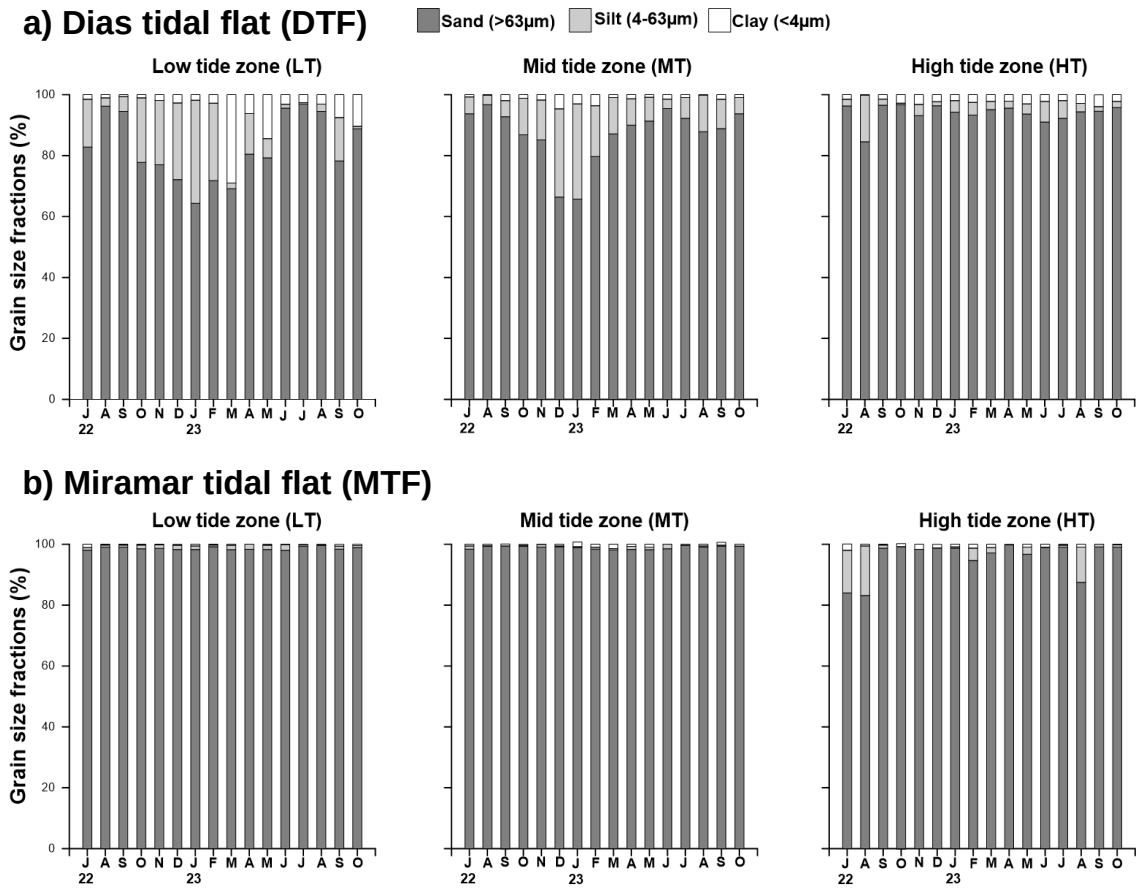


Figure 3.1. Plot showing sediment grain size in low, mid, and high-tide zones at a) Dias tidal flat and b) Miramar tidal flat during the study period.

The temperature and salinity showed a similar trend, with lower values observed during monsoon and higher values in post-monsoon and pre-monsoon. The average chlorophyll-*a* values were lower in MTF than in DTF. Seasonally, the lowest chlorophyll-*a* values were recorded during the monsoon seasons, whereas the highest values were recorded during the pre-monsoon and post-monsoon seasons of 2022 and 2023 at both tidal flats. However, at MTF, relatively higher chlorophyll-*a* values were recorded only at the HT zone during the 2022 monsoon season than in the 2023 monsoon (Figure 3.2a-d).

At DTF, the average SW and interstitial water temperature (28.1^{o}C and 28.0^{o}C) and salinity (22.4 and 23.1 PSU) showed no significant difference in 2019. The average sediment temperature in 2022-23 showed a similar range between tidal zones (28.1-28.8^{o}C). Similarly, the average SW salinity (27.7-28.4 PSU) showed no significant variation between SW and interstitial water. The average chlorophyll-*a* values were similar in LT (0.23±0.29 mg/g) and MT (0.23±0.20 mg/g) and low in HT (0.12±0.13 mg/g). In 2022-23, the average nitrate (NO_3) concentration showed a gradually decreasing trend from SW (1.16±1.13 µM) to interstitial water (0.69±0.56 µM); the average nitrite (NO_2) concentration in the SW (0.30±0.18 µM) was higher than the interstitial water (0.17±0.24 µM); the average phosphate (PO_4) concentration was higher in interstitial water (4.08±1.29 µM) than the SW (1.76±0.77 µM); the average silicate (SiO_2) concentration was higher in interstitial water (32.0±6.9 µM) than SW (10.5±6.4 µM) (Figure 3.2).

At MTF, the average SW and interstitial water temperature (27.3^{o}C and 27.2^{o}C) and salinity (28.3 and 27.5 PSU) showed no significant difference in 2019. In 2022-23, the average temperature was marginally higher in HT (29.1±3.8^{o}C) but showed no significant differences between SW (28.4±1.9^{o}C), LT (28.5±1.9^{o}C), and MT (28.5±2.8^{o}C). On the contrary, the average interstitial water salinity was higher (27.3±6.3 PSU) than SW (22.0±13.0 PSU). The HT sediment was very dry and devoid of interstitial water. The average chlorophyll-*a* values were lowest in HT (0.05±0.08 mg/g), followed by LT (0.06±0.13 mg/g), and highest in MT (0.09±0.08 mg/g) (Figure 3.2e-h). In 2022-23, the average nitrate (NO_3), nitrite (NO_2), phosphate (PO_4) and silicate (SiO_2) concentration were higher in interstitial water (NO_3:2.61±4.59µM; NO_2:1.13±1.01 µM; PO_4: 3.77±0.95 µM; SiO_2: 29.9±4.5 µM) than in SW (NO_3:1.45±1.60 µM; NO_2:0.33±0.33 µM; PO_4: 1.73±0.66 µM; SiO_2: 14.16±7.15 µM) (Figure 3.2).

Inter-seasonal variations

Pre-monsoon

The average temperature recorded in the SW, LT, and MT during pre-monsoon was marginally higher in 2019 than in 2022 at both tidal flats. Similarly, the average salinity recorded in the SW and MT interstitial water during pre-monsoon was marginally higher in 2019 than in 2022 at both tidal flats. However, the DTF showed slightly higher temperature and salinity values than the MTF, but the differences were insignificant.

At DTF, the average SW temperature during pre-monsoon was marginally higher in 2019 (30.0±0.97ºC) than in 2022 (29.5±2.0ºC), in LT 2019 was marginally lower (30.0±0.97ºC) than in 2022 (30.3±0.3ºC), in MT 2019 was lower (19.5±15.1ºC) than in 2022 (28.9±3.9ºC). The average SW salinity during pre-monsoon was marginally higher in 2019 (35±0.4 PSU) than in 2022 (34±0.8 PSU), and in interstitial water, salinity was slightly higher in 2019 (33±2.5 PSU) than in 2022 (30±3.2 PSU).

At MTF, the average SW temperature during pre-monsoon was marginally higher in 2019 (28.9±0.12ºC) than in 2022 (29.0±1.6ºC), in LT 2019 was marginally lower (28.9±0.12ºC) than in 2022 (29.0±1.8ºC), in MT 2019 was lower (28.6±0.29ºC) than in 2022 (29.0±1.4ºC). The average SW salinity during pre-monsoon was marginally higher in 2019 (35.7±0.52 PSU) than in 2022 (33±1.2 PSU), interstitial water salinity was slightly higher in 2019 (36±0.89 PSU) than in 2022 (35±0.7 PSU) (Figure 3.2).

Monsoon

The average temperature recorded in the SW during monsoon was marginally lower in 2019, followed by 2022 and 2023 at both tidal flats. In LT, sediment temperature was marginally lower in 2022, followed by 2019 and 2023; in MT, 2019 and 2022 were slightly lower than 2023, and in HT, 2022 and 2023 were similar at both tidal flats. The average salinity recorded in the SW during monsoon was significantly lower in 2019, followed by 2022 and 2023 at both tidal flats. The interstitial water salinity was significantly lower in 2019, followed by 2023 and 2022 at both tidal flats. The average rainfall recorded in 2019 (400±578 mm) was the highest, followed by 2023 (229±328 mm) and the least in 2022 (86±119 mm). In 2019, the monsoon months (June-September) recorded 637-1654 mm of rainfall; in 2022, 142-313 mm of rainfall; and in 2023, 389-956 mm of rainfall.

At DTF, the average SW temperature during monsoon was marginally lower in 2019 (26.0±2.0ºC), followed by 2022 (27.0±1.1ºC) and 2023 (28.0±2.0ºC). In LT, sediment temperature was marginally lower in 2022 (26.0±0.9ºC), followed by 2019 (26.2±2.02ºC) and 2023 (28.0±1.5ºC), in MT 2019 (26.0±0.19ºC) and 2022 (26.0±0.8ºC) was slightly lower than 2023 (27.0±1.3ºC) and in HT 2022 (26.0±0.9ºC) was lower than 2023 (27.0±1.2ºC). The average SW salinity during monsoon was significantly lower in 2019 (10±5.5 PSU), followed by 2022 (22±6.9 PSU) and 2023 (24±7.9 PSU). The interstitial water salinity was significantly lower in 2019 (13±6.5 PSU), followed by 2023 (26±6.4 PSU) and 2022 (27±1.5 PSU).

At MTF, the average SW temperature during monsoon was marginally lower in 2019 (26.0±0.68ºC), followed by 2022 (27.0±0.5ºC) and 2023 (27.0±2.2ºC). In LT, sediment temperature was marginally lower in 2022 (26.0±0.3ºC), followed by 2019 (26.0±0.68ºC) and 2023 (28.0±1.6ºC), in MT 2019 (27.7±0.27ºC) and 2022 (26.0±0.8ºC) was slightly lower than 2023 (27.0±1.1ºC) and in HT 2022 (27.0±0.3ºC) and 2023 (27.0±0.1ºC) was similar. The average SW salinity during monsoon was significantly lower in 2019 (4±2.5 PSU), followed by 2022 (8±7.4 PSU) and 2023 (15±16.1 PSU). The interstitial water salinity was significantly lower in 2019 (19.3±15.8 PSU), followed by 2022 (23±6.1 PSU) and 2023 (26±6.9 PSU).

Post-monsoon

The average temperature recorded in the SW and the interstitial water in the post-monsoon season was marginally higher in 2023 than in 2022 at both tidal flats. The average temperature in LT, MT, and HT surface sediment showed no significant differences between 2022 and 2023 at both tidal flats. In post-monsoon, the average salinity recorded in the SW and interstitial water was marginally higher in 2023 than in 2022 at DTF, whereas, at MTF, the SW was marginally higher in 2023 than in 2022, and interstitial water was marginally higher in 2022 than in 2023.

At DTF, the average SW temperature during post-monsoon was marginally higher in 2023 (30.0±0.9ºC) than in 2022 (29.0±2.0ºC); in the interstitial water, no difference was found between the years. The average LT sediment temperature was similar for both the years (30.0±1.5ºC); for MT and HT 2023 (31.0±2.1ºC), it was slightly higher than in 2022 (29.0-30.0±1.5ºC). The average SW and the interstitial water salinity during both post-monsoon years were marginally higher in 2023 (33 PSU) than in 2022 (29-32±2.1-3.0 PSU).

At MTF, the average SW and interstitial water temperature during post-monsoon were marginally higher in 2023 (30.0ºC) than in 2022 (29.0±2.1ºC). The average surface sediment temperature of LT was marginally higher in 2023 (30.0±0.5ºC) than in 2022 (29.0±2.1ºC); for MT, it was similar in both the years (31.0ºC) and for HT, 2022 (33.0±1.3ºC) was slightly higher than 2023 (32.0±1.9ºC). The average SW salinity was marginally higher in 2023 (31 PSU) than in 2022 (27±1.8 PSU), and the interstitial water during both years was higher in 2022 (28±4.2 PSU) than in 2023 (22 PSU).

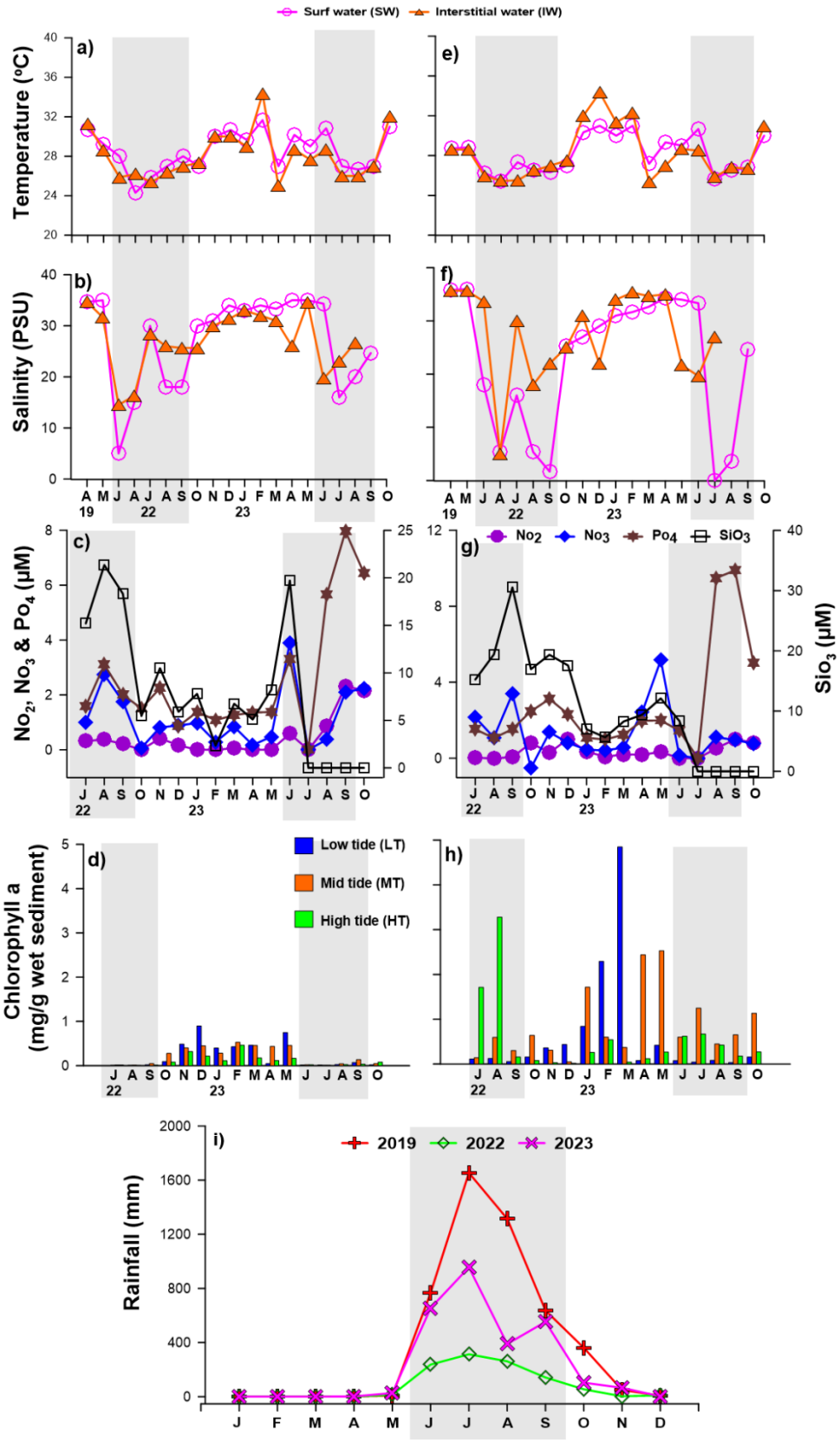


Figure 3.2. Plots showing environmental variables during the study period: a) and e) Temperature, b) and f) Salinity, c) and g) Nutrients, d) and h) Chlorophyll *a* and i) Rainfall at both DTF (a-d) and MTF (e-f). Shaded and unshaded regions represent the monsoon and non-monsoon seasons (pre- and post-monsoon).

3.1.3.2. The phytoplankton and microphytobenthos assemblage of Dias and Miramar tidal flat

Intra-annual variations of phytoplankton in tidal flats

The surf water of MTF encountered relatively more phytoplankton (species count, diversity, and abundance) than DTF, but the differences were insignificant. Further, ANOVA revealed significant ($p<0.05$) seasonal variations in abundance (except MTF) and diversity indices. Both tidal flats recorded A higher phytoplankton abundance during the non-monsoon seasons. The seasonal differences were significant and insignificant at DTF ($p<0.001$) and MTF, respectively. The species count (S), richness (d), evenness (J'), and diversity (H') were significantly ($p<0.05$) higher in the pre-monsoon and post-monsoon seasons than in the monsoon season at both tidal flats.

Altogether, 92 phytoplankton species (23 pennate, 51 centric, and 18 dinoflagellates) were recorded at both tidal flats, of which 45 species were common. Maximum species were recorded at MTF (84 species, 67 diatoms, and 17 dinoflagellates; 91%) belonging to 55 genera than DTF (53 species, 47 diatoms, and 6 dinoflagellates; 58%) belonging to 48 genera. In MTF, an additional 31 phytoplankton species (~34%) were recorded, which are not recorded at DTF). In both the tidal flats, diatoms (DTF – 99.7%; MTF - 98%) followed by dinoflagellates (0.3 – 2 %) dominated the community. Among the diatoms, centric dominated (DTF - 52%; MTF - 63%), but the composition differed between the tidal flats, whereas the pennate diatom composition (DTF – 47.7%; MTF - 35%) remained similar. During the study period, the average centric pennate ratio (C:P) values were 4.0±1.15, with the lowest and highest values recorded in October 2022 (0.08, caused by *Pseudonitzschia* spp. bloom) and in April 2023 (13.17, caused by *L. undulatum* and *B. malleus* blooms), respectively at DTF. In contrast, the average C:P values were 12.17±5.5, with the lowest and highest values recorded in October 2023 (0.01, caused by *Navicula* sp.) and in June 2023 (87.8, caused by *C. curvisetus* and *C. debilis* blooms), respectively at MTF. Interestingly, a C:P value >1 was recorded for 11 months, indicating centric diatom dominance at both tidal flats.

At DTF, pennate diatom *Pseudonitzschia* spp. (~0.7 $x10^4$ cells/L; 35%) dominated the community, followed by centric diatoms *Bellerochea malleus* (~0.5 $x10^4$ cells/L; 26%), *Lithodesmium undulatum* (~0.3 $x10^4$ cells/L; 6%), and *Skeletonema* sp. (~0.2 $x10^4$ cells/L; 6%). *Pyrocystis* sp. (0.004 $x10^4$ cells/L; 0.2%) was the dominant species among the dinoflagellates. During the study period, the bloom of *Pseudonitzschia* spp. (~12.5$x10^4$ cells/L; October 2022) and *B. malleus* (~4.4$x10^4$ cells/L; December 2022)

were observed (Figure 3.3). The cluster analysis of the phytoplankton contributing >1% revealed three main groups at 90% similarity. The first group was formed by the bloom-forming diatoms (*Pseudonitzschia* spp. and *B. malleus*, contributing 61%), the second group formed two sub-groups representing second (*Lithodesmium undulatum*, *Skeletonema*, and *Navicula* sp., contributing 16%) and third (*Cocconeis* sp. and *Lithodesmium* sp., contributing 6%) most abundant species and the third group (contributing 11%) formed two sub-groups consisting of remaining major contributors (Figure 3.4a).

At MTF, pennate diatom *Pseudonitzschia* spp. (~1.7 x10^4 cells/L; 31%) dominated the community, followed by centric diatoms *Skeletonema* sp. (~1.2 x10^4 cells/L; 22%), *Chaetoceros curvisetus* (~0.6 x10^4 cells/L; 12%), and *Chaetoceros debilis* (~0.5 x10^4 cells/L; 10%). Among the dinoflagellates, *Tripos furca* (~0.05 x10^4 cells/L; 0.7%) was the dominant species. During the study period, the bloom of *Pseudonitzschia* spp. (~28.2x10^4 cells/L; October 2022) and various *Chaetoceros* spp. (e.g., *C. curvisetus*, *C. debilis*, *C. decipiens*, *C. didymus*, and *C. socialis*; June 2023) (up to ~8.8x10^4 cells/L) were recorded (Figure 3.5). The cluster analysis of the phytoplankton species contributing >1% revealed two main groups at 90% similarity. The first group formed two sub-groups consisting of the major bloom-forming diatoms (*Skeletonema* sp., *C. curvisetus*, *C. debilis*, *Pseudonitzschia* spp., contributing 75%), and the second group formed two sub-groups consisting of remaining major contributors (contributing 19%) (Figure 3.4b). Interestingly, *Pseudonitzschia* spp. and *Skeletonema* sp. were the commonly recorded dominant diatoms at both tidal flats.

Intra-annual variations of MPB

Altogether, 57 MPB species (22 pennate, 24 centric, and 11 dinoflagellates) were recorded at both tidal flats, of which 34 species were common. More MPB species and relatively less abundance were recorded at MTF than at DTF; however, the differences were insignificant. A higher MPB abundance was recorded during the non-monsoon than monsoon seasons at both tidal flats; however, the seasonal differences were significant only at DTF ($p<0.001$) but not at MTF. The species count (S), species richness (d), and diversity (H') of MPB showed a decreasing trend from LT to HT at both tidal flats. In contrast, abundance was higher in HT, followed by LT and MT at MTF, whereas a decreasing trend for abundance was observed from LT to HT at DTF. Moreover, the MPB abundance was higher in the LT and MT but not in HT at DTF than MTF (Figure 3.6).

Similarly, a significant difference ($p<0.001$) in MPB abundance, species count, and diversity was recorded between the tidal zones for both tidal flats and between LT-HT and MT-HT; however, differences were not significant between LT-MT at DTF. On the contrary, no significant differences were observed between the tidal zones at MTF.

In DTF, 45 MPB species (36 diatoms and 9 dinoflagellates) belonging to 40 genera were recorded overall. A slightly higher number of MPB species were recorded at LT (36 species, 31 diatoms, and 5 dinoflagellates) and MT (36 species, 31 diatoms, and 5 dinoflagellates) than at HT (33 species, 27 diatoms, and 6 dinoflagellates). In MTF, 48 MPB species (39 diatoms and 9 dinoflagellates) belonging to 40 genera were recorded. A higher number of MPB species were recorded at LT (41 species, 27 diatoms, and 8 dinoflagellates), followed by MT (36 species, 27 diatoms, and 9 dinoflagellates) and HT (33 MPB species, 25 diatoms, and 8 dinoflagellates). At DTF, centric diatoms dominated LT-MT, and pennate dominated the HT zone. Consequently, a higher centric-to-pennate ratio (C:P) was observed in LT-MT (i.e., >1, LT-3.3±0.90 and MT-3.4±0.86) than in the HT zone (<1, HT-0.7±0.25). In contrast, at MTF, centric diatoms dominated in LT and pennate in MT-HT, revealed by higher C:P values (i.e., >1 in LT-1.3±0.61 and <1 in MT-0.76±0.34 and HT-0.59±0.33). Centric and pennate diatoms co-dominated at LT (24-65%), centric diatoms at MT (65%), and pennate diatoms at HT (83%) in DTF, whereas pennate diatoms (69-91%) were predominant at all tidal zones at MTF (Figure 3.3a-b; 3.5a-b). The abundance of epipelic forms decreased from LT to MT and increased in HT, whereas epipsammic forms decreased from LT to HT at DTF. Meanwhile, at MTF, the abundance of epipelic and epipsammic forms decreased from LT to MT and increased in HT (Figures 3.3c and 3.5c).

In DTF, the MPB community in LT was co-dominated by *Navicula* spp. (24%) and *Thalassiosira* sp. (23%), followed by *B. malleus* (21%) and *L. undulatum* (17%), in MT, co-dominated by *L. undulatum* (25%) and *Thalassiosira* sp. (24%), followed by *Navicula* spp. (21%) and *B. malleus* (14%) and in HT, pennate diatom *Navicula* spp. (65%) was the dominant species, followed by *Nitzschia* sp. (14%) and *Thalassiosira* sp. (9%). Further, in October 2022, a high abundance of *Pseudonitzschia* spp. (also observed in SW during the same period) in LT (1123 cells/g of WS), MT (982 cells/g of WS), and HT (1143 cells/g of WS) were observed, respectively. The cluster analysis of the MPB community (considering species contributing >1%) at LT, MT, and HT revealed two main groups at 90% similarity. At all the tidal zones, the first group was formed by the most abundant diatoms, and the second group consisted of the remaining major contributors

(Figure 3.7). The common diatoms found in the first group at all tidal zones were *Pseudonitzschia* spp. (20-35%), *Navicula* sp. (16-39%), *Thalassiosire* sp. (21-24%), *B. malleus* (22-26%), and *Lithodesmium* sp. (5-18%).

In MTF, the MPB community in the LT was dominated by *Navicula* spp. (54%) followed by *Thalassiosira* sp. (18%), in MT, by *Navicula* spp. (51%), *Nitzschia* sp. (22%) and *Thalassiosira* sp. (13%), and in HT, *Navicula* spp. (58%) and *Nitzschia* sp. (31%) were the dominant species. Dinoflagellate contribution was negligible, with a relatively higher contribution at MTF (1% with 9 species) than at DTF (>1% with 9 species). At MTF, the pennate diatom abundance peaked in Jan-March 2023 (1190-1730 cells/g of WS) for LT, in Oct 2022, Jan and Aug 2023 (694-974 cells/g of WS) for MT, and in July-Aug 2022 and May-June 2023 (2060-2255 cells/g of WS) for HT all dominated by *Navicula* spp. and *Nitzschia* sp. The cluster analysis of the MPB community (considering species contributing >1%) at LT, MT, and HT revealed two main groups at 70% similarity. The most abundant diatoms formed the first group, and the second group comprised the remaining major contributors (Figure 3.8). The common diatoms found in the first group at all tidal zones were *Navicula* sp. (51-58%), *Nitzschia* sp. (23-31%), *Thalassiosira* sp. (13-19%), and *Chaetoceros* sp. (3-7%). Interestingly, *Navicula* sp. and *Thalassiosira* sp. were the commonly recorded dominant diatoms found in the first group at both tidal flats.

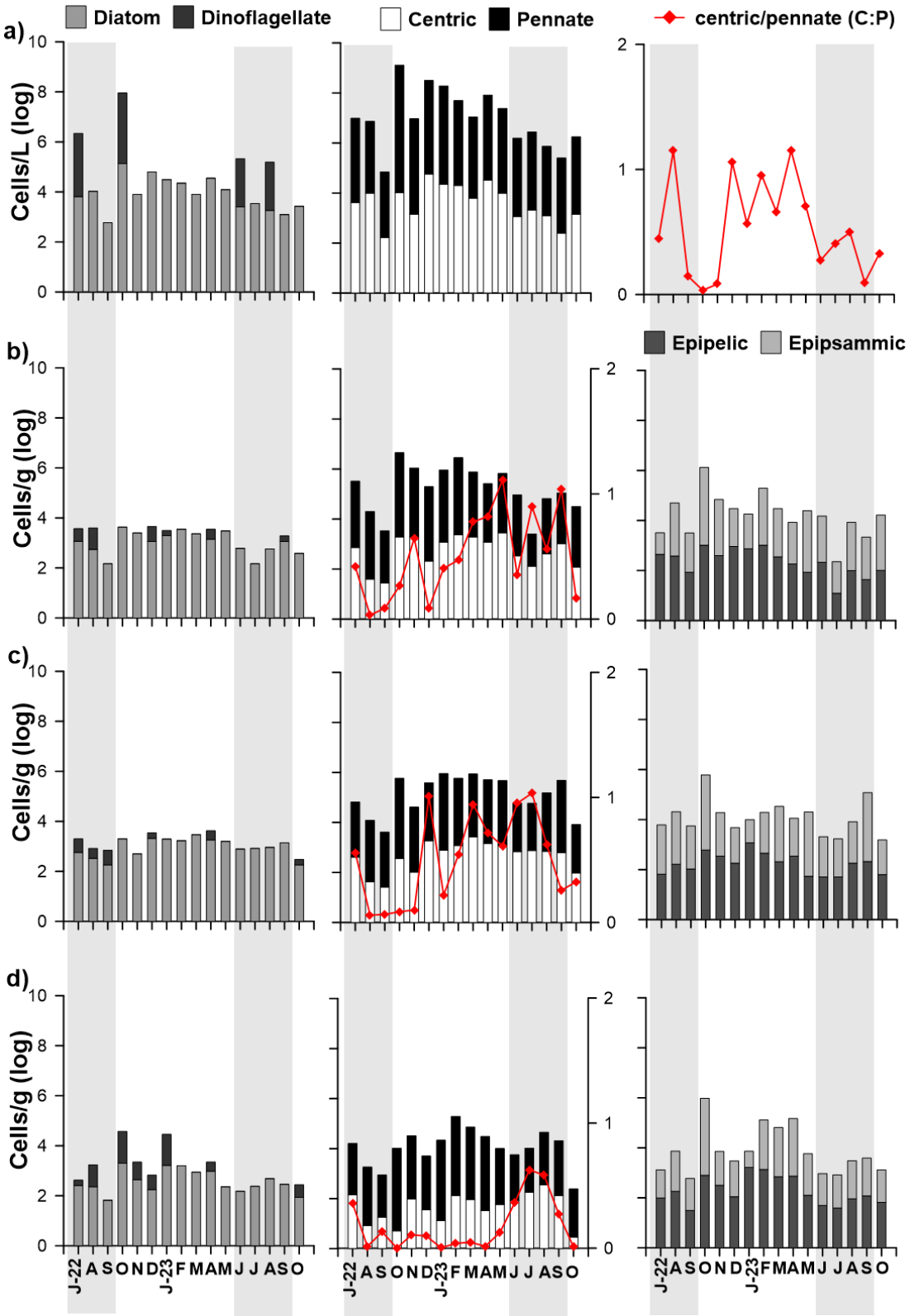


Figure 3.3. Plots showing inter-annual variability in diatoms and dinoflagellates, centric and pennate diatoms, and abundance of epipelic and episammasic diatoms in a) surf water, b) low-tide, c) mid-tide, and d) high-tide zones during the study period at DTF. Shaded regions represent the monsoon seasons.

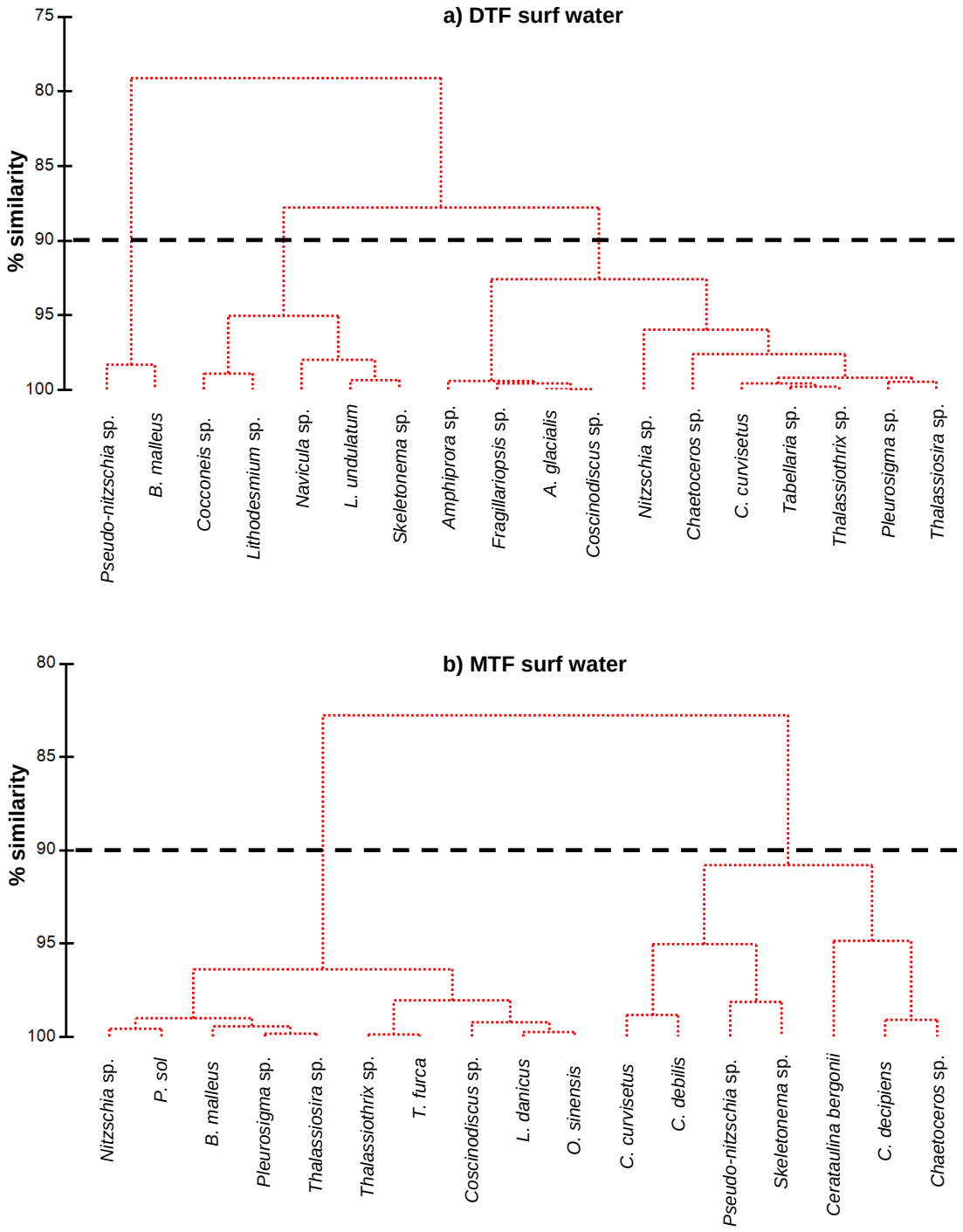


Figure 3.4. Plots showing cluster analysis of the dominant phytoplankton species in the surf water of a) DTF and b) MTF.

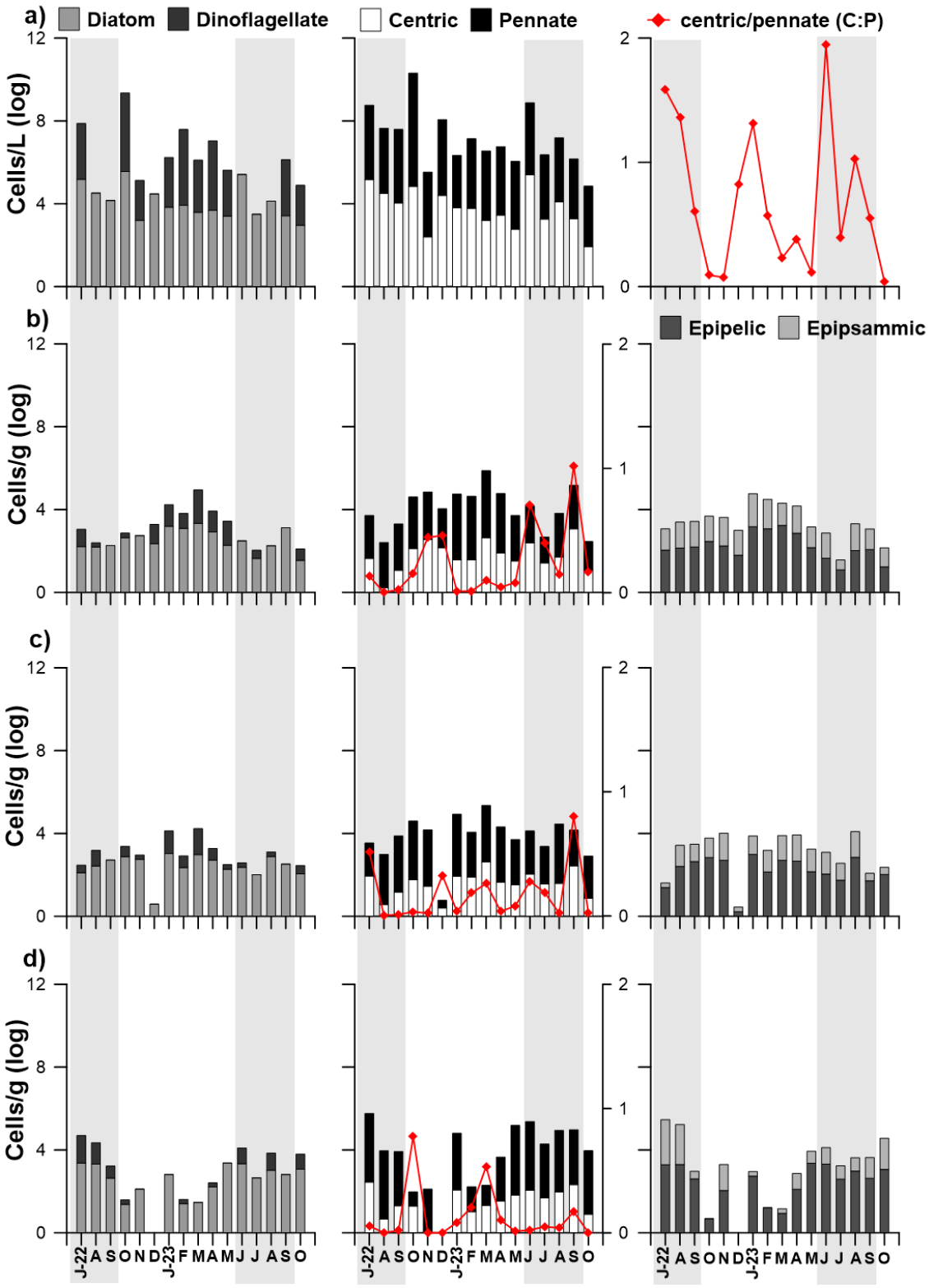


Figure 3.5. Plots showing inter-annual variability in diatoms and dinoflagellates, centric and pennate diatoms, and abundance of epipelic and episammasic diatoms in a) surf water, b) low-tide, c) mid-tide, and d) high-tide zones during the study period at MTF. Shaded regions represent the monsoon seasons.

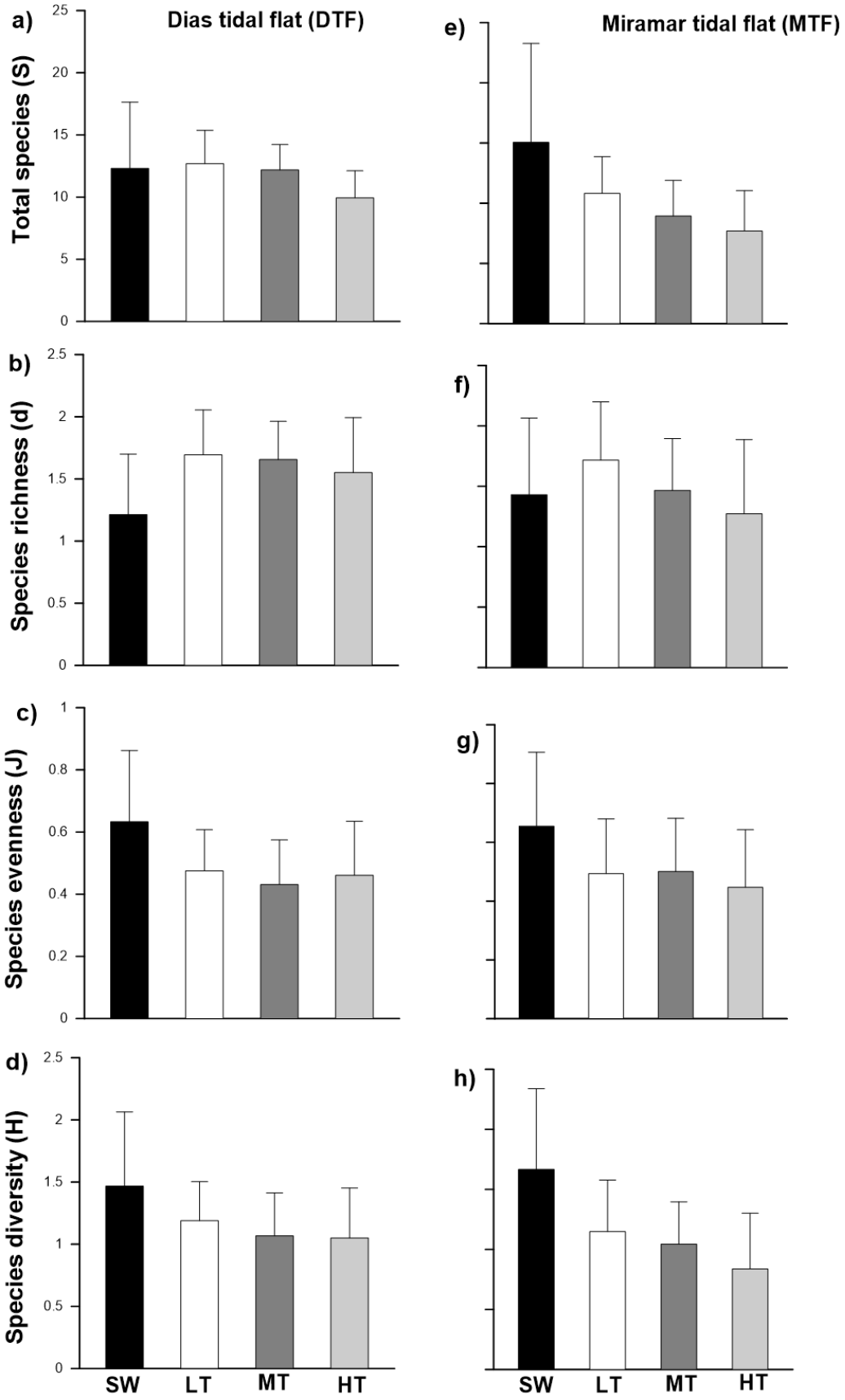


Figure 3.6. Plots showing diversity indices of surf water (SW), low-tide (LT), mid-tide (MT), and high-tide (HT) zones during the study period at Dias tidal flat (a-d) and Miramar tidal flat (e-h).

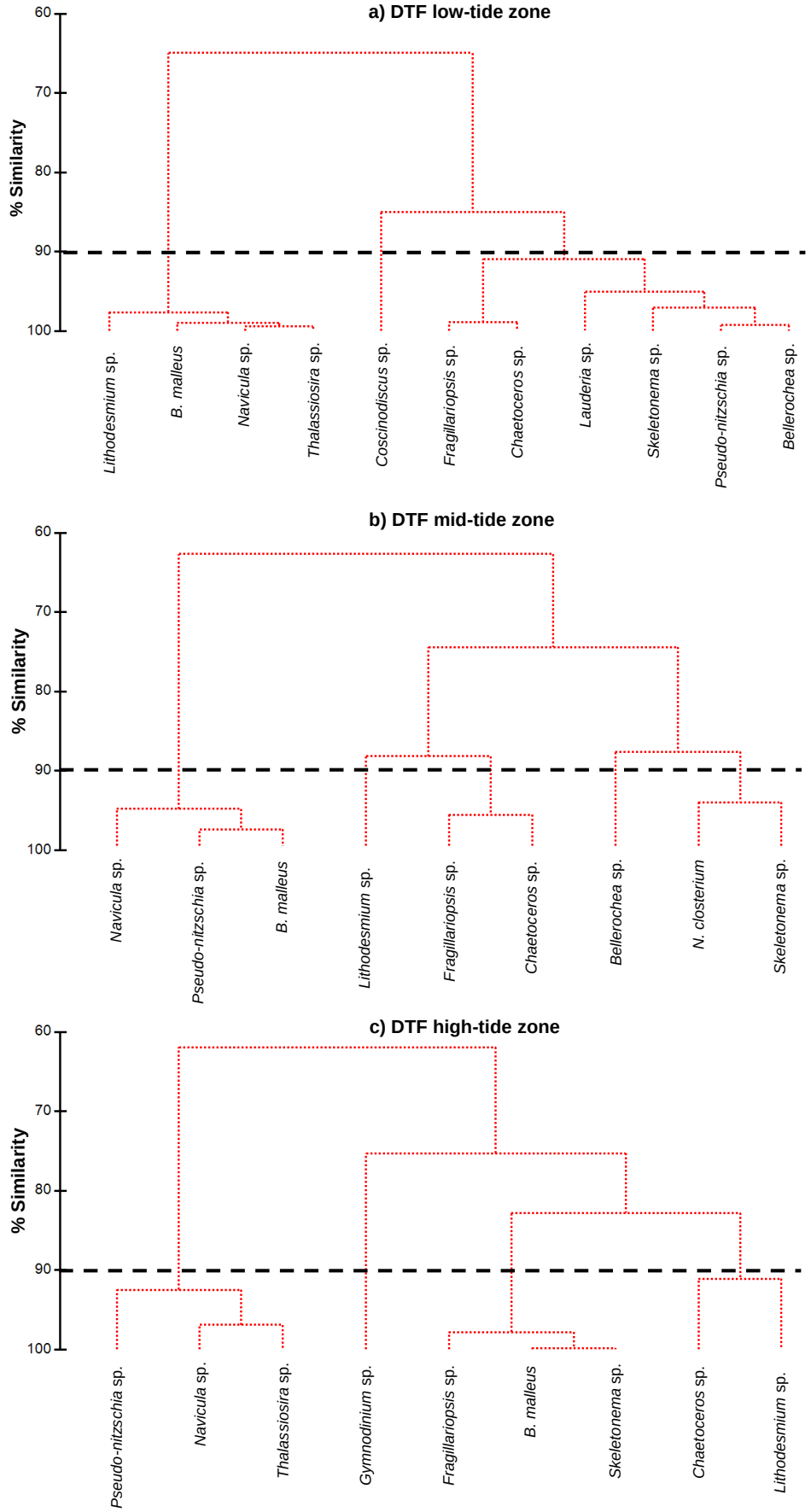


Figure 3.7. Plots showing cluster analysis of the dominant MPB species in a) low-tide, b) mid-tide, and c) high-tide zone of DTF.

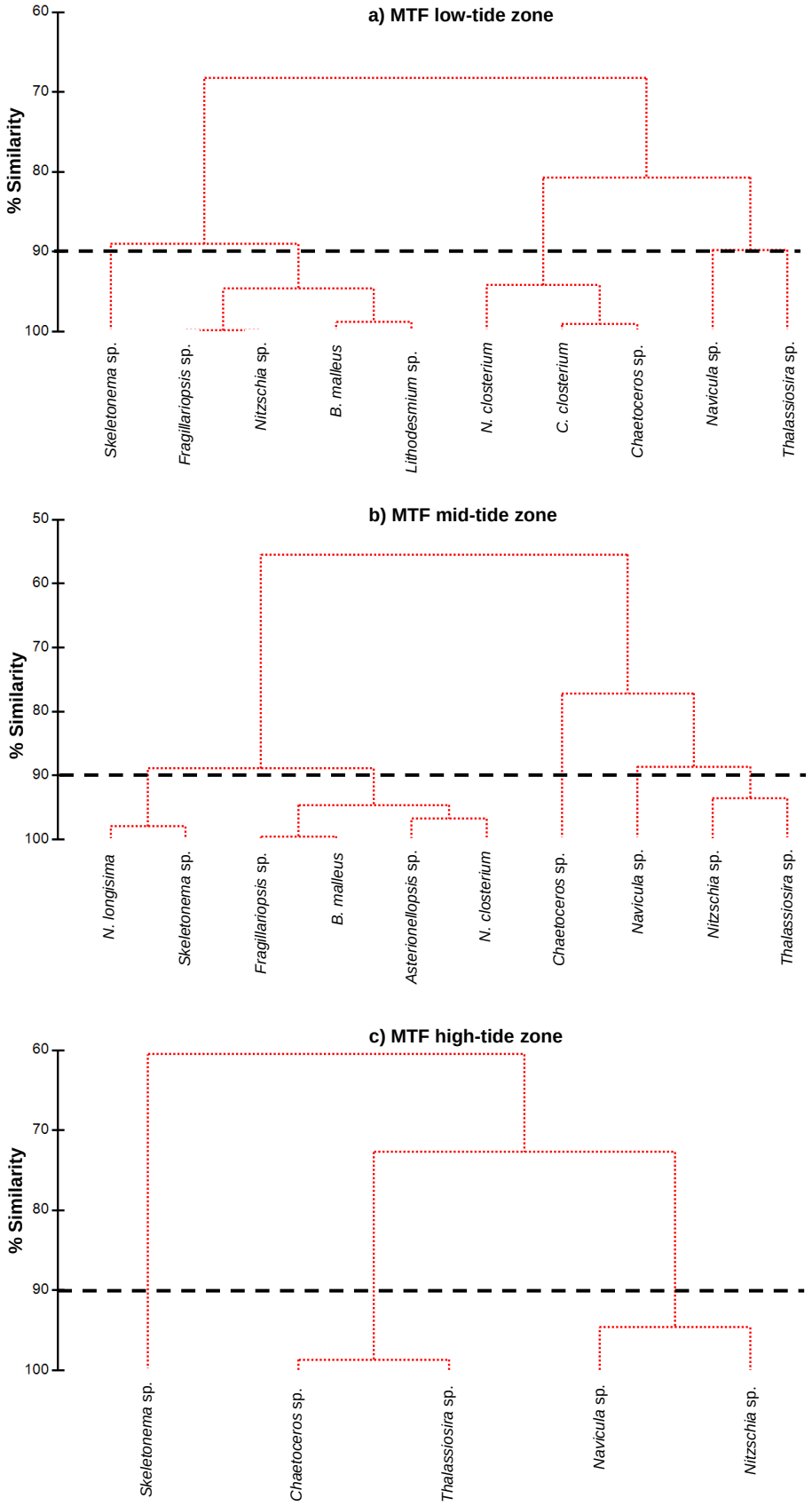


Figure 3.8. Plots showing cluster analysis of the dominant MPB species in a) low-tide, b) mid-tide, and c) high-tide zone of MTF.

Inter-seasonal variations of phytoplankton

Pre-monsoon

The pre-monsoon season of 2019 (April-May; ~1.5 x10^4 cells/L) recorded lower phytoplankton abundance than in 2023 (February-May; ~1.9 x10^4 cells/L) at DTF, whereas at MTF, the pre-monsoon season of 2019 (1.2 x10^4 cells/L) recorded higher phytoplankton abundance than in 2023 (~0.7 x10^4 cells/L); however, the differences were not significant. Centric diatoms dominated the community at DTF in 2019 and 2023 with similar dominant taxa. For instance, in 2019, *L. undulatum* and *Skeletonema* sp., whereas in 2023, *B. malleus* and *L. undulatum* were the dominant diatoms. Meanwhile, centric and pennate diatoms co-dominated in 2019, and dinoflagellate and pennate co-dominated in 2023 at MTF. In 2019, *Chaetoceros* sp. and *Navicula* sp., whereas in 2023, *Tripos furca* and *Navicula* spp. were the dominant phytoplankton. The species count (S), richness (d), evenness (J'), and diversity (H') were higher in the pre-monsoon season of 2023 than in 2019 at both tidal flats (Figures 3.9 and 3.10). Overall, the observed differences between 2019 and 2023 pre-monsoon were not significant.

Monsoon

The 2022 monsoon season (July-September) recorded the highest phytoplankton abundance (~6.0 x10^4 cells/L), followed by 2019 (July-August; ~2.5 x10^4 cells/L), and the least in 2023 (June-September; ~2.2 x10^4 cells/L) at DTF. Whereas, in MTF, the 2023 monsoon season recorded the highest phytoplankton abundance (~6.9 x10^4 cells/L), followed by 2022 (~6.5 x10^4 cells/L), and the least in 2019 (~1.0 x10^4 cells/L). Interestingly, the variation between the 2019, 2022, and 2023 monsoons was insignificant at DTF and MTF. Centric diatoms in 2022, pennate and centric in 2023, and pennate diatoms in 2019 co-dominated at DTF. Centric diatoms dominated the community during all monsoon seasons at MTF; however, the dominant species differed. Centric diatoms dominated the community in the 2022-23 monsoon in DTF, whereas in 2019, pennate was the dominant diatom. In 2019, *Nitzschia* spp. and *Navicula* spp.; in 2022, *Skeletonema* sp.; and in 2023, *Navicula* spp., *Thalassiosira* sp., and *Coscinodiscus* sp. were the most dominant diatoms. In MTF, centric diatoms dominated the community during all monsoon seasons (i.e., 2019, 2022, and 2023); however, the dominant species differed. For instance, *Chaetoceros* sp., *Navicula* spp., and *Leptocylindrus danicus* in 2019, *Skeletonema* sp., *Chaetoceros* sp., and *L. danicus* in 2022, and *Chaetoceros debilis*, *Chaetoceros curvisetus*, *Coscinodiscus* sp., and *Skeletonema* sp. in 2023 were the

dominant diatom species. There was no significant difference in the species count (S), whereas species richness (d) was higher in 2023, followed by 2022, and least in 2019 at both tidal flats. Evenness (J') was higher in both 2022-2023 and lower in 2019, and diversity (H') was higher in 2023, followed by 2019 and least in 2022 at DTF, whereas evenness (J') and diversity (H') were higher in 2019, followed by 2023 and 2022 at MTF (Figures 3.9 and 3.10). Overall, abundance and species count showed no significant differences, but species richness, evenness, and diversity were significantly ($p<0.05$) influenced by the monsoon season at both tidal flats.

Post-monsoon

The 2022 post-monsoon season (October-December; ~69.0 $x10^4$ cells/L) recorded the highest phytoplankton abundance than in 2023 (January and October; ~16.0 $x10^4$ cells/L) with insignificant differences at DTF. In contrast, the 2022 post-monsoon season (October-December; ~13.0 $x10^4$ cells/L) recorded the highest phytoplankton abundance than in 2023 (January and October; ~0.4 $x10^4$ cells/L) with significant differences at MTF. Pennate diatoms dominated the community in 2022 and centric diatoms in 2023 at both tidal flats. In DTF, pennate (*Pseudonitzschia* sp.) and centric (*L. undulatum* and *Cocconeis* sp.) diatoms dominated in 2022 and 2023, respectively. In MTF, pennate diatoms dominated the community in 2022 (*Pseudonitzschia* sp.), whereas centric diatoms in 2023 (*Chaetoceros decipiens*). The species count (S), abundance, and species richness (d) were higher in the post-monsoon season of 2022 than in 2023, except diversity (H') and evenness (J'), which was higher in 2023 than in 2022 at both the tidal flats (Figures 3.9 and 3.10). Overall, the 2022-2023 post-monsoon season influenced the abundance significantly at MTF ($p<0.05$) but not at DTF.

Inter-seasonal variations of MPB

Pre-monsoon

The DTF showed higher MPB abundance than the MTF during the pre-monsoon seasons. The MPB abundance was lower in 2019 (DTF: 71-97 cells/g of WS; MTF: 37-72 cells/g of WS) than in 2023 (DTF: 835-2588 cells/g of WS; MTF: 474-1114 cells/g of WS) at all tidal zones, with significant differences ($p<0.05$) between both tidal flats but differences were insignificant between the tidal zones. The MPB abundance from LT to HT gradually increased and decreased in 2019 and 2023, respectively, at DTF, whereas it increased from LT to MT and further decreased in HT in 2019 and decreased from LT

to HT in 2023 at MTF however, the differences were insignificant (Figure 3.9 and 3.10). At DTF, the C:P values at HT were <1 (pennate dominance) and >1 at LT to MT, respectively, during both 2019 and 2023. While at MTF, the C:P values were <1 at all the tidal zones in 2019 and 2023 (Figure 3.3 and 3.5). Centric diatoms dominated LT and MT (*L. undulatum* and *Thalassiosira* sp.), and pennate diatoms dominated HT (*Navicula* spp. and *Nitzschia* spp. in 2019; *Navicula* spp., *Pseudonitzschia* spp., and *Amphora* sp. in 2023) in both years at DTF. In contrast, the centric diatom in 2019 dominated at the LT and HT (*Chaetoceros* spp.) and the pennate diatom (*Navicula* spp.) at the MT zone, whereas in 2023, the pennate diatom in LT, MT (*Navicula* spp.), and HT zones (*Nitzschia* spp.) dominated at MTF. The species richness (d), evenness (J'), and diversity (H') were higher in the pre-monsoon season of 2019 than in 2023, with only evenness showing a significant difference ($p<0.05$). In contrast, species count (S) was significantly higher ($p<0.05$) in 2023 than in 2019 in all the tidal zones at both tidal flats (Figures 3.11 and 3.12).

Monsoon

The MTF showed higher MPB abundance than the DTF during all the monsoon seasons. The MPB abundance was significantly lower ($p<0.05$) in 2019 and significantly higher ($p<0.05$) in 2022 compared to the 2023 monsoon in all tidal zones at both tidal flats. In DTF, the LT zone recorded the highest MPB abundance in 2022 (625 cells/g of WS), followed by 2023 (619 cells/g of WS) and 2019 (76 cells/g of WS) with significant differences ($p<0.05$) between 2019-2022 and 2019-2023 but not between 2022-2023 (Figure 3.9). Whereas the MT and HT zones recorded the highest MPB abundance in 2023 (289-978 cells/g of WS), followed by 2022 (185-362 cells/g of WS) and 2019 (86-94 cells/g of WS). Interestingly, abundance showed significant differences ($p<0.05$) between 2019-2022 and 2019-2023 only for MT, but the differences were insignificant for HT. In MTF, the LT and MT zones recorded the highest MPB abundance in 2023 (353-456 cells/g of WS) followed by 2022 (168-1614 cells/g of WS) and 2019 (78-135 cells/g of WS), whereas the HT zone showed higher abundance in 2022 (1614 cells/g of WS) followed by 2023 (1080 cells/g of WS) and 2019 (479 cells/g of WS). Interestingly, the differences were significant ($p<0.05$) between 2019-2022 and 2019-2023 but not between 2022-2023 for all the tidal zones (Figure 3.10). The MPB abundance gradually increased from LT to MT and decreased in HT in 2019 and 2023, whereas it gradually decreased from LT to HT in 2022 with insignificant differences at DTF. While in MTF,

an opposite trend was observed. At DTF, the C:P values were <1 (pennate dominance) in 2019 and 2022 but >1 (centric dominance) in 2023 at all the tidal zones. At MTF, the C:P values were <1 (pennate dominance) in 2019 and 2022 at all the tidal zones but >1 (centric dominance) in 2023 except HT (Figure 3.3 and 3.5). Pennate diatoms dominated the community in 2019 and 2022 (*Navicula* spp., *Nitzschia* spp., *Fragillariopsis* sp., and *Amphora* sp.), and centric diatoms in 2023 (*Thalassiosira* sp.) were present in all the tidal zones at DTF. In comparison, pennate diatoms (*Navicula* spp. and *Nitzschia* spp.) dominated the community in 2019, 2022, and 2023 in all the tidal zones except LT and MT in 2023, where centric diatom (*Thalassiosire* sp.) dominated at MTF. At DTF, the species count (S), evenness (J'), and diversity (H') were higher in 2023, followed by 2022 and 2019, and the differences were significant ($p<0.05$) at all the tidal zones. Whereas species richness (d) was higher in 2023, followed by 2022 and 2019 at all tidal zones, but the differences were insignificant (Figure 3.11). At MTF, species count (S), species richness (d), evenness (J'), and diversity (H') were higher in 2023, followed by 2022 and 2019. However, the differences were significant ($p<0.001$) only for the 2019 monsoon season for species count (S) and diversity (H'), significant ($p<0.001$) among all the seasons for species richness (d), and insignificant for evenness (J') (Figure 3.12).

Post-monsoon

The MPB abundance was higher in DTF than in MTF during post-monsoon seasons. The 2022 (1518-2637 cells/g of WS) post-monsoon season recorded the highest MPB abundance in the LT and MT than in 2023 (1062-1166 cells/g of WS), whereas in HT, the abundance was marginally higher in 2023 (881 cells/g of WS) than 2022 (876 cells/g of WS) with insignificant differences at DTF. Whereas the 2023 (592-914 cells/g of WS) post-monsoon season recorded the highest MPB abundance in all the tidal zones compared to 2022 (50-433 cells/g of WS), the differences were insignificant except in the HT zone at MTF. The MPB abundance gradually decreased from LT to HT in both years at DTF (Figure 3.9). At MTF, abundance gradually increased from LT to MT and decreased in HT in 2022, and was the opposite in 2023 with insignificant differences. At DTF, the C:P values were ≥1 (centric dominance) in LT for both the years, >1 for MT 2022, and <1 (pennate dominance) for MT 2023, and HT 2022. At MTF, the C:P values were >1 (centric dominance) and <1 (pennate dominance) in 2022 and 2023, respectively, for LT and HT, and <1 (pennate dominance) in MT for both years (Figure 3.3 and 3.5). In LT, centric diatoms (*B. malleus* and *L. undulatum*) dominated in both years; in MT,

centric dominated in 2022 (*B. malleus* and *Thalassiosira* sp.) and pennate in 2023 (*Navicula* spp.) and in HT, pennate diatoms dominated in both years (*Navicula* spp. and *Pseudonitzschia* sp.) at DTF, whereas Pennate diatoms (*Navicula* spp.) dominated in both years in all the tidal zones except LT in 2022, where centric dominated (*Chaetoceros* sp.) at MTF. At DTF, the species count (S), species richness (d), evenness (J'), and diversity (H') were higher in the post-monsoon season of 2022 than in 2023 for MT and HT, whereas LT showed an opposite trend with insignificant differences (Figures 3.11). At MTF, the species count (S), species richness (d), evenness (J'), and diversity (H') were higher in the post-monsoon season of 2022 than in 2023 for all the tidal zones with insignificant differences (Figure 3.12).

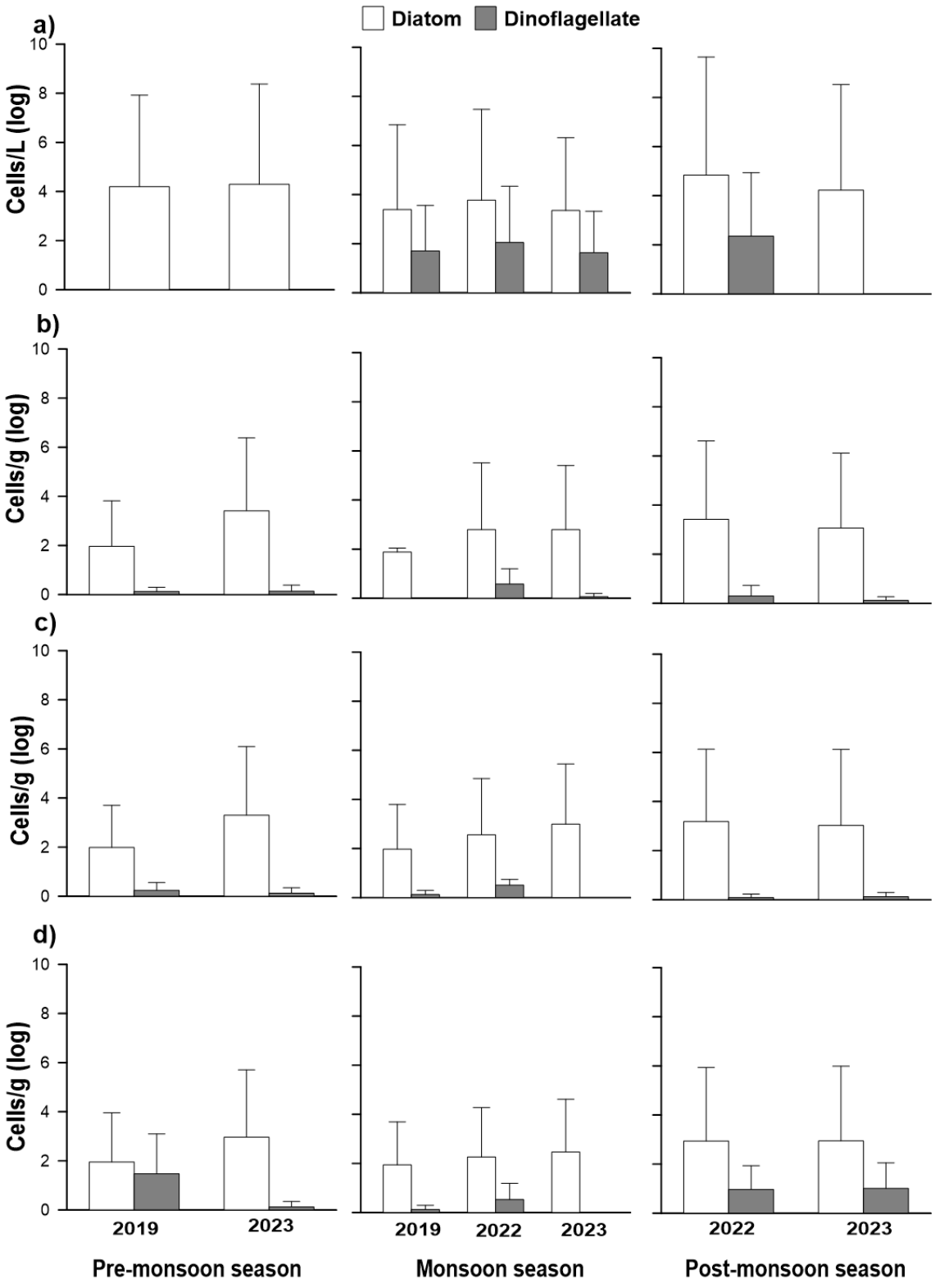


Figure 3.9. Plots showing seasonal variability of phytoplankton in a) surf water and in microphytobenthos in b) low-tide, c) mid-tide, and d) high-tide zones during pre-monsoon, monsoon, and post-monsoon season at DTF. Data presented here is the months' average in the respective seasons and years.

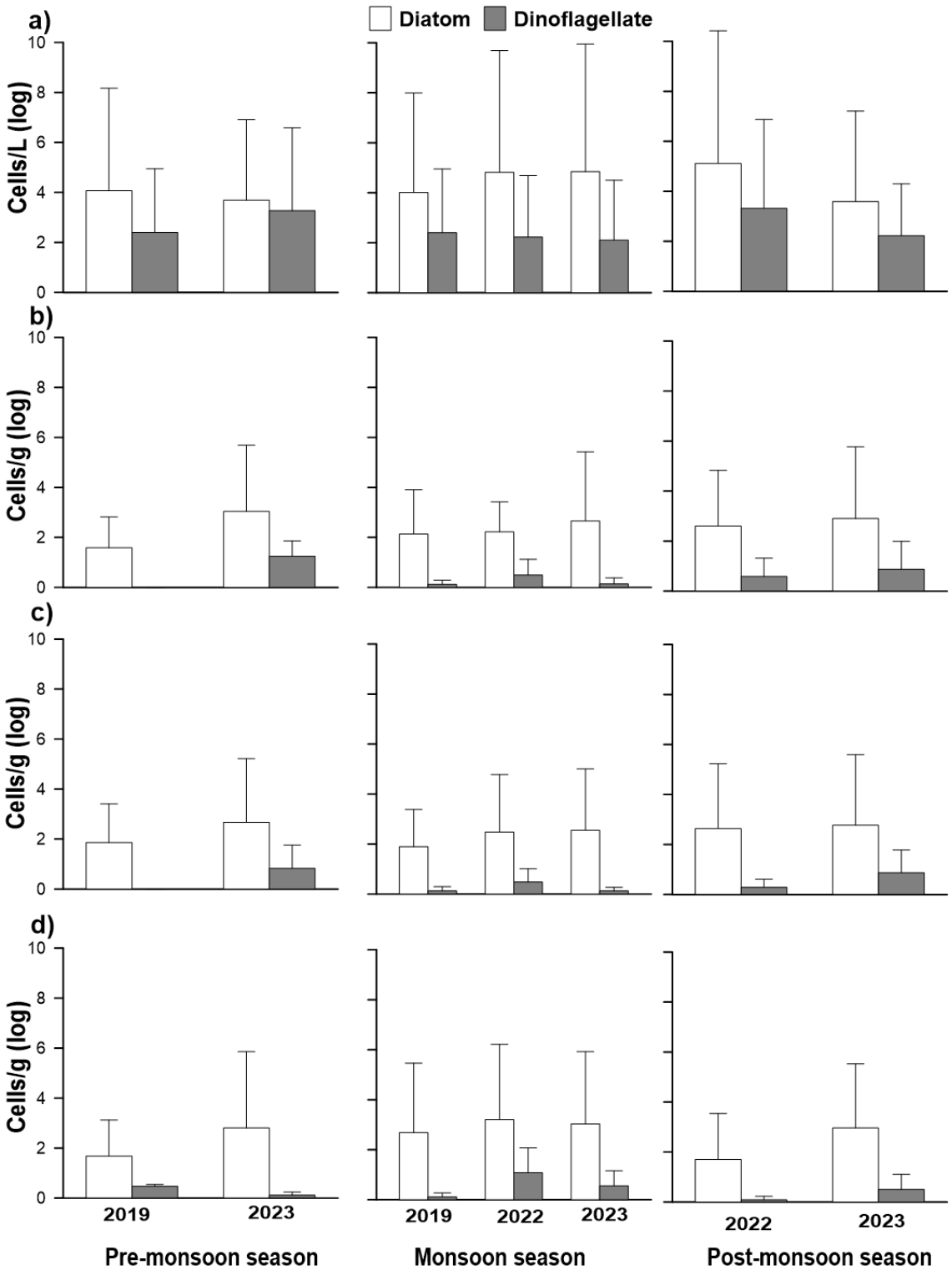


Figure 3.10. Plots showing seasonal variability of phytoplankton in a) surf water and in microphytobenthos in b) low-tide, c) mid-tide, and d) high-tide zones during pre-monsoon, monsoon, and post-monsoon season at MTF. Data presented here is the months' average in the respective seasons and years.

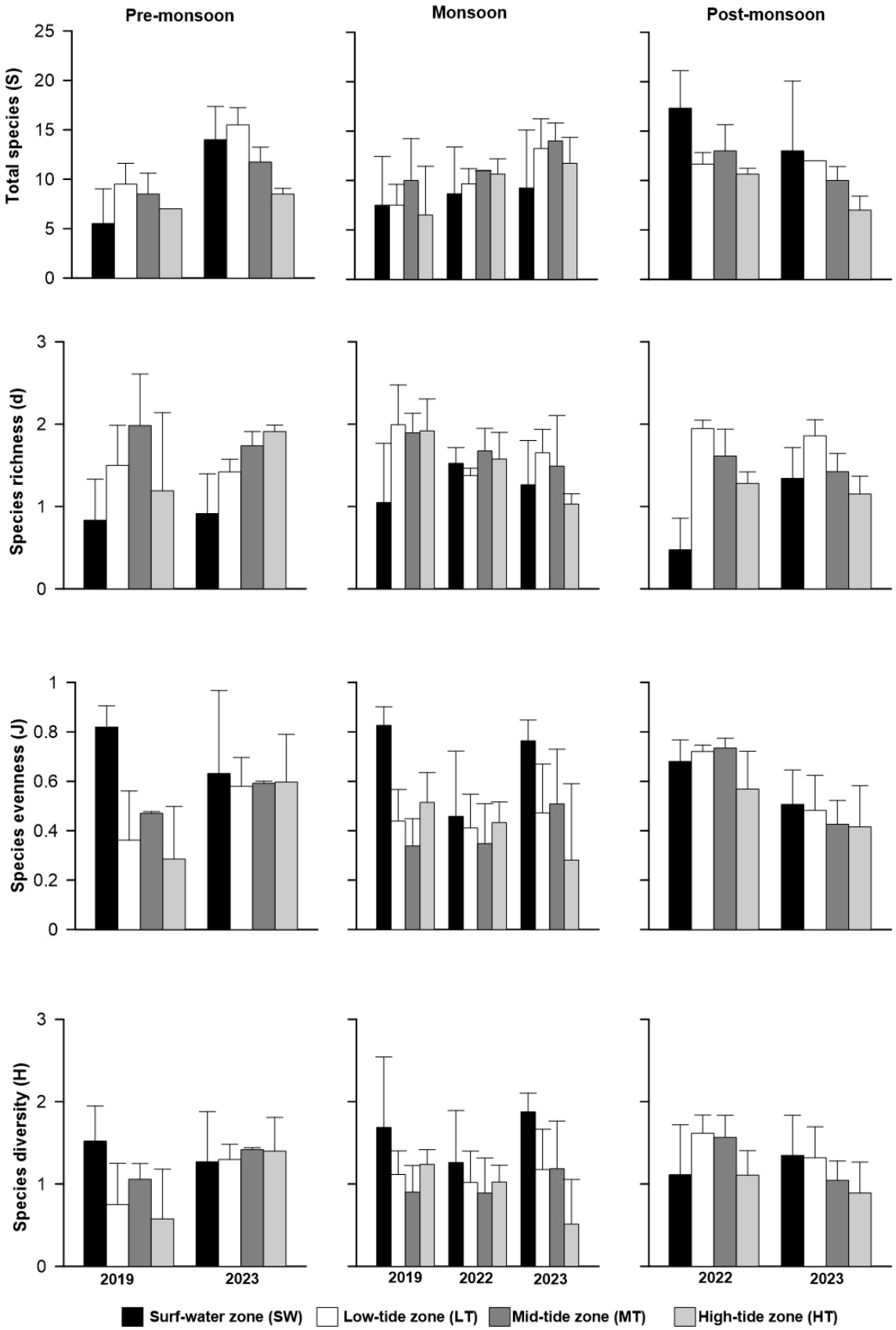


Figure 3.11. Plots showing seasonal diversity indices of surf water, low-tide, mid-tide, and high-tide zones in pre-monsoon, monsoon, and post-monsoon seasons at Dias tidal flat.

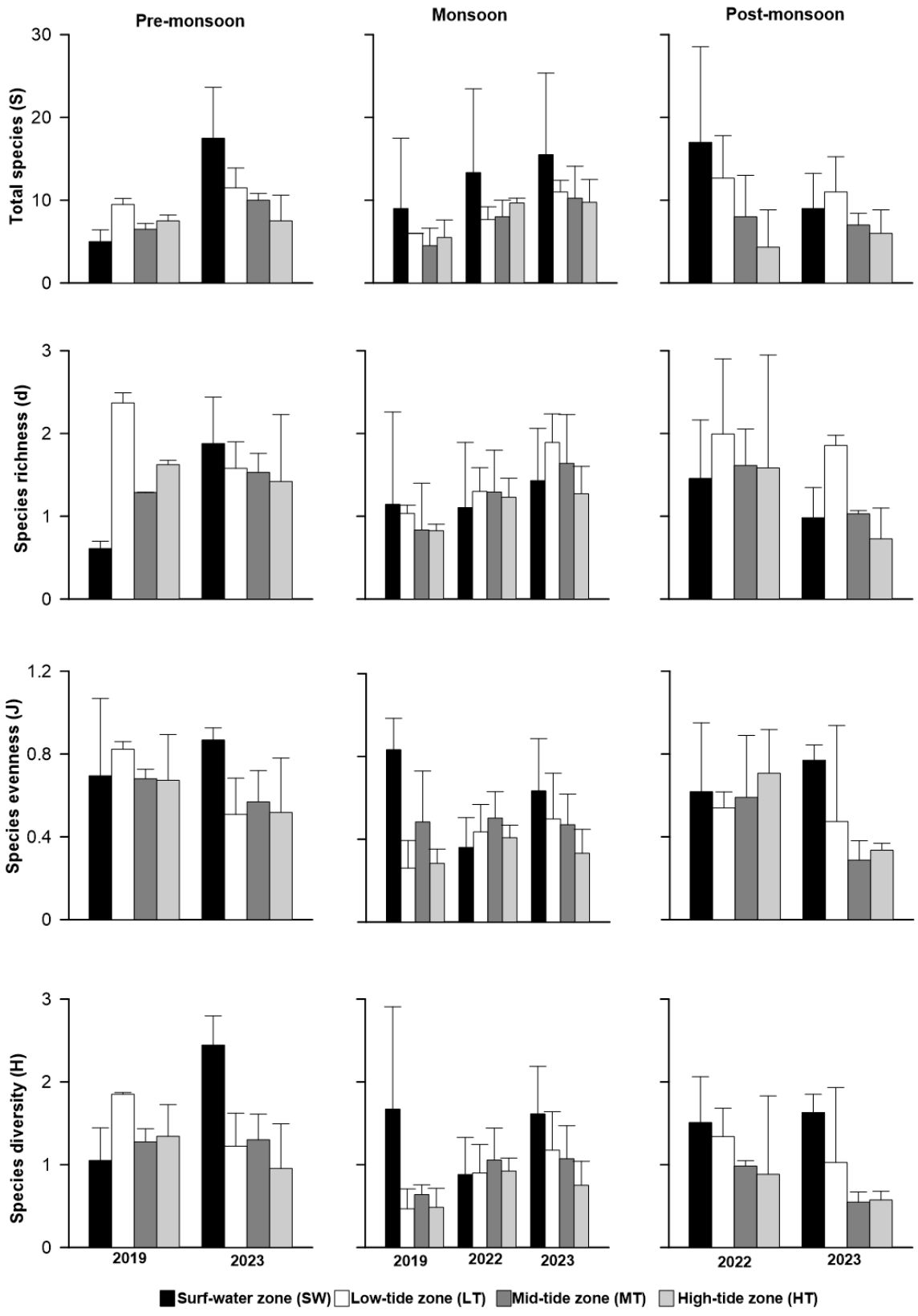


Figure 3.12. Plots showing seasonal diversity indices of surf water, low-tide, mid-tide, and high-tide zones in pre-monsoon, monsoon, and post-monsoon seasons at Miramar tidal flat.

3.1.3.3. Influence of surf water on MPB assemblage

At DTF, 25 species (34%) were common between SW and the tidal flat, whereas 26 MPB species (58%) were common across the tidal flat (i.e., among LT, MT, and HT). Only 6 (13%) (*Gamphonema* sp., *Nitzschia* sp., *Campylodiscus* sp., *Chaetoceros curvisetus*, *Streptotheca* sp. and *Scrippseilla* sp.), 3 (0.07%) (*Cyclotella* sp., *Rhizosolenia* sp. and *Ankistrodinium* sp.), and 3 (0.07%) (*Thalassiothrix* sp., *Dinophysis* sp. and *Gyrodinium* sp.) MPB species were specific to LT, MT, and HT, respectively. The regression analysis showed a significant ($p<0.001$) positive correlation between SW phytoplankton and LT, MT, and HT MPB communities. Interestingly, the SW-centric diatoms showed no correlation, but SW pennate diatoms showed a significant ($p<0.001$) positive correlation with LT, MT, and HT pennate diatoms in the tidal flat (Figure 3.13). Therefore, the SW phytoplankton community contributed significantly to the MPB, especially the pennate assemblages.

At MTF, 32 species (32%) were common between the SW and tidal flat, whereas 24 MPB species (52%) were common across the tidal zones. Only 10 (21%) (*Pleurosigma* sp., *Asteromphalus* sp., *Ditylum* sp., *Guinardia* sp., *Melosira moniliformis*, *Odontella* sp., *Oestrupia* sp., *Streptotheca* sp., *Amphidinium* sp., and *Dinophysis* sp.), 1 (0.02%) (*Chaetoceros didymus*), and 2 (0.04%) (*Cyclotella* sp., *Planktoniella sol* and *Pyrophacus* sp.) MPB species were specific to LT, MT, and HT, respectively. The regression analysis showed no correlation between SW phytoplankton and MPB communities at the tidal flat. Therefore, the SW phytoplankton community showed no significant contribution to the MPB assemblages (Figure 3.13). Only 24 (32%) and 33 (34%) phytoplankton species were found in the MPB community at DTF and MTF, respectively. A total of 45 (49%) phytoplankton species, 29 (50%), 23 (40%), and 20 (33%) MPB species were common in SW, LT, MT, and HT of DTF and MTF, respectively. Only 17 MPB species (30%) were common between both the tidal flats, whereas 9 (16%) (*Achnanthes* sp., *Gamphonema* sp., *Licmophora* sp., *Licmophora abbrebeata, Campylodiscus* sp., *Odontella obtuse, Rhizosolenia* sp., *Gyrodinium* sp., and *Prorocentrum* sp.) and 12 (21%) (*Asterionellopsis* sp., *Biddulphia* sp., *Nitzschia longisima, Striatella* sp., *Chaetoceros didymus, Ditylum* sp., *Guinardia* sp., *Lauderia annulate, Oestrupia* sp., *Planktoniella sol*, *Amphidinium mootonorum,* and *Pyrophacus* sp.) were specific to DTF and MTF, respectively (Table 3.1).

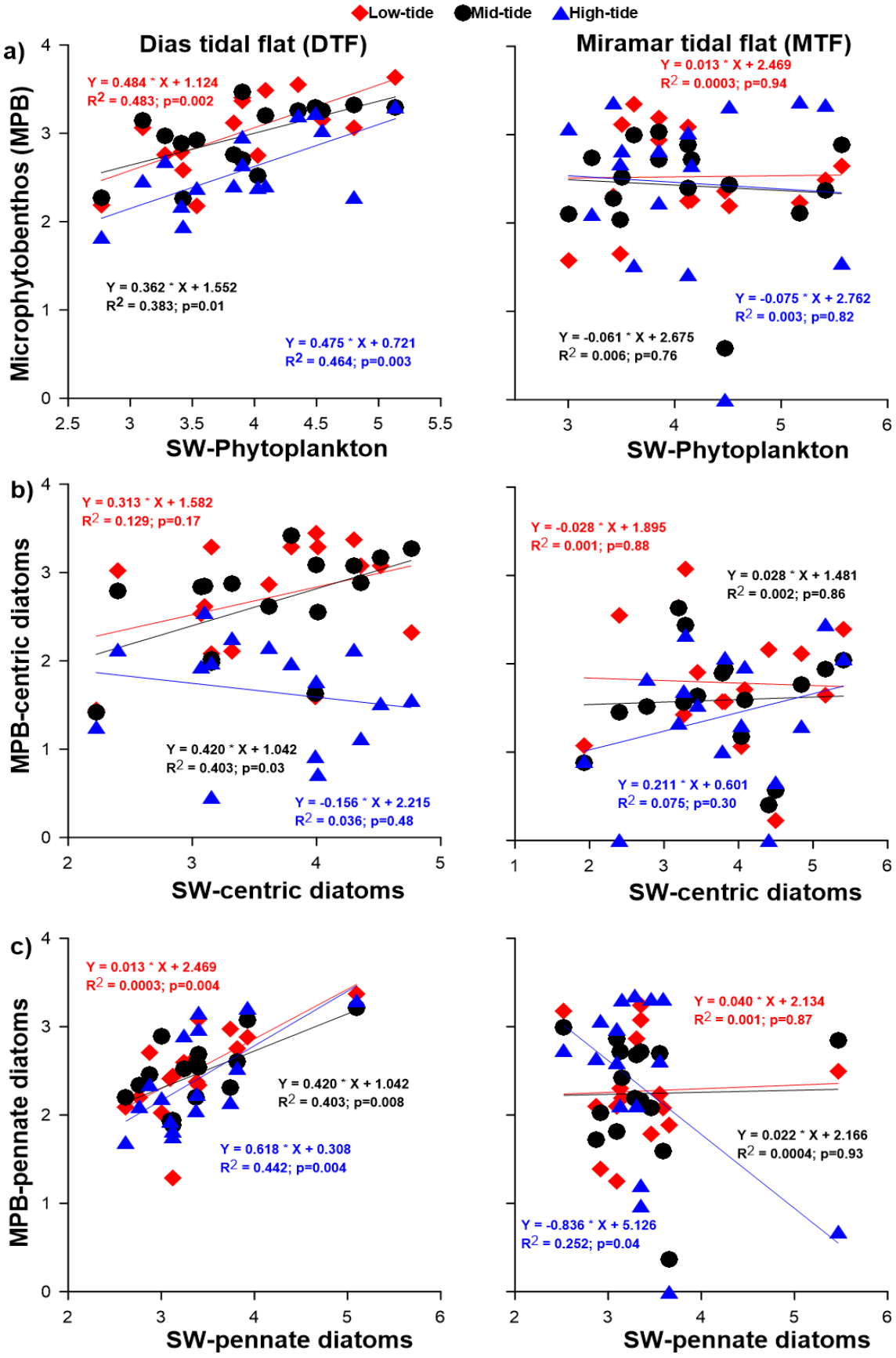


Figure 3.13. Regression plot showing correlation between a) microphytobenthos and SW-phytoplankton, b) MPB-centric and SW-centric diatoms, and c) MPB-pennate and SW-pennate diatoms of Dias and Miramar tidal flat.

Table 3.1. Table showing phytoplankton and microphytobenthos taxa recorded in surf water (SW), low-tide (LT), mid-tide (MT), and high-tide (HT) zones during the study period and also indicates percentage contribution at both DTF and MTF.

		Dias tidal flat (DTF)				Miramar tidal flat (MTF)			
	Pennate diatoms	**SW**	**LT**	**MT**	**HT**	**SW**	**LT**	**MT**	**HT**
1	*Achnanthes* sp.	0.05	0.06	0.12	-	0.02	-	-	-
2	*Amphiprora* sp.	0.55		0.06	0.16			0.07	0.01
3	*Amphora* sp.		1.10	1.46	8.87	0.34	0.93	0.99	2.10
4	*Bacillaria* sp.	0.29							
5	*Biddulphia* sp.						0.08	0.10	0.02
6	*Cylindrotheca closterium*		0.06	0.07	0.08	0.01	6.21	0.24	0.02
7	*Diploneis* sp.	0.07				0.02			
8	*Fragillariopsis* sp.	0.60	1.79	2.65	1.67	0.00	1.58	0.92	0.15
9	*Gamphonema* sp.		0.02						
10	*Grammatophora* sp.	0.19							
11	*Gyrodinium* sp.	0.38				0.02			
12	*Licmophora* sp.	0.22	0.02	0.04	0.16				
13	*L. abbrebeata*			0.06	0.16				
14	*Lioloma* sp.					0.02			
15	*Membraneis* sp.	0.24				0.29			
16	*Navicula* sp.	4.48	25.63	38.76	16.48	1.07	54.62	51.55	58.43
17	*Nitzschia* sp.	0.86	0.03			0.60	1.57	22.65	31.06
18	*N. longisima*	0.19					0.19	0.65	0.03
19	*N. closterium*		0.09	0.56	0.19	0.01	4.24	1.24	0.03
20	*Pleurosigma* sp.	1.17	0.01	0.03		0.51	0.01		
21	*P. normanii*	0.05				0.03			
22	*Pseudo-nitzschia* sp.	34.79	1.09	19.66	35.16	31.50	0.11	0.04	0.02
23	*Striatella* sp.						0.11	0.01	
24	*Surirella* sp.	0.12				0.05			
25	*Tabellaria* sp.	1.29	0.12	0.26	0.09	0.13	0.01	0.05	0.02
26	*Thalassionema* sp.	0.38	0.04	0.06		0.20	0.09	0.01	0.01
27	*T. nitzschoides*		0.07	0.02	0.13		0.01	0.03	0.01
28	*Thalassiothrix* sp.	1.32			0.16	0.74		0.02	0.01
29	*Trachyneis* sp.	0.02				0.01			
	Centric diatoms								
30	*Asterionellopsis* sp.						0.07	1.08	0.13
31	*A. glacialis*	0.58				0.06			
32	*Asterionella japonica*		0.01	0.06	0.05		0.01	0.09	0.03
33	*Asteromphalus* sp.		0.02	0.03	0.37	0.01	0.01		
34	*Bacteriastrum* sp.					0.11			
35	*Bellerochea* sp.		1.13	1.09	0.21	0.10			
36	*B. malleus*	26.08	22.08	25.54	1.84	0.55	1.17	0.94	
37	*Campylodiscus* sp.		0.03						
38	*Cerataulina bergonii*					2.15			

39	*C. bicornis*					0.21			
40	*C. pelagica*					0.03			
41	*Chaetoceros* sp.	1.68	1.67	2.03	3.20	4.31	6.64	4.10	3.42
42	*C. affinis*	0.10				0.14			
43	*C. curvisetus*	1.37	0.03			11.76	0.01	0.08	0.08
44	*C. danicus*					0.03			
45	*C. debilis*					9.65			
46	*C. decipiens*					4.95			
47	*C. didymus*					0.38		0.01	
48	*C. peruvianus*					0.02		0.00	
49	*C. socialis*					0.16		0.00	
50	*Cocconeis* sp.	2.97				0.02			
51	*Coscinodiscus* sp.	0.58	0.51	0.21	0.22	0.88	0.44	0.14	0.02
52	*Cyclotella* sp.			0.06		0.03			
53	*Dactyliosolen fragillismus*					0.35			
54	*Ditylum* sp.	0.12				0.04	0.02		
55	*D. brightwelli*	0.14				0.01			
56	*Guinardia* sp.	0.02				0.11	0.01		
57	*G. striata*	0.12				0.28			
58	*Hemiaulus* sp.	0.19				0.02			
59	*H. sinensis*					0.06			
60	*Hemidiscus cuneiformis*	0.00				0.02			
61	*Lauderia* sp.		0.79	0.04	0.13				
62	*L. annulata*	0.38				0.19	0.04		0.01
63	*Leptocylindrus danicus*	0.34	0.01	0.06	0.37	0.98	0.01	0.05	0.19
64	*L. minimus*					0.04			
65	*Lithodesmium* sp.	2.59	18.22	5.07	5.14	0.02	1.24	0.50	0.03
66	*L. undulatum*	6.21				0.01			
67	*Melosira moniliformis*	0.22	0.13	0.33	0.48	0.04	0.01		
68	*Odontella* sp.	0.07	0.03	0.04	0.06	0.01	0.01		
69	*O. aurita*	0.12				0.11			
70	*O. obtusa*		0.05	0.10	0.05				
71	*O. mobiliensis*	0.19				0.35			
72	*O. sinensis*	0.12				0.95			
73	*Oestrupia* sp.						0.09		
74	*Paralia sulcata*	0.24				0.18			
75	*Planktoniella sol*	0.34				0.58			0.02
76	*Proboscia alata*					0.02			
77	*Rhizosolenia* sp.	0.36		0.06		0.22			
78	*R. imbricata*					0.01			
79	*R. setigera*					0.02			
80	*Skeletonema* sp.	5.66	0.94	0.71	1.82	22.07	0.83	0.70	0.67
81	*Streptotheca* sp.		0.05			0.01	0.02		
82	*Striatella* sp.	0.36							

83	*S. unipunctata*					0.01			
84	*Thalassiosira* sp.	1.25	24.03	0.45	21.04	0.52	18.62	13.05	3.13
85	*Triceratium* sp.					0.01			
	Dinoflagellates								
86	*Akashiwo sanguinea*					0.01			
87	*Amphidinium* sp.		0.03	0.04	0.33	0.15	0.02	0.00	0.13
88	*A. mootonorum*						0.40	0.06	
89	*Ankistrodinium* sp.			0.06			0.02	0.16	
90	*Dinophysis* sp.				0.16	0.03	0.01		
91	*D. acuminata*					0.11			
92	*D. caudata*					0.05			
93	*Gonyaulax* sp.					0.02			
94	*Gymnodinium* sp.		0.01	0.06	0.89	0.02	0.06	0.06	0.09
95	*Gyrodinium* sp.				0.08				
96	*Peridinium* sp.		0.06	0.12		0.08	0.32	0.10	0.02
97	*P. quinquecorne*					0.09			
98	*Prorocentrum* sp.	0.02			0.11				
99	*P. gracile*	0.02				0.05			
100	*P. micans*					0.02			
101	*P. lima*					0.01			
102	*Protoperidinium* sp.	0.05	0.04	0.02	0.14	0.16	0.07	0.13	0.11
103	*Pyrocystis* sp.	0.19				0.08			
104	*Pyrophacus* sp.					0.01			
105	*Scrippseilla* sp.		0.03				0.11	0.17	
106	*Tripos furca*	0.02				0.73			
107	*T. fusus*	0.02				0.03			

3.1.4. Discussion

The MPB plays key ecological roles in supporting the upper levels of trophic food webs (Kang et al., 2015), sequestering large amounts of carbon (Mao et al., 2020; Moritsch et al., 2021), and acting as nature-based solutions to climate change (James et al., 2024). Therefore, recently, the studies related to MPB have gained momentum. However, the enumeration of MPB from sediment samples is challenging, unlike the enumeration of phytoplankton from the water column, where direct methods can be used. Direct examination of the sediment samples is difficult as often algal species are embedded in aggregates or obscured by detritus and sediment particles (Kranck & Milligan, 1988). Therefore, various indirect techniques, such as the most probable number (MPN) technique, the sieving method, or chlorophyll-*a* estimation, are used to enumerate or estimate sediment microalgae. The MPN technique was initially used to enumerate bacterial samples (Colwell, 1979). Further, the MPN technique was modified and used for enumerating sediment microalgae (An et al., 1992; Larrazabal et al., 1990; Erard-Le Denn et al., 1993), including diatom resting stages in the sediments (Imai et al., 1984, 1990; An et al., 1992; Larrazabal et al., 1990). However, studies have shown that even though the MPN method gives only relative abundance, it is the most effective and feasible technique for MPB quantification, identification, and viability check (Harris et al., 1998; McQuoid, 2002; Mitbavkar & Anil, 2006) and was adopted in this study.

The MPB has been extensively studied from the Asian continent, and most of the studies are conducted in South Korea, Japan, and China (Park et al., 2014). Despite India having a vast coastline (~5423 km), which consists of around 43% sandy beaches and 46% mud flats and marshy coastline (Kumar et al., 2006), studies on MPB are limited (Mitbavkar & Anil, 2002, 2004, 2006; Sanilkumar et al., 2009; Balasubramaniam et al., 2017; Jeslin et al., 2021). Among the Indian studies, the MPB enumeration methods varied significantly, with only a few using the MPN method (Mitbavkar & Anil, 2002, 2004, & 2006) while others used Chlorophyll-*a* biomass (Sanilkumar et al., 2009; Balasubramaniam et al., 2017) and the sieving method (Jeslin et al., 2021) for the quantification of MPB. Since the present study aimed to study the MPB dynamics and compare the findings with previous studies (which also used the MPN method), a slightly modified MPN method for the MPB enumeration (McQuoid, 2002) was selected. Interestingly, MPB species and abundance were comparable with previous MPN-based studies (Mitbavkar & Anil, 2002, 2004 & 2006), proving the reliability and effectiveness of this method. The MPN method was adopted to understand the MPB dynamics at

contrasting sandy tidal flats, and the findings of different temporal scales are discussed with a schematic (Figures 3.14 and 3.15) in the subsequent sections.

3.1.4.1. Inter-annual variations

The abundance of MPB and phytoplankton in overlying SW showed significant inter-annual variations, with diatoms as the dominant groups. The MPB abundance was highest in LT, followed by MT and HT at DTF, whereas an opposite trend was observed at MTF. This tidal zone variation in MPB abundance could be attributed to the distinct tidal flat structure. At DTF, the entire tidal zone (i.e., LT-HT) is well submerged by the diurnal tidal fluctuations, and a sea wall restricts the HT zone. At MTF, the SW reaches the HT zone only during the spring tide period, leaving the HT zone undisturbed. Hence, it can be assumed that tidal influence on microalgae in HT is more significant at DTF than at MTF. A similar abundance pattern was also reported in other studies (Jesus et al., 2009; Cartaxana et al., 2006), where higher biomass was found in the sandy upper shore sites. However, MPB abundance is strongly affected by local conditions, and generalization between sites is difficult (e.g., Defew et al., 2002; Van der Grinten et al., 2004). Additionally, the SW phytoplankton influences the MPB community, which was evident in this study. Generally, centric and pennate diatoms dominate the SW and MPB communities, respectively, and were also observed at both DTF and MTF. Similar diatom dominance to biomass, diversity, and production is also reported in various studies (e.g., Oh & Koh, 1995; MacIntyre et al., 1996; Underwood & Kromkamp, 1999; Agatz et al., 1999; Du et al., 2009; Mitbavkar & Anil, 2002; Azovsky et al., 2020). Further, the bloom events in SW greatly influence MPB (particularly at LT and MT) through deposition and vice versa through resuspension in SW. For instance, during the study period, bloom events of pennate diatom *Pseudonitzschia* spp. (in both DTF and MTF), and centric diatom *B. malleus* (in DTF) was reflected in the tidal flats as evidenced by the high centric: pennate (C:P) ratio and taxonomic composition (Figure 3.5). Assuming centric (C) and pennate (P) diatoms represent planktonic and benthic forms, respectively. C:P values can be a potential indicator for understanding the diatom exchange between MPB and SW community, particularly during bloom periods. Further, the regression analysis between the SW and tidal flat diatom community revealed interdependency between them (Figure 3.13). For instance, interdependency was observed only for pennate diatoms but not with centric diatoms at all tidal zones in DTF. This is because a significant tidal influence is observed for the entire flat up to the HT zone. Meanwhile, at MTF, interdependency was observed only for pennate diatom between the SW and HT zones

but not in the LT and MT zones due to more tidal disturbances in the latter than the former. These findings suggest that the interdependency of the diatom community between MPB and SW community is tidal flat specific and dependent on the topography of the tidal flat.

Moreover, in the present study, around 24 (32%) and 33 (35 %) phytoplankton species were common between SW and tidal flats of all the tidal zones at DTF and MTF, respectively. Further, at DTF, 25 (47%), 4 (0.1%), 2 (0.05%), and 2 (0.06%) species were specific to SW, LT, MT, and HT, whereas at MTF, 50 (59%) and 1 (0.025%) species were specific to SW and LT. MacIntyre et al. (1996) have noticed that many phytoplankton in the SW are also permanent components of the MPB community. Previous studies have reported the benthic-pelagic coupling where phytoplankton cells from the adjacent waters are observed in the sediment and vice versa (de Jonge & van Beusekom, 1992; Mitbavkar & Anil, 2002). This exchange can be caused by the wave and tidal actions responsible for the sediment's deposition and resuspension (Delgado et al., 1991; de Jonge & van Beusekom, 1992, 1995; de Jonge, 1992). The vigorous mixing caused by these processes can resuspend and redistribute the diatom-attached sediment particles and free-living diatom cells on or within the sediment. It might cause an exchange of diatom cells between SW and the sediment layer. Since the MTF has a gentle slope, the waves first brake over the sand bars, reform, and brake again before reaching the tidal flat, reducing the wave action (Loveson et al., 2014). Therefore, vigorous mixing, which usually resuspends and redistributes the diatom-attached sediment particles and free-living diatom cells between surf water and the sediment layer, is inefficient at MTF. However, the wave actions are comparatively vigorous during the monsoon seasons, drastically changing the beach topography (Loveson et al., 2014).

Additionally, MPB recorded is mainly represented by epipsammic (smaller and attached to sand grains) and epipelic (larger and motile forms within sediments) forms. However, their distribution with tidal zones differed between tidal flats. The abundance of epipsammic and epipelic forms gradually decreased and increased from LT to HT, respectively, at DTF. In contrast, at MTF, it marginally decreased from LT to MT and increased significantly from MT to HT, respectively. Further, epipsammic and epipelic can be potential indicators for sediment texture as their abundance ratios are associated with sediment texture. Previous studies have suggested that the epipelic forms are more abundant in finer sediment, whereas epipsammic forms are in coarser sediment (Oh & Koh, 1995; Mitbavkar & Anil, 2002; Stal, 2003; Skinner et al., 2006; Facca & Sfriso, 2007; Du et al., 2009). In DTF, the sediment texture gradually changed from a mixed type

(i.e., sandy-silt) to a primarily sandy type from LT to HT. In contrast, at MTF, it remained sandy throughout the study period. However, numerous epipelic and epipsammic species occur across a range of sediment types (Azovsky et al., 2020) and are well documented in various literature (MacIntyre et al., 1996; Paterson & Hagerthey, 2001; Méléder et al., 2007; Jesus et al., 2009; Ribeiro et al., 2013; Cibic et al., 2019). Moreover, smaller epipsammic diatoms are less prone to damage by collisions with sand grains than the larger motile forms (epipelic). Such adaptation might give epipsammon an advantage to flourish in unstable sandy sediments (Delgado et al., 1991; Cibic et al., 2019). Further, light penetration is deeper in sandy sediment than muddy, allowing photosynthesis to continue even during tidal submersion, which might not be true in muddy sediment. Few studies have also pointed out that the epipsammic forms are capable of regulating their photopigment composition and activity in changing light conditions, whereas epipelic forms are low light-acclimated (Jesus et al., 2009; Cartaxana et al., 2011, 2016).

MPB showed similar seasonal distribution (i.e., low and high MPB during monsoon and non-monsoon, respectively) at both tidal flats. These findings are in agreement with previous studies (Rasmussen et al., 1983; Wolfstein et al., 2000; Mitbavkar & Anil, 2002, 2004, 2006; Woelfel et al., 2007; Ha et al., 2018; Redzuan & Underwood, 2021). The monsoon season adds nutrients to the tidal flat, but the intensive wave action and runoff wash the top few centimeters of the sediment, making the conditions less conducive for MPB growth. Further, reduced salinity can also cause osmotic shock and hinder MPB growth during the monsoon period. In contrast, non-monsoon (pre- and post-monsoon) conditions are the most conducive, with stable environmental conditions at both water-column and tidal flats. Another interesting aspect of MTF is the beach profile changes during the monsoon and post-monsoon seasons (Loveson et al., 2014). The sediment transport rates during pre-monsoon and post-monsoon were 0.016 x 10^6 m^3/year to 0.62 x 10^6 m^3/year (Jayakumar et al. 2002; Seelam et al. 2014) and ~0.02 x 10^6 m^3/year to 0.04 x 10^6 m^3 /year (Jayakumar et al. 2002) at MTF. A study at MTF by Seelam et al. (2014) showed 13 m^3 of sediment erosion between December and January. Unlike MTF, beach profile studies are scarce for DTF. The only study by Rodrigues (1984) reported the beach slope to be gradual and decreased further during the monsoon season. The sediment erosion starts towards the end of the pre-monsoon season and continues till the end of the monsoon season (Rodrigues, 1984). Such seasonal changes in the beach profile can affect the sand-dwelling communities and have been reported in various studies (Jesus et al., 2009; Paterson & Hagerthey, 2001)

Various studies have established using MPB as a potential indicator of anthropogenic impacts (Dalu et al., 2020; Du et al., 2017; Barinova et al., 2019). Daly Yahia-Kéfi et al. (2005) have reported *Bellerochea horologicalis* and *Lithodesmium polymorpha* from both water and sediment, associated with eutrophic conditions with phosphate-rich water and used as indicator species in the southwestern zone of the Bay of Tunis. In DTF, *B. malleus* and *L. undulatum* dominance in the MPB community was found to be associated with elevated phosphate values, both in the SW (1.76±0.77 µM) and interstitial water (4.08±1.29 µM), indicating as potential eutrophic indicator species. Mitbavkar and Anil (2002) have also recorded *Bellerochea* sp. in the upper sediment (0-5 cm), with abundance peaking in monsoon and post-monsoon season, where nutrients are usually more, but *L. undulatum* was not noticed at DTF. On the other hand, the rampant developmental activities at MTF have already resulted in ecosystem degradation (Mascarenhas & Ingole, 2009). The MTF inhabit various intertidal burrowing forms (e.g., bivalves, polychaetes, and small crustaceans) (Ingole, 2002, 2003, 2004). However, the biodiversity decline, such as the loss of exotic species since the 1980s (Ingole, 2002) and the decline in foraminiferal abundance and diversity between 1994-2001 (Nigam et al., 2005), are already reported from the tidal flat. Changes are not only observed in the biotic but also the abiotic attributes like an extraordinary increase in the suspended load (i.e., 2.0 mg/l in 1972 to 114.50 mg/l in 1990; Nigam et al., 2002) and shoreline changes (~40m to ~280m width since the 1950s; Loveson et al., 2014). These changes in the beach profile, shoreline, and benthic biodiversity are attributed to the iron ore mining activities taking place in the hinterland of the Mandovi River catchment area (Nigam et al., 2002 and 2005; Loveson et al., 2014). Further, a few studies have also pointed out that the MTF is also affected by oil spills and tar-ball pollution (Rekadwad & Khobragade, 2015; Ansari & Ingole, 2002). However, there are no studies on the MPB status from this tidal flat, and this study provides the baseline data on the MPB assemblages. However, compared to other undisturbed and protected tidal flat (i.e., DTF) on the same coastline, MTF shows low abundance and diversity (Mitbavkar & Anil, 2002). Interestingly, higher dinoflagellate species (including 3 potential HAB taxa, e.g., *Amphidinium* sp., *Gymnodinium* sp., and *Peridinium quinquecorne*) are recorded in MTF but not recorded in DTF. Hence, the proliferation of HAB species in the MTF could be a precursor of HAB events in the adjacent water column and raise concerns. Therefore, regular monitoring of MPB will be crucial in coastal ecosystem monitoring and management.

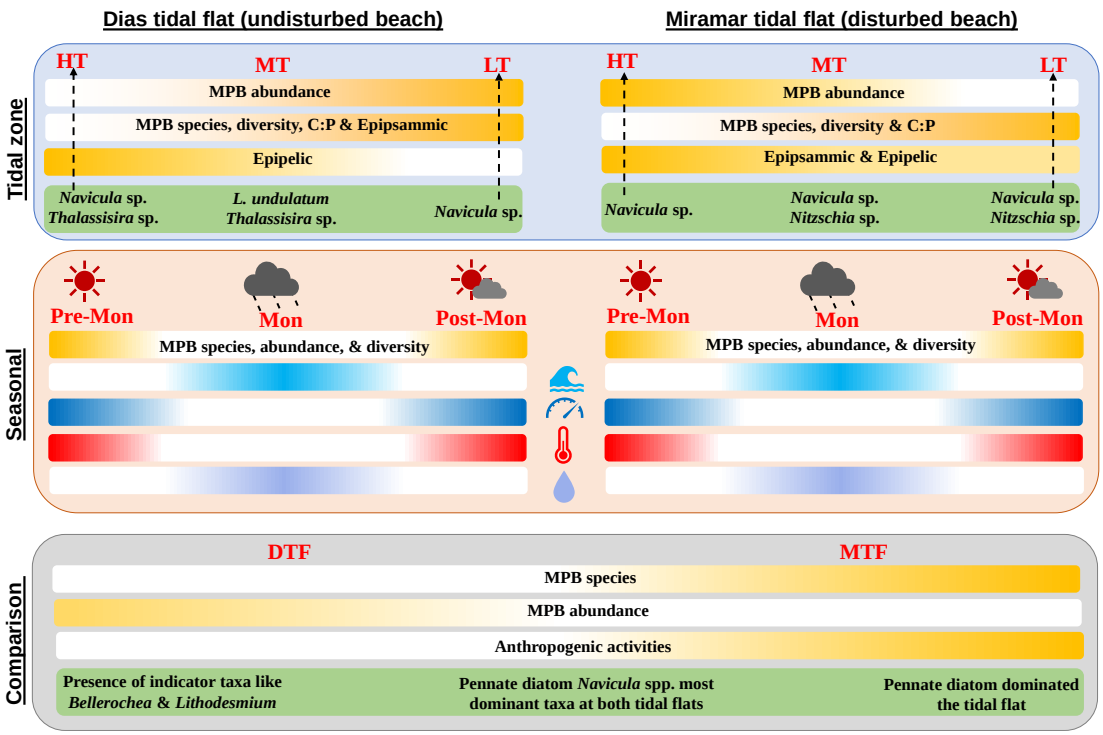


Figure 3.14. The schematic shows tidal zone, seasonal, and comparative inter-annual variations between the Dias tidal flat (DTF) and Miramar tidal flat (MTF). The darker, slightly light, and light color shades represent the highest, comparatively low, and lowest values of different parameters. The wave symbol indicates wave intensity, the meter symbol indicates salinity, the thermometer indicates temperature and the droplet indicates nutrients.

3.1.4.2. Inter-seasonal variations

During the study period, environmental parameters revealed distinct variations between the seasons (monsoon, post-monsoon, and pre-monsoon) of different years (i.e., 2019,2022 and 2023). Among the seasons, the most prominent variations in environmental conditions were observed for the monsoon season. The inter-annual variability in rainfall (both intensity and duration as well as its onset and withdrawal) and the associated physical changes (e.g., strong waves) are the primary reasons for bringing drastic variations in the environmental conditions. For instance, the rainfall was highest in 2019, followed by 2023 and 2022, and these events resulted in significant variations in the temperature and salinity of the surf and interstitial waters (Figure 3.2). Moreover, the monsoon season's extended precipitation duration and intensity often influence the early phase of the post-monsoon season (i.e., October-November), as evidenced by salinity. For instance, the post-monsoon of 2022 was relatively stable and without any episodic

precipitation, whereas episodic precipitation with overcast conditions was observed in the 2023 post-monsoon, resulting in a relative decrease in salinity. For the pre-monsoon season of 2019 and 2023, the environmental variables almost showed similar trends with negligible freshening of surf waters. Hence it is assumed that the influence of such environmental conditions would also be observed on MPB. Further, the MPN method used in this study for MPB quantification relies on relative abundance instead of absolute abundance. However, to delineate the year-wise variations for different seasons, absolute abundance data are generally desirable over relative abundance to depict inter-seasonal variations. Despite methodological constraints, the relative MPB abundance and diversity, derived from the MPN method, showed significant variability between different years of the monsoon seasons (i.e., low in 2019, followed by 2022 and 2023) at both tidal flats. However, the taxa dominance (i.e., *Navicula* spp.) remained unchanged in all the monsoonal years at both the tidal flats. Nevertheless, the MPN method, which uses relative abundance for MPN quantification, is good enough for qualitative and diversity studies. Overall, no tidal zone variations between different years or different seasons were observed except in MTF, which showed a unique response to the year-wise monsoonal changes. For instance, the MPB abundance showed a lower abundance at the LT and MT zones and higher at the HT zone during the monsoonal years. The HT zone, which was mostly dry, benefitted from rainfall by getting abrupt nutrient input without much sediment disturbance caused by the wave actions. Unlike monsoon season, MPB abundance and diversity didn't show much variation between 2022 and 2023 post-monsoons. Interestingly, even though the MPB diversity was similar, the community composition was distinct. The disparity could be due to the non-uniform sampling months for the post-monsoon season. For instance, only two months were sampled in 2023 compared to three months in 2022 during the post-monsoon season, which might have undermined the observations. On the other hand, in the pre-monsoon seasons of 2019 and 2023 the abundance, taxa, evenness, and species varied significantly between the years despite the season in both years being the most stable. However, the environmental conditions were found to be conducive to MPB growth, hence recording the highest abundance at both tidal flats.

Overall, during the non-monsoon season, the dominant taxa and assemblages varied greatly between different years for both the tidal flats. In benthic, centric diatoms dominated the pre-monsoon seasons in 2019, post-monsoon in 2022, and 2023 at DTF, pennate diatoms in all the non-monsoon seasons at MTF and only the pre-monsoon 2023

at DTF. These taxa dominance was mostly governed by the periodic bloom events occurring in the non-monsoon seasons at both tidal flats. Occurrences of blooms in the non-monsoon seasons due to local environmental factors could influence the variations in the MPB community. Nevertheless, generating absolute data, which is challenging, is the need of the hour to understand the impact of anthropogenic activities and climate change on the MPB dynamics and benthic-pelagic ecosystem functioning *per se*.

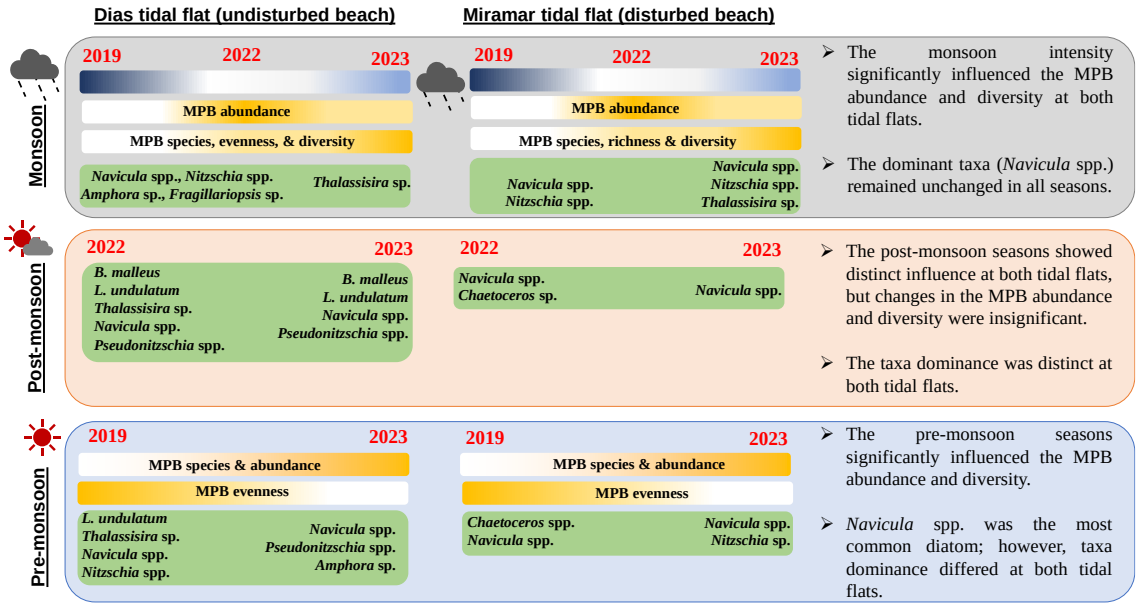


Figure 3.15. The schematic shows pre-monsoon, monsoon, and post-monsoon inter-seasonal variations between the Dias tidal flat (DTF) and the Miramar tidal flat (MTF). The darker, slightly light, and light color shades represent the highest, comparatively low, and lowest values of different parameters.

3.1.4.3. Decadal variations in MPB

To understand the decadal variation, only MPB data from the current and ~2.5 decade-old previous studies (Mitbavkar and Anil 2002, 2006) from DTF are considered as MPN-based studies. The comparison revealed that the previous study (Mitbavkar and Anil, 2002 & 2006) recorded fewer MPB species than the present study. To bring uniformity in both data sets, dinoflagellate species data were excluded from comparison. In both studies, diatoms were the dominant components of the MPB assemblage. However, comparing MPB taxa based on clustering of presence/absence data revealed significant differences in the MPB species assemblage. Only 28% (SW), 24% (LT), 29% (MT), and

35% (HT) MPB species were common in the previous and present studies. In the previous study, *Navicula* spp., *Amphora* sp., and *Thalassiosira* sp. were found to be most abundant and were recorded throughout the study period, whereas in the present study, *Navicula* spp., *Thalassiosira* sp., *B. malleus*, *L. undulatum*, and *Nitzschia* spp. were dominant and were recorded throughout the study period, whereas *Amphora* sp. contribution was minimal (0.8-4%). Interestingly, the previously documented minor contributors (*Bellerochea* sp., *Chaetoceros* sp., and *Skeletonema* sp.) or not documented species (*Lithodesmium* sp.) were predominant in the present study, suggesting a significant shift in the species dominance and assemblage due to changing environmental conditions (e.g., monsoon-driven changes, eutrophication, increase in seawater intrusion, etc.). For instance, there has been a rise in eutrophication indicator species such as *Bellerochea* sp. and *Lithodesmium* sp. (Daly Yahia-Kefi et al., 2005). Another interesting finding is that the previous studies have reported *Chaetoceros* sp. and *Skeletonema* sp. only from the SW and LT zone in the sediment, whereas in the present study, though not as dominant taxa, they were predominant in all the tidal zones, suggesting the increased level of seawater intrusion.

Further, several studies reported that rare species are important reservoirs of genetic and ecological diversity in the coastal marine environment (Boero, 1994), and the compensatory growth of rare species supports the stability and diversity of the population (Floder et al., 2010). According to the insurance theory proposed by Weithoff (2003), rare phytoplankton species are a backup for species' functional diversity and respond quickly to disturbances, making the ecosystem more resilient. In recent studies, intertidal flats have emerged as one of the non-classical blue carbon ecosystems (Chen et al., 2020; Sasmito et al., 2020; James et al., 2024), which can sequester and store large amounts of carbon at climate-relevant time scales (Mao et al., 2020; Moritsch et al., 2021) and have been termed nature-based solutions (NBS) to climate change (James et al., 2024). Hence, monitoring the MPB assemblages can help in coastal management programs and potentially aid in climate change impact studies.

3.1.5. Conclusion

This study concludes that MPB and SW phytoplankton abundance showed significant inter-annual and seasonal variations, with diatoms as the dominant groups at undisturbed (DTF) and disturbed (MTF) tidal flats. Further, MPB showed significant variations between low (LT), mid (MT), and high (HT) tide zones at both DTF and MTF. Generally,

centric and pennate diatoms dominate the SW and MPB communities, respectively, and were also observed at both DTF and MTF. The SW phytoplankton influenced the MPB community through deposition and vice versa through resuspension in SW. C:P values can be a potential indicator for understanding the diatom exchange between MPB and SW community, particularly during bloom periods. However, the interdependency of the diatom community between MPB and SW community is tidal flat specific and dependent on the topography of the tidal flat. Further, epipsammic and epipelic abundance can be potential indicators for sediment texture as their abundance ratios are associated with sediment texture. Interestingly, potential eutrophic indicator species associated with elevated phosphate values were observed at DTF. Meanwhile, the anthropogenically disturbed MTF showed lower abundance and diversity than DTF, along with potential HAB dinoflagellate taxa (*Amphidinium* sp., *Gymnodinium* sp., and *Peridinium quinquecorne*), which were not recorded in DTF. Further, the relative MPB abundance and diversity showed significant interseasonal variability for monsoon and pre-monsoon seasons at both tidal flats. However, the taxa dominance (i.e., *Navicula* spp.) remained unchanged and differed for monsoon and non-monsoon seasons, respectively. Further, a decadal shift in the MPB community was observed at an undisturbed tidal flat (DFT). Interestingly, a ~2.5-decade-old study documented minor contributors or non-documented species that were predominant in the present study, suggesting a significant shift in the species' dominance and assemblage due to changing environmental conditions due to natural (e.g., monsoon variability) and anthropogenic activities (e.g., tourism). These findings highlight that the regular monitoring of MPB is the need of the hour to understand the impact of anthropogenic activities and climate change on the MPB dynamics and benthic-pelagic ecosystem functioning, *per se*.

3.2. The pelagic ecosystem

3.2.1. Introduction

Among the eukaryotic protists, dinoflagellates are characterized by two flagella comprising an accountable proportion of plankton biomass (Taylor, 1987), forming essential components of both marine and freshwater ecosystems. As part of their life cycle or as a preparatory measure for a dormant period, ~12-13% of dinoflagellate species are known to produce organic-walled and calcareous resting cysts, which are refractory and subsequently settle in the sediment (Head, 1996; Dale, 1996). The dinoflagellate cysts act as a repository for environmental information for modern marine (e.g., Rochon et al., 1999; Dale et al., 2002; Pospelova et al., 2008; Bringue et al., 2013; Zonneveld et al., 2013) and freshwater (Kouli et al., 2001; McCarthy et al., 2011; Mertens et al., 2012a) ecosystems and are extensively used in past reconstruction of oceanographic conditions (e.g., Pospelova et al., 2002; Marret & Zonneveld, 2003; Pospelova et al., 2005; Hallegraeff & Gollasch, 2006; Marret et al., 2009; Mertens et al., 2009a). In the shallow regions, these dinoflagellate cysts can act as seed banks for blooms (including harmful algal blooms) and help in unwanted bio-invasions by remaining viable for many years (Matsuoka & Fukuyo, 2000; Lundholm et al., 2011; Delebecq et al., 2020) whereas, in the deeper regions, they contribute majorly in the export of organic matter (Mouradian et al., 2007).

The Indian Ocean (IO) comprises the Arabian Sea (AS) on the west, the Bay of Bengal (BoB) on the east, equatorial IO (EIO) from 4^{o}N to 4^{o}S, and south tropical IO (STIO) up to 30^{o}S. The IO is intensely influenced by seasonal monsoonal forcing, weak equatorial upwelling, and significant freshwater influx from major rivers (Schott & McCreary, 2001). The IO plays a vital role in the global ocean in the transport of heat, salt, carbon, and about 15-20% of global primary production despite being the smallest oceanic basin (Behrenfield & Falkowski, 1997; Regaudie-de-Gioux et al., 2014). The IO can broadly be divided into North IO (i.e., NIO) comprising AS and BoB and South IO (i.e., SIO) comprising EIO and STIO. The NIO is relatively more productive than the SIO (Dalabehara & Sarma, 2021), and the circulation patterns differ significantly. The NIO shares similar atmospheric forcing and seasonal wind patterns driven by monsoons (Prasad, 2004), whereas the SIO receives a very low supply of nutrients from rivers and atmospheric deposition and has no influence of the monsoon winds. These contrasting atmospheric and hydrographic settings make the NIO and SIO very interesting ocean basins. The reflection of these contrasting atmospheric and hydrographic settings is

highly anticipated in the dinoflagellate cyst assemblages. However, the dinoflagellate cysts studies in IO are primarily restricted to coastal regions viz, coastal regions of the eastern AS (Godhe et al., 2000; D'costa et al., 2008; D'silva et al., 2011, 2012; Narale et al., 2015; Rodrigues et al., 2019, 2022), western AS (Zonneveld et al. 1997, and 2013; Zonneveld & Jurkschat, 1999), BoB (Naidu et al., 2012; D'Silva et al., 2013; Narale et al., 2013; Uddandam et al., 2015; Uddandam et al., 2017; Narale & Anil, 2017; Uddandam et al., 2020), and within south-east Asian regions (Matsuoka, 1981; Kumar, 1996; Matsuoka et al., 1999; Azanza et al., 2004; Kawamura, 2004; Furio et al., 2006; Hessler et al., 2013). Since some dinoflagellate species are known to cause harmful blooms that threaten fisheries and coastal human populations, the studies (including cysts) mentioned above are mostly concentrated in the coastal regions. Dinoflagellate cyst studies also help address various coastal management-related issues (Shin et al., 2011), making coastal studies inevitable. Generally, the species-specific dinoflagellate cyst morphology is extensively used in field and lab-based studies as a proxy for change in environmental factors like temperature and salinity (Ellegaard et al., 2002; Mertens et al., 2009a, 2009b, 2010 and 2012a, b; Verleye et al., 2012; Rodrigues & Patil, 2021). However, such studies are important; field-based morphometric studies representing larger ocean basins from the pelagic regions with different oceanographic settings are limited. However, such studies might be challenging in the oligotrophic pelagic regions, which are limited by the lesser cyst concentrations. Moreover, the compilation of a global dataset on dinoflagellate cysts by Zonneveld et al. (1997 and 2013), Marret and Zonneveld (2003), and Marret et al. (2020) have pointed out the geographical data gap from the pelagic regions of the IO. Studies on dinoflagellate cyst distribution in the surface sediments at a larger basin scale can provide detailed information for a better understanding of the environmental drivers of dinoflagellate cyst species (de Vernal et al., 2001; Marret & Zonneveld, 2003; Zonneveld et al., 2013; de Vernal et al., 2020; Marret et al., 2020).

Given this, an extensive surface sample from the pelagic regions of the IO is analyzed to evaluate (i) the cyst assemblages from deep-sea sediments from various bioregions, (ii) differences or similarities existing among the bioregions, and (iii) variations in morphometry of cosmopolitan dinoflagellate cysts. The geographical coverage in the present study encompasses the AS, BoB, equatorial IO, and STIO up to 30^{o}S. Therefore, this study reduces the geographical data gap from the IO pelagic regions,

as Marret and Zonneveld (2003) identified, and addresses various ecological issues relevant to dinoflagellate cyst ecology.

3.2.2. Methodology

The details of the sampling site, sample collection, and analysis from the deep-sea sediment to study dinoflagellate cysts are presented in Chapter 2 subsection 2.2.2.

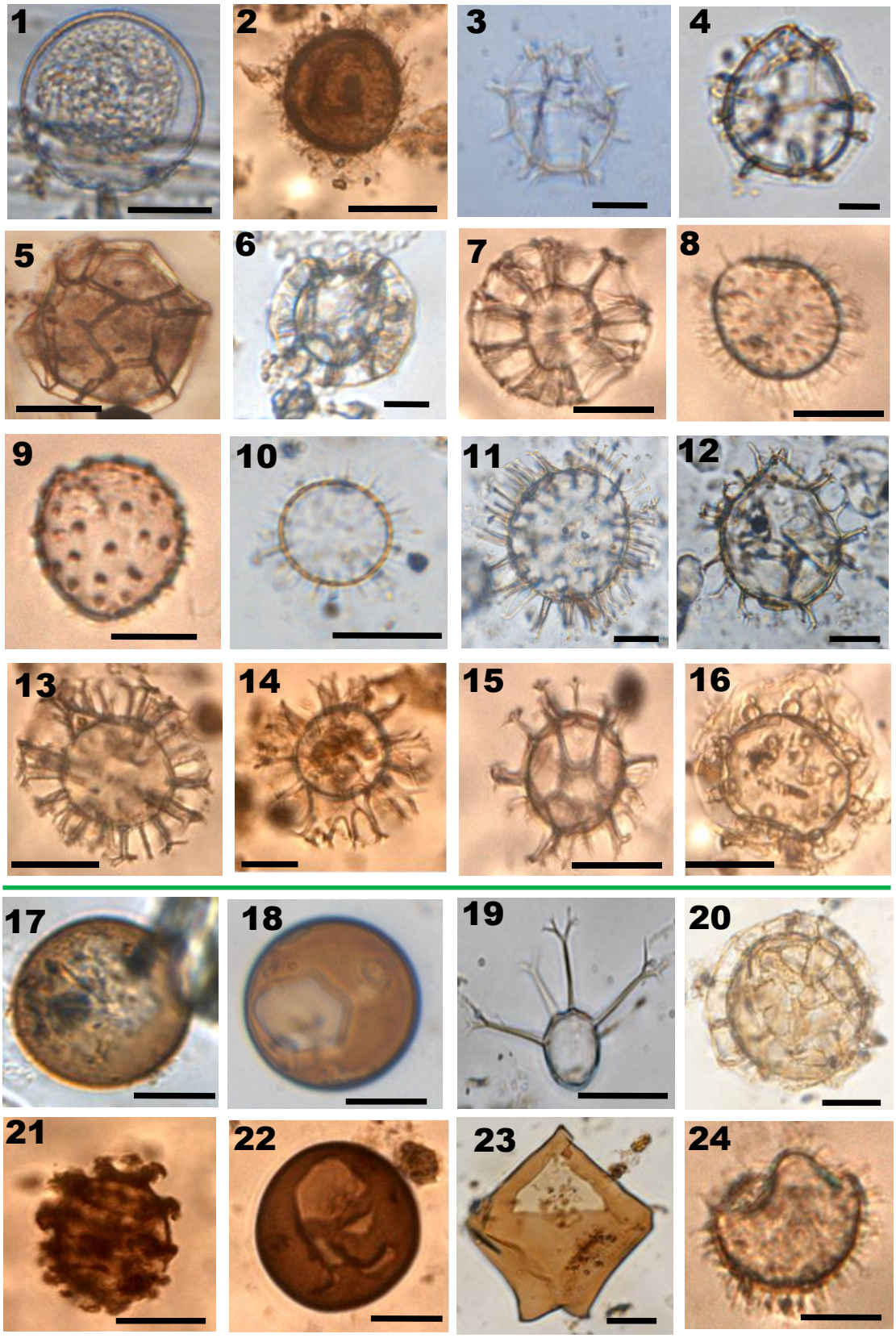
Data analysis

Dinoflagellate cysts community indices (species count or number of species, Shannon–Wiener's diversity index (H′), Pielous evenness, and Margalef's species richness) for each station and region (oligotrophic-AS, OMZ-AS, BoB, EIO, and STIO) were determined using PRIMER – version 6 (PRIMER–E Ltd. Plymouth, UK).

3.2.3. Results

3.2.3.1. Dinoflagellate cyst diversity and distribution

Altogether 48 dinoflagellate cyst species were recorded, of which 41 cysts belonging to 18 genera in AS (17 autotrophic, 3 mixotrophic, and 21 heterotrophic), 28 cysts belonging to 16 genera in BoB (10 autotrophic, 3 mixotrophic, and 15 heterotrophic), 19 cysts belonging to 11 genera in EIO (12 autotrophic, 1 mixotrophic, and 6 heterotrophic), and 12 cysts belonging to 8 genera in STIO (10 autotrophic, and 2 heterotrophic) were found in this study (Figure 3.17a-b, Table 3.2) Therefore, the NIO recorded more species (i.e., 48 species) than the SIO (20 species). The maximum concentration of dinoflagellate cyst was recorded in the coastal-AS (231 cysts g^{-1}) followed by OMZ-AS (124 cysts g^{-1}), oligotrophic-AS (90 cysts g^{-1}), BoB (13 cysts g^{-1}), and least in STIO (9 cysts g^{-1}) and EIO (6 cysts g^{-1} each) (Figure 3.18a). *Spiniferites ramosus* and *Spiniferites* sp. in NIO, and *Pentapharsodinium dalei* in SIO were the dominant taxa. The autotrophic cysts dominated in AS (73%-82%), EIO (84%), and STIO (98%), whereas heterotrophic cysts in BoB (49%) (Figure 3.18b). The higher species count, evenness, richness, and diversity in NIO than in SIO signifies distinct geographic patterns in planktonic dinoflagellate production (Figures 3.17c-f). Interestingly, the dinoflagellate cyst assemblage showed distinct geographic variations. For instance: (i) *Impagidinium strialatum*, *Operculodinium centrocarpum*, *Spiniferites* sp., and *Echinidinium* sp. were the common occurrence in the IO, (ii) *Spiniferites hyperacanthus*, *Spiniferites merabilis*, cyst of *Protoperidinium* sp., *Lingulodinium machaerophorum*, *Trinovantedinium applanatum*, and cyst of *Polykrikos hartmannii* were common only in NIO.



Continue…..

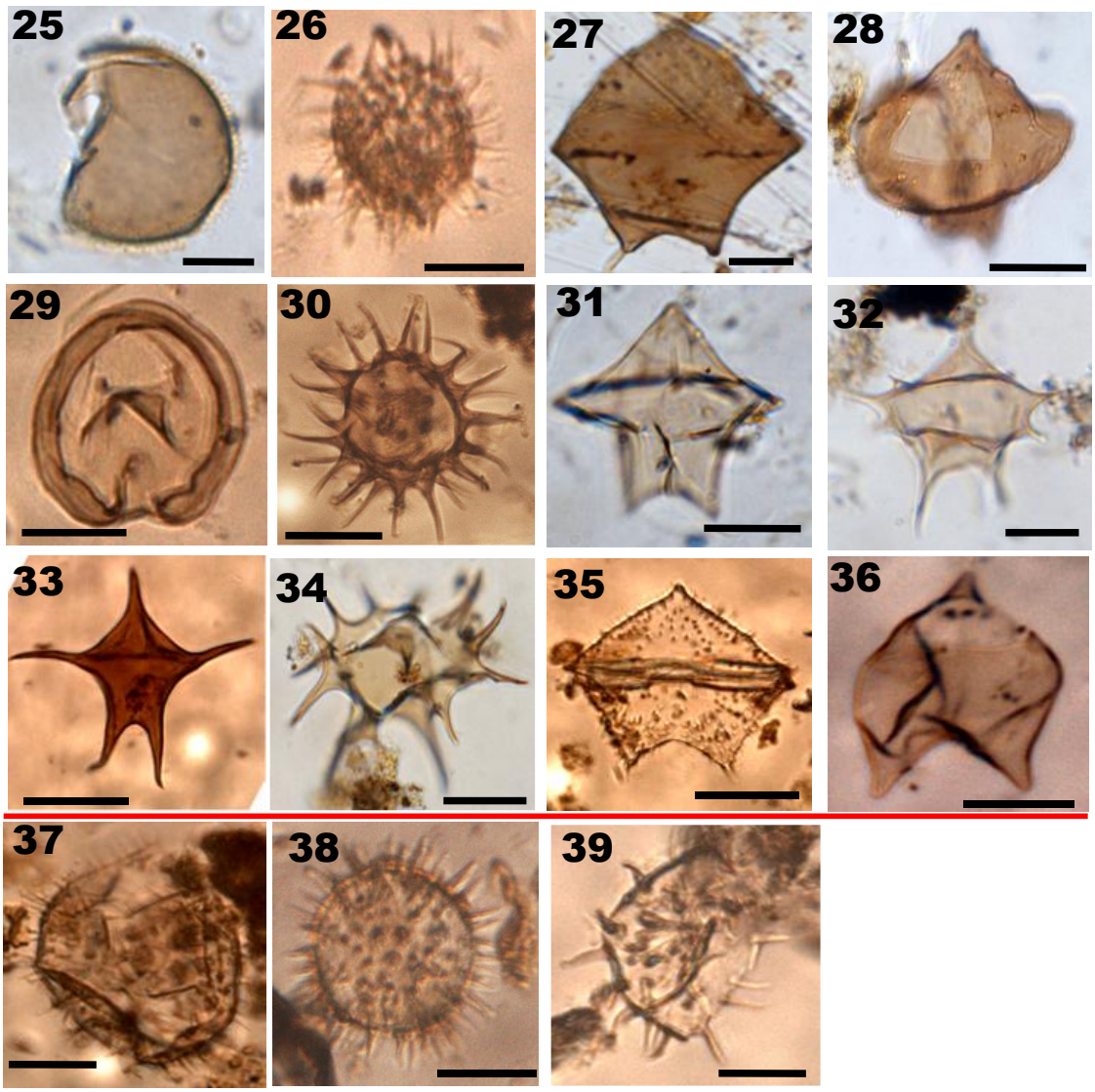


Figure 3.16. Micrograph of dinoflagellate cysts **A) Autotrophic:** 1) Cyst of *Alexandrium* sp., 2) *Bitectatodinium spongium*, 3) *Impagidinium aculeatum*, 4) *Impagidinum paradoxum*, 5) *Impagidinum patulum*, 6) *Impagidinum strialatum* 7) *Nematosphaeropsis labyrinthus*, 8) *Operculodinium centrocarpum*, 9) *Operculodinium janduchenei*, 10) Cyst of *Pentapharsodinium dalei*, 11) *Polysphaeridium zoharyi*, 12) *Spiniferites bentorii*, 13) *Spiniferites hyperacanthus*, 14) *Spiniferites mirabilis*, 15) *Spiniferites ramosus*, 16) *Tuberculodinium vancampoae*, **B) Heterotrophic:** 17) *Brigantedinium simplex*,18) *Brigantedinium sp., 19*) Cyst of *Cladopyxis sp.*, 20) Cyst of *Polykrikos kofoidii*, 21) Cyst of *Polykrikos schwartzii*, 22) Cyst of *Protoperidinium denticulatum*, 23) Cyst of *Protoperidinium latissimum*, 24) Cyst of *Protoperidinium monospinum*, 25) Cyst of *Diplopelta* sp., 26) *Echinidinium* sp., 27) *Lejeunecysta sabrina*, 28) *Quinquecuspis pentagonum*, 29) *Selenopemphix nephroides*, 30) *Selenopemphix quanta*, 31) *Stelladinium abei*, 32) *Stelladinium bifurcatum*, 33) *Stelladinium reidii*, 34) *Stelladinium stellatum*, 35) *Trinovantedinium applanatum*, 36) *Votadinium calvum*, **C) Mixotrophic:** 37) Cyst of *Polykrikos hartmannii*, 38) *Lingulodinium machaerophorum*, 39) *Ligulodinium* sp. (all scale bar 20 micron).

In the AS oligotrophic region, maximum species count (24 species) and diversity index H' (2.7) were recorded in stations 2 and 5, respectively. The other three stations in AS oligotrophic regions, where the depth varied from 2000-4600m, recorded 15-22 species, 68-155 cysts g^{-1}, and 1.6-2.0 diversity index H' of dinoflagellate cysts. Station 4 (depth 4607m) recorded a relatively lower species count (only 16) and concentration (68 cysts g^{-1}). In the AS-OMZ region, the species count was higher in station 8 (i.e., 22 taxa) followed by stations 6 and 7 (recorded 21 and 20 taxa, respectively). Station 8 recorded the maximum cyst concentration (140 cysts g^{-1}), followed by stations 7 (123 cysts g^{-1}) and 6 (108 cysts g^{-1}). The cysts of autotrophic taxa dominated the assemblages than heterotrophic taxa in all the AS regions. Cysts produced by autotrophic taxa contribute 83%, 77%, and 74% to the total dinoflagellate cysts in the coastal, oligotrophic, and OMZ regions of the AS, respectively. The heterotrophic to autotrophic ratio (H/A) showed a slightly higher value in the OMZ (0.37) than in the oligotrophic (0.36) and coastal (0.20) regions of the AS. In the AS coastal and oligotrophic region, cyst assemblage was mostly dominated by autotrophic species like *Spiniferites* spp., cysts of *Gonyaulax Spinifera* complex, *S. ramosus,* and *S. mirabilis,* and mixotrophic species like *Lingulodinium* sp. representing 56% of the total dinoflagellate cyst assemblage.

On the contrary, in the AS-OMZ region, the species count was higher in station 8 (i.e., 22 taxa) followed by stations 6 and 7 (recorded 21 and 20 taxa, respectively). Station 8 recorded the maximum cyst concentration (140 cysts g^{-1}), followed by stations 7 (123 cysts g^{-1}) and 6 (108 cysts g^{-1}). The AS-OMZ region cyst assemblage was mostly dominated by autotrophic species like *Spiniferites* spp., *Spiniferites ramosus*, *Lingulodinium* sp., *Echinidinium* sp., *Nematosphaeropsis* sp., *Impagidinium paradoxum* which represent 75% of the total dinoflagellate cyst assemblage. Among the five HAB species, three species in both station 6 (*Operculodinium centrocarpum, Gonyaulax Spinifera* complex and cyst of *Polykrikos hartmannii*) and station 7 (*Operculodinium centrocarpum*, *Gonyaulax Spinifera* complex and *Lingulodinium machaerophorum*) and all in station 8 were recorded. The comparison of cyst assemblage data revealed that the species count and abundance recorded in this study were low compared to the EAS and WAS (Figure 3.19). In the BoB, coastal station 1 showed maximum cyst concentration (19 cysts g^{-1}), number of species (18 species), and diversity (2.5), whereas stations 2 and 3 (14 species) showed an equal number of species but cyst concentration was slightly higher in the former (15 cysts g^{-1}) than the latter (7 cysts g^{-1}). All the stations were dominated by *Spiniferites* sp. and cyst of *Protoperidinium* sp.

Table 3.2. Dinoflagellate cysts concentration (cysts g^{-1} dry weight) in the Arabian Sea (AS), Bay of Bengal (BoB), Equatorial Indian Ocean (EIO), and South tropical Indian Ocean (STIO) A: autotrophic, H: heterotrophic, M: mixotrophic, C: coastal, O: oligotrophic, OMZ: oxygen minimum zone, NIO: North Indian Ocean and SIO: South Indian Ocean. (*): Indicates potentially HAB species. The motile affinity is based on Li et al., 2023; Marret et al., 2020; Ramírez-Valencia et al., 2021; Rigel et al., 2022.

Sl. No.	**Trophic status**	**Biological name**	**Paleontological name**	**AS**	**BoB**	**EIO**	**STIO**	**NIO**	**SIO**
1	A	Unknown	*Bitectatodinium spongium*	3.3	0.0	0.0	0.0	9.8	0.0
2	A	*Alexandrium* sp.	Cyst of *Alexandrium* sp.*	0.0	0.0	0.0	0.0	0.0	0.0
3	A	*Pentapharsodinium dalei*	Cyst of *Pentapharsodinium dalei*	2.8	0.0	1.3	1.0	8.3	2.3
4	A	*Gonyaulax* sp. Indet.	*Impagidinium aculeatum*	6.6	0.1	0.9	0.4	19.8	1.3
5	A	*Gonyaulax* sp. Indet.	*Impagidinium paradoxum*	0.9	0.0	0.2	0.0	2.8	0.2
6	A	*Gonyaulax* sp. Indet.	*Impagidinium patulum*	0.5	0.5	0.4	0.3	1.8	0.7
7	A	*Gonyaulax* sp. Indet.	*Impagidinium* sp.	2.4	0.2	0.8	0.9	7.3	1.7
8	A	*Gonyaulax* sp. Indet.	*Impagidinium strialatum*	3.6	0.0	0.2	0.0	10.8	0.2
9	A	*Gonyaulax spiniferites* complex	*Nematosphaeropsis labyrinthus*	2.3	0.0	0.0	0.0	7.0	0.0
10	A	Unknown	*Nematosphaeropsis* sp.	3.7	0.4	0.3	0.0	11.4	0.4
11	A	*Protoperidinium reticulatum*	*Operculodinium centrocarpum**	1.5	0.4	0.0	0.0	4.9	0.0
12	A	Unknown	*Operculodinium janduchenei*	0.2	0.0	0.0	0.0	0.7	0.0
13	A	Unknown	*Operculodinium* sp.	0.3	0.1	0.1	6.0	1.0	6.1

14	A	*Pyrodinium bahamense*	*Polysphaeridium zoharyi**	0.0	0.0	0.0	0.0	0.1	0.0
15	A	*Gonyaulax nezaniae*	*Spiniferites bentorii*	0.0	0.2	0.0	0.0	0.3	0.0
16	A	*Gonyaulax whaseongensis*	*Spiniferites hyperacanthus*	6.3	0.0	0.0	0.0	18.9	0.0
17	A	*Gonyaulax spiniferites* complex	*Spiniferites merabilis*	18.2	0.2	0.0	0.0	54.7	0.0
18	A	*Gonyaulax spiniferites* complex	*Spiniferites ramosus*	36.4	0.0	0.0	0.0	109.1	0.0
19	A	*Gonyaulax spiniferites* complex	*Spiniferites* sp.	27.4	3.7	1.0	0.1	85.9	1.1
20	A	*Pyrophacus steinii*	*Tuberculodinium vancampoae*	1.4	0.2	0.0	0.0	4.5	0.0
21	H	*Protoperidinium avellana*	*Brigantedinium cariacoense*	0.0	0.5	0.0	0.0	0.5	0.0
22	H	*Protoperidinium conicoides*	*Brigantedinium simplex*	0.1	0.4	0.0	0.0	0.6	0.0
23	H	*Protoperidinium* sp.	*Brigantedinium* sp.	0.0	0.2	0.0	0.0	0.3	0.0
24	H	*Cladopyxis* sp.	Cyst of *Cladopyxis* sp.	0.0	0.0	0.0	0.0	0.1	0.1
25	H	*Diplopelta* sp.	Cyst of *Diplopelta* sp.	0.0	0.1	0.0	0.0	0.2	0.0
26	H	*Polykrikos kofoidii*	Cyst of *Polykrikos kofoidii*	1.1	0.0	0.0	0.0	3.2	0.0
27	H	*Polykrikos schwartzii*	Cyst of *Polykrikos schwartzii*	0.5	0.0	0.0	0.0	1.6	0.0
28	H	*Protoperidinium denticatum*	Cyst of *Protoperidinium denticulatum*	0.1	0.0	0.0	0.0	0.3	0.0
29	H	*Protoperidinium latissimum*	Cyst of *Protoperidinium latissimum*	0.3	0.0	0.0	0.0	0.8	0.0
30	H	*Protoperidinium monospinum*	Cyst of *Protoperidinium monospinum*	2.8	2.3	0.5	0.0	10.6	0.5
31	H	*Protoperidinium* sp.	Cyst of *Protoperidinium* sp.	0.0	0.1	0.0	0.0	0.1	0.0

32	H	Diplopsalid or Protoperidinioid group	*Echinidinium* sp.	8.0	1.0	0.2	0.1	25.0	0.3
33	H	*Protoperidinium leonis*	*Lejeunecysta sabrina*	0.3	0.0	0.0	0.0	0.8	0.0
34	H	*Protoperidinium* sp.	*Quinquecuspis pentagonum*	2.1	0.1	0.0	0.0	6.3	0.0
35	H	*Protoperidinium* sp.	*Quinquecuspis* sp.	0.0	0.1	0.0	0.0	9.1	0.0
36	H	*Protoperidinium subinerme*	*Selenopemphix nephroides*	0.2	0.5	0.0	0.0	1.1	0.0
37	H	*Protoperidinium conicum*	*Selenopemphix quanta*	3.0	0.3	0.0	0.0	3.8	0.0
38	H	Unknown	*Selenopemphix* sp.	0.2	0.0	0.1	0.0	0.5	0.1
39	H	*Protoperidinium* sp.	*Stelladinium abei*	0.0	0.2	0.0	0.0	0.2	0.0
40	H	Unknown	*Stelladinium bifurcatum*	0.0	0.0	0.0	0.0	0.1	0.0
41	H	*Protoperidinium* sp.	*Stelladinium reidii*	0.8	0.3	0.0	0.0	2.8	0.0
42	H	*Protoperidinium compressum*	*Stelladinium stellatum*	0.5	0.3	0.1	0.0	1.9	0.1
43	H	*Protoperidinium pentagonum*	*Trinovantedinium applanatum*	0.6	0.2	0.0	0.0	1.9	0.0
44	H	*Protoperidinium oblongum*	*Votadinium calvum*	0.9	0.0	0.0	0.0	2.6	0.0
45	H	*Protoperidinium steidinferae*	*Votadinium* sp.	0.0	0.0	0.0	0.0	0.1	0.0
46	M	*Polykrikos hartmannii*	Cyst of *Polykrikos hartmannii**	0.8	0.4	0.0	0.0	2.9	0.0
47	M	*Lingulodinium polyedrum*	*Lingulodinium machaerophorum**	1.1	0.1	0.0	0.0	3.4	0.0
48	M	*Lingulodinium* sp.	*Lingulodinium* sp.	7.3	0.3	0.1	0.0	22.3	0.1
				149	13.3	6.3	9.1	462	15

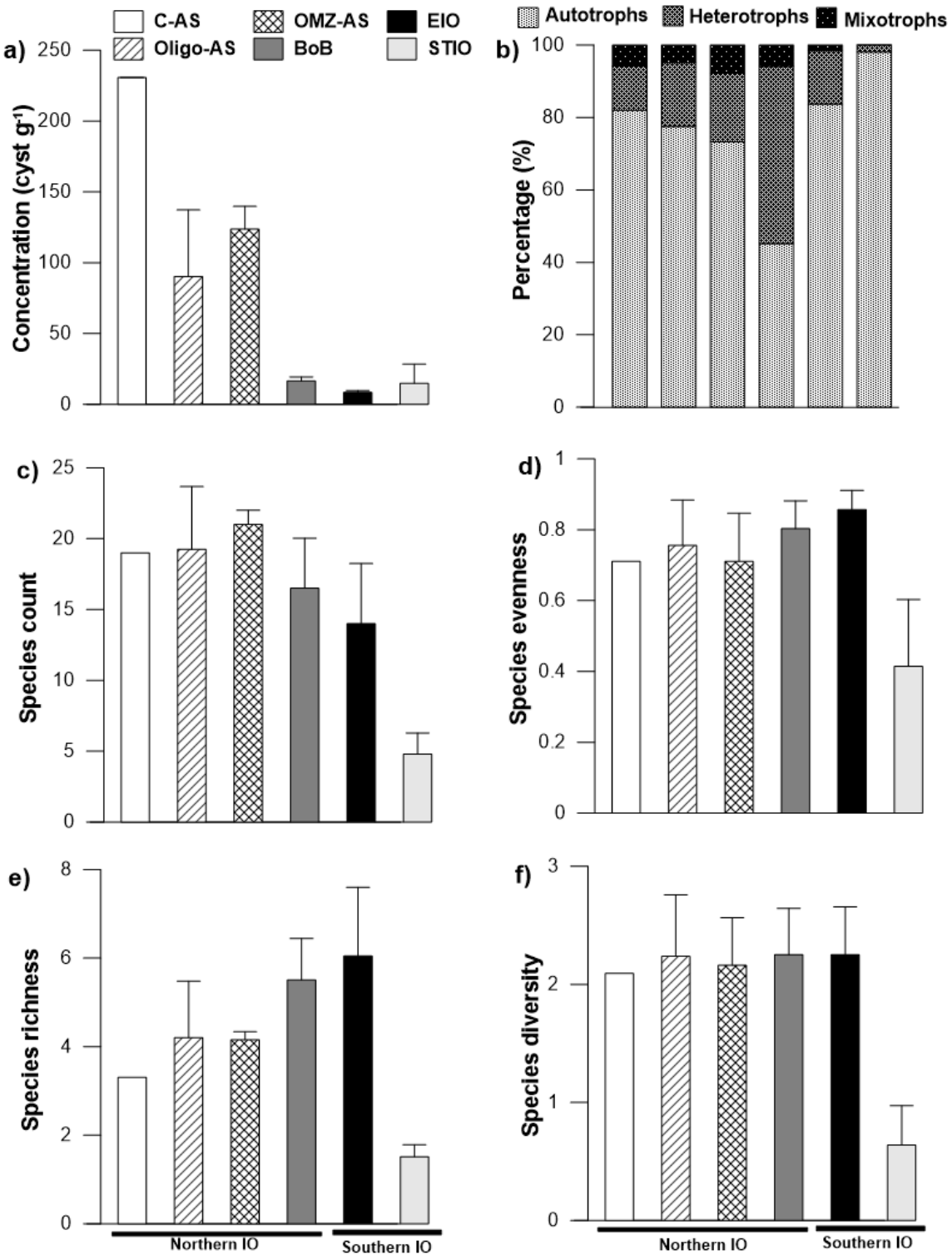


Figure 3.17. Variations in dinoflagellate cyst a) abundance, b) Autotrophic, heterotrophic, and mixotrophic forms, c) species count, d) species evenness, e) species richness, and f) species diversity in the Indian Ocean. C-AS: coastal Arabian Sea, O-AS: oligotrophic Arabian Sea, OMZ-AS: oxygen minimum zone Arabian Sea, BoB: Bay of Bengal, EIO: the equatorial Indian Ocean, and STIO: south tropical Indian Ocean.

In EIO, the western south-equatorial station (i.e., station 16) showed maximum cyst concentration (9 cysts g^{-1}) and number of species (17 species) and diversity (2.5) followed by the eastern south-equatorial station (i.e., station 4; 8 cysts g^{-1}; 11 species; diversity 1.8). All the stations in EIO were dominated by *Impagidinium* spp. (*I. paradoxum* and *I. aculeatum*). In STIO, station 10 showed maximum cyst concentration (39 cysts g^{-1}) followed by station 7 (11 cysts g^{-1}), station 11 (10 cysts g^{-1}), station 9 (8 cysts g^{-1}), and station 8 (7 cysts g^{-1}), whereas the remaining stations (station 6, 12, 13 and 14) recorded lowest cyst concentration (0.27-4 cysts g^{-1}). A maximum number of species was recorded in station 10 (7 species), followed by station 12 (6 species) and stations 7 and 11 (5 species each). Maximum diversity was recorded in station 7 (1.2), followed by station 10 (0.67), station 11 (0.53), and station 8 (0.41). All the stations in STIO were dominated by *Impagidinium* spp. (*I. strialatum* and *I. aculeatum*), *Pentapharsodinium dalei,* and cyst of *Cladopyxis* sp.

This study recorded cysts of four autotrophic and two mixotrophic potential HAB species (cyst of *Alexandrium* sp., cysts of *Gonyaulax* spp., *Operculodinium centrocarpum*, *Polysphaeridium zoharyi,* cyst of *Polykrikos hartmannii*, and *Lingulodinium machaerophorum*) of which five were present in AS except for cyst of *Alexandrium* sp., four in BoB except cyst of *Alexandrium* sp., and *Polysphaeridium zoharyi*, and only two in EIO (cyst of *Gonyaulax* sp., and *Operculodinium centrocarpum*) and STIO (cyst of *Alexandrium* sp. and *Operculodinium centrocarpum*) (Figure 3.19).

3.2.3.2. Comparison with previous studies

A comparison of cyst data with other regions of AS revealed that 32 species are common for both western and eastern AS (Table 3.3). Among them, 27 species recorded in this study were documented from both the western and eastern AS, indicating their widespread occurrence in the region. Also, 7 (cyst of *Cladopyxis* sp., cyst of *Protoperidinium latissimum, Lejeunecysta sabrina, Operculodinium janduchenei,* cyst of *Protoperidinium denticulatum, Protoperidinium monospinum,* and *Stelladinium bifurcatum*) and 6 (cyst of *Cladopyxis* sp., *Impagidinium patulum, Impagidinium strialatum, Operculodinium janduchenei, Protoperidinium monospinum,* and *Stelladinium bifurcatum*) species recorded in this study were not reported from western and eastern AS, respectively. Further, four species (cyst of *Cladopyxis* sp., *Operculodinium janduchenei, Stelladinium bifurcatum,* and *Protoperidinium monospinum*) are found to be reported for the first time from the AS (Table 3.3).

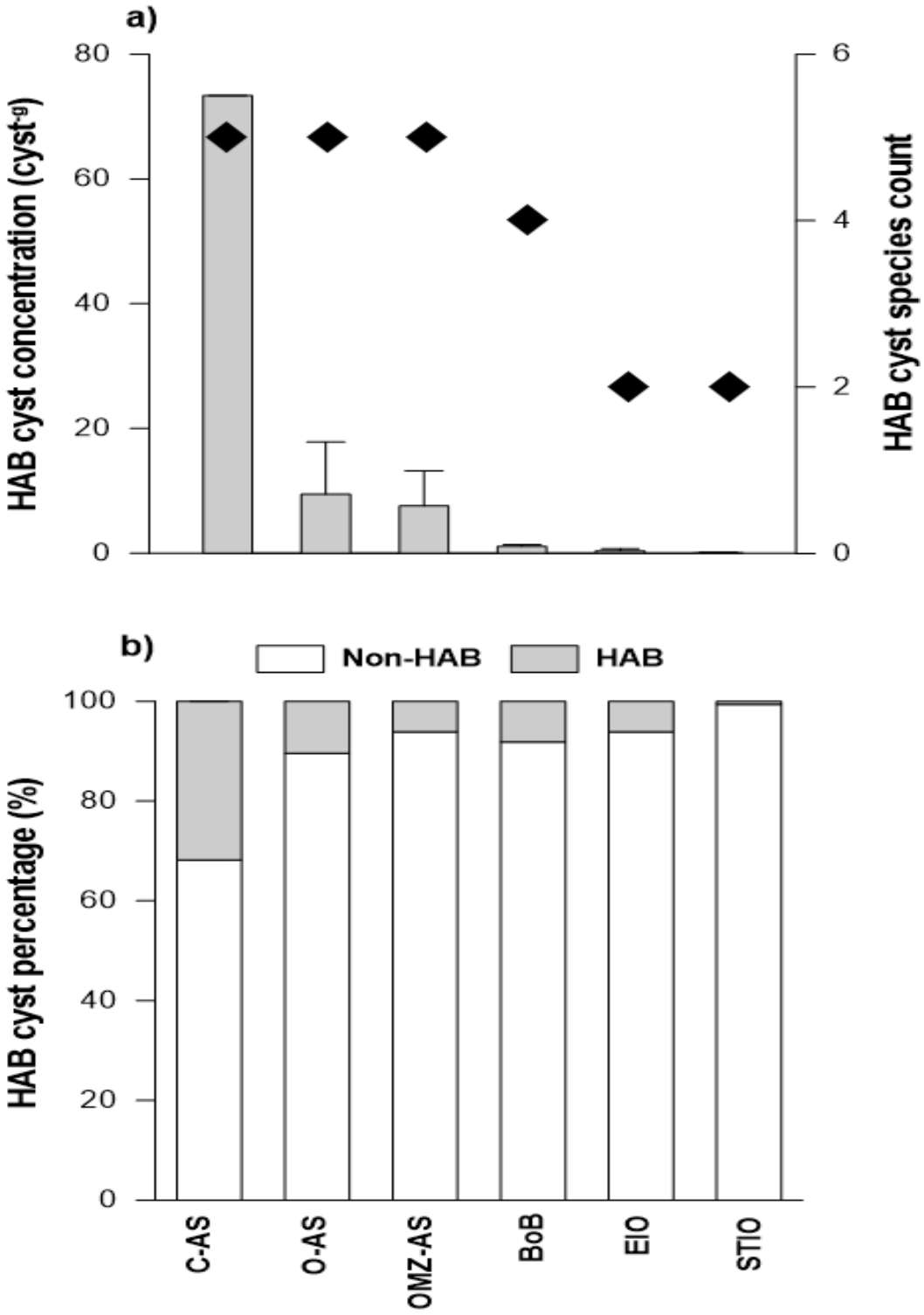


Figure 3.18. Bar plots showing a) HAB cyst concentration and species count and b) percentage contribution in different bioregions of the Indian Ocean. C-AS: coastal Arabian Sea, O-AS: oligotrophic Arabian Sea, OMZ-AS: oxygen minimum zone Arabian Sea, BoB: Bay of Bengal, EIO: equatorial Indian Ocean, and STIO: south-tropical Indian Ocean.

Table 3.3. The table shows dinoflagellate cysts abundance (cysts g^{-1} dry weight) in transects 1 and 2 of the Arabian Sea. A: Autotrophs; M: Mixotrophs; H: Heterotrophs; EAS: eastern Arabian Sea; WAS: western Arabian Sea. Trophic status is given following Marret et al., 2020. The motile affinity is based on Li et al., 2023; Marret et al., 2020; Ramírez-Valencia et al., 2021; Rigel et al., 2022. Indet: indeterminate, + means previously reported.

	Trophic status	**Motile affinity**	**Paleontological name**	**T1**	**T2**	**EAS**	**WAS**
1	A	Unknown	*Bitectatodinium spongium*[4,5&6]	2.0	0.0	+	+
2	A	*Gonyaulax* sp. Indet.	*Impagidinium aculeatum*[4&6]	3.8	3.5	+	+
3	A	*Gonyaulax* sp. Indet.	*Impagidinium paradoxum*[4&6]	9.6	7.8	+	+
4	A	*Gonyaulax* sp. Indet.	*Impagidinium patulum*[6]	1.8	0.5		+
5	A	*Gonyaulax* sp. Indet.	*Impagidinium* sp.	1.1	0.0	+	+
6	A	*Gonyaulax* sp. Indet.	*Impagidinium strialatum*[6]	1.0	4.7		+
7	A	*Gonyaulax spiniferites* complex	*Nematosphaeropsis labyrinthus*[4&6]	5.3	4.1	+	+
8	A	Unknown	*Nematosphaeropsis sp.*	0.0	7.0	+	+
9	A	*Protoperidinium reticulatum*	*Operculodinium centrocarpum*[1-6]	4.2	4.0	+	+
10	A	Unknown	*Operculodinium janduchenei**	1.2	3.0		
11	A	Unknown	*Operculodinium* sp.	0.3	0.3	+	+
12	A	*Pyrodinium bahamense*	*Polysphaeridium zoharyi*[3,5&6]	0.6	0.1	+	+
13	A	*Gonyaulax nezaniae*	*Spiniferites bentorii*[4&6]	0.1	0.0	+	+

14	A	*Gonyaulax whaseongensis*	*Spiniferites hyperacanthus*[4]	4.0	1.0	+	+
15	A	*Gonyaulax spiniferites* complex	*Spiniferites mirabilis*[1,3,4&6]	12.1	2.2	+	+
16	A	*Gonyaulax spiniferites* complex	*Spiniferites ramosus*[1,3,4&6]	27.2	22.5	+	+
17	A	*Gonyaulax spiniferites* complex	*Spiniferites* sp.	17.5	30.6	+	+
18	A	*Pyrophacus steinii*	*Tuberculodinium vancampoae*[2,3,5&6]	2.5	0.0	+	+
19	M	*Polykrikos hartmannii*	Cyst of *Polykrikos hartmannii*[1-3, 5&6]	0.5	0.1	+	+
20	M	*Lingulodinium polyedrum*	*Lingulodinium machaerophorum*[1-6]	1.4	0.4	+	+
21	M	*Lingulodinium* sp.	*Lingulodinium* sp.	4.4	9.2	+	+
22	H	*Protoperidinium* sp.	*Brigantedinium simplex*[5&6]	0.2	0.0	+	+
23	H	*Protoperidinium conicoides*	*Brigantedinium* sp.[2,5&6]	0.0	0.1	+	+
24	H	*Cladopyxis* sp.	Cyst of *Cladopyxis* sp.*	0.1	0.0		
25	H	*Polykrikos kofoidii*	Cyst of *Polykrikos kofoidii*[2-5]	0.1	0.0	+	+
26	H	*Polykrikos schwartzii*	Cyst of *Polykrikos schwartzii*[1-3,5&6]	0.6	0.0	+	+
27	H	*Protoperidinium denticatum*	Cyst of *Protoperidinium denticatum*[3&5]	0.3	0.0	+	
28	H	*Protoperidinium latissimum*	Cyst of *Protoperidinium latissimum*[1,3&5]	0.2	0.0	+	

29	H	*Protoperidinium monospinum*	Cyst of *Protoperidinium monospinum**	0.6	0.0		
30	H	*Protoperidinium* sp.	Cyst of *Protoperidinium* sp.	1.9	4.2	+	+
31	H	Diplopsalid or Protoperidinioid group	*Echinidinium* sp.[4&6]	6.8	11.8	+	+
32	H	*Protoperidinium leonis*	*Lejeunecysta sabrina*[5]	0.2	0.0	+	
33	H	*Protoperidinium subinerme*	*Selenopemphix nephroides*[1-6]	2.4	3.2	+	+
34	H	*Protoperidinium conicum*	*Selenopemphix quanta*[2-6]	1.8	0.1	+	+
35	H	Unknown	*Selenopemphix* sp.	0.0	0.5	+	+
36	H	Unknown	*Stelladinium bifurcatum**	0.0	0.1		
37	H	*Protoperidinium* spp.	*Stelladinium reidii*[4&6]	1.5	0.6	+	+
38	H	*Protoperidinium compressum*	*Stelladinium stellatum*[2-4&6]	0.1	1.4	+	+
39	H	*Protoperidinium pentagonum*	*Trinovantedinium applanatum*[1-6]	0.3	0.1	+	+
40	H	*Protoperidinium oblongum*	*Votadinium calvum*[1,3,5&6]	0.5	0.7	+	+
41	H	*Protoperidinium steidinferae*	*Votadinium* sp.	0.1	0.0	+	+
			Sum	**118**	**124**		

Note: Superscript numbers indicate species previously reported in those references, i.e., 1. Godhe et al., 2000; 2. D'costa et al., 2008; 3. D'silva et al., 2011; 4. Narale et al., 2015 5. Rodrigues et al., 2022 and 6. Zonneveld et al., 2013.

Overall, the comparison of cyst assemblage data revealed that the species count (including HAB species) and cyst concentration recorded in this study is low compared to the previous studies (Figure 3.19). This study revealed the widespread occurrence of 21 species in IO (NIO and SIO). Most cosmopolitan dinoflagellate cyst species are autotrophic (67%), belonging to motile dinoflagellates of the *Gonyaulax* genus. Among all the recorded species, 47 (98%) and only 21 (44%) were recorded in NIO and SIO, respectively. Also, 27 species (56%) were restricted to NIO, and only 1 species (2%) to SIO. Previously, 43 species (90%) in AS, 34 species (71%) in BoB, and 31 species (65%) in SIO were reported from the regions, respectively. In the NIO one (*Stelladinium abei*) and SIO 4 (cyst of *Alexandrium* sp., *Pentapharsodinium dalei,* cyst of *Cladopyxis* sp., and *Stelladinium stellatum*), dinoflagellate cyst species were not reported previously.

3.2.3.3. Morphometric variability in the cosmopolitan species

The body size of *Operculodinium centrocarpum* showed significant variability ($p>0.001$) among all the bioregions except STIO, whereas the process length was significantly different ($p>0.001$) in all the regions (C-AS: d=36 µm, and PL=2 µm; O-AS: d=33±4 µm, and PL=7±2 µm; OMZ-AS: d=31±4 µm, and PL=6±1 µm; BoB: d=50±13 µm, and PL=12±4 µm; EIO: d=31±9 µm, and PL=7±2 µm; STIO: d=38±0.6 µm, and PL=8±0.2 µm). The highest body size and process length were recorded in BoB and the least in OMZ-AS and C-AS, respectively (Figure 3.20a-b). However, the variations were within the reported size ranges (d=33-48 µm and PL=7-14 µm). The body size of *Nematosphaeropsis labyrinthus* showed no significant differences among the bioregions except between O-AS and OMZ-AS, whereas process length varied significantly ($p>0.05$) among the bioregions except between OMZ-AS and EIO (O-AS: d=24 µm, and PL=12 µm; OMZ-AS: d=22 µm, and PL=11 µm; EIO: d=23±0.6 µm, and PL=11±2 µm; STIO: d=27±1.2 µm, and PL=17±2.2 µm). The highest body size and process length were recorded in STIO, and the lowest in OMZ-AS (Figure 3.20c-d). However, the variations were within the reported size ranges (d=27-42 µm and PL=11-23 µm). The body size and process length of *Impagidinium patulum* showed significant variability ($p>0.001$) only between O-AS and EIO (O-AS: W=57±4 µm, and PL=6±1 µm; OMZ-AS: W=51±7 µm, and PL=5±1 µm; STIO: W=50 µm, and PL=4±1 µm; EIO: W=44±10 µm, and PL=5±2 µm). The highest body size and process length were recorded in O-AS and the least in EIO and STIO, respectively. The body size of *Impagidinium strialatum* showed no significant differences among the bioregions, whereas process length varied significantly

(p>0.05) among BoB, EIO, and STIO (STIO: PL=6±1 µm; EIO: PL=5±1 µm; OMZ-AS: PL=5±0.4 µm; O-AS: PL=5±1 µm; BoB: PL=4±0.3 µm).

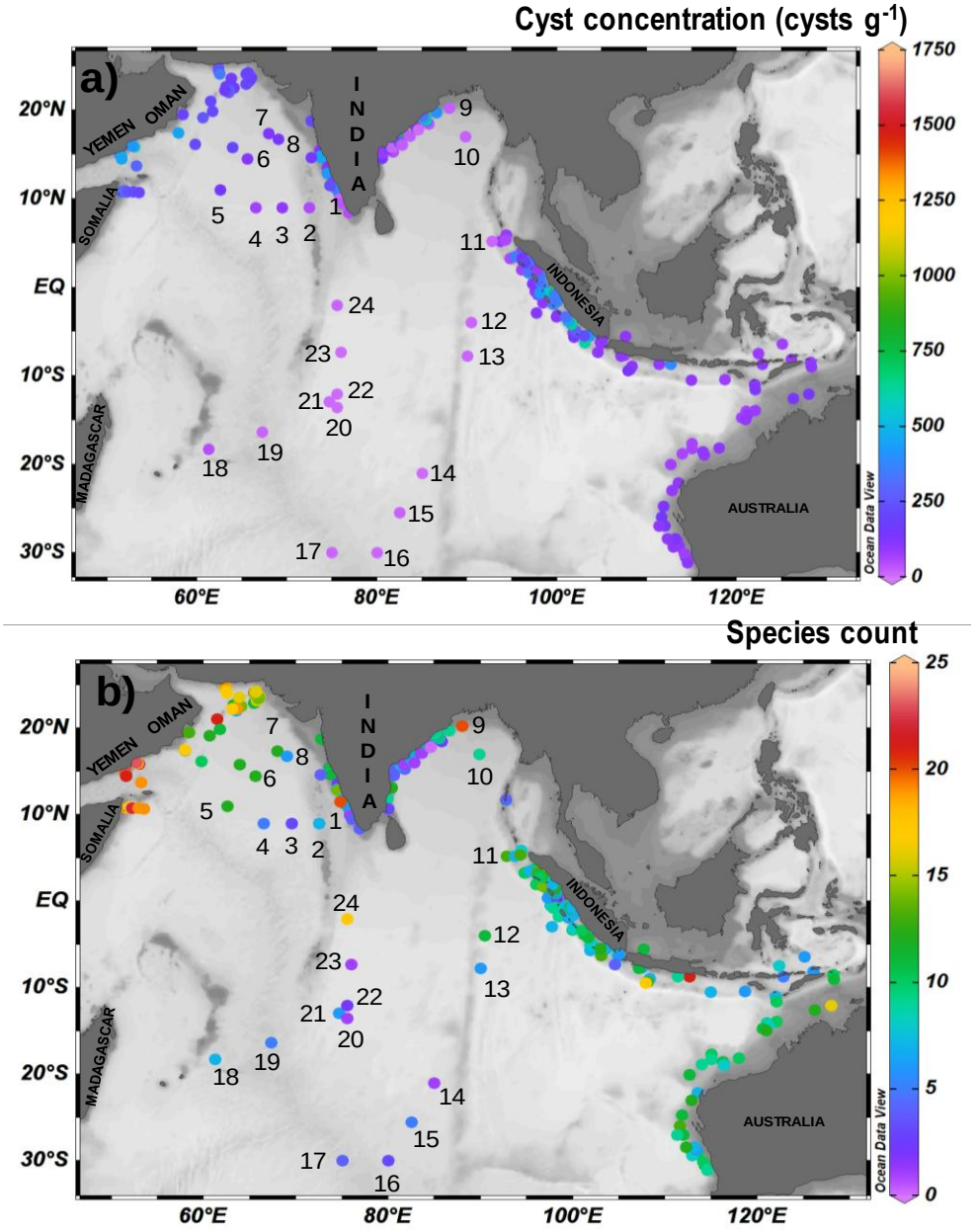


Figure 3.19. Plots showing comparative data for dinoflagellate cysts in the Indian Ocean a) dinoflagellate cyst concentration (cysts g^{-1}) and b) Species count. Present study locations are represented using numbers, and unnumbered dots represent previous studies. Data for species count and concentration for comparison are taken from Zonneveld et al., 2013; D'Silva et al., 2011; Narale et al., 2015; Dcosta et al., 2008 and Rodrigues et al., 2022.

The highest process length was recorded in STIO, and the lowest was in BoB. The body size and process length of the cyst of *Pentapharsodinium dalei* varied significantly ($p>0.05$) between BoB and STIO, showing smaller sizes in BoB than in STIO (STIO: d=28±3 µm and PL=6±1 µm; EIO: d=25±1 µm; BoB: d=19±0.1 µm, and PL=4±0.3 µm). The body size and process length of *Spiniferites hypercanthus-merabilis* varied significantly ($p>0.05$) between AS and BoB, showing smaller sizes in BoB than in AS (AS: PL=5±1 µm; BoB: PL=4±0.3 µm; BoB: d=19±0.1 µm, and PL=4±0.3 µm). The other cosmopolitan dinoflagellate cysts showed no significant morphometric variations in the bioregions of the IO.

3.2.3.4. Plankton drift simulations to track the origin of dinoflagellate cysts

The planktondrift simulations of dinoflagellate cysts revealed different transport patterns for the stations located in the AS, BoB, EIO, and STIO regions, suggesting different origins. The transport scenarios for the AS dinoflagellate cysts revealed different transport patterns for the stations located in coastal, oligotrophic, and OMZ regions, suggesting different origins. For instance, the lateral transport of the dinoflagellate cysts in coastal station 1 and station 2 is confined over a small region, whereas stations 3 and 4 show some overlapping, and station 5 has the maximum lateral transport even from the western AS and OMZ region. However, in OMZ stations (6, 7, and 8), the lateral transport of the dinoflagellate cysts was also relatively large but confined to the OMZ region to a larger extent.

The lateral transport of dinoflagellate cysts in the coastal BoB station (9) was confined to a small region, contrary to the other two stations where the lateral transport covered a larger area. For instance, in station 10, the spread was from the adjacent coastal region to the pelagic region, in station 11, the lateral transport shows contribution from the Andaman Sea and the northern coastal regions of Indonesia. The lateral transport was over a much larger area in the EIO (stations 12, 13, 23, and 24) than in the STIO, with all the stations overlapping each other. The four stations between 20^{o}S-30^{o}S (stations 15-17) in the STIO overlapped but were more confined in the area (Figure 3.21).

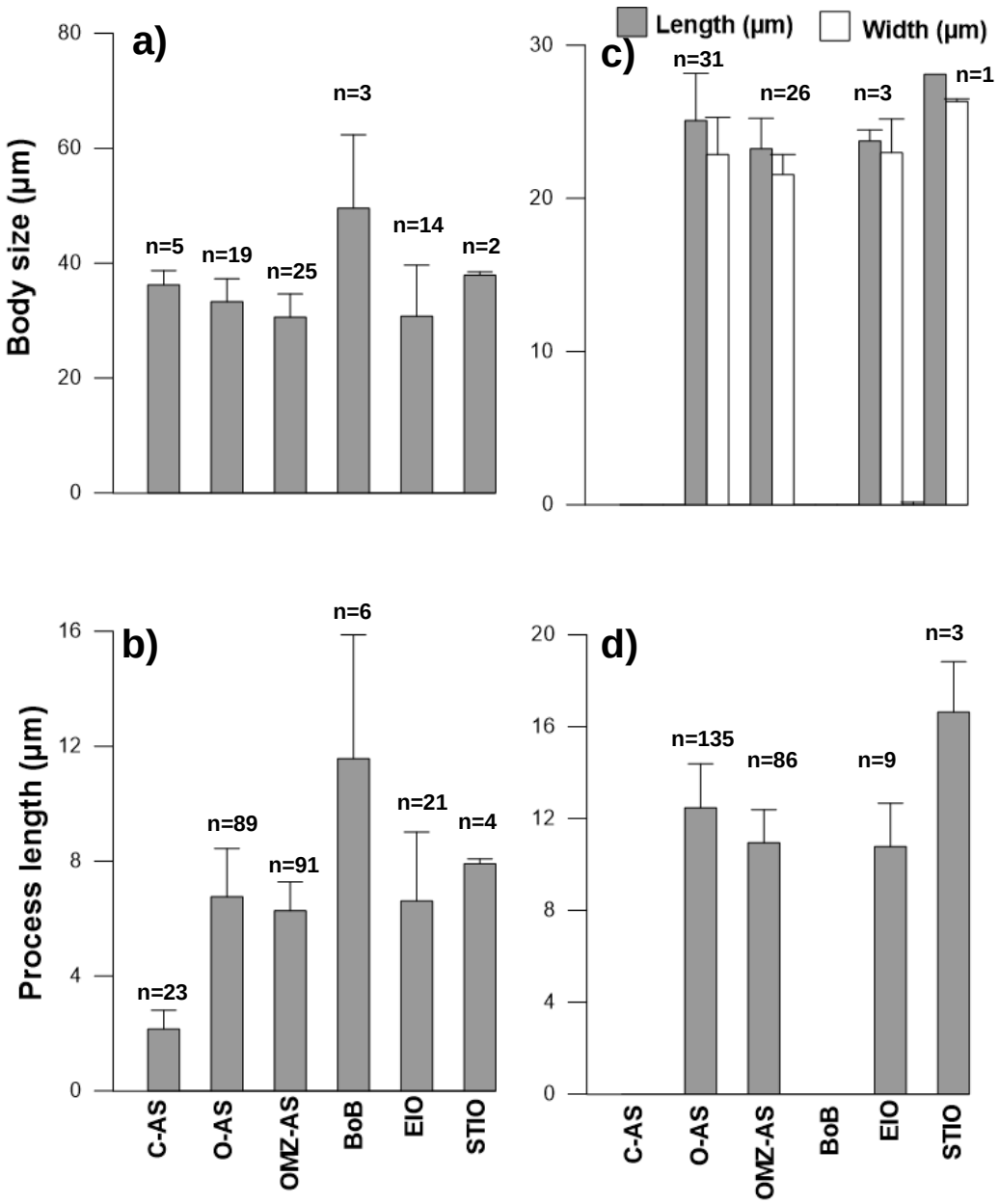


Figure 3.20. The plot shows morphometric measurements of dinoflagellate cyst body size (L=length, W=width, and D=diameter) and process length (PL) in the Indian Ocean. **i)** *Operculodinium centrocarpum* a) body size (diameter) and b) process length, and **ii)** *Nematosphaeropsis labyrinthus* c) body size (length and width) and d) process length. C-AS: coastal Arabian Sea, O-AS: oligotrophic Arabian Sea, OMZ-AS: oxygen minimum zone Arabian Sea, BoB: Bay of Bengal, EIO: the equatorial Indian Ocean, and STIO: south tropical Indian Ocean.

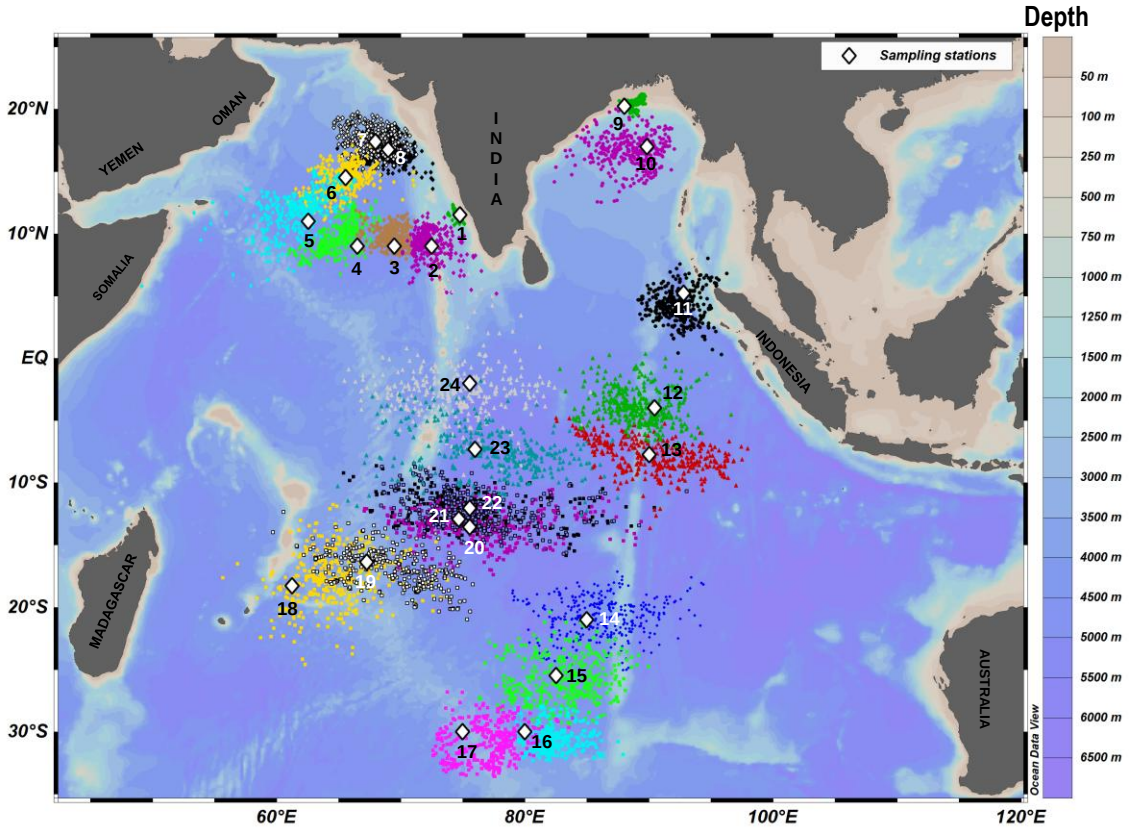


Figure 3.21. The map shows the possible surface origin locations of the sinking particles by the ocean currents for a sinking speed of 11 m/day. The data points are generated from the planktondrift.science.uu.nl website and plotted in the ODV using a surface plot.

3.2.4. Discussion

3.2.4.1. Dinoflagellate cyst diversity and distribution

The study on dinoflagellate cyst diversity and distribution from the recent sediments of the IO revealed 48 species. The highest dinoflagellate cyst concentration was recorded at 113m in the coastal AS (in NIO) and the lowest at 5200m in the EIO (in SIO). The AS in the NIO is known to be more productive than the oligotrophic EIO and STIO regions of the SIO (Dalabehara & Sarma, 2021). Therefore, the upper water column productivity can determine the dinoflagellate cyst concentration in the underlying sediment. Additionally, the low oxygen in the OMZ depths might also help in better preservation and low microbial degradation of the dinoflagellate cyst (Wendler et al., 2002), which is otherwise susceptible to oxidative degradation like organic matter (Zonneveld et al., 1997). Interestingly, the NIO is well known for two OMZ regions, one in the Arabian Sea and the other in the Bay of Bengal. The particulate organic carbon (POC) sinking flux to the deep sea (>2500 m) is reported to be one of the highest in the NIO (4-13 mg m^{-2} d^{-1}; Sarma et al., 2007) and one of the lowest in SIO (0.50 mg m^{-2} d^{-1}; Harms et al., 2021) among the world oceans. Therefore, less dinoflagellate cyst concentration in the sediment of the oligotrophic region (i.e., SIO) than in the relatively productive region (i.e., NIO) is obvious. It signifies distinct geographic patterns of dinoflagellate production in the water column and their preservation in the underlying sediment influenced by the OMZ regions.

The NIO dinoflagellate cyst community was dominated by *Spiniferites ramosus* and *Spiniferites* sp. The *Spiniferites* is one of the most common dinoflagellate cyst genera reported from recent and past dinoflagellate cyst populations (de Vernal et al., 2018). It has also been reported in higher concentrations from the northwest AS (Zonneveld & Brummer, 2000). Also, *Spiniferites* are known to be moderately sensitive to the presence of oxygen (Zonneveld & Brummer, 2000), and the presence of OMZ in the NIO might play a significant role in its preservation in the underlying sediment. The *Spiniferites* sp. are characteristic of neritic environments but are also reported from open ocean sites (Rochon et al., 1999; Marret & Zonneveld, 2003). However, due to the large morphological variability among different species of *Spiniferites* it has been difficult to assign them to specific species correctly. Therefore, many researchers represent their results after grouping several species of *Spiniferites* at the genus level (Hessler et al., 2013; de Vernal et al., 2018; Pespelova et al., 2018), which might have distinct ecological preferences (de Vernal et al., 2018). Therefore, the inferences linking *Spiniferites* to specific environmental conditions could be speculative and must be treated cautiously.

Contrary to *Spiniferites*, *Spiniferites ramosus* is very distinct and easy to identify and occurs in a wide range of environmental conditions (8.5-17.2^{o}C; 33.2 ± 5.2 PSU). The distribution of *S. ramosus* is also cosmopolitan (Zonneveld et al., 2013) and reported from mid-latitudes (de Vernal et al., 2018) to low latitudes (Hessler et al., 2013).

The dinoflagellate cyst of *Pentapharsodinium dalei* dominated the assemblages in the SIO. cyst of *P. dalei* is also considered to be a cosmopolitan species (Marret & Zonneveld, 2003) and has been reported from coastal to deep-sea in all the latitudes (Radi et al., 2001; Marret & Zonneveld, 2003; Pospelova et al., 2008). Though the cyst of *P. dalei* is considered a cold-water species, it has previously been reported from outer harbor regions in the BoB associated with low nutrient conditions (D'Silva et al., 2013) and China Sea with several genetically and morphologically different morphospecies (Gu et al., 2013). However, cyst of *P. dalei* shows a preference for cool temperate to sub-polar conditions and can occur in a wide range of temperatures (0-29.6^{o}C) and salinity (21.3-36.7 PSU) (Candel et al., 2012; Marret & Zonneveld, 2003; Radi & de Vernal, 2008). The proximity of SIO stations (especially STIO) to the polar region might have contributed to the assemblage in the bottom sediment. Further, many stations in the SIO region recorded a very low dinoflagellate cyst concentration. Two reasons might contribute to such low cyst concentration: i) planktonic dinoflagellate abundance and their cyst-forming potential (Dale, 1983; Dale, 2001), and ii) the prevailing sediment texture in the area. The SIO region is well-known to be an oligotrophic region (Dalabehara & Sarma, 2021; Harms et al., 2021) with coarser sediment dominated by silicious ooze (Pattan & Jauhari, 2001). However, the present study's sediment texture analysis revealed finer-grained sediments (mostly silty-clayey) prevailing in SIO. Though various studies have reported higher dinoflagellate cyst concentration in finer-grained (silt and clayey) sediment than in coarser sediment (Dale, 1976; Dale, 1983; Hallegraeff et al., 2003; Narale et al., 2013; Narale & Anil, 2017), such inferences might not be valid for pelagic regions with prevalent oligotrophic conditions in the upper water column.

The other most common dinoflagellate cysts were *Impagidinium aculeatum* and *Nematosphaeropsis labyrinthus*, majorly reported from the oligotrophic pelagic regions of the IO. These two dinoflagellate cysts are mostly reported from the outer neritic to oceanic environments (Matthiessen, 1995; Zonneveld & Brummer, 2000; Eldrett & Harding, 2009) and are characterized by oligotrophic surface waters (Zonneveld et al., 1997). *I. aculeatum* and *N. labyrinthus* are also moderately resistant to oxygen availability and are often characterized as oceanic species (Zonneveld & Brummer, 2000). Their

presence throughout the surface sediments of the AS, though in low concentrations, has been previously reported (Zonneveld, 1997; Zonneveld & Brummer, 2000).

Interestingly, the IO dinoflagellate cyst assemblage was dominated by autotrophic species except BoB, which the heterotrophic dinoflagellate cyst dominated. The autotrophic dominance of the dinoflagellate cyst in the pelagic region is opposite to the heterotrophic dominance in the coastal region of the IO (except BoB). The previous studies on dinoflagellate cyst (D'Silva et al., 2013; Narale et al., 2013; Uddandam et al., 2015; Uddandam et al., 2017) from the BoB (including the Andaman Sea) have also reported the dominance of heterotrophic forms which agrees with our findings. Generally, the dominance of autotrophs is attributed to higher planktonic production (Dale, 1983; Anderson et al., 1995; Joyce et al., 2005), whereas the dominance of heterotrophs is attributed to the availability of prey (e.g., diatoms) (Matsuoka et al., 2003; Godhe & McQuoid, 2003), and reduced light intensity (Dale, 2001b). The BoB is known for suspended riverine load causing low light penetration (Narale et al., 2013) and diatom dominance (Madhu et al., 2006); heterotrophic dinoflagellate cyst dominance is inevitable. Several harmful dinoflagellates are known to produce cysts, which might settle in the sediment and can serve as the precursor for blooms. Therefore, dinoflagellate cysts are meticulously monitored for HAB monitoring (Anderson et al., 2012; Ribeiro et al., 2012), and this study provides an overview of the geographic distribution of potential HAB species from the IO.

3.2.4.2. Transport scenarios for dinoflagellate cyst in the IO

The dinoflagellate cyst accumulation and distribution in the sediment also depend on the lateral transport during their sinking through the water column or re-suspension by bottom currents (Anderson et al., 1985; Zonneveld & Brummer, 2000; Hessler et al., 2013). The dinoflagellate cysts might be transported over a long distance from their original location of formation by moving water masses. Nooteboom et al. (2019) have reported the displacement of dinoflagellate cyst up to 1570 km under the influence of currents from the surface origin till they reach the ocean floor. Such large-scale transportation can assume a direct relationship between cysts in bottom sediments and prevailing environmental conditions in the immediately overlying surface waters, which is a challenge (Dale, 1996; Verleye et al., 2012). Therefore, the extent of lateral transport of dinoflagellate cyst should be considered when interpreting surface water conditions using sediment. Based on the prevailing known conditions, the NIO (AS and BoB) shares similar monsoonal forcing and seasonal wind patterns (Prasad, 2004) and is also

characterized by OMZ in the water column (Naqvi et al., 2006; Sarma et al., 2013). The persistence of lateral intrusion of the Persian Gulf Water (PGW) and Red Sea water (RSW) in the AS can also transport dinoflagellate cyst from the Northwestern AS to the ocean basin. However, few previous studies (Abidi, 1997; Zonneveld & Brummer, 2000) have suggested no long-distance lateral transport of dinoflagellate cysts in the West Indian Ocean and Northwestern AS. Abidi's (1997) argument is based on the match found between oceanographic boundaries and the recorded cyst assemblages and similar biogeographic distributions of dinoflagellate cyst taxa and foraminifer taxa. In contrast, the planktondrift simulation in the present study showed basin-wide lateral transport of dinoflagellate cysts in the AS basin. The dinoflagellate cyst's surface origin and lateral transport are well discussed in Paul and Patil (2024) for the AS basin. The planktondrift simulations (Figure 7) broadly revealed the following: (i) The dinoflagellate cyst in the BoB showed large-scale lateral transport (except for the coastal station), which could be due to the East Indian Coastal Current (EICC), which reverses directions twice a year and forms the western boundary current of a basin-wide anticyclonic gyre, (ii) in SIO, the bottom layers are occupied by the Antarctic Bottom Water (ABW), Indian deep waters (IDW), and upper ocean waters from the Pacific Ocean entering through the Indonesian Through Flow (ITF) (Qian et al., 2004) might be influencing the lateral transport of dinoflagellate cyst in the basin. However, the planktondrift simulations showed more lateral transport over a larger area for EIO and few stations of STIO (above 20^{o}S), whereas four stations in STIO (20^{o}S-30^{o}S) showed much confined small-scale lateral transport of the dinoflagellate cyst considering 11 m/day sinking speed scenarios (Figure 3.12). Therefore, basin-wide lateral transport could have influenced the distribution of more cosmopolitan dinoflagellate cysts in the NIO than in the SIO. Thus, the present study attempted to understand the lateral transport scenarios and their possible contribution to controlling the dinoflagellate cyst assemblages in the pelagic regions of the IO for the first time.

3.2.4.3. Comparison of dinoflagellate cyst assemblages with previous studies in the IO

The global studies on dinoflagellate cysts from the world oceans are aptly compiled by Zonneveld et al. (1997 and 2013) and Marret and Zonneveld (2003). The compilations help understand the biogeographical distribution of dinoflagellate cysts and highlight the study gaps. Though dinoflagellate cysts have been thoroughly studied from the coastal regions of the eastern AS (Godhe et al., 2000; D'costa et al., 2008; Dsilva et al., 2011, 2012; Narale et al., 2015; Rodrigues et al., 2019, 2022), western AS (Zonneveld et al.

1997, and 2013; Zonneveld & Jurkschat, 1999), and BoB (Naidu et al., 2012; D'Silva et al., 2013; Narale & Anil, 2017; Narale et al., 2013; Uddandam et al., 2017; Uddandam et al., 2015; Uddandam et al., 2020), and coastal areas within south-east Asian regions (Matsuoka, 1981; Kumar, 1996; Matsuoka et al., 1999; Azanza et al., 2004; Kawamura, 2004; Furio et al., 2006; Hessler et al., 2013), studies from the pelagic regions are none and have been pointed out several times in various studies (Marret & Zonneveld, 2003; Zonneveld et al., 2013; Marret et al., 2020). This study from the least studied pelagic IO regions revealed 21 dinoflagellate cysts as cosmopolitan, while 27 and 1 dinoflagellate cyst species are confined to NIO and SIO, respectively. The comparison revealed that 9%, 32%, and 38% of dinoflagellate cysts were not reported previously and recorded only in the present study. Moreover, one dinoflagellate cyst species in NIO (*Stelladinium abei*) and four in SIO (cyst of *Alexandrium* sp., cyst of *Pentapharsodinium dalei,* cyst of *Cladopyxis* sp. and *Stelladinium stellatum*) were not reported previously. So far 16 potential HAB cyst species have been reported from the coastal regions of AS and BOB (e.g., *Alexandrium affine, Alexandrium minutum, Alexandrium tamarense, Alexandrium cf. tamiyavanichi, Gonyaulax spinifera* complex, *Gymnodinium catenatum, Lingulodinium machaerophorum, Operculodinium centrocarpum, Polysphaeridium zoharyi, Scrippsiella trochoidea, Pheopolykrikos hartmannii, Gymnodinium cf. catenatum, Blixaea quinquecornis, Gonyaulax scrippsae, Scrippsiella acuminata,* and *Diplopsalis lenticula*) (D'Silva et al., 2013; Narale et al., 2013; Narale & Anil, 2017; Uddandam et al., 2017; Hessler et al., 2013; D'costa et al., 2008; D'silva et al., 2011; Rodrigues et al., 2022). All 16 species are documented from coastal AS and only 11 from BoB (except *Gymnodinium cf. catenatum, Blixaea quinquecornis, Gonyaulax scrippsae, Scrippsiella acuminata,* and *Diplopsalis lenticula*). Interestingly, of the 16 species, only 6 (~37%) are reaching deeper depths (>5000m). Further, their contribution was higher in NIO (8%-32%) than in EIO (6%) and STIO (>1%). Given this, HAB species might be of concern for the coastal stations rather than the deeper stations (i.e., SIO) despite some reaching deeper parts. Among the recorded 6 potential HAB species, 5 (e.g., *Polysphaeridium zoharyi, Lingulodinium machaerophorum* as well as cysts of *Alexandrium* sp., *Gonyaulax* spp., and *Polykrikos hartmannii*) are region specific while the lone *Operculodinium centrocarpum* was widespread in NIO and SIO. *O. centrocarpum,* known for producing yessotoxin, is one of the dominant cosmopolitan species reported from both hemispheres, with relatively higher abundance in temperate and polar regions than in subtropical and tropical regions (Marret et al., 2020). It has been

reported from the Pacific and Atlantic Oceans and many seas (except Caspian and Aral seas). Previously, *O. centrocarpum* was reported from the coastal NIO, and this study expanded its biogeographic distribution to deeper depths. While this study forms a benchmark, more in-depth studies from different core depths using approaches such as morphometrics, metagenomics, and germination are warranted for understanding their biogeographic distribution as they are of greater importance for reconstructing past climates in palaeoceanographic (Bijl et al., 2021) and species dispersal studies (Nooteboom et al., 2019).

3.2.4.4. Morphometric variabilities in cosmopolitan dinoflagellate cysts and potential proxy

The morphological variations reported in the dinoflagellate cyst show a relationship with water properties, particularly the process length changes as a function of salinity and temperature (Mertens et al., 2012a; Mertens, 2013; Verleye et al., 2012). The first dinoflagellate cyst, used as a proxy for its variable process length in response to salinity, was *Lingulodinium machaerophorum* from the Black Sea (Wall et al., 1973). There are other dinoflagellate cyst species in which the process length (reduced) indicates lower salinity conditions like *Operculodinium centrocarpum* (Dale, 1996; Nehring, 1997; Ellegaard, 1998), cysts of *Pentapharsodinium dalei* (Nehring, 1994; 1997) and several *Spiniferites* species (Wall et al., 1973; Dale, 1996; Lewis et al., 1999; Ellegaard et al., 2002). The present study observed morphological variations in a few cosmopolitan dinoflagellate cysts, which varied according to cyst type. For instance, cosmopolitan potential HAB cysts, *O. centrocarpum* showed body size and process length variations among all the bioregions except STIO. The highest process length was recorded in BoB (station 3), and the lowest was C-AS. Interestingly, the sea surface salinity in C-AS was found to be lower (34 PSU) than BoB (station 3; 35 PSU), though salinity was lowest in the coastal stations of BoB (stations 1 and 2; 31 PSU), but unfortunately, cyst of *O. centrocarpum* was not recorded in those stations. Further, the cyst of *Pentapharsodinium dalei* showed significant morphometric variability in both body size and process length, whereas BoB showed smaller sizes than in STIO. In this case, the cyst of *P. dalei* was recorded from station 2 in BoB with a lower surface salinity (31 PSU) than STIO (35 PSU). Similarly, the body size and process length of *Spiniferites mirabilis-hyperacanthus* also varied significantly between AS and BoB, showing smaller sizes in the latter than the former in response to the lower (31 PSU) and relatively higher salinity (35 PSU) in the respective regions. The *Impagidinium strialatum* and *Nematosphaeropsis labyrinthus*

cysts showed significant differences in the process length but not in body size, recording the highest process length in STIO and the lowest in BoB and OMZ-AS, respectively. However, there are no studies available on the morphometric variability of *I. strialatum* and *N. labyrinthus* to salinity, but few studies have reported their association with higher surface temperature (Zonneveld, 1997; Crouch et al., 2010; Gallagher & Wagstaff, 2021). However, the morphometric variabilities in these pelagic dinoflagellate cyst species (*I. strialatum* and *N. labyrinthus*) are measured from a small number of cysts (<10), so the results might not be reproducible (Verleye et al., 2012). Therefore, cyst morphometric studies from low cyst concentrations in oligotrophic pelagic regions might be a challenge. Hence, it can be assumed that most cosmopolitan dinoflagellate cysts showed morphological variability in IO. Several studies across the oceans have documented morphological variability in dinoflagellate cysts (e.g., Ellegaard et al., 2002; Mertens et al., 2009a, 2009b, 2010, and 2012a, b; Mertens, 2013), and so far, only a few from IO (Rodrigues & Patil, 2021; Paul & Patil, 2024). However, morphological variability-related studies require a higher concentration of dinoflagellate cysts; therefore, such studies from low cyst concentration areas like SIO become challenging. Hence, more studies, especially from SIO, would facilitate the application of morphometry as a proxy in the pelagic regions. Nonetheless, this study will serve as the baseline data from a less-studied pelagic region of the IO.

3.2.5. Conclusion

This study provides the first account of dinoflagellate cyst distribution and diversity from the pelagic regions of productive NIO and oligotrophic SIO. The findings reveal the presence of dinoflagellate cysts in the deepest depths (~5000m) of the IO. NIO harbors more cysts (including HAB types) than SIO, with autotrophic dinoflagellates dominating the community (except for BOB). Almost 40% of identified cysts (*Impagidinium strialatum*, *Operculodinium centrocarpum*, *Spiniferites* sp., *Nematosphaeropsis labyrinthus*, and *Echinidinium* sp.) were cosmopolitan, while the remaining were region-specific. Further, 9%, 32%, and 38% of dinoflagellate cysts are reported for the first time from AS, BoB, and SIO, respectively. The lateral transport of dinoflagellate cyst and its influence on the assemblage is studied for the first time. Moreover, variability in the morphology of some cosmopolitan dinoflagellate cysts (including potential yessotoxin-producing *O. centrocarpum*) was observed, indicating potential environmental proxies

for IO. Nevertheless, this study will contribute to the growing knowledge of dinoflagellate cyst biogeography and fill a long-overdue research gap, particularly from the IO.

Chapter 4

Delineating the phytoplankton distribution patterns based on taxonomic and functional classification

Chapter 4: Delineating the phytoplankton distribution patterns based on taxonomic and functional classification

The phytoplankton distribution and community assemblages are generally studied based on taxa without emphasizing the morphological traits and their role in the functional classifications. Even though the functional classification based on morphological traits has great potential to increase our insight into the organization of ecological communities and to predict their reorganization under any environmental change. The functional classification-based approach in studying phytoplankton community assemblages has become more popular in freshwater ecosystems (Margalef, 1978; Reynolds, 1988; Weithoff, 2003; Salmaso & Padisak, 2007; Litchman & Klausmeier, 2008; Kruk et al., 2010; Naselli-Flores & Barone, 2011, Martini et la., 2021; Laraib et al., 2023; Naselli-Flores & Padisak, 2024) than in marine ecosystems (Stanca et al., 2013; Barton et al., 2013; Litchman et al., 2007, 2015; Finkel et al., 2010; Mao et al., 2024), and so far, no studies from the Indian subcontinent. Given the above, the phytoplankton morphological traits and adaptations were studied from different marine habitats (i.e., intertidal and pelagic). The phytoplankton morphological traits and adaptations from different habitats might provide holistic knowledge about their adaptive strategies and lead to a better understanding of phytoplankton ecology. This chapter is divided into two sub-chapters, 4.1 and 4.2, describing results from the intertidal and pelagic ecosystems.

4.1. The intertidal ecosystem

In this sub-chapter, phytoplankton distribution based on morphological traits was studied from two intertidal ecosystems, rock pools, and tidal flats, and the details are described in subsequent sections 4.1.1. and 4.1.2.

4.1.1. Rockpools and tidal flats

4.1.1.1. Introduction

Rock pools (RPs) are a prominent component of any rocky intertidal habitat and are extensively studied for their diverse invertebrate fauna. The microalgal community assemblage, dynamics, and structure on a temporal and spatial scale, various biotic (grazing and interactions with different rock pool inhabitants) and abiotic (nutrient, light, temperature, salinity, tidal influence, pool size, and dimensions) factors influencing the assemblages and succession (Huggett & Griffiths, 1986; Metaxas & Scheibling, 1993, 1994, 1996a, b; Underwood & Skilleter, 1996; Norberg, 1998; Therriault & Kolasa, 2001;

Martins et al., 2007; Anusa et al., 2012; Soininen & Meier, 2014; Haggqvist & Lindholm, 2015, 2016; Rishworth et al., 2017; DaSilva et al., 2020) of rock-pools have been extensively studied throughout the world in fresh, brackish and marine ecosystems but not in the Indian sub-continent. The small size with well-defined boundaries, rock pools can serve as perfect mesocosms to study the phytoplankton community dynamics (Metaxas & Scheibling, 1994, 1996a). Microalgae from the adjacent waters are introduced into the rock pools because of the tidal action and remain isolated from the adjacent seawater depending on the tidal amplitude and location of the rock pools on the shore (Metaxas & Scheibling, 1994). The importance of the tidal cycle in deciding the biotic and abiotic components of the rock pools is greatly acknowledged (Metaxas & Scheibling, 1993). Even though the Indian coastline has a significant number of rocky shores (~600 km) abundant with rock pools, it has not received the attention for microalgal research. Rock pools play a very important role in the intertidal ecosystem and can serve as a seed bank (Baig et al., 2006; Patil et al., 2017) or even cause toxic algae bloom, causing fishkill (Murray et al., 2015). Since RP microalgae experience/tolerate various orders of environmental variability (like temperature, salinity, light, and anthropogenic disturbances) on a very short temporal scale, they are referred to as eurythermal, euryhaline, and euryphotic (Patil et al., 2017). Therefore, to cope with such extreme conditions, RP microalgae constantly compete through various physiological, morphological, and biochemical adaptations, like changes in morphology and shape, producing specific enzymes/pigments/compounds, different nutrient acquisition strategies (like mixotrophy) and vertical migration (Legrand et al., 2003). Among them, the prevalence of physiological adaptation (photoprotection and photoinhibition) in RP microalgae was reported in a separate study (Patil et al., 2017). However, the present study characterizes the phytoplankton community based on the species composition and the morphological traits of the RPs located at different tidal levels. Also, the role of the allelopathic effect of dominant microalgae on the selected planktonic and benthic microalgae was elucidated. Various functional traits are being used to understand the functional role of a particular organism in a given ecosystem (Padisak et al., 2003; Litchman & Klausmeier, 2008). Phytoplankton assemblages under variable environmental conditions can perhaps be shaped by size and form selection in natural environments (Morabito et al., 2007). Various geometric shapes of microalgae co-existing together in an ecosystem is a form of adaptive strategy responding to the fluctuating environment (Margalef, 1978; Reynolds, 2006; Naselli-Flores et al., 2007).

The functional classification approach has already been applied to understand the rock-pool microalgal assemblage and has proved useful (Haggqvist & Lindholm, 2015). Shape, being the simplest morphological attribute, carries ecological information as the environmental forcing influences it significantly (Grover, 1989; Sommer, 1998; Padisak et al., 2003; Naselli-Flores et al., 2007; Karp-Boss & Boss, 2016). Using microalgae shapes can make understanding the rock pool and microphytobenthos (MPB) assemblage easier and help in predictive studies. The effects of climate change start at the cellular level (Hochachka & Somero, 2002) and, following a domino effect, rise to individual organism and population levels, ultimately affecting the metabolic rates, survival, and various life-history traits (O'Connor et al., 2007). Such global changes are bound to affect the coastal ecosystem inevitably. The Indian summer monsoon plays a major role in controlling the coastal and open ocean productivity. However, under the ongoing climate change scenarios, the Indian summer monsoon has changed drastically (Maharana et al., 2021). The MPB, which cannot evade such unfavorable climate change conditions, is bound to use various combinations of adaptations like phenotypic plasticity, functional redundancy, and rapid evolution of traits suited for those conditions (Bernhard & Leslie, 2013). Although geometric shapes (morphological traits) have also been used to decipher the ecological understanding in marine waters (Stanca et al., 2013), they have never been used before to understand community dynamics, particularly in a rock pool and tidal flat ecosystem.

Knowing that the west coast of India is rich in rocky shores and tidal flats, a dearth of studies concerning the microalgal community of rock pools and tidal flats exist; this study explored (1) how the tidal levels and variations affect the rock-pool microalgal and MPB assemblages. (2) Does the geometric shape serve as a morphological trait to understand the distribution of rock-pool microalgae and the MPB community? Further, the microscopic observation of unpreserved samples during the sampling period indicated blooms of *Amphidinium carterae* sensu stricto (a potentially harmful dinoflagellate) and *Bysmatrum gregarium* in the rock pool (Patil et al., 2017). The literature search revealed that the toxicity and allelopathy of *Amphidinium carterae* are studied and reported around the world, but not all the strains are found to be toxic (Jeong et al., 2001; Baig et al., 2006; Mandal et al., 2011; Murray et al., 2015). Given this, experiments were also performed to confirm whether the bloom formations of *Amphidinium carterae* in RPs have any toxic or allelopathic effect on the dominant microalgal groups in the adjacent waters.

4.1.1.2. Methodology

The details of the sampling site, sample collection, and analysis from the tidal flats situated at both Zuari Estuary (Dias tidal flat; DTF) and Mandovi Estuary (Miramar tidal flat; MTF) are presented in Chapter 2, subsection 2.1.1 and for rock pools are presented in Chapter 2, subsection 2.1.2.

Data analysis

Univariate measures such as species count (S), Shannon–Wiener's index (H'), species richness (d), and evenness (J') were performed on log-transformed data for both species-wise and shape-wise data for rock pool and MPB abundance data. Further, these data and abundance data (log-transformed data) were subjected to a two-way analysis of variance (ANOVA) to evaluate the variation between the location of RPs, the periods of flushing and non-flushing, between tidal zones and tidal flats. The clustering of RP microalgae was performed through the Bray–Curtis similarity and group average methods. Log (x+1) transformations were used for the analysis, and the grouping was done at a 50% level to show the significant similarities shape-wise between the flushing/non-flushing period. For the allelopathy experiment, ANOVA followed by a post-hoc test was performed on the data normalized to day 0 values and the significant differences among the treatments. Univariate measures calculation and clustering analysis were performed using statistical software PRIMER version 6 and ANOVA using Statistica software (release 8).

4.1.1.3. Results

4.1.1.3a. Distribution of microalgae based on taxonomic nomenclature in rockpool

Altogether, 79 microalgal species comprising 68 diatoms and 11 dinoflagellate species were recorded. However, the RP microalgal community exhibited distinct variations between (i) the years of sampling (i.e., 2014 and 2015), (ii) the location of the rock pools at different tidal levels (LT, MT, and HT-RPs), and (iii) with the occurrence of tidal flushing in LT, MT, and HT-RPs with the adjacent water during the sampling period. More microalgal species numbers and abundances were recorded during 2015 compared to 2014 (Figure 4.1), and the lower salinity due to the precipitation (pre-monsoon showers) could probably be the reason. Interestingly, HT-RPs harbored high microalgal abundance during both years compared to LT and MT-RPs. In contrast, univariate measures such as the number of species, diversity index, and species richness revealed lower values for HT-RPs than MT and LT-RPs, and this trend was observed in both years. ANOVA for total abundance, number of species, species richness, and diversity revealed

significant variations ($p < 0.001$) for inter-annual, location of pools, and periods of flushing and non-flushing. The microalgae composition of LT-RPs (74% and 61% in 2014 and 2015, respectively) and MT-RPs (50% and 64% in 2014 and 2015, respectively) were dominated by diatoms (of which pennate diatoms contribution was highest, i.e., 23–59% in both the years) followed by dinoflagellates (i.e., 26–36%) of which thecate dinoflagellates were the maximum contributors (9–65%). However, the composition was completely different in HT-RPs, wherein the community was dominated by dinoflagellates (83–96%) in both years. The pennate diatom community in LT and MT-RPs was mostly represented by *Pseudonitzschia* spp., *Nitzschia* spp., *Thalassionema* spp., and *Licmophora* sp., whereas the dinoflagellate community of HT-RPs was dominated by high abundance of *A. carterae* and *B. gregarium* (refer Patil et al. 2017 for details on identification). It was further observed that in each pool, during both years, the phytoplankton abundance and composition showed significant temporal variations (particularly during the flushing (F) and non-flushing (NF) periods and was mainly due to the variations in the intensity of the tidal flushing.

The NF period recorded the least number of species in all the RPs compared to the F period, in which 2014 showed the least compared to 2015 (Figure 4.2a). The species richness index shows higher species richness in the F period in all the RPs than in the NF period, in which LT-RPs show the highest value, followed by MT and HT-RPs for both years (Figure 4.2b). The Pielou's evenness (J') index values revealed that the population in MT and LT-RPs are evenly distributed (J' close to 1) compared to HT-RP's (negligible J' value) and it was consistent during F and NF periods (Figure 4.2c). The uneven distribution in HT-RPs was mainly due to the high abundance of *Bysmatrum* (in 2014) and *A. carterae* (in 2015) (Figure 4.1 and Table 4.1). Using taxonomic data, the cluster analysis at a 50% Bray–Curtis similarity level revealed two groups represented by LT and MT-RPs and the other by HTRP (not shown).

4.1.1.3b. Microalgal composition and distribution based on geometric shape as a trait in the rockpool

The diversity indices for shapes show that the total number of shapes was more in 2015 (i.e., all 12 shapes recorded) compared to 2014, wherein only nine shapes were recorded (Figure 4.3). In 2014, LT-RPs were dominated by Gam (37–59%) shape followed by B (12–25%), and MT-RPs were dominated by Gam (up to 36%), Elli (up to 64%) and B (up to 47%) (Figure 4.3). In both the RPs, 6–8 shape types were recorded during flushing (Fa and Fb) and non-flushing periods.

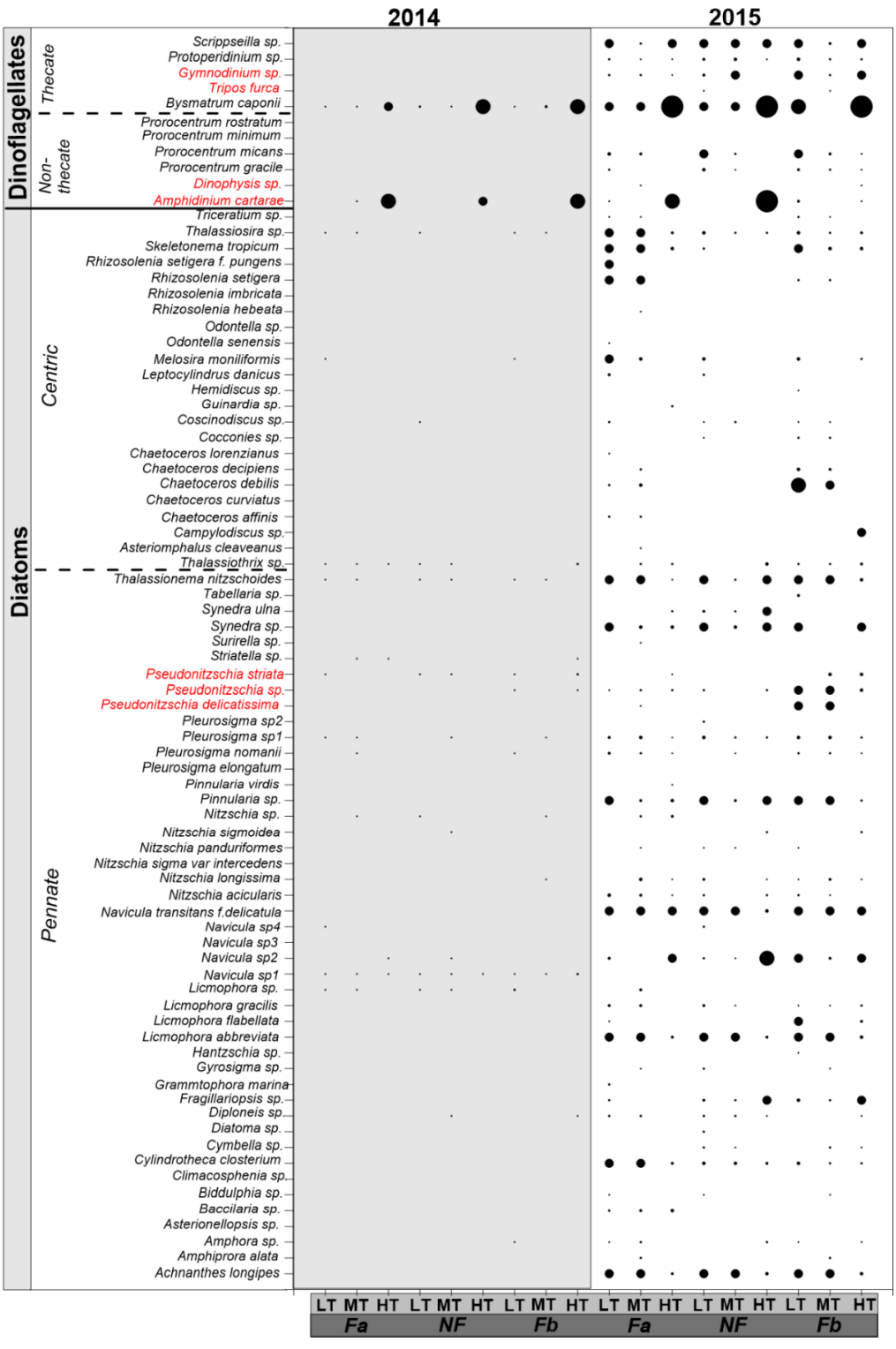


Figure 4.1. Bubble plot of the temporal (2014 & 2015) and spatial (among low-tide (LT), mid-tide (MT), and high-tide (HT) rock pools) variation of the total rock pool phytoplankton abundance. The maximum symbol diameter corresponds to 70 x 10^3 cells L^{-1}. Fa: flushing during the first five days, NF: non-flushing, and Fb: flushing during the last five days of the 15-day sampling. Species highlighted in red are known to be toxic or harmful species.

Table 4.1. Phytoplankton abundance (cells L^{-1}) in low (LT), mid (MT), and high (HT) tide rock pools during non–flushing (NF) and flushing (Fa – before NF; and Fb – after NF) periods in the summer months of both years (2014 and 2015)

Microalgae species	2014 (cells L^{-1})									2015 (cells L^{-1})								
	Fa			NF			Fb			Fa			NF			Fb		
	LT	MT	HT	LT	MT	HT	LT	MT	HT	LT	MT	HT	LT	MT	HT	LT	MT	HT
Pennate Diatoms																		
Achnanthes longipes	0	0	0	0	0	0	0	0	0	223	153	32	490	140	77	550	248	62
Amphiprora alata	0	0	0	0	0	0	0	0	0	10	15	0	0	0	0	0	15	0
Amphora sp.	0	0	0	0	0	0	1	1	0	7	18	0	0	10	27	7	10	5
Asterionellopsis sp.	5	0	0	0	0	0	0	0	0	0	0	0	0	0	0	0	0	0
Baccilaria sp.	0	0	0	0	0	0	0	0	0	23	35	52	0	0	0	0	0	0
Biddulphia sp.	0	0	0	0	0	0	0	0	0	7	0	0	3	0	0	0	3	0
Climacosphenia sp.	0	0	1	0	0	0	0	0	0	0	0	0	0	0	0	0	0	0
Cylindrotheca closterium	0	0	0	0	0	0	0	0	0	270	357	42	97	55	32	98	17	15
Cymbella sp.	0	0	0	0	0	0	0	0	0	0	0	0	12	8	0	0	15	5
Diatoma sp.	0	0	0	0	0	0	0	0	0	0	0	0	23	0	0	0	0	0
Diploneis sp.	1	0	0	0	1	0	0	0	2	27	27	0	17	13	5	10	0	3
Fragillariopsis sp.	0	0	0	0	0	0	0	0	0	13	0	0	42	25	417	62	13	103
Grammatophora marina	0	0	0	0	0	0	0	0	0	13	0	0	0	0	0	0	0	0
Gyrosigma sp.	0	0	0	0	0	0	0	0	0	0	3	0	25	0	0	0	5	0
Hantzschia sp.	0	0	0	0	0	0	0	0	0	0	0	0	0	0	0	5	0	0
Licmophora abbreviata	0	0	0	0	0	0	0	0	0	672	245	47	490	128	32	968	225	80
L. flabellata	0	0	0	0	0	0	0	0	0	8	0	0	0	0	0	168	50	48
L. gracilis	0	0	0	0	0	0	0	0	0	32	32	0	43	7	0	3	5	20
Licmophora sp.	8	3	0	5	1	0	11	0	0	0	32	0	0	0	0	0	0	0
Navicula sp1	5	2	4	1	2	3	4	4	14	0	0	0	0	0	0	0	0	0
Navicula sp2	1	0	1	1	3	0	0	0	11	45	0	127	20	5	3542	152	40	113
Navicula sp3	0	0	0	0	0	0	0	0	0	0	0	0	0	0	0	0	0	0
Navicula sp4	2	1	0	0	0	0	0	0	0	0	0	0	13	0	0	0	0	0
Navicula transitans f.delicatula	0	0	0	0	0	0	0	0	0	700	313	107	457	288	88	650	357	210
Nitzschia acicularis	0	0	0	0	0	0	0	0	0	85	40	3	18	0	18	18	3	0
N. longissima	0	0	0	0	0	0	0	1	0	0	77	7	37	10	7	8	35	8
N. sigma var intercedens	0	0	0	1	1	0	0	0	0	0	0	0	0	0	0	0	0	0
N. panduriformes	0	0	0	0	0	0	0	0	0	0	5	0	3	3	0	3	0	0
N. sigmoidea	0	1	0	0	1	0	0	0	0	0	0	0	0	0	27	0	0	15
Nitzschia sp.	0	2	0	2	0	0	0	5	0	0	27	38	0	0	0	0	0	0
Pinnularia sp.	0	0	0	0	0	0	0	0	0	103	47	82	178	42	195	163	150	25
P. virdis	0	0	0	0	0	0	0	0	0	0	0	3	0	0	0	0	0	0
Pleurosigma elongatum	0	0	0	0	0	0	0	0	0	0	0	0	0	0	0	0	0	0

P. nomanii	1	2	1	0	1	0	1	1	0	45	15	7	0	3	0	25	12	7
Pleurosigma sp1	3	3	0	1	2	0	0	2	0	35	90	7	58	18	12	52	52	25
Pleurosigma sp2	0	0	0	0	0	0	0	0	0	0	0	0	12	0	0	0	0	0
Pseudonitzschia delicatissima	0	0	0	0	0	0	0	0	0	0	5	0	0	0	0	360	292	0
Pseudonitzschia sp.	0	0	0	0	0	0	6	1	3	7	22	20	12	0	22	142	115	95
P. striata	2	1	1	4	4	0	2	0	23	0	0	8	0	0	0	0	72	60
Striatella sp.	0	3	5	0	0	0	0	0	9	0	0	0	0	0	0	0	0	0
Surirella sp.	0	0	0	0	0	0	0	0	0	0	3	0	0	0	0	0	0	0
Synedra sp.	0	0	0	0	0	0	0	0	0	183	68	92	187	77	267	103	0	375
S. ulna	0	0	0	0	0	0	0	0	0	0	0	23	37	15	423	0	0	0
Tabellaria sp.	0	0	0	0	0	0	0	0	0	0	0	0	0	0	0	45	0	0
Thalassionema nitzschoides	10	3	0	8	9	0	7	2	0	173	128	5	165	27	268	260	148	58
Thalassiothrix sp.	1	2	2	2	1	0	0	0	14	0	12	17	0	0	97	27	13	43
Centric Diatoms																		
Asteriomphalus cleveanus	0	0	0	0	0	0	0	0	0	0	2	0	0	0	0	0	0	0
Campylodiscus sp.	0	0	0	0	0	0	0	0	0	0	0	0	0	0	0	0	0	950
Chaetoceros affinis	0	0	0	0	0	0	0	0	0	13	23	0	0	0	0	0	0	0
C. curviatus	0	0	0	0	0	0	0	0	0	30	0	0	0	0	0	0	0	0
C. debilis	0	0	0	0	0	0	0	0	0	12	67	0	0	0	0	2570	207	0
C. decipiens	0	0	0	0	0	0	0	0	0	0	22	0	0	0	0	68	32	0
C. lorenzianus	0	0	0	0	0	0	0	0	0	7	0	0	0	0	0	0	0	0
Cocconies sp.	0	0	0	0	0	0	0	0	0	0	0	0	7	0	0	13	13	0
Coscinodiscus sp.	0	0	0	1	1	0	0	0	0	17	10	0	3	13	0	8	8	0
Guinardia sp.	0	0	0	0	0	0	0	0	0	0	0	13	0	0	0	0	0	0
Hemidiscus sp.	0	0	0	0	0	0	0	1	0	0	0	0	0	0	0	2	0	0
Leptocylindrus danicus	0	0	0	0	0	0	1	0	0	45	0	0	23	0	0	0	0	0
Melosira moniliformis	1	0	0	0	0	0	2	0	0	310	67	0	67	0	0	70	0	20
Odontella senensis	0	0	0	0	0	0	0	0	0	3	0	0	0	0	0	0	0	0
Odontella sp.	0	0	0	0	0	0	0	0	0	0	0	0	0	0	0	10	0	0
Rhizosolenia hebeata	0	0	0	0	0	0	0	0	0	0	5	0	0	0	0	0	0	0
R. imbricata	0	0	0	0	0	0	1	0	0	0	0	0	0	0	0	0	0	0
R. setigera	0	0	0	0	0	0	0	0	0	183	620	100	0	0	0	12	17	0
R. setigera f. pungens	0	0	0	0	0	0	0	0	0	330	0	0	0	0	0	0	0	0
Skeletonema tropicum	0	0	0	0	0	0	0	0	0	150	157	67	15	0	0	190	70	57
Thalassiosira sp.	2	2	0	2	1	0	4	3	0	160	180	40	57	23	17	58	23	42
Triceratium sp.	0	0	0	0	0	0	0	0	0	3	8	0	0	0	0	15	3	0
Dinoflagellates																		
Amphidinium cartarae	0	5	3928	0	0	419	0	0	3360	8	0	2142	0	0	10742	45	0	7
Dinophysis sp.	0	0	0	0	0	0	0	0	0	0	3	0	0	0	0	0	0	5
Prorocentrum gracile	0	0	0	0	0	0	0	0	0	28	0	0	73	3	0	48	18	3
P. micans	1	0	0	1	0	0	0	0	0	73	38	0	210	13	0	322	38	8

P. minimum	0	0	0	0	0	0	0	0	0	0	0	0	0	0	0	0	0	0	
P. rostratum	0	0	0	0	0	0	1	0	0	0	0	0	0	0	0	0	0	0	
Bysmatrum caponii	4	5	177	19	4	1226	10	39	1559	813	613	37403	660	368	62578	3292	30	30090	
Tripos furca	0	0	0	1	0	0	0	0	0	0	0	0	3	0	0	0	3	0	
Gymnodinium sp.	0	0	0	0	0	0	0	0	0	28	17	8	32	278	0	158	15	743	
Protoperidinium sp.	0	0	0	0	0	0	0	0	0	20	3	3	43	87	5	70	27	18	
Scrippseilla sp.	0	0	0	0	0	0	0	0	0	287	22	658	167	120	827	402	38	485	

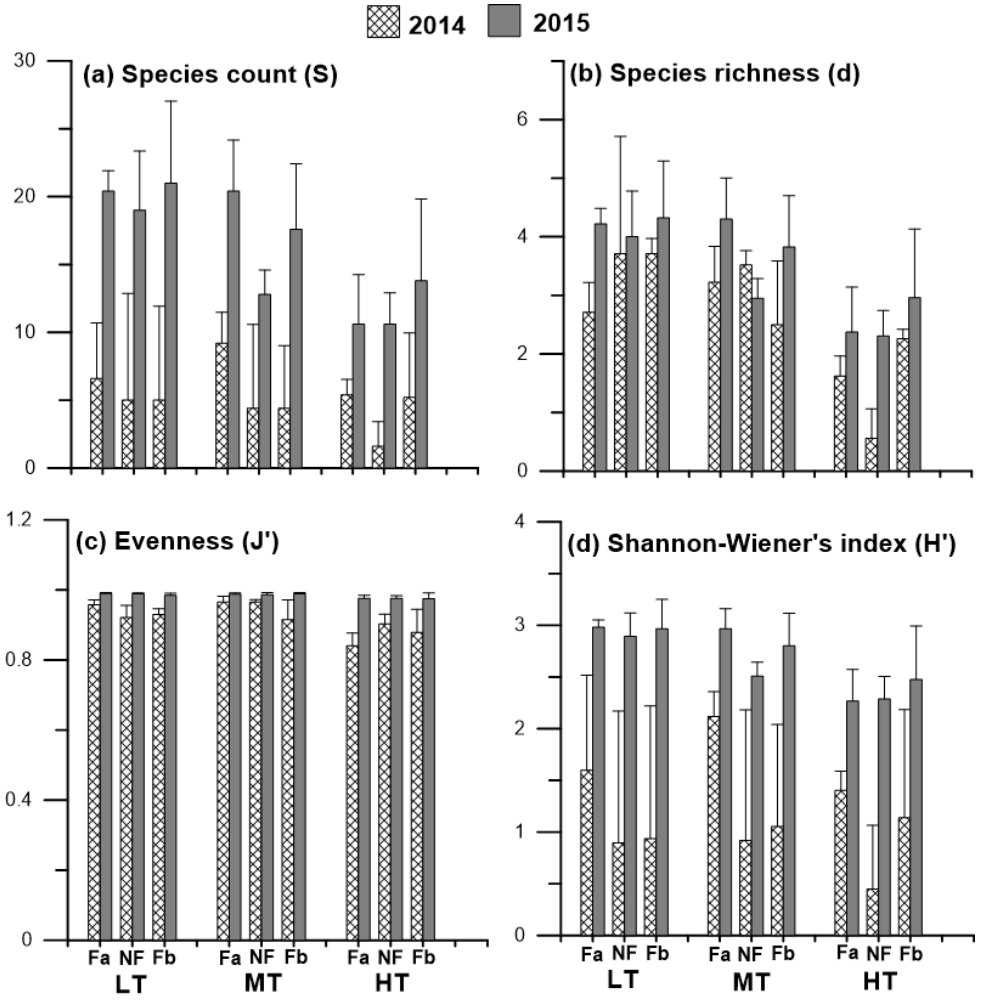


Figure 4.2. Taxonomy-wise diversity indices of RP microalgae. S: species count, d: species richness, J': evenness, H': Shannon–Weiner's index, Fa, and Fb: flushing period, NF: non-flushing period, LT: low-tide, MT: mid-tide and HT: high-tide.

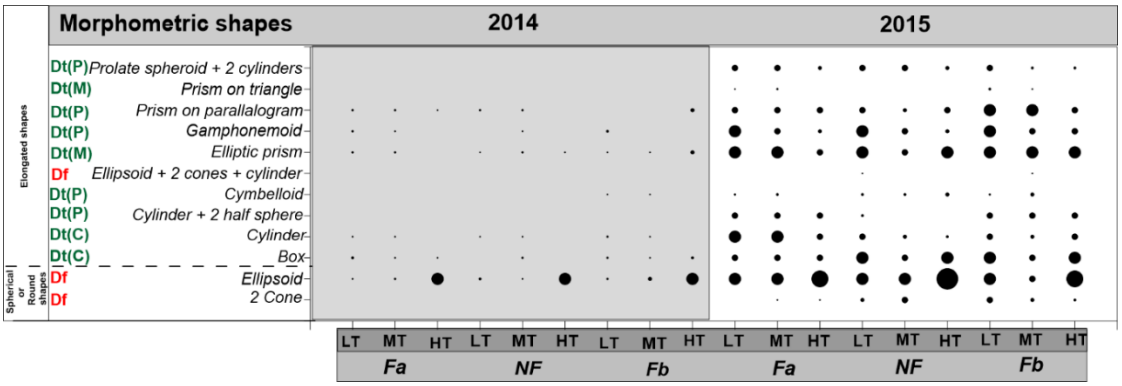


Figure 4.3. Bubble plot showing the temporal (2014 and 2015) and spatial (among low-tide (LT), mid-tide (MT), and high-tide (HT) rock pools) variation of the total rock pool phytoplankton abundance based on shapes. The maximum symbol diameter corresponds up to 809x10^3 cells L^{-1}. Fa: flushing during the first five days, NF: non-flushing, and Fb: flushing during the last five days of the 15-day sampling. Df: dinoflagellates; Dt(P): pennate diatoms; Dt(C): centric diatoms; Dt(M): both pennate and centric diatoms.

In contrast, HT-RPs were dominated by Elli (99%) shape during both the F (six shape types in Fa and seven shape types in Fb) and NF (2 shape types) periods (Figure 4.4). ANOVA revealed insignificant variations in shape diversity and richness for flushing and non-flushing periods. However, in the year 2015, LT-RPs were dominated by Ps2Cyl (up to 26%), Gam (up to 17%), Elli (27–38%), and Gam (up to 18%), whereas MT-RPs were dominated by Ps2Cyl (up to 40%), Cyl2Hs (up to 18%), Cyl2Hs (20%), Gam (20%), Elli (up to 33%) and 2C (up to 25%). Interestingly, similar to 2014, the HT-RPs were dominated by Elli (97%) during flushing and non-flushing periods. Similar to 2014, ANOVA revealed insignificant variations in shape diversity and richness for flushing and non-flushing periods. During the 2015 sampling, the number of shapes recorded was relatively less in HT-RPs (9–10 shapes) compared to LT-RPs (11 shapes) and MTRPs (12 shapes) (Figure 4.4).

Thus, the shape diversity gradually decreased from LT-RPs to HT-RPs. The HT-RP was consistently dominated by the Elli shape, which is majorly represented by dinoflagellates (*A. carterae* and *B. gregarium*) in both years (Figure 4.4). The Gam shape was chiefly represented by *Licmophora* spp. in both the years. Shape PoP (representing *Nitzschia* spp., *Pseudonitzschia* spp., and *Pleurosigma* spp., i.e., mostly pennate diatoms) is the most diverse geometric shape comprising 10 species and 3 genera, followed by EliP (9 species and 6 genera), Elli (7 species and 5 genera) and Cyl (5 species and 5 genera)

in 2014. The most diverse shape in 2015 ElliP (represented by a mixed group of pennate and centric diatoms), comprises 23 species and 14 genera, followed by PoP (14 species and 4 genera), Elli (11 species and 7 genera), Cyl (11 species and 8 genera) and B (9 species and 7 genera). Hence, the simple shapes dominated in terms of taxa richness in both years.

The shape-wise clustering of the RP microalgae population for 2014 at 50% Bray–Curtis similarity level revealed only one group showing Cyl, B, ElliP, and PoP to be significantly similar (Figure 4.5). However, shape-wise clustering of RP microalgae for the year 2015 at 50% Bray–Curtis similarity level revealed five major groups in which group I (B and ElliP), group II (Gam and Ps2Cyl), group III (2C and PoP), group IV (Cyl and Cyl2Hs) showed significant similarities, but group V (Elli) formed a single group in the cluster (Figure 4.5). Like taxonomic data, the cluster analysis using shape data at 50% Bray–Curtis similarity level also revealed two groups: one represented by LT and MT-RPs and the other by HT-RP (Figure 4.6).

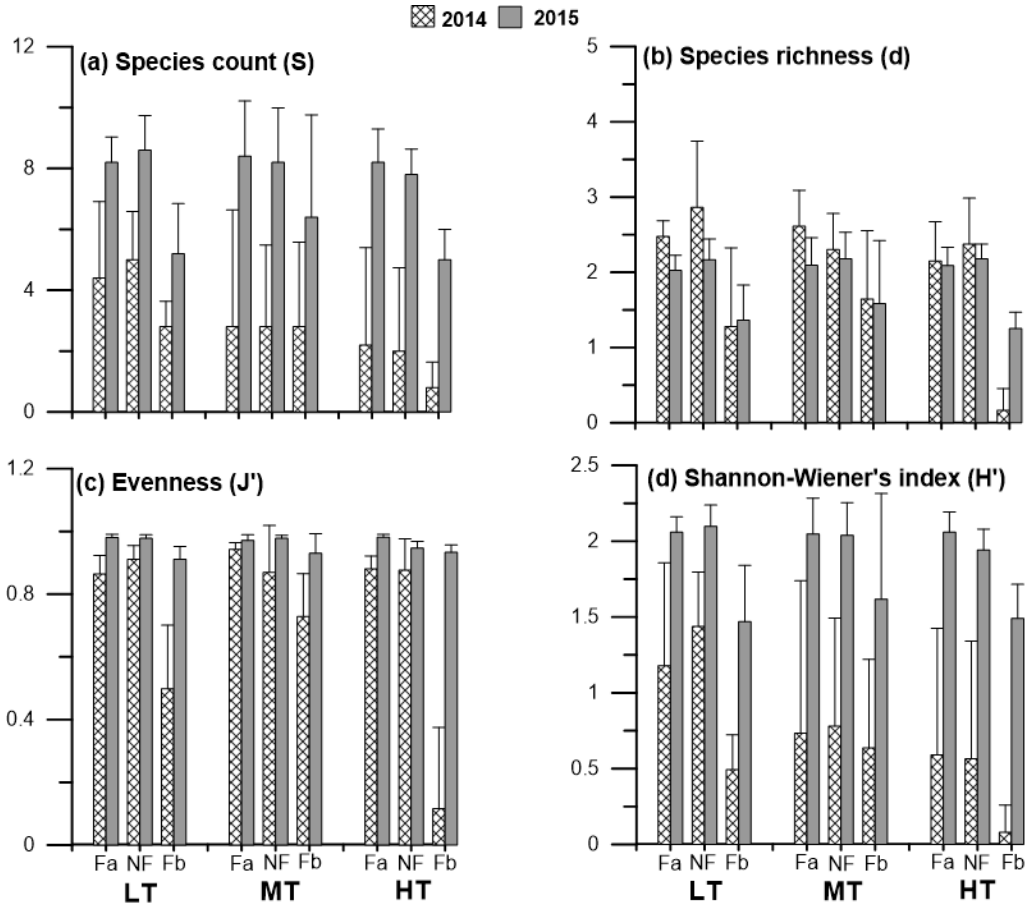


Figure 4.4. Diversity indices of RP microalgae based on shapes. S: species count, d: species richness, J': evenness, H': Shannon–Weiner's index, Fa, and Fb: flushing period, NF: non-flushing period, LT: low-tide, MT: mid-tide and HT: high-tide.

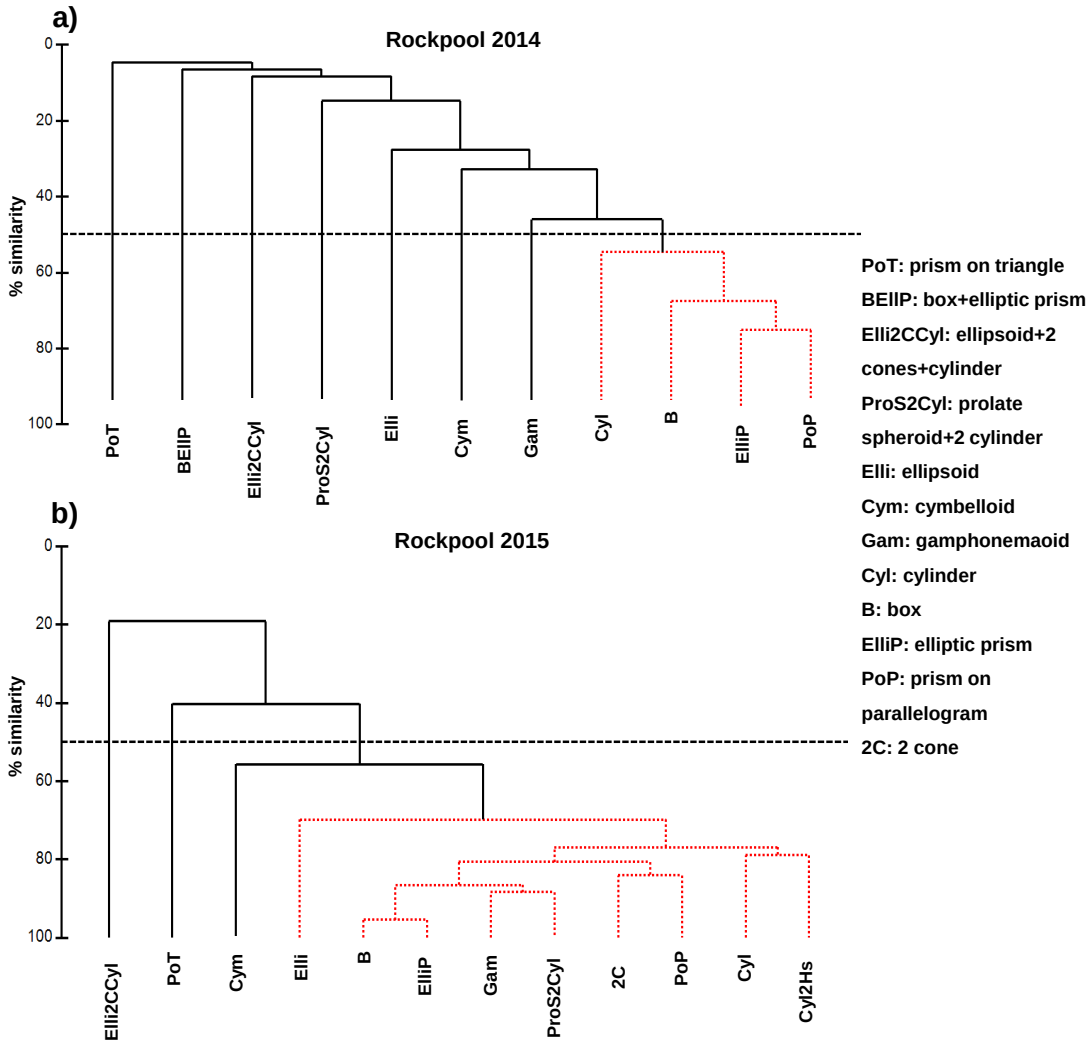


Figure 4.5. Cluster dendrogram based on geometric shapes for the years 2014 (a) and 2015 (b) using the Bray–Curtis similarity coefficient and group average method: grouping done at 50% similarity (data is log transformed; LT: low-tide, MT: mid-tide, HT: high-tide, Fa, and Fb: flushing period and NF: non-flushing period).

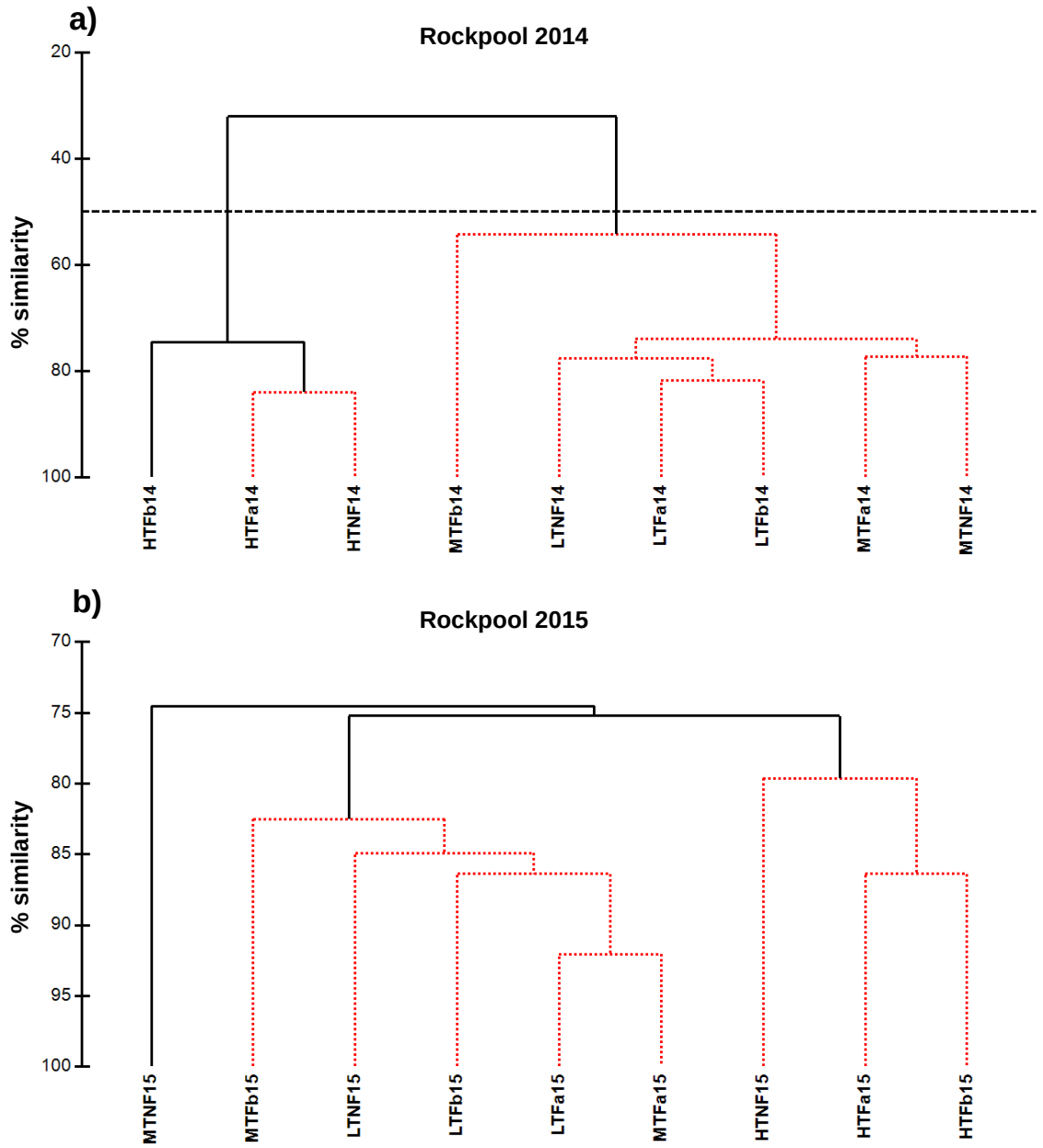


Figure 4.6. Cluster dendrogram based on geometric shapes with respect to flushing (Fa and Fb) and non-flushing (NF) period for the year (a) 2014 and (b) 2015 using the Bray–Curtis similarity co-efficient and group average method: grouping done at 50% similarity. Data is log-transformed: LT: low-tide, MT: mid-tide, HT: high-tide.

4.1.1.3c. The phytoplankton shape variability in the surf water of tidal flats

The phytoplankton shapes showed significant inter-annual variability at both tidal flats. Overall, 11 shapes (DTF: 8 simple and 3 complex, MTF: 7 simple and 4 complex) were recorded, but the dominance differed at both tidal flats. For instance, DTF was co-dominated by PoP (37%; *Pseudonitzschia* sp.) and PoT (36%; *Bellerochea malleus*) whereas MTF was co-dominated by ElliP (34%; *C. curvisetus* and *Navicula* spp.), PoP (33%; *Pseudonitzschia* sp. and *Nitzschia* spp.), and Cyl2Hs (22%; *Skeletonema* sp.). The highest number of shapes were recorded in July and October 2022 (8 shapes each) and October 2022 (10 shapes each), and the lowest was in September 2023 (2 shapes) and July 2023 (3 shapes) at DTF and MTF, respectively. Among the shapes, ElliP (7 months) followed by PoT (6 months) dominated at DTF, whereas in MTF, ElliP (6 months) followed by PoP (3 months) dominated. In both tidal flats, the maximum phytoplankton species corresponds to ElliP (DTF: 18 species, MTF: 22 species) and Cyl (DTF: 10 species, MTF: 21 species). The shapes in which only one MPB species were recorded were 2C, Gam, Cyl2Hs, and Cym at DTF and ProS2Cyl and Cyl2Hs at MTF.

The phytoplankton shape assemblage showed seasonal variability in the shape dominance, but the number of shapes was similar at both the tidal flats. In the pre-monsoon season, MTF (8 shapes) recorded higher shapes than DTF (6 shapes). At DTF, PoT (81%), whereas at MTF Cyl (24%) and ElliP (20%) dominated. At DTF, PoT was dominated by *B. malleus* and *L. undulatum*, whereas Cyl and ElliP were by *Paralia sulcata* and *Navicula* sp. at MTF. In the monsoon seasons, a similar number of shapes (9 shapes) were recorded at both tidal flats. At DTF, 9 shapes were recorded in 2022, and only 7 shapes in 2023. At MTF, 9 shapes were recorded in 2022 and only 8 in 2023. The monsoon seasons of 2022 and 2023 showed no significant difference in shape assemblage; however, the dominance varied at both tidal flats. At DTF, Cyl2Hs (*Skeletonema* sp.) and ElliP (*Navicula* spp.) dominated in 2022 and 2023, whereas, at MTF, Cyl2Hs (*Skeletonema* sp.) in 2022 and ElliP in 2023 (*C. debilis* and *C. curvisetus*) dominated. In the post-monsoon seasons, 10 shapes (all in 2022 at both tidal flats) were recorded, and only 7 and 8 in 2023 at DTF and MTF, respectively. The post-monsoon seasons of 2022 and 2023 showed no significant difference in shape assemblage and dominance; however, the dominant taxa varied slightly at both tidal flats. For instance, *Pseudonitzschia* sp. dominated PoP at both tidal flats in 2022, whereas *Cocconeis* sp. and *Chaetoceros decipiens* dominated ElliP in 2023 at DTF and MTF, respectively.

4.1.1.3d. MPB shape variability in the tidal flats

The MPB shape showed significant variability between the tidal zones at both tidal flats. More shapes were documented at DTF (12 shapes; 9 simple and 3 complex) than at MTF (10 shapes; 7 simple and 3 complex). Among the shapes, ElliP followed PoT, Cyl and PoP were the major contributors. Interestingly, some dominant shapes were dominated by distinct taxa, and similar taxa represented some. For instance, ElliP was mostly represented by *Navicula* spp., *Fragillariopsis* sp. (in DTF), and *Chaetoceros* sp. (in MTF); Cyl was represented by *Thalassiosira* sp. at both tidal flats; PoT by *Lithodesmium* sp. and *Bellerochea* sp. in DTF; ProS2Cyl by *Cylindrotheca closterium*, and PoP by *Nitzschia Closterium* and *Nitzschia* spp. in MTF. Interestingly, the shape dominance varied at both tidal flats despite the number of shapes recorded at different tidal zones remained the same. For instance, at DTF, PoT dominated LT (38%) and MT (38%) and ElliP (67%) in HT. In contrast, at MTF, ProS2Cyl (38%) and ElliP (32%) dominated LT, PoP (37-44%), and ElliP (36-37%) dominated both MT and HT.

Temporally, the MPB assemblage showed seasonal shape variability. The monsoon recorded a maximum number of shapes (9-12 shapes), followed by non-monsoons (7-10 shapes), whereas among the tidal zones, MT (DTF: 8-12, and MTF: 7-9 shapes) recorded higher shapes than LT (DTF:10-11, MTF: 8-10 shapes) and HT (DTF: 7-12, MTF: 7-8 shapes). At DTF, the pre-monsoon season was dominated by PoT and Cyl in the LT-MT zone and ElliP in the HT zone, Cyl and ElliP dominated the monsoon season in all the tidal zones, and ElliP and PoT dominated the post-monsoon-season in all the tidal zones (Figure 4.7a-d). At MTF, the pre-monsoon season was dominated by ProS2Cyl and ElliP in LT, PoP and ElliP in MT, and PoP in HT zone; the monsoon season was dominated by Cyl and ElliP in LT, PoP and ElliP in MT and HT zone, and ElliP and PoP dominated the post-monsoon season at all the tidal zones (Figure 4.7e-h).

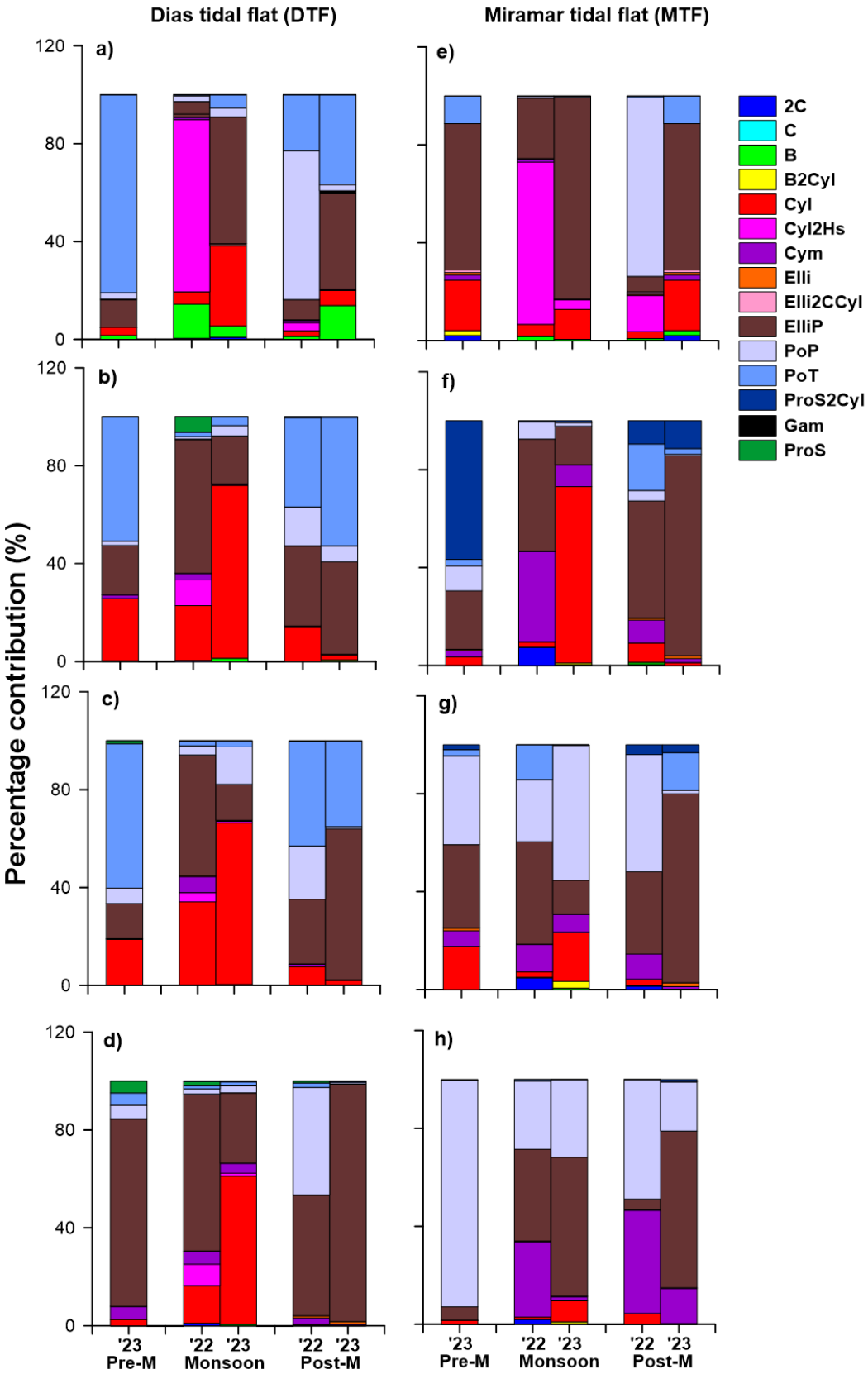


Figure 4.7. Plots showing percentage contribution of phytoplankton geometric shapes in pre-monsoon, monsoon, and post-monsoon seasons in a & e) surf water, b & f) low-tide, c & g) mid-tide, and d & h) high-tide zones of DTF (a-d) and MTF (e-h). The data presented here is the month's average for the respective seasons and years.

4.1.1.3e. Effect of A. carterae cell-free filtrate on other rockpool microalgae

The allelopathic effect of *A. carterae* cell-free filtrate was evaluated against the three microalgal cultures (i.e., *S. costatum, B. gregarium,* and *D. tertiolecta*) and the results revealed that the allelopathy effect was species-specific. In the case of *S. costatum*, the maximum growth was observed in control (i.e., 0%) compared to those grown in cell filtrates. Inhibition of *Skeletonema* growth increased with increased strength of the cell-free filtrates (Figure 4.8). Additionally, the morphological changes were also evident; for example, the larger chains containing 16–17 cells were seen only in control, and for those with reduced filtrate strength, the chain length was shorter, containing 4–5 cells. Similar to *S. costatum*, growth inhibition (up to 76%) in *B. gregarium* was also observed at higher concentrations (100% and 75%) of cell-free filtrate compared to control (Figure 4.8). The number of cells in 100% filtrate strength was 6.5 cells/ml, whereas, in control, density was 26 cells/ml on the 4th day. This suggests that, despite the slow growth of *B. gregarium*, the growth in the control was four times more than that observed in 100% filtrate concentration. Moreover, *B. gregarium* cells also showed some distinct morphological changes at higher concentrations (100%, 75%, and 50%) wherein the cells formed a dormant structure and remained non-motile, but in control, the cell morphology and motility remained intact. ANOVA revealed that, in the case of *S. costatum* and *B. gregarium*, significant inhibition with respect to filtrate strength ($p < 0.01$) and the highest was observed at 100% followed by 75% filtrate strength. Unlike *S. costatum* and *B. gregarium*, *D. tertiolecta* showed no growth inhibition or morphological changes, even at the highest concentration. ANOVA also revealed an insignificant variation between the cell filtrate strength and control. Surprisingly, the maximum growth was observed in 100% cell-free filtrate, and the growth in 100% cell-free filtrate was ~30% more compared to the control on the 4th day, suggesting a stimulatory effect (Figure 4.8).

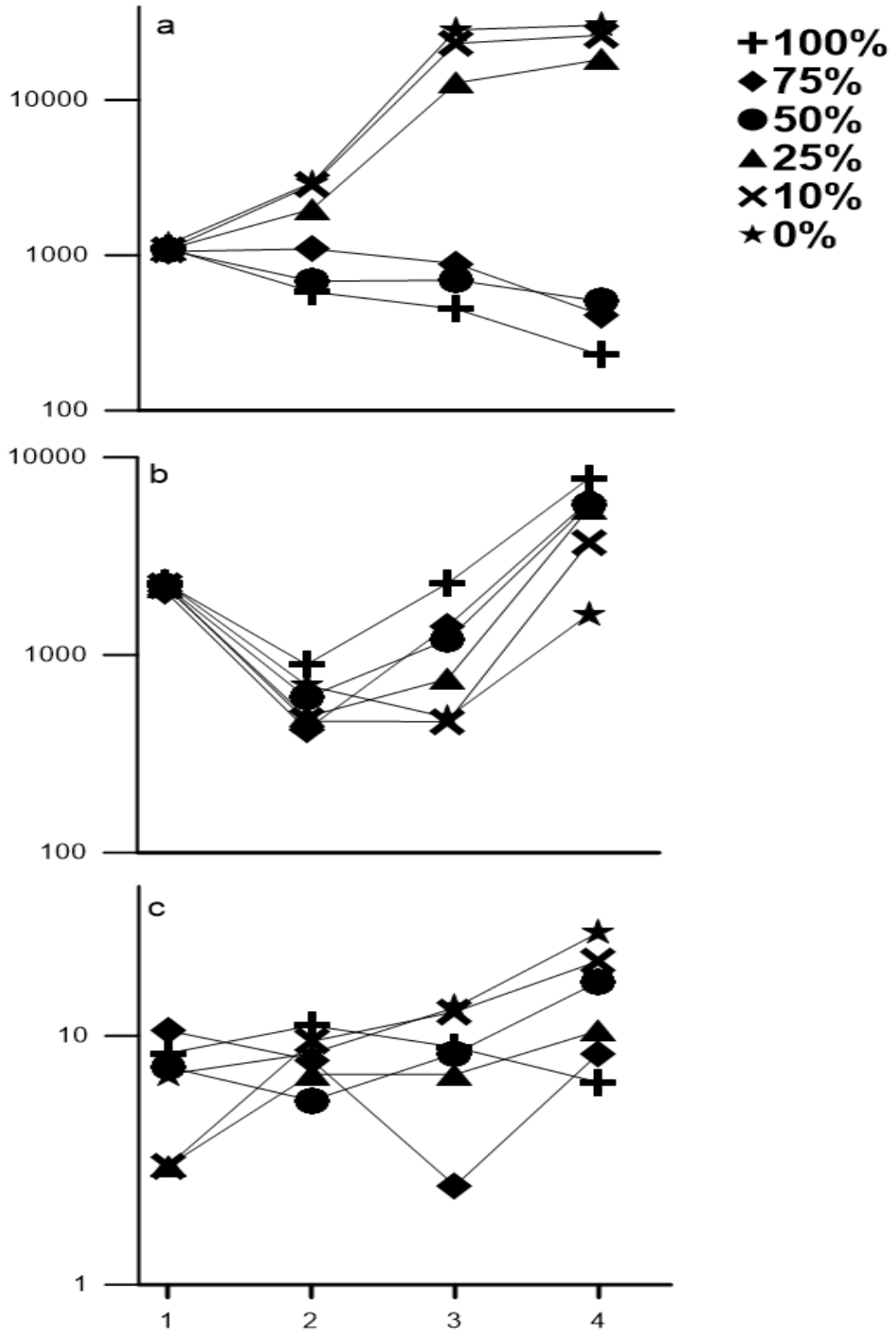


Figure 4.8. Effect of *A. carterae* cell-free filtrate on the growth of (a) *Skeletonema costatum*, (b) *Dunaliella tertiolecta*, and (c) *Bysmatrum gregarium* in different filtrate concentrations.

4.1.1.4. Discussion

4.1.1.4a. Influence of location on the microalgal community based on taxonomic nomenclature

The intertidal microalgal community fluctuated greatly among the tidal locations at both habitats. Microalgae are introduced in the rock pools and tidal flats by the tidal action from the adjacent seawater, and the assemblages change consequently depending on the period of non-flushing. Tidal flushing based on the rock pools' location is a significant factor (Underwood & Skilleter, 1996) in shaping and controlling the microalgal community on a very short temporal scale (Metaxas & Scheibling, 1994). However, several factors influence assemblage during such short timescales (Metaxas & Scheibling, 1994).

Tidal flushing brings the organisms from the adjacent sea and adds fresh nutrients to the LT and MT zones, which support rich phytoplankton assemblage compared to the HT zones (Soininen & Meier, 2014). In our study, during both years, diatoms with higher species diversity were dominant in the LT and MT-RPs and dinoflagellates, with lesser species diversity, in the HT-RPs (Figure 4.1). In contrast, diatoms were the most dominant group in all the tidal zones at tidal flats. The diatom dominance in LT and MT-RPs has also been reported in other studied RPs (Anusa et al., 2012; Soininen & Meier, 2014; Rishworth et al., 2017). Among the diatoms, pennate species dominated LT and MT-RPs, and they were represented mainly by elongated, chain-forming, or branching types such as *Licmophora* spp., *Pseudonitzschia* spp., *Synedra* spp., *Navicula* spp., *Thalassionema* spp. and *Thalassiothix* spp. However, in the tidal flat habitats, except for a couple of dominant pennate diatoms (*Navicula* spp., *Nitzschia* spp.) the community structure differed from the RP habitat. For instance, the dominance of chain-forming diatoms like *Chaetoceros* sp., *Lithodesmium* sp., *Bellerochea* sp. and *Cylindrotheca closterium* were dominant. Since LT and MT-RPs are the most turbulent and frequently flushed pools, the dominance of pennate forms (Padisak et al., 2003) with benthic lineage is not unusual (Metaxas & Lewis, 1992; Metaxas & Scheibling, 1996a, b). Whereas, the dominance of dinoflagellates in HT-RPs was mainly due to the blooms of *A. carterae* and *B. gregarium* (Patil et al., 2017). In contrast to HT-RPs, the HT zone in the tidal flats was pennate diatom dominated, and dinoflagellate contribution was negligible. Though *Amphidinium* sp. was recorded from the tidal flats, its bloom was not observed. The RPs and tidal flats are distinct habitats and harbor distinct microalgal communities. Both these intertidal habitats experience extreme environmental conditions (desiccation, monsoon-driven

fluctuations, tidal actions, etc.). These communities have adapted according to their respective habitats and prevalent hydrological conditions. For example, the HT-RPs selected in this study are relatively smaller compared to the LT and MT-RPs and, therefore, will experience higher environmental stress (temperature up to 40°C and salinity up to 67 PSU) and less frequent tidal flushing, which in turn will influence the microalgal assemblage in the HT-RPs (Patil et al., 2017). The dinoflagellates *A. carterae* and *B. gregarium* (both are newly reported from Indian waters) were found to be euryhaline, eurythermal and euryphotic (Patil et al., 2017). The photoprotection mechanism of these HT-RP dinoflagellates, detailed in Patil et al. (2017), points out their adaptive capabilities to a varying light regime. The dinoflagellate blooms exhibited typical characteristics of S-strategists, i.e., species utilizing nutrients efficiently under resource-limited conditions (Reynolds, 2006), and this was the case in HT-RPs due to non-flushing for a considerable time. These findings are also consistent with Margalef's proposal (1978), which states that centric and pennate diatoms should dominate in high turbulence and flagellates should dominate under low turbulence conditions (Kiorboe, 1993). Interestingly, the adaptation of diatoms in the tidal flat habitat was different. The pennate diatoms often undergo vertical migration within a few centimeters of the sediment layers to avoid harsh conditions such as wave washout, desiccation, and nutrient limitation (Mitbavkar and Anil, 2004, 2006).

4.1.1.4b. Microalgal community based on geometric shapes at different tidal zones in the intertidal regions

The present study is the first attempt to use the geometric shape as a trait to determine phytoplankton and MPB dynamics in the rock-pool and tidal flat ecosystem. Our results show that the intertidal regions (both RPs and tidal flats) of the Goa coast are characterized by high morphological diversity in shape. The LT and MT zones are relatively more diverse in shape than HT zones (Figures 4.3 and 4.4). All the recorded microalgae taxa were classified into 12 geometric shapes (Hillebrand et al., 1999; Sun & Liu, 2003), and the morphological differences have a functional meaning which is well reflected in phytoplankton adaptive strategies (Lewis, 1976; Margalef, 1978; Naselli-Flores et al., 2007). Even though there is no specific literature suggesting a particular shape to be either spherical or elongated, many of the pre-defined shapes have been categorized based on the various published literature (Stanca et al., 2013; Karp-Boss & Boss, 2016) to fall in either of the following categories spherical/round and elongated shape. Therefore, in the present study, it is assumed that shapes like 2 cones and ellipsoids

can be classified as spherical or near-spherical shapes, whereas the rest of the shapes are elongated shapes. Any deviation from a perfect sphere is considered an advantage for resource acquisition. The sphere represents the smallest boundary area occupying a given space; therefore, distortion from the spherical shape can increase the area of the surface, which might represent a competitive adaptation to conserve an optimum surface-to-volume ratio, i.e., S:V (Lewis, 1976; Reynolds, 2006; Karp-Boss & Boss, 2016). For instance, distortion of spherical shape diatoms to achieve an optimum S:V can allow them to sink more slowly than spheres of equivalent size and can also help to out-compete smaller ones for resource acquisition (Grover, 1989; Padisak et al., 2003). It has also been reported that shapes such as elongated and round or combined shapes are prevalent in flushed and stagnant nutrient-limited regions, respectively (Sommer, 1998; Morabito et al., 2007), and is also evident in this study. For instance, the dominance of elongated and nonspherical shapes like Gam, PoP, B, PoT, and Cym in the frequently flushed LT and MT zones prove the success of these shapes in exploiting the abrupt nutrient input as well as surviving the frequent turbulence caused by tidal action (Naselli-Flores et al., 2007; Naselli-Flores & Barone, 2007). In HT-RPs, the dominance of the Elli shape suggests the prevalence of more stable, stratified, and nutrient-deprived water. In contrast, in the HT zone of the tidal flats, the dominance of the ElliP shape dominated by pennate diatoms suggests more unfavorable and nutrient-deprived conditions. This means that under such conditions, the elongated shapes will be replaced with round or combined shapes mainly represented by flagellates (dinoflagellate *A. carterae* and *B. gregarium* in this study), which competes poorly for inorganic nutrients (Litchman & Klausmeier, 2008; Stanca et al., 2013) in the RP habitat but not at tidal flats. However, shapes from intertidal RP habitats showed less temporal and seasonal variability than the tidal flats. The MPB shape variabilities were more significant between tidal zones at the MTF than at the DTF. This difference was mostly due to natural (monsoon-driven changes, beach morphology, sediment texture, bioturbation, sediment erosion, and deposition process, etc.) and anthropogenic pressure (e.g., tourism, development activities, etc.). Moreover, RP habitats provide a stable substrate for the phytoplankton to evade the tidal washout or flushing. However, tidal flat surface sediments are prone to frequent washout, and MPB can evade such conditions only by migrating to the deeper layers. Therefore, it can be presumed that the intertidal flats selected in this study are more dynamic habitats than the RPs, and specific studies from diverse tidal flats are required to understand their shape dynamics.

Another interesting finding of this study is that even though the taxonomic assemblage changed temporally (from 2014 to 2015), the shape dominance remained more or less consistent at both intertidal habitats, i.e., ElliP and PoP were the most taxa-rich shapes, indicating the importance of shape as a robust morphological trait in microalgal studies enabling easy, less complicated non-taxonomic approach for better understanding of community dynamics. This also suggests that these particular morphological traits are selected by environmental pressure and must have some selective advantages compared to other shapes, such as spherical shapes (Karp-Boss & Boss, 2016). Periodic measurements of morphological trait succession can provide information on the health of the ecosystem (e.g., underwater light climate; Naselli-Flores & Barone, 2007), essential functional processes (e.g., community assemblage; Salmaso & Padisak, 2007), ecological characteristics of phytoplankton organisms (Naselli-Flores et al., 2007) and act as a helpful monitoring tool without any mind-boggling taxonomic skills (Stanca et al., 2013).

4.1.1.4c. Allelopathy of bloom-forming dinoflagellate Amphidinium against other microalgae

Various *Amphidinium* strains have shown toxic effects on other microalgae, nauplii larvae, and even fish (Baig et al., 2006; Murray et al., 2015), and the production of toxin is also considered a type of physiological trait to deter predators (Litchman & Klausmeier, 2008). The literature revealed that the toxicity and allelopathy of *A. carterae* are studied and reported worldwide (Jeong et al., 2001; Baig et al., 2006; Mandal et al., 2011; Murray et al., 2015). It has also been reported that *A. carterae*, which released substances or allelochemicals into the culture medium or environment, inhibited or altered the growth of the co-cultured or co-existing microalgae (Xiaoqing et al., 2012). Further, the prevalence of high levels of cryptic diversity within the *Amphidinium* sensu stricto (Murray et al., 2012) and variability in toxicity in some of them (Baig et al., 2006) is well documented. Given this, the present study was conducted to confirm whether the blooming of *A. carterae* (local strain) suppressed the growth of other microalgae present in the HT zones by producing some antagonistic allelopathic chemical. This is the first attempt to find out the allelopathic effect of cell-free filtrate of local strain *A. carterae* on various commonly occurring phytoplankton species. This study confirms that the cell-free filtrate of *A. carterae* does produce some allelochemicals, which have species-specific effects. The species specificity of the toxic effect of allelochemical is reported in a few studies elsewhere (Baig et al., 2006; Poulson et al., 2010). The maximum inhibition

of growth by cell-free filtrate of *A. carterae* was noticed in *Skeletonema* cells, followed by *Bysmatrum* (Figure 4.8). However, results showed a stimulatory effect of cell-free filtrate of *A. carterae* on the green algae *Dunaliella* (Figure 4.8). The stimulatory effect of allelochemicals from other algae and cyanobacteria are also reported (Rice, 1984; Suikkanen et al., 2005; Poulson et al., 2010). The allelopathy is often used to get an upper hand to compete for limited resources and helps in the organism's bloom formation (Graneli & Hansen, 2006; Pavaux et al., 2020). Hence, it is assumed that the *A. carterae* might have used allelopathy as a physiological trait to suppress competitors in the HT zones, in addition to its eurytolerant adaptive capability against extreme temperature, salinity, and light (Patil et al., 2017). Such a strategy might have enabled to compete against the limited resources to form blooms in the RPs, as evident from the composition data. These findings suggest that such a physiological trait (allelopathy) can also be related to 'competitor's suppression' and 'predator's avoidance' as proposed by Litchman and Klausmeier (2008). It was also observed that *Skeletomena* was the most sensitive to allelochemical, followed by *Bysmatrum*. However, the inhibition in growth was observed only at a higher strength of *A. carterae* filtrate, suggesting that the tidal action (through dilution) could play a great role in the effectiveness of allelopathy as a competitive strategy in HT-RPs.

The morphological changes observed in *Bysmatrum*, like temporary cyst-like structures induced by the cell-free filtrate of *A. carterae*, might explain the coping mechanism of *Bysmatrum gregarium*, which also co-existed with *A. carterae* in the HT-RPs. Temporary cyst formation, which is used as a defense mechanism to resist allelochemicals, is also reported in *Scrippsiella* (which is almost identical to *Bysmatrum*; Jeong et al., 2012) as well (Fistarol et al., 2004). A separate study also showed a weaker allelopathy effect by *A. carterae* filtrate on *Amphora coffeaeformis*, a biraphid benthic pennate, and biofilm-forming diatom (Modi & Patil, 2019 dissertation). Nevertheless, the present study indicated that *Amphidinium* blooms in rock pools will have a varying effect on planktonic and biofilm microalgae. However, further studies with mixed microalgal assemblage and the faunal component will lead to a better understanding of the impact on the microalgal community. Since *Amphidinium* experiences extreme environments in the rock pools (Patil et al., 2017), elucidating the role of environmental parameters (e.g., temperature and salinity) on the allelochemical production and their effects need further attention.

4.1.1.5. Conclusion

This study highlights that the location and nature of RPs and tidal flats determine the nature of phytoplankton assemblage. In both the intertidal habitats, less microalgal diversity (including shapes) and the number of species were recorded in the HT zone, followed by MT and LT in RPs and LT and MT in tidal flats. Interestingly, even though the taxonomic assemblage changed temporally, the shape dominance remained consistent, suggesting the latter a robust morphological trait for RPs but not in tidal flats. The microalgae assemblages followed distinct trends in RPs and tidal flats. For instance, in frequently flushed RPs (MT and LT), pennate diatoms (*Pseudonitzschia*, *Nitzschia*, *Thalasionema*, *Navicula*, and *Licmophora*) representing elongated types dominated, whereas in stagnant HT-RPs spherical/combined shaped dinoflagellates (*Amphidinium* sensu stricto and *Bysmatrum gregarium*) dominated. However, in the tidal flats, LT and MT zones were dominated by elongated type chain forming taxa (*Thalassiosira* sp., *Bellerochia* sp., *Lithodesmium* sp., and *Chaetoceros* spp.) and HT zone by pennate diatoms (*Navicula* spp., and *Nitzschia* spp.). Since tidal flats are diverse based on sediment texture, beach profile, and other local factors, more studies are required to delineate the variations. Further, species-specific allelopathy on other microalgae by *Amphidinium* (known harmful algae of concern and dominant in HT-RPs) highlights a type of physiological trait to suppress competitors. It might be one of the reasons for its predominance in HT-RPs experiencing varying environmental (light, temperature, and salinity) conditions. Therefore, it can be concluded that the microalgae in intertidal flats are a highly dynamic than the rockpools.

4.2. The pelagic ecosystem

In this sub-chapter, the phytoplankton distribution based on taxa, shape, size, and morphometric traits (surface-to-volume ratio; S:V, greatest axial linear dimension; GALD) were studied from a) different oceanographic settings (convective mixing and oligotrophic regions), and b) sea-surface and sub-surface chlorophyll maximum layer (SCML) occurring at different depths in different bioregions of the pelagic ecosystems. The findings are discussed in the subsequent sections 4.2.1 and 4.2.2, respectively.

4.2.1. Different oceanographic settings

4.2.1.1. Introduction

Phytoplankton, which are vital in ecosystem functioning, food-web dynamics, fisheries, and biogeochemical cycling of essential micro and macronutrients, are not only taxonomically diverse but also show amazing Intra and inter-specific morphological diversity with organisms ranging greatly in the magnitude of size (Finkel et al., 2010) and a wide range of shapes (Hillebrand et al., 1999; Sun & Liu, 2003). Traditionally, the morphological attributes are used only for taxonomic studies but do not reflect the ecological functions (Naselli-Flores et al., 2007; Salmaso & Padisak, 2007). Lewis (1976) first noted the ecological value of morphological descriptors in phytoplankton resource acquisition (light and nutrient uptake) under the pressure of natural selection and competition. The adaptive value of the morphological variability and differences in morphology adopted for diverse ecological strategies by phytoplankton was studied by Margalef (1978) and later explored by Reynolds (1997). Few shapes are better adapted to certain environmental conditions than others, so the phytoplankton with such shapes should have better fitness and diversity (Ryabov et al., 2021). The aquatic ecosystem's ecological state can be assessed by understanding the adaptive value of different phytoplankton morphologies; therefore, morphological diversity can be considered a key factor allowing a particular ecological group to withstand the various environmental conditions experienced in the ecosystem (Naselli-Flores, 2014).

The trait-based approaches in phytoplankton ecology have become common. Such approaches can increase our insight into the organization of ecological communities and predict their reorganization under any environmental change (Litchman & Klausmeier, 2008). This is because phytoplankton are relatively simple and have well-defined traits that determine their ecological niche (Litchman & Klausmeier, 2008). The well-defined commonly used traits in phytoplankton can be classified into three categories (Litchman

& Klausmeier, 2008; Weithoff & Beisner, 2019): (i) morphological- size, shape, greatest axial linear dimension (GALD), biovolume, mucilage presence/absence, and biological form (unicellular/colonial/filament/chains); (ii) physiological- presence/absence of silica demand, heterocysts (N_2-fixation), mixotrophy, toxin production, resting stages, dominant pigment type, nutrient, and/or light uptake parameters; and (iii) behavioral- presence/absence of flagella and aerotypes. Among all the abovementioned traits, morphometric traits like size and shape are considered master traits (Weithoff & Beisner, 2019), which affect nutrient acquisition, sinking, and grazer susceptibility (Grover, 1989; Smayda, 1970; Thingstad et al., 2005). Size and shape are also plastic in nature and depend on many environmental variables, such as light levels, nutrient concentrations, and grazing pressure (Chisholm, 1992; Duarte et al., 1990).

Furthermore, in trait-based studies, species sharing similar adaptive traits are grouped even if they are taxonomically distinct (Simberloff & Dayan, 1991). From the phytoplankton viewpoint, the pelagic habitat, its main representative phyla, and their ecology are relatively similar across marine and freshwater ecosystems (Weithoff & Beisner, 2019). Despite such similarity, the focus of research differed between systems, i.e., the majority of research in the marine considered how traits and trait distribution derive processes that determine the environmental conditions (like biogeochemistry), but it is the opposite in the freshwater where the focus is on how communities respond to the environment and which environmental factors drive the trait-based community assembly (Weithoff & Beisner, 2019). For instance, the increasing uses of trait-based studies to explain and understand phytoplankton community is limited to distribution (Kruk et al., 2010), seasonal dynamics (Salmaso & Padisak, 2007), diversity, and community structure (Litchman & Klausmeier, 2008) in freshwater, whereas in the marine ecosystem, the studies are limited to spatiotemporal variation (Stanca et al., 2013), biogeographic trait patterns (Barton et al., 2013), biogeochemical processes such as primary production and nitrogen fixation (Breton et al., 2017), oceanic biogeochemistry (Litchman et al., 2007, 2015; Finkel et al., 2010), and phytoplankton dynamics (Alexander et al., 2015). Many morphological traits might be strategic and help explain phytoplankton differences and patterns under contrasting hydrodynamic conditions (Fraisse et al., 2013). Thus, morphological traits are pivotal in determining phytoplankton ecological niches (Aubry et al., 2017). The morphological adaptive strategy that responds to environmental changes helps differently-sized phytoplankton organisms coexist, making it like a geometric concurrence (Roselli & Basset, 2015; Segura et al., 2013). However, to our knowledge,

the information on the variations in phytoplankton shapes concerning different hydrographic settings in the marine pelagic systems is not available and was addressed in the present study by selecting the eastern Arabian Sea in the Northern India Ocean, a well-studied system, as a reference. A similar approach was attempted to study the rockpool micro-phytoplankton community from the intertidal zone (Paul et al., 2021), but studies from the open ocean are limited even though there exist few datasets on cell volumes (Chitari & Anil, 2017).

The Arabian Sea (AS) is considered one of the unique oceanic basins owing to its high productive periods in winter (WM) and summer monsoon (SM) caused by the seasonal reversal of wind direction and associated drastic changes in the surface currents (Banse, 1987) and the data presented here corresponds to winter monsoon from eastern AS (EAS). The physical change in the water column associated with the reversal of monsoonal winds governs the productivity of the Arabian Sea (Wiggert et al., 2005). During WM, the hydrographic conditions in the northern and southern regions of EAS are significantly different, i.e., currents bring in high nutrients through convective mixing in the NEAS, which supports phytoplankton production (including bloom; Banse, 1987; Sarma et al., 2019) and was also noticed in this study, i.e., higher in NEAS (both open and coastal) than SEAS-O (Tables 4.2 and 4.3). The convective mixing in NEAS is triggered by the cold-dry north-easterly continental wind blowing over the surface waters, causing evaporation (Madhupratap et al., 1996; Weller et al., 2002). The convective mixing during winter monsoons deepens the mixed layer depth and enhances nutrient availability (Sawant & Madhupratap, 1996). Whereas in SEAS, WM is defined by the existence of seasonal down-welling Rossby waves (Shankar et al., 2002) which, along with its associated currents, brings the nutrient-enriched low saline water mass from the western boundary of the Bay of Bengal (Shenoi et al., 2002) and triggers primary producers (Kumar et al., 2004; Amol, 2018) in the otherwise warmer oligotrophic waters (Vijayan et al., 2021). Additionally, the mesoscale features such as sea surface temperature (SST) fronts supporting rich phytoplankton biomass compared to the adjoining non-fronts are also prevalent in AS. However, more SST fronts are reported in NEAS than in SEAS (Kurian et al., 2020). Therefore, in the present study, an attempt has been made to understand the distribution of phytoplankton shapes and species composition between contrasting hydrographic settings such as (a) nutrient-rich coastal and open ocean systems, (b) oligotrophic and non-oligotrophic ocean systems, and (c) SST fronts and non-fronts from both coastal and ocean ecosystems. This study explores

the possibility of using phytoplankton shapes (>5 microns) as ecological indicators in marine pelagic systems.

Table 4.2. Hydrography and nutrient concentration at surface and sub-surface in NEAS-O, NEAS-C, and SEAS-O in winter monsoon. The mean value is calculated for temperature, salinity, and oxygen concentration. The median value is used for nutrient concentration. The numbers in parenthesis indicate the parameter's range values, and the * indicates the chlorophyll concentration value.

Regions of EAS	**Cruise**	**Temperature (ºC)**	**Salinity (PSU)**	**Oxygen (mL L^{-1})**	**Fluorescence (mg/m^3)**	**Nitrate (µM)**	**Phosphate (µM)**
NEAS-O	(0m)	26.1 (25.1-27.0)	36.3 (35.8-36.5)	4.3 (4.0-4.5)	0.54 (µg L^{-1})*	0.95 (0.56-3.23)	0.27 (0.09-0.45)
	(100m)	23.7 (19.5-25.0)	36.5 (36.2-36.7)	3.0 (0.3-4.1)	-	5.80 (3.17-17.0)	0.82 (0.41-1.77)
NEAS-C	(0m)	26.8 (26.3-27.3)	36.3 (35.5-36.7)	4.2 (3.7-4.6)	1.1 (0.2-3.0)	-	-
	(100m)	25.9 (24.0-27.1)	36.6 (36.3-36.7)	2.5 (0.9-4.1)	0.3 (0.2-0.5)	-	-
SEAS-O	T1 (0m)	28.9 (28.5-29.7)	35.4 (35.1-36.5)	4.4 (4.2-4.6)	0.6 (0.1-1.7)	0.96 (0.15-1.67)	0.24 (0.06-0.69)
	T1 (100m)	20.3 (18.8-21.6)	35.2 (35.0-35.7)	0.61 (0.07-0.93)	0.06 (0.003-0.2)	15.1 (10-20.9)	1.2 (1.0-1.9)
	T2 (0m)	29.1 (28.6-29.4)	33.8 (18.6-35.7)	4.3 (3.1-4.5)	0.62 (0.14-1.04)	-	-
	T2 (100m)	18.3 (16.5-21.5)	35.2 (35.1-35.3)	0.7 (0.5-1.0)	0.11 (0.002-0.24)	-	-

Table 4.3. Hydrography and nutrient concentration at surface and sub-surface frontal and non-frontal regions of NEAS-C and SEAS-O in winter monsoon. The mean value is calculated for temperature, salinity, and oxygen concentration. The median value is used for nutrient concentration. The numbers in parentheses indicate the range values of the parameter.

Regions of EAS	Cruise	Temperature (^oC)	Salinity (PSU)	Oxygen (mL L^{-1})	Fluorescence (mg/m^3)
NEAS-C	East Front (0m)	26.6 (26.4-27.1)	36 (35.6-36.6)	4.2 (3.9-4.6)	1.7 (1.1-3)
	East Front (100m)	25.7 (24.8-26.4)	36.5 (36.4-36.6)	2.2 (1.6-3.1)	0.2 (0.2-0.3)
	West Front (0m)	26.8 (26.3-27.1)	36.5 (36.1-36.7)	4.1 (3.7-4.2)	0.6 (0.4-0.9)
	West Front (100m)	26.1 (24.9-27)	36.6 (36.5-36.7)	2.5 (0.5-4.1)	0.4 (0.2-0.5)
	Main Front (0m)	26.7 (26.4-27.1)	36.2 (35.5-36.6)	4.2 (3.8-4.6)	1.4 (0.8-2.2)
	Main Front (100m)	26.1 (25.4-26.8)	36.5 (36.3-36.6)	2.7 (1.6-3.9)	0.3 (0.2-0.4)
	Non-Front (0m)	27.1 (27-27.3)	36.7 (36.6-36.7)	4.2 (4.1-4.2)	1.4 (0.2-9.4)
	Non-Front (100m)	25.7 (24-27.1)	36.6 (36.5-36.7)	2.4 (1.1-4.1)	0.3 (0.2-0.5)
SEAS-O	Non-front West (0m)	29.1 (28.8-29.5)	35.8 (35.3-36.5)	4.3 (4.2-4.4)	0.3 (0.1-0.7)
	Non-front West (100m)	19.6 (18.8-20.6)	35.6 (35.5-35.7)	0.11 (0.07-0.14)	0.18 (0.15-0.20)
	Front (0m)	28.9 (28.5-29.7)	35.3 (35.2-35.3)	4.5 (4.3-4.6)	0.8 (0.3-1.7)
	Front (100m)	20.3 (19-21.2)	35.1 (35-35.1)	0.7 (0.5-0.9)	0.02 (0.003-0.06)
	Non-front East (0m)	28.9 (28.7-29.2)	35.4 (35.1-35.8)	4.4 (4.3-4.5)	0.5 (0.1-0.8)
	Non-front East (100m)	21.1 (20.7-21.6)	35.2 (35.1-35.2)	0.8 (0.7-0.9)	0.1 (0.06-0.1)

4.2.1.2. Methodology

The details of the sampling site, sample collection, and analysis are presented in Chapter 2, sub-section 2.2.1.

Data analysis

Univariate measures such as species count, abundance, Shannon-Wiener's diversity, species richness, and evenness were performed on log-transformed species and shape data. The frontal and non-frontal phytoplankton clustering was performed through the Bray-Curtis similarity and group average methods. Log (x+1) transformed species and shape data were used for the analysis, and the grouping was done at a 50% level to find the significant similarities. Furthermore, the log-transformed taxa and shape data were subjected to a two-way analysis of variance (ANOVA) to evaluate the variation between regions and between the frontal and non-frontal regions. The relationship between the greatest axial linear dimension (GALD) and S:V was determined using linear regression on log(x+1) transformed data. The significance level was set at $p<0.05$, and the determination coefficient (R^2) was considered the proportion of variation in S:V, which can be attributed to GALD, whereas the slope (b) showed the degree to which the S:V would vary as GALD increases. If the slope (b) value is very low, for instance, $b = -0.06$ for PoP, that means a decrease in S:V of 0.06 μm^{-1} for each μm increase in GALD. The negative correlation between GALD and S:V, in general, means that as the GALD increases, the S:V decreases, and vice versa. Univariate measures calculation and clustering analysis were performed using statistical software PRIMER 6, ANOVA was performed using Statistica software (release 8), linear regression analysis and box plots were plotted using R program (R core Team, 2020), and ODV plots were plotted using Ocean Data View 4 (Schlitzer, 2015).

4.2.1.3. Results

4.2.1.3a. Taxonomic and shape diversity of the north-eastern Arabian Sea (NEAS)

A total of 133 (belonging to 63 genera) and 83 (belonging to 48 genera) species were recorded in the open ocean (NEAS-O) and coastal (NEAS-C) regions, respectively (Table 4.4). In NEAS-O, diatoms (81%) comprising 54 species (36 centric and 18 pennate species), followed by dinoflagellates (19%) comprising 89 species dominated the community, whereas in NEAS-C, diatoms (94%) comprising 44 species (30 centric and 14 pennate species) followed by dinoflagellates (6%) comprising 39 species dominated the phytoplankton community. Despite diatom dominance, the contribution to the total

community was higher in the open ocean (82–98%) than in the coastal (77%) (Figure 4.9). ANOVA revealed significant differences in phytoplankton community structure and species dominance between the open ocean and coastal region ($p = 0.003$). The diversity analysis reveals that the species count, richness, evenness, and diversity were higher in the NEAS-O than in NEAS-C, except for the abundance, which showed an opposite trend for taxonomy and shape (Figure 4.10a–j).

In the NEAS-O, centric diatoms *Rhizosolenia styliformis* and *Probosica alata* of Cyl shape followed by pennate diatoms *Lioloma* sp. of B shape and *Navicula* spp. of ElliP shape and dinoflagellate species *Protoperidinium* spp of 2C shape were the major contributors. Whereas in NEAS-C, centric diatom *Skeletonema* sp. of Cyl2Hs shape and *Leptocylindrus* sp. of Cyl shape followed by pennate diatom *Pseudonitzschia* spp. of PoP shape and *Thalassionema nitzschoides* of B shape and dinoflagellate species *Protoperidinium* spp. of 2C shape dominated the community. It is notably interesting that despite the overall phytoplankton community being diatom-dominated, the community structure was quite different within diatoms except for the dinoflagellates.

All the recorded phytoplankton species are categorized into 19 (11 simple and 8 combined) and 16 (11 simple and 5 combined) morphometric shapes from NEAS-O and NEAS-C, respectively. Simple-shaped (88%) phytoplankton dominated in NEAS-O, whereas combined-shaped (55%) in NEAS-C. Among the simple shapes, Cyl (54%) was the dominant shape, followed by ElliP (9%), B (9%), Elli (6%), and ElliP4Cs (5%) in NEAS-O. Maximum species diversity was observed in Elli2CCyl, representing 36 phytoplankton species (all dinoflagellates), followed by Cyl with 27 species (22 centric diatoms and 5 dinoflagellates), Elli with 20 species (all dinoflagellate), and ElliP with 16 species (11 centric and 5 pennate diatoms). Among the combined shaped phytoplankton, Cyl2Hs (53%) was dominant, followed by PoP (12%), ElliP (12%), and Cyl (12%) in NEAS-C. The maximum species diversity was observed in Cyl with 17 species (all centric diatoms), followed by ElliP with 14 species (11 centric and 3 pennate diatoms) and Elli with 14 species (all dinoflagellates).

Table 4.4. Micro-phytoplankton abundance (depth-averaged cells L^{-1}) and the corresponding shape in the open ocean and coastal region of North-eastern Arabian Sea (NEAS-O and NEAS-C) and open ocean of South-eastern Arabian Sea (SEAS-O). Species in bold font indicate diatoms, and normal font indicates dinoflagellates; numbers in parenthesis are numbers of shapes recorded.

Sl No.	Species	NEAS-O	NEAS-C	SEAS-O	Shapes
1.	*Gonyaulax sp*	38	14	24	2 Cones (1)
2.	*G. polygrammum*	0	0	4	
3.	*G. kofoidii*	0	2	2	
4.	*Protoperidinium sp1*	378	398	203	
5.	*Protoperidinium sp2*	109	0	0	
6.	*P. diabolus*	9	0	0	
7.	*P. pallidum*	0	0	22	
8.	*P. tenuissimum*	0	0	44	
9.	***Lioloma sp***	1312	0	0	Box (2)
10.	***Synedra sp***	4	0	34	
11.	***Tabellaria sp.***	0	468	0	
12.	***Thalassionema nitzschioides***	6	4562	24	
13.	***Thalassiothrix sp***	107	65	875	
14.	***T. longissima***	60	0	0	
15.	***Pinnularia***	0	134	0	
16.	***Asterionella sp.***	1	39	0	Box + 2 Cylinder (3)
17.	***Climacosphenia sp***	38	0	0	Box + Elliptic prism (4)
18.	*Podolampus sp*	12	16	0	Cone (5)
19.	*P. palmipes*	2	12	0	
20.	*P. spinifera*	3	0	0	
21.	*Pronoctiluca sp*	1	0	0	Cone + Half sphere (6)

22.	*Amphisolenia sp*	5	0	0	
23.	*A. asrragalus*	5	0	0	
24.	*A. asymmetric*	2	0	0	
25.	*A. bidentata*	0	1	0	
26.	*A. globifera*	3	0	0	
27.	***Asteriomphalus sp***	7	27	20	
28.	***Bacteriastrum sp***	1	0	0	
29.	***Ceratulina sp***	207	216	502	
30.	***Coscinodiscus sp***	326	105	85	
31.	***Cyclotella sp***	22	0	0	
32.	***Dactylosolen sp***	0	26	0	
33.	***Guinardia sp***	36	60	0	
34.	***Guinardia flaccida***	0	0	2	
35.	***Guinardia striata***	190	4	2	
36.	***Lauderia sp.***	0	76	0	Cylinder (7)
37.	***Leptocylindrus sp***	22	2958	4	
38.	***Melosira sp***	6	0	0	
39.	***Planktonella sol***	56	0	11	
40.	***Rhizosolenia sp***	34	0	4	
41.	***R. alata***	1220	6	78	
42.	***R. bergonii***	411	2	37	
43.	***R. calcar-avis***	351	3	27	
44.	***R. castracanei***	6	0	0	
45.	***R. hebetata***	479	9	5	
46.	***R. imbricata***	55	97	18	
47.	***R. robusta***	10	0	0	
48.	***R. setigera***	309	969	13	
49.	***R. stolterfothii***	84	0	0	
50.	***R. styliformis***	1509	15	18	
51.	***Thalassiosira sp***	691	2823	236	
52.	***Corethron sp***	5	13	0	Cylinder + 2 Half sphere (8)
53.	***Skeletonema sp***	548	34126	0	
54.	***Amphora sp***	1	82	0	Cymbelloid (9)
55.	*Hemidiscus sp*	19	0	0	

56.	*Alexandrium sp*	9	7	0	
57.	*Amphidinium sp*	10	0	0	
58.	*Ceratoperidinium sp*	58	0	0	
59.	*Dinophysis sp*	85	3	15	
60.	*D. acuminata*	0	2	3	
61.	*D. caudata*	0	0	13	
62.	*D. miles*	0	4	0	
63.	***Diplonies sp***	22	8	0	
64.	*Dissodinium sp.*	0	1	0	
65.	*D. bicorme*	2	0	0	
66.	*D. elegans*	46	0	0	
67.	*Gymnodinium sp*	14	51	98	
68.	*Gyrodinium sp*	127	162	230	Ellipsoid (10)
69.	*Karlodinium sp*	0	4	0	
70.	*Prorocentrum sp*	43	103	95	
71.	*P. compressum*	0	0	2	
72.	*P. dentatum*	0	26	55	
73.	*P. gracile*	1	7	23	
74.	*P. micans*	8	148	33	
75.	*Pyrocystis sp*	67	2	0	
76.	*P. fusiformis f. fusiformis*	6	0	2	
77.	*P. bamulum*	41	0	0	
78.	*P. fusiformis f. lanceolata*	25	0	0	
79.	*Pyrophacus sp*	9	1	2	
80.	*Scrippsiella sp*	147	123	142	
81.	*Sinophysis sp.*	38	0	6	
82.	*Tripos sp*	64	1	0	
83.	*T. biceps*	1	1	2	
84.	*T. azoricum*	1	0	0	Ellipsoid+2 Cone+ Cylinder (11)
85.	*T. bochmii*	1	18	0	
86.	*T. borridum*	2	0	0	
87.	*T. breve var breve*	0	0	6	
88.	*T. breve var pulchellum*	0	0	4	
89.	*T. bumile*	0	0	4	

90.	*T. candelabrum var. candilabrum*	3	0	2	
91.	*T. contrarium*	2	0	0	
92.	*T. declinatum var angusiicorrum*	1	0	0	
93.	*T. declinatum var declinatum*	0	0	11	
94.	*T. deflexum*	0	2	8	
95.	*T. eherenbergii*	3	0	0	
96.	*T. extensum*	5	0	0	
97.	*T. furca var. berghii*	11	53	50	
98.	*T. furca var. eugrammum*	31	12	0	
99.	*T. fusus*	8	8	31	
100.	*T. fusus var. fusus*	5	0	0	
101.	*T. fusus var. schucttii*	3	0	0	
102.	*T. gravidum*	1	0	0	
103.	*T. humile*	2	0	0	
104.	*T. lineatum*	0	1	2	
105.	*T. longirostrum*	2	0	0	
106.	*T. longissimum*	1	0	0	
107.	*T. lunula var. lunula*	2	0	0	
108.	*T. macroceros var. gallicum*	0	0	8	
109.	*T. massiliense var. massiliense*	1	0	0	
110.	*T. pentagonum var. subrobustum*	4	0	0	
111.	*T. pentagonum var. tenerum*	6	37	4	
112.	*T. petersi*	0	0	6	
113.	*T. ramipes var. palmatum*	4	0	0	
114.	*T. symmetricum var. coaractatum*	3	0	0	
115.	*T. teres*	20	2	0	
116.	*T. trichoceros*	62	0	0	
117.	*T. tripos var. atlanticum*	63	0	51	
118.	*T. tripos var. indicum*	0	0	2	
119.	*T. tripos var. pulchellum*	124	0	8	
120.	*T. vultur var japonicum*	1	0	0	
121.	***Amphiproroa sp.***	1	13	0	

122.	***Chaetoceros sp***	273	6125	487	
123.	***C. atlanticum***	35	2	0	
124.	***C. coaractatus***	43	0	0	
125.	***C. laciniosus***	23	0	0	
126.	***C. peruvianus***	0	0	7	
127.	***Eucampia sp***	1	23	0	
128.	***Fragilaria sp***	222	3	15	
129.	***Hemiaulus sp***	122	6	0	
130.	***H. hauckii***	0	36	0	Elliptic prism (12)
131.	***H. membranceae***	0	44	0	
132.	***Meuneria sp***	186	14	0	
133.	***Navicula sp***	501	1146	483	
134.	***N. transistans***	39	0	0	
135.	***Odontella sp***	45	4	3	
136.	***O. mobilensis***	0	34	2	
137.	***O. sinensis***	0	1	0	
138.	***Surirella sp***	36	0	0	
139.	***Trachyneis aspera***	2	0	0	
140.	***Climacodium sp***	431	31	47	Elliptic prism+ 4 Cones (13)
141.	*Ceratocorys sp*	17	0	4	Half sphere (14)
142.	*C. armata*	1	0	0	
143.	*Ornithocercus sp*	139	0	5	
144.	***Nitzschia sp***	34	102	14	Prism on parallelogram (15)
145.	***Pleurosigma sp***	70	160	16	
146.	***Pseudonitzschia sp***	158	7529	1180	
147.	***Ditylum sp***	0	97	0	Prism on triangle (16)
148.	*Triceratium sp*	4	0	5	
149.	*Oxytoxum sp*	43	27	3	Prolated spheroid (17)
150.	*O. caudatum*	6	0	0	
151.	*O. cf. crassum*	2	2	0	
152.	*O. cf. globosum*	1	2	0	
153.	*O. challengeroides*	1	0	0	
154.	*O. curvatum*	1	13	0	

155.	*O. curvicaudatum*	20	2	0	
156.	*O. diploconus*	6	0	3	
157.	*O. lanticeps*	3	0	0	
158.	*O. longum*	21	0	0	
159.	*O. parvum*	0	0	4	
160.	*O. scolopax*	17	6	12	
161.	*O. tesselatum*	21	4	3	
162.	***Cylindrotheca closterium***	13	657	30	Prolated spheroid + 2 Cylinders (18)
163.	*Cladopyxis sp*	1	0	0	Sphere (19)
164.	*Noctiluca sp*	169	1	0	
	Total	**12606**	**64204**	**5541**	

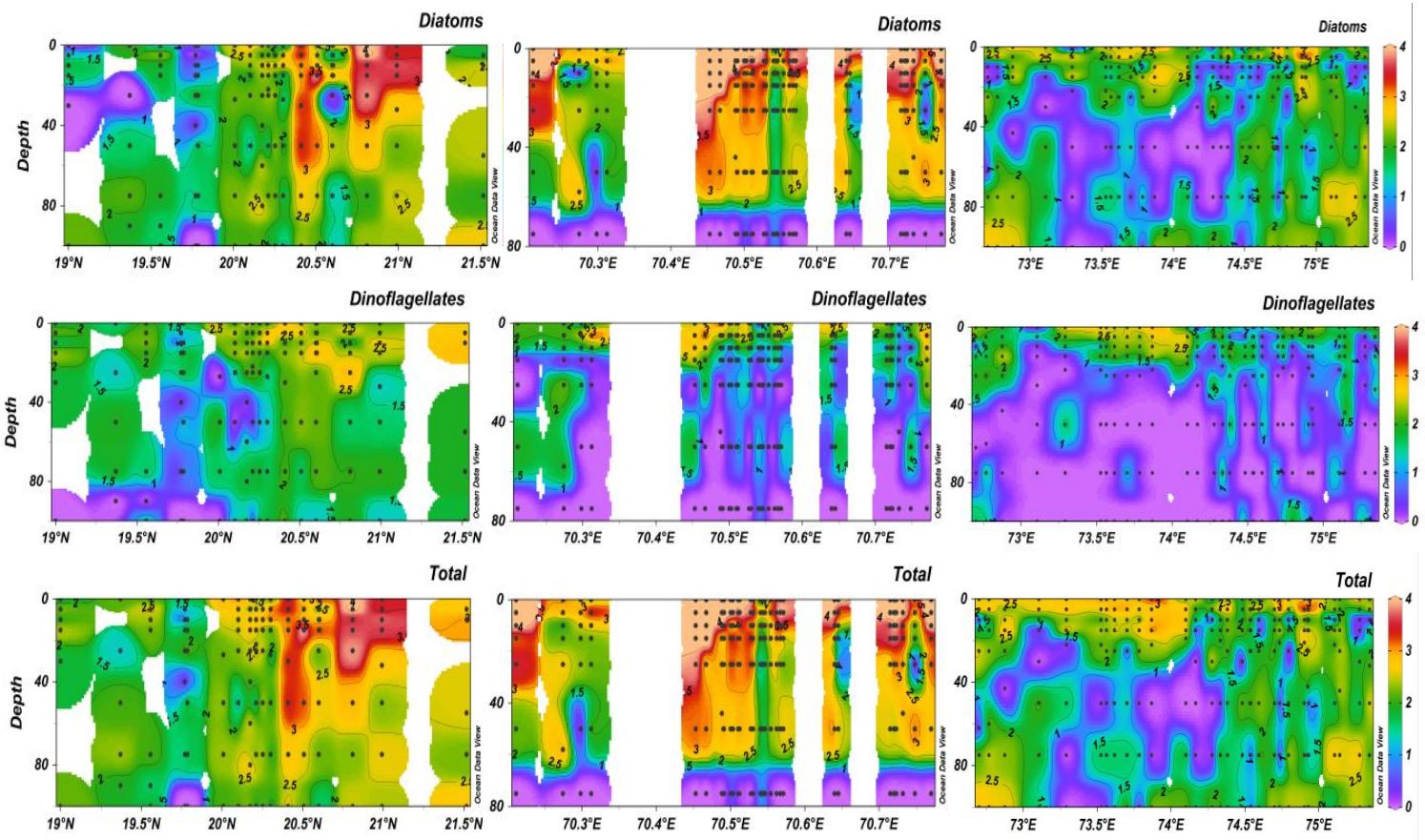


Figure 4.9. Groupwise distribution of phytoplankton in the water column of NEAS and SEAS. NEAS-O: North-eastern Arabian Sea open ocean; NEAS-C: North-eastern Arabian Sea coastal region and SEAS-O: South-eastern Arabian Sea open ocean.

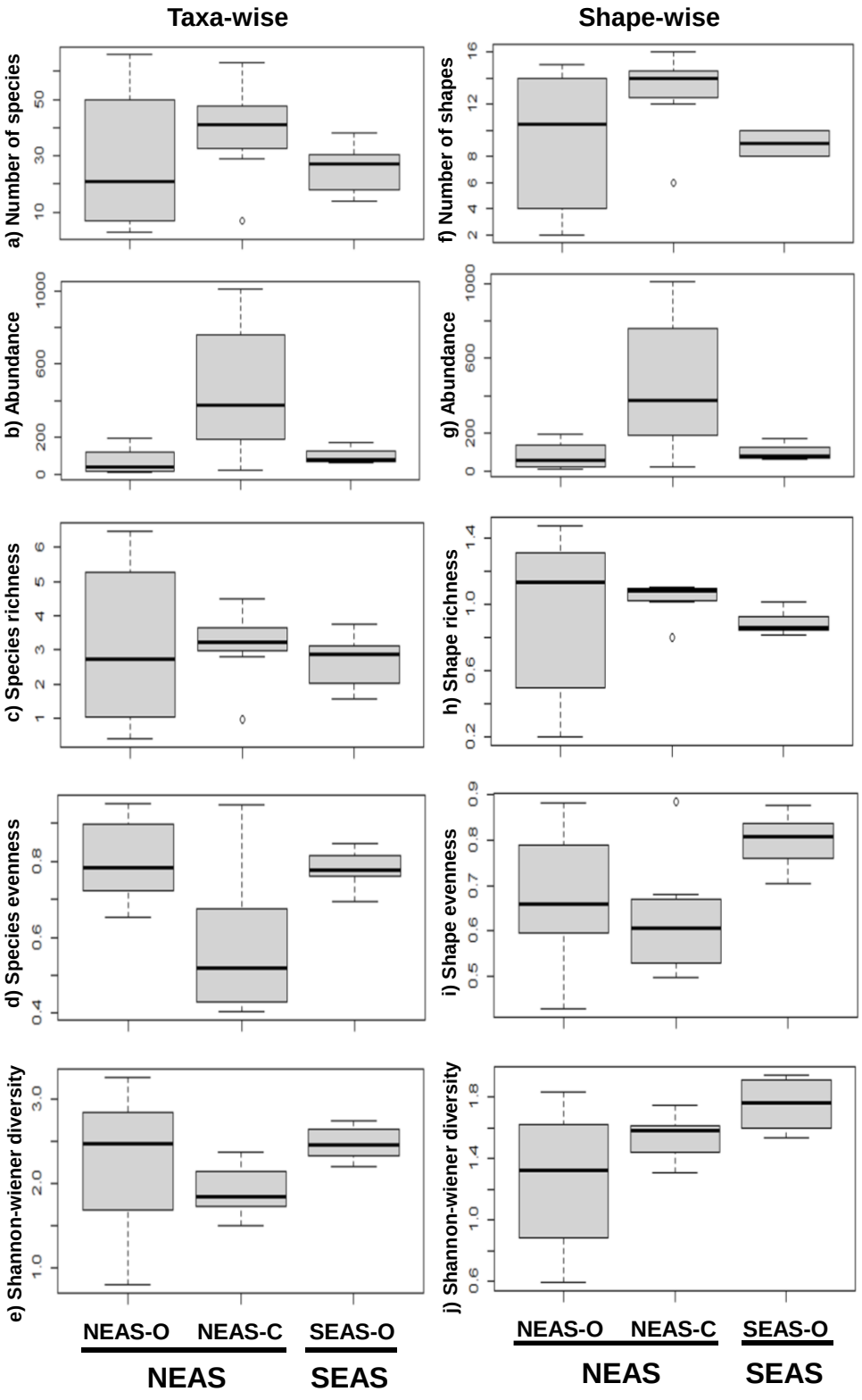


Figure 4.10. Univariate measures of phytoplankton (both taxonomy and shape-wise) from NEAS (both coastal and open ocean) and SEAS (open ocean). Station data are pooled and presented here.

The linear regression analysis of dominant phytoplankton shapes (abundance ≥ 60%) from NEAS-O revealed a significant negative correlation between GALD and S:V ($p < 0.05$), whereas no significant correlation was observed for NEAS-C (Figure 4.11). In the NEAS-O, the determination of coefficient (R^2) for dominant shapes showed low values. However, in the present study, the dominant shapes (Cyl, ElliP, and PoP) of both coastal and open ocean ecosystems in NEAS adopted high S:V with a low GALD strategy. The results point out that all the dominant shapes in NEAS-O are attenuated (Cyl, ElliP, and PoP) and have adapted the strategy to conserve the optimal S:V, which changes very minimally as the GALD increases (Figure 4.11).

Additionally, the sampling at 38 stations in the NEAS-C region encompasses both frontal and non-frontal regions and is categorized and presented accordingly as follows: (a) east front (EF) comprising 7 stations, (b) west front (WF) comprising 5 stations, (c) main front (MF) comprising 18 stations, and (d) non-front (NF) comprising of 8 stations (Figure 4.12). It is evident from the comparative community and diversity analysis that the frontal waters showed high abundance and species composition compared to the non-frontal waters (Figure 4.13a–e). Among all the stations, MF recorded the maximum number of phytoplankton species, followed by EF, NF, and WF waters. The phytoplankton abundance was higher in all the frontal stations compared to NF. Interestingly, species richness, evenness, and diversity were higher in the NF stations compared to all the frontal stations (MF, EF, and WF) (Figure 4.13c–f).

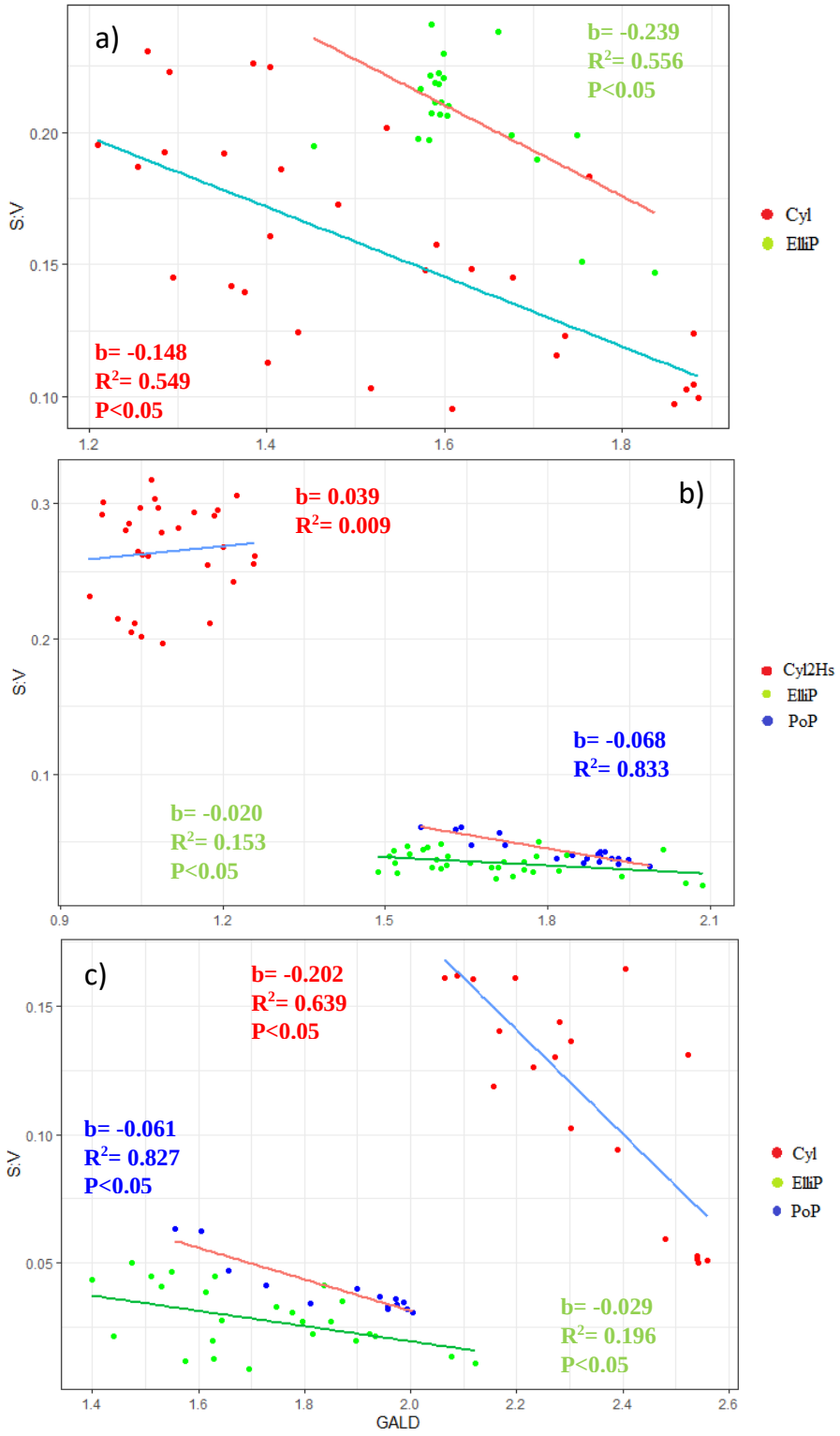


Figure 4.11. Relationship between GALD and S:V for the 8 dominant shapes recorded in North-eastern (NEAS-O and NEAS-C) and South-eastern Arabian Sea during the study period. a) NEAS-O: North-eastern Arabian Sea open-ocean, b) NEAS-C: North-eastern Arabian Sea coastal waters, and c) SEAS-O: South-eastern Arabian Sea open ocean; Cyl: Cylinder; ElliP: Elliptic prism; Cyl2Hs: Cylinder + 2 Half sphere; PoP: Prism on parallelogram.

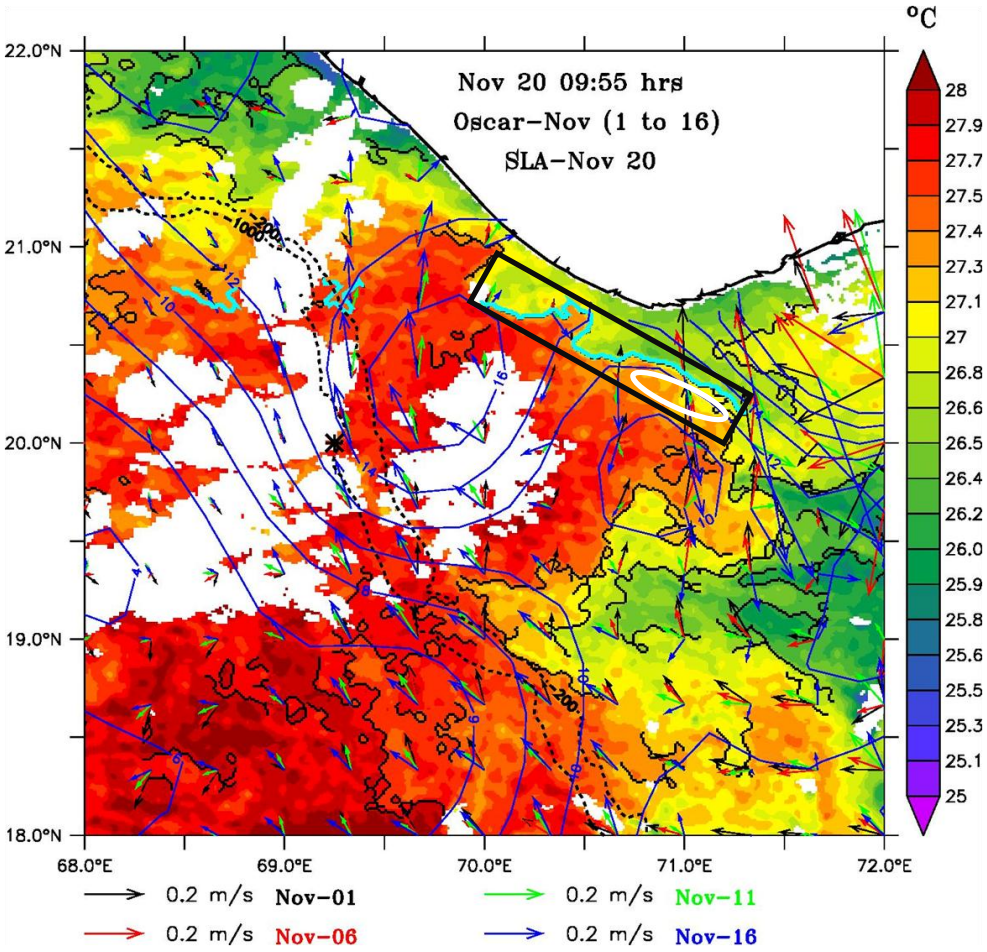


Figure 4.12. Map showing Sea level anomaly (SLA) plot with SST frontal and non-frontal regions in coastal region of NEAS. The blue line is showing the location of the fronts, the black rectangle and white oval shapes showing the frontal and non-frontal part sampled in the present study.

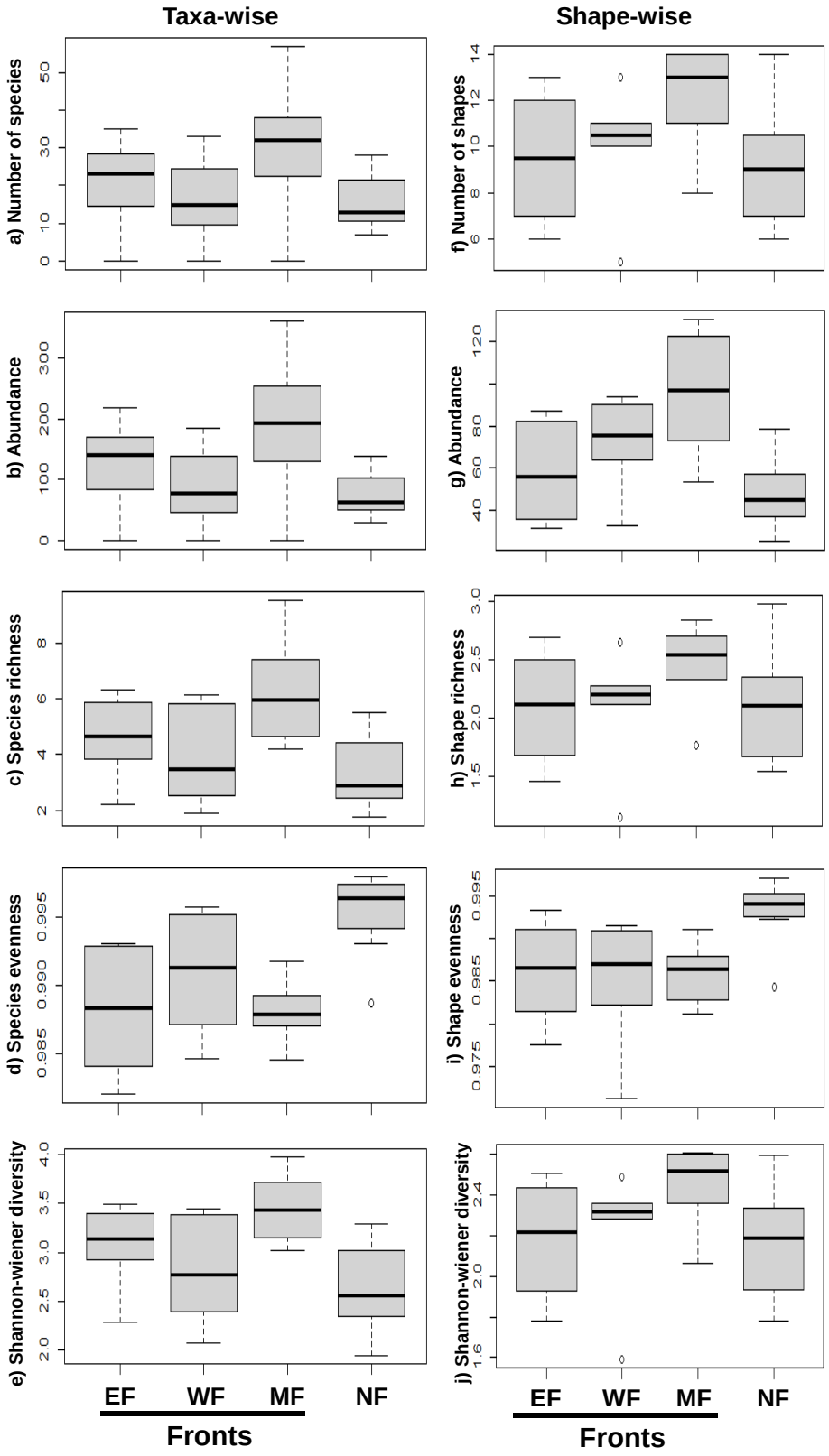


Figure 4.13. Univariate measures of phytoplankton (both taxonomy and shape-wise) from frontal and non-frontal in the coastal region of NEAS. EF: East front; WF: West front; MF: Main front and NF: Non-front. Station data from the frontal and non-frontal regions are pooled and presented here.

A total of 67 phytoplankton species (39 diatoms (26 centric and 13 pennate) and 28 dinoflagellate species) representing 44 genera were recorded in the MF, followed by EF with 52 species (32 diatoms (20 centric and 12 pennate) and 20 dinoflagellate species) from 38 genera, NF 50 species (27 diatom (18 centric and 9 pennate) and 23 dinoflagellate species) from 34 genera, and WF 49 species (31 diatom (19 centric and 12 pennate) and 18 dinoflagellate species) from 36 genera. Diatoms in the frontal waters, contributing 90–98% of the total abundance, dominated the entire phytoplankton community, whereas dinoflagellates contributed only 2–10%. The non-frontal waters were also diatom-dominated, contributing 81% of the total abundance, and dinoflagellates contributed the remaining 19%.

The shape-based morphometric analysis from the frontal and non-frontal regions of NEAS-C reveals that simple shapes dominated the WF (56%) and NF (69%), whereas combined shapes dominated the EF (57%) and MF (55%). The dominant shapes in all the frontal regions (except NF) were Cyl2Hs (43-56%), followed by PoP (11-15%), ElliP (11-12%), and Cyl (11-15%). The dominant shape in the NF region was Cyl (23%) followed by Cyl2Hs (22%), PoP (17%), and ElliP (15%). The maximum shape diversity in all the frontal (11-14 species) and non-frontal (13 species) regions was observed in the Cyl shape. However, the univariate measurement reveals that the shape richness, evenness, and diversity were higher in the non-frontal regions than in the frontal regions, except for the abundance (N), which was higher in the frontal region (Figure 4.13f–j).

The dominant shapes such as Cyl2Hs (centric diatom *Skeletonema* sp.), PoP (*Pseudonitzschia* spp.), ElliP (*Chaetoceros* spp. and *Navicula* spp), and Cyl (*Thalassiosira* spp. and *Leptrocylindrus* spp.) in the frontal region are represented by diatoms. In the non-frontal region, Cyl was the dominant shape and is majorly represented by *Leptocylindrus* spp. and *Thalassiosira* spp. Taxonomically, the centric diatom community was dominated by *Skeletonema* sp. and *Leptocylindrus* spp., whereas the pennate community was dominated by *Pseudonitzschia* spp. and *Navicula* spp. The dinoflagellate communities in both frontal and non-frontal waters were dominated by *Protoperidinium* spp. The cluster analysis for both taxonomy and shape show two distinct clusters in which all the frontal stations (MF, EF, and WF) showed significant taxonomic similarity and formed one single cluster and NF as another cluster (Figure 4.14); however, the number of shapes was insignificant between the frontal and non-frontal regions. ANOVA also revealed significant ($p = 0.0001$) taxonomic differences between MF and

NF regions but significant shape dissimilarity between frontal and non-frontal regions was not found ($p > 0.05$).

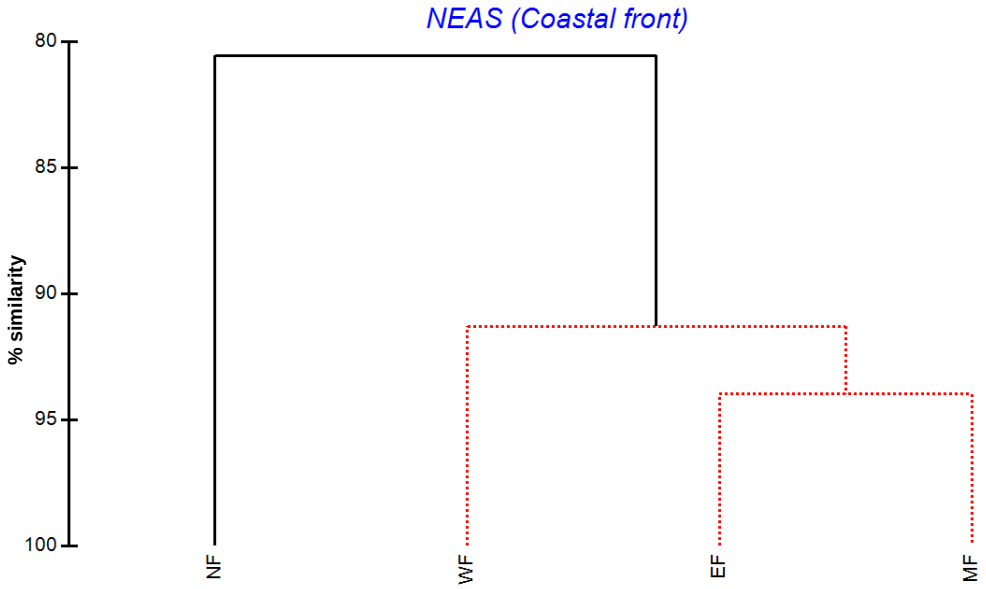


Figure 4.14. Shape-wise cluster plot of micro-phytoplankton community of frontal and non-frontal coastal NEAS. WF: West front, EF: East front, MF: Main front and NF: Non-front.

4.2.1.3b. Taxonomic and shape diversity of the south-eastern Arabian Sea (SEAS)

In SEAS-O, 74 phytoplankton species belonging to 35 genera were recorded from two transects (T1 and T2). Of the 74 species, 30 and 44 species were represented by diatoms (21 centric and 9 pennate species) and dinoflagellates, respectively; despite the high number of dinoflagellate species, the phytoplankton community was dominated by diatoms (77%). Unlike NEAS-O, the percentage contribution revealed the maximum contribution by pennate diatoms (48%) followed by centric diatoms (29%) and dinoflagellates (23%). *Cerataulina* sp. and *Chaetoceros* spp. dominated the centric diatom community, whereas *Pseudonitzschia* spp. and *Thalassiothrix* sp. dominated the pennate diatom community. *Gyrodinium* sp., *Protoperidinium* spp., and *Scrippsiella* sp dominated the dinoflagellate community. Between the transects, transect 1 (T1) comprising 19 stations showed a slightly higher abundance than transect 2 (T2) comprising 12 stations. 68 species belonging to 35 genera and 42 species belonging to 28 genera were recorded from T1 and T2, respectively. Of the 68 species in T1, 28 and 40 species were represented by diatoms (19 centric and 9 pennate species) and dinoflagellate,

respectively. Meanwhile, in T2, they were represented by an equal number of species, i.e., 21 diatom species (13 centric and 8 pennate species) and dinoflagellates. In both transects, diatoms (76% in T1 and 84% in T2) dominated the community, followed by dinoflagellates (24% in T1 and 16% in T2). Among the diatoms, the pennate contribution was higher than centric diatoms. Also, the community in both transects is represented by the same dominant species. For instance, in T1, the centric diatom community was dominated by *Cerataulina* sp., *Chaetoceros* spp., and *Thalassiosira* sp., whereas *Pseudonitzschia* spp. and *Navicula* sp. dominated among pennate diatoms. The dinoflagellate community was dominated by *Protoperidinum* sp., *Gyrodinium* sp., and *Scrippsiella* sp. In T2, *Chaetoceros* spp. and *Thalassiosira* sp. were the dominant centric diatoms, whereas *Pseudonitzschia* sp. and *Thalasiothrix* sp. dominated the pennate diatom community. *Gyrodinium* spp. and *Protoperidinium* spp. dominated the dinoflagellate community. Univariate measures revealed that T1 showed higher species number, abundance, richness, diversity, and evenness than T2 (Figure 4.15a–e). All the recorded 74 phytoplankton species categorized into 12 morphometric shapes (9 simple and 3 combined) were recorded in the SEAS-O. Simple shapes showed maximum contribution (93–97%) compared to the combined shapes (3–7%). Considering the T1 and T2 transect, Cyl (23%) followed by PoP (19%), ElliP (18%), Elli, and B (14% each) dominated the phytoplankton community. T1 and T2 recorded similar shapes, but Cyl (29%) dominated the former and PoP (32%) in the latter. ElliP2CCyl and Cyl showed maximum diversity, representing 16 species each in T1, and Cyl (9 species) and Elli (7 species) in T2 showed the maximum diversity. The most dominant shape (Cyl) in T1 was represented by centric diatoms *Cerataulina* spp. and *Thalassiosira* spp., and the dominant shape PoP in T2 was represented by pennate diatom *Pseudonitzschia* spp. The diversity analysis of T1 and T2 revealed that shape abundance, evenness, and diversity were higher in T1 except for richness (d) which was higher in T2 (Figure 4.15f–j). Similar to NEAS-O, the linear regression analysis of dominant phytoplankton shapes (abundance $\geq 60\%$) revealed a significant negative correlation between GALD and S:V ($p < 0.05$) (Figure 4.11) with the highest determination of coefficient (R^2) was recorded for PoP followed by Cyl. The dominant shapes (Cyl, ElliP, and PoP) of SEAS-O adopted low S:V with a high GALD strategy. The results point out that all the dominant shapes in SEAS-O are attenuated (Cyl, ElliP, and PoP) and have adapted the strategy to conserve the optimal S:V, which changes very minimally as the GALD increases (Figure 4.11).

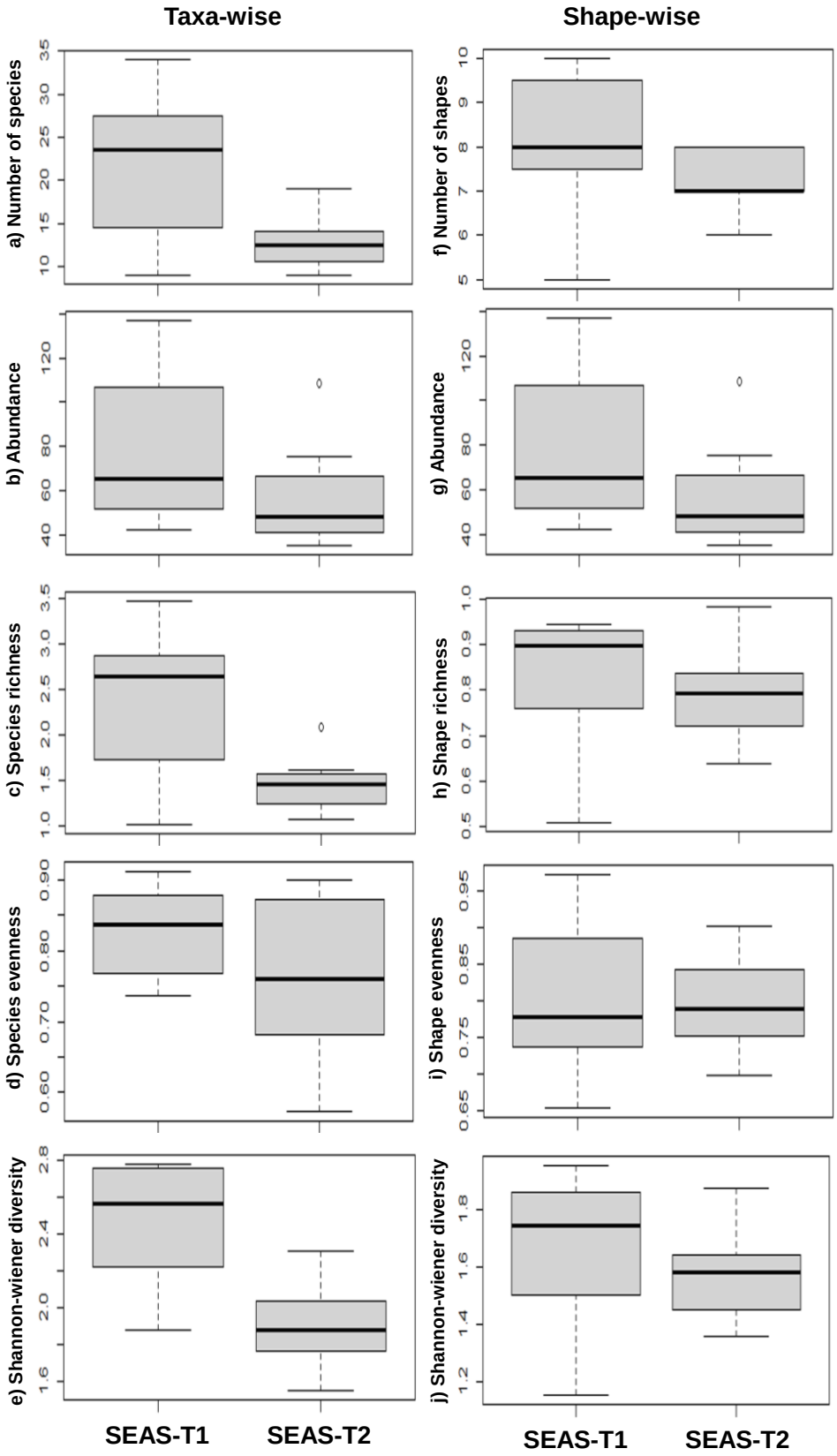


Figure 4.15. Univariate measures of phytoplankton (both taxonomy and shape-wise) from transects T1 and T2 of SEAS (open ocean). Station data are pooled and presented here.

Additionally, T1 in SEAS-O encompasses 19 stations in both frontal (F) and non-frontal (NF) regions, and the results are presented accordingly. Of the 19 stations, 10 stations were frontal (F) and 9 stations were non-frontal (NF). Furthermore, the NF region was again divided into two zones, NF-west (NFW) and NF-east (NFE). The diversity analysis shows that the species count, richness, evenness, and diversity are higher in the frontal region than in the NF regions, except for the abundance, which is higher in the NFE (Figure 4.16a–e). A total of 45 species belonging to 24 genera and 38 belonging to 27 (in NFW) and 26 (in NFE) genera were recorded in F and NF, respectively. Of the 45, 18 and 27 species correspond to diatoms (13 centric and 5 pennate species) and dinoflagellates, respectively, in F, whereas in NF, 20 diatoms (12 centric and 8 pennate species) plus 18 dinoflagellates and 16 diatoms (10 centric and 6 pennate species) plus 22 dinoflagellates were recorded from NFW and NFE, respectively. In all the regions, diatoms dominated the phytoplankton community, i.e., 70%, 79%, and 77% in frontal, NFW, and NFE, respectively. In the frontal region, pennate diatom (*Pseudonitzschia* spp.) dominated, whereas centric diatoms (*Chaetoceros* spp. and *Cerataulina* sp.) dominated the NF (NFE and NFW) regions. *Gyrodinium* sp. and *Protoperidinium* spp. dominated the dinoflagellate community in both frontal and NF regions. The cluster analysis shows that frontal and NFE are significantly similar and form a single cluster in the dendrogram (Figure 4.17). Between non-frontal (both NFW and NFE) and frontal, 11 and 10 morphometric shapes were recorded in the former and later, respectively. Simple-shaped phytoplankton dominated (92–95%) both the frontal and non-frontal regions, whereas combined shape contributed only 5–8%. Among the simple shapes, Cyl-shaped phytoplankton dominated (28–41%) the non-frontal regions, whereas frontal regions were co-dominated by Elli (26%) and Cyl (21%) shape (Figure 4.18). Interestingly, the species structure was different although Cyl-shape was most dominant in both the frontal and non-frontal regions. In NFW, Cyl-shape was represented by *P. alata* and *Cerataulina* spp. and NFE was dominated only by *Cerataulina* spp. The Elli shape was mostly represented by dinoflagellates (*Gyrodinium* spp. and *Scrippsiella* spp.) in the frontal regions. Maximum diversity among shapes in the frontal regions was observed with Cyl, Elli, and ElliP2CCyl, which were represented by 11 species each, whereas maximum species diversity among the non-frontal regions was observed with Cyl (7–10 species) and Elli (7–9 species) shapes. The diversity analysis reveals that NFE and NFW have a similar number of shapes, and richness is relatively higher than in the frontal regions (Figure 4.16f & d). NFE showed the maximum abundance, followed by front and NFW. The

cluster analysis showed that the non-frontal regions are similar to each other but dissimilar to the frontal regions, but ANOVA does not show any significant dissimilarity ($p > 0.05$) (Figure 4.17).

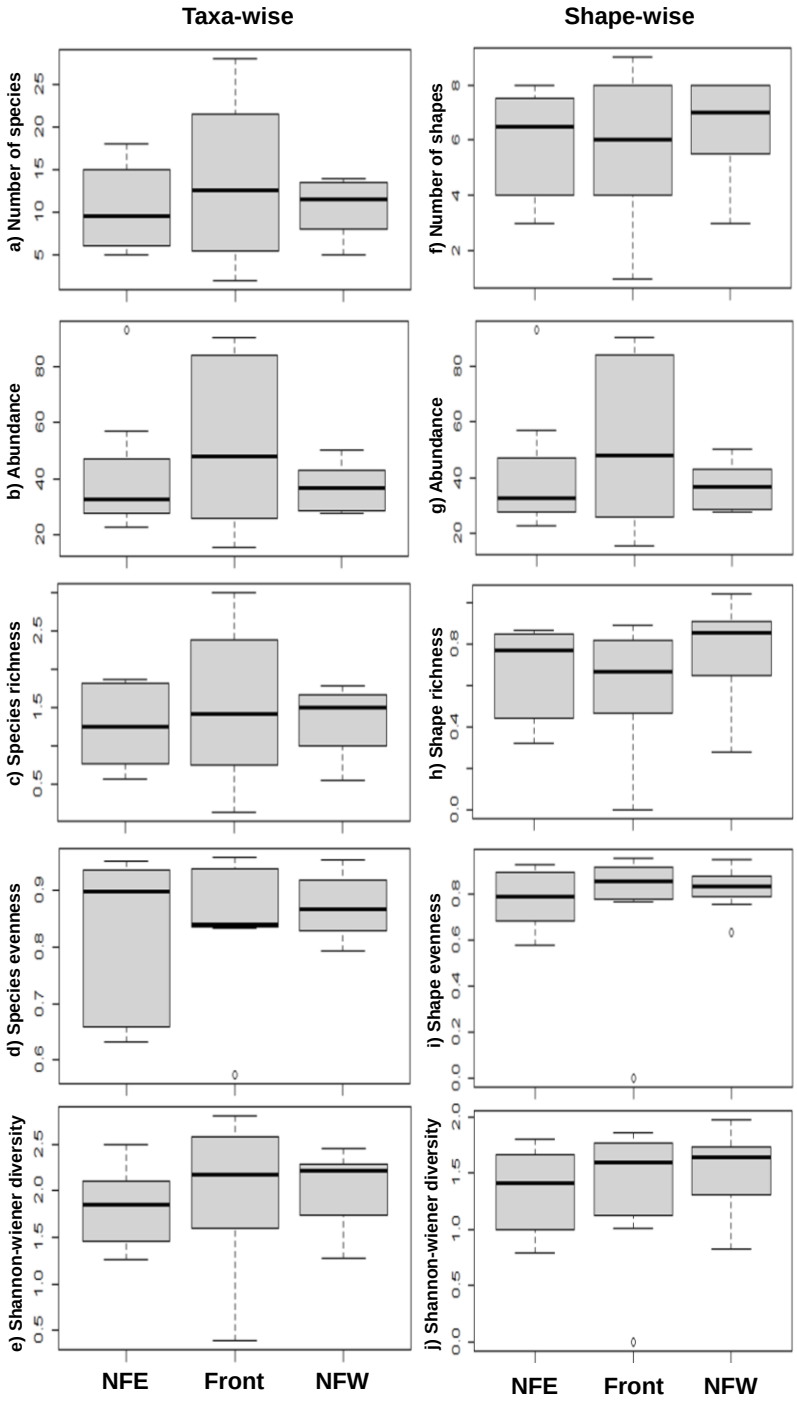


Figure 4.16. Univariate measures of phytoplankton (both taxonomy and shape-wise) from frontal and non-frontal in the oceanic region of SEAS. NFW: Non-front West; F: Frontal region and NFE: Non-front East. Station data from the frontal and non-frontal regions are pooled and presented here.

4.2.1.3c. Taxonomic and shape diversity comparison between NEAS-O and SEAS-O

The chain-forming centric diatoms (e.g., *P. alata* and *R. styliformis*; 62%) dominated the NEAS-O, whereas pennate diatoms (*Pseudonitzschia* spp.; 48%) dominated in the SEAS-O. The percentage contributions of diatom and dinoflagellates differed in the NEAS-O and SEAS-O, where dinoflagellates contributed less (2%) in the former than the latter (23%). The dinoflagellate community was dominated by a single genus (*Protoperidinium* spp.) in NEAS-O, whereas *Gyrodinium* spp., *Protoperidinium* spp., and *Scrippsiella* spp. co-dominated the community in the SEAS-O. The abundance, species richness, evenness, and diversity were higher in the NEAS-O than in SEAS-O (Figure 4.10a-e). The cluster analysis based on Bray–Curtis similarity shows that the NEAS-O and SEAS-O are significantly dissimilar (Figure 4.19). The shape richness was higher in NEAS-O (19 shapes) than in SEAS-O (12 shapes) (Figure 4.10f-j). The most dominant shape was Cyl, comprising 27 phytoplankton species (22 centric diatoms and 5 dinoflagellate species) and PoP, comprising 3 pennate diatom species in NEASO and SEAS-O, respectively (Figure 4.20). The most species diverse shape Elli2CCyl comprised 36 and 16 dinoflagellate species in NEAS-O and SEAS-O, respectively. The univariate analysis revealed that the number of shapes, abundance, and shape richness was higher in NEAS-O than in SEAS-O, but shape evenness and diversity showed an opposite trend (Figure 4.10f-j).

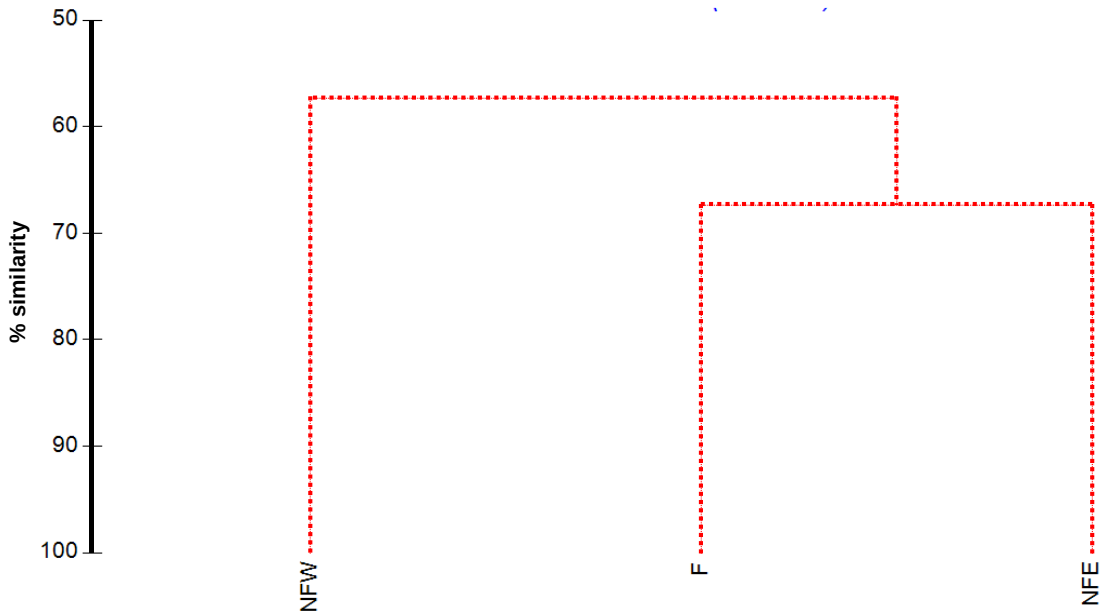


Figure 4.17. Taxonomy wise Cluster plot of open ocean frontal and non-frontal region micro-phytoplankton community of SEAS. NFW: Non-front West, F: Frontal region and NFE: Non-front East.

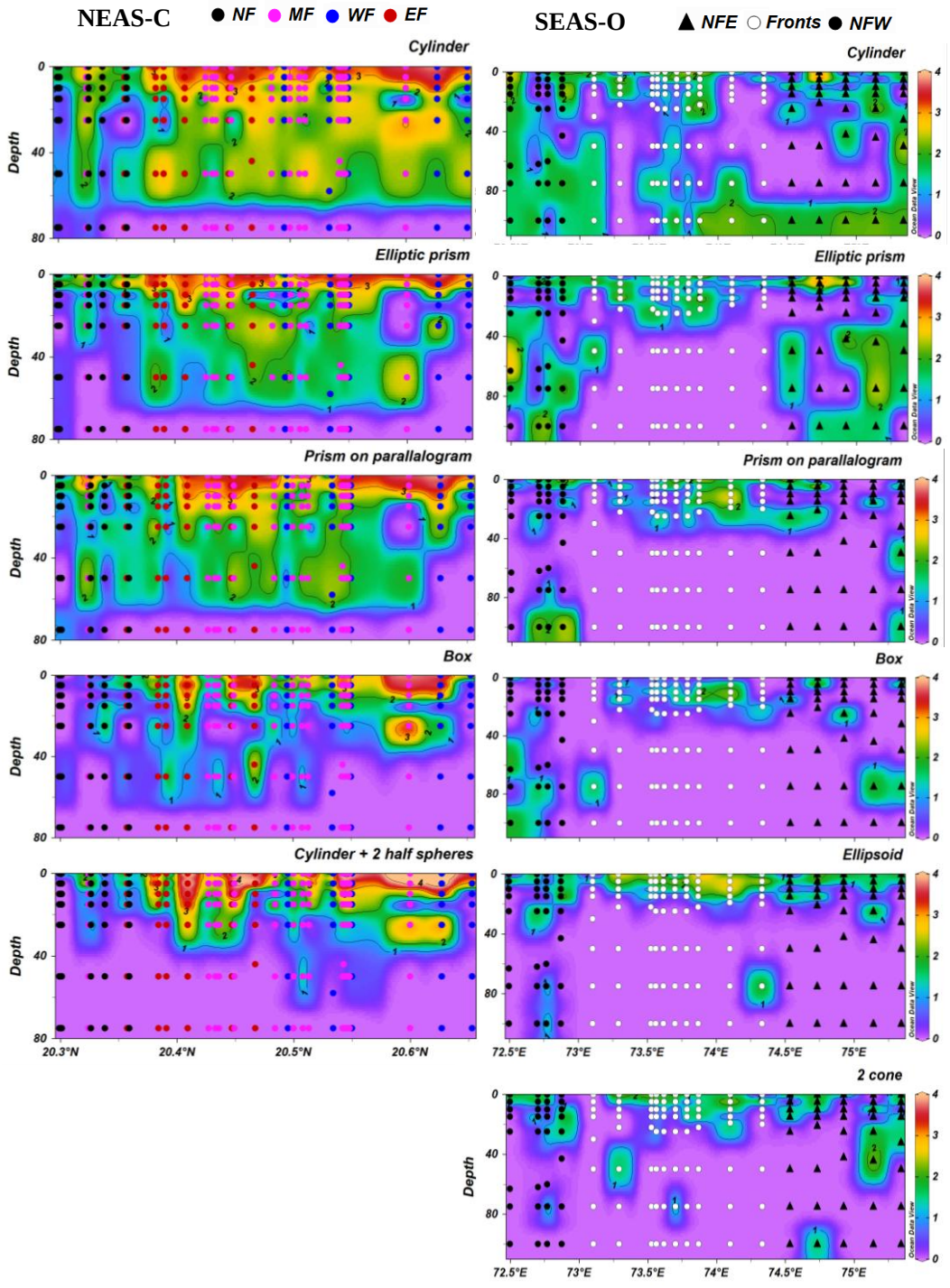


Figure 4.18. Distribution of dominant phytoplankton shape in the frontal and non-frontal water column of NEAS and SEAS. NEAS-C: Coastal North-eastern Arabian Sea; SEAS-O: Open Ocean South-eastern Arabian Sea; NF: Non-front; MF: Main front; WF: West front; EF: East front; NEF: Non-front East and NFW: Non-front West.

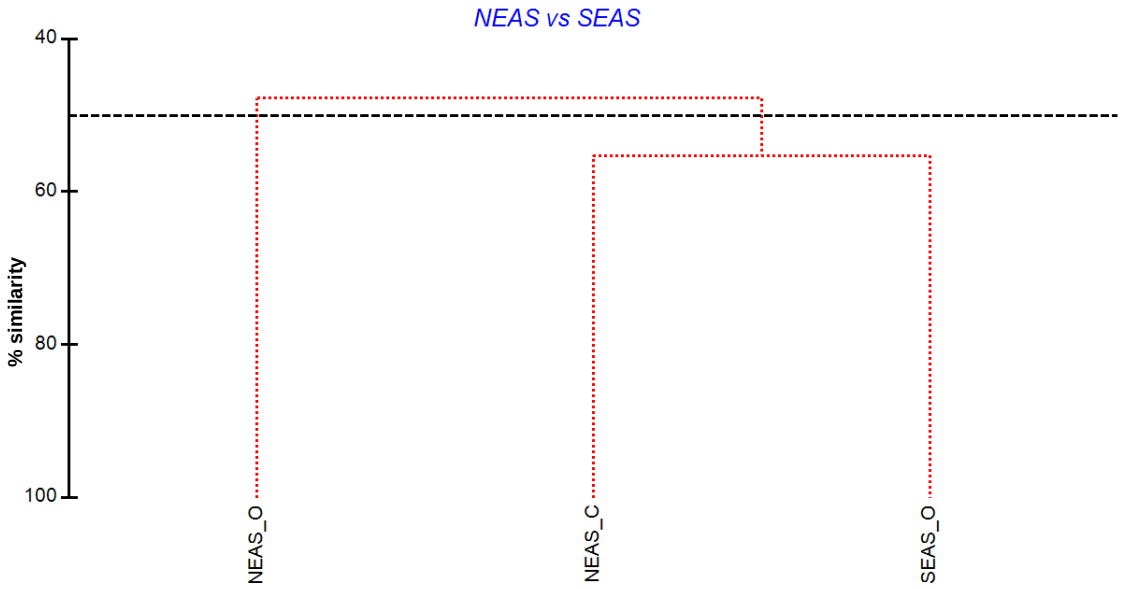


Figure 4.19. Taxonomy-wise cluster plot of micro-phytoplankton community of NEAS and SEAS. NEAS-O: North-eastern Arabian Sea open ocean, NEAS-C: North-eastern Arabian Sea coastal region, and SEAS-O: South-eastern Arabian Sea open ocean.

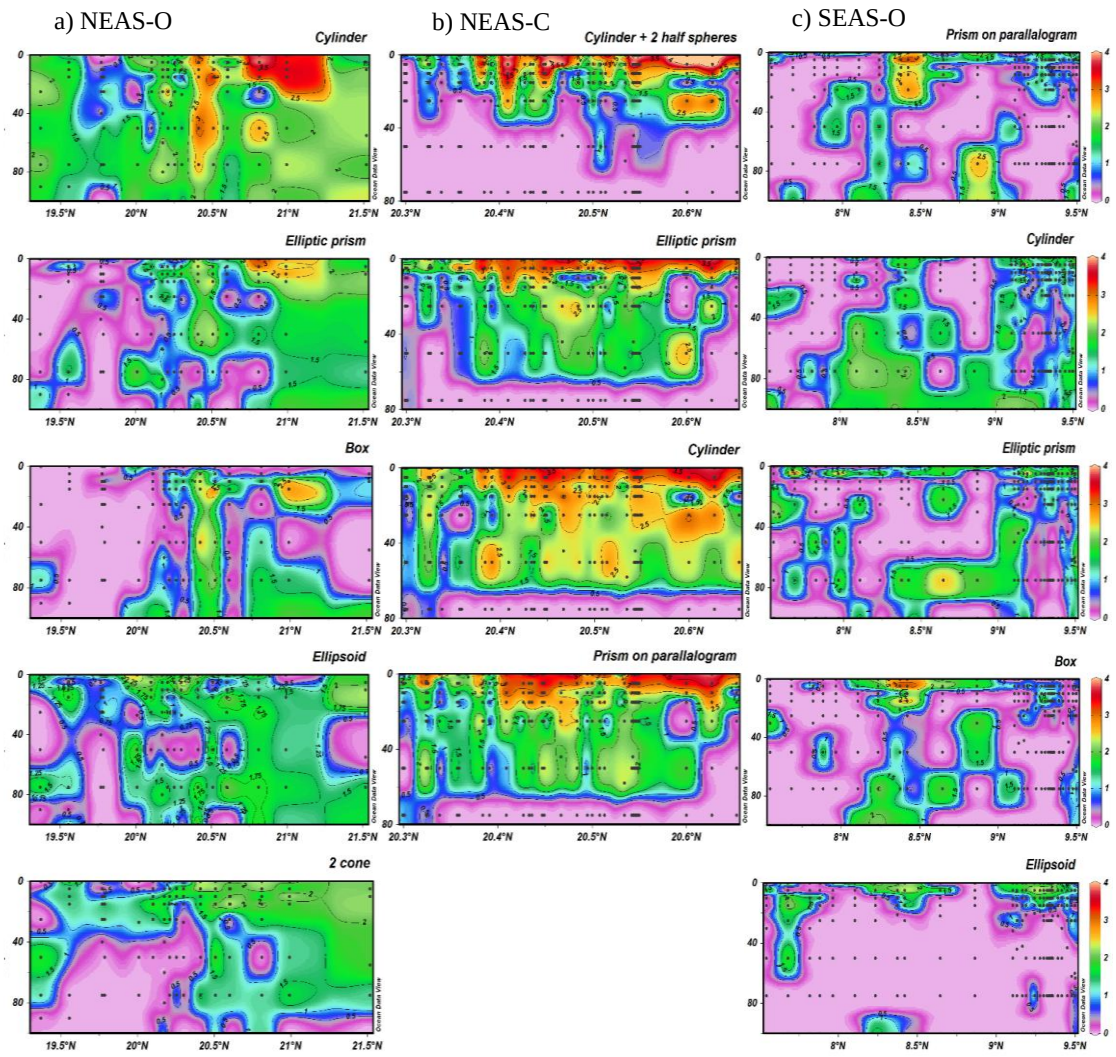


Figure 4.20. Distribution of dominant phytoplankton shape in the water column of NEAS and SEAS. NEAS-O: North-eastern Arabian Sea open ocean; NEAS-C: North-eastern Arabian Sea coastal region and SEAS-O: South-eastern Arabian Sea open ocean.

4.2.1.4. Discussion

This study recorded 164 species and represents most (accounting for up to 71%) of the geometric shapes (22 out of 31 described shapes of Sun and Liu (2003)) described for phytoplankton in literature (Table 4.4). The remaining unrecorded 9 shapes are mostly represented by the freshwater species or the phytobenthos in the sunlit zone or belong to groups (e.g., flagellates, Euglenophyceae, Chlorophyceae) that were not recorded due to known technical limitations (e.g., preservatives) through microscopy approach. The latter may be significant as the present study deals with species from marine pelagic systems but not freshwater or benthic habitats. The phytoplankton marker pigment data for the

eastern Arabian Sea, including from the presented NEAS-O transect (Sarma et al., 2018) and available literature (Bemal et al., 2019; Chandrasekhararao et al., 2018; Roy et al., 2015), indicated the presence of groups such as non-thecate dinoflagellates (peridinin), Chrysophyceae (19′-butanoyloxyfucoxanthin), haptophytes (19′-hexanoyloxyfucoxanthin), cyanobacteria (zeaxanthin), Prochlorococcus (divinyl chlorophyll-*a* and -*b*), chlorophytes (chl-*b*), and prasinophytes (prasinoxanthin). Since the present study is based on microscopic analysis, only the dominant groups (>5 μm), like diatoms and thecate dinoflagellates, are possible to consider, but not the above-mentioned groups (except picophytoplankton) due to methodological limitations (Lugols-Iodine and Formalin; Williams et al., 2016). Also, picophytoplankton are not considered, and *Trichodesmium* preserved well with the fixative but was not found in this study. Considering methodological limitations in the microscopic method, the phytoplankton shape data are generally underestimated, and even then, they are successfully used and tested to understand the phytoplankton dynamics in both freshwater (mostly community-related) and marine systems (process-related) (e.g., Aubry et al., 2017; Stanca et al., 2013). Despite methodological limitations, this study also revealed that EAS harbors most of the described phytoplankton shapes and species showing dissimilar spatial distribution patterns concerning abundance, composition, and diversity. In this study, the variability in distribution patterns between bioregions having distinct hydrographic conditions is discussed in the subsequent sections.

4.2.1.4a. Variability between coastal and open ocean ecosystems

The contrast in the oceanographic conditions is well reflected in both taxa and morphology for the NEAS-C and NEAS-O phytoplankton communities. The diatom dominance (also reported in previous studies, e.g., by Vijayan et al., 2021 and references therein) is represented by different species and morphotypes, but NEAS-O harbored rich species and shape diversity compared to the NEAS-C. Such high variability in geometric shape is not a coincidence but a morphological adaptation to environmental conditions. Similar findings are also reported from the coastal waters of the Salento Peninsula (Italy) where the phytoplankton shapes were dependent on environmental conditions and strongly varied with the season (Stanca et al., 2013). The winter convective mixing and advection induced the availability of high nitrate and phosphate concentration (Bemal et al., 2018; Sarma et al., 2018) favored high species and shape variability in the NEAS. Furthermore, the Rhizosolenoid diatom devoid of nitrogen-fixing endosymbionts (*Richelia*) also signifies nitrate availability (Padmakumar et al., 2010a, b). Among the

recorded phytoplankton morphotypes, species with Cyl and Cyl2Hs dominated the NEAS-O and co-dominated the NEAS-C, where the chain-forming (*Skeletonema* sp. and *Leptocylindrus* spp.) and nonchain forming (Rhizosolenoid) centric diatoms dominated in NEAS-C and NEAS-O, respectively, showing spatial variations. In NEAS-C, the Cyl2Hs-shape (solely represented by *Skeletonema*) contributed more than half (53%) of the shape diversity. However, its distribution was restricted only to the upper water column (<40 m) (Figure 4.20), suggesting that Cyl2Hs-shape is the best fit only in the shallow waters or might have had a very strong mechanism to remain afloat in the sunlit zone to exploit the available resources (Durante et al., 2019; Smayda & Boleyn, 1966). For instance, in *Skeletonema*, a high S:V (0.8; Smayda & Boleyn, 1966) and large colony formation are the key features to reducing the sinking rate. The sinking rate is generally lower in elongated shapes (like Cyl, Cyl2Hs) than in spherical shapes (Durante et al., 2019). Whereas in the open ocean, the presence of apical process in Cyl-shape, i.e., *Rhizosolenia* sp. (as shown in *Rhizosolenia setiger* by Smayda & Boleyn, 1966) might have helped reduce the sinking rate. Another experimental study demonstrates that the spine reduces the sinking rate (Padisak et al., 2003). The dominant (48%) Cyl-shaped diatom in NEAS-O was found to be evenly distributed throughout the water column (Figure 4.20), making it a successful and best-adapted shape among all the 19 shapes reported. The success of Cyl-shaped phytoplankton can also be inferred by its morphometric traits and adaptive strategies like conserving optimum S:V and high S:V with low GALD, respectively. The regression analysis revealed that the Cyl-shape showed a negative correlation between GALD and S:V with a very low slope (b = 0.131) value. This means a decrease in S:V of 0.131 μm^{-1} for each μm increase in GALD, pointing out that the dominant shape in the NEAS-O ecosystem was attenuated and has adapted the strategy to conserve the optimal S:V, which changes very minimally as the GALD increases.

4.2.1.4b. Variability in contrasting oceanographic settings

Our study finds that both the taxonomic and shape diversity of phytoplankton were higher in the productive non-oligotrophic NEAS-O compared to the nonproductive oligotrophic SEAS-O. Cyl-shaped centric diatoms dominated and co-dominated in NEAS-O and SEAS-O, respectively. However, the species representing Cyl-shape are different but were mostly dominated by centric diatoms. In NEAS-O, Rhizosolenoid (like *P. alata* and *R. styliformis*) diatoms dominated, whereas in SEAS-O *Cerataulina* sp., *P. alata*, and *Thalassiosira* sp. co-dominated with elliptic prism-shaped (*Chaetoceros* spp.) diatoms.

Cerataulina spp. representing the Cyl-shape is well known for its bloom formation in nutrient-depleted turbulent waters (Ault et al., 2000; Lauria et al., 1999). Such spatial variability in morphotype dominance can be attributable to the prevalence of different hydrographic conditions in NEAS-O (biochemical changes driven by winter convective mixing) and SEAS-O (oligotrophic conditions). The oligotrophic conditions in the SEAS-O have resulted in the low abundance and chain-forming small pennate diatoms, which are known to have advantages over large phytoplankton cells under nutrient-limited conditions making them dominant (Finkel, 2007; Grover, 1989). The oligotrophic condition of SEAS-O is also revealed by the increased percentage contribution of dinoflagellate species (23%) known to be better adapted in nutrient-limited conditions and use their flagella in exploiting a stratified water column. Among the 12 shapes, simple and attenuated shapes like Cyl (23%), PoP (19%), and ElliP (18%) dominated the phytoplankton communities. The less shape diversity reflects the prevailing environmental conditions (oligotrophic waters), which could not afford to support the variety of other shapes, and only the best-adapted shapes flourished. However, it is interesting to note that even if the NEAS-O and SEAS-O showed very different hydrographical conditions and diversity, the shape dominance remained the same: simple attenuated shapes like Cyl or ElliP dominated across this vast gradient. All the dominant shapes have adopted the strategy of conserving their optimum S:V by showing negative correlation and minimal variations as the linear dimension changes (Figure 4.11). Moreover, the adaptive strategies opted by the dominant shapes (Cyl, ElliP, and PoP) in NEAS-O and SEAS-O varied. In the NEAS-O, the dominant shapes (Cyl, ElliP, and PoP) opted for high S:V with low GALD, but the dominant shapes in SEAS-O opted for the opposite. Such consistency in morphological traits composition compared to species composition is also reported in various studies (Naselli-Flores & Barone, 2007; Weithoff & Gaedke, 2017; Salmaso & Padisak, 2007), pointing out the importance of trait-based studies. Therefore, it can be said that the phytoplankton cell geometry or shape in the eastern Arabian Sea (NEAS-O and SEAS-O) showed a high level of redundancy. Redundancy, in this case, means that even if the taxonomic diversity was high, only a small number of shapes dominated. The trait-based studies allow the quantitative assessment of community or ecosystem resistance or resilience to changes through functional redundancy (Lavorel & Garnier, 2002; McGill et al., 2006), which in turn can increase the predictability of future ecosystem function projections than the species-centered taxonomic approaches (Levine, 2016; Martini et al., 2021). Furthermore, the

eastern Arabian Sea (NEAS-O and SEAS-O) is well known for the occurrence of large-scale phytoplankton blooms (D'Silva et al., 2012), and the species causing blooms are generally characterized by simple shapes. For example, spherical-shape Noctiluca bloom (Gomes et al., 2008; Sarma et al., 2019) and Cyl-shape *Trichodesmium* (Padmakumar et al., 2010b; Prabhu et al., 1965; Ramanamurthy et al., 1972). Therefore, it can be assumed that because of such bloom events, the shape diversity could be heavily influenced and skewed towards the bloom-forming dominant shape in the study area (NEAS-O and SEAS-O). Even considering such events, the eastern AS (NEAS-O and SEAS-O) is dominated by simple shape phytoplankton, particularly the Cyl-shape, suggesting it is the most adapted shape irrespective of the oceanographic regions and hydrographic conditions. The Cyl-shape has a wide morphological variability associated with wide taxonomic variability and is also considered a more attenuated shape capable of conserving the optimum S:V ratio very efficiently, therefore making it the best fit with the prevailing environmental conditions (Aubry et al., 2017).

4.2.1.4c. Variability in frontal and non-frontal regions

The mesoscale features (fronts or filaments), which are used to generate potential fisheries zone (PFZ) advisories, are considered hotspots for phytoplankton bloom (Franks, 1992; Hesse et al., 1989) and its formation both in coastal (Sarma et al., 2018; Vipin et al., 2015) and open ocean (Amol, 2018; Roy et al., 2015) regions of EAS is well documented. The phytoplankton community studies on frontal regions of the EAS are mostly based on marker pigments (Bemal et al., 2019; Kurian et al., 2020; Roy et al., 2015). However, detailed taxa and morphometry-based studies of the phytoplankton community variability in coastal and open ocean frontal regions are lacking, and an attempt has been made to delineate frontal influence on phytoplankton shape dominance in EAS.

The phytoplankton shapes in EAS showed significant morphometric variability between NEAS-C and SEAS-O frontal regions. The frontal regions in NEAS-C were dominated by Cyl2Hs (43–56% and are solely represented by *Skeletonema*), and its dominance can be explained by the background condition or preexisting phytoplankton community theory (Sarma et al., 2018). This suggests that Cyl2Hs-shaped phytoplankton was best adapted to exploit the frontal hydrographic conditions. The morphometric adaptations like high S:V (0.8) associated with low GALD in Cyl2Hs might have a major role. The dominance of chain-forming diatoms in the coastal frontal regions is also reported in the South China Sea (Liu et al., 2021) and EAS (Sarma et al., 2018). However, the non-frontal (NF) regions were equally dominated by Cyl (*Leptocylindrus* being the

dominant one), Cyl2Hs (23–22%, PoP (17%), and ElliP (15%) shapes. This suggests that the NF regions have a higher competition among the species for the limited resources where all the major shapes flourished similarly to their potential, whereas the Cyl2H shape competes with others in frontal conditions. However, it should be noted that the phytoplankton response to the frontal conditions is subjected to the prevailing background conditions and community (Kurian et al., 2020; Sarma et al., 2018). The background phytoplankton community is dominated by chain-forming centric diatoms but the percentage contribution and abundance were relatively less. Also, the species composition (particularly diatoms) was slightly different in the non-front regions compared to the frontal regions. Such morphological shift towards a more attenuated shape (like long chain-forming *Skeletonema*) is a type of adaptation that shows minimal variations in the S:V ratio to maximize chloroplast exposition to light, i.e., opting for the most elongated shape by maintaining the shortest diameter (Naselli-Flores & Barone, 2011).

In contrast to NEAS-C fronts, the shape dominance in the oligotrophic SEAS-O front is different despite both T1 and T2 transects showing the least shape diversity (only 12 shapes) with the former transect cutting across the frontal waters but not in the latter, i.e., T2 transect without fronts (Bemal et al., 2019). SEAS is seldom enriched by Rossby wave-associated fronts, bringing in changes in hydrographic conditions, but is less favorable to phytoplankton growth than the NEAS (Table 4.3). Nevertheless, this study points out the influence of Rossby fronts on phytoplankton shape dominance and biological productivity per se. The frontal stations in SEASO showed a slight increase in abundance and diversity compared to non-frontal stations on the western side (NFW) but not those on the eastern side (NFE). The availability of relatively higher inorganic nitrogen in frontal (2.06 μM) and NFE (1.54 μM) than NFW (1.02 μM) could be the reason for the differences in phytoplankton abundance. In NFE, the increased abundance can also be due to the reminiscence of frontal signature (Amol, 2018; Bemal et al., 2019; Vipin et al., 2015) along the path as the sampled front was associated with a strong current that was drifting at 40–50 cm s^{-1} westward (Bemal et al., 2019). The Rossby waves were drifting westward towards the offshore, which means that the NFE should have the reminiscence of the Rossby front, and NFW (yet to be influenced by the Rossby front) is the true non-frontal region which is also evident from the salinity profile of water mass as explained in Bemal et al. (2019) in details. The reminiscence effect of the westward

propagating Rossby front is also well reflected in the morphological and species diversity of the associated phytoplankton community.

The dominance of the Cyl (41%) shape in the NFE and also the existence of the Elli-shape (7% though in less abundance) set the necessary background for the phytoplankton community, which took advantage of the Rossby front and co-dominated the frontal region. The frontal regions of SEAS-O were co-dominated by Elli (26%) and Cyl (21%) shapes representing dinoflagellate and centric diatoms, respectively. Even though dinoflagellates are considered poor competitors for inorganic nutrients (Litchman & Klausmeier, 2008), they are generally predominant in low-nutrient waters, as observed in this study. For instance, the ability of *Gyrodinium* spp., Elli-shaped mixotrophic dinoflagellate, to rapidly increase almost three times and respond to the abrupt resource enrichment associated with the Rossby front proves that Elli-shaped phytoplankton has the required adaptive strategies (flagella and mixotrophy) to flourish in the given environmental conditions.

4.2.1.5. Conclusion

This study concludes that the phytoplankton cell shape in the eastern Arabian Sea showed a high level of redundancy by choosing only a few dominant shapes associated with high taxonomic diversity. The integrated approach (taxonomy and morphology) adopted in the present study revealed higher taxonomic and shape diversity in the convective mixing influenced non-oligotrophic NEAS-O than adjoining NEAS-C and oligotrophic SEAS-O. Interestingly, the shape diversity and dominance (Cyl, ElliP, and PoP) remained the same between NEASO and SEAS-O, and among the fronts, the combined and simple shaped phytoplankton out-competed in NEAS-C and SEAS-O. The assessment of morphological properties based on S:V and its relationship with GALD suggested the prevalence of different adaptive strategies to cope with respective hydrographic conditions in the open ocean (NEAS-O and SEAS-O) and coastal (NEAS-C) by conserving S:V despite the increase in GALD in the former and no change in the latter.

4.2.2. The sea surface and sub-surface chlorophyll maximum layers in different bioregions

4.2.2.1. Introduction

Phytoplankton, which contributes to almost half of the global primary production (Smayda, 1970), are adapted to live in suspension in turbulent water masses and fluctuating light and nutrient regimes in various water bodies (Reynolds, 2006). Even though many indispensable resources can limit phytoplankton growth, nutrient availability (N, P, and Si) and light are the main drivers (Tilman et al., 1982). Other factors like grazing and parasitic infections (Kagami et al., 2007) are important loss processes. Various morphological and physiological specializations developed in phytoplankton species have helped them adapt to their environment (Reynolds, 2007). The phytoplankton size and shape expressed by greatest axial linear dimension (GALD) and surface-to-volume ratio (S:V) reflect their ability to obtain nutrients, light, resist sinking, and reduce grazing pressure (Lewis, 1976; Naselli-Flores et al., 2007). Therefore, morphological traits are directly related to phytoplankton's life strategies (Irwin et al., 2006) and are readily used to describe and identify functional groups and trait-based studies (Reynolds et al., 2002; Padisak et al., 2009). In recent decades, application of morphometric traits to explain and understand phytoplankton community distribution is well-explored in freshwater (Margalef, 1978; Reynolds, 1988; Weithoff, 2003; Salmaso & Padisak, 2007; Litchman & Klausmeier, 2008; Kruk et al., 2010; Naselli-Flores & Barone, 2011), estuarine (O'Farrell et al., 2007; Kruk et al., 2015) and marine (Stanca et al., 2013; Barton et al., 2013; Litchman et al., 2007, 2015; Finkel et al.,2010; Paul et al., 2021, 2023) ecosystems. In trait-based studies, taxonomically distinct species are grouped based on their similar adaptive traits (Simberloff & Dayan, 1991). Morphological traits (i.e., cell shape and size) affect various aspects of phytoplankton survival like grazing by zooplankton (Sunda & Hardison, 2010; Pancic & Kiorboe, 2018; Petrucciani et al., 2022), diffusion and sinking (Padisak et al., 2003; Durante et al., 2019), growth rates (Wirtz, 2011), nutrient uptake (Grover, 1989; Karp-Boss & Boss, 2016) and light harvesting (Naselli-Flores & Barone, 2007, 2011). The key phytoplankton traits (cell size and shape) are controlled by environmental conditions (like nutrients, light, temperature, species interactions, and grazers), making shape and size crucial determinants of fitness (Naselli-Flores et al., 2007; Zohary et al., 2010; Stanca et al., 2013; Leonilde et al., 2017). The effect of nutrients and grazing on phytoplankton morphological attributes (like shape,

size, S:V, and GALD) are investigated in various reservoirs (Naselli-Flores & Barone., 2007; Xiao et al., 2011; Butts et al., 2022). There are few studies on shape variability from marine systems (Paul et al., 2021; Paul et al., 2023), but specific studies on morphological attributes considering SCML from a vast marine pelagic system, particularly Indian Ocean (IO) are scarce.

The IO's unique geographical, physical, and meteorological features distinguish it from the world's two major oceans i.e., Pacific and Atlantic. The tropical IO encompasses the northern IO (Arabian Sea and Bay of Bengal on the west and east, respectively), equatorial IO from 4^{o}N-4^{o}S, and southern tropical IO up to 30^{o}S. Among them, northern IO is surrounded by Asian land masses and is profoundly influenced by seasonal monsoonal forcing, weak equatorial upwelling, and significant freshwater influx from major rivers (Schott & McCreary, 2001). The IO is the smallest oceanic basin and plays important roles in the global ocean i.e., the transport of heat, salt, carbon, and about 15-20% of global primary production (Behrenfield & Falkowski, 1997; Regaudie-de-Gioux et al., 2014). The existence of an upper low-chlorophyll, a nutrient-depleted mixed layer where productivity is limited (Dugdale & Goering, 1967), followed by a light-limited, nutricline-associated with elevated chlorophyll known as subsurface chlorophyll maximum layer (SCML) is common in stratified waters (Herbland & Voituriez, 1979; Cullen, 1982). According to Cullen (2015), SCMLs are the local chl-maxima, formed in layers and maintained by ecological interactions like autecological processes (growth, photosynthetic acclimation, and sinking or swimming of phytoplankton) and grazing control that modulates phytoplankton concentrations over days to weeks. The primary production at sea surface can also be limited due to photoinhibition (Kirk, 1994). Consequently, phytoplankton accumulation occurs at distinct water depths, which do not necessarily correspond to the maximum in either irradiance or nutrient concentration (Cullen, 1982), forming SCML. SCML is a ubiquitous ocean feature in tropical (Shah et al., 2020), subtropical (Mignot et al., 2014), and polar regions (McLaughlin & Carmack, 2010; Baldry et al., 2020). However, SCML depth varies globally, forming at depths >80 m in the subtropical and tropical (30^{o}S to 30^{o}N), 40-80 m in tropics, Southern Ocean (south of 40^{o}S), and <40 m in the northern subarctic (north of 40^{o}N) (Yasunaka et al., 2022). The existence of such biological feature and its significant contribution to the column primary production is already reported in the IO (Garg et al., 2024; Shah et al., 2020; Jayaram et al., 2021; Sarma & Aswanikumar, 1991; Shulenberger & Reid, 1981; Goldman et al., 2003; Revelante & Gilmartin, 1995; Hanson et al., 2007). The SCML is

greatly influenced by the prevailing physical processes, mixing, stratification, and the phytoplankton groups (Shah et al., 2020; Fu et al., 2018). Though most of these studies have focused on the formation and maintenance of SCML, either satellite-based (Shah et al., 2020) or argo-float-based (Jayaram et al., 2021) data, the community-based studies are lacking (Sarma et al., 2021). A recent study based on the HPLC-based phytoplankton pigment data from the northern IO reported that micro-phytoplankton are the major contributors to increasing Chl_{max} (Gerg et al., 2024). However, an integrated taxonomic and morphological trait-based (shape, size, S:V and GALD) study of micro-phytoplankton community from sea surface and SCML within different geographic regions of the IO and at various SCML depths (20-140 m) is not available. Therefore, the present study focuses on the applicability of oceanic micro-phytoplankton morphological traits to infer if forms can be related to ecological functions/changes, how traits vary in different sub-chlorophyll maximum layer depths, and their usefulness as tracers in changing oceanic ecosystems. As oceans are vulnerable to climate change, phytoplankton adaptive capabilities from ecological and global change perspectives are becoming vital.

4.2.2.2. Methodology

The details of the sampling site, sample collection, and analysis are presented in Chapter 2, sub-section 2.2.1.

Data analysis

Univariate measures such as species count, Shannon–Wiener's diversity, species richness, and evenness were performed on log-transformed data for both taxa and PGS. The clustering of different regions and between SCML depths was performed with SIMPROF (Similarity Profile Analysis; significance level at 0.05) through the Bray–Curtis similarity and group average method. The data were grouped at a 50% level to ascertain significant similarities or dissimilarities concerning PGS and taxa. Univariate and clustering analyses were performed using the statistical software PRIMER 6. The two-way analysis of variance (ANOVA) was performed using Statistica software (release 8) on log-transformed data to evaluate the variations between regions and SCML depths. The relationship between S:V and GALD was determined using power law regression on log-transformed data. The functional relationship between two measured quantities, where a relative change in one quantity results in a relatively proportional change in other, is often expressed as a power law equation (allometric equation) representing scale symmetry:

$$y=kx^b \text{ or } \log y = b \log x + \log k$$

Where b is the scaling exponent of the law.

Here GALD was taken as a function (i.e., y), S:V is variable (i.e., x), b is the order of scaling (i.e., the exponent), and k is a constant. So, if b= -0.15, a 100% change (i.e., doubling) in GALD is associated with a 15% decrease in S:V. The multivariate relationship of environmental variables with PGSs, S:V and GALD) corresponding to sea surface and SCML depths were evaluated by performing Redundancy Analysis (RDA) using CANOCO v4.5 software (Ter Braak & Smilauer, 2002). To identify best ordination model, detrended correspondence analysis (DCA) was conducted, and based on the lengths of environmental gradient (< 2 standard deviations), a linear response model (i.e., RDA) was selected. Based on the direct gradient technique of RDA and using forward selection (and a Monte Carlo permutation test, n=499), significant environmental variables that explained most variances were determined. The arrow length (environmental variables, PGSs, S:V, and GALD) and orientation determine their relative importance and approximate correlations to the axes (Leps & Smilauer, 2003).

Data presentation

The stations were grouped into six regions based on geographical locations (Table 4.5). AS stations are grouped in two transects, i.e., AST1 (stations in East-West direction) and AST2 (OMZ), stations from BoB and the Andaman Sea are grouped as BoB, stations 2^{o}N-7^{o}N are grouped as NEIO, 1^{o}S-10^{o}S as SEIO and 10^{o}S-30^{o}S as STIO. Furthermore, all stations are categorized as shallow (20-50m), intermediate (50-100m), and deep (>100m) SCMLs to study the variations at different depths of occurrences (Table 4.6).

Table 4.5. Station details with regions, geographic positions, mixed layer depth, and nitracline depth.

Station No.	Latitude	Longitude	Mixed layer depth (MLD)	Nitracline depth	Regions
1	9°N	75°5E	35	60	Arabian Sea transect 1 (AST1) Oligotrophic transect
2	9°N	74°0E	9	70	
3	9°N	72°5E	28	100	
4	9°N	69°5E	44	95	
5	9°N	68°E	32	40	
6	9°N	66°5E	67	75	
7	9°N	65°E	43	40	
8	9°N	63°5E	67	60	
9	9°N	62°E	55	40	
10	9°N	60°E	43	20	
11	11°N	62°57E	85	35	Arabian Sea transect 2 (AST2) OMZ transect
12	14°50N	65°57E	72	105	
13	16°75N	69°E	91	20	
14	17°38N	67°95E	39	20	
15	17°N	89°85E	13	20	Bay of Bengal (BoB)
16	20°22N	88°04E	22	65	
17	10°40N	92°64E	31	100	
18	7°99N	92°38E	22	50	
19	7°N	75°58E	34	20	North Equatorial Indian Ocean (NEIO)
20	5°19N	92°81E	35	62	
21	2°91N	92°15E	-	95	
22	1°98S	90°47E	78	85	South Equatorial Indian Ocean (SEIO)
23	2°03S	75°56E	71	50	
24	4°S	90°46E	31	55	
25	7°32S	75°98E	17	100	
26	7°76S	90°02E	45	150	
27	9°99S	89°63E	61	150	

28	16°05S	88°29E	48	150	South Tropical Indian Ocean (STIO)
29	20°99S	85°E	60	150	
30	25°50S	82°53E	66	150	
31	30°S	80°E	56	80	
32	30°S	75°E	48	150	
33	30°S	69°99E	59	75	
34	18°27S	61°25E	46	80	
35	16°36S	67°27E	50	75	
36	12°93S	74°67E	66	80	
37	13°55S	75°55E	60	92	
38	16°05S	88°29E	60	-	

Table 4.6. Stations are grouped according to varying depths of SCML.

Regions of the IO	Cruise	Stations	Depth of SCML [m]	
AST2_1	SSD069	15	35	20-50m
AST2_2	SSD069	16	26	
AST2_3	SSD069	17	20	
AST2_4	SSD069	18	28	
BoB_1	SSD079	1	43	
AST1_1	SSD069	3	60	50-100m
AST1_2	SSD069	4	58	
AST1_3	SSD069	5	56	
AST1_4	SSD069	7	95	
AST1_5	SSD069	8	92.5	
AST1_6	SSD069	9	75	
AST1_7	SSD069	10	72	
AST1_8	SSD069	11	75	
AST1_9	SSD069	12	80	
AST1_10	SSD069	14	72	
BoB_2	SSD079	2	65	
BoB_3	SSD079	3	75	
BoB_4	SSD079	4	50	
NEIO_1	SSD079	5	50	
NEIO_2	SSD079	6	70	
NEIO_3	SSD079	24	58	
SEIO_1	SSD079	7	95	
SEIO_2	SSD079	8	85	
SEIO_3	SSD079	9	50	
SEIO_4	SSD079	10	55	
SEIO_5	SSD079	22	60	
SEIO_6	SSD079	23	92	
STIO_1	SSD079	11	100	

STIO_7	SSD079	17	65	
STIO_9	SSD079	19	75	
STIO_10	SSD079	20	75	
STIO_11	SSD079	21	80	
STIO_2	SSD079	12	115	>100m
STIO_3	SSD079	13	140	
STIO_4	SSD079	14	115	
STIO_5	SSD079	15	125	
STIO_6	SSD079	16	120	
STIO_8	SSD079	18	120	

4.2.2.3. Results

4.2.2.3a. Hydrographic condition of the Indian Ocean

Overall, the surface water of IO was warmer than that of SCML. The equatorial region (NEIO and SEIO) surface water was the warmest, followed by AST1, BoB, AST2, and STIO, the coolest. In the SCML, AST1 was the warmest, followed by BoB, NEIO, AST2, SEIO, and least in STIO. The salinity of surface and SCML was lowest in BoB, followed by equatorial, STIO, and AS (maximum) transects. Maximum surface DO was recorded in BoB, followed by NEIO, STIO, SEIO, AST2, and least in AST1, whereas, in SCML, STIO showed the maximum DO, followed by AST2, BoB, AST1, NEIO, and SEIO. The MLD was shallow in BoB (12±6m), NEIO (31±4m) and deepening in SEIO (36±27m), AST1 (42±6m), STIO (53±7m) and AST2 (72±12m). The nitracline depth was shallow in AST2 (45±41m), NEIO (58±38m), BoB (59±33m), AST1 (60±26m) and deeper in SEIO (98±44m) and STIO (108±36m).

The median NO_3 concentration for surface waters ranged from 0.57-1.4 µM, recording maximum in NEIO (1.4±0.15 µM), followed by BoB (1.24±0.62 µM), AST1 (1.02±0.51 µM), SEIO (0.96±1.7 µM), STIO (0.85±0.19 µM) and least in AST2 (0.57±0.25 µM) and in SCML from 0.7-5.0 µM recording maximum in NEIO (5.0±0.5 µM), followed by BoB (2.9±1.8 µM), SEIO (2.4±0.6 µM), AST1 (1.8±2.0 µM), STIO (1.2±0.3 µM) and least in AST2 (0.7±0.9 µM).

The median PO_4 concentration for surface waters ranged from 0.5-1.4 µM recording maximum in AST1 (1.4±0.15 µM), followed by BoB (1.2±0.42 µM), NEIO (0.8±0.36 µM), SEIO (0.7±1.4 µM) and least in STIO and AST2 (0.5±0.2 µM) and in SCML from 0.3-2.2 µM recording maximum in NEIO (2.2±0.8 µM), followed by BoB (1.4±0.9 µM), SEIO (1.3±0.3 µM), AST1 (1.1±1.1 µM), STIO (0.8±0.2 µM) and least in AST2 (0.3±0.5 µM) (see Table 4.7).

The intermediate SCML was warmest (26.3±0.5ºC) than shallow (25.9±0.3ºC) and deep (18.5±1.05ºC) SCML. The deep SCML was more oxygen saturated (4.7±0.16 mgL^{-1}) than shallow (3.2±0.41 mgL^{-1}) and intermediate (3.3±0.13 mgL^{-1}), which did not show much variation. The salinity variation was insignificant among SCML depths. The mean concentration of Si, PO_4, NO_2+NO_3, and N:P was maximum in the intermediate, followed by shallow and least in deep SCML (see Table 4.8).

Table 4.7. The environmental parameters and nutrient concentration at the sea surface and SCML of different regions of the Indian Ocean. The values of environmental parameters are mean, and nutrients are median. The range values are given in parentheses.

Regions of IO	**Temperature (^{O}C)**	**Salinity (PSU)**	**Oxygen (mL L^{-1})**	**NO_3 (µM)**	**NO_2 (µM)**	**PO_4 (µM)**
AST1 (0m)	28.7 (27.8-29.3)	35.1 (34.2-35.5)	3.7 (3.6-3.8)	1.02 (0.49-5.64)	0.21 (0.04-0.42)	1.45 (0.84-2.49)
AST1 (SCML)	27.8 (26.5-28.9)	35.9 (35.5-35.9)	3.2 (2.5-3.6)	1.8 (0.26-18.4)	0.1 (0.05-0.45)	1.1 (0.55-2.73)
AST2 (0m)	26.1 (25.0-26.8)	36.3 (36.2-36.5)	3.6 (3.5-3.7)	0.57 (0.41-1.5)	0.46 (0.24-0.48)	0.55 (0.28-1.23)
AST2 (SCML)	26.0 (25.0-26.8)	36.3 (36.2-36.5)	3.6 (3.6-3.7)	0.7 (0.65-3.27)	0.4 (0.24-0.45)	0.3 (0.21-1.83)
BoB (0m)	28.7. (27.4-29.7)	32.4 (31.8-32.9)	4.5 (4.4-4.7)	1.17 (0.7-3.47)	0.17 (0.15-0.24)	0.69 (0.56-1.66)
BoB (SCML)	27.1 (25.6-27.9)	33.6 (33.4-34.1)	3.3 (1.6-4.0)	2.9 (1.2-9.2)	0.3 (0.2-0.39)	1.4 (0.9-4.6)
NEIO (0m)	29.8 (29.8)	34.8 (34.7)	4.4 (4.36)	1.41 (1.19-1.72)	0.19 (0.15-0.22)	0.82 (0.65-1.79)
NEIO (SCML)	26.8 (25.3-28.3)	34.4 (34.1-34.7)	3.1 (2.6-3.6)	5.0 (4.5-6.2)	0.3 (0.21-0.36)	2.2 (1.8-4.3)
SEIO (0m)	28.9 (28.9-30.0)	34.2 (34.1-34.9)	4.3 (3.4-4.4)	0.96 (0.79-10.88)	0.17 (0.13-0.32)	0.71 (0.59-9.35)
SEIO (SCML)	24.2 (21.0-28.2)	35.0 (34.7-35.2)	3.0 (1.9-4.0)	2.4 (0.9-5.0)	0.5 (0.26-0.61)	1.3 (0.8-2.6)
STIO (0m)	26.1 (22.5-28.0)	35.0 (33.9-35.9)	4.3 (3.3-4.7)	0.85 (0.32-2.69)	0.17 (0.13-0.34)	0.49 (0.37-2.65)
STIO (SCML)	20.4 (14.7-24.5)	35.3 (34.8-35.7)	4.1 (2.5-5.1)	1.2 (0.6-3.9)	0.3 (0.11-0.37)	0.8 (0.53-2.05)

Table 4.8. The environmental parameters and nutrient concentration at varying depths of SCML of the Indian Ocean. The values of environmental parameters are mean, and for nutrients, it is median along with standard error.

Depth of SCML	Temperature (^{O}C)	Salinity (PSU)	Oxygen (mL L^{-1})	NO_2 (µM)	NO_3 (µM)	PO_4 (µM)	Si (µM)	N:P
>50m	25.9±0.29	35.9±0.45	3.2±0.41	0.37±0.08	3.44±1.7	1.74±0.9	5.96±3.4	2.21±0.5
50-100m	26.2±0.51	35.1±0.18	3.4±0.13	0.29±0.03	3.69±0.8	1.6±0.4	9.88±1.5	2.60±0.8
<100m	18.5±1.05	35.6±0.06	4.7±0.16	0.22±0.03	0.91±0.1	0.67±0.05	6.19±1.1	1.38±0.1

4.2.2.3b. Relationship between PGS, morphological traits, and environmental variables

The RDA results revealed that the dominant PGSs at sea surface were limited by SiO_4 availability and high light (PAR) conditions. Similarly, S:V and GALD were controlled by only nutrient limitation, but in SCML, both nutrient and light availability were the controlling factors. Interestingly, S:V and GALD of the dominant PGS in shallow and intermediate SCML were positively correlated with nutrients and light, whereas in the deep SCML, nutrients were positively and the light was negatively correlated. Further, the temperature was also one of the controlling parameters in the deep SCML, and it negatively correlated with GALD and PGS, which means increasing temperature will result in smaller phytoplankton cells. Therefore, the morphometric attributes (S:V and GALD) were strongly influenced by the SCML occurrence depth and the prevailing environment (Figures 4.21a-c).

4.2.2.3c. PGS diversity of surface waters

The PGSs in the surface water were relatively similar (Figure 4.22a). Altogether, 13 PGSs (9 simple and 4 complex), corresponding to 108 micro-phytoplankton species were recorded. Simple PGSs contributed 81-98% and complex 4-19% in the IO. A few simple (Cyl, ElliP, and PoP) and complex (2C and Elli2CCyl) PGSs were common, irrespective of the regions. However, the maximum PGS was recorded in AST1 (12 PGS; 8 simple and 4 complex) followed by SEIO (11 PGS; 7 simple and 4 complex), BoB (10 PGS; 7 simple and 3 complex), AST2, NEIO and STIO (9 PGS; 6 simple and 3 complex each). Among the PGS, Cyl, and Ellip were dominant compared to other prominent PGS like PoP, Elli, 2C, and ElliP4C (Table 4.9). However, species responsible for corresponding

PGS differed with bioregions (Table 4.9). All these PGSs cumulatively contributed up to 87% of the total community in all the regions.

Shape type	PGSs	Depth	AST1	AST2	BoB	NEIO	SEIO	STIO
Simple	Cylinder	Surface	43% *Bacteriastrum* sp. *R. styliformis*	31% *Bacteriastrum* sp. *R. styliformis*	40% *Leptocylindrus* sp. *Probosica alata*	32% *P. alata* *R. hebetate*	19% *P. calcar-avis* *Coscinodiscus* sp.	9% *Coscinodiscus* sp. *Asteromphalus* sp.
		SCML	42% *G. striata* *Bacteriastrum* sp.	20% *P. alata* *R. hebetate*	30% *Bacteriastrum* sp. *Dactylosolen* sp.	19% *Thalassiosira* sp. *Bacteriastrum* sp.	21% *Coscinodiscus* sp. *Bacteriastrum* sp.	17% *Coscinodiscus* sp.
	Elliptic prism	Surface	12% *Chaetoceros* sp.	13% *C. peruvianus*	32% *Navicula* sp. *Chaetoceros* sp.	43% *C. didymus* *H. sinensis*	43% *Navicula* sp. *C. curvisetus*	32% *Navicula* sp.
		SCML	32% *C. curvisetus* *Chaetoceros* sp.	12% *C. peruvianus*	47% *C. messanensis* *Chaetoceros* sp.	23% *Chaetoceros* sp. *C. lanciniosus*	31% *Navicula* sp.	37% *Navicula* sp.
	PoP	Surface	2% *Pseudonitzschia* sp.	29% *Pseudonitzschia* sp.	1% *Pleurosigma* sp *Nitzschia* sp	4% *Pseudonitzschia* sp.	4% *Pseudonitzschia* sp.	35% *Nitzschia* sp.
		SCML	12% *Pseudonitzschia* sp.	36% *Pseudonitzschia* sp.	10% *Pseudonitzschia* sp.	36% *Pseudonitzschia* sp.	36% *Pseudonitzschia* sp.	26% *Pseudonitzschia* sp.
	Ellipsoid	Surface	15% *Prorocentrum* sp.	-	4% *Gymnodinium* sp.	5% *Prorocentrum* sp.	10% *Prorocentrum* sp.	2% *Dinophysis* sp. *Scrippsiella* sp.
		SCML	5% *Prorocentrum* sp.	3% *Dinophysis* sp. *Gyrodinium* sp. *P. minusculum*	1% *Prorocentrum* sp.	1% *Dinophysis* sp.	1% *Gymnodinium* sp	1% *Dinophysis* sp.
	Box	Surface	1% *Lioloma* sp. *T. bacillare*	7% *Lioloma* sp.	1% *Thalassiothrix* sp.	-	1% *T. nitzschioides*	-
		SCML	4% *Lioloma* sp.	7% *Lioloma* sp.	5% *Thalassiothrix* sp.	6% *T. nitzschioides*	6% *Thalassiothrix* sp.	6% *Thalassiothrix* sp. *T. nitzschioides*
Complex	2 Cones	Surface	6% *Protoperidinium* sp. *Gonyaulax* sp.	1% *Protoperidinium* sp.	15% *Protoperidinium* sp. *Gonyaulax* sp.	6% *Gonyaulax* sp.	3% *Protoperidinium* sp.	4% *Protoperidinium* sp.
		SCML	1% *Protoperidinium* sp. *P. stenii* *P. tenuissimum* *Corythodinium* sp.	4% *Protoperidinium* sp.	0.4% *Gonyaulax* sp. *P. tenuissimum* *Protoperidinium* sp.	0.2% *Protoperidinium* sp.	1% *Protoperidinium* sp.	9% *Protoperidinium* sp.
	Ellipsoid + 2 Cones + Cylinder	Surface	3% *T. feres*	5% *T. deflexus* *T. tripos*	1% *T. tripos var. atlanticum*	3% *T. fusus var. fusus*	3% *T. pentagonus*	2% *T. trichoceros*
		SCML	1% *T. longirostrus*	11% *T. tripos*	0.3% *T. breve* *T. contrarium*	0.2% *T. vultur*	0.5% *T. horridus*	1% *T. horridius*

Table 4.9. The table shows the percentage contribution of PGSs and dominant taxa in the sea surface and SCML of the Indian Ocean bioregions.

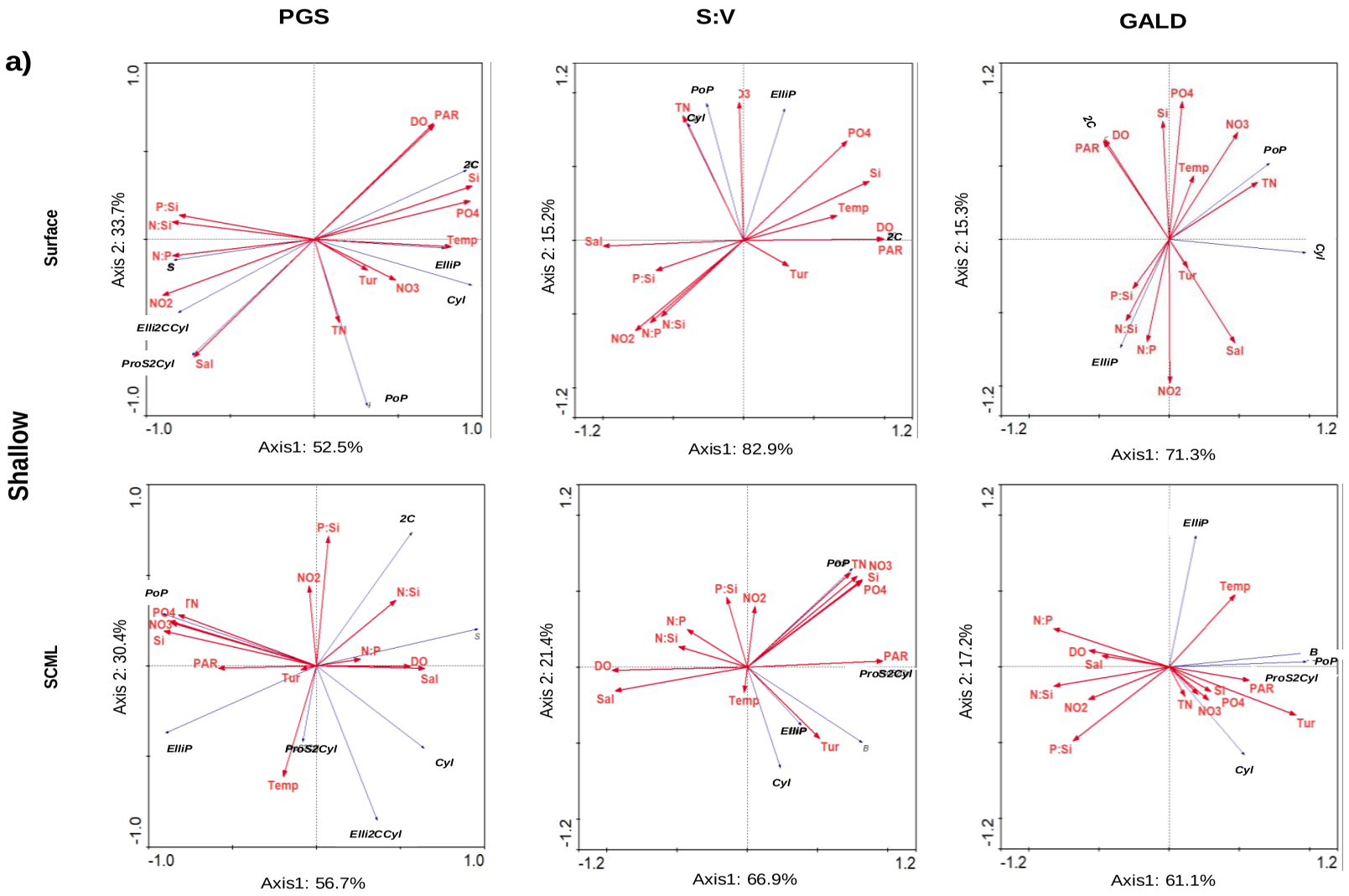


Figure 4.21a. RDA results show the relationship between environmental variables and dominant PGS and morphometric traits (S:V and GALD) in shallow surface and SCML. PGS: phytoplankton geometric shape, S:V: surface-to-volume ratio, and GALD: greatest axial linear dimension.

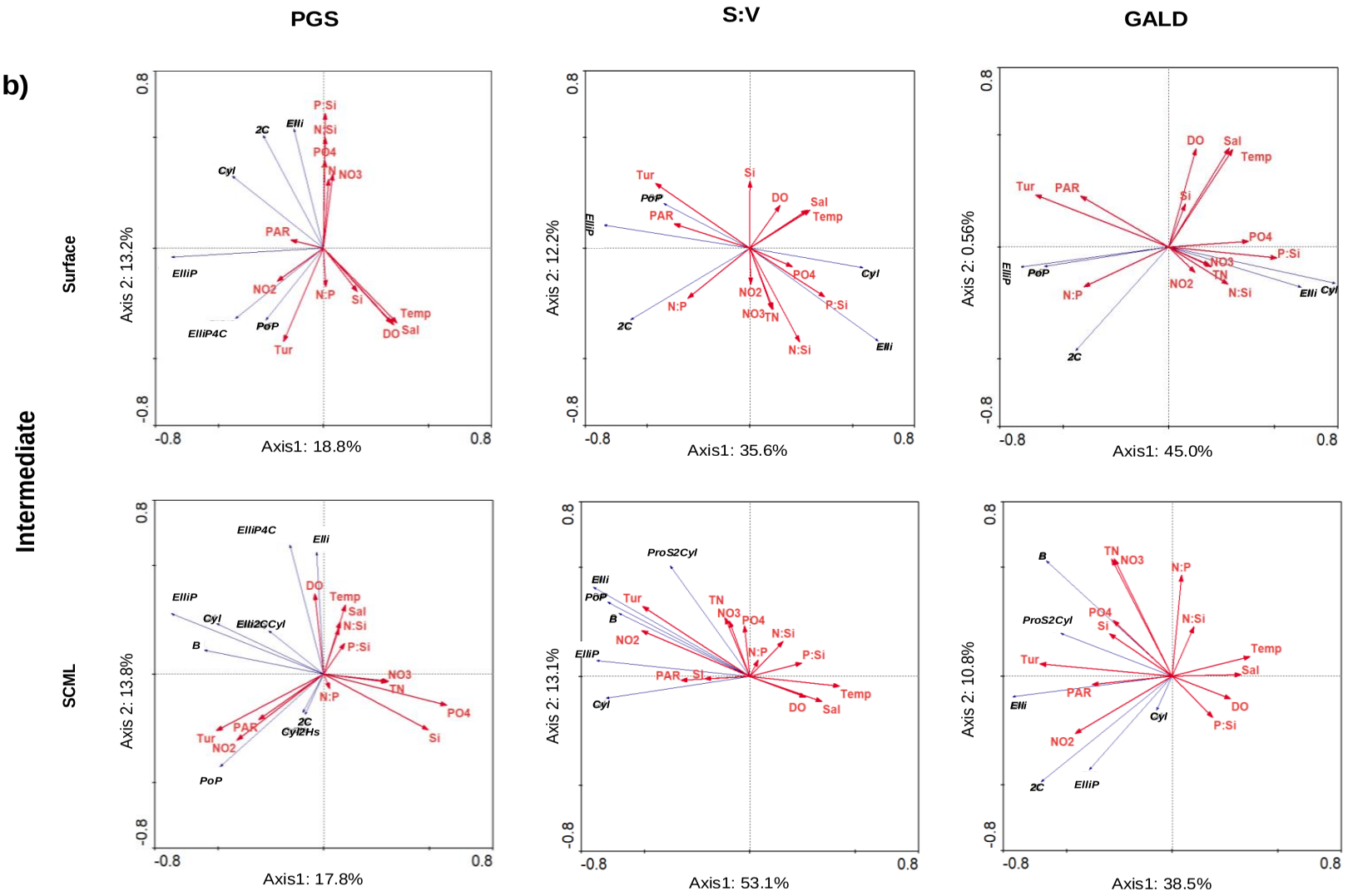


Figure 4.21b. RDA results show the relationship between environmental variables and dominant PGS and morphometric traits (S:V and GALD) in Intermediate surface and SCML. PGS: phytoplankton geometric shape, S:V: surface-to-volume ratio, and GALD: greatest axial linear dimension.

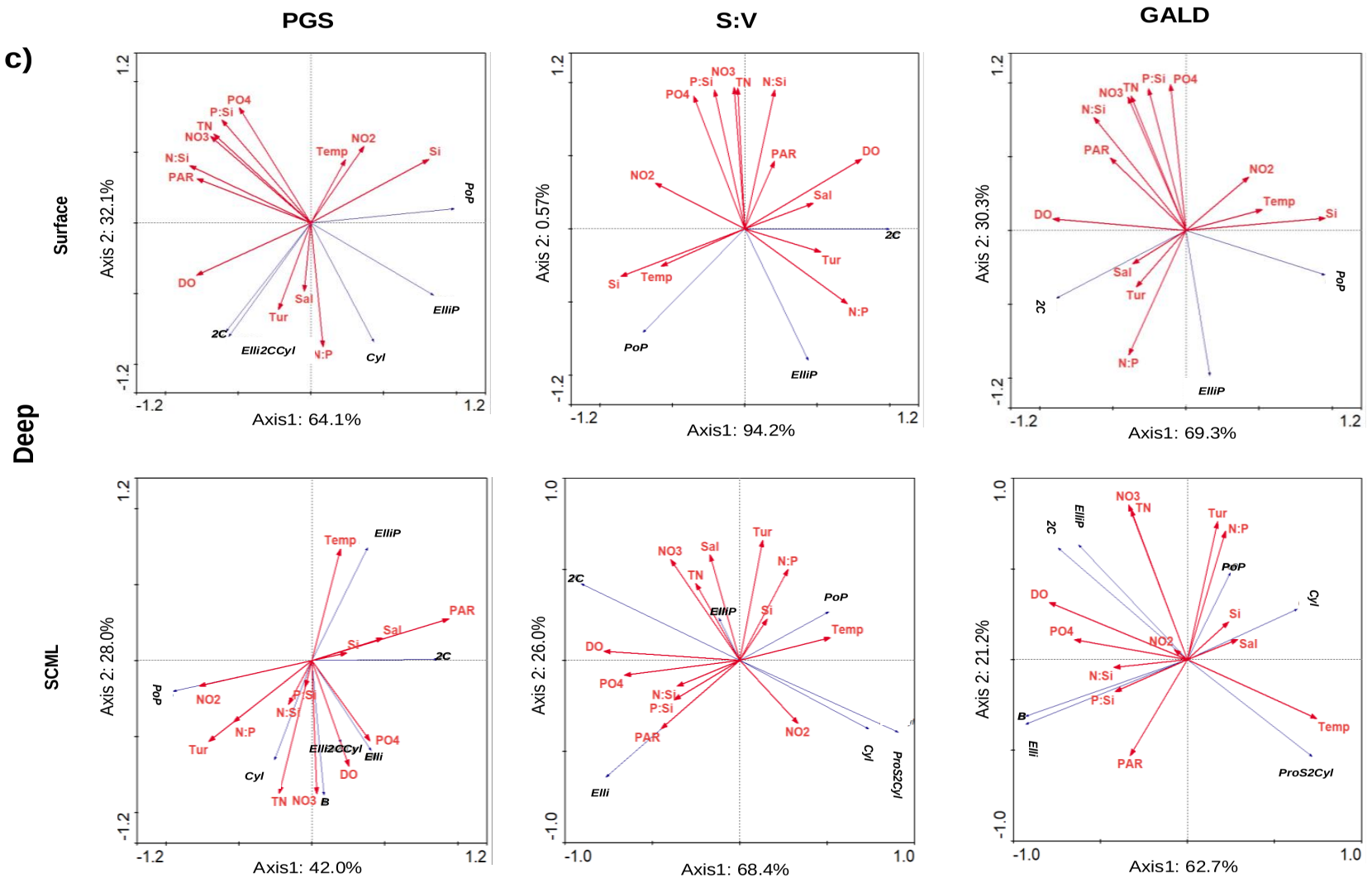


Figure 4.21c. RDA results show the relationship between environmental variables and dominant PGS and morphometric traits (S:V and GALD) in Deep surface and SCML. PGS: phytoplankton geometric shape, S:V: surface-to-volume ratio, and GALD: greatest axial linear dimension.

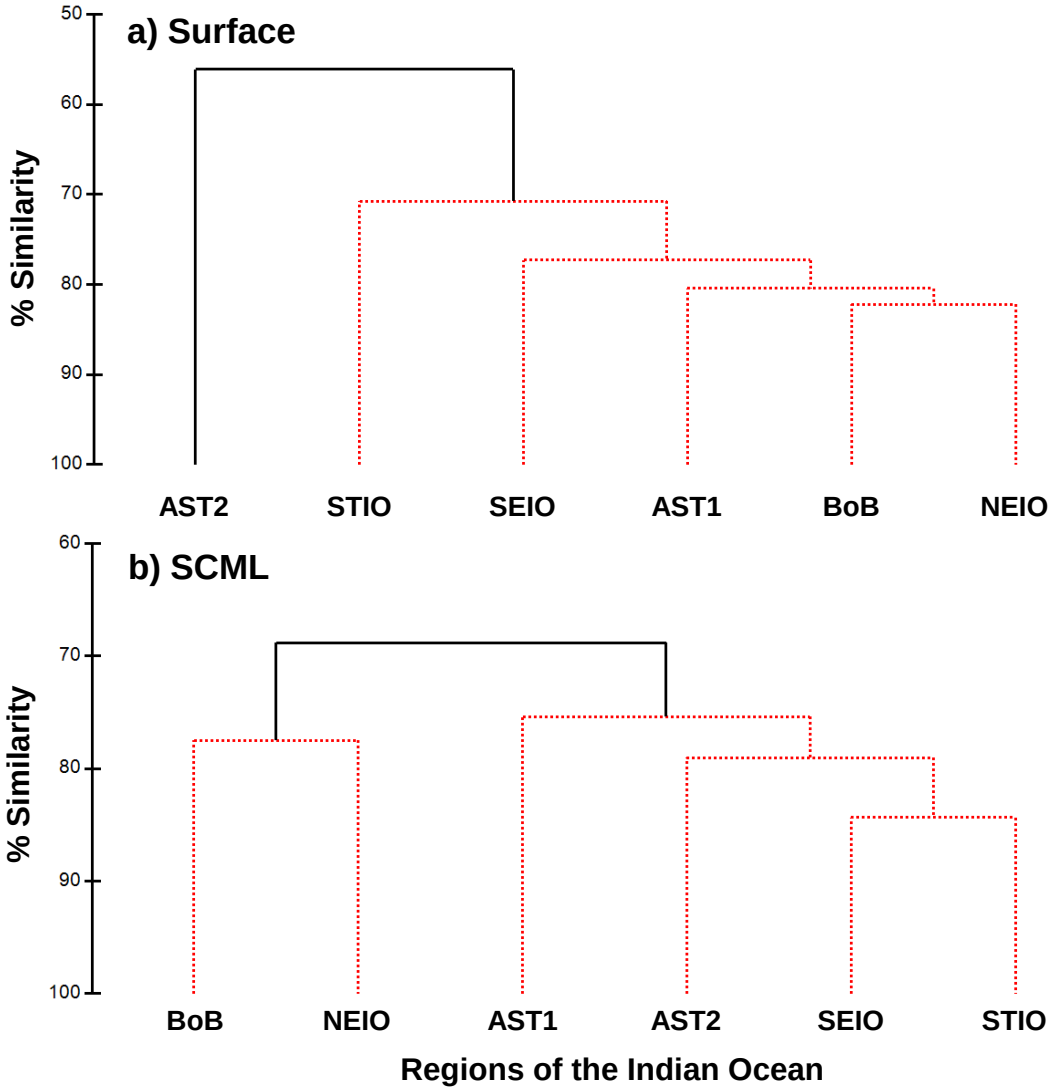


Figure 4.22. Dendrogram based on PGS of the micro-phytoplankton community of a) surface and b) SCML waters among the different regions of the Indian Ocean (IO). AST1: Arabian Sea transect 1, AST2: Arabian Sea transect 2, BoB: Bay of Bengal, NEIO: North equatorial Indian Ocean, SEIO: South equatorial Indian Ocean, STIO: South tropical Indian Ocean.

Maximum species diversity was observed in Cyl for AST1 (15 centric diatom species), AST2 (8 centric diatom species), BoB (13 centric diatom species), and STIO (10 centric diatom species) whereas ElliP (9 diatom species;8 centric and 1 pennate) and Elli (6 dinoflagellate species) showed maximum diversity in NEIO and SEIO, respectively. The univariate analysis revealed similar PGSs among the regions. PGS richness and diversity were highest in BoB, followed by AST1 and NEIO, AST2 and STIO, and least in SEIO. The number of PGS was highest in BoB, followed by AST1, AST2, NEIO, and STIO, and least in SEIO (Figure 4.23g-i). The S:V and GALD of dominant PGS, which cumulatively represented more than 50% in surface waters, were Cyl, ElliP, and 2C. The S:V of Cyl and 2C significantly increased from northern to southern IO, and the maximum was in STIO ($0.59\mu m^{-1}$) and SEIO ($4.33\mu m^{-1}$), respectively, whereas ElliP remained relatively similar, ranging between 0.43-$0.70\mu m^{-1}$. However, GALD of Cyl, ElliP, and 2C decreased significantly from northern to southern IO, and the maximum was in AST2 for both (373 and 86 µm) and AST1(1056µm), respectively.

The regression analysis of the dominant PGSs in surface (Cyl, ElliP, and PoP) showed a significant negative correlation between S:V and GALD for Cyl and ElliP but not for PoP, which was not significant. Interestingly, the scaling exponent (i.e., b), which can be used to quantify the amount of change of dependent variable (i.e., S:V in this case), showed significant variation in surface for both Cyl (-0.09 to -0.41) and ElliP (-0.16 to -0.32) but not for PoP (-0.09 to 0.05) (Figure 4.24).

4.2.2.3d. PGSs in varying depths of SCML

Like sea surface, SCML PGS were similar (Figure 4.22b), and 17 PGSs (12 simple and 5 complex) belonging to 134 species were recorded. Simple and complex PGSs contributed 86-98% and 2-14%, respectively. Among the 17 PGSs, five simple (Cyl, ElliP, PoP, Elli, and B) and two complex (2C, and Elli2CCyl) PGSs were common. The SCML corresponding to different regions were categorized as shallow (20-50m; represented by all stations in AST2 and one in BoB), intermediate (50-100m; represented by all stations in AST1, NEIO, and SEIO, three stations in BoB and five stations in STIO)

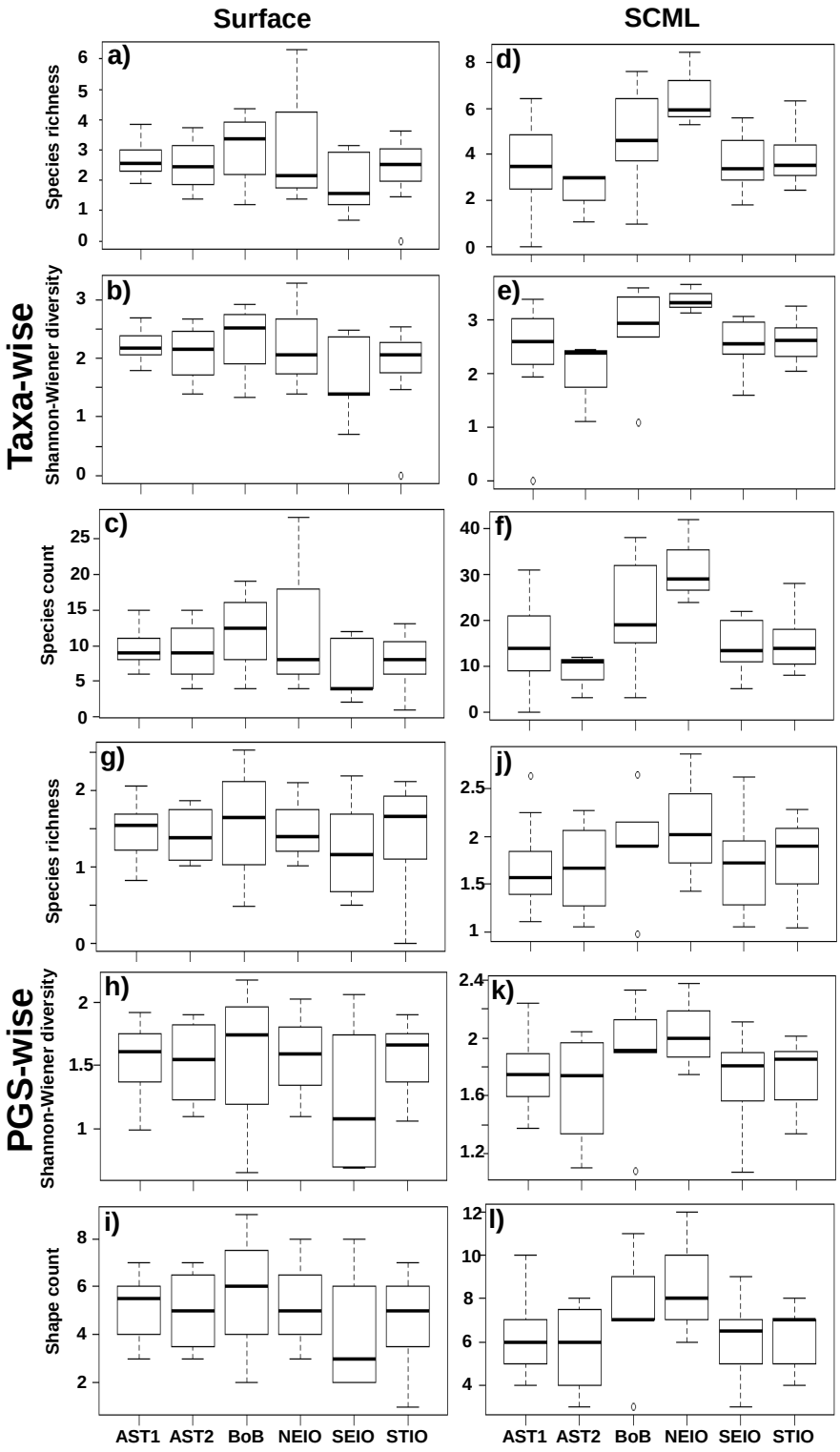


Figure 4.23. Box plot based on taxonomy and PGS from the Sea surface and SCML waters of different regions in the Indian Ocean. a,d,g,j) Margalef's species richness, b,e,h,k) Shannon-Wiener diversity, c,f,I,l) number of species. AST1: Arabian Sea transect 1, AST2: Arabian Sea transect 2, BoB: Bay of Bengal, NEIO: North equatorial Indian Ocean, SEIO: South equatorial Indian Ocean, STIO: South tropical Indian Ocean and SCML: sub-surface chlorophyll maximum layer.

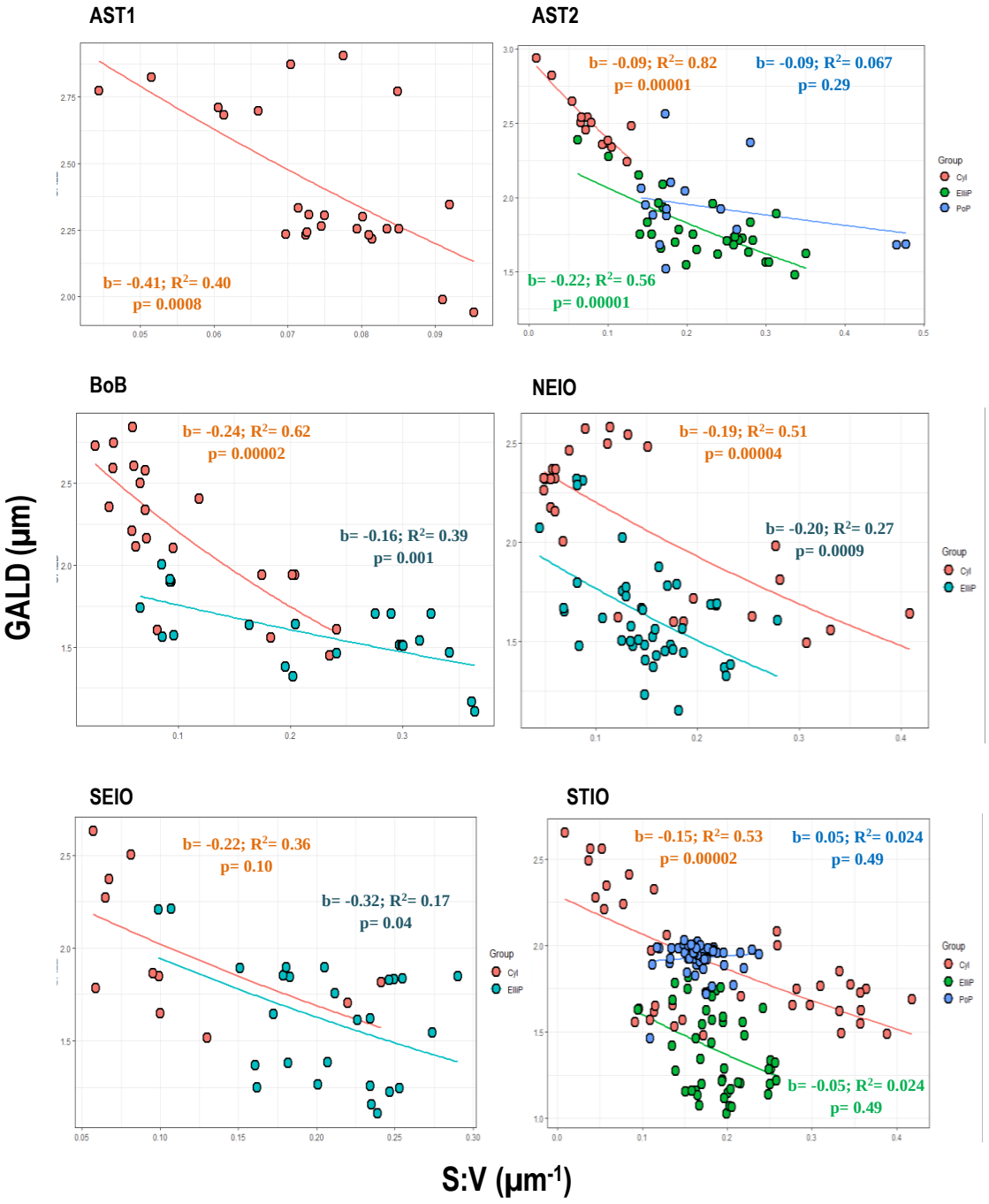


Figure 4.24. Non-linear regression of dominant PGS in surface waters of the IO. AST1: Arabian Sea transect 1, AST2: Arabian Sea transect 2, BoB: Bay of Bengal, NEIO: North equatorial Indian Ocean, SEIO: South equatorial Indian Ocean, STIO: South tropical Indian Ocean, S:V: surface-to-volume ratio and GALD: greatest-axial-linear-dimension. ElliP: elliptic prism, Cyl: cylinder and PoP: prism on parallelogram.

and deep (>100m; represented by six stations in STIO) SCML (Table 4.8). PGSs were maximum in intermediate NEIO (13 PGS: 8 simple and 5 complex) followed by intermediate BoB (12 PGS: 7 simple and 5 complex), shallow AST2, intermediate AST1, and deep STIO (11 PGS each), intermediate SEIO (10 PGS: 7 simple and 3 complex), shallow BoB and intermediate STIO (9 PGS each). The PGSs in shallow, intermediate, and deep SCML corresponded to 50 (37 diatoms and 13 dinoflagellates), 113 (72 diatoms and 41 dinoflagellates), and 48 (34 diatoms and 14 dinoflagellates) micro-phytoplankton species, respectively. Like sea surface, among the PGS, ElliP, and Cyl were the most dominant compared to other prominent PGS like PoP, Elli, B, 2C, and Elli2CCyl (Table 4.9). However, the species responsible for corresponding PGS differed with SCML depths in different bioregions (Table 4.10). All these PGS cumulatively contribute up to 96%, 93%, and 94% in shallow, intermediate, and deep SCML of total abundance, respectively.

Table 4.10. The table shows the percentage contribution of PGSs and dominant taxa in different depths of SCML.

Shape type	**PGSs**	**Shallow SCML (20-50 m)**	**Intermediate SCML (50-100 m)**	**Deep SCML (>100 m)**
Simple	**Cylinder**	30% *Bacteriastrum* sp. *Dactyliosolen* sp.	26% *Bacteriastrum* sp. *Coscinodiscus* sp.	24% *Bacteriastrum* sp. *Coscinodiscus* sp.
	Elliptic prism	41% *C. peruvianus* *C. curvisetus*	31% *Chaetoceros* sp. *C. messanensis*	36% *Navicula* sp.
	Prism on parallelogram	15% *Pseudonitzschia* sp.	26% *Pseudonitzschia* sp.	13% *Pseudonitzschia* sp.
	Ellipsoid	0.6% *Dinophysis* sp. *Gyrodinium* sp.	2.5% *Prorocentrum* sp.	4% *Dinophysis* sp.
	Box	6% *Thalassiothrix* sp.	5.5% *T. nitzschioides*	7.1% *Thalassiothrix* sp.
Complex	**2 Cones**	0.7% *Protoperidinium* sp.	1.7% *Protoperidinium* sp.	6.7% *Protoperidinium* sp.
	Ellipsoid + 2 Cones + Cylinder	2.2% *T. tripos*	0.5% *T. longirostrum* *T. horridius*	3.1% *T. teres* *T. horridius*

4.2.2.3e. S:V and GALD of PGSs in varying depths of SCML

The variability in S:V and GALD of PGS showed distinct variability with respect to SCML depths. For instance, S:V of Cyl showed a significant increase, ElliP and Elli showed a minor increase, and PoP and B showed a significant decrease with increasing depth of SCML. The GALD of Cyl and ElliP significantly decreased, PoP showed a minor decline, B showed a minor increase, and Elli showed no trend with increasing SCML depth.

The regression analysis between S:V and GALD revealed a significant negative for Cyl, ElliP, and Elli2CCyl, a significant positive for PoP and no significant negative correlation for B in shallow depth, significant negative for Cyl, ElliP, PoP, B, and 2C, no significant negative and positive correlation for Elli and Elli2CCyl respectively in the intermediate and significant negative for Cyl, ElliP, Elli, and 2C, not significant positive for PoP and not significant negative correlation for B and Elli2CCyl in deep SCML. Interestingly, the scaling exponent 'b' showed a decreasing trend from shallow to deep SCML for Cyl (-0.45, -0.33, and -0.22), an increasing trend from shallow to deep SCML for B (-0.13, -0.27 and -0.52), Elli (-0.22 and -0.27) and 2C (-1.94 and -3.55), decreasing from shallow to intermediate and again increasing in deep SCML for ElliP (-0.30, -0.24, and -0.56) and no trend for PoP and Elli2CCyl (Figure 4.25 and 4.26).

4.2.2.3f. Comparative results between the sea surface and SCML

The SCML recorded more PGS (17 PGS) than the corresponding surface waters (13 PGS). In shallow, 12 (8 simple and 4 complex) and 15 (10 simple and 5 complex) PGSs belonging to 34 and 50 species of micro-phytoplankton were recorded in surface and SCML, respectively. Simple PGSs contributed 87% and 96%, whereas complex PGSs contributed 13% and 4% in shallow regions of the sea surface and SCML. Three simple (Cyl, ElliP, and PoP) and two complex (2C and Elli2CCyl) PGSs were common. Among simple PGSs, Cyl contributed 32%, co-dominated by *Rhizosolenia styliformis*, *Bacteriastrum* sp., and *Probosica alata* on the surface, and 30%, co-dominated by *Bacteriastrum* sp., *Dactyliosolen* sp., and *Thalassiosira* sp. in SCML. ElliP contributed 25%, co-dominated by *Navicula* sp. and *Chaetoceros peruvianus* on the surface, and 41%, dominated by various *Chaetoceros* species (e.g., *C. messanensis,* and *C. curvisetus*) in SCML.

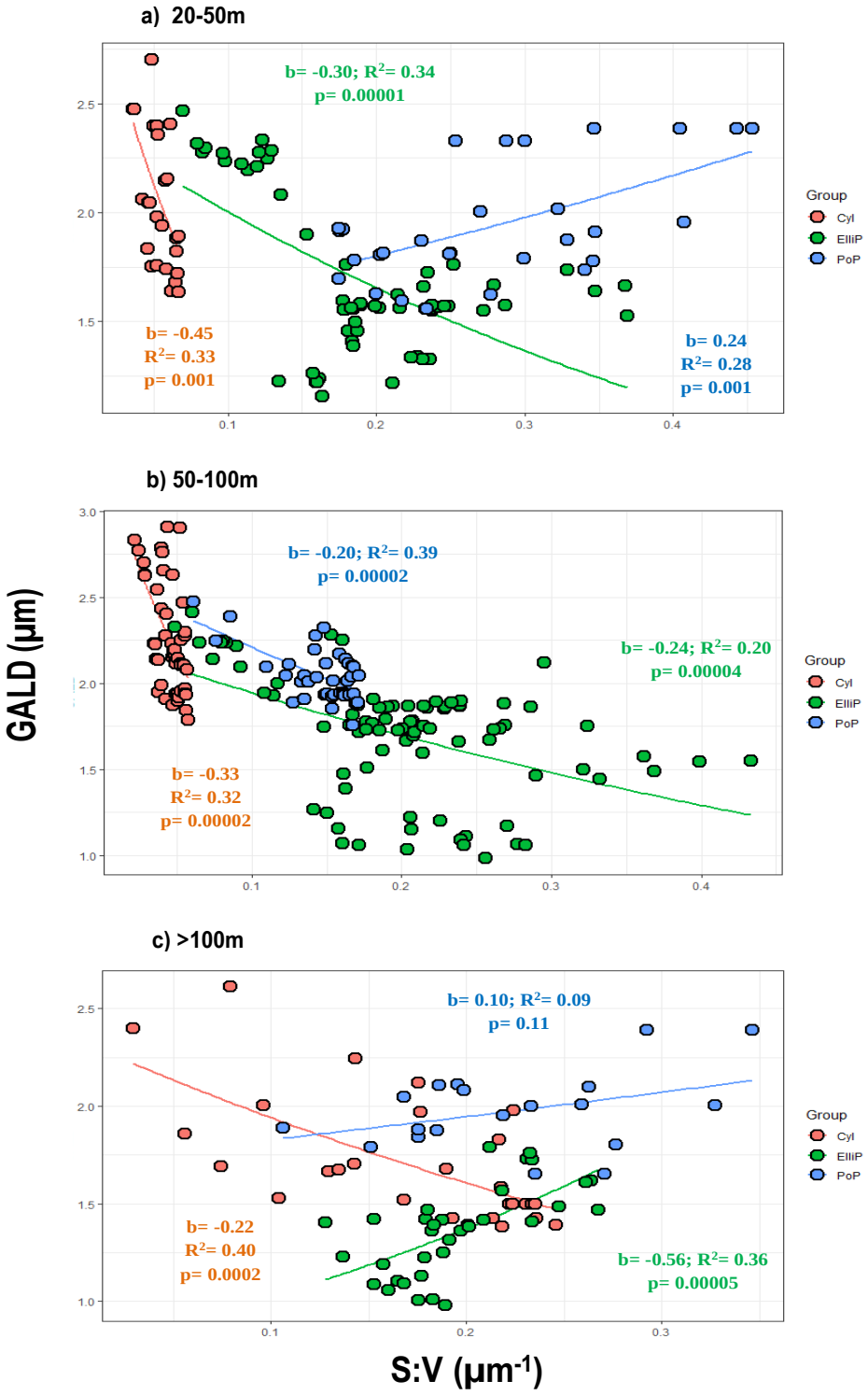


Figure 4.25. Non-linear regression of dominant PGS in varying depths of SCML in the IO. S:V: surface-to-volume ratio, GALD: greatest-axial-linear-dimension, ElliP: elliptic prism, Cyl: cylinder, and PoP: prism on parallelogram.

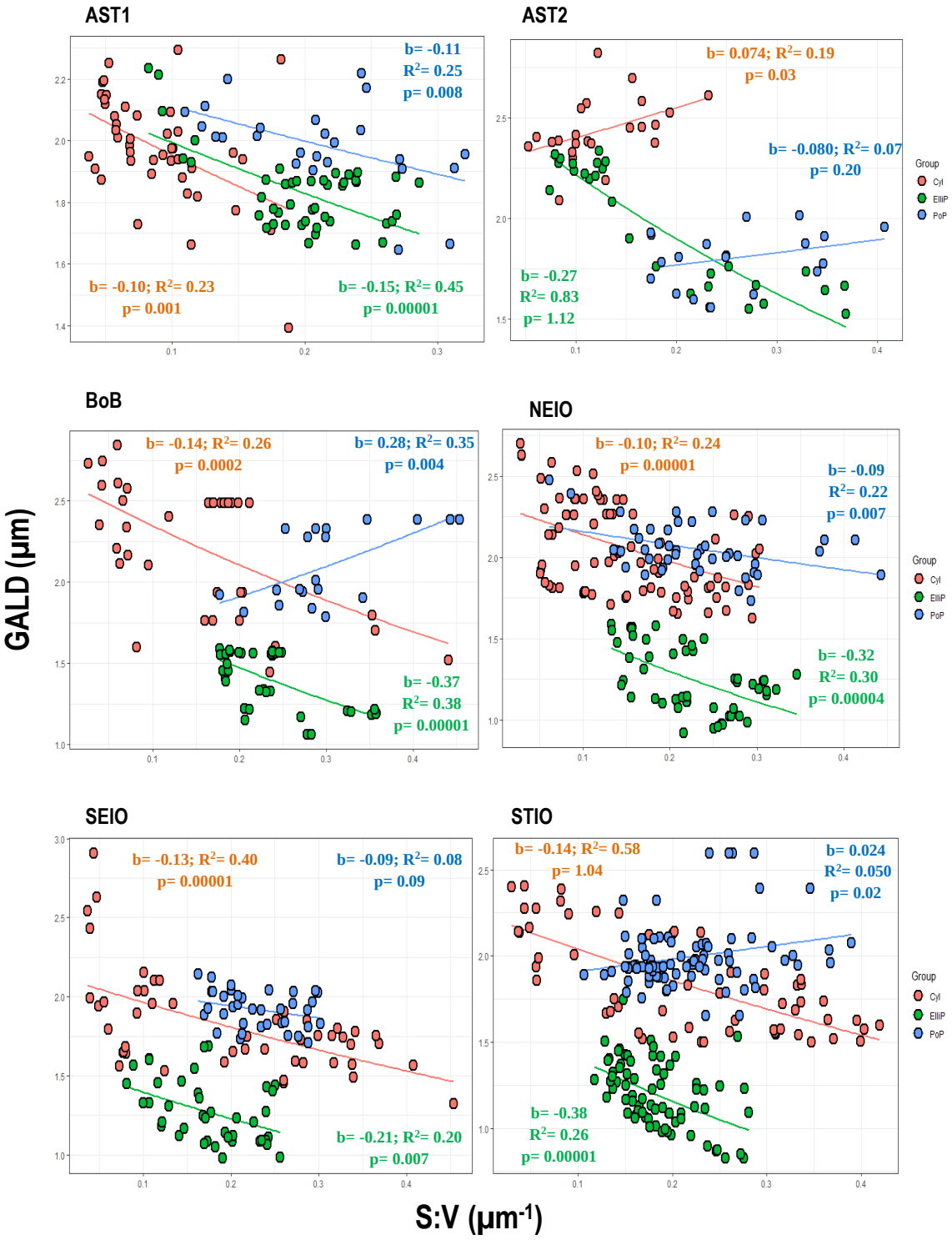


Figure 4.26. Non-linear regression of dominant PGS in surface waters of the IO. AST1: Arabian Sea transect 1, AST2: Arabian Sea transect 2, BoB: Bay of Bengal, NEIO: North equatorial Indian Ocean, SEIO: South equatorial Indian Ocean, STIO: South tropical Indian Ocean, S:V: surface-to-volume ratio, GALD: greatest-axial-linear-dimension, ElliP: elliptic prism, Cyl: cylinder and PoP: prism on parallelogram.

PoP contributed 17% and 15% in surface and SCML, respectively, dominated by *Pseudonitzschia* sp. Regarding complex PGSs, 2C contributed 5%, dominated by *Protoperidinium* sp. in surface waters, whereas Elli2CCyl contributed 3% and 2% in surface and SCML, respectively dominated by *Tripos* species (e.g., *T. tripos*, *T. deflexus*, and *T. pentagonus*). Simple PGSs like Cyl showed no change in S:V and a significant decrease in GALD, PoP showed a significant increase in S:V and GALD, and ElliP showed a significant decrease in S:V and GALD (Figure 4.27), whereas complex PGS, 2C showed no change in S:V and a significant decrease in GALD between surface and SCML.

In the intermediate region, 13 (8 simple and 5 complex) PGSs in surface and SCML belonging to 96 and 113 micro-phytoplankton species were recorded. Simple PGSs contributed 78% and 95%, whereas complex 12% and 5% in the intermediate region of surface and SCML. Four simple (Cyl, ElliP, Elli, and PoP) and three complex (2C, ElliP4C, and Cyl2Hs) PGSs were common. Among simple PGSs, Cyl contributed 32%, co-dominated by *Coscinodiscus* sp., *Leptocylindrus* sp., *Thalassiosira* sp., *Bacteriastrum* sp., and *Guinardia cylindrus* in surface and 26% in SCML, co-dominated by *Bacteriastrum* sp., *Coscinodiscus* sp., and *Thalassiosira* sp. ElliP contributed 27%, co-dominated by *Navicula* sp., *Chaetoceros* sp., and *Hemiaulus sinensis* in surface, and 31% in SCML, dominated by various *Chaetoceros* species (e.g., *C. messanensis*, and *C. lasiniosus*). Elli contributed 9% in surface water, dominated by *Prorocentrum* sp., and PoP contributed 26% in SCML, dominated by *Pseudonitzschia* sp. Regarding complex PGSs, 2C contributed 7% and 2% in surface and SCML, both dominated by *Protoperidinium* sp. and *Gonyaulax* sp. ElliP4C contributed 6% in surface, dominated by *Climacodium frauenfeldianum* and Cyl2Hs contributed 2% in SCML, dominated by *Corethron* sp. Simple PGSs like Cyl and ElliP showed a significant increase in S:V and a decrease in GALD, PoP showed a significant increase in both S:V and GALD (Figure 4.27) whereas, in complex PGSs, 2C showed no change in S:V and a significant decrease in GALD between surface and SCML.

In deep region, 8 (5 simple and 3 complex) and 11 (8 simple and 3 complex) PGSs in surface and SCML belonging to 25 and 48 micro-phytoplankton species were recorded. Simple PGSs contributed 83% and 88%, whereas complex 17% and 12% in deep region of surface and SCML. Three simple (Cyl, ElliP, and PoP) and three complex (2C, Elli2CCyl, and Cyl2Hs) PGSs were common. Among simple PGSs, Cyl contributed 12% in surface, co-dominated by *Asteromphalus* sp., *Rhizosolenia clevei*, and *Rhizosolenia*

hebetata, and 24% in SCML, co-dominated by *Bacteriastrum* sp. and *Coscinodiscus* sp. ElliP contributed 48% in surface, co-dominated by *Navicula* sp. and *Chaetoceros dadayi*, and 36% in SCML, dominated by *Chaetoceros simplex*. PoP contributed 20% in surface, dominated by *Nitzschia* sp., and 13% in SCML, dominated by *Pseudonitzschia* sp. Regarding complex PGSs, Cyl2Hs contributed 8% on the surface, dominated by *Corethron* sp., 2C 6% and 7% on the surface and SCML, respectively, dominated by *Protoperidinium* sp., and Elli2CCyl contributed 3% in SCML, co-dominated by *Tripos teres* and *Tripos horridius*. Simple PGSs like Cyl showed a significant increase in S:V and a decrease in GALD, PoP showed a significant increase in S:V and GALD, and ElliP showed no significant change in S:V and a decrease in GALD (Figure 4.27), whereas, in complex PGSs, 2C showed no change in S:V and GALD between surface and SCML.

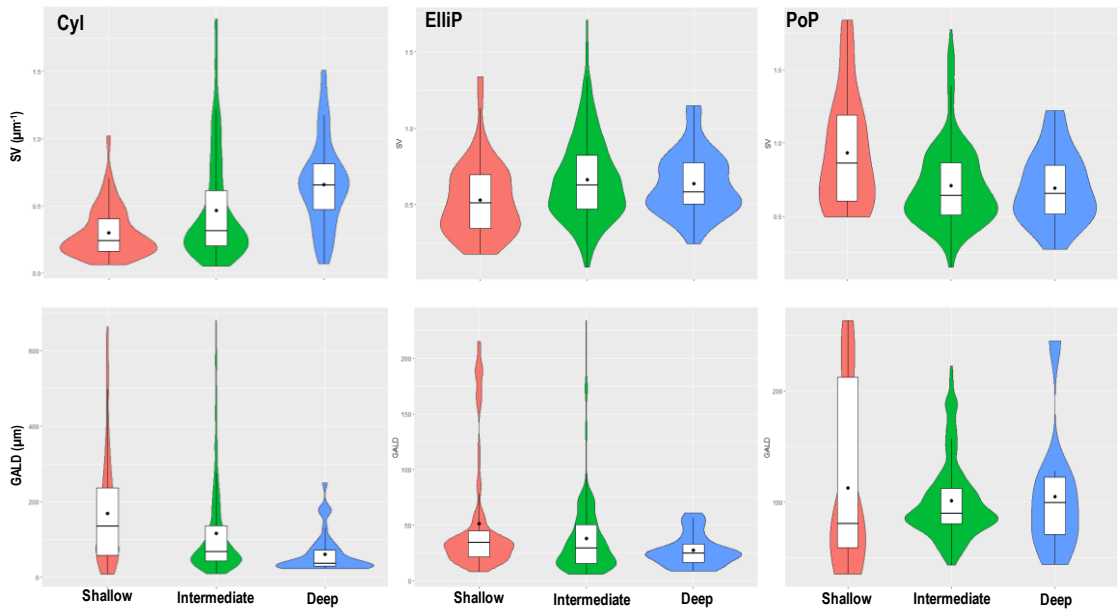


Figure 4.27. Violin plot of morphological attributes (S:V and GALD) in dominant PGS from varying SCML depths. S:V: surface-to-volume ratio, GALD: greatest-axial-linear-dimension, SCML: sub-surface chlorophyll maximum layer, Cyl: cylinder, ElliP: elliptic prism, and PoP: prism on parallelogram.

The surface waters of shallow, intermediate, and deep regions recorded lower micro-phytoplankton and PGSs than SCML, all dominated by simple shapes. The simple (Cyl, ElliP, and PoP) and complex (2C, Elli2CCyl, and Cyl2Hs) PGS were common in both layers, irrespective of the regions. However, Cyl dominated the surface and ElliP in the SCML of both shallow and intermediate regions, respectively. ElliP was dominant in the deep region (surface and SCML). The S:V in Cyl showed no change in shallow, increase in intermediate and deep regions, ElliP showed a decrease in shallow, increase in intermediate and no change in deep, PoP showed an increase, and 2C showed no change in all the regions between surface and SCML. The GALD showed a decrease in Cyl, ElliP, 2C and an increase in PoP for all the areas except 2C, which showed no change only in the deep region.

4.2.2.4. Discussion

The existence of permanent SCML in IO (AS, BoB, equatorial IO, and STIO) has been well documented (Shulenberger & Reid, 1981) primarily focused on the formation and maintenance of SCML using satellite (Shah et al., 2020) or argo-float data (Jayaram et al., 2021). Fu et al. (2018) emphasized that the phytoplankton community structure defines the understanding of SCML characteristics. The phytoplankton species show high morphological plasticity, optimizing their performance in response to environmental variabilities. Therefore, morphological analysis could be used to estimate the ecological variability within which a species can persist. Moreover, in the past two decades, analyzing spatial and temporal patterns of phytoplankton assemblages using trait-based methods has become popular (see Naselli-Flores & Padisak, 2023 and references therein). Hence, it is crucial to establish an understanding of the morphological trait variability and community structure between the sea surface and SCML as various taxa play a pivotal role in biogeochemical processes, like carbon transfer to depth or higher trophic level, in new primary production (Goldman et al., 2003; Revelante & Gilmartin, 1995) and could help in predictions of ecosystem response to future climate changes (Barnett et al., 2019).

This study recorded 108 and 134 species representing only 45% and 55% of the geometric shapes (14 and 17 out of 31 described shapes of Sun and Liu (2003)) described for phytoplankton in literature in surface and SCML, respectively. The unrecorded 14 shapes are represented mainly by the freshwater species or phytobenthos in the sunlit zone or belong to groups (e.g., flagellates, Euglenophyceae, Chlorophyceae) that were not recorded due to known technical limitations (e.g., preservatives and sample collection

above 20 micron) through microscopy approach. Despite methodological limitations, this study revealed that SCML harbors most of the described phytoplankton shapes and species, showing dissimilar spatial distribution patterns concerning abundance, composition, and diversity. A better understanding of the SCML micro-phytoplankton community, along with key taxa and their morphological adaptations, will be necessary to assess climate warming impact across IO effectively. The pelagic ecosystem trophic pathways could be modified if any variation in biomass, species composition, and size structure of the phytoplankton community within the SCML takes place (Legendre & Rassoulzadegan, 1996). Therefore, to better anticipate the community shifts and the functional implications for the ecosystem in changing global climate scenarios, it is of utmost importance to understand the relationship and variability of morphometric traits and taxonomy. This study discusses the variability in distribution patterns between bioregions and variable depths of SCML in the IO, having distinct hydrographic conditions in the subsequent sections.

4.2.2.4a. Variability of diversity and morphological traits of PGS in sea surface

Simple elongated shapes (e.g., Cyl, ElliP, and PoP) followed by complex shapes dominated in IO. ElliP and Cyl were the most prevalent PGSs in the surface waters but showed an opposite trend in distribution. For instance, Cyl showed a clear dominance in the northern (NIO, i.e., AS, BoB, and NEIO) than the southern IO (SIO, i.e., SEIO and STIO) and vice versa for ElliP. Interestingly, Cyl displayed taxonomic gradation where chain-forming taxa with or without setae dominated the NIO and solitary bigger taxa in SIO. While ElliP showed no such taxonomic variability (dominated by various species of *Chaetoceros*). Whereas in complex PGSs, the distribution was sporadic, and they are primarily present in the oligotrophic AST1, NEIO, SEIO, and STIO. The complex PGSs (Elli, 2C, and ElliP4C), which are mostly dominated by various pennate and dinoflagellate species, are known for their adaptive capabilities (presence of flagella and capability to survive in low nutrient conditions) in oligotrophic sea surface conditions. Since oligotrophic conditions are widespread in marine pelagic systems, PGS variability will also be similar. On the other hand, the morphological traits (S:V and GALD), which encode even the smallest environmental changes in their adaptive measures, are well reflected i.e., low S:V ($0.42\pm0.18\mu m^{-1}$) and high GALD ($219\pm89\mu m$) values under mesotrophic conditions (i.e., in NIO) and high S:V ($0.51\pm0.07\mu m^{-1}$) and low GALD ($102\pm6\mu m$) under oligotrophic conditions (i.e., in SIO) (Figure 4.28). The nutrients flow across cell boundary might not increase with meagre increase of S:V as it also depends

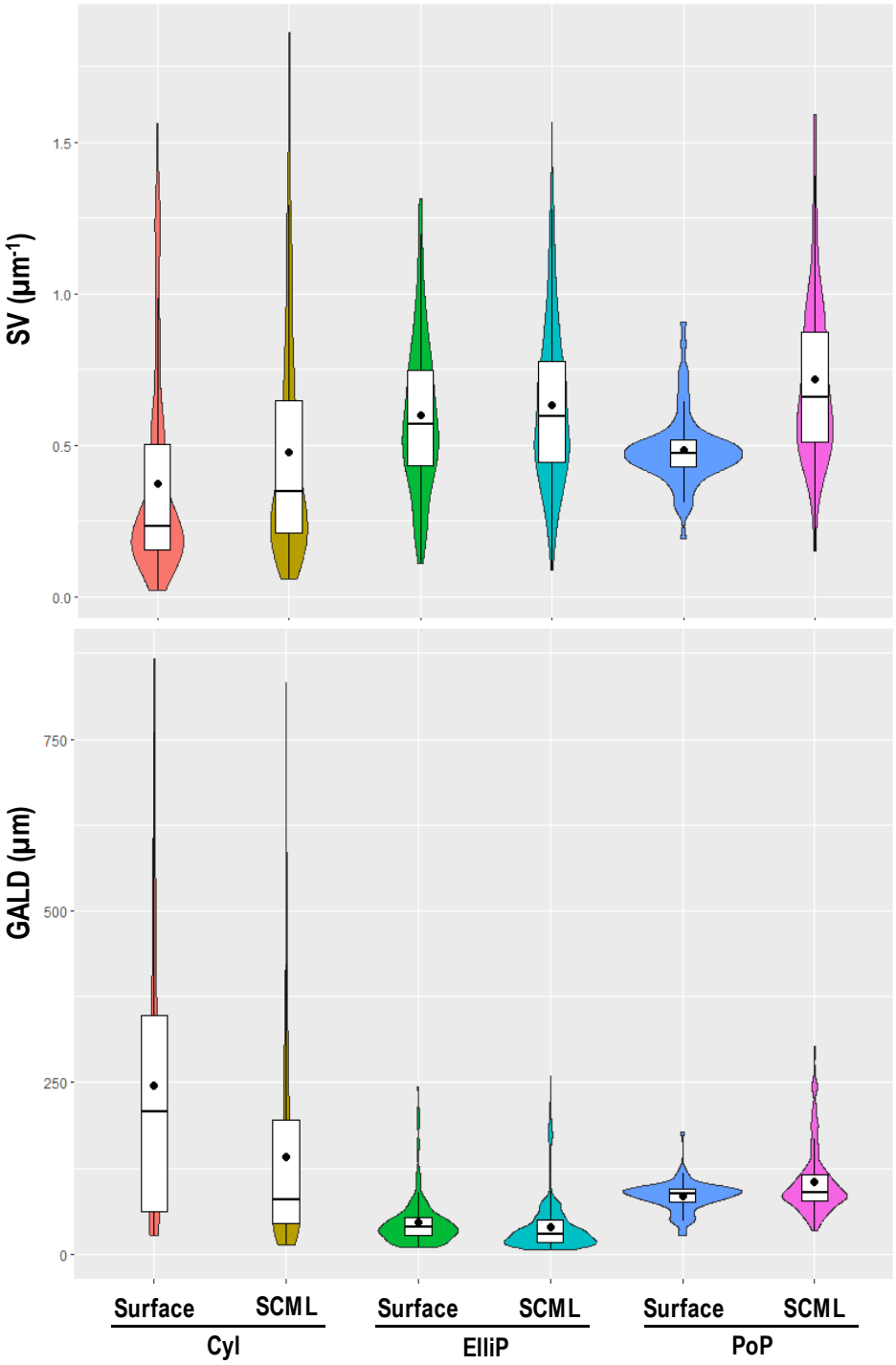


Figure 4.28. Violin plot of morphological attributes (S:V and GALD) in dominant PGS from sea surface and SCML waters. S:V: surface-to-volume ratio, GALD: greatest-axial-linear-dimension, SCML: sub-surface chlorophyll maximum layer, Cyl: cylinder, ElliP: elliptic prism, and PoP: prism on parallelogram.

on the cell shape (nutrient flow declines as cell curvature decreases, i.e., cell radius increases; Kiorboe, 2008); therefore, elongated prolate cells can provide large nutrient flow compared to oblate cells with same surface area and volume (Karp-Boss & Boss, 2006). Hence, elongated shapes richness is greater than oblate ones in general (Ryabov et al., 2021).

Interestingly, individual PGSs show distinct patterns in their morphometric traits. For instance, the S:V of Cyl significantly increased from northern to southern IO, showing maximum values for STIO, whereas ElliP showed no such pattern (Figure 4.29). The trends observed in Cyl could have been caused by environmental gradients (the trophic conditions and stratification). The water column becomes more stratified and oligotrophic as towards equatorial regions. It is known that environmental conditions like nutrients, light, and temperature influence the shape and size distribution of phytoplankton (Naselli-Flores et al., 2007; Stanca et al., 2013), making size and shape as crucial determinants of fitness. Kruk and Segura (2012) also concluded that environmental factors select specific phytoplankton morphological groups. However, this study shows that such patterns are PGS-specific and majorly determined by the dominant taxa. For example, non-setae-bearing taxa like *Rhizosolenia*, *Pseudosolenia*, *Coscinodiscus*, and *Probosica* or taxa with short (*Bacteriastrum* in Cyl) and long setae (*Chaetoceros* in ElliP). Former ones seldom form chains, and depend more on their morphological attributes for survival whereas later chain lengths are independent of morphological attributes and therefore show no specific patterns or trends. Since the S:V decreases with cell volume, it has been assumed that natural selection should favour elongated PGSs (Lewis, 1976; Niklas, 2000). Hence, morphological attributes reflect the environmental variability more robustly in simple PGS like Cyl than other PGSs (like ElliP, PoP) and can act as a potential ecological proxy for the pelagic ocean.

4.2.2.4b. Variability of diversity and morphological traits of PGS in varying depths of SCML

Like sea surface, PGSs are dominated by simple elongated shapes (e.g., Cyl, ElliP, and PoP) irrespective of the SCML depths and bioregions. ElliP, Cyl, and PoP were the most prevalent PGSs in shallow, intermediate, and deep SCML. The intermediate SCML harbored the maximum PGSs and taxa than shallow and deep. Though the dominance remained constant, the percentage contribution of simple PGSs (ElliP, Cyl, PoP, and B) gradually decreased except for Elli, which showed an opposite trend. In contrast, the contribution of complex PGSs (2C and Elli2CCyl)

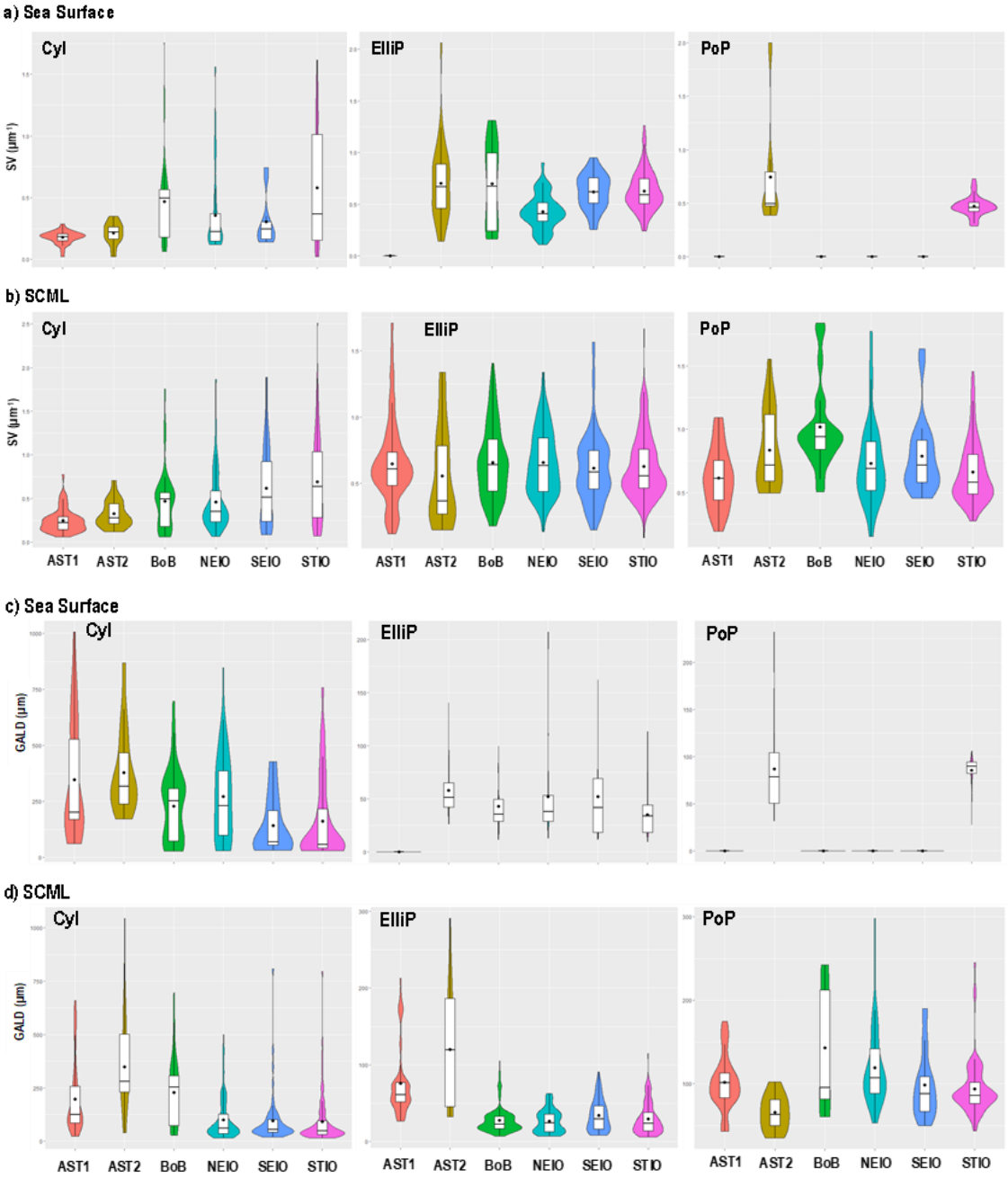


Figure 4.29. Violin plot of morphological attributes (S:V and GALD) in dominant PGSs from the sea surface and SCML of different regions in the Indian Ocean. AST1: Arabian Sea transect 1, AST2: Arabian Sea transect 2, BoB: Bay of Bengal, NEIO: North equatorial Indian Ocean, SEIO: South equatorial Indian Ocean, STIO: South tropical Indian Ocean, S:V: surface-to-volume ratio, GALD: greatest-axial-linear-dimension, Cyl: cylinder, ElliP: elliptic prism, and PoP: prism on parallelogram.

gradually increased with the increasing depth of SCML. However, the taxa in various SCML depths showed significant similarity between shallow and intermediate and dissimilarity to deep SCMLs. This similarity can be explained by the nutrient availability (N:P), which was relatively higher in shallow and intermediate but less in deep SCML. These two layers (shallow and intermediate) were dominated by *Pseudonitzschia* spp., which is well adapted to grow in varying light conditions (Bates et al., 1998; Houliez et al., 2023). Whereas the deep SCML was dominated by a heterotrophic dinoflagellate (*Protoperidinium* spp.), well known as a key contributor to the SCML community (Durham & Stocker, 2012; Cullen, 2015). Few microscopic observations have also reported increased dinoflagellate abundance in the SCML (Estrada et al., 2016; Barnett et al., 2019; Decembrini et al., 2020). The motility of dinoflagellates (response to resource gradients) can act as an essential trait in compensating for physiological disadvantages compared to diatoms (Ross & Sharples, 2007). *Protoperidinium* spp. is also known to be species-specific feeders and prefers to feed on diatoms majorly (Buskey, 1997). Some of the *Protoperidinium* species (*P. depressum*) have also shown survival for extended periods (up to 71 days) in conditions of starvation (Jakobsen & Hansen, 1997; Menden-Deuer et al., 2005). However, the capability to endure extended starvation is a useful strategy, especially for a species-specific feeder; their presence might not indicate optimal growth conditions (Gribble et al., 2007). *Chaetoceros simplex* was also found abundantly in deeper SCML. The presence of *Chaetoceros simplex* in low light and nutrient-poor conditions is also reported from the deeper waters of the western Pacific Ocean (Mou et al., 2022). On the other hand, ElliP and PoP were most prevalent PGS in SCML and were dominated by spore-forming (e.g., *Chaetoceros* spp., *Bacteriastrum* spp.; Bosak et al., 2015) and low light-adapted taxa (e.g., *Pseudonitzschia* spp.).

The relation between morphological traits (S:V vs GALD) differed between SCML depths, suggesting different adaptive strategies to cope with prevailing conditions. The PGS in shallow SCML showed low S:V and high GALD, while in intermediate and deep SCML, PGS showed high S:V and low GALD (Figure 4). For instance, high S:V and low GALD observed in deep and intermediate SCML could be due to low nutrient and light conditions (O'Farrell et al., 2007; Morabito et al., 2007) and vice versa for shallow SCML. Kurk et al. (2015) reported from subtropical estuary that the S:V ratio increased with the vertical attenuation coefficient and, supposedly, the extent of light limitation. Cell elongation gives micro-phytoplankton a competitive advantage by diminishing sinking velocity (Padisak et al., 2003), better nutrient absorption without affecting S:V

ratio (Kleparski et al., 2022), enhancing light capture (Naselli-Flores & Barone, 2011) and can also be an adaptation to grazing (Petrucciani et al., 2022). The morphometric traits of the dominant PGSs between SCML depths show specific morphometric adaptation (like the ability to maintain an optimum S:V and GALD). For example, in shallow SCML, all dominant species in their respective PGSs maintained a low S:V (0.15-0.67 μm^{-1}) and high GALD (40-158 µm) whereas in deep SCML, high S:V (0.37-0.90 μm^{-1}) and low GALD (27-72 µm) strategy was prevalent. The intermediate SCML S:V (0.20-0.92 μm^{-1}) and GALD (28-111 µm) values were higher than shallow but lower than deep SCML. Such trait variability could be due to nutrient limitation as amount of light availability is the same at all SCML depths (i.e., 1-2%). Though many studies have shown a strong effect of light (Kruk et al., 2015; O'Farrell et al., 2007) and nutrients (Naselli-Flores & Barone, 2011) on the phytoplankton morphology but under constant low light conditions, nutrients act as a strong controlling factor (Morabito et al., 2007; Charalampous et al., 2018). Moreover, the spectral quality of light (within range of photosynthetic active radiation; PAR, 400-700 nm) other than the intensity plays a major role for phytoplankton (Hintz et al., 2021). The spectral range of light shifts from a full spectrum at the surface to a limited (predominantly blue spectrum) in deeper layers (Kirk, 2011; Holtrop et al., 2021). Therefore, the spectral quality of light in shallow, intermediate, and deep SCML might be subjected to such spectral shifts, which may also be an additional factor influencing morphometric traits.

Additionally, variability in S:V was also observed for different PGSs between SCML depths, similar to that observed for surface waters. For instance, S:V of Cyl increased significantly, and ElliP and Elli showed a minor increase, whereas PoP and B decreased significantly with increasing depth of SCML. The shallow and intermediate SCMLs were less stratified and nutrient-depleted than the deep SCMLs. Such environmental differences in SCMLs are strongly reflected in a similar pattern in the morphological attributes of Cyl, ElliP, and Elli, whereas PoP and B show opposite trends. Ryabov et al. (2021) have considered PGSs like Cyl, and ElliP as elongated and PoP and B as oblate shapes. They have argued that the rate of nutrient diffusion declines as cell curvature decreases; therefore, an elongated cell can provide a larger nutrient flow than oblate cells. They also observed that the maximum surface extension for oblate shapes are smaller than the elongated ones. Moreover, the opposite trends observed in PoP and B might also be because of the pennate diatom taxa (e.g., *Pseudonitzschia*, *Thalassiothirx*, and *Thalassionema*) that dominate these PGSs. These taxa are either known to be well

adapted to thrive in low light conditions or form chains to overcome their geometric constraints. Hence, the elongated PGSs are more prevalent with robust morphological attributes responding to environmental conditions than the oblate PGSs. The observations suggest that light (both quantity and quality) and nutrients have a strong limiting influence on the morphological attributes of micro-phytoplankton in the oligotrophic pelagic system of IO.

4.2.2.4c. Sea surface vs SCML

The surface and SCML taxa also differed and were governed by the prevailing environmental conditions in both layers. The trophic conditions are different across IO, like eutrophic conditions (North-eastern AS, mesotrophic conditions (central and southeastern AS, and BoB), and oligotrophic conditions (equatorial and STIO); therefore, the taxa are expected to be different (Sarma et al., 2021). The micro-phytoplankton assemblages between the surface and SCML reveal that the SCML community is well adapted to the subsurface environments by showing distinct assemblages from the surface. Few studies have reported that assemblage might be similar if SCML is formed due to growing cell accumulation near the surface. However, if SCML is formed due to active growth, then the species assemblage may differ from the upper layer (Furuya & Marumo, 1983). In this study, except for AST2, all the SCML have formed below MLD, suggesting major environmental constraints governing community differences.

Additionally, morphometric traits (S:V and GALD) showed interesting results. For instance, S:V of dominant PGSs (e.g., Cyl, ElliP, and PoP) showed no specific pattern or trends between shallow SCML and the corresponding sea surface. Probably environmental conditions showed similarity as shallow SCML is within MLD. In contrast, the PGS of intermediate and deep SCML showed distinct patterns with the corresponding sea surface due to differences in environmental conditions. For instance, dominant PGSs showed an increasing and decreasing trend in their S:V and GALD values, respectively. However, no such changes or patterns were noticed in complex PGSs like 2C, which correspond to dinoflagellates that can overcome any vertical environmental gradient by using their flagella for migration. An increase in S:V helps improve the nutrient uptake in general (Kruk et al., 2015; Raven, 1999); therefore, the observed patterns in S:V and GALD might be in response to the nutrient availability. The allometric scaling analysis of dominant PGSs in which the functional relationship between two measured quantities (S:V and GALD in this study), where a relative change in one quantity results in a relative proportional change in the other, in surface and SCML

revealed interesting information. For all dominant PGS, any change in GALD was associated with very minimal change (decrease) in S:V (Figures 4.24-4.26), suggesting the adaptation by dominant PGSs to conserve S:V. The degree of change in S:V was even less for SCML than the surface. Similar strategies have been reported previously from the north and southeastern Arabian Sea (Paul et al., 2023), the Mediterranean micro-tidal lagoon (Aubry et al., 2017), and the coast of the Salento peninsula (Stanca et al., 2013). However, in AS, nutrient availability and the prevailing hydrographic conditions determined the adaptive strategies adopted by dominant PGSs. The variations in allometric patterns are not evolutionary but result from random variations or local adaptive differences among populations (Neustupa, 2016). These variations have been identified as essential factors in morphological evolutions as individual allometric trajectories may act as constraints canalizing evolutionary change of morphology (Klingenberg, 2010; Wilson, 2013; Pelabon et al., 2014). Reynold has implicitly recognized morphological traits as "master traits" because physiological and ecological features are strongly regulated by shape and size (Reynolds, 2006; Weithof & Beisner, 2019) and represent organisms' response to environmental changes affecting ecosystem functioning (Kruk et al., 2021). The morphological attributes and their variability help species to increase their fitness to varying environmental factors. This morphological variability is known as "phenotypic plasticity" and can be produced by a single genotype (West-Eberhard, 1989). The realized niches can be made unstable by a species using phenotypic plasticity over space and time (Marrone et al., 2023). Therefore, given the above arguments, this study argues that S:V and GALD can act as robust morphological traits in the pelagic regions of IO. PGSs like Cyl and PoP respond very strongly, and ElliP sporadically to environmental factors aided by their morphological traits, making them proxies to map the phenotypic plasticity in large pelagic systems, which is predicted to change due to global warming.

Several modelling-based studies suggest climate warming will increase ocean stratification, reducing nutrient exchange between the deep ocean and the upper mixed layer (Bopp et al., 2001; Sarmiento et al., 2004). The stratification in the upper 200m has increased by 5.3% in the global ocean (in recent decades, i.e., 1960-2018), caused mainly by temperature changes (Li et al., 2020). According to Dutkiewicz et al. (2005), ocean stratification will deepen the nitracline, reducing nutrient supply to the euphotic layer by the end of this century and oceanic primary productivity by 14%. Nonetheless, predicting the impact of such changes on marine ecosystems is elusive. Cermeño et al. (2008)

predicted that enhanced nutrient limitation would reduce the competitive advantages of diatoms. As revealed in our study, the SCML formed at depths coincided with 1-2% PAR and nitracline depth (within 10m depth above or below). RDA analysis revealed the tight coupling for deep SCML PGS (including S:V and GALD) with nutrients and light (PAR). Further, N:P values at different SCML depths varied according to nitracline, i.e., higher in shallow (2.21±1.12) and intermediate (2.50±4.32) than in deep (1.38±0.33) SCML. The N:P value at deep SCML was low because it formed above the nitracline depth, and the gap between them was also greater. Further, the temperature negatively correlated with GALD and PGS, suggesting relatively higher temperatures favored smaller phytoplankton cells. Therefore, under the predicted global warming scenario, deepening of nitracline might affect the different size and shape primary producers in the following ways: (i) smaller spherical phytoplankton (e.g., picoplankton, coccolithophores): these have less nutrient requirements and might be relatively less affected as they are well adapted to low light and low nutrient condition (known to have low Reynolds numbers with high S:V and low GALD, making nutrient uptake much easier; Fogg, 1991), (ii) bigger flagellated phytoplankton with complex PGS (like dinoflagellates) with high S:V and GALD: these cells might be moderately affected as they are equipped with various nutrition modes (e.g., autotrophy, heterotrophy, and mixotrophy) and can also evade low nutrient conditions using flagella for motility, and (iii) bigger simple PGS phytoplankton (without flagella; e.g., diatoms) with low to moderate S:V and GALD: these forms are dominant (80-90%), possess distinct phenotypic plasticity, have higher nutrient requirements and might be severely affected by light and nutrient limitation. Therefore, their morphometric traits can offer a potential ecological proxy in predicted oceanic climate change scenarios (deeper nitracline with very low light and a relatively shallow SCML with low nutrients). Under such conditions, the morphological traits (S:V and GALD) can be useful tracers to delineate the adaptive strategies by different PGSs, i.e., PGS with high morphometric plasticity (like cylinder and prism on parallelogram) will have the upper hand over other PGS (like an elliptic prism) with limited plasticity. Nonetheless, further studies unraveling the dynamics of S:V and GALD of PGS with nitracline depth and PAR under the predicted future scenarios will provide more insights into the resilience or vulnerability of SCML micro-phytoplankton, biological pump efficiency *per se*, to the global change predictions.

4.2.2.5. Conclusion

This study concludes that the simple elongated PGSs (e.g., Cyl, ElliP, and PoP) were cosmopolitan, having similar dominance (with varying percentage contribution) patterns in the sea surface, SCML, and between the deep SCML and corresponding sea surface. However, they showed latitudinal gradients at the sea surface, i.e., north-south and south-north gradients for Cylindrical and Elliptic-prism PGS, respectively. In contrast, the complex PGS showed sporadic distribution. Further, the similarity between the PGS (community and morphological trait) of SCML and the corresponding sea surface is based on the location of the former concerning MLD. Among SCMLs, the occurrence depth determined PGS dominance and its morphological attributes. Simple and complex PGS contribution gradually decreases and increases, respectively, with increasing SCML depth. Also, PGS in shallow SCML showed low S:V and high GALD, while in intermediate and deep SCML, high S:V and low GALD, indicating adaptive strategy, i.e., phenotypic plasticity behavior by dominant PGSs to capture light. Between the SCML depths, only simple PGS (Cylinder followed by Elliptic-prism and Prism on parallelogram) showed profound variability in morphological traits showcasing strong phenotypic plasticity behavior and as a potential ecological proxy in oceanic systems. Since micro-phytoplankton are significant contributors to SCML, this study facilitates a better understanding of SCML ecology and biogeochemistry *per se* in predicted ocean change scenarios.

Chapter 5

Photo-physiological adaptation of microalgae from different bioregions

Chapter 5: Photo-physiological adaptation of microalgae from different bioregions.

5.1. Introduction

In functional classification, microalgal physiology is also considered one of the important traits in addition to shape and size. The phytoplankton photosynthesis and growth are controlled by various indispensable resources and nutrient availability (N, P, and Si), and light is the main driver (Tilman et al., 1982). The incident light regime is highly dynamic concerning the quantity and spectral composition. For instance, microalgae inhabiting intertidal regions and shallow water bodies (e.g., rock pools) experience extreme saturating irradiance compared to pelagic areas. Nevertheless, microalgae might have acquired a unique photo-adaptation strategy in each system. Various factors like seasonal and diurnal cycles, stratospheric ozone, meteorology (e.g., aerosols, clouds), attenuation by water-column, and vertical mixing are responsible for the light dynamics (Denman & Gargett, 1983; Kirk, 1994; Harrison & Smith, 2009). The perceived light for phytoplankton can fluctuate on a time scale varying from seconds to hours with full sunlight to complete darkness.

Phytoplankton residing on the sea surface are generally exposed to high PAR (photosynthetically active radiation; 400–700 nm) and short wavelengths like ultraviolet A (UV-A) radiation (315–400 nm) and ultraviolet B (UV-B) radiation (280–315 nm) of the solar spectrum. The UVR is attenuated faster in the water column than PAR, causing a vertical gradient in the spectral composition, and is highly dependent on the turbulence of the water column (Neale et al., 1998, 2003). When exposed to excessive irradiance, the phytoplankton undergoes inactivation of PSII reaction centers, and this phenomenon is known as photoinhibition, where the ability to perform photosynthesis reduces (Osmond, 1994) and prolonged exposure can also cause viability loss (van De Poll et al., 2005). Moreover, combining excess PAR with other stressors (e.g., suboptimal temperature, UVR) can increase photoinhibition than PAR alone (Heraud & Beardall, 2000). According to Gao et al. (2007), the size structure of the community and cloudiness determine the impact of UVR on phytoplankton photosynthesis. Thus, the response of UVR depends not only on the phytoplankton assemblage sensitivity but also on the combination of other environmental variables. To avoid the inactivation of the PSII centers over broad radiation conditions, phytoplankton have developed various physiological and biochemical mechanisms of photoprotection (Roy, 2000; Banaszak,

2003; Aro et al., 1994) however, it is a complex, metabolically expensive and time taking process (Raven, 1989, 2011). The phytoplankton community uses three known mechanisms for photoprotection (all or a combination of the three). Those mechanisms involve (i) dynamic photo-inhibition (i.e., quick PSII reaction center recovery from damage; Gorbunov et al., 2001), (ii) non-photochemical quenching (NPQ; dissipation of excess energy through thermal dissipation using xanthophyll cycle; van De Poll et al., 2010), and (iii) the production of photo-protective pigments (Falkowski & Chen, 2003). The NPQ involves the conversion of violaxanthin to zeaxanthin through antheraxanthin for green algae and higher plants (Demmig et al., 1988) and the conversion of diadinoxanthin to diatoxanthin (Arsalane et al., 1994; Olaizola et al., 1994) in Chl-*c*–containing algae, known as the xanthophyll cycle activity (Ruban et al., 2004).

The photo-physiology and photoprotection mechanism measured on natural phytoplankton communities have provided vital information about the fitness and health of the ecosystem (Moore et al., 2005; Patil & Anil, 2019). A higher photoprotective capability might benefit the phytoplankton community under variable light conditions. For instance, in the highly mixed water column (e.g., coastal), the short-term photo-response is activated more often than in a more stratified and stable oceanic ecosystem, and this characteristic can be a determining factor for the competitive performance of some phytoplankton (Dimier et al., 2007). The studies related to the photo-physiology of phytoplankton have been studied from various oceanic regions, like the Atlantic and Pacific Atlantic oceans (e.g., Behrenfeld et al., 2006; Moore et al., 2008; Browning et al., 2014; Lin et al., 2016), Southern Ocean (Holeton et al., 2005; Suggett et al., 2009; Lin et al., 2016), as well as during phytoplankton blooms (Moore et al., 2005; Suggett et al., 2006) and mesoscale eddies (Bibby et al., 2008). However, there are no studies from the oceanic regions of the Indian Ocean except a few representative studies that have been conducted on the coastal habitat of the Arabian Sea, such as rockpools (Patil et al., 2017) and monsoon-influenced estuaries (Patil & Anil, 2019). Therefore, in the present study, the photo-physiological adaptations of natural phytoplankton communities from two contrasting oceanic regions (i.e., productive Arabian Sea and oligotrophic south tropical Indian Ocean) were studied for the first time using photo-physiological parameters (F_v/F_m and σ_{PSII}) and HPLC-derived pigment concentrations. The purpose of this study is to evaluate the following: (i) the photoprotective response of sea surface and SCML water phytoplankton communities to natural sunlight, (ii) the effect of only PAR and

PAR+UVR treatment on the photoprotective mechanism, and (iii) to evaluate photoprotective mechanism among different bioregions of the Indian Ocean. The knowledge gained on photo-physiology could better understand phytoplankton adaptation, carbon assimilation, and photo-acclimation capacity, mainly when the surface mixed layer shallows in the future global warming scenario.

5.2. Methodology

The details of the sampling site, sample collection, experimental design, and analysis for the present objective are presented in Chapter 2, subsection 2.2.3.

Data analysis

To evaluate the variations in treatments and locations of the bioregions, multifactorial ANOVA followed by a post hoc Tukey test was performed on the PSII parameters (F_0, F_v/F_m, and σ_{PSII}). A one-way ANOVA was performed using Statistica software (release 8) to assess variations in the pigment ratios (DT + DD/Chl-*a*, DT/DT + DD, PPC/PSC) concerning the location of the bioregions.

5.3. Results

5.3.1. Phytoplankton community

The microscopic analysis revealed that the experimental phytoplankton community was diatom-dominated (AS: 94-99%; STIO: 50-99%) and low dinoflagellates contribution (AS: 1-6%; STIO: 1-10%) at both the bioregions (Figure 5.1a and 5.2a). However, the dinoflagellate contribution was higher (50%) in the only PAR treatment of the surface experiment (i.e., station 13) at STIO. Centric diatoms were the significant contributors in the first experiment (i.e., station 16), whereas pennate diatoms were in the second experiment (i.e., station 17) at the AS. Whereas, pennate diatoms contributed significantly in both experiments (i.e., stations 11 and 13) for surface and SCML at STIO. However, based on the size-fractionated diagnostic pigments, the initial samples showed micro-22%, nano-10%, and pico-68% at AS and micro-28% and pico-72-100% contribution at STIO. Interestingly, in response to the nutrient's addition, the contribution significantly changed for micro-68-71%, nano-3-4%, and pico-24-29%, respectively, at AS (Figure 5.1c-f). The contribution of pico- and micro-phytoplankton significantly changed to 19-90% and 47-98%, respectively, at STIO. Similarly, the total Chl-*a* increased from an

initial value of 0.58 μgL^{-1} to a final value of 1.15-6.5 μgL^{-1} at AS. Whereas at STIO, total Chl-*a* increased from an initial value of 0.10-0.31 μgL^{-1} in surface and 0.47 μgL^{-1} in SCML to a final value of 0.21-0.63 μgL^{-1} in surface and 1.03 μgL^{-1} in SCML experimental setup.

5.3.2. Effect of solar radiation on PSII parameters

The PAR and UVR values were lowest in the early morning, followed by evening, and highest at noon. The early morning, evening, and noon PAR and UVR values were PAR= 80 $mWcm^{-2}$; UVR= 0.001 $mWcm^{-2}$, PAR= 267 $mWcm^{-2}$; UVR= 0.05 $mWcm^{-2}$, and PAR= 1937 $mWcm^{-2}$, UVR= 4.378 $mWcm^{-2}$, respectively in the AS (Figures 5.1a). Similarly, the early morning, evening, and noon PAR and UVR values were PAR= 0.03-18.9 $mWcm^{-2}$; UVR= 0.01-0.05 $mWcm^{-2}$, PAR= 28.4 $mWcm^{-2}$; UVR= 0.05 $mWcm^{-2}$, and PAR= 1607-2004 $mWcm^{-2}$; UVR: 3.6-4.2 $mWcm^{-2}$, respectively in the STIO (Figures 5.2c).

The measurements of the photosynthetic parameters revealed distinct variations over the 72-hour incubation period at both bioregions. The photosynthetic parameters (F_0, F_v/F_m, and σ_{PSII}) showed characteristic diurnal patterns (a morning high to noon low and a reciprocal increase in the evening) for both treatments at both bioregions. In F_v/F_m and σ_{PSII}, diurnal patterns were characterized by a rapid recovery for both locations at the AS. Interestingly, the recovery of F_v/F_m was gradual, but the same pattern was not observed for σ_{PSII} at the STIO. The F_0 values increased from 0.99 to 1.25 and 0.40 to 3.95 for only PAR treatment and from 0.99 to 1.84 and 0.40 to 3.72 for PAR+UVR treatment at both locations, respectively, in the AS. Similarly, the F_0 values increased from 0.30 to 0.72 and 0.67 to 0.87 for only PAR treatment with surface water and from 0.67 to 0.75 for PAR+UVR treatment with SCML water in both experiments in the STIO (Figure 5.3. and Figure 5.4.).

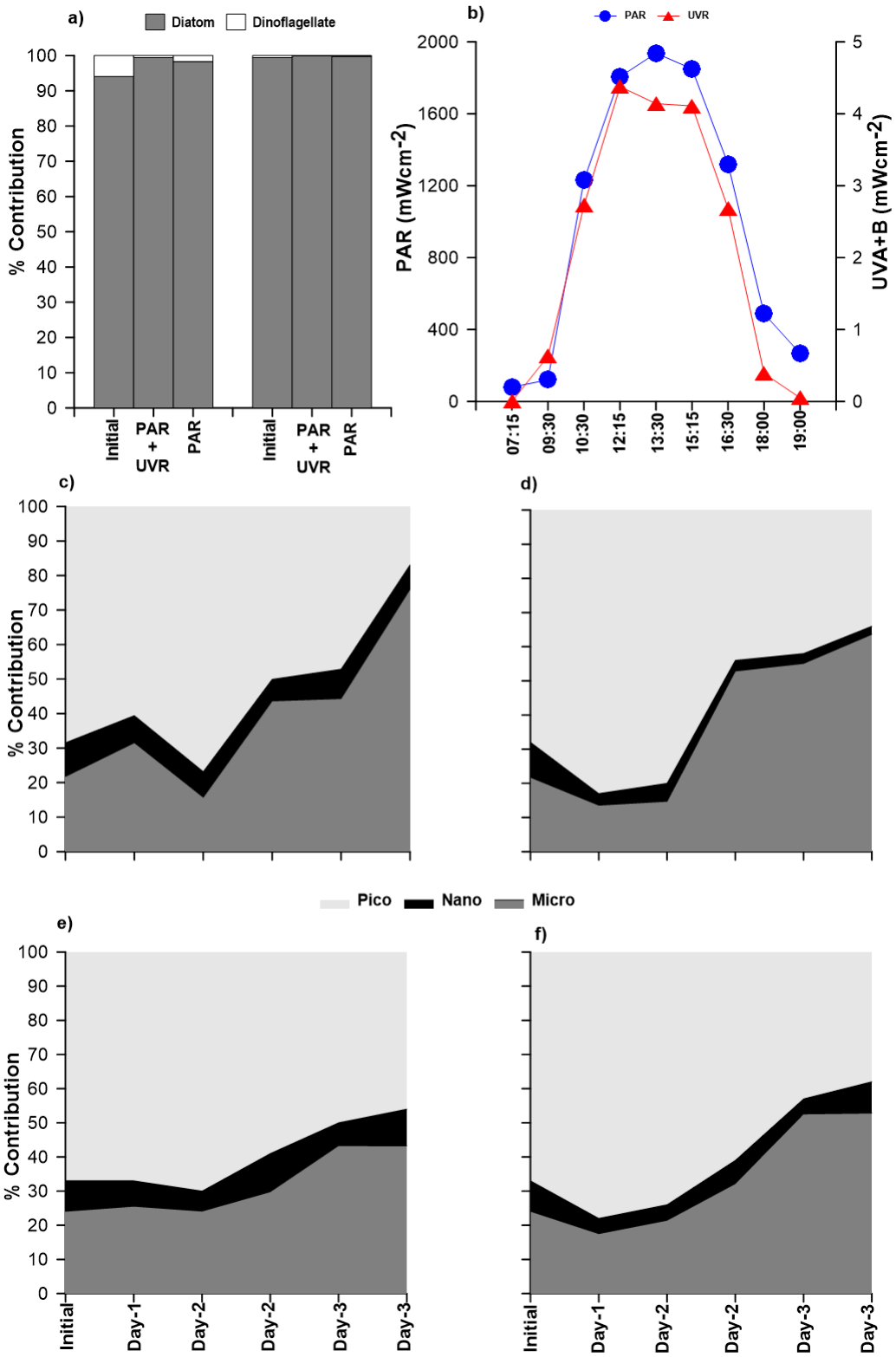


Figure 5.1. Plots showing a) pennate and centric percentage contribution, b) dial variation in solar radiation and c-f) percentage contribution of pico-, nano-, and micro-phytoplankton based on marker pigment in PAR and PAR+UVR treatment during the incubation period in the Arabian Sea.

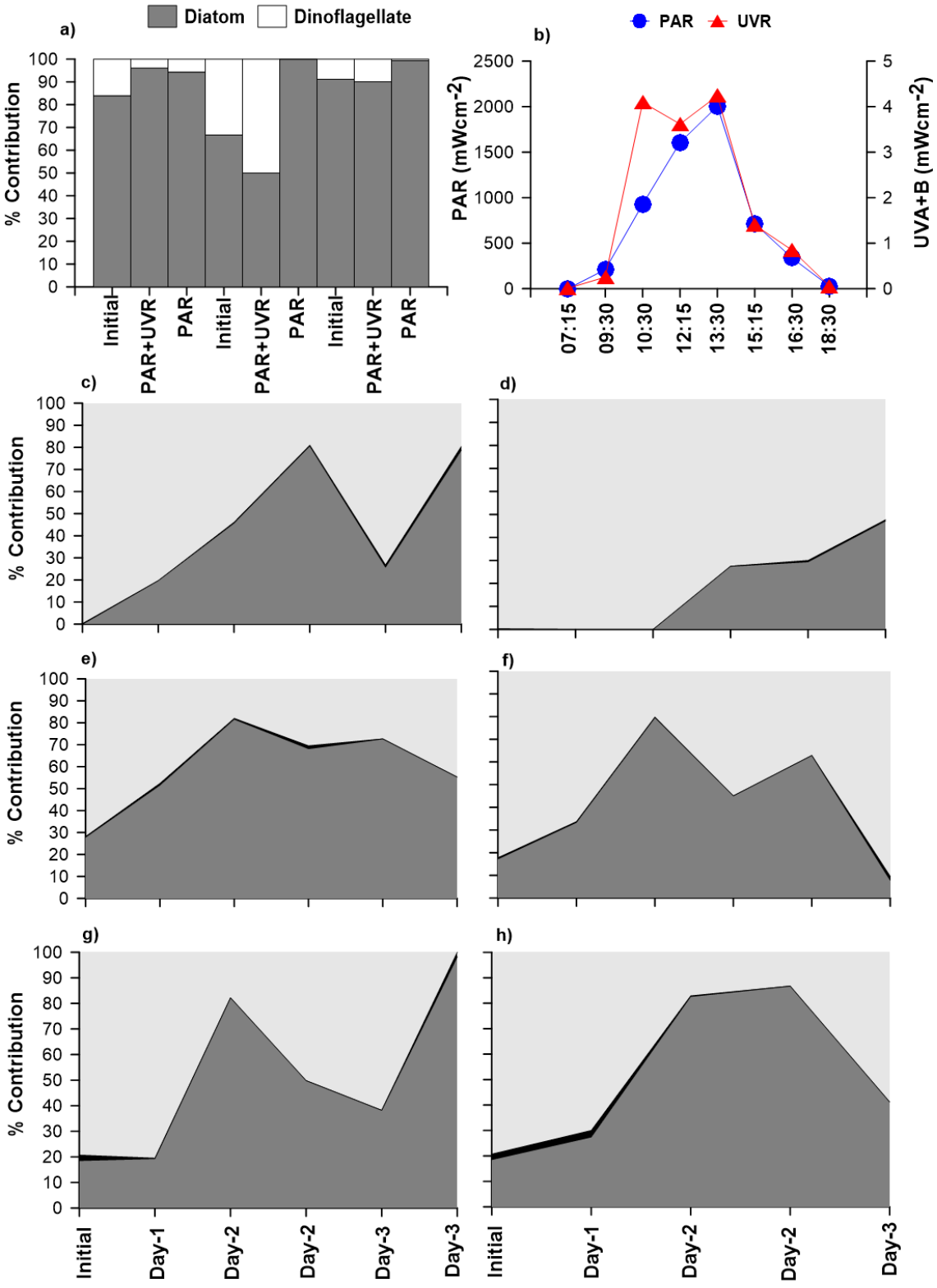


Figure 5.2. Plots showing a) diatom and dinoflagellate percentage contribution, b) dial variation in solar radiation, and c-h) percentage contribution of pico-, nano-, and micro-phytoplankton based on marker pigment in PAR and PAR+UVR treatment during the incubation period in the South-tropical Indian Ocean.

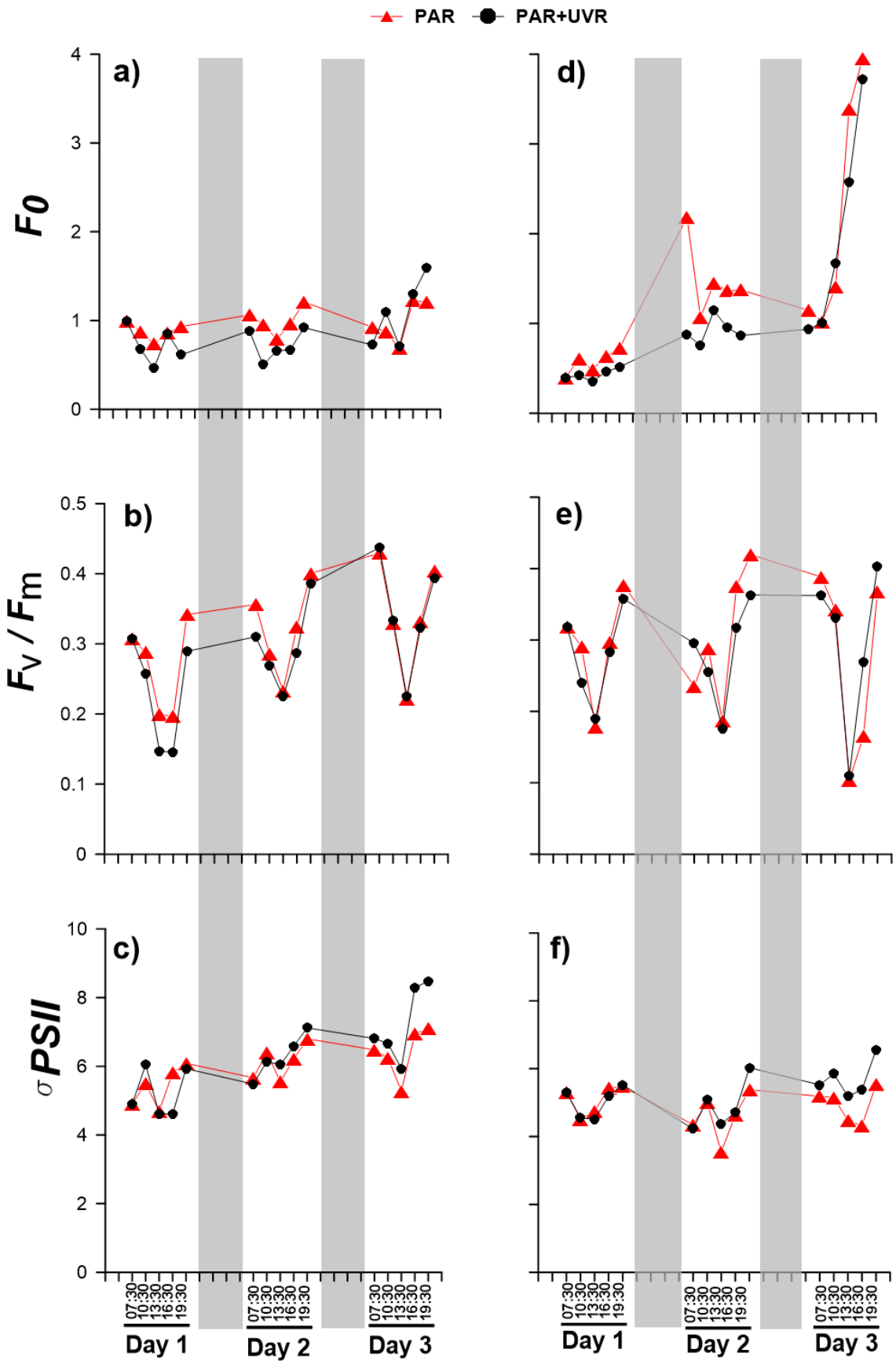


Figure 5.3. PSII parameters during the three days incubation in the Arabian Sea.

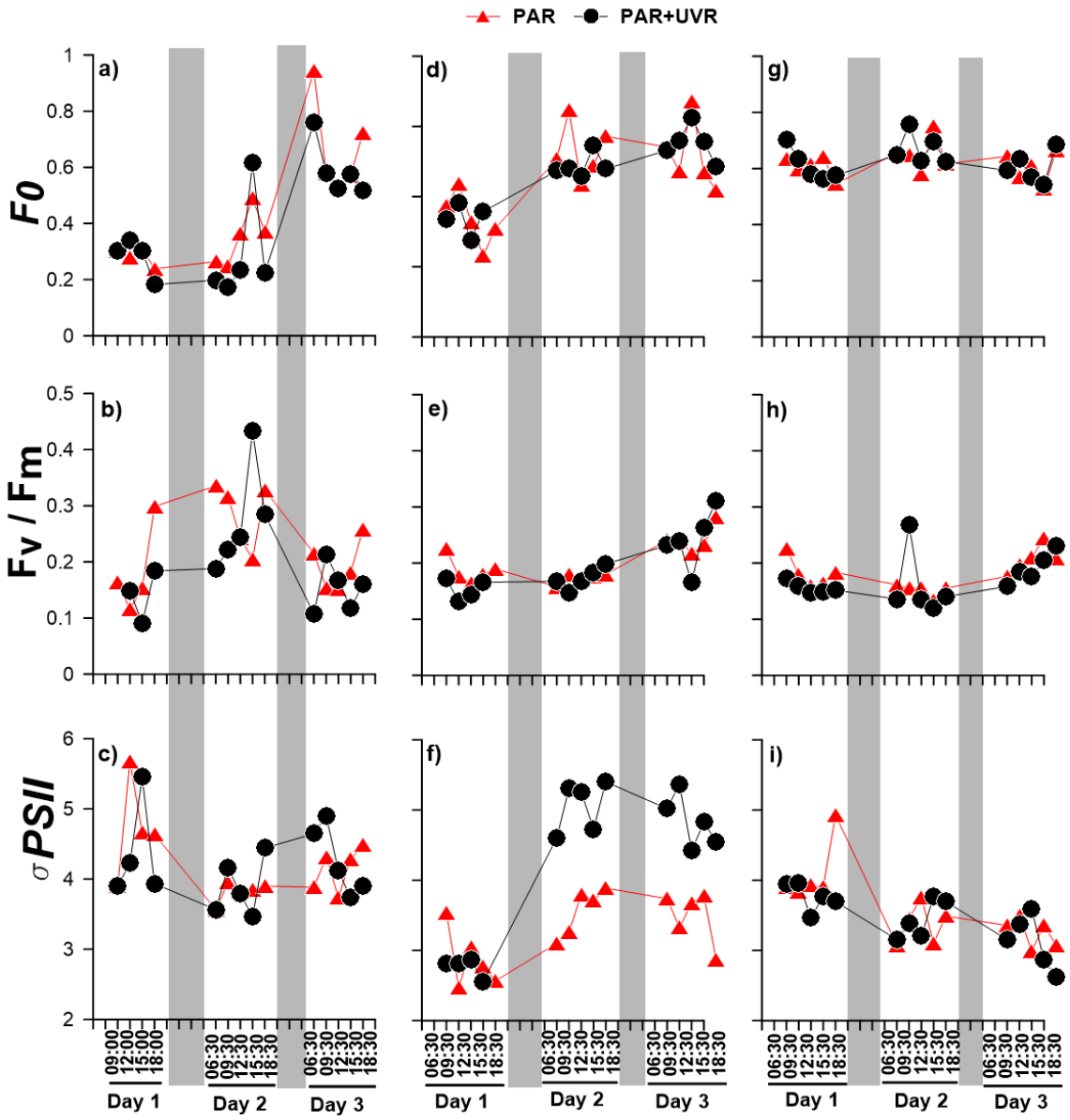


Figure 5.4. PSII parameters during the three days incubation in the South-tropical Indian Ocean.

The increase in F_0 values was related to biomass increase due to phytoplankton growth at both bioregions. However, the growth was not significant for the second experiment at STIO. The ANOVA revealed that the F_v/F_m and σ_{PSII} values of the afternoon were significantly lower ($p < 0.05$) than the morning and late evening values for all the experiments at both bioregions. Interestingly, the ANOVA revealed insignificant differences only for the second experiment with both surface and SCML water at STIO. All the above-observed trends were similar for both the treatments (i.e., only PAR and PAR+UVR); however, the values were much lower in the PAR+UVR treatment than only PAR, but the differences were insignificant at both bioregions. The reduction of high

morning F_v/F_m and σ_{PSII} values under high solar radiation in the noon and its subsequent recovery by evening shows the ability of the AS and STIO phytoplankton community for a photo-protection mechanism using dynamic photo-inhibition. The decrease in the F_v/F_m value was associated with a decrease in σ_{PSII} values, indicating the quenching in the antennae bed of the reaction center at both locations at the AS. In contrast, the decrease in the F_v/F_m value was not associated with any change in σ_{PSII} values, indicating the quenching within the reaction center for both experiments at the STIO.

5.3.3. Effect of solar radiation on photoprotective pigments

The distinct variations in photoprotective pigment ratios (DT + DD/Chl-*a* and PPC:PSC) and the phytoplankton de-epoxidation state (DT/DT + DD) were also observed in the AS. The photoprotective pigment ratios and the de-epoxidation state of the microalgae showed distinct variations between the experiments at different locations in the STIO. In the AS, the photo-protective pigment ratios showed lower values in the morning and higher in the evening for both locations. However, the phytoplankton community exposed to PAR+UVR treatments produced higher concentrations of PPC than the only PAR treatment at both locations. When irradiance increases, there is a significant increment in the proportion of photo-protective carotenoids and, consequently, in the PPC:PSC index. In STIO, in the first location (i.e., station 11), the photo-protective pigment ratios showed no variation for both the treatments (i.e., PAR and PAR+UVR) with surface water, but the de-epoxidation state showed variation only for PAR+UVR treatment. In the second location (i.e., station 13), the photo-protective pigment ratios and the de-epoxidation state showed lower values in the morning and higher values in the evening for both the treatments (i.e., PAR and PAR+UVR) with surface and SCML water. Interestingly, the non-photochemical quenching (NPQ) mechanism was not evident at both locations in the AS (Figure 5.5) but was observed at both locations with surface and SCML water in the STIO (Figure 5.6).

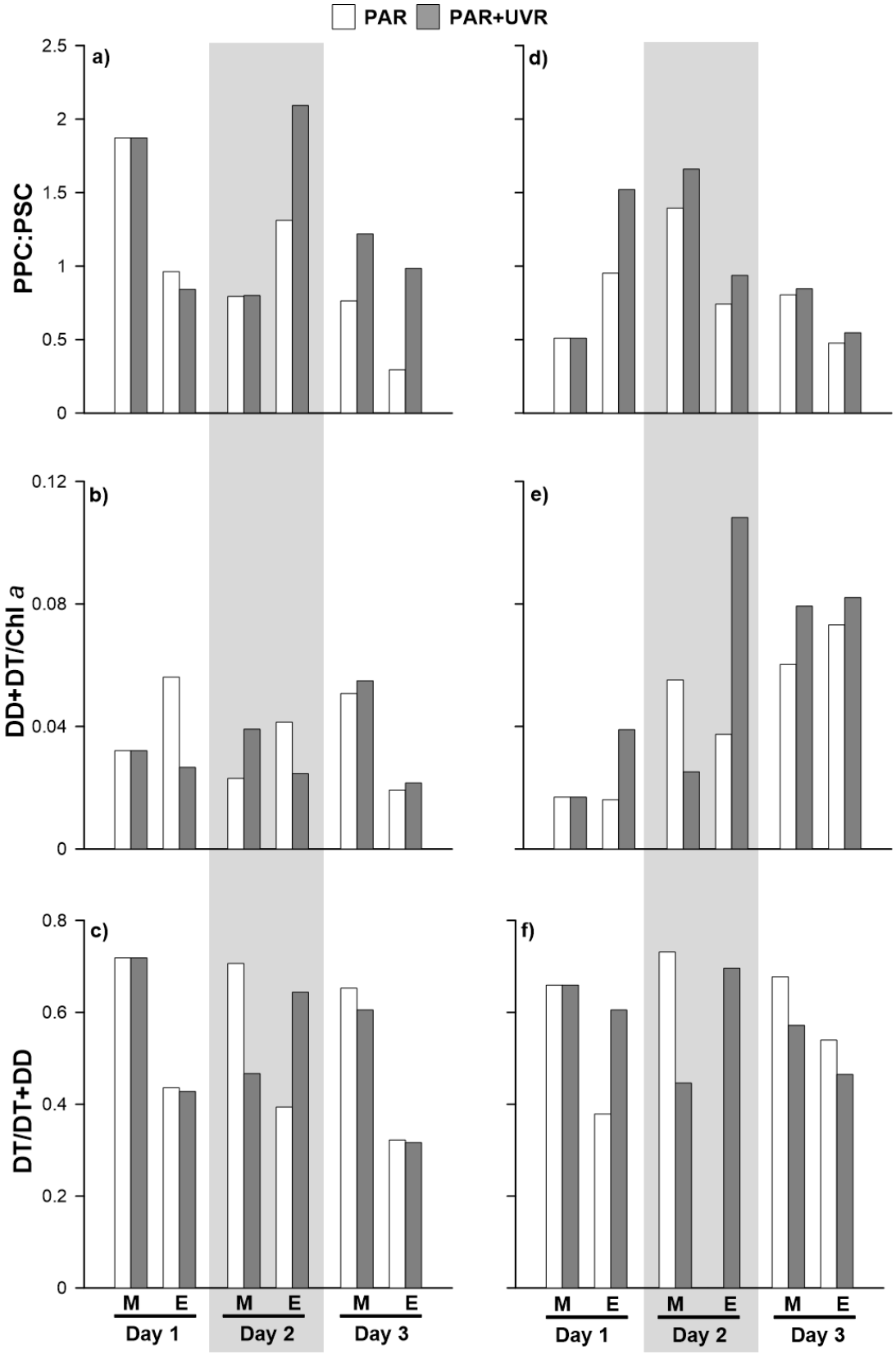


Figure 5.5. Plot showing values of a) photoprotective carotenoids (PPC) to photosynthetic carotenoids (PSC), b) photoprotective pigment ratios, i.e., DD + DT/Chlorophyll-*a*, and c) de-epoxidation of the xanthophyll cycle pigment DD, i.e., DT/DD + DT during the incubation period in the Arabian Sea. DT: Diatoxanthin, DD: Diadinoxanthin; M: Morning and E: Evening.

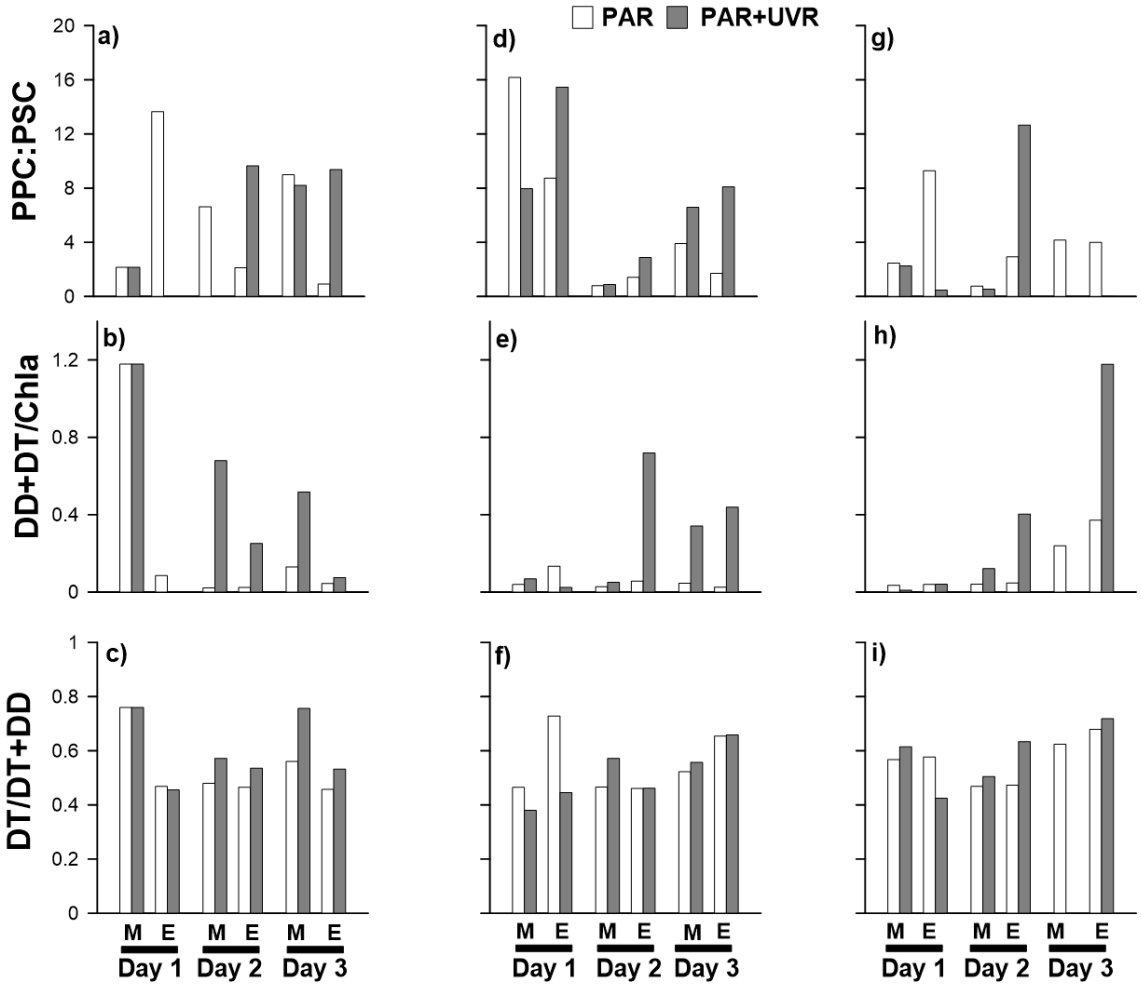


Figure 5.6. Plot showing values of a) photoprotective carotenoids (PPC) to photosynthetic carotenoids (PSC), b) photoprotective pigment ratios, i.e., DD + DT/Chlorophyll-*a*, and c) de-epoxidation of the xanthophyll cycle pigment DD, i.e., DT/DD + DT during the incubation period in the South-tropical Indian Ocean. DT: Diatoxanthin, DD: Diadinoxanthin; M: Morning, and E: Evening.

5.4. Discussion

5.4.1. Effect of solar radiation on PSII parameters and photoprotective pigments

Light plays a significant role in phytoplankton growth, productivity, and ecology, yet light availability (both quantitative and qualitative) depends on the organisms' location in the aquatic environment. Generally, phytoplankton experience variable irradiance in the open ocean. For instance, the phytoplankton communities on the sea surface are exposed to a higher irradiance than the SCML communities. In this study, the response of phytoplankton to the variable PAR and PAR+UVR treatments varied with the community and locations. For instance, the centric and pennate diatom-dominated community in the

AS experienced higher UVR and comparatively less PAR. In contrast, the pennate diatom-dominated community in the STIO experienced higher PAR and comparatively lower UVR due to cloudy weather. Therefore, one can expect distinct photosynthetic performance from the AS and STIO communities. The fluorescence measurements show that the AS and STIO phytoplankton are photosynthetically active; however, the response magnitude was different for sea surface and SCML waters and between the locations. The magnitude of diel variations was higher in the sea surface of the AS than in STIO and between the sea surface and SCML of STIO. This trend was persistent in both only-PAR and PAR+UVR treatments. The distinct response observed between the locations can be attributed to the differences in phytoplankton composition and irradiance. The phytoplankton communities at the sea surface are generally exposed to high solar irradiance, both ultraviolet (UVR and PAR); therefore, they should have a well-defined photoprotection mechanism. Such photoprotective mechanisms can be selectively activated based on the exposure length and are species-specific (Halac et al., 2014; Dimier et al., 2007). Phytoplankton species with flagella (e.g., dinoflagellates) can avoid the excessive radiation by moving downward (Roy, 2000; Richter et al., 2007); however, in highly stratified water columns, they might be physically forced to stay at the water surface with high radiation. The variable fluorescence measurements (F_0, F_v/F_m, and σ_{PSII}) and pigment ratios (DT + DD/Chl-*a*, PPC:PSC, and DT/DT + DD) revealed that the dynamic photoinhibition, NPQ and photoprotective pigments accumulation were the prominent photo-adaptive strategies to regulate excess light.

Interestingly, in all the locations, the F_v/F_m value of the sea surface and SCML phytoplankton communities showed a morning high, mid-day low, and a consequent recovery to the maximum in the evening. These results confirm the involvement of dynamic photoinhibition, which plays an essential role in the photoprotection of phytoplankton. Dynamic photoinhibition is attributed to the rapid recovery (on a timescale of tens of minutes to hours) of PSII reaction centers from transient damage (Gorbunov et al., 2001). The dynamic photoinhibition as the photoprotection mechanism is widely known in phytoplankton (Falkowski, 1994), macroalgae (Hanelt et al., 1993), and corals (Ralph et al., 1999; Gorbunov et al., 2001). However, the magnitude of F_v/F_m recovery was higher for the AS sea surface, followed by the STIO sea surface, and least in STIO SCML. This could be due to the prevalence of low F_v/F_m ratios in STIO SCML followed by AS and STIO sea surface. The synthesis or accumulation of photoprotective pigments (i.e., non-photosynthetic active pigments; Babin et al., 1996) can cause low or

mid-day depression in F_v/F_m. Generally, the photoprotective pigments absorb PAR, but this energy is not transferred to Photosystems (I or II), causing reduced F_v/F_m. Various studies suggest that the increased accumulation of photoprotective (PP) carotenoids and xanthophylls under high PAR and UVR (e.g., Van de Poll et al., 2006; Dimier et al., 2007; Villafañe et al., 2008) and the same was evident in this study. Since the STIO locations were exposed to high PAR and UVR, the accumulation of PP was also higher, which is evident in the PP and photosynthetic (PS) ratio. The low F_v/F_m ratios in STIO sea surface and SCML waters could also be due to the taxonomic dominance of picophytoplankton, as evidenced by the diagnostic pigment HPLC data and is also observed in previous studies (Moore et al., 2005, 2006; Suggett et al., 2009). Fishwick et al. (2006) have shown that the cross-shelf trends of F_v/F_m and σ_{PSII} from the south-west coast of South Africa are broadly correlated with community structure, and the values changed as the community changed from diatoms to picoeukaryote dominant. However, the picoeukaryote groupings used by Fishwick et al. (2006) contain organisms like pelagophytes (19'-butanoyloxyfucoxanthin) and chlorophytes (Chl-*b*), which have very different PSII antenna structures, which might have caused the observed variability. Similarly, low F_v/F_m ratios can indicate a stressed phytoplankton community and are highly dependent on the contributing taxa (Patil & Anil, 2019; Giannini et al., 2021).

Further, the mechanism of thermal dissipation of excess excitation energy either in the light-harvesting antennae or the reaction centers of PSII can also cause the mid-day reduction in chlorophyll fluorescence (Vassiliev et al., 1994). The quenching within the reaction center is shown by a decrease in F_v/F_m without changing σ_{PSII}, whereas quenching in the antennae bed decreases σ_{PSII} values (Vassiliev et al., 1994) and is correlated with the xanthophyll cycle (Demmig-Adams & Adams, 1996). In the present study, at both the locations in the AS, a low F_v/F_m value was associated with a low σ_{PSII} value, pointing out that the thermal dissipation of excess excitation energy occurred in the antennae bed for both treatments. Whereas, for sea surface and SCML at STIO, the decrease in F_v/F_m was associated without a change in $\sigma_{PSII,}$ indicating that the thermal dissipation of excess excitation energy occurred in the reaction centers of PSII for both treatments. However, the involvement of the xanthophyll cycle by producing xanthophyll pigments (i.e., diatoxanthin-DT and diadinoxanthin-DD) in dissipating the excess energy was variable between AS and STIO. For instance, the dissipation of excess energy by the xanthophyll cycle was not observed in the AS locations, whereas the xanthophyll cycle was active in the STIO locations for both sea surface and SCML waters. The lower DT and higher

DD+DT pool, as shown by the accumulation of DD, signified the prevalence of NPQ of reaction centers in the AS location. This could be because DT is a quencher of excitation energy within the antenna, and its formation can reduce the effective absorption cross-section of PSII (Falkowski & Raven, 2007). Generally, DT is involved in the thermal dissipation of excess energy without transferring it to chlorophylls (Demmig-Adams, 1990; Olaizola et al., 1994), and DD plays a role in light harvesting by transferring energy to chlorophylls. Surprisingly, even though the thermal dissipation of excess excitation energy occurred in the antennae bed in the AS locations, the involvement of the xanthophyll cycle in dissipating the excess energy was not found. This might have been caused by the high UVR recorded in the AS, which might inhibit the xanthophyll cycle and cause decreased DT concentration (Brunet et al., 2011). Similar inhibition of the xanthophyll cycle by UVR has been stated in various studies (Helbling et al., 2001; Buma et al., 2009; Halac et al., 2014).

5.4.2. Comparison of photoprotection mechanism from habitats receiving extremely high light

The phytoplankton communities inhabiting different marine habitats are distinct concerning taxa, dominance, diversity, and physiological adaptations. The light regimes (solar radiation) experienced by the phytoplankton communities in an intertidal rockpool and an open ocean are completely different and might be driven by the prevalent hydrological conditions. For instance, intertidal rockpools are shallow water bodies that experience saturating solar radiation, whereas open oceans are vast water bodies, and solar radiation gradually decreases as the depth increases. Consequently, the rockpool phytoplankton communities have little or no choice but to adapt to the saturating light regime, whereas the open ocean communities can sink deeper to avoid such saturating solar radiation. The sinking of oceanic phytoplankton communities could also be hindered by the stratification of the water column, leaving no choice but to adapt to the prevailing light regimes. Therefore, distinct photo-physiological adaptations are inevitable in rockpool and oceanic phytoplankton communities.

Here, the findings of a previous study on the photoprotection mechanism of the rockpool phytoplankton (Patil et al., 2017) are compared with the present study to delineate the differences or similarities existing in the photoprotection mechanism between two distinct phytoplankton communities from contrasting marine habitats. As revealed by the AS and STIO sea surface and SCML phytoplankton communities, the

intertidal rockpool communities also exhibited dynamic photoinhibition, NPQ of reaction centers, or the accumulation of photoprotective pigments to regulate the excess solar radiation. The decrease of F_v/F_m from a morning high to a mid-day low and its subsequent recovery in the evening was consistent in all the marine habitats (i.e., AS, STIO, and rockpools), which signifies the role of dynamic photoinhibition in the photoprotection across environmental gradients and habitats. Further, the thermal dissipation of excess excitation energy occurred in PSII reaction centers for rockpool and STIO, which was associated with a decrease in F_v/F_m and an increase in σ_{PSII}, whereas in the AS quenching was observed in the antennae bed, leading to a decrease in σ_{PSII}. The antennae bed quenching mostly correlates with a xanthophyll cycle; however, it was not observed in the AS or the rockpools (high tide rockpools). The reason could be the inhibition of the xanthophyll cycle by excessive UVR in both habitats. In contrast, the xanthophyll cycle was functional in the STIO, possibly because the relatively low UVR caused no damage or because smaller phytoplankton (e.g., pennate diatoms or picophytoplankton) were dominant in STIO during incubation. Since σ_{PSII} for smaller phytoplankton is higher, it could be more susceptible to photoinactivation of PSII (Key et al., 2010). Therefore, an added photoprotection mechanism like the xanthophyll cycle can reduce the photoinactivation and increase the adaptability. However, it was noticed that the recovery magnitude of F_v/F_m was lower in STIO and higher in AS and rockpools. This could be attributed to the phytoplankton community differences recorded in these habitats. According to Key et al. (2010), the diatoms have a higher PSII repair rate than the picophytoplankton (e.g., *Prochlorococcus* and *Synechoccocus* spp.). The photosynthetic apparatus structure and composition differences can cause taxonomic differences in the PSII repair rates (Six et al., 2007). Temperature is another factor affecting the recovery magnitude of F_v/F_m, and a lower temperature can also inhibit the metabolic PSII repair rates (Key et al., 2010). The temperature was relatively lower in the STIO locations compared to AS and rockpools; therefore, it might have reduced the metabolic rate, reducing the PSII repair rates.

Moreover, Capotondi et al. (2012) have predicted increased sea surface temperature, resulting in a stratified upper mixed layer in the marine ecosystem, consequently exposing phytoplankton to higher PAR and UVR. This higher or often ambient intensity of PAR and UVR is sufficient to cause sporadic photoinhibition to the surface phytoplankton (Harrison & Smith, 2009). The UVR alone is reported to cause photoinhibition of total primary production by 10-30% in coastal (Helbling et al., 2003;

Li et al., 2009) and 15-27% in open ocean waters (Helbling et al., 1992; Li et al., 2009). However, the natural Antarctic phytoplankton assemblages suffer a higher (34-44%) photoinhibition caused by solar radiation (Boucher & Prézelin, 1996; Holm-Hansen, 1997). A study in the oligotrophic regions of the Indian Ocean showed that solar UVR significantly affects the phytoplanktonic production of particulate organic carbon and dissolved organic carbon despite being genetically adapted (Fuentes-Lema et al., 2015). Aardema et al. (2024) concluded that low-light adaption in temperate to subpolar latitudes and in (sub-) tropical upwelling regions can cause phytoplankton communities to increase the light-harvesting capacity. Therefore, growth and primary productivity can be optimized by photophysiological plasticity, allowing the phytoplankton community to fine-tune its light capture. Hence, the variability in marine photosynthesis can be different based on oceanographic regions, daily cycles, and environmental drivers.

Nevertheless, these results confirm that the photoprotection mechanisms depend highly on the habitat type, prevailing dominant taxa, and hydrographic conditions. Further, the fast recovery capability from PSII inhibition by surface phytoplankton assemblages could be advantageous in adapting to fluctuating light regimes when the surface mixed layer shallows and phytoplankton cells are exposed to increased light intensities in the future. These findings can provide important insights and improve our understanding and predictions of climate change on marine ecosystems and biological productivity.

5.5. Conclusion

This study concludes that PAR+UVR treatment had a more prominent effect on photo-physiology than only PAR treatment, irrespective of the bioregions; however, the differences are insignificant. Dynamic photo-inhibition (F_v/F_m), NPQ, and accumulation of photo-protective pigments (DT+DD/Chl-*a* and PPC/PSC) were found to be the prominent photo-adaptive strategies, but the magnitude and mechanism differed between the bioregions. In IO, the phytoplankton communities used all or a combination of the photoprotection mechanisms. Dynamic photo-inhibition was a primary photoprotection mechanism observed in all the bioregions; however, the magnitude was region-specific (i.e., rapid in AS and gradual in STIO). The thermal dissipation of excess excitation energy using the NPQ occurred in the reaction centers of PSII for STIO, whereas in the AS, quenching was observed in the antennae bed. Further, the photo-protection mechanism using the xanthophyll cycle (DT/DD+DT) was region-specific (i.e., observed

only in STIO but not in AS) whereas at STIO, the response was similar between surface and SCML waters. A similar photo-physiological adaptation in extremely high-light adapted phytoplankton in smaller water bodies like tropical rock pools (facing eastern AS) highlights dominant taxonomic groups, habitat type, prevailing hydrographic conditions, and magnitude of solar flux determine the mechanism involved in the photoprotection.

Chapter 6
Summary

Chapter 6: Summary

The microscopic and photosynthetic algae in the sunlit zone of water bodies and sediment are known as microalgae. Microalgae are the primary producers and can be found in various ecologically distinct ecosystems (e.g., intertidal, sub-tidal, coastal, and pelagic). The intertidal and pelagic ecosystems are distinct in biological, hydrological, and environmental settings. Rock pools and tidal flats are unique but ecologically distinct habitats among the intertidal ecosystem. The diversity, distribution, and composition of microalgae have been thoroughly studied in these ecosystems, but studies related to the morpho-physiological adaptations have not been conducted. These habitats are dominated by various microalgae taxa equipped with habitat-specific morpho-physiological adaptations. Similarly, the pelagic ecosystems are characterized by distinct hydrological and environmental factors that tightly regulate the microalgae assemblages and their morpho-physiological adaptations. The size and shape of the microalgae are some of the determining traits that help in morpho-physiological adaptations. However, there are no studies from the Indian subcontinent that delineate these morpho-physiological traits in both intertidal and pelagic ecosystems. Therefore, the present study delineates the morph-physiological adaptations of microalgae from intertidal (rockpools and tidal flats) and pelagic ecosystems encompassing a wide range of environmental settings. In the pelagic ecosystem, the dormant benthic forms (i.e., dinoflagellate cysts) and the dominant planktonic forms (i.e., micro-phytoplankton) from the contrasting regions of the Indian Ocean (up to 30^{o} S) were addressed. Additionally, the photo-physiological adaptations of phytoplankton from the Arabian Sea and the south tropical Indian Ocean were studied using an onboard mesocosm experimental approach. The findings of these studies are summarized in the subsequent sections.

Overall, the abundance of MPB and phytoplankton in overlying surf waters (SW) showed significant inter-annual and seasonal variations, with diatoms as the dominant groups at both undisturbed (DTF) and disturbed (MTF) tidal flats. DTF harbored higher MPB species diversity than adjacent SW, whereas an opposite trend was observed at MTF. Further, MPB showed significant variations between low (LT), mid (MT), and high (HT) tide zones. At DTF, MPB is dominated by centric diatoms in the SW, LT, and MT zones and pennate diatoms in the HT zone. Meanwhile, at MTF, MPB was co-dominated by centric and pennate diatoms in SW and pennate diatoms in LT, MT, and HT zones. Both pennate (*Navicula* spp. and *Nitzschia* spp.) and centric diatoms (*Thalassiosira* sp., *Bellerochea malleus*, and *Lithodesmium undulatum*) co-dominated the MPB community,

irrespective of the tidal zones at both tidal flats. The regression analysis between the SW phytoplankton and MPB community revealed that the influence of the former on the latter (particularly at LT and MT) and vice versa was also observed through deposition and resuspension, respectively. Centric-to-pennate (C:P) ratios can be a potential indicator for understanding the diatom exchange between MPB and SW community, particularly during bloom periods. However, the interdependency of the diatom community between MPB and SW community is tidal flat specific and dependent on the topography of the tidal flat. Further, epipsammic and epipelic abundance can be potential indicators for sediment texture as their abundance ratios are associated with sediment texture. MPB showed similar seasonal distribution (i.e., low and high MPB during monsoon and non-monsoon, respectively) at both tidal flats. Interestingly, potential eutrophic indicator species (*Bellerochea* and *Lithodesmium*) associated with elevated phosphate values were observed at DTF. Meanwhile, the anthropogenic disturbed MTF showed lower abundance and diversity than DTF, along with potential harmful algal bloom (HAB) dinoflagellate taxa (e.g., *Amphidinium* sp., *Gymnodinium* sp. and *Peridinium quinquecorne*) not recorded in DTF. Further, the environmental parameters revealed distinct variations between the seasons (monsoon, post-monsoon, and pre-monsoon) of different years (i.e., 2019,2022 and 2023) and so with the MPB. Despite methodological constraints, the relative MPB abundance and diversity, derived from the MPN method, showed significant inter-seasonal variability only for monsoon seasons at both tidal flats. However, the taxa dominance (i.e., *Navicula* spp.) remained unchanged and differed for monsoon and non-monsoon seasons, respectively. Further, a decadal shift in the MPB community was observed at an undisturbed tidal flat (DFT). Interestingly, a ~2.5-decade-old study documented minor contributors or non-documented species that were predominant in the present study, suggesting a significant shift in the species' dominance and assemblage due to changing environmental conditions due to natural (e.g., changing monsoonal patterns, increasing sea levels, etc.) and anthropogenic activities (e.g., increased nutrient loading). Another interesting finding is that the predominance of *Chaetoceros* sp. and *Skeletonema* sp. in all the tidal zones of DTF compared to the previous studies (restricted to SW and LT zones) suggests the increased level of seawater intrusion. Nevertheless, the study highlights that the generation of absolute abundance MPB data, which is challenging, is the need of the hour to understand the impact of anthropogenic activities and climate change on the MPB dynamics and benthic-pelagic ecosystem functioning, *per se*.

In the pelagic ecosystems, diatoms followed by dinoflagellates dominated in the upper photic zone of the water column, and diatom frustules and dinoflagellate cysts in the underlying sediments. Assessment of cysts producing dinoflagellate assemblage from pelagic systems revealed a lower number of cysts (i) at deeper depths (up to 5000m) than shallow depths (<200m) and (ii) in oligotrophic regions than oxygen minimum zone (OMZ) and the region located close to high productive regions (e.g., upwelling, OMZ). Overall, more dinoflagellate cyst species (including potential harmful species), cyst concentration, and diversity were recorded in the North Indian Ocean-NIO (i.e., the Arabian Sea and the Bay of Bengal) than in the South Indian Ocean-SIO (i.e., Equatorial and South Tropical Indian Ocean). Dinoflagellate cyst assemblage showed distinct geographic variations (i.e., cosmopolitan and region-specific) due to the prevalence of large and small-scale lateral transport in the Indian Ocean. Altogether, a total of 48 cyst types (22 genera) were recorded, of which 21 are cosmopolitan (e.g., *Impagidinium strialatum*, *Operculodinium centrocarpum*, *Spiniferites* sp., and *Echinidinium* sp), and the remaining 27 are region-specific to NIO. Interestingly, only a few cosmopolitan cyst species, like *Operculodinium centrocarpum* (between NIO-SIO and coastal-open ocean regions), cyst of *Pentapharsodinium dalei* (between NIO-SIO), and *Lingulodinium machaerophorum* (between coastal-open ocean regions) showed significant morphometric variability among the different bioregions highlighting its potential as an ecological proxy.

The assessment of microalgal adaption in the different habitats of intertidal regions indicated that the location and nature of the habitat (rock pools – RPs and tidal flats) determine the nature of the assemblage. In both the intertidal habitats, less microalgal diversity (including shapes) and the number of species were recorded in the HT zone, followed by MT and LT in RPs and LT and MT in tidal flats. Interestingly, even though the taxonomic assemblage changed temporally, the shape dominance remained consistent, suggesting the latter a robust morphological trait for RPs but not in tidal flats. The microalgae assemblages followed distinct trends in RPs and tidal flats. For instance, in frequently flushed RPs (MT and LT), pennate diatoms (*Pseudonitzschia*, *Nitzschia*, *Thalasionema*, *Navicula*, and *Licmophora*) representing elongated types dominated, whereas in stagnant HT-RPs spherical/combined shaped dinoflagellates (*Amphidinium* sensu stricto and *Bysmatrum gregarium*) dominated. However, in the tidal flats, LT and MT zones were dominated by elongated type chain forming taxa (*Thalassiosira* sp., *Bellerochia* sp., *Lithodesmium* sp., and *Chaetoceros* spp.) and HT zone by pennate

diatoms (*Navicula* spp., and *Nitzschia* spp.). Since tidal flats are diverse based on sediment texture, beach profile, and other local factors, more studies are required to delineate the variations. Further, species-specific allelopathy on other microalgae by *Amphidinium* (known harmful algae of concern and dominant in HT-RPs) highlights a type of physiological trait to suppress competitors. It might be one of the reasons for its predominance in HT-RPs experiencing varying environmental (light, temperature, and salinity) conditions. Therefore, it can be concluded that the microalgae in intertidal flats are more dynamic than the rockpools.

Further, the phytoplankton communities from pelagic systems were assessed to explore the potential of using commonly used traits (such as cell geometric shape and taxa) as ecological function indicators from the data generated during the winter monsoon in the eastern Arabian Sea (AS). The study concludes that the phytoplankton cell shape in the eastern Arabian Sea showed a high level of redundancy by choosing only a few dominant shapes associated with high taxonomic diversity. The integrated approach (taxonomy and morphology) adopted revealed higher taxonomic and shape diversity in the convective mixing influenced non-oligotrophic northeastern AS-open ocean (NEAS-O) than adjoining northeastern AS-coastal (NEAS-C) and oligotrophic southeastern AS-open ocean (SEAS-O). Interestingly, the shape diversity and dominance remained the same between NEAS-O and SEAS-O, and among the fronts, the combined and simple-shaped phytoplankton out-competed in NEAS-C and SEAS-O. The assessment of morphological properties based on the surface-to-volume ratio (S:V) and its relationship with greatest-axial-linear-dimension (GALD) suggested the prevalence of different adaptive strategies to cope with respective hydrographic conditions in the open ocean (NEAS-O and SEAS-O) and coastal (NEAS-C) by conserving S:V despite the increase in GALD in the former and no change in the later.

In the pelagic ecosystem of the Indian Ocean (IO), (i) simple phytoplankton geometric shapes (PGS) and morphological traits, i.e., S:V and GALD, showed a north-south gradient in the Indian Ocean, and (ii) despite different taxonomic composition, the PGS showed similar distribution and dominance in the Indian Ocean bioregions. Further, the PGS (community and morphological trait) of the sub-surface chlorophyll maximum layer (SCML) and the corresponding sea surface will be similar or dissimilar if the former is located within or deeper than the mixed layer depth. Among the SCML, the depth of occurrences determined the morphological attributes and phytoplankton shape dominance. For instance, (i) simple and complex PGS contribution gradually decreases

and increases, respectively, with increasing depth, and (ii) the PGS in shallow SCML showed low S:V and high GALD while in intermediate and deep SCML high S:V and low GALD were observed due to the phenotypic plasticity behavior by dominant PGSs to capture light. The analysis of phytoplankton morphological traits from different ecosystems suggests that S:V ratio and GALD are good indicators of "phenotypic plasticity" and can act as robust morphological traits for marine microalgae.

Variable fluorescence and diagnostic pigments confirm the prevalence of contrasting physiological adaptations in different oceanic regions, further indicating the utility of the former as a potential physiological trait of microalgae. Dynamic photo-inhibition (F_v/F_m), non-photochemical quenching (NPQ), and accumulation of photo-protective pigments (DT+DD/Chl-*a* and PPC/PSC) were found to be the prominent photo-adaptive strategies, but the magnitude and mechanism differed between the IO regions. Dynamic photo-inhibition was a primary photoprotection mechanism observed in all the bioregions; however, the magnitude was region-specific (i.e., rapid in AS and gradual in STIO). The thermal dissipation of excess excitation energy using the NPQ occurred in the reaction centers of PSII for STIO, whereas in the AS, quenching was observed in the antennae bed. The photo-protection mechanism using the xanthophyll cycle (DT/DD+DT) was region-specific, i.e., observed only in STIO but not in AS. Further, the photoprotection mechanism was similar between surface and SCML waters of the STIO region. A similar photo-physiological adaptation in extremely high-light adapted phytoplankton in smaller water bodies like tropical rock pools (facing eastern AS) highlights dominant taxonomic groups, habitat type, prevailing hydrographic conditions, and magnitude of solar flux determine the mechanism involved in the photoprotection. Moreover, the fast recovery capability from PSII inhibition by surface phytoplankton assemblages could be advantageous in adapting to fluctuating light regimes when the surface mixed layer shallows and phytoplankton cells are exposed to increased light intensities in the future.

Therefore, this study highlights that the morpho-physiological adaptation of microalgae plays a significant role in better understanding the nature of habitat functioning. The morphology-based studies can help simplify the understanding of ecosystem functioning and species succession without entering the taxonomical details. The various life strategies, like cyst formations, can better elucidate the benthic-pelagic coupling and give a better understanding of seasonal bloom formation. The understanding of photo-adaptation in microalgae from contrasting habitats will have implications in

studies related to ecological surveillance and primary productivity. Overall, this study highlights that morphometry (including dinoflagellate cysts) and photo-physiology of microalgae can be used as potential indicators in ecological studies. Moreover, the present study aptly points out a new way of looking at microalgae ecology and also aids in a better understanding of microalgae ecology holistically.

Bibliography

Bibliography

Aardema, H.M., Slagter, H.A., Hrabe de Angelis, I., Calleja, M.L., Dragoneas, A., Moretti, S., Schuback, N., Heins, L., Walter, D., Weis, U., Haug, G.H., 2024. On the variability of phytoplankton photophysiology along a latitudinal transect in the North Atlantic surface ocean. Journal of Geophysical Research: Biogeosciences, 129 (9), p.e2023JG007962.

Abidi, N., 1997. Les Kystes de dinoflagelles marqueurs de l'environnement océanique: repartition actuelle dans l'ocean Indien occidental et application a deux sequences sedimentaires du Canal de Mozambique (Doctoral dissertation, Paris 6).

Agatz, M., Asmus, R.M., Deventer, B., 1999. Structural changes in the benthic diatom community along a eutrophication gradient on a tidal flat. Helgoland Marine Research 53, 92–101.

Ahmed, A., Kurian, S., Gauns, M., Chndrasekhara Rao, A.V., Mulla, A., Naik, B., Naik, H., Naqvi, S.W.A., 2016. Spatial variability in phytoplankton community structure along the eastern Arabian Sea during the onset of south-west monsoon. Cont. Shelf Res., 119: 30-39.

Alexander, H., Rouco, M., Haley, S.T., Wilson, S.T., Karl, D.M., Dyhrman, S.T., 2015. Functional group-specific traits drive phytoplankton dynamics in the oligotrophic ocean. Proceedings of the National Academy of Sciences, 112(44), E5972–E5979.

Amal, K.S., Benny, N., Ajayakumar, P., Thomas, L.C., Padmakumar, K.B., 2024. Ephemeral analysis on microphytobenthos in an estuarine system along the southwest coast of India. Aquatic Ecology, 58(4), 1049-1065.

Amol, P., 2018. Impact of Rossby waves on chlorophyll variability in the southeastern Arabian Sea. Remote Sensing Letters, 9(12), 1214–1223.

An, K. H., Lassus, P., Maggi, P., Bardouil, M., & Truquet, P. (1992). Dinoflagellate cyst changes and winter environmental conditions in Vilaine Bay, Southern Brittany (France).

Anderson, D.M., Butman, B., Fong, D., Franks, P.J.S., Geyer, W.R., Keafer, B.A., Loder, T., Signeil, E.L.P., 1995. Sources, transport, and nutrient environment of toxic red tide' populations in the Western Gulf of Maine. In: Gulf of Maine News. Regional Association for Research on the Gulf of Maine, pp. 6–9.

Anderson, D.M., Cembella, A.D., Hallegraeff, G.M., 2012. Progress in understanding harmful algal blooms: paradigm shifts and new technologies for research, monitoring, and management. Ann Rev of Mar Sci 4, 143–176.

Anderson, D.M., Lively, J.J., Reardon, E.M., Price, C.A., 1985. Sinking characteristics of dinoflagellate cysts. Limnol and Oceanogra, 30(5), 1000–1009.

Anil, A.C., Mitbavkar, S., D'Silva, M.S., Hegde, S., D'Costa, P.M., Meher, S.S., Banerjee, D., 2007. Effect of ageing on survival of benthic diatom propagules. J. Exp. Mar. Biol. Ecol., 343:37–43.

Ansari, Z. A., Ingole, B., 2002. Effect of an oil spill from MV Sea Transporter on intertidal meiofauna at Goa, India. Marine Pollution Bulletin, 44(5), 396-402.

Anusa, A., Ndagurwa, H.G.T., Magadza, C.H.D., 2012. The influence of pool size on species diversity and water chemistry in temporary rock pools on Domboshawa Mountain, northern Zimbabwe; Afr. J. of Aqua. Sci. 37 (1) 89-99.

Arkema, K.K., Guannel, G., Verutes, G., Wood, S.A., Guerry, A., Ruckelshaus, M., Kareiva, P., Lacayo, M., Silver, J.M., 2013. Coastal habitats shield people and property from sea-level rise and storms. Nature climate change, 3(10), 913-918.

Aro, E.M., McCaffery, S., Anderson, J.M., 1994. Recovery from photoinhibition in peas (Pisum sativum L.) acclimated to varying growth irradiances (role of D1 protein turnover). Plant Physiology, 104(3), 1033-1041.

Arsalane, W., Rousseau, B., Duval, J.C., 1994. Influence of the pool size of the xanthophyll cycle on the effects of light stress in a diatom: competition between photoprotection and photoinhibition. Photochem. Photobiol. 60:237–43.

Arunpandi, N., Jyothibabu, R., Jagadeesan, L., Gireesh Kumar, T.R., Karnan, C., Naqvi, S.W.A., 2017. Noctiluca and copepods grazing on the phytoplankton community in a nutrient-enriched coastal environment along the southwest coast of India. Environ. Monit. Assess., 189(7).

Aubry, B.F., Pugnetti, A., Roselli, L., Stanca, E., Acri, F., Finotto, S., Basset, A., 2017. Phytoplankton morphological traits in a nutrient-enriched, turbulent Mediterranean microtidal lagoon. J. Plankton Res., 39(3), 564–576.

Ault, T., Velzeboer, R., Zammit, R., 2000. Influence of nutrient availability on phytoplankton growth and community structure in the Port Adelaide River, Australia: Bioassay assessment of potential nutrient limitation. Hydrobiologia, 429, 89–103.

Azanza, R.V., Siringan, F.P., San Diego-Mcglone, M.L., Yniguez, A.T., Macalalad, N.H., Zamora, P.B., Agustin, M.B., Matsuoka, K., 2004. Horizontal dinoflagellate cyst distribution, sediment characteristics and benthic flux in Manila Bay, Philippines. Phycol. Res. 52, 376–386.

Azovsky, A.I., Mazei, Y.A., Saburova, M.A., Sapozhnikov, P.V., 2020. Patterns in diversity and composition of the microbenthos of subarctic intertidal beaches with different morphodynamics. Marine Ecology Progress Series, 648, 19-38.

Babin, M., Morel, A., Claustre, H., Bricaud, A., Kolber, Z., Falkowski, P.G. 1996. Nitrogen-and irradiance-dependent variations of the maximum quantum yield of carbon fixation in eutrophic, mesotrophic and oligotrophic marine systems. Deep Sea Research Part I: Oceanographic Research Papers, 43(8), 1241-1272.

Baig, H.S., Saifullah, S.M., Dar, A., 2006. Occurrence and toxicity of *Amphidinium carterae* Hulburt in the North Arabian Sea; Harm. Alg. 5 (2) 133–140.

Balasubramaniam, J., Prasath, D., Jayaraj, K.A., 2017. Microphytobenthic biomass, species composition and environmental gradients in the mangrove intertidal region of the Andaman Archipelago, India. Environmental monitoring and assessment, 189, 1-19.

Baldry, K., Strutton, P.G., Hill, N.A., Boyd, P.W., 2020. Subsurface chlorophyll-a maxima in the southern ocean. Front. Mar. Sci. 7, 671.

Banaszak, A.T., 2003. Photoprotective physiological and biochemical responses of aquatic organisms. In: Helbling EW, Zagarese HE (eds) UV effects in aquatic organisms and ecosystems. The Royal Society of Chemistry, Cambridge, pp 329–356.

Banse, K., 1987. Seasonality of phytoplankton chlorophyll in the central and northern Arabian Sea. Deep-Sea Research, 34(5–6), 713–723.

Barinova, S., Bondarenko, A., Ryabushko, L., Kapranov, S., 2019. Microphytobenthos as an indicator of water quality and organic pollution in the western coastal zone of the Sea of Azov. Oceanological and Hydrobiological Studies, 48(2), 125-139.

Barlow, R., Stuart, V., Lutz, V., Sessions, H., Sathyendranath, S., Platt, T., Kyewalyanga, M., Clementson, L., Fukasawa, M., Watanabe, S., Devred, E., 2007. Seasonal pigment patterns of surface phytoplankton in the subtropical southern hemisphere. Deep Sea Research Part I: Oceanographic Research Papers, 54(10),1687-1703.

Barnett, M.L., Kemp, A.E.S., Hickman, A.E., Purdie, D.A., 2019. Shelf sea subsurface chlorophyll maximum thin layers have a distinct phytoplankton community structure. Cont. Shelf Res. 174, 140–157.

Barton, A.D., Pershing, A.J., Litchman, E., Record, N.R., Edwards, K.F., Finkel, Z.V., Kiørboe, T., Ward, B.A., 2013. The biogeography of marine plankton traits. Ecology Letters, 16(4), 522–534.

Bates, S.S., Garrison, D.L., Horner, R.A., 1998. Bloom dynamics and physiology of domoic-acid-producing *Pseudonitzschia* species. NATO ASI series G ecological sciences, 41, 267-292.

Baula, I.U., Azanza, R.V., Fukuyo, Y., Siringan, F.P., 2011. Dinoflagellate cyst composition, abundance and horizontal distribution in Bolinao, Pangasinan, Northern Philippines. Harmful Algae, 11, 33-44.

Behrenfield, M.J., Falkowski, P.G., 1997. Photosynthetic rates derived from satellite-based chlorophyll concentration; Limnol. Oceanogr. 42 1–10.

Bemal, S., Anil, A.C., Amol, P., 2019. Picophytoplankton variability: Influence of Rossby wave propagation in the southeastern Arabian Sea. Journal of Marine Systems, 199, 103–221.

Bemal, S., Anil, A.C., Shankar, D., Remya, R., Roy, R., 2018. Picophytoplankton variability: Influence of winter convective mixing and advection in the northeastern Arabian Sea. Journal of Marine Systems, 180, 37–48.

Benny, N., Thomas, L.C., Padmakumar, K.B., 2021. Community structure of microphytobenthos associated with mangrove ecosystems along the southwest coast of India. Estuaries and Coasts, 44(5), 1380-1391.

Bere, T., Mangadze, T., Mwedzi, T., 2014. The application and testing of diatom-based indices of stream water quality in Chinhoyi Town, Zimbabwe. Water SA, 40(3), 503-512.

Bharathi, M.D., Sarma, V.V.S.S., Ramaneswari, K., 2018. Intra-annual variations in phytoplankton biomass and its composition in the tropical estuary: Influence of river discharge. Marine Pollution Bulletin, 129(1): 14-25.

Bibby, T.S., Gorbunov, M.Y., Wyman, K.W., Falkowski, P.G., 2008. Photosynthetic community responses to upwelling in mesoscale eddies in the subtropical North Atlantic and Pacific Oceans. Deep Sea Research Part II: Topical Studies in Oceanography, 55(10-13), 1310-1320.

Bijl, P.K., Frieling, J., Cramwinckel, M.J., Boschman, C., Sluijs, A., Peterse, F., 2021. Maastrichtian–Rupelian paleoclimates in the southwest Pacific–a critical re-evaluation of biomarker paleothermometry and dinoflagellate cyst paleoecology at Ocean Drilling Program Site 1172. Clim. Past. 17(6), 2393-2425.

Blum, M.D., Roberts, H.H., 2009. Drowning of the Mississippi Delta due to insufficient sediment supply and global sea-level rise. Nature geoscience, 2(7), 488-491.

Boero, F., 1994. Fluctuations and variations in coastal marine environments. Marine Ecology, 15(1), 3-25.

Bolch, C.J., 2022. Impact of molecular approaches on dinoflagellate taxonomy and systematics. In *Advances in Phytoplankton Ecology* (pp. 81-117). Elsevier.

Bopp, L., Monfray, P., Aumont, O., Dufresne, J.L., Le Treut, H., Madec, G., Terray, L., Orr, J.C., 2001. Potential impact of climate change on marine export production. Global Biogeochemical Cycles, 15(1), pp.81-99.

Bosak, S., Šupraha, L., Nanjappa, D., Kooistra, W.H., Sarno, D., 2015. Morphology and phylogeny of four species from the genus Bacteriastrum (Bacillariophyta). Phycol. 54(2), 130-148.

Boucher, N.P., Prézelin, B.B., 1996. An in situ biological weighting function for UV inhibition of phytoplankton carbon fixation in the Southern Ocean. Marine ecology progress series, 144, 223-236.

Breton, E., Christaki, U., Bonato, S., Didry, M., Artigas, L.F., 2017. Functional trait variation and nitrogen use efficiency in temperate coastal phytoplankton. Marine Ecology Progress Series, 563, 35–49.

Brewin, R.J., Sathyendranath, S., Jackson, T., Barlow, R., Brotas, V., Airs, R., Lamont, T., 2015. Influence of light in the mixed-layer on the parameters of a three-component model of phytoplankton size class. Remote Sensing of Environment, 168, 437-450.

Bringue, M., Pospelova, V., Pak, D., 2013. Seasonal production of organic-walled dinoflagellate cysts in an upwelling system: a sediment trap study from the Santa Barbara Basin, California. Mar. Micropaleontol. 100:34–51.

Browning, T.J., Bouman, H.A., Moore, C.M., Schlosser, C., Tarran, G.A., Woodward, E.M.S., Henderson, G.M., 2014. Nutrient regimes control phytoplankton ecophysiology in the South Atlantic. Biogeosciences, 11(2), 463-479.

Brunet, C., Johnsen, G., Lavaud, J., Roy, S., 2011. Pigments and photoacclimation processes. *Phytoplankton pigments: characterization, chemotaxonomy and applications in oceanography*.

Buma, A.G., Visser, R.J., Van De Poll, W.H., Villafane, V.E., Janknegt, P.J., Walter Helbling, E., 2009. Wavelength-dependent xanthophyll cycle activity in marine microalgae exposed to natural ultraviolet radiation. European Journal of Phycology, 44(4), 515-524.

Buskey, E.J., 1997. Behavioral components of feeding selectivity of the heterotrophic dinoflagellate Protoperidinium pellucidum. Mar. Ecol. Prog. Ser. 153, 77-89.

Butts, T.J., Moody, E.K., Wilkinson, G.M., 2022. Contribution of zooplankton nutrient recycling and effects on phytoplankton size structure in a hypereutrophic reservoir. J. Plankton Res. 44(6), 839-853.

Cahoon, L., 1999. The role of benthic microalgae in neritic ecosystems. Oceanography and Marine Biology, 37, 47–86.

Candel, M.S., Radi, T., de Vernal, A., Bujalesky, G., 2012. Distribution of dinoflagellate cysts and other aquatic palynomorphs in surface sediments from the Beagle Channel, Southern Argentina. Mar. Micropaleontol. 96, 1-12.

Capblancq, J., Catalan, J., 1994. Phytoplankton: Which, and how much? In R. Margalef (Ed.), Limnology Now: A Paradigm of Planetary Problems (pp. 9–36). Elsevier Science B.V.

Capotondi, A., Alexander, M.A., Bond, N.A., Curchitser, E.N., Scott, J.D., 2012. Enhanced upper ocean stratification with climate change in the CMIP3 models. Journal of Geophysical Research: Oceans, 117(C4).

Cartaxana, P., Mendes, C.R., van Leeuwe, M.A., Brotas, V., 2006. Comparative study on microphytobenthic pigments of muddy and sandy intertidal sediments of the estuary. Estuarine, Coastal and Shelf Science 66 (1–2), 225–230.

Cartaxana, P., Ribeiro, L., Goessling, J.W., Cruz, S., Kühl, M., 2016. Light and O_2 microenvironments in two contrasting diatom-dominated coastal sediments. Marine Ecology Progress Series, 545, 35-47.

Cartaxana, P., Ruivo, M., Hubas, C., Davidson, I., Serôdio, J., Jesus, B., 2011. Physiological versus behavioral photoprotection in intertidal epipelic and epipsammic benthic diatom communities. Journal of Experimental Marine Biology and Ecology, 405(1-2), 120-127.

Cermeño, P., Dutkiewicz, S., Harris, R.P., Follows, M., Schofield, O., Falkowski, P.G., 2008. The role of nutricline depth in regulating the ocean carbon cycle. Proceedings of the National Academy of Sciences, 105(51), 20344-20349.

Chandrasekhararao, A.V., Kurian, S., Vidya, P.J., Gauns, M., Shenoy, D.M., Mulla, A., Naik, H., Reddy, T.V., Naqvi, S.W.A., 2018. Phytoplankton response to the contrasting physical regimes in the eastern Arabian Sea during northeast monsoon. Journal of Marine Systems, 182, 56–66.

Chapman, M.G., Tolhurst, T.J., Murphy, R.J., Underwood, A.J., 2010. Complex and inconsistent patterns of variation in benthos, micro-algae and sediment over multiple spatial scales. Marine Ecology Progress Series, 398, 33–47.

Charalampous, E., Matthiessen, B., Sommer, U., 2018. Light effects on phytoplankton morphometric traits influence nutrient utilization ability. J. Plankton Res. 40(5), 568-579.

Chen, J., Wang, D., Li, Y., Yu, Z., Chen, S., Hou, X., White, J. R., Chen, Z., 2020. The carbon stock and sequestration rate in tidal flats from coastal China. Global Biogeochemical Cycles, 34(11), e2020GB006772.

Chisholm, S.W., 1992. Phytoplankton size. Primary productivity and biogeochemical cycles in the sea, Plenum Press, New York, G.P. Falkowski, A.D. Woodhead (Eds.) 213–237.

Chitari, R.R., Anil, A.C., 2017. Estimation of diatom and dinoflagellate cell volumes from surface water of the Northern Indian Ocean. Oceanologia, 59, 389–395.

Cho, H.J., Matsuoka, K., 2001. Distribution of dinoflagellate cysts in surface sediments from the Yellow Sea and East China Sea. Marine Micropaleontology, 42(3-4), 103-123.

Cibic, T., Fazi, S., Nasi, F., Pin, L., Alvisi, F., Berto, D., Viganò, L., Zoppini, A., Del Negro, P., 2019. Natural and anthropogenic disturbances shape benthic phototrophic and heterotrophic microbial communities in the Po River Delta system. Estuarine, Coastal and Shelf Science, 222,168-182.

Colwell, R.R., 1979. Enumeration of specific populations by the most-probable-number (MPN) method. In Native aquatic bacteria: Enumeration, activity, and ecology. ASTM International.

Crouch, E.M., Mildenhall, D.C., Neil, H.L., 2010. Distribution of organic-walled marine and terrestrial palynomorphs in surface sediments offshore eastern New Zealand. Mar. Geol. 270(1-4), 235-256.

Cullen, J.J., 1982. The deep chlorophyll maximum - comparing vertical profiles of chlorophyll-a. Can. J. Fish. Aquat. Sci. 39, 791–803.

Cullen, J.J., 2015. Subsurface chlorophyll maximum layers: enduring enigma or mystery solved? Annu. Rev. Mar. Sci. 7, 207–239.

D’Silva, M.S., Anil, A.C., D'Costa, P.M., 2011. An overview of dinoflagellate cysts in recent sediments along the west coast of India. Indian J. Geo-Mar. Sci. 40, 697–709.

D’Silva, M.S., Anil, A.C., Naik, R.K., D’Costa, P.M., 2012. Algal blooms: A perspective from the coasts of India. Natural Hazards, 63, 1225–1253.

D’Silva, M.S., Anil, A.C., Sawant, S.S., 2013. Dinoflagellate cyst assemblages in recent sediments of Visakhapatnam harbour, east coast of India: Influence of environmental characteristics. Mar. pol. Bull. 66(1-2), 59-72.

Dalabehara, H.B., Sarma, V.V.S.S., 2021. Physical forcing controls spatial variability in primary production in the Indian Ocean. Deep-Sea Res. II.: Top. Stud. in Oceanogra. 183, 104906.

Dale, B., 1976. Cyst formation, sedimentation, and preservation: factors affecting dinoflagellate assemblages in recent sediments from Trondheims fjord, Norway. Rev. Palaeobot. Palyno. 22(1):39–60.

Dale, B., 1996. Dinoflagellate cyst ecology: modeling and geological applications. In: Jansonius, J., McGregor, D.C. (Eds.), Palynology: Principles and Applications. AASP Foundation, pp. 1249–1275.

Dale, B., Dale, A.L., Jansen, J.H.F., 2002. Dinoflagellate cysts as environmental indicators in surface sediments from the Congo deep-see fan and adjacent regions. Palaeogeogr. Palaeo climatol. Palaeoecol. 185:309–38.

Dalu, T., Adams, J.B., Taylor, J.C., Bate, G.C., Nunes, M., Froneman, P.W., Wasserman, R.J., 2018. Overview and status of estuarine microphytobenthos ecological research in South Africa. African Journal of Marine Science, 40(1), 1-12.

Dalu, T., Magoro, M.L., Naidoo, L.S., Wasserman, R.J., Human, L.R., Adams, J.B., Perissinotto, R., Deyzel, S.H., Wooldridge, T., Whitfield, A.K., 2020. Microphytobenthos diversity and community structure across different micro-estuaries and micro-outlets: Effects of environmental variables on community structure. Environmental Pollution, 260, p.114097.

Daly Yahia-Kéfi, O., Souissi, S., De Stefano, M., Daly Yahia, M.N., 2005 "*Bellerochea horologicalis* and *Lithodesmioides polymorpha* var. *tunisiense* var. nov.

(Coscinodiscophyceae, Bacillariophyta) in the Bay of Tunis: ultrastructural observations and spatio-temporal distribution" Botanica Marina, vol. 48, no. 1, 58-72.

D'Costa, P.M., Anil, A.C., Patil, J.S., Hegde, S., D'Silva, M.S., Chourasia, M., 2008. Dinoflagellates in a mesotrophic tropical environment influenced by monsoon. Estuar. Coast. Shelf Sci. 77, 77–90.

de Boyer Montegut, C., Madec, G., Fischer, A.S., Lazar, A., Iudicone, D., 2004. Mixed layer depth over the global ocean: An examination of profile data and a profile-based climatology. J. Geophy. Res.: Oceans, 109(C12).

De Clerck, O., Guiry, M.D., Leliaert, F., Samyn, Y., Verbruggen, H., 2013. Algal taxonomy: a road to nowhere? J. Phycol. 49: 215–225.

de Jonge, V.N., 1992. Physical processes and dynamics of microphytobenthos in the Ems estuary (The Netherlands). PhD thesis, University of Groningen, Groningen.

de Jonge, V.N., van Beusekom, J.E.E., 1992. Contribution of resuspended microphytobenthos to total phytoplankton in the Ems estuary and its possible role for grazers. Neth J Sea Res 30:91-105.

de Jonge, V.N., van Beusekom, J.E.E., 1995. Wind-and tide-induced resuspension of sediment and microphytobenthos from tidal flats in the Ems estuary. Limnol Ocenogr 40:766-778.

de Vernal, A., Eynaud, F., Henry, M., Limoges, A., Londeix, L., Matthiessen, J., Marret, F., Pospelova, V., Radi, T., Rochon, A., Van Nieuwenhove, N., Zaragosi, S., 2018. Distribution and (palaeo) ecological affinities of the main Spiniferites taxa in the mid-high latitudes of the Northern Hemisphere. Palynology. 42(sup1), 182-202.

de Vernal, A., Henry, M., Matthiessen, J., Mudie, P.J., Rochon, A., Boessenkool, K.P., Eynaud, F., Grosfjeld, K., Guiot, J., Hamel, D., Harland, R., Head, M.J., Kunz-Pirrung, M., Levac, E., Loucheur, V., Peyron, O., Pospelova, V., Radi, T., Turon, J.L., Voronina, E., 2001. Dinoflagellate cyst assemblages as tracers of sea-surface conditions in the northern North Atlantic, Arctic and sub-Arctic seas: the new ‘n=677’ data base and its application for quantitative palaeoceanographic reconstruction. J Quat Sci 16, 681–698.

de Vernal, A., Radi, T., Zaragosi, S., Van Nieuwenhove, N., Rochon, A., Allan, E., De Schepper, S., Eynaud, F., Head, M.J., Limoges, A., Londeix, L., Marret, F., Matthiessen, J., Penaud, A., Pospelova, V., Price, A., Richerol, T., 2020. Distribution of common modern dinoflagellate cyst taxa in surface sediments of the Northern Hemisphere in relation to environmental parameters: the new n = 1968 database. Mar Micropaleontol 159, 101796.

Decembrini, F., Caroppo, C., Bergamasco, A., 2020. Influence of lateral advection on phytoplankton size-structure and composition in a Mediterranean coastal area. Continent. Shelf Res. 209, 104216.

Defew, E.C., Tolhurst, T.J., Paterson, D.M., 2002. Site-specific features influence sediment stability of intertidal flats. Hydrology and Earth System Sciences 6 (6), 971–982.

Delebecq, G., Schmidt, S., Ehrhold, A., Latimier, M., Siano, R., 2020. Revival of ancient marine dinoflagellates using molecular biostimulation. J. Phycol. 56 (4), 1077-1089.

Delgado, M., de Jonge, V.N., Peletier, H., 1991. Effect of sand movement on the growth of benthic diatoms. J Exp Mar Biol Ecol145:221-231.

Demers, S., et al., 1991. Rapid light-induced changes in cell fuorescence and in xanthophyll-cycle pigments of Alexandrium excavatum (Dinophyceae) and *Talassiosira pseudonana* (Bacillariophyceae): a photo-protection mechanism. Mar. Ecol. Prog. Ser. 76:185–193.

Demmig-Adams, B., 1990. Carotenoids and photoprotection: a role for the xanthophyll zeaxanthin. Biochim Biophys Acta Bioenerg 1020:1–24.

Demmig-Adams, B., Adams, W.W., 1996. The role of xanthophyll cycle carotenoids in the protection of photosynthesis. Trends Plant Sci 1:21–26.

Denman, K.L., Gargett, A.E., 1983. Time and space scales of vertical mixing and advection of phytoplankton in the upper ocean. Limnology and oceanography, 28(5), 801-815.

Dimier, C., Corato, F., Tramontano, F., Brunet, C., 2007. Photoprotection and xanthophyll-cycle activity in three marine diatoms 1. Journal of Phycology, 43(5), 937-947.

Du, G., Son, M., Yun, M., An, S., Chung, I.K., 2009. Microphytobenthic biomass and species composition in intertidal flats of the Nakdong River estuary, Korea. Estuarine, Coastal and Shelf Science, 82(4), 663-672.

Du, G., Yan, H., Dupuy, C., 2017. Microphytobenthos as an indicator of environmental quality status in intertidal flats: case study of coastal ecosystem in Pertuis Charentais, France. Estuarine, Coastal and Shelf Science, 196, 217-226.

Duarte, C.M., Agusti, S., Canfield, D.E. Jr., 1990. Size plasticity of freshwater phytoplankton: Implications for community structure. Limnology and Oceanography, 35(8), 1846–1851.

Dugdale, R.C., Goering, J.J., 1967. Uptake of new and regenerated forms of nitrogen in primary productivity. Limnol. Oceanogr. 12, pp. 196-206.

Durante, G., Basset, A., Stanca, E., Roselli, L., 2019. Allometric scaling and morphological variation in sinking rate of phytoplankton. J. Phycol., 55, 1386–1393.

Durham, W.M., Stocker, R., 2012. Thin phytoplankton layers: characteristics, mechanisms, and consequences. Annu. Rev. Mar. Sci. 4, 177–207.

Dutkiewicz, S., Sokolov, A., Stone, P., Scott, J., 2005. Joint Program of the Science and Policy of Global Change Report, 122 (Massachusetts Institute of Technology, Cambridge, MA).

Eldrett, J.S., Harding, I.C., 2009. Palynological analyses of Eocene to Oligocene sediments from DSDP Site 338, Outer Vøring Plateau. Mar. Micropaleontol. 73(3-4), 226-240.

Ellegaard, M., 1998. Dinoflagellate cysts from Danish marine sediments — with emphasis on Gymnodinium catenatum-like cysts. PhD Thesis, University of Copenhagen.

Ellegaard, M., Lewis, J., Harding, I., 2002. Cyst–theca relationship, life cycle, and effects of temperature and salinity on the cyst morphology of Gonyaulax baltica sp. nov. (Dinophyceae) from the Baltic Sea Area. J. Phycol. 38, 775–789.

Erard-Le Denn, E., Desbruyeres, E., Olu, K., 1993. *Alexandrium minutum*: Resting cyst distribution in the sediments collected along the Brittany coast, France. *DEV. MAR. BIOL. 1993.*

Estrada, M., Delgado, M., Blasco, D., Latasa, M., Cabello, A.M., Benítez-Barrios, V., Vidal, M., 2016. Phytoplankton across tropical and subtropical regions of the Atlantic, Indian and Pacific oceans. PLoS One, 11(3), e0151699.

Facca, C., Sfriso, A., 2007. Epipelic diatom spatial and temporal distribution and relationship with the main environmental parameters in coastal waters. Estuarine, Coastal and Shelf Science, 75(1-2), 35-49.

Fagherazzi, S., Mariotti, G., Banks, A.T., Morgan, E.J., Fulweiler, R.W., 2014. The relationships among hydrodynamics, sediment distribution, and chlorophyll in a mesotidal estuary. Estuarine, Coastal and Shelf Science, 144, 54–64.

Falkowski, P.G., 1994. Light utilization and photoinhibition of photosynthesis in marine phytoplankton. Photoinhibition of photosynthesis, 407-432.

Falkowski, P.G., Chen, Y.B., 2003. Photoacclimation of light harvesting systems in eukaryotic algae. In Light-harvesting antennas in photosynthesis (pp. 423-447). Dordrecht: Springer Netherlands.

Falkowski, P.G., Raven, J.A., 2013. Aquatic photosynthesis. Princeton University Press.

Faraloni, C., Torzillo, G., 2017. Synthesis of antioxidant carotenoids in microalgae in response to physiological stress. In: Cvetkovic, D.J., Nikolic, G.S. (Eds.), Carotenoids. In Tech, p. Ch. 09.

Finkel, Z.V., 2007. Does phytoplankton cell size matter? The evolution of modern marine food webs. Evolution of Primary Producers in the Sea, 1, 333–350.

Finkel, Z.V., Beardall, J., Flynn, K.J., Quigg, A., Rees, T.A.V., Raven, J.A., 2010. Phytoplankton in a changing world: Cell size and elemental stoichiometry. J. Plankton Res., 32(1), 119–137.

Fishwick, J.R., Aiken, J., Barlow, R., Sessions, H., Bernard, S., Ras, J., 2006. Functional relationships and bio-optical properties derived from phytoplankton pigments, optical and photosynthetic parameters; a case study of the Benguela ecosystem. Journal of the Marine Biological Association of the United Kingdom, 86(6), 1267-1280.

Fistarol, G.O., Legrand, C., Rengefors, K., Granéli, E., 2004. Temporary cyst formation in phytoplankton: a response to allelopathic competitors? Environ. Microbial. 6 (8) 791-798.

Floder, S., Jaschinski, S., Wells, G., Burns, C.W., 2010. Dominance and compensatory growth in phytoplankton communities under salinity stress. Journal of Experimental Marine Biology and Ecology, 395(1-2), 223-231.

Fogg, G.E., 1991. The phytoplanktonic ways of life. New phytol., 118(2), 191-232.

Folk, R.L., 1974. The petrology of sedimentary rocks. Austin, Texas, Hemphill Publishing Co., 182 pp.

Folk, R.L., Andrews, P.B., Lewis, D.W., 1970. Detrital sedimentary rock classification and nomenclature for use in New Zealand. New Zealand Journal of Geology and Geophysics 13 (4), 937–968.

Fraisse, S., Bormans, M., Lagadeuc, Y., 2013. Morphofunctional traits reflect differences in phytoplankton community between rivers of contrasting flow regime. Aquatic Ecology, 47(3), 315–327.

Franks, P.J., 1992. Phytoplankton blooms at fronts: Patterns, scales, and physical forcing mechanisms. Reviews in Aquatic Sciences, 6, 121–137.

Fu, M., Sun, P., Wang, Z., Wei, Q., Qu, P., Zhang, X., Li, Y., 2018. Structure, characteristics and possible formation mechanisms of the subsurface chlorophyll maximum in the Yellow Sea Cold Water Mass. Cont. Shelf Res., 165, 93-105.

Fuentes-Lema, A., Sobrino, C., González, N., Estrada, M., Neale, P.J., 2015. Effect of solar UVR on the production of particulate and dissolved organic carbon from phytoplankton assemblages in the Indian Ocean. Marine Ecology Progress Series, 535, 47-61.

Furio, E.F., Matsuoka, K., Mizushima, K., Baula, I., Chan, K.W., Puyong, A., Srivilai, D., Sidharta, B.R., Fukuyo, Y., 2006. Assemblage and geographical distribution of dinoflagellate cysts in surface sediments of coastal waters of Sabah, Malaysia. Coast. Mar. Sci. 30 (1), 62–73.

Furuya, K., Marumo, R.,1983. The structure of the phytoplankton community in the subsurface chlorophyll maxima in the western North Pacific Ocean. J. Plankton Res., 5, 393 – 406.

Galbraith, H., Jones, R., Park, R., Clough, J., Herrod-Julius, S., Harrington, B., Page, G., 2002. Global climate change and sea level rise: potential losses of intertidal habitat for shorebirds. Waterbirds, 25(2), 173-183.

Gallagher, S.J., Wagstaff, B.E., 2021. Quaternary environments and monsoonal climate off northwest Australia: Palynological evidence from Ocean Drilling Program Site 765. Quat. Sci. Rev. 259, 106917.

Gao, K., Li, G., Helbling, E.W., Villafanẽ, V.E., 2007. Variability of UVR effects on photosynthesis of summer phytoplankton assemblages from a tropical coastal area of the South China Sea. Photochem Photobiol 83:802–809.

Gao, Y., Fang, H., Dong, Y., Li, H., Pu, C., Zhan, A., 2017. An improved method for the molecular identification of single dinoflagellate cysts. PeerJ, 5, e3224.

Garg, S., Gauns, M., Pratihary, A.K., 2024. Response of oceanic subsurface chlorophyll maxima to environmental drivers in the Northern Indian Ocean. Environ. Res. 240, 117528.

Giannini, F., Mendes, C.R.B., Garcia, C.A.E., Carvalho, A.C.O., Ciotti, A.M., 2021. Phytoplankton community and the fluorescence-derived photo-physiological parameters in the South Atlantic Ocean. Journal of Marine Systems, 218, 103538.

Gibson, R., Atkinson, R., Gordon, J., 2007. Loss, status and trends for coastal marine habitats of Europe. Oceanography and Marine Biology: an annual review, 45, 345-405.

Godhe, A., Karunasagar, I., Karlson, B., 2000. Dinoflagellate cysts in recent marine sediments from SW India. Bot. Mar. 43, 39–48.

Godhe, A., McQuoid, M.R., 2003. Influence of benthic and pelagic environmental factors on the distribution of dinoflagellate cysts in surface sediments along the Swedish west coast, Aquat. Microb. Ecol. 32, 185–201.

Goldman, J.C., McGillicuddy, D.J., 2003. Effect of large marine diatoms growing at low light on episodic new production. Limnol. Oceanogr. 48, 1176–1182.

Gomes, H.R., Goes, J.I., Matondkar, S.G.P., Parab, S.G., Al-Azri, A.R.N., Thoppil, P.G., 2008. Blooms of Noctiluca miliaris in the Arabian Sea—An in situ and satellite study. Deep-Sea Research-I, 55, 751–765.

Goodwin, P., Mehta, A.J., Zedler, J.B., 2001. Tidal wetland restoration: an introduction. J. Coastal Res. SI, 1–6.

Gorbunov, M.Y., Kolber, Z.S., Lesser, M.P., Falkowski, P.G., 2001. Photosynthesis and photoprotection in symbiotic corals. Limnology and Oceanography, 46(1), 75-85.

Granéli, E., Hansen, P.J., 2006. Allelopathy in Harmful Algae: A mechanism to compete for resources? Ecol. Stud., Granéli E and Turner J T (Eds.) Ecol. of Harm. Algae. 189-201.

Grasshoff, K., Ehrhardt, M., Kremling, K., 1983. Determination of nutrients. Methods Seawater Anal., 2:125-88.

Gribble, K.E., Nolan, G., Anderson, D.M., 2007. Biodiversity, biogeography and potential trophic impact of *Protoperidinium* spp. (Dinophyceae) off the southwestern coast of Ireland, J. Plankton Res. Volume 29, Issue 11, Pages 931–947.

Grover, J.P., 1989. Influence of cell shape and size on algal competitive ability. J. Phycol., 25, 402–405.

Gu, H., Luo, Z., Zeng, N., Lan, B., Lan, D., 2013. First record of Pentapharsodinium (Peridiniales, Dinophyceae) in the China Sea, with description of *Pentapharsodinium dalei* var. *aciculiferum*. Phycolo. Res. 61(4), 256-267.

Gu, H., Zheng, J., Huang, S., Morquecho, L., Krock, B., Shin, H.H., Li, Z., Derrien, A., Mertens, K.N., 2024. A new dinoflagellate *Gonyaulax pospelovana* with resting

cysts resembling Spiniferites delicatus and its biogeography and ecology revealed by DNA metabarcoding. Phycologia. 63(1), pp.74-88.

Guillard, R.R.L., Ryther, J.H., 1962. Studies on marine planktonic diatoms, I. *Cyclotella nana* Hustedt and *Detonula confervaceae* (Cleve) Gran Can J Microbiol 8: 229-239.

Guiry, M.D. 2012. How many species of algae are there? J. Phycol. 48, 1057–1063.

Ha, H.J., Kim, H., Noh, J., Ha, H.K., Khim, J.S., 2018. Rainfall effects on the erodibility of sediment and microphytobenthos in the intertidal flat. Environmental pollution, 242, 2051-2058.

Häggqvist, K., Lindholm, T., 2015. Phytoplankton communities in rock pools on the Åland Islands, SW Finland – environmental variables, functional groups and strategies. Biodivers. 16 (1) 15-26.

Häggqvist, K., Lindholm, T., 2016. Phytoplankton, physical and chemical microscale variations in three brackish rock pools; Phycol. Res. 64 241-250.

Halac, S.R., Villafañe, V.E., Gonçalves, R.J., Helbling, E.W., 2014. Photochemical responses of three marine phytoplankton species exposed to ultraviolet radiation and increased temperature: role of photoprotective mechanisms. Journal of Photochemistry and Photobiology B: Biology, 141, 217-227.

Hallegraeff, G., Gollasch, S., 2006. Anthropogenic introductions of microalgae. In Graneli, E. and Turner, J. T. (eds), Ecology of Harmful Algae, Springer, Berlin, Heidelberg, pp. 379–390.

Hallegraeff, G.M., Anderson, D.M., Cembella, A.D., Enevoldsen, H.O. 2003. Manual on harmful marine microalgae. Unesco.

Hanelt, D., Huppertz, K., Nultsch, W., 1993. Daily course of photosynthesis and photoinhibition in marine macroalgae investigated in the laboratory and field. Marine ecology progress series. Oldendorf, 97(1), 31-37.

Hanson, C.E., Pesant, S., Waite, A.M., Pattiaratchi, C.B., 2007. Assessing the magnitude and significance of deep chlorophyll maxima of the coastal eastern Indian Ocean. Deep Sea Res. Part II: Topical Studies in Oceanography, 54(8-10), 884-901.

Hardikar, R., Haridevi, C.K., Chowdhury, M., Shinde, N., Ram, A., Rokade, M.A., Rakesh, P.S., 2017. Seasonal distribution of phytoplankton and its association with physico-chemical parameters in coastal waters of Malvan, west coast of India. Environ. Monit. Assess., 189.

Harms, N.C., Lahajnar, N., Gaye, B., Rixen, T., Schwarz-Schampera, U., Emeis, K.C., 2021. Sediment trap-derived particulate matter fluxes in the oligotrophic subtropical gyre of the South Indian Ocean. Deep-Sea Res. II.: Top. Stud. in Oceanogra. 183, 104924.

Harris, A.S.D., Jones, K.J., Lewis, J., 1998. As assessment of the accuracy and reproducibility of the most probable number (MPN) technique in estimating numbers of nutrient stressed diatoms in sediment samples. J. Exp. Mar. Biol. Ecol. 231:21–30.

Harrison, J.W., Smith, R.E., 2009. Effects of ultraviolet radiation on the productivity and composition of freshwater phytoplankton communities. Photochemical & Photobiological Sciences, 8(9), 1218-1232.

Helbling, E.W., Buma, A.G., de Boer, M.K., Villafañe, V.E., 2001. In situ impact of solar ultraviolet radiation on photosynthesis and DNA in temperate marine phytoplankton. Marine Ecology Progress Series, 211, 43-49.

Helbling, E.W., Gao, K., Gonçalves, R.J., Wu, H., Villafañe, V.E., 2003. Utilization of solar UV radiation by coastal phytoplankton assemblages off SE China when exposed to fast mixing. Marine Ecology Progress Series, 259, 59-66.

Helbling, E.W., Villafane, V., Ferrario, M., Holm-Hansen, O., 1992. Impact of natural ultraviolet radiation on rates of photosynthesis and on specific marine phytoplankton species. Marine Ecology Progress Series, 89-100.

Heraud, P., Beardall, J., 2000. Changes in chlorophyll fluorescence during exposure of *Dunaliella tertiolecta* to UV radiation indicate a dynamic interaction between damage and repair processes. Photosynthesis Research, 63, 123-134.

Herbland, A., Voituriez, B., 1979. Hydrological structure analysis for estimating the primary production in the tropical Atlantic Ocean. J. Mar. Res. 37, 10–87.

Herman, P.M., Middelburg, J.J., Heip, C.H., 2001. Benthic community structure and sediment processes on an intertidal flat: results from the ECOFLAT project. Continental Shelf Research, 21(18-19), 2055-2071.

Hesse, K.J., Liu, Z.L., Schaumann, K., 1989. Phytoplankton and fronts in the German Bight. Scientia Marina, 53, 187–196.

Hessler, I., Young, M., Holzwarth, U., Mohtadi, M., Lückge, A., Behling, H., 2013. Imprint of eastern Indian Ocean surface oceanography on modern organic-walled dinoflagellate cyst assemblages. Mar. Micropaleontol. 101, 89-105.

Hillebrand, H., Durselen, C.D., Kirschtel, D., Pollingher, U., Zohary, T., 1999. Biovolume calculation for pelagic and benthic microalgae. Journal of Phycology, 35, 403–424.

Hintz, N.H., Zeising, M., Striebel, M., 2021. Changes in spectral quality of underwater light alter phytoplankton community composition. Limnol. Oceanogra., 66(9), 3327-3337.

Hochachka, P.W., Somero, G.N., 2002. *Biochemical adaptation: mechanism and process in physiological evolution*. Oxford university press.

Holeton, C.L., Nedelec, F., Sanders, R., Brown, L., Moore, C.M., Stevens, D.P., Heywood, K.J., Statham, P.J., Lucas, C.H., 2005. Physiological state of phytoplankton communities in the Southwest Atlantic sector of the Southern Ocean, as measured by fast repetition rate fluorometry. Polar Biology, 29, pp.44-52.

Holm-Hansen, O., 1997. Short- and long-term effects of UVA and UVB on marine phytoplankton productivity. Photochemistry and Photobiology, 65(2), 266-268.

Holtrop, T., Huisman, J., Stomp, M., Biersteker, L., Aerts, J., Grébert, T., Partensky, F., Garczarek, L., Woerd, H.J., 2021. Vibrational modes of water predict spectral niches for photosynthesis in lakes and oceans. Nat. Ecol. Evol., 5:55–66.

Hope, J.A., Paterson, D.M., Thrush, S.F., 2020. The role of microphytobenthos in soft-sediment ecological networks and their contribution to the delivery of multiple ecosystem services. Journal of Ecology, 108(3), 815-830.

Hopes, A., Mock, T., 2015. Evolution of microalgae and their adaptations in different marine ecosystems. In eLS, John Wiley & Sons, Ltd.

Houliez, E., Schmitt, F.G., Breton, E., Skouroliakou, D.I., Christaki, U., 2023. On the conditions promoting *Pseudo-nitzschia* spp. blooms in the eastern English Channel and southern North Sea. Harmful Algae, 102424.

Huggett, J., Griffiths, C.L., 1986. Some relationships between elevation, physic-chemical variables and biota of intertidal rock pools; *Mar. Ecol. Prog. Ser.* **29** 189–197.

Imai, I., Itakura, S., Itoh, K., 1990. Distribution of diatom resting cells in sediments of Harima-Nada and northern Hiroshima Bay, the Seto Inland Sea, Japan (in Japanese with English abstract). Bull Coast Oceanogr 28:75-84.

Imai, I., Itoh, K., Antaku, M., 1984. Extinction dilution method for the enumeration of dormant cells of red tide organisms in marine sediments. Bull Plankton Soc Jpn 31:123-124.

Ingole, B.S., 2002. Miramar beach is no more habitat for exotic species. The Navahind Times, v. XXXIX, 354, 1/14.

Ingole, B.S., 2003. Benthic life on the tropical sandy shore: Miramar beach a case study. Discovery Publishing House.

Ingole, B.S., 2004. Coastal benthic ecology of Goa. In: A.G. Untawale (Ed.), Know your shore: Goa, Goa Government Publication, 51-61.

Irwin, A.J., Finkel, Z.V., Schofield, O.M., Falkowski, P.G., 2006. Scaling-up from nutrient physiology to the size-structure of phytoplankton communities. J. Plankton res., 28(5), 459-471.

Ishikawa, A., Tamaguchi, A., 1994. The role of cysts on population dynamics of *Scrippsiella* spp. (Dinophyceae) in Onagawa Bay, northeast Japan. Mar Biol 119:39-44.

Itakura, S., Imai, I., Itoh, K., 1997. “Seed bank” of coastal planktonic diatoms in bottom sediments of Hiroshima Bay, Seto Inland Sea, Japan. Mar Biol 128:497-508.

Jagadeesan, L., Jyothibabu, R., Arunpandi, N., Parthasarathi, S., 2017. Copepod grazing and their impact on phytoplankton standing stock and production in a tropical

coastal water during the different seasons. Environmental Monitoring and Assessment, 189(3).

Jakobsen, H.H., Hansen, P.J., 1997. Prey size selection, grazing and growth response of the small heterotrophic dinoflagellate *Gymnodinium* sp. and the ciliate *Balanion comatum*—a comparative study, Mar. Ecol. Prog. Ser., vol. 158, pg.75-86.

James, K., Macreadie, P.I., Burdett, H.L., Davies, I., Kamenos, N.A., 2024. It's time to broaden what we consider a 'blue carbon ecosystem'. Glob. Change Biol. 30, e17261.

Jayakumar, S., Raju, N.S.N., Gowthaman, R., AshokKumar, K., Anand, N.M., 2002. Daily beach profiles and littoral environmental observations off Baga, Calangute and Miramar beaches during November-December 1999. Goa: NIO.

Jayaram, C., Udaya Bhaskar, T.V.S., Chacko, N., Prakash, S, Rao K.H., 2021. Spatio-temporal variability of chlorophyll in the northern Indian Ocean: A biogeochemical argo data perspective. Deep–Sea Res. II., 183, 104928.

Jeffrey, S., Wright, S., Zapata, M., 2011. Microalgal classes and their signature pigments. In: Roy, S., Llewellyn, C., Egeland, E., Johnsen, G. (Eds.), Phytoplankton Pigments: Characterization, Chemotaxonomy and Applications in Oceanography. Cambridge Environmental Chemistry Series. Cambridge University Press, pp. 3–77.

Jeong, H.J., Jang, S.H., Kang, N.S., Yoo, Y.D., Kim, M.J., Lee, K.H., Yoon, E.Y., Potvin, E., Hwang, Y.J., Kim, J.I., Seong, K.A., 2012. Molecular characterization and morphology of the photosynthetic dinoflagellate *Bysmatrum caponii* from two solar Saltons in Western Korea; Ocean Sci. J. 47(1) 1–18.

Jeong, H.J., Kang, H., Shim, J.H., Park, J.K., Kim, J.S., Song, J.Y., Choi, H.J., 2001. Interactions among the toxic dinoflagellate *Amphidinium carterae*, the heterotrophic dinoflagellate *Oxyrrhis marina*, and the calanoid copepods *Acartia* spp. Mar. Ecol. Prog. Ser. 218 77–86.

Jeslin, I.J., Benny, N., Thomas, L.C., Padmakumar, K.B., 2021. Short-term spatio-temporal variabilities of microphytobenthic assemblages in the mangrove

ecosystems along the southwest coast of India. Wetlands Ecology and Management, 29(5), 689-702.

Jin, E., Polle, J.E.W., Lee, H.K., Hyun, S.M., Chang, M., 2003. Xanthophylls in microalgae: from biosynthesis to biotechnological mass production and application. J. Microbiol. Biotechn. 13:165–174.

Joyce, L.B., Pitcher, G.C., du Randt, A., Monteiro, P.M.S., 2005. Dinoflagellate cysts from surface sediments of Saldanha Bay, South Africa: an indication of the potential risk of harmful algal blooms. Harmful Algae. 4 (2), 309–318.

Kagami, M., de Bruin, A., Ibelings, B. W., Van Donk, E., 2007. Parasitic chytrids: their effects on phytoplankton communities and food-web dynamics. Hydrobiol., 578, 113-129.

Kang, C.K., Park, H.J., Choy, E.J., Choi, K.S., Hwang, K., Kim, J.B., 2015. Linking intertidal and subtidal food webs: consumer-mediated transport of intertidal benthic microalgal carbon. PloS one, 10(10), e0139802.

Karp-Boss, L., Boss, E., 2016. The elongated, the squat and the spherical: Selective pressures for phytoplankton shape. In: Aquatic Microbial Ecology and Biogeochemistry: A Dual Perspective (eds. Glibert, P.M. and Kana, T.M.). Springer International Publication, Geneva, Switzerland, pp. 25–34.

Kawamura, H., 2004. Dinoflagellate cyst distribution along a shelf to slope transect of an oligotrophic tropical sea (Sunda Shelf, South China Sea). Phycol. Res. 52, 355–375.

Key, T., McCarthy, A., Campbell, D.A., Six, C., Roy, S., Finkel, Z.V., 2010. Cell size trade-offs govern light exploitation strategies in marine phytoplankton. Environmental microbiology, 12(1), 95-104.

Kiorboe, T., 1993. Turbulence, phytoplankton cell size, and the structure of pelagic food webs; *Adv. Mar. Biol.* 29 l-72.

Kiorboe, T., 2008. A mechanistic approach to plankton ecology. Princeton University Press.

Kirk, J.T.O., 1994. Light and Photosynthesis in Aquatic Ecosystems, second ed. Cambridge University Press, Cambridge, 509pp.

Kirk, J.T.O., 2011. Light and photosynthesis in aquatic ecosystems. Cambridge University Press, New York

Kirwan, M.L., Megonigal, J.P., 2013. Tidal wetland stability in the face of human impacts and sea-level rise. Nature, 504(7478), 53-60.

Kleparski, L., Beaugrand, G., Edwards, M., Schmitt, F.G., Kirby, R.R., Breton, E., Gevaert, F., Maniez, E., 2022. Morphological traits, niche-environment interaction and temporal changes in diatoms. Prog. Oceanogra., 201, 102747.

Klingenberg, C.P., 2010. There's something afoot in the evolution of ontogenies. BMC Evol. Biol., 10, 221.

Koh, C.H., Khim, J.S., Araki, H., Yamanishi, H., Mogi, H., Koga, K., 2006. Tidal resuspension of microphytobenthic chlorophyll a in a Nanaura mudflat, Saga, Ariake Sea, Japan: flood–ebb and spring–neap variations. Marine Ecology Progress Series, 312, 85-100.

Kornman, B.A., de Deckere, E.M.G.T., 1998. Temporal variation in sediment erodibility and suspended sediment dynamics in the Dollard estuary. Geological Society, London, Special Publications, 139, 231–241.

Kouli, K., Brinkhuis, H., Dale, B., 2001. *Spiniferites cruciformis*: a freshwater dinoflagellate cyst? Rev. Palaeobot. Palynol. 113:273–86.

Koyama, Y., Kuki, M., Andersson, P.O., Gillbro, T., 1996. Singlet excited states and the light-harvesting function of carotenoids in bacterial photosynthesis. Photochem. Photobiol. 63: 243–256.

Kranck, K., Milligan, T.G., 1988. Macroflocs from diatoms: in situ photography of particles in Bedford Basin, Nova Scotia. Mar. Ecol. Progr. Ser. 44, 183–189.

Kromkamp, J., Peene, J., van Rijswijk, P., Sandee, A., Goosen, N., 1995. Nutrients, light and primary production by phytoplankton and microphytobenthos in the eutrophic, turbid Westerschelde estuary (The Netherlands). Hydrobiologia, 311, 9–19.

Kruk, C., Devercelli, M., Huszar, V.L., 2021. Reynolds Functional Groups: a trait-based pathway from patterns to predictions. Hydrobiol., 848, 113-129.

Kruk, C., Huszar, V.L., Peeters, E.T., Bonilla, S., Costa, L., Lürling, M., Reynolds, C.S., Schefer, M., 2010. A morphological classification capturing functional variation in phytoplankton. Fresh. Biol., 55(3), 614–627.

Kruk, C., Martínez, A., Nogueira, L., Alonso, C., Calliari, D., 2015. Morphological traits variability reflects light limitation of phytoplankton production in a highly productive subtropical estuary (Río de la Plata, South America). Mar. Biol., 162, 331-341.

Kruk, C., Segura, A.M., 2012. The habitat template of phytoplankton morphology-based functional groups. Hydrobiol., 698: 191–202.

Kumar, P.S., Narvekar, J., Kumar, A., Shaji, C., Anand, P., Sabu, P., Rijomon, G., Josia, J., Jayaraj, K., Radhika, A., 2004. Intrusion of the Bay of Bengal water into the Arabian Sea during winter monsoon and associated chemical and biological response. Geophysical Research Letters, 31, 15.

Kumar, V.S., Pathak, K.C., Pednekar, P.N.S.N., Raju, N.S.N., Gowthaman, R., 2006. Coastal processes along the Indian coastline. Current science, 530-536.

Kurian, S., Chndrasekhararao, A.V., Vidya, P.J., Shenoy, D.M., Gauns, M., Uskaikar, H., Aparna, S.G., 2020. Role of oceanic fronts in enhancing phytoplankton biomass in the eastern Arabian Sea during an oligotrophic period. Marine Environmental Research, 160, 105023.

Kusum, K.K., Vineetha, G., Madhu, N.V., Anil, P., Dayana, M., Shihab, B.K., Muhsin, A.I., Riyas, C., Raveendran, T.V., 2017. Variability in the phytoplankton community of Kavaratti reef ecosystem (northern Indian Ocean) during peak and waning periods of El Nino 2016. Environ. Monit. Assess., 189:(12).

Larrazabal, M.E., Lassus, P., Maggi, P., Bardouil, M., 1990. Kystes modernes de dinoflagellés en baie de Vilaine-Bretagne sud (France). Cryptogamie Algologie, 11(3), 171-185.

Lauria, M.L., Purdie, D.A., Sharples, J., 1999. Contrasting phytoplankton distribution controlled by tidal turbulence in an estuary. Journal of Marine Systems, 21, 189–197.

Lavorel, S., Garnier, E., 2002. Predicting changes in community composition and ecosystem functioning from plant traits: Revisiting the Holy Grail. Functional Ecology, 16, 545–556.

Lefebvre, S., Leal, J.C.M., Dubois, S., Orvain, F., Blin, J.L., Bataille, M.P., Ourry, A., Galois, R., 2009. Seasonal dynamics of trophic relationships among co-occurring suspension-feeders in two shellfish culture dominated ecosystems. Estuarine, Coastal and Shelf Science, 82(3), 415-425.

Legendre, L., Rassoulzadegan, F., 1996. Food-web mediated export of biogenic carbon in oceans: environmental control. Mar. Ecol. Prog. Ser., 145, 179–193.

Leonilde, R., Elena, L., Elena, S., Francesco, C., Alberto, B., 2017. Individual trait variation in phytoplankton communities across multiple spatial scales. J. Plankton Res., 39(3), 577-588.

Lepš, J., Šmilauer, P., 2003. Multivariate analysis of ecological data using CANOCO. Cambridge university press.

Levine, J.M., 2016. A trail map for trait-based studies. Nature,529, 163–164.

Lewis, J., Rochon, A., Harding, I., 1999. Preliminary observations of cyst-theca relationships in *Spiniferites ramosus* and *Spiniferites membranaceus* (Dinophyceae). Grana, 38(2-3), 113-124.

Lewis, W.M., 1976. Surface/volume ratio: implication for phytoplankton morphology. Science, 192, 885–887.

Li, G., Cheng, L., Zhu, J., Trenberth, K.E., Mann, M.E., Abraham, J.P., 2020. Increasing ocean stratification over the past half-century. Nat. Clim. Change, 10(12), 1116-1123.

Li, G., Wu, Y., Gao, K., 2009. Effects of Typhoon Kaemi on coastal phytoplankton assemblages in the South China Sea, with special reference to the effects of solar UV radiation. Journal of Geophysical Research: Biogeosciences, 114(G4).

Li, Z., Pospelova, V., Kawamura, H., Luo, C., Mertens, K.N., Hernández-Almeida, I., Yin, K., Wu, Y., Wu, H., Xiang, R., 2020. Dinoflagellate cyst distribution in surface sediments from the South China Sea in relation to hydrographic conditions and primary productivity. Mar. Micropaleontol. 159, p.101815.

Li, Z., Pospelova, V., Mertens, K.N., Liu, L., Wu, Y., Li, C., Gu, H., 2023. Evaluation of organic-walled dinoflagellate cyst distributions in coastal surface sediments of the China Seas in relation with hydrographic conditions for paleoceanographic reconstruction. Quat. Internat. 661, 60-75.

Lin, H., Kuzminov, F.I., Park, J., Lee, S., Falkowski, P.G., Gorbunov, M.Y., 2016. The fate of photons absorbed by phytoplankton in the global ocean. Science, 351(6270), 264-267.

Litchman, E., de Tezanos Pinto, P., Edwards, K.F., Klausmeier, C.A., Kremer, C.T., Thomas, M.K., 2015. Global biogeochemical impacts of phytoplankton: a trait-based perspective. J. Ecol., 103(6).

Litchman, E., Klausmeier, C.A., 2008. Trait-based community ecology of phytoplankton. The Ann. Rev. of Ecol. Evol. and System, 39. 615–639.

Litchman, E., Klausmeier, C.A., Schofield, O.M., Falkowski, P.G., 2007. The role of functional traits and trade-offs in structuring phytoplankton communities: Scaling from cellular to ecosystem level. Ecology Letters, 10(12), 1170–1181.

Liu, D., Shi, Y., Di, B., Sun, Q., Wang, Y., Dong, Z., Shao, H., 2012. The impact of different pollution sources on modern dinoflagellate cysts in Sishili Bay, Yellow Sea, China. Mar. Micropaleontol. 84, 1-13.

Liu, X., Liu, Y., Chai, Z., Hu, Z., Tang, Y. Z., 2023. A combined approach detected novel species diversity and distribution of dinoflagellate cysts in the Yellow Sea, China. Mar. Pol. Bull. 187, 114567.

Liu, Z., Li, Q. P., Ge, Z., Shuai, Y., 2021. Variability of plankton size distribution and controlling factors across a coastal frontal zone. Progress in Oceanography, 197, 102665.

Lovelock, C.E., Feller, I.C., Reef, R., Hickey, S., Ball, M.C., 2017. Mangrove dieback during fluctuating sea levels. Scientific Reports, 7(1), 1680.

Loveson, V.J., Gujar, A.R., Iyer, S.D., Udayaganesan, P., Luis, R.A.A., Gaonkar, S.S., Chithrabhanu, P., Tirodkar, G.M., Singhvi, A.K., 2014. Beach dynamics and oscillations of shoreline position in recent years at Miramar Beach, Goa, India: a study from a GPR survey. Natural hazards, 73, pp.2089-2106.

Lundholm, N., Ribeiro, S., Andersen, T.J., Koch, T., Godhe, A., Ekelund, F., Ellegaard, M., 2011. Buried alive -germination of up to a century-old marine protist resting stages. Phycologia. 50 (6), 629-640.

MacIntyre, H.L., Geider, R.J., Miller, D.C., 1996. Microphytobenthos: The ecological role of the "Secret Garden" of unvegetated, shallow-water marine habitats. I. Distribution, abundance and primary production. Estuaries and Coasts, 19, 186–201.

Madhu, N.V., Jyothibabu, R., Maheswaran, P.A., Gerson, V.J., Gopalakrishnan, T.C., Nair, K.K.C., 2006. Lack of seasonality in phytoplankton standing stock (chlorophyll a) and production in the western Bay of Bengal. Cont. Shelf Res. 26(16), 1868–1883.

Madhupratap, M., Kumar, S.P., Bhattathiri, P.M.A., Kumar, M.D., Raghukumar, S., Nair, K.K.C., Ramaiah, N., 1996. Mechanism of the biological response to winter cooling in the northeastern Arabian Sea. Nature, 384(6609), 549–552.

Maharana, P., Agnihotri, R., Dimri, A.P., 2021. Changing Indian monsoon rainfall patterns under the recent warming period 2001–2018. Climate Dynamics, *57*(9), 2581-2593.

Mandal, S.K., Singh, R.P., Patel, V., 2011. Isolation and characterization of exopolysaccharide secreted by a toxic dinoflagellate, *Amphidinium carterae* Hulburt 1957 and its probable role in harmful algal blooms (HABs); *Microb. Ecol.* **62** 518–527.

Mandal, A., Dutta, A., Das, R., Mukherjee, J. 2021. Role of intertidal microbial communities in carbon dioxide sequestration and pollutant removal: A review. Marine Pollution Bulletin, 170, 112626.

Mao, J., Burdett, H.L., McGill, R.A.R., Newton, J., Gulliver, P., Kamenos, N.A., 2020. Carbon burial over the last four millennia is regulated by both climatic and land use change. Global Change Biology, 26(4), 2496–2504.

Mao, Y., Guo, C., Yu, L., Gong, X., Sun, J., 2024. The impact of eddies and spring warm pool on sinking rates of phytoplankton with different shapes and sizes. Marine Biology, 171(5), 100.

Margalef, R., 1978. Life-forms of phytoplankton as survival alternatives in an unstable environment. Oceanol. Acta. 1, 493–509.

Marret, F., Bradley, L., de Vernal, A., Hardy, W., Kim, S.Y., Mudie, P., Penaud, A., Pospelova, V., Price, A.M., Radi, T., Rochon, A., 2020. From bi-polar to regional distribution of modern dinoflagellate cysts, an overview of their biogeography. Mar. Micropaleontol. 1, 159:101753.

Marret, F., de Vernal, A., Benderra, F., Harland, R., 2001. Late Quaternary sea-surface conditions at DSDP Hole 594 in the southwest Pacific Ocean based on dinoflagellate cyst assemblages. J. of Quat. Sci.: Published for the Quaternary Research Association, 16(7), 739-751.

Marret, F., Mudie, P., Aksu, A., Hiscott, R.N., 2009. A Holocene dinocyst record of a two-step transformation of the Neoeuxinian brackish water lake into the Black Sea. Quat. Int. 197, 72–86.

Marret, F., Zonneveld, K.A.F. 2003. Atlas of modern organic-walled dinoflagellate cyst distribution. Rev. Palaeobot. Palynol. 125, 1–200.

Marrone, F., Fontaneto, D., Naselli-Flores, L., 2023. Cryptic diversity, niche displacement, and our poor understanding of taxonomy and ecology of aquatic microorganisms. Hydrobiol., 850 (6), 1221-1236.

Martini, S., Larras, F., Boyé, A., Faure, E., Aberle, N., Archambault, P., Bacouillard, L., Beisner, B. E., Bittner, L., Castella, E., Danger, M., 2021. Functional trait-based approaches as a common framework for aquatic ecologists. Limnology and Oceanography, 66(3), 965–994.

Martins, G.M., Hawkins, S.J., Thompson, R.C., Jenkins, S.R., 2007. Community structure and functioning in intertidal rock pools: effects of pool size and shore height at different successional stages. Mar. Ecol. Prog. Ser. 329, 43–55.

Mascarenhas, A., Ingole, B., 2009. Miramar (Goa) beach management project: An oceanographic evaluation. Coastal Environments: Problems and Perspectives, 212-225.

Matsuoka, K., 1981. Dinoflagellate cysts and pollen in pelagic sediments of the northern part of the Philippine Sea. Bull. of Facul. of Lib. Arts. Nagasaki University 21 (2), 59–70.

Matsuoka, K., 1999. Eutrophication process recorded in dinoflagellate cyst assemblages - a case of Yokohama Port, Tokyo Bay, Japan. Sci Total Environ 231 (1), 17–35.

Matsuoka, K., Fukuyo, Y., 2000. Technical Guide for Modern Dinoflagellate Cyst Study WESTPAC-HAB/WESTPAC/IOC. Japan Society for the Promotion of Science, 29 pp.

Matsuoka, K., Fukuyo, Y., Praseno, D.P., Adnan, Q., Masaki, K., 1999. Dinoflagellate cysts in surface sediments of Jakarta Bay, off Ujung Pandang and Larantuka of Flores Islands, Indonesia, with special reference of *Pyrodinium bahamense*. Bull. of the Facul. of Fisheries. 80, 49–56.

Matsuoka, K., Joyce, L.B., Kotani, Y., Matsuyama, Y., 2003. Modern dinoflagellate cysts in hypertrophic coastal waters of Tokyo Bay, Japan. J. Plankton Res. 25(12), 1461–1470.

Matthiessen, J., 1995. Distribution patterns of dinoflagellate cysts and other organic-walled microfossils in recent Norwegian-Greenland Sea sediments. Mar. Micropaleontol. 24(3-4), 307-334.

McCarthy, F.M.G., Mertens, K.N., Ellegaard, M., Sherman, K., Pospelova, V., Ribeiro, S., Blasco, S., Vercauteren, D., 2011. Resting cysts of freshwater dinoflagellates in southeastern Georgian Bay (Lake Huron) as proxies of cultural eutrophication. Rev. Palaeobot. Palynol. 166:46–62.

McGill, B.J., Enquist, B.J., Weiher, E., Westoby, M., 2006. Rebuilding community ecology from functional traits. Trends in Ecology & Evolution, 21, 178–185.

McLaughlin, F.A., Carmack, E.C., 2010. Deepening of the nutricline and chlorophyll maximum in the Canada Basin interior, 2003–2009. Geophys. Res. Lett., 37 (24).

McQuoid, M.R., 2002. Pelagic and benthic environmental controls on the spatial distribution of a viable diatom propagule bank on the Swedish west coast. J. Phycol. 38: 881–893.

Méléder, V., Rincé, Y., Barillé, L., Gaudin, P., Rosa, P., 2007. Spatiotemporal changes in microphytobenthos assemblages in a macrotidal flat (Bourgneuf Bay, France) 1. Journal of phycology, 43(6), 1177-1190.

Menden-Deuer, S., Lessard, E.J., Satterberg, J., Grünbaum, D., 2005. Growth rates and starvation survival of three species of the pallium-feeding, thecate dinoflagellate genus *Protoperidinium*. Aquat. Microb. Ecol., 41(2), 145-152.

Mertens, K.N., 2013. Morphological variation in dinoflagellate cysts: current status and future challenges, in: AASP-CAP-NAMS-CIMP-DINO10 joint meeting, San Francisco, USA, 137–137.

Mertens, K.N., Bradley, L.R., Takano, Y., Mudie, P.J., Marret, F., Aksu, A.E., Hiscott, R.N., Verleye, T.J., Mousing, E.A., Smyrnova, L.L., Bagheri, S., 2012. Quantitative estimation of Holocene surface salinity variation in the Black Sea using dinoflagellate cyst process length. Quat Sci Rev 39, 45–59.

Mertens, K.N., Bringué, M., Van Nieuwenhove, N., Takano, Y., Pospelova, V., Rochon, A., de Vernal, A., Radi, T., Dale, B., Patterson, R.T., Weckström, K., Andrén, E., Louwye, S., Matsuoka, K., 2012a. Process length variation of the cyst of the dinoflagellate Protoceratium reticulatum in the North Pacific and Baltic-Skagerrak region: Calibration as an annual density proxy and first evidence of pseudo-cryptic speciation. J. Quaternary Sci. 27, 734–744.

Mertens, K.N., Dale, B., Ellegaard, M., Jansson, I.M., Godhe, A., Kremp, A., Louwye, S., 2010. Process length variation in cysts of the dinoflagellate *Protoceratium reticulatum* from surface sediments of the Baltic-Kattegat-Skagerrak estuarine system: a regional salinity proxy. Boreas. 40, 242–255.

Mertens, K.N., Gonzalez, C., Delusina, I., Louwye, S., 2009a. 30000 years of productivity and salinity variations in the late quaternary Cariaco Basin revealed by dinoflagellate cysts. Boreas. 38, 647–662.

Mertens, K.N., Rengefors, K., Moestrup, Ø., Ellegaard, M., 2012b. A review of recent freshwater dinoflagellate cysts: taxonomy, phylogeny, ecology and palaeocology. Phycologia. 51:612–9.

Mertens, K.N., Ribeiro, S., Bouimetarhan, I., Caner, H., Combourieu Nebout, N., Dale, B., De Vernal, A., Ellegaard, M., Filipova, M., Godhe, A., Goubert, E., 2009b. Process length variation in cysts of a dinoflagellate *Lingulodinium machaerophorum* in surface sediments: investigating its potential as salinity proxy. Mar. Micropaleontol. 70, 54–69.

Metaxas, A., Lewis, A.G., 1992. Diatom communities in tidepools: the effect of Intertidal height. Bota. mari. 35, l-10.

Metaxas, A., Scheibling, R.E., 1993. Community structure and organization of tidepools. Mar. Ecol. Prog. Ser. 98, 187–198.

Metaxas, A., Scheibling, R.E., 1994. Changes in phytoplankton abundance in tidepools over the period of tidal isolation. Bota. mari. 37, 301–314.

Metaxas, A., Scheibling, R.E., 1996a Spatial heterogeneity of phytoplankton assemblages in tidepools: effects of abiotic and biotic factors. Mar. Ecol. Prog. Ser. 130, 179–199.

Metaxas, A., Scheibling, R.E., 1996b. Top-down and bottom-up regulation of phytoplankton assemblages in tidepools. Mar. Ecol. Prog. Ser. 145, 161–177.

Meyer, A. A., Tackx, M. Daro, N., 2000. Xanthophyll cycling in *Phaeocystis globosa* and *Thalassiosira* sp.: a possible mechanism for species succession. J. Sea Res. 43: 373–384.

Michelberger, T., Mezzadrelli, E., Bellan, A., Perin, G., Morosinotto, T., 2024. The Xanthophyll Cycle balances Photoprotection and Efficiency in the seawater alga Nannochloropsis oceanica. *bioRxiv*, 2024-10.

Mignot, A., Claustre, H., Uitz, J., Poteau, A., d'Ortenzio, F., Xing, X., 2014. Understanding the seasonal dynamics of phytoplankton biomass and the deep chlorophyll maximum in oligotrophic environments: a Bio-Argo float investigation. Global Biogeochem. Cycles, 28 (8), 856–876.

Mitbavkar, S., Anil, A.C., 2002. Diatoms of the microphytobenthic community: population structure in a tropical intertidal sand flat. Marine Biology 140, 41–57.

Mitbavkar, S., Anil, A.C., 2004. Vertical migratory rhythms of benthic diatoms in a tropical intertidal sand flat: influence of irradiance and tides. Marine biology, 145, 9-20.

Mitbavkar, S., Anil, A.C., 2006. Diatoms of the microphytobenthic community in a tropical intertidal sand flat influenced by monsoons: spatial and temporal variations. Marine Biology, 148, 693-709.

Modi, J.S., Patil, J.S., 2019. Allelopathic effect of the dinoflagellate *Amphidinium carterae* filtrates on diatoms. (Master dissertation, CSIR-NIO, India), unpublished.

Moisan, T.A., Olaizola, M., Mitchell, B.G., 1998. Xanthophyll cycling in *Phaeocystis antarctica*: changes in cellular fuorescence. Mar. Ecol. Prog. Ser. 169: 113–121.

Moore, C.M., Lucas, M.I., Sanders, R., Davidson, R., 2005. Basin-scale variability of phytoplankton bio-optical characteristics in relation to bloom state and community structure in the Northeast Atlantic. Deep Sea Research Part I: Oceanographic Research Papers, 52(3), 401-419.

Moore, C.M., Mills, M.M., Langlois, R., Milne, A., Achterberg, E.P., La Roche, J., Geider, R.J., 2008. Relative influence of nitrogen and phosphorous availability on phytoplankton physiology and productivity in the oligotrophic sub-tropical North Atlantic Ocean. Limnology and Oceanography, 53(1), 291-305.

Moore, C.M., Suggett, D.J., Hickman, A.E., Kim, Y.N., Tweddle, J.F., Sharples, J., Geider, R.J., Holligan, P.M., 2006. Phytoplankton photoacclimation and photoadaptation in response to environmental gradients in a shelf sea. Limnology and Oceanography, 51(2), pp.936-949.

Morabito, G., Oggioni, A., Caravati, E., Panzani, P., 2007. Seasonal morphological plasticity of phytoplankton in Lago Maggiore (N. Italy). Hydrobiol., 578, 47-57.

Moritsch, M.M., Young, M., Carnell, P., Macreadie, P.I., Lovelock, C., Nicholson, E., Raimondi, P.T., Wedding, L.M., Ierodiaconou, D., 2021. Estimating blue carbon

sequestration under coastal management scenarios. Science of the Total Environment, 777, 145962.

Mou, S., Zhang, Z., Zhao, H., Nair, S., Li, Y., Xu, K., Zhang, Y., 2022. A dark-tolerant diatom (*Chaetoceros*) cultured from the deep Sea. J. Phycol., 58(2), 208-218.

Mouradian, M., Panetta, R. J., De Vernal, A., Gélinas, Y., 2007. Dinosterols or dinocysts to estimate dinoflagellate contributions to marine sedimentary organic matter? Limnol. and oceanogr. 52(6), 2569-2581.

Murray, N.J., Phinn, S.R., DeWitt, M., Ferrari, R., Johnston, R., Lyons, M.B., Clinton, N., Thau, D., Fuller, R.A., 2019. The global distribution and trajectory of tidal flats. Nature, 565(7738), 222-225.

Murray, S.A., Garby, T., Hoppenrath, M., Neilan, B.A., 2012. Genetic diversity, morphological uniformity and polyketide production in Dinoflagellates (Amphidinium, Dinoflagellata); PLoS ONE 7(6) e38253,

Murray, S.A., Kohli, G.S., Farrell, H., Spiers, Z.B., Place, A.R., Dorantes-Aranda, J.J., Ruszczy, K.J., 2015. A fish kill associated with a bloom of *Amphidinium carterae* in a coastal lagoon in Sydney, Australia. Harm. Alg. 49, 19–28.

Murty, C.S., Das, P.K., Nair, R.R., Veerayya, M., Varadachari, V.V.R., 1976. Circulation and sedimentation processes in and around the Aguada Bar. Indian J Mar Sci.

Naidu, P.D., Patil, J.S., Narale, D.D., Anil, A.C., 2012. A first look at the dinoflagellate cysts abundance in the Bay of Bengal: implications on Late Quaternary productivity and climate change. Curr. Sci. 495-499.

Naqvi, S.W.A., Naik, H., Pratihary, A., D'Souza, W., Narvekar, P.V., Jayakumar, D.A., Devol, A.H., Yoshinari, T., Saino, T., 2006. Coastal versus open-ocean denitrification in the Arabian Sea. Biogeosciences, 3 (4), pp. 621-633.

Narale, D.D., Anil, A.C., 2017. Spatial distribution of dinoflagellates from the tropical coastal waters of the South Andaman, India: Implications for coastal pollution monitoring. Mar. Poll. Bul. 115(1-2), 498-506.

Narale, D.D., Naidu, P.D., Anil, A.C., Godad, S.P., 2015. Evolution of productivity and monsoonal dynamics in the eastern Arabian Sea during the past 68ka using

dinoflagellate cyst records. Palaeogeogr. Palaeoclimatol. Palaeoecol. 435, 193–202.

Narale, D.D., Patil, J.S., Anil, A.C., 2013. Dinoflagellate cyst distribution in recent sediments along the south-east coast of India. Oceanologia, 55(4), 979-1003.

Naselli-Flores, L., 2014. Morphological analysis of phytoplankton as a tool to assess ecological state of aquatic ecosystems: The case of Lake Arancio, Sicily. Italy. Inland Waters, 4(1), 15–26.

Naselli-Flores, L., Barone, R., 2007. Pluriannual morphological variability of phytoplankton in a highly productive Mediterranean reservoir (Lake Arancio, Southwestern Sicily). Hydrobiol. 578, 87–95.

Naselli-Flores, L., Barone, R., 2011. Fight on plankton! or, phytoplankton shape and size as adaptive tools to get ahead in the struggle for life. Cryptogamie, Algologie, 32(2), 157–204.

Naselli-Flores, L., Padisak, J., 2024. Analysis of morphological traits as a tool to identify the realized niche of phytoplankton populations: what do the shape of planktic microalgae, Anna Karenina and Vincent van Gogh have in common? Hydrobiol., 1-17.

Naselli-Flores, L., Padisak, J., Albay, M., 2007. Shape and size in phytoplankton ecology: Do they matter? Hydrobiologia, 578, 157–161.

Neale, P.J., Davis, R.F., Cullen, J.J., 1998. Interactive effects of ozone depletion and vertical mixing on photosynthesis of Antarctic phytoplankton. Nature, 392(6676), 585-589.

Neale, P.J., Helbling, E.W., Zagarese, H.E., 2003. Modulation of UVR exposure and effects by vertical mixing and advection.

Nehring, S., 1994. Spatial distribution of dinoflagellate resting cysts in recent sediments of Kiel Bight, Germany (Baltic Sea). Ophelia, 39(2), 137-158.

Nehring, S., 1997. Dinoflagellate resting cysts from recent German coastal sediments. 307-324.

Neustupa, J., 2016. Static allometry of unicellular green algae: scaling of cellular surface area and volume in the genus Micrasterias (Desmidiales). J. Evol. Biol., 29, 292–305.

Nigam, R., Nayak, G.N., Naik, S., 2002. Does mining pollution affect foraminiferal distribution in Mandovi estuary, Goa, India. Rev Paleobiol Geneve 21:673–677

Nigam, R., Panchang, R., Banerjee, P., 2005. Foraminifera in surface sediments of Mandovi River Estuary: indicators for mining pollution and high sea stand in Goa, India. J Coast Res 21:853–859.

Niklas, K.J., 2000. The evolution of plant body plans—a biomechanical perspective. Ann. Bot., 85(4), 411-438.

Nooteboom, P.D., Bijl, P.K., Van Sebille, E., Von Der Heydt, A.S., Dijkstra, H.A., 2019. Transport bias by ocean currents in sedimentary microplankton assemblages: Implications for paleoceanographic reconstructions. Paleoceanogr. Paleoclimatol. 34(7), 1178-1194.

Nooteboom, P.D., Delandmeter, P., Van Sebille, E., Bijl, P.K., Dijkstra, H.A., Von Der Heydt, A.S., 2020. Resolution dependency of sinking Lagrangian particles in ocean general circulation models. PLoS ONE 15(9): e0238650.

Norberg, J., 1998. Effects of temperature and light on the composition of brackish-water rock pool ecosystem. Aqua. Ecol. 32, 323-334.

O'Connor, M.P., Agosta, S.J., Hansen, F., Kemp, S.J., Sieg, A.E., McNair, J.N., Dunham, A.E., 2007. Phylogeny, regression, and the allometry of physiological traits. The American Naturalist, 170(3), 431-442.

O'Farrell, I., de Tezanos Pinto, P., Izaguirre, I., 2007. Phytoplankton morphological response to the underwater light conditions in a vegetated wetland. Hydrobiol., 578, 65-77.

Oakes, J.M., Rysgaard, S., Glud, R.N., Eyre, B.D., 2016. The transformation and fate of sub-Arctic microphytobenthos carbon revealed through 13C-labeling. Limnology and Oceanography, 61(6), 2296-2308.

Oh, S.H., Koh, C.H., 1995. Distribution of diatoms in the surficial sediments of the Mangyung-Dongjin tidal flat, west coast of Korea (Eastern Yellow Sea). Marine Biology 122, 487–496.

Olaizola, M., La Roche, J., Kolber, Z., Falkowski, P.G., 1994. Nonphotochemical fluorescence quenching and the diadinoxanthin cycle in a marine diatom. Photosynth Res 41(2):357–370.

Osmond, C.B., 1994. What is photoinhibition? Insights from comparisons of shade and sun plants. Photoinhibition of photosynthesis from molecular mechanisms to the field.

Padisak, J., 1992. Seasonal succession of phytoplankton in a large shallow lake (Balaton, Hungary)—a dynamic approach to ecological memory, its possible role and mechanisms. J. Ecology 80: 217–230.

Padisak, J., Crossetti, L.O., Naselli-Flores, L., 2009. Use and misuse in the application of the phytoplankton functional classification: a critical review with updates. Hydrobiol., 621, 1-19.

Padisak, J., Soroczki-Pinter, E., Rezner, Z., 2003. Sinking properties of some phytoplankton shapes and the relation of form resistance to morphological diversity of plankton – an experimental study. Hydrobiol. 500, 243–257.

Padmakumar, K.B., Menon, N.R., Sanjeevan, V.N., 2010a. Occurrence of endosymbiont *Richelia intracellularis* (Cyanophyta) within the diatom *Rhizosolenia hebetatain* Northern Arabian Sea. International Journal of Biodiversity and Conservation, 2(4), 70–74.

Padmakumar, K.B., Smitha, B.R., Thomas, L.C., Fanimol, C.L., SreeRenjimma, G., Menon, N.R., Sanjeevan, V.N., 2010b. Blooms of *Trichodesmium erythraeum* in the South Eastern Arabian Sea during the onset of 2009 Summer Monsoon. Ocean Science Journal, 45(3), 151–157.

Pancic, M., Kiørboe, T., 2018. Phytoplankton defence mechanisms: traits and trade-offs: Defensive traits and trade-offs. Biol. Rev., 93,1269–1303.

Park, J., Kwon, B., Kim, M., Hong, S., Ryu, J., Song, S.J., Khim, J.S., 2014. Microphytobenthos of Korean tidal flats: A review and analysis on floral distribution and tidal dynamics. Ocean and coastal management 102: 471-482.

Parry, M.L. (Ed.)., 2007. Climate change 2007-impacts, adaptation and vulnerability: Working group II contribution to the fourth assessment report of the IPCC (Vol. 4). Cambridge University Press.

Passeri, D.L., Hagen, S.C., Medeiros, S.C., Bilskie, M.V., Alizad, K., Wang, D., 2015. The dynamic effects of sea level rise on low-gradient coastal landscapes: A review. Earth's Future, 3(6), 159-181.

Paterson, D.M., 1994. Biological mediation of sediment erodibility: ecology and physical dynamics. Cohesive sediments.

Paterson, D.M., Hagerthey, S.E., 2001. Microphytobenthos in Constrasting Coastal Ecosystems: Biology and Dynamics. In: Reise, K. (eds) Ecological Comparisons of Sedimentary Shores. Ecological Studies, vol 151. Springer, Berlin, Heidelberg.

Patil, J.S., Anil, A.C., 2019. Assessment of phytoplankton photo-physiological status from a tropical monsoonal estuary. Ecological indicators, 103, 289-300.

Patil, J.S., Rodrigues, R.V., Paul, P., Sathish, K., Rafi, M., Anil, A.C., 2017. Benthic dinoflagellate blooms in tropical intertidal rock pools: Elucidation of photoprotection mechanisms. Marine Biology, 164, 1-19.

Pattan, J.N., Jauhari, P., 2001. Major, trace, and rare earth elements in the sediments of the Central Indian Ocean Basin: Their source and distribution. Mar. geores. Geotech. 19(2), 85-106.

Paul, P., Patil, J.S., 2024. Geographic distribution of modern dinoflagellate cysts in surface sediments of the Arabian Sea: significance of taxa and morphometry as potential ecological indicators. Environmental Science and Pollution Research, 1-19.

Paul, P., Patil, J.S., Anil, A.C., 2021. Phytoplankton communities in marine intertidal rock-pools: Effect of location, geometric shapes and allelopathy. Journal of Earth System Science, 130(3), 128.

Paul, P., Patil, J.S., Anil, A.C., 2023. Variability in phytoplankton shape dominance in marine pelagic systems: prevalence of different adaptive strategies in the eastern Arabian Sea during the winter monsoon. Environ. Monit. Assess., 195(4), 528.

Pavaux, A-S., Berdalet, E., Lemée, R., 2020. Chemical Ecology of the Benthic Dinoflagellate Genus Ostreopsis: Review of Progress and Future Directions. Front. Mar. Sci. 7, 498.

Pelabon, C., Firmat, C., Bolstad, G.H., Voje, K.L., Houle, D., Cassara, J., Rouzic, A.L., Hansen, T.F., 2014. Evolution of morphological allometry. Annu. N. Y. Acad. Sci., 1320: 58–75.

Perkins, R., Underwood, G., Brotas, V., Snow, G., Jesus, B., Ribeiro, L., 2001. Responses of microphytobenthos to light: Primary production and carbohydrate allocation over an emersion period. Marine Ecology Progress Series, 223, 101–112.

Petrucciani, A., Chaerle, P., Norici, A., 2022. Diatoms Versus Copepods: Could Frustule Traits Have a Role in Avoiding Predation? Front. Mar. Sci., 8:804960.

Pinckney, J.L., 2018. A mini-review of the contribution of benthic microalgae to the ecology of the continental shelf in the South Atlantic Bight. Estuaries and Coasts, 41(7), 2070–2078.

Pospelova, V., Chmura, G.L., Boothman, W.S., Latimer, J.S., 2002. Dinoflagellate cyst records and human disturbance in two neighboring estuaries New Bedford harbour and Apponagansett Bay Massachusetts (USA). Sci. Total Environ. 298 (1), 81–102.

Pospelova, V., Chmura, G.L., Boothman, W.S., Latimer, J.S., 2005. Spatial distribution of modern dinoflagellate cysts in polluted estuarine sediments from Buzzards Bay (Massachusetts,USA) embayments. Mar. Ecol. Prog. Ser. 292, 23–40.

Pospelova, V., Chmura, G.L., Walker, H.A., 2004. Environmental factors influencing the spatial distribution of dinoflagellate cyst assemblages in shallow lagoons of southern New England (USA). Rev Palaeobot Palynol 128, 7–34.

Pospelova, V., de Vernal, A. Pedersen, T.F., 2008. Distribution of dinoflagellate cysts in surface sediments from the north eastern Pacific Ocean (43-25° N) in relation to

sea-surface temperature, salinity, productivity and coastal upwelling. Mar. Micropalentol. 68:21–48.

Pospelova, V., Pedersen, T.F., de Vernal, A., 2006. Dinoflagellate cysts as indicators of climatic and oceanographic changes during the past 40 kyr in the Santa Barbara Basin, southern California. Paleoceanogr 21, 1–16.

Pospelova, V., Price, A.M., Pedersen, T.F., 2015. Palynological evidence for late quaternary climate and marine primary productivity changes along the California margin. Paleoceanogr 30:877–894.

Pospelova, V., Zonneveld, K.A., Heikkilä, M., Bringué, M., Price, A.M., Esenkulova, S., Matsuoka, K., 2018. Seasonal, annual, and inter-annual Spiniferites cyst production: a review of sediment trap studies. Palynol. 42(sup1), 162-181.

Poulson, K.L., Sieg, R.D., Prince, E.K., Kubanek, J., 2010. Allelopathic compounds of a red tide dinoflagellate have species-specific and context-dependent Impacts on phytoplankton. Mar. Ecol. Prog. Ser. 416, 69–78.

Prabhu, M.S., Ramamurthy, S., Kuthalingam, M.D.K., Dhulkhed, M.H., 1965. On an unusual swarming of the planktonic blue-green algae *Trichodesmium* spp., off Mangalore. Current Science, 34(3), 95–95.

Prasad, T.G., 2004. A comparison of mixed-layer dynamics between the Arabian Sea and Bay of Bengal: One-dimensional model results. J. of Geophy. Res.: Oceans, 109(C3).

Price, A.M., Gurdebeke, P.R., Mertens, K.N., Pospelova, V., 2016. Determining the absolute abundance of dinoflagellate cysts in recent marine sediments III: Identifying the source of Lycopodium loss during palynological processing and further testing of the Lycopodium marker-grain method. Rev. Palaeobot. Palynol. 226, 78-90.

Qian, S., Arnold, L.G., Martin, V., 2004. Spreading of the Indonesian Throughflow in the Indian Ocean. J. Phys. Oceanogr. 34 (4), pp. 772-792.

R core Team., 2020. R: A language and environment for statistical computing. R foundation for statistical computing, Vienna, Austria. https:// www.R- proje ct. org/

Radi, T., Bonnet, S., Cormier, M.A., de Vernal, A., Durantou, L., Faubert, E., Head, M.J., Henry, M., Pospelova, V., Rochon, A., 2013. Operational taxonomy and (paleo-) autecology of round, brown, spiny dinoflagellate cysts from the Quaternary of high northern latitudes. Mar. Micropaleontol. 98, 41–57.

Radi, T., de Vernal, A., 2004. Dinocyst distribution in surface sediments from the northeastern Pacific margin (40–60◦ N) in relation to hydrographic conditions, productivity and upwelling. Rev Palaeobot Palynol 128, 169–193.

Radi, T., de Vernal, A., 2008. Dinocysts as proxy of primary productivity in mid–high latitudes of the Northern Hemisphere. Mar. Micropaleontol. 68(1-2), 84-114.

Radi, T., Vernal, A. D., Peyron, O., 2001. Relationships between dinoflagellate cyst assemblages in surface sediment and hydrographic conditions in the Bering and Chukchi seas. Journal of Quaternary Science: Published for the Quaternary Research Association, 16(7), 667-680.

Ralph, P.J., Gademann, R., Larkum, A.W.D., Schreiber, U., 1999. In situ underwater measurements of photosynthetic activity of coral zooxanthellae and other reef-dwelling dinoflagellate endosymbionts. Marine Ecology Progress Series, 180, 139-147.

Ramanamurthy, V.D., Selvakumar, R.A., Bhargava, R.M.S., 1972. Studies on the blooms of *Trichodesmium erythraeum* (Ehr.) in the waters of the central west coast of India. Current Science, 41, 803–804.

Ramírez-Valencia, V., Paez-Reyes, M., Salgado, J., Sangiorgi, F., Zúñiga-González, A.C., Amézquita, A., Ibarra-Ávila, H., González-Arango, C., 2021. Distribution of organic-walled dinoflagellate cysts in surface sediments of the southern Caribbean and the eastern tropical Pacific and its environmental implications. Mar Micropaleontol 167, 102000.

Rasmussen, M.B., Henriksen, K., Jensen, A., 1983. Possible causes of temporal fluctuations in primary production of the microphytobenthos in the Danish Wadden Sea. Marine Biology, 73, 109-114.

Raven, J.A., 1989. Flight or flight: the economics of repair and avoidance of photoinhibition of photosynthesis. Functional Ecology, 5-19.

Raven, J.A., 1999. Picophytoplankton. Prog. Phycol. Res., 13, 33–106.

Raven, J.A., 2011. The cost of photoinhibition. Physiologia plantarum, 142(1), 87-104.

Redzuan, N.S., Underwood, G.J., 2021. The importance of weather and tides on the resuspension and deposition of microphytobenthos (MPB) on intertidal mudflats. Estuarine, Coastal and Shelf Science, 251, 107190.

Regaudie-de-Gioux, A., Lasternas, S., Agustí, S., Duarte, C.M., 2014. Comparing marine primary production estimates through different methods and development of conversion equations. Front. Mar. Sci., 1, 19.

Rekadwad, B.N., Khobragade, C.N., 2015. A case study on effects of oil spills and tar-ball pollution on beaches of Goa (India). Marine Pollution Bulletin, 100(1), 567-570.

Revelante, N., Gilmartin, M., 1995. The relative increase of large phytoplankton in subsurface chlorophyll maximum of the northern Adriatic Sea. J. Plankton Res., 17 (17), 1535-1562.

Reynolds, C.S., 1988. Functional morphology and the adaptive strategies of freshwater phytoplankton. Growth and reproductive strategies of freshwater phytoplankton, 388-433.

Reynolds, C.S., 1997. Vegetation processes in the pelagic: A model for ecosystem theory. Ecology Institute, Oldendorf Luhe, Germany, 371.

Reynolds, C.S., 2006. Ecology of Phytoplankton. Cambridge: Cambridge University Press.

Reynolds, C.S., 2007. Variability in the provision and function of mucilage in phytoplankton: facultative responses to the environment. Hydrobiol., 578(1), 37-45.

Reynolds, C.S., Huszar, V., Kruk, C., Naselli-Flores, L., Melo, S., 2002. Towards a functional classification of the freshwater phytoplankton. J. Plankton Res., 24(5), 417-428.

Ribeiro, L., Brotas, V., Rincé, Y., Jesus, B., 2013. Structure and diversity of intertidal benthic diatom assemblages in contrasting shores: a case study from the Tagus estuary1. Journal of Phycology, 49(2), 258-270.

Ribeiro, S., Amorim, A., Andersen, T.J., Abrantes, F., Ellegaard, M., 2012. Reconstructing the history of an invasion: the toxic phytoplankton species *Gymnodinium catenatum* in the Northeast Atlantic. Biol. Invasions. 5, 969–985.

Rice, E.L., 1984. Allelopathy. Academic Press, Orlando.

Richter, P.R., Häder, D.P., Gonçalves, R.J., Marcoval, M.A., Villafane, V.E., Helbling, E.W., 2007. Vertical migration and motility responses in three marine phytoplankton species exposed to solar radiation. Photochemistry and photobiology, 83(4), 810-817.

Rigel, C.Q., Javier, H., Ernesto, G.M., Rafael, R.M., 2022. Assemblages of dinoflagellate resistance cysts and copepod eggs in superficial sediments at the upper Gulf of California. Conti. Shelf. Res. 235, 104648.

Rishworth, G.M., Perissinotto, R., Miranda, N.A.F., Bornman, T.G., Steyn, P.P., 2017. phytoplankton community dynamics within peritidal pools associated with living Stromatolites at the freshwater–marine interface. Aquat. Sci. 79, 357–370.

Rochon, A., de Vernal, A., Turon, J.L., Matthiessen, J. Head, M.J., 1999. Distribution of recent dinoflagellate cysts in surface sediments from the North Atlantic Ocean and adjacent seas in relation to sea-surface parameters. American Association of Stratigraphic Palynologists Foundation, Contribution series 35, Dallas, TX, pp. 152.

Rodrigues, C., 1984. Community structure of intertidal fauna at Dona Paula beach (Goa, India). PhD thesis, University of Poona, Poona.

Rodrigues, R.V., Patil, J.S., 2021. Salinity changes may influence dinoflagellate cyst morphometry: data from monsoon-influenced tropical coastal ecosystems. J. Plankton. Res. 43(6), 853-864.

Rodrigues, R.V., Patil, J.S., Anil, A.C., 2022. Dinoflagellates cyst assemblage concerning trophic index for eutrophication from major ports along the west coast of India. Mar. Pol. Bull. 176, 113423.

Rodrigues, R.V., Patil, J.S., Sathish, K., Anil, A.C., 2019. Dinoflagellate planktonic-motile-stage and benthic-cyst assemblages from a monsoon-influenced tropical harbour: elucidating the role of environmental conditions. Estuar. Coast. Shelf Sci. 226, 106253.

Roselli, L., Basset, A., 2015. Decoding size distribution patterns in marine and transitional water phytoplankton: From community to species level. PLoS ONE, 10(5), e0127193.

Ross, O.N., Sharples, J., 2007. Phytoplankton motility and the competition for nutrients in the thermocline. Mar. Ecol. Prog. Ser., 347, 21–38.

Roy, R., Chitari, R., Kulkarni, V., Krishna, M.S., Sarma, V.V.S.S., Anil, A.C., 2015. CHEMTAX-derived phytoplankton community structure associated with temperature fronts in the northeastern Arabian Sea. Journal of Marine Systems, 144, 81–91.

Roy, S., 2000. Strategies for the minimization of UV-induced damage. In: De Mora SJ, Demers S, Vernet M (eds) The effects of UV radiation in the marine environment. Cambridge University Press, Cambridge, pp 177–205.

Ruban, A.V., Lavaud, J., Rousseau, B., Guglielmi, G., Horton, P., Etienne, A.L., 2004. The super-excess energy dissipation in diatom algae: comparative analysis with higher plants. Photosynth. Res. 82:165–75.

Ryabov, A., Kerimoglu, O., Litchman, E., Olenina, I., Roselli, L., Basset, A., Stanca, E., Blasius, B., 2021. Shape matters: the relationship between cell geometry and diversity in phytoplankton. Ecol. Lett., 24, 847–861.

Salmaso, N., Naselli-Flores, L., Padisak, J., 2015. Functional classifications and their application in phytoplankton ecology. Freshwater Biology, 60(4), 603-619.

Salmaso, N., Padisak, J., 2007. Morpho-functional groups and phytoplankton development in two deep lakes (Lake Garda, Italy and Lake Stechlin, Germany). Hydrobiol., 578, 97–112.

Sanilkumar, M.G., Saramma, A.V., Joseph, K.J., 2009. Vertical distribution of microphytobenthos in Cochin estuary. Journal of the Marine Biological Association of India, 51(1), 61-68.

Sarma, V., Krishna, M., Viswanadham, R., Rao, G., Rao, V., Sridevi, B., Kumar, B., Prasad, V., Subbaiah, C.V., Acharyya, T., 2013. Intensified oxygen minimum zone on the western shelf of Bay of Bengal during summer monsoon: influence of river discharge. J. of Oceanogra. 69(1):45–55.

Sarma, V.V., Aswanikumar, V., 1991. Subsurface chlorophyll maxima in the north-western Bay of Bengal. J. plankton Res., 13(2), 339-352.

Sarma, V.V.S.S., Desai, D.V., Patil, J.S., Khandeparker, L., Aparna, S.G., Shankar, D., D'Souza, S., Dalabehera, H.B., Mukherjee, J., Sudharani, P., Anil, A.C., 2018. Ecosystem response in temperature fronts in the northeastern Arabian Sea. Progress in Oceanography, 165, 317–331.

Sarma, V.V.S.S., Dileep Kumar, M., Saino, T., 2007. Impact of sinking carbon flux on accumulation of deep-ocean carbon in the Northern Indian Ocean. Biogeochem. 82, 89-100.

Sarma, V.V.S.S., Patil, J.S., Shankar, D., Anil, A.C., 2019. Shallow convective mixing promotes massive *Noctiluca scintillans* bloom in the northeastern Arabian Sea. Marine Pollution Bulletin, 138, 428–436.

Sarma, V.V.S.S., Prasad, M.H.K., Dalabehera, H.B., 2021. Influence of phytoplankton pigment composition and primary production on pCO2 levels in the Indian Ocean. J. Earth Syst. Sci., 130:85.

Sarmiento, J.L., Slater, R., Barber, R., Bopp, L., Doney, S.C., Hirst, A.C., Kleypas, J., Matear, R., Mikolajewicz, U., Monfray, P., Soldatov, V., 2004. Response of ocean ecosystems to climate warming. Global Biogeochemical Cycles, 18(3).

Sasmito, S.D., Kuzyakov, Y., Lubis, A.A., Murdiyarso, D., Hutley, L.B., Bachri, S., Friess, D.A., Martius, C., Borchard, N., 2020. Organic carbon burial and sources in soils of coastal mudflat and mangrove ecosystems. Catena, 187, 104414.

Sawant, S., Madhupratap, M., 1996. Seasonality and composition of phytoplankton in the Arabian Sea. Current Science, 71, 11.

Schlitzer, R., 2015. Data analysis and visualization with Ocean Data View. CMOS Bulletin SCMO, 43(1), 9-13.

Schott, F.A., McCreary Jr., J.P., 2001. The monsoon circulation of the Indian Ocean. Prog. Oceanogr. 51 (1), 1–123.

Seelam, J.K., Yadhunath, E.M., Jishad, M., Gowthaman, R., Rajasekaran, C., Pednekar, P.S., 2014. Post-monsoon equilibrium beach profiles and longshore sediment transport rates at Candolim, Miramar and Keri beaches of Goa, India. Current Science, pp.408-416.

Segura, A.M., Kruk, C., Calliari, D., Fort, H., 2013. Use of a morphology-based functional approach to model phytoplankton community succession in a shallow subtropical lake. Freshwater Biology, 58(3), 504–512.

Shah, H.M., Smitha, B.R., Mohammad Hatha, A.A., Sudhakar, M., 2020. Subsurface chlorophyll maxima in the North Eastern Arabian Sea: Simulation on impact of warming. Ecol. Indic., 110, 105858.

Shankar, D., Vinayachandran, P., Unnikrishnan, A., 2002. The monsoon currents in the north Indian Ocean. Progress in Oceanography, 52, 63–120.

Shenoi, S., Shankar, D., Shetye, S., 2002. Differences in heat budgets of the near-surface Arabian Sea and Bay of Bengal: Implications for the summer monsoon. Journal of Geophysical Research: Oceans, 107, 1–14.

Shin, H.H., Yoon, Y.H., Kim, Y.O., Matsuoka, K., 2011. Dinoflagellate cysts in surface sediments from southern coast of Korea. Estuaries and Coasts, 34, 712-725.

Shulenberger, E., Reid, J.L., 1981. The Pacific shallow oxygen maximum, deep chlorophyll maximum, and primary productivity, reconsidered. Deep-Sea Res. Part A: Oceanographic Research Papers, 28(9), 901-919.

Simberlof, D., Dayan, T., 1991. The guild concept and the structure of ecological communities. Annu. Rev. Ecol. Syst., 22, 115–143.

Six, C., Finkel, Z.V., Irwin, A.J., Campbell, D.A., 2007. Light variability illuminates niche-partitioning among marine picocyanobacteria. PLoS One, 2(12), e1341.

Skinner, T., Adams, J.B., Gama, P.T., 2006. The effect of mouth opening on the biomass and community structure of microphytobenthos in a small oligotrophic estuary. Estuarine, Coastal and Shelf Science, 70(1-2), 161-168.

Smayda, T.J., 1970. The suspension and sinking of phytoplankton in the Sea. Oceanography and Marine Biology, An Annu. Rev., 8, 353–414.

Smayda, T.J., Boleyn, B.J., 1966. Experimental observations on the flotation of marine diatoms. II. *Skeletonema costatum* and *Rhizosolenia setigera*. Limnology and Oceanography, 11(1), 18–34.

Soininen, J., Meier, S., 2014. Phytoplankton richness is related to nutrient availability, not to pool size, in a subarctic rock pool system. Hydrobiol. 70, 137-145.

Solbrig, O.T., 1993. Plant traits and adaptive strategies: their role in ecosystem function. In Schulze, E. D. & H. A. Mooney (eds), Biodiversity and Ecosystem Function. Ecological Studies. Springer-Verlag, Berlin: 97–116.

Sommer, U., 1998. Silicate and the functional geometry of marine phytoplankton. J. of Plank. Res. 20, 1853–1859.

Sonneman, J.A., Hill, D.R.A., 1997. A taxonomic survey of cyst-producing dinoflagellates from recent sediments of Victorian coastal waters Australia. Bot. Mar. 40 (1–6), 149–178.

Stal, L.J., 2003. Microphytobenthos, their extracellular polymeric substances, and the morphogenesis of intertidal sediments. Geomicrobiology Journal, 20(5), 463-478.

Stanca, E., Cellamare, M. Basset, A., 2013. Geometric shape as a trait to study phytoplankton distributions in aquatic ecosystems. Hydrobiol., 701, 99–116.

Strzepek, F.R., Harrison, J.P., 2004. Photosynthetic architecture differs in coastal and oceanic diatoms. Nature, 431.

Suggett, D.J., Moore, C.M., Hickman, A.E., Geider, R.J., 2009. Interpretation of fast repetition rate (FRR) fluorescence: signatures of phytoplankton community structure versus physiological state. Marine Ecology Progress Series, 376, 1-19.

Suggett, D.J., Moore, C.M., Marañón, E., Omachi, C., Varela, R.A., Aiken, J., Holligan, P.M., 2006. Photosynthetic electron turnover in the tropical and subtropical Atlantic Ocean. Deep Sea Research Part II: Topical Studies in Oceanography, 53(14-16), 1573-1592.

Suikkanen, S., Fistaro, G.O., Granéli, E., 2005. Effects of cyanobacterial allelochemicals on a natural plankton community. Mar. Ecol. Prog. Ser. 287, 1–9.

Sun, J., Liu, D., 2003. Geometric models for calculating cell biovolume and surface area for phytoplankton. J. Plankton Res. 25(11), 1331–134.

Sunda, W.G., Hardison, D.R., 2010. Evolutionary tradeoffs among nutrient acquisition, cell size, and grazing defense in marine phytoplankton promote ecosystem stability. Mar. Ecol. Prog. Ser., 401,63–76.DOI:

Syvitski, J.P., Kettner, A.J., Overeem, I., Hutton, E.W., Hannon, M.T., Brakenridge, G.R., Day, J., Vörösmarty, C., Saito, Y., Giosan, L. Nicholls, R.J., 2009. Sinking deltas due to human activities. Nature Geoscience, 2(10), 681-686.

Syvitski, J.P., Vörösmarty, C.J., Kettner, A.J., Green, P., 2005. Impact of humans on the flux of terrestrial sediment to the global coastal ocean. science, 308(5720), 376-380.

Taylor, F.J.R., 1973. General features of dinoflagellate material collected by the "Anton Bruun" during the International Indian Ocean Expedition. The biology of the Indian Ocean (pp. 155–169). Springer.

Taylor, F.J.R., 1987. Ecology of dinoflagellates: general and marine ecosystems. In Taylor, F. J. R. [Ed.] The Biology of Dinoflagellates. Botanical Monographs 21, Blackwell Scientific Publications, Oxford, pp. 398–502.

Ter Braak, C.J., Smilauer, P., 2002. CANOCO reference manual and CanoDraw for Windows user's guide: software for canonical community ordination (version 4.5). www.canoco.com.

Therriault, T.W., Kolasa, J., 2001. Desiccation frequency reduces species diversity and predictability of community structure in coastal rock pools. Israel J. of Zoo. 47, (4) 477-489.

Thingstad, T.F., Krom, M.D., Mantoura, R.F.C., Flaten, G.F., Groom, S., Herut, B., Kress, N., Law, C.S., Pasternak, A., Pitta, P., Psarra, S., 2005. Nature of phosphorus limitation in the ultraoligotrophic eastern Mediterranean. Science, 309(5737), 1068–1071.

Throndsen, J., 1978. The dilution-culture method. In: Sournia A (ed) Phytoplankton manual. Museum National d'Histoire Naturelle, Paris, 218-224.

Tilman, D., Kilham, S.S., Kilham, P., 1982. Phytoplankton community ecology: the role of limiting nutrients. Annu. Rev. Ecol. Syst., 13(1), 349-372.

Tomas, C.R. (Ed.). 1997. Identifying marine phytoplankton. Academic Press.

Ubertini, M., Lefebvre, S., Gangnery, A., Grangeré, K., Le Gendre, R., Orvain, F., 2012. Spatial variability of benthic-pelagic coupling in an estuary ecosystem: consequences for microphytobenthos resuspension phenomenon. PLoS ONE 7(8): e44155.

Uddandam, P., Prasad, V., Rai, J., Joshi, H., 2015. A study of the distribution pattern of dinoflagellate cysts from the Bay of Bengal. Journal of the Palaeontological Society of India, 60(2), 11-19.

Uddandam, P.R., Prasad, V., Manoj, M.C., 2020. New dinoflagellate cysts from the recent sediments of northern Indian Ocean. Journal of the Palaeontological Society of India, 65(1), 15-26.

Uddandam, P.R., Prasad, V., Rai, J., 2017. Dinoflagellate cyst distribution in sediments of western Bay of Bengal: Role of sea surface conditions. Palaeogeogr. Palaeoclimatol. Palaeoecol. 483, 31-48.

Underwood, A.J., Skilleter, G.A., 1996. Effects of patch size on the structure of assemblages in rock pools J. Exp. Mar. Biol. Ecol. 197, 63–90.

Underwood, G.J.C., Kromkamp, J., 1999. Primary production by phytoplankton and microphytobenthos in estuaries. Adv Ecol Res 29:93−153.

Van De Poll, W.H., Alderkamp, A.C., Janknegt, P.J., Roggeveld, J., Buma, A.G., 2006. Photoacclimation modulates excessive photosynthetically active and ultraviolet radiation effects in a temperate and an Antarctic marine diatom. Limnology and Oceanography, 51(3), 1239-1248.

Van De Poll, W.H., Buma, A.G., Visser, R.J., Janknegt, P.J., Villafañe, V.E., Helbling, E.W., 2010. Xanthophyll cycle activity and photosynthesis of *Dunaliella tertiolecta* (Chlorophyceae) and *Thalassiosira weissflogii* (Bacillariophyceae) during fluctuating solar radiation. Phycologia, 49(3), 249-259.

Van De Poll, W.H., Van Leeuwe, M.A., Roggeveld, J., Buma, A.G., 2005. Nutrient limitation and high irradiance acclimation reduce PAR and UV-induced viability loss in the antarctic diatom *Chaetoceros brevis* (bacillariophyceae) 1. Journal of Phycology, 41(4), 840-850.

Van der Grinten, E., Simis, S., Barranguet, C., Admiraal, W., 2004. Dominance of diatoms over cyanobacterial species in nitrogen-limited biofilms. Archiv fur Hydrobiologie 161 (1), 98–111.

Van Heukelem, L., 2002. HPLC phytoplankton pigments: sampling, laboratory methods, and quality assurance procedures. In: Mueller J, Fargion G (eds) Ocean optics protocols for satellite ocean color sensor, Revision 3, volume 2, Chap. 16, NASA Technical Memorandum 2002–2004, vol. 2, pp 258–268

Vassiliev, I.R., Prasil, O., Wyman, K.D., Kolber, Z., Hanson, A.K., Prentice, J.E., Falkowski, P.G., 1994. Inhibition of PSII photochemistry by PAR and UV radiation in natural phytoplankton communities. Photosynth Res 42:51–64.

Verleye, T.J., Mertens, K.N., Young, M.D., Dale, B., McMinn, A., Scott, L., Zonneveld, K.A., Louwye, S., 2012. Average process length variation of the marine dinoflagellate cyst *Operculodinium centrocarpum* in the tropical and Southern Hemisphere Oceans: assessing its potential as a palaeosalinity proxy. Mar. Micropaleontol. 86, pp.45-58.

Vijayan, A.K., Reddy, B.B., Sudheesh, V., Marathe, P.H., Nampoothiri, V.N., Harikrishnachari, N.V., Kavya, P., Gupta, G.V.M., Ramanamurthy, M.V., 2021. Phytoplankton community structure in a contrasting physicochemical regime along the eastern Arabian Sea during the winter monsoon. Journal of Marine Systems, 215, 103501.

Villafañe, V.E., Janknegt, P.J., de Graaff, M., Visser, R.J., van de Poll, W.H., Buma, A.G., Walter Helbling, E., 2008. UVR-induced photoinhibition of summer marine phytoplankton communities from Patagonia. Marine Biology, 154, 1021-1029.

Vipin, P., Sarkar, K., Aparna, S.G., Shankar, D., Sarma, V.V.S.S., Gracias, D.G., Krishna, M.S., Srikanth, G., Mandal, R., Rama Rao, E.P., Rao, S.N., 2015. Evolution and subsurface characteristics of a sea-surface temperature filament and front in the

northeastern Arabian Sea during November–December 2012. Journal of Marine Systems, 150, 1–11.

Wall, D., Dale, B., 1968. Modern dinoflagellate cysts and evolution of the peridiniales. Micropaleontol. 14 (3), 265–304.

Wall, D., Dale, B., Harada, K., 1973. Descriptions of new fossil dinoflagellates from the Late Quaternary of the Black Sea. Micropaleontol. 18-31.

Wang, Z., Matsuoka, K., Qi, Y., Chen, J., Lu, S., 2004. Dinoflagellate cyst records in recent sediments from Daya Bay, South China Sea. Phycological Research, 52(4), 396-407.

Weithoff, G., 2003. The concepts of 'plant functional types' and 'functional diversity' in lake phytoplankton – a new understanding of phytoplankton ecology? Freshwat. Biol., 48, 1669–1675.

Weithoff, G., Beisner, B.E., 2019. Measures and approaches in trait-based phytoplankton community ecology–From freshwater to marine ecosystems. Front. Mar. Sci., 6, 40.

Weithoff, G., Gaedke, U., 2017. Mean functional traits of lake phytoplankton reflect seasonal and inter-annual changes in nutrients, climate and herbivory. Journal of Plankton Research, 39, 509–517.

Welbara, D.E., Gebre-Meskel, D.K., Hailu, T.F., 2024. Morpho-functional traits of phytoplankton functional groups: a review. Biologia, 79(7), 1983-1998.

Weller, R.A., Fischer, A.S., Rudnick, D.L., Eriksen, C.C., Dickey, T.D., Marra, J., Fox, C., Leben, R., 2002. Moored observations of upper-ocean response to the monsoons in the Arabian Sea during 1994–1995. Deep Sea Research Part II: Topical Studies in Oceanography, 49(12), 2195–2230.

Wendler, I., Zonneveld, K.A., Willems, H., 2002. Oxygen availability effects on early diagenetic calcite dissolution in the Arabian Sea as inferred from calcareous dinoflagellate cysts. Glob. Planet. Change, 34(3-4), 219-239.

West-Eberhard, M.J., 1989. Phenotypic plasticity and the origins of diversity. Annu. Rev. Ecol. Syst., 20: 249–278.

Wiggert, J.D., Hood, R.R., Banse, K., Kindle, J.C., 2005. Monsoon-driven biogeochemical processes in the Arabian Sea. Progress in Oceanography, 65(2–4), 176–213.

Williams, O.J., Beckett, R.E., Maxwell, D.L., 2016. Marine phytoplankton preservation with Lugol's: A comparison of solutions. Journal of Applied Phycology, 28(3), 1705–1712.

Wilson, L.A.B., 2013. Allometric disparity in rodent evolution. Ecol. Evol., 3, 971–984.

Wirtz, K.W., 2011. Non-uniform scaling in phytoplankton growth rate due to intracellular light and CO2 decline. J. Plankton Res., 33, 1325–1341.

Woelfel, J., Schumann, R., Adler, S., Hübener, T., Karsten, U., 2007. Diatoms inhabiting a wind flat of the Baltic Sea: species diversity and seasonal succession. Estuarine, Coastal and Shelf Science, 75(3), 296-307.

Wolfstein, K., Colijn, F., Doerffer, R., 2000. Seasonal dynamics of microphytobenthos biomass and photosynthetic characteristics in the northern German Wadden Sea, obtained by the photosynthetic light dispensation system. Estuarine, Coastal and Shelf Science, 51(5), 651-662.

Xiao, L.J., Wang, T., Hu, R., Han, B.P., Wang, S., Qian, X., Padisák, J., 2011. Succession of phytoplankton functional groups regulated by monsoonal hydrology in a large canyon-shaped reservoir. Water Res., 45(16), 5099-5109.

Xiaoqing, J.I., Xiaotian, H., Baijuan, Y., Zhiming, Y., 2012. Analysis on allelochemicals in the cell-free Filtrates of *Amphidinium carterae.* Acta Ecologica Sinica 32(6) 1745–1754.

Yamochi, S., 1989. Distribution of benthic cells of *Skeletonema costatum* and *Heterosigma akashiwo* in Osaka Bay. Bull Plankton Soc Jpn 36:47-51.

Yasunaka, S., Ono, T., Sasaoka, K., Sato, K., 2022. Global distribution and variability of subsurface chlorophyll a concentration. Ocean Sci., 18(1), 255–268.

Zhuang, Y., Jin, H., Chen, J., Ren, J., Zhang, Y., Lan, M., Zhang, T., He, J., Tian, J., 2020. Phytoplankton community structure at subsurface chlorophyll maxima on the western Arctic shelf: patterns, causes, and ecological importance. J. Geophy. Res.: Biogeosciences, 125(6), e2019JG005570.

Zohary, T., Padisák, J., Naselli-Flores, L., 2010. Phytoplankton in the physical environment: beyond nutrients, at the end, there is some light. Hydrobiol, 639, 261-269.

Zonneveld, K.A.F., 1997a. Dinoflagellate cyst distribution in surface sediments from the Arabian Sea (northwestern Indian Ocean) in relation to temperature and salinity gradients in the upper water column. Deep-Sea Res II 44, 1411–1443.

Zonneveld, K.A.F., Brummer, G.J.A., 2000. (Palaeo-)ecological significance, transport and preservation of organic-walled dinoflagellate cysts in the Somali Basin, NW Arabian Sea. Deep-Sea Res. II: Top. Stud. Oceanogra. 47, 2229–2256.

Zonneveld, K.A.F., Jurkschat, T., 1999. Bitectatodinium spongium (Zonneveld, 1997) Zonneveld et Jurkschat, comb. nov. from modern sediments and sediment trap samples of the Arabian Sea (northwestern Indian Ocean): taxonomy and ecological affinity. Rev. Palaeobot. and Palynol. 106(3-4), 153-169.

Zonneveld, K.A.F., Marret, F., Versteegh, G.J.M., Bogus, K., Bonnet, S., Bouimetarhan, I., Crouch, E., de Vernal, A., Elshanawany, R., Edwards, L., Esper, O., Forke, S., Grøsfjeld, K., Henry, M., Holzwarth, U., Kielt, J., Kim, S., Ladouceur, S., Ledu, D., Chen, L., Limoges, A., Londeix, L., Lu, S., Mahmoud, M.S., Marino, G., Matsouka, K., Matthiessen, J., Mildenhal, D.C., Mudie, P., Neil, H.L., Pospelova, V., Qi, Y., Radi, T., Richerol, T., Rochon, A., Sangiorgi, F., Solignac, S., Turon, J., Verleye, T., Wang, Y., Wang, Z., Young, M., 2013. Atlas of modern dinoflagellate cyst distribution based on 2405 data points. Rev Palaeobot Palynol 191, 1–197.

Zonneveld, K.A.F., Sebastian Meier, K.J., Esper, O., Siggelkow, D., Wendler, I., Willems, H., 2005. The (palaeo) environmental significance of modern calcareous dinoflagellate cysts: a review. Paläontologische Zeitschrift, 79, 61-77. https://doi.org/10.1007/BF03021754.

Zonneveld, K.A.F., Susek, E., Fischer, G., 2010. Seasonal variability of the organic-walled dinoflagellate cyst production in the coastal upwelling region off Cape Blanc (Mauritania): a five-year survey. J Phycol 46, 202–215.

Zonneveld, K.A.F., Versteegh, G., Kodrans-Nsiah, M., 2008. Preservation and organic chemistry of Late Cenozoic organic-walled dinoflagellate cysts: a review. Mar Micropaleontol 68(1-2), 179-197.

Zonneveld, K.A.F., Versteegh, G.J., de Lange, G.J., 1997. Preservation of organic-walled dinoflagellate cysts in different oxygen regimes: a 10,000 year natural experiment. Mar. micropaleontol. 29(3-4), 393-405.

Zonneveld, K.A.F., Grotheer, H., Versteegh, G.J.M., 2022. Dinoflagellate cysts production, excystment and transport in the upwelling off Cape Blanc (NW Africa). Front. Mar. Sci. 9:915755.

Publications

List of publications

Paul P., Patil, J.S. & Anil, A.C. Phytoplankton communities in marine intertidal rock pools: effect of location, geometric shapes, and allelopathy. *Journal of Earth System Science* 130, 128 (2021).

Paul, P., Patil, J. S., & Anil, A. C. Variability in phytoplankton shape dominance in marine pelagic systems: prevalence of different adaptive strategies in the eastern Arabian Sea during the winter monsoon. *Environmental Monitoring and Assessment*, 195(4), 528 (2023).

Paul, P., & Patil, J. S. Geographic distribution of modern dinoflagellate cysts in surface sediments of the Arabian Sea: significance of taxa and morphometry as potential ecological indicators. *Environmental Science and Pollution Research*, 31(44), 56253-56271 (2024).

Paul, P., & Patil, J. S. Delineating morphological traits of oceanic micro-phytoplankton as potential ecological indicators. *Marine Pollution Bulletin*, 208, 116952 (2024).

Conferences presentation

Paul, P., Patil, J.S. & Anil, A.C. Phytoplankton distribution in intertidal rock pools: the importance of location, environmental variables, and allelopathy. International Symposium on Advances in Coastal Research with Special Reference to Indo-Pacific-2019 (oral presentation).

Paul, P., Patil, J.S. & Anil, A.C. Morphological and taxonomic diversity of micro-phytoplankton from the south-eastern Arabian Sea during 2020 winter monsoon: elucidation from surface and sub-surface chlorophyll maximum layers. 7th National Conference of the Ocean Society of India (poster + flash presentation).

Paul, P. & Patil, J.S. Micro-phytoplankton communities from contrasting oceanographic conditions in the eastern Arabian Sea during the winter monsoon. International Indian Ocean Science Conference (poster presentation).

Paul, P. & Patil, J.S. Distribution of modern dinoflagellate cysts in surface sediment from central and South-eastern Arabian Sea. 8th National Conference of the Ocean Society of India (poster presentation).

Paul, P. & Patil, J.S. Dinoflagellate cysts assemblages in surface sediment from the deeper depths of the Indian Ocean, first scholar's meet Samudramanthan (poster + flash presentation).

Paul, P. & Patil, J.S. Delineating micro-phytoplankton morphometry as potential ecological indicators in the Indian Ocean: elucidation from sea surface and variable sub-surface chlorophyll maxima. World Ocean Science Congress (poster + flash presentation).

Marine Pollution Bulletin 208 (2024) 116952



Contents lists available at ScienceDirect

Marine Pollution Bulletin

journal homepage: www.elsevier.com/locate/marpolbul



Delineating morphological traits of oceanic micro-phytoplankton as potential ecological indicators

Pranoy Paul [a,b], Jagadish S. Patil [a,*]

[a] CSIR-National Institute of Oceanography, Dona Paula 403004, Goa, India
[b] School of Earth, Ocean and Atmospheric Sciences, Goa University, Taleigao Plateau 403 206, Goa, India

ARTICLE INFO

Keywords:
Ocean
Phytoplankton geometric shape
Morphological trait
Sub-surface chlorophyll maximum
Sea surface
Surface to volume ratio
Greatest axial linear dimension

ABSTRACT

The micro-phytoplankton (>20 μm) adaptations and resilience were assessed using morphological traits (shape, surface-to-volume ratio; S:V, and greatest-axial-linear-dimension; GALD) from sea-surface and different SCML-depths (shallow:20-50 m, intermediate:50-100 m, and deep:100-140 m) across different bioregions of Indian Ocean. The dominant simple elongated phytoplankton-geometric-shapes (PGSs) and morphological traits showed distinct north-south distribution and varied with light and nutrient availability. Further, SCML and corresponding sea-surface PGS will be similar or dissimilar if the former is located within or deeper than mixed-layer depth. Also, simple and complex PGS contribution gradually decreases and increases with increasing depth. Additionally, shallow SCML-PGS showed low-S:V and high-GALD while vice-versa for intermediate/deep SCML-PGS due to phenotypic plasticity behavior. Overall, only simple-PGS (cylinder, elliptic-prism, and prism-on-parallelogram) showed strong adaptive behavior through phenotypic plasticity and were highlighted as potential ecological tracers to address ecological impact of oceanographic processes (including coastal eutrophication, and aerosol deposition) linked to nutrient and light availability in predicted ocean change scenarios.

1. Introduction

Phytoplankton, which contributes to almost half of the global primary production (Smayda, 1970), are adapted to live in suspension in turbulent water masses and fluctuating light and nutrient regimes in various water bodies (Reynolds, 2006). Even though many indispensable resources can limit phytoplankton growth, nutrient availability (N, P, and Si) and light are the main drivers (Tilman et al., 1982). Other factors like grazing and parasitic infections are important loss processes (Kagami et al., 2007). Various morphological and physiological specializations developed in phytoplankton species have helped them adapt to their environment (Reynolds, 2007). The phytoplankton size and shape expressed by greatest axial linear dimension (GALD) and surface-to-volume ratio (S:V) reflect their ability to obtain nutrients, light, resist sinking, and reduce grazing pressure (Lewis, 1976; Naselli-Flores et al., 2007). Therefore, morphological traits are directly related to phytoplankton's life strategies (Irwin et al., 2006) and are readily used to describe and identify functional groups and trait-based studies (Reynolds et al., 2002; Padisak et al., 2009). In recent decades, the application of morphometric traits to explain and understand phytoplankton community distribution is well-explored in freshwater (Margalef, 1978; Reynolds, 1988; Weithoff, 2003; Salmaso and Padisak, 2007; Litchman and Klausmeier, 2008; Kruk et al., 2010; Naselli-Flores and Barone, 2011), estuarine (O'Farrell et al., 2007; Kruk et al., 2015) and marine (Litchman et al., 2007, 2015; Finkel et al., 2010; Stanca et al., 2013; Barton et al., 2013; Paul et al., 2021, 2023) ecosystems. In trait-based studies, taxonomically distinct species are grouped based on their similar adaptive traits (Simberlof and Dayan, 1991). Morphological traits (i.e., cell shape and size) affect various aspects of phytoplankton survival like grazing by zooplankton (Sunda and Hardison, 2010; Pancic and Kiørboe, 2018; Petrucciani et al., 2022), diffusion and sinking (Padisak et al., 2003; Durante et al., 2019), growth rates (Wirtz, 2011), nutrient uptake (Grover, 1989; Karp-Boss and Boss, 2016) and light harvesting (Naselli-Flores and Barone, 2007, 2011). The key phytoplankton traits (cell size and shape) are controlled by environmental conditions (like nutrients, light, temperature, species interactions, and grazers), making shape and size crucial determinants of fitness (Naselli-Flores et al., 2007; Zohary et al., 2010; Stanca et al., 2013; Leonilde et al., 2017). The effect of nutrients and grazing on phytoplankton morphological attributes (like shape, size, S:V, and GALD) are investigated in various reservoirs (Naselli-Flores and Barone, 2007; Xiao et al., 2011; Butts et al., 2022). There are few studies on

* Corresponding author.
E-mail address: patilj@nio.res.in (J.S. Patil).

https://doi.org/10.1016/j.marpolbul.2024.116952
Received 24 July 2024; Received in revised form 4 September 2024; Accepted 4 September 2024
Available online 30 September 2024
0025-326X/© 2024 Elsevier Ltd. All rights are reserved, including those for text and data mining, AI training, and similar technologies.

shape variability from marine systems (Paul et al., 2021; Paul et al., 2023), but specific studies on morphological attributes considering SCML from a vast marine pelagic system, particularly the Indian Ocean (IO), are scarce.

The IO's unique geographical, physical, and meteorological features distinguish it from the world's two major oceans, i.e., Pacific and Atlantic. The tropical IO encompasses the northern IO (Arabian Sea and Bay of Bengal on the west and east, respectively), equatorial IO from 4°N-4°S, and southern tropical IO up to 30°S. Among them, northern IO is surrounded by Asian land masses and is profoundly influenced by seasonal monsoonal forcing, weak equatorial upwelling, and significant freshwater influx from major rivers (Schott and McCreary Jr., 2001). The IO is the smallest oceanic basin and plays important roles in the global ocean, i.e., the transport of heat, salt, carbon, and about 15–20 % of global primary production (Behrenfield and Falkowski, 1997; Regaudie-de-Gioux et al., 2014). The existence of an upper low-chlorophyll, a nutrient-depleted mixed layer where productivity is limited (Dugdale and Goering, 1967), followed by a light-limited, nutricline-associated with elevated chlorophyll known as subsurface chlorophyll maximum layer (SCML) is common in stratified waters (Herbland and Voituriez, 1979; Cullen, 1982). According to Cullen (2015), SCMLs are the local chlorophyll-maxima, formed in layers and maintained by ecological interactions like autecological processes (growth, photosynthetic acclimation, and sinking or swimming of phytoplankton) and grazing control that modulates phytoplankton concentrations over days to weeks. The primary production at sea surface can also be limited due to photoinhibition (Kirk, 1994). Consequently, phytoplankton accumulation occurs at distinct water depths, which do not necessarily correspond to the maximum in either irradiance or nutrient concentration (Cullen, 1982), forming SCML. SCML is a ubiquitous ocean feature in tropical (Shah et al., 2020), subtropical (Mignot et al., 2014), and polar regions (McLaughlin and Carmack, 2010; Baldry et al., 2020). However, SCML depth varies globally, forming at depths >80 m in the subtropical and tropical (30°S to 30°N), 40–80 m in the tropics, Southern Ocean (south of 40°S), and < 40 m in the northern subarctic (north of 40°N) (Yasunaka et al., 2022). The existence of such biological feature and its significant contribution to the column primary production has already been reported in the IO (Shulenberger and Reid, 1981; Sarma and Aswanikumar, 1991; Revelante and Gilmartin, 1995; Goldman and McGillicuddy, 2003; Hanson et al., 2007; Shah et al., 2020; Jayaram et al., 2021; Garg et al., 2024). The SCML is greatly influenced by the prevailing physical processes, mixing, stratification, and phytoplankton groups (Fu et al., 2018; Shah et al., 2020). Though most of these studies have focused on the formation and maintenance of SCML, either satellite-based (Shah et al., 2020) or argo-float-based (Jayaram et al., 2021) data, the community-based studies are lacking (Sarma et al., 2021). A recent study based on the HPLC-based phytoplankton pigment data from the northern IO reported that micro-phytoplankton are the major contributors to increasing Chl_{max} (Garg et al., 2024). However, an integrated taxonomic and morphological trait-based (shape, size, S:V and GALD) study of micro-phytoplankton community from sea surface and SCML within different geographic regions of the IO and at various SCML depths (20–140 m) is not available. Therefore, the present study focuses on the applicability of oceanic micro-phytoplankton morphological traits to infer if forms can be related to ecological functions/changes, how traits vary in different sub-chlorophyll maximum layer depths, and their usefulness as tracers in changing oceanic ecosystems. As oceans are vulnerable to climate change, phytoplankton adaptive capabilities from ecological and global change perspectives are becoming vital.

2. Materials and methods

2.1. Study area and sampling strategies

The observations were made during two cruises onboard *R/V Sindhu Sadhana* in the Southeastern and oxygen minimum zone (OMZ) of the Arabian Sea (AS) (SSD069; 12 January-11 February 2020), Bay of Bengal (BoB) and North and South Equatorial Indian Ocean up to 30°S (NEIO, SEIO and STIO) in a three-month long cruise (SSD079; 14 March-5 June 2021) (Fig. 1; Table 1). The water samples were collected at 38 stations (AS-14, BoB-4, NEIO-3, SEIO-6, and STIO-11) from the sea surface and sub-surface chlorophyll maximum layers (SCML) with 10 L Niskin bottles attached to 32 Carousel Water Sampler (Sea-bird Electronics Inc.; SBE), which is operated with SBE 911 plus CTD equipped with sensors such as temperature (SBE 3 plus SN5552; ±0.001 °C), conductivity (SBE 4 SN4088; ±0.0003 S m^{-1}), dissolved oxygen (SBE 43SN2288; ±2 % of saturation), transmissometer (WET Labs C-star), fluorometer (Seapoint Sensors; 0.02 μg L^{-1}) and surface PAR (LI-COR Biospherical; μmol photons m^{-2} s^{-1}) for real-time data acquisition.

2.2. Micro-phytoplankton collection

The collected 5 L water samples from the sea surface and SCML were passed through a 20 μm mesh, concentrated to 100 mL, and preserved with 4 % acidic Lugol's iodine for further analysis. A known aliquot (2–5 mL) of sample volume was analyzed in duplicates using an inverted microscope (IX73 Olympus Make) at 200-400× to assess micro-phytoplankton composition and abundance. Microalgal identification was performed using standard identification keys (Tomas, 1997; Taylor, 1973).

The morphological measurements such as length, width, breadth, area, volume, surface-to-volume ratio (S:V), and greatest axial linear dimension (GALD) of ~30 cells for each micro-phytoplankton were measured according to geometric shapes (Hillebrand et al., 1999; Sun and Liu, 2003) at 200×-600× using pre-calibrated Olympus cellSens standard software digital camera adapter system (Qimaging MicroPublisher 5.0 RTV) attached to the inverted microscope (Olympus IX73). These measurements were then utilized for cell volume (V; μm^3) and surface area (S; μm^2) calculation (Hillebrand et al., 1999; Sun and Liu, 2003). The S:V and GALD (μm) are calculated as Paul et al. (2023) described, and morphometric shapes are hereafter referred to as phytoplankton geometric shapes (PGS; Salmaso et al., 2015).

Overall, 17 PGS were identified among which 12 were simple (Box-B, Cone-C, Cylinder-Cyl, Cymbelloid-Cym, Ellipsoid-Elli, Elliptic prism-ElliP, Gamphonemoid-Gam, Half sphere-Hs, Prism on parallelogram-PoP, Prism on triangle-PoT, Prolate spheroid-Ps and Sphere-S) and 5 were combined/complex (Cylinder+2 Half spheres-Cyl2Hs, Ellipsoid+2 Cones+ Cylinder-Elli2CCyl, Elliptic prism+4 Cones-ElliP4C, Prolate spheroid+2 Cylinders-Ps2Cyl and 2 Cones-2C).

2.3. Environmental variables

Seawater samples for dissolved inorganic nutrient analysis were collected in 4.5 mL cryo-vials in 4 replicates and frozen at -20 °C until analysis. Samples were thawed to room temperature before analysis, and nutrients (nitrate, nitrite, phosphate, and silicate) were measured using an auto-analyzer (Model: Skalar Analytical SAN^{++}, Netherlands) following standard colorimetric methods (Grasshoff et al., 1992). The onboard-operated CTD profiler obtained other environmental parameters (temperature, salinity, oxygen, and PAR). The SCML depth was determined using fluorescence downward profiles generated by a fluorometer (Seapoint Sensors; 0.02 μg L^{-1}) attached to the CTD profiler. The mixed layer depth (MLD) was calculated using a 0.03 kg m^{-3} density difference from the surface (de Boyer Montegut et al., 2004), and nitracline depth was taken where the nitrate concentration reached 1 μM L^{-1} (Zhuang et al., 2020).

2.4. Data analysis

Univariate measures such as species count, Shannon–Wiener's diversity, species richness, and evenness were performed on log-

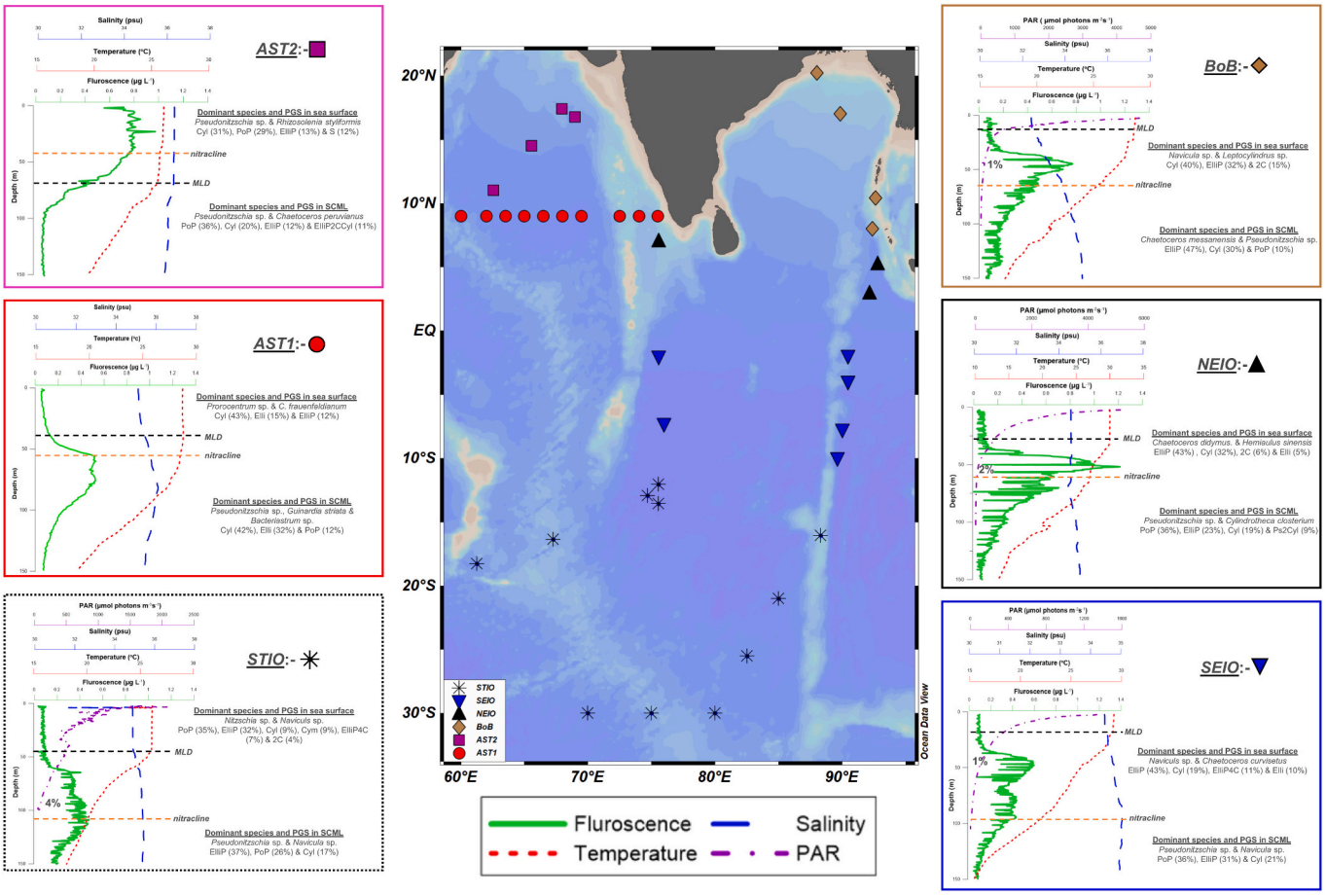


Fig. 1. Schematic showing map of the study area along with the fluorescence profile of different regions of the Indian Ocean. Dominant species and PGS are denoted for surface and SCML in each subsequent profile. Cyl: cylinder, ElliP: elliptic prims, Elli: ellipsoid, PoP: prism on parallelogram, S: sphere, ElliP2CCyl: elliptic prism+2cones + cylinder, Cym: cymbeloid, ElliP4C: elliptic prism+4 cones, Ps2Cyl: prolate spheroid+2 cylinders, 2C: 2 cones, AST1: Arabian Sea transect 1, AST2: Arabian Sea transect 2, BoB: Bay of Bengal, NEIO: North equatorial Indian Ocean, SEIO: South equatorial Indian Ocean and STIO: South tropical Indian Ocean. The black dotted line shows mixed layer depth (MLD), and the orange dotted line shows nitracline depth.

transformed data for both taxa and PGS. The clustering of different regions and between SCML depths was performed with SIMPROF (Similarity Profile Analysis; significance level at 0.05) through the Bray–Curtis similarity and group average method. The data were grouped at 50 % to ascertain significant similarities or dissimilarities concerning PGSs and taxa. Univariate and clustering analyses were performed using the statistical software PRIMER 6 (Clarke and Gorley, 2006; Clarke and Warwick, 2001). The two-way analysis of variance (ANOVA) was performed using Statistica software (release 8) on log-transformed data to evaluate the variations between regions and SCML depths. The relationship between S:V and GALD was determined using power law regression on log-transformed data. The functional relationship between two measured quantities, where a relative change in one quantity results in a relatively proportional change in another, is often expressed as a power law equation (allometric equation) representing scale symmetry:

$$y = kx^b \text{ or } \log y = b \log x + \log k$$

where b is the scaling exponent of the law.

Here GALD was taken as a function (i.e., y), S:V is variable (i.e., x), b is the order of scaling (i.e., the exponent), and k is a constant. So, if $b = -0.15$, a 100 % change (i.e., doubling) in GALD is associated with a 15 % decrease in S:V. The multivariate relationship of environmental variables with PGSs, S:V, and GALD corresponding to the sea surface and SCML depths were evaluated by performing Redundancy Analysis (RDA) using CANOCO v4.5 software (Ter Braak and Smilauer, 2002). To identify the best ordination model, detrended correspondence analysis (DCA) was conducted, and based on the lengths of environmental gradient (< 2 standard deviations), a linear response model (i.e., RDA) was selected. Based on the direct gradient technique of RDA and using forward selection (and a Monte Carlo permutation test, $n = 499$), key environmental variables were determined. The arrow length (environmental variables, PGSs, S:V, and GALD) and orientation determine their relative importance and approximate correlations to the axes (Lepš and Šmilauer, 2003).

2.5. Data presentation

The stations were grouped into six regions based on geographical locations (Table 1). AS stations are grouped in two transects, i.e., AST1 (stations in East-West direction) and AST2 (OMZ), stations from BoB and the Andaman Sea are grouped as BoB, stations 2°N-7°N are grouped as NEIO, 1°S-10°S as SEIO and 10°S-30°S as STIO. Furthermore, all stations are categorized as shallow (20-50 m), intermediate (50-100 m), and deep (>100 m) SCMLs to study the variations at different depths of occurrences (See Supplementary Table 1).

Table 1
Station details with regions and geographic positions.

Station No.	Latitude	Longitude	Regions
1	9°N	75°5E	
2	9°N	74°0E	
3	9°N	72°5E	
4	9°N	69°5E	
5	9°N	68°E	Arabian Sea transect 1 (AST1)
6	9°N	66°5E	Oligotrophic transect
7	9°N	65°E	
8	9°N	63°5E	
9	9°N	62°E	
10	9°N	60°E	
11	11°N	62°57E	Arabian Sea transect 2 (AST2)
12	14°50N	65°57E	OMZ transect
13	16°75N	69°E	
14	17°38N	67°95E	
15	17°N	89°85E	
16	20°22N	88°04E	Bay of Bengal (BoB)
17	10°40N	92°64E	
18	7°99N	92°38E	
19	7°N	75°58E	North Equatorial Indian Ocean (NEIO)
20	5°19N	92°81E	
21	2°91N	92°15E	
22	1°98S	90°47E	
23	2°03S	75°56E	
24	4°S	90°46E	South Equatorial Indian Ocean (SEIO)
25	7°32S	75°98E	
26	7°76S	90°02E	
27	9°99S	89°63E	
28	16°05S	88°29E	
29	20°99S	85°E	
30	25°50S	82°53E	
31	30°S	80°E	
32	30°S	75°E	
33	30°S	69°99E	South Tropical Indian Ocean (STIO)
34	18°27S	61°25E	
35	16°36S	67°27E	
36	12°93S	74°67E	
37	13°55S	75°55E	
38	16°05S	88°29E	

3. Results

3.1. Hydrographic condition of the Indian Ocean

Overall, the IO sea surface water was warmer than that of SCML. The equatorial region (NEIO and SEIO) sea surface water was the warmest, followed by AST1, BoB, AST2, and STIO, the coolest. In the SCML, AST1 was the warmest, followed by BoB, NEIO, AST2, SEIO, and least in STIO. The salinity of the sea surface and SCML was lowest in BoB, followed by equatorial, STIO, and AS (maximum) transects. Maximum sea surface DO was recorded in BoB followed by NEIO, STIO, SEIO, AST2, and least in AST1, whereas, in SCML, STIO showed the maximum DO followed by AST2, BoB, AST1, NEIO, and SEIO. The MLD was shallow in BoB (12 ± 6 m), NEIO (31 ± 4 m) and deepening in SEIO (36 ± 27 m), AST1 (42 ± 6 m), STIO (53 ± 7 m) and AST2 (72 ± 12 m). The nitracline depth was shallow in AST2 (45 ± 41 m), NEIO (58 ± 38 m), BoB (59 ± 33 m), AST1 (60 ± 26 m) and deeper in SEIO (98 ± 44 m) and STIO (108 ± 36 m).

The median NO_3 concentration for sea surface waters ranged from 0.57 to 1.4 μM, recording maximum in NEIO (1.4 ± 0.15 μM), followed by BoB (1.24 ± 0.62 μM), AST1 (1.02 ± 0.51 μM), SEIO (0.96 ± 1.7 μM), STIO (0.85 ± 0.19 μM) and least in AST2 (0.57 ± 0.25 μM). In SCML, concentrations ranged from 0.7 to 5.0 μM, recording maximum in NEIO (5.0 ± 0.5 μM), followed by BoB (2.9 ± 1.8 μM), SEIO (2.4 ± 0.6 μM), AST1 (1.8 ± 2.0 μM), STIO (1.2 ± 0.3 μM) and least in AST2 (0.7 ± 0.9 μM).

The median PO_4 concentration for sea surface waters ranged from 0.5 to 1.4 μM recording maximum in AST1 (1.4 ± 0.15 μM), followed by BoB (1.2 ± 0.42 μM), NEIO (0.8 ± 0.36 μM), SEIO (0.7 ± 1.4 μM) and least in STIO and AST2 (0.5 ± 0.2 μM). In SCML, concentrations ranged from 0.3 to 2.2 μM, recording maximum in NEIO (2.2 ± 0.8 μM), followed by BoB (1.4 ± 0.9 μM), SEIO (1.3 ± 0.3 μM), AST1 (1.1 ± 1.1 μM), STIO (0.8 ± 0.2 μM) and least in AST2 (0.3 ± 0.5 μM) (Table 2).

The intermediate SCML was warmer (26.3 ± 0.5 °C) than shallow (25.9 ± 0.3 °C) and deep (18.5 ± 1.05 °C) SCML. The deep SCML was more oxygen saturated (4.7 ± 0.16 mgL^{-1}) than shallow (3.2 ± 0.41 mgL^{-1}) and intermediate (3.3 ± 0.13 mgL^{-1}), which did not show much variation. The salinity variation was insignificant among SCML depths. The mean concentration of SiO_4, PO_4, NO_2 + NO_3, and N:P was maximum in the intermediate, followed by shallow and least in deep SCML (Table 3).

3.2. Relationship between PGS, morphological traits, and environmental variables

The RDA results revealed that the dominant PGSs at the sea surface were limited by SiO_4 availability and high light (PAR) conditions. Similarly, S:V and GALD were controlled by only nutrient limitation, but in SCML, both nutrient and light availability were the controlling factors. Interestingly, S:V and GALD of the dominant PGSs in shallow and intermediate SCML were positively correlated with nutrients and light, whereas in the deep SCML, nutrients were positively and the light was negatively correlated. Further, the temperature was also one of the controlling parameters in the deep SCML, and it negatively correlated with GALD and PGSs, which means increasing temperature will result in smaller phytoplankton cells. Therefore, the morphometric attributes (S:V and GALD) were strongly influenced by the SCML depth and the prevailing environment (Supplementary Fig. 1a–c).

3.3. PGS diversity of the sea surface waters

The PGSs in the sea surface water were relatively similar (Supplementary Fig. 2a). Altogether, 13 PGSs (9 simple and 4 complex) were recorded, corresponding to 108 micro-phytoplankton species. Simple PGSs contributed 81–98 % and complex 4–19 % in the IO. A few simple (Cyl, ElliP, and PoP) and complex (2C and Elli2CCyl) PGSs were common, irrespective of the regions. However, the maximum PGSs were recorded in AST1 (12 PGSs; 8 simple and 4 complex) followed by SEIO (11 PGSs; 7 simple and 4 complex), BoB (10 PGSs; 7 simple and 3 complex), AST2, NEIO and STIO (9 PGSs; 6 simple and 3 complex each).

Among the PGSs, Cyl and ElliP were dominant compared to other prominent PGSs like PoP, Elli, 2C, and ElliP4C (Supplementary Table 2). However, species responsible for corresponding PGSs differed with bioregions (Supplementary Table 2). All these PGSs cumulatively contributed up to 87 % of the total community in all the regions. Maximum species diversity was observed in Cyl for AST1 (15 centric diatom species), AST2 (8 centric diatom species), BoB (13 centric diatom species), and STIO (10 centric diatom species) whereas ElliP (9 diatom species; 8 centric and 1 pennate) and Elli (6 dinoflagellate species) showed maximum diversity in NEIO and SEIO, respectively. The univariate analysis revealed similar PGSs among the regions. PGS richness and diversity were highest in BoB, followed by AST1 and NEIO, AST2 and STIO, and least in SEIO. The number of PGS was highest in BoB, followed by AST1, AST2, NEIO, and STIO, and least in SEIO (Supplementary Fig. 3g–i).

The S:V and GALD of dominant PGSs, cumulatively representing >50 % in the sea surface waters, were Cyl, ElliP, and 2C. The S:V of Cyl and 2C significantly increased from northern to southern IO, and the maximum was in STIO (0.59 μm^{-1}) and SEIO (4.33 μm^{-1}), respectively, whereas ElliP remained relatively similar, ranging between 0.43 and 0.70 μm^{-1}. However, GALD of Cyl, ElliP, and 2C decreased significantly from northern to southern IO, and the maximum was in AST2 for both Cyl (373 μm) and ElliP (86 μm) and in AST1 for 2C (1056 μm), respectively.

The regression analysis of the dominant PGSs in the sea surface (Cyl,

Table 2
The environmental parameters and nutrient concentration at the sea surface and SCML of different regions of the Indian Ocean. The values of environmental parameters are mean, and nutrients are median. The range values are given in parentheses.

Regions of IO	Temperature (°C)	Salinity (PSU)	Oxygen (mL L^{-1})	NO_3 (μM)	NO_2 (μM)	PO_4 (μM)
AST1	28.7	35.1	3.7	1.02	0.21	1.45
(0m)	(27.8–29.3)	(34.2–35.5)	(3.6–3.8)	(0.49–5.64)	(0.04–0.42)	(0.84–2.49)
AST1	27.8	35.9	3.2	1.8	0.1	1.1
(SCML)	(26.5–28.9)	(35.5–35.9)	(2.5–3.6)	(0.26–18.4)	(0.05–0.45)	(0.55–2.73)
AST2	26.1	36.3	3.6	0.57	0.46	0.55
(0m)	(25.0–26.8)	(36.2–36.5)	(3.5–3.7)	(0.41–1.5)	(0.24–0.48)	(0.28–1.23)
AST2	26.0	36.3	3.6	0.7	0.4	0.3
(SCML)	(25.0–26.8)	(36.2–36.5)	(3.6–3.7)	(0.65–3.27)	(0.24–0.45)	(0.21–1.83)
BoB	28.7.	32.4	4.5	1.17	0.17	0.69
(0m)	(27.4–29.7)	(31.8–32.9)	(4.4–4.7)	(0.7–3.47)	(0.15–0.24)	(0.56–1.66)
BoB	27.1	33.6	3.3	2.9	0.3	1.4
(SCML)	(25.6–27.9)	(33.4–34.1)	(1.6–4.0)	(1.2–9.2)	(0.2–0.39)	(0.9–4.6)
NEIO	29.8	34.8	4.4	1.41	0.19	0.82
(0m)	(29.8)	(34.7)	(4.36)	(1.19–1.72)	(0.15–0.22)	(0.65–1.79)
NEIO	26.8	34.4	3.1	5.0	0.3	2.2
(SCML)	(25.3–28.3)	(34.1–34.7)	(2.6–3.6)	(4.5–6.2)	(0.21–0.36)	(1.8–4.3)
SEIO	28.9	34.2	4.3	0.96	0.17	0.71
(0m)	(28.9–30.0)	(34.1–34.9)	(3.4–4.4)	(0.79–10.88)	(0.13–0.32)	(0.59–9.35)
SEIO	24.2	35.0	3.0	2.4	0.5	1.3
(SCML)	(21.0–28.2)	(34.7–35.2)	(1.9–4.0)	(0.9–5.0)	(0.26–0.61)	(0.8–2.6)
STIO	26.1	35.0	4.3	0.85	0.17	0.49
(0m)	(22.5–28.0)	(33.9–35.9)	(3.3–4.7)	(0.32–2.69)	(0.13–0.34)	(0.37–2.65)
STIO	20.4	35.3	4.1	1.2	0.3	0.8
(SCML)	(14.7–24.5)	(34.8–35.7)	(2.5–5.1)	(0.6–3.9)	(0.11–0.37)	(0.53–2.05)

Table 3
The environmental parameters and nutrient concentration at varying depths of SCML of the Indian Ocean. The values of environmental parameters are mean and for nutrient is median along with standard error.

Depth of SCML	Temperature (°C)	Salinity (PSU)	Oxygen (mL L^{-1})	NO_2 (μM)	NO_3 (μM)	PO_4 (μM)	Si (μM)	N:P
>50 m	25.9 ± 0.29	35.9 ± 0.45	3.2 ± 0.41	0.37 ± 0.08	3.44 ± 1.7	1.74 ± 0.9	5.96 ± 3.4	2.21 ± 0.5
50–100 m	26.2 ± 0.51	35.1 ± 0.18	3.4 ± 0.13	0.29 ± 0.03	3.69 ± 0.8	1.6 ± 0.4	9.88 ± 1.5	2.60 ± 0.8
<100 m	18.5 ± 1.05	35.6 ± 0.06	4.7 ± 0.16	0.22 ± 0.03	0.91 ± 0.1	0.67 ± 0.05	6.19 ± 1.1	1.38 ± 0.1

ElliP, and PoP) showed a significant negative correlation between S:V and GALD for Cyl and ElliP but not for PoP, which was not significant. Interestingly, the scaling exponent (i.e., b), which can be used to quantify the amount of change of the dependent variable (i.e., S:V in this case), showed significant variation in the sea surface for both Cyl (−0.09 to −0.41) and ElliP (−0.16 to −0.32) but not for PoP (−0.09 to 0.05) (Fig. 2).

3.4. PGSs in varying depths of SCML

Like the sea surface, SCML PGSs were similar (Supplementary Fig. 2b), and 17 PGSs (12 simple and 5 complex) belonging to 134 species were recorded. Simple and complex PGSs contributed 86–98 % and 2–14 %, respectively. Among the 17 PGSs, five simple (Cyl, ElliP, PoP, Elli, and B) and two complex (2C and Elli2CCyl) PGSs were common. The SCML corresponding to different regions were categorized as shallow (20-50 m; represented by all stations in AST2 and one in BoB), intermediate (50-100 m; represented by all stations in AST1, NEIO, and SEIO, three stations in BoB and five stations in STIO) and deep (>100 m; represented by six stations in STIO) SCML (Supplementary Table 1). PGSs were maximum in intermediate NEIO (13 PGSs: 8 simple and 5 complex) followed by intermediate BoB (12 PGSs: 7 simple and 5 complex), shallow AST2, intermediate AST1, and deep STIO (11 PGSs each), intermediate SEIO (10 PGSs: 7 simple and 3 complex), shallow BoB and intermediate STIO (9 PGSs each). The PGSs in shallow, intermediate, and deep SCML corresponded to 50 (37 diatoms and 13 dinoflagellates), 113 (72 diatoms and 41 dinoflagellates), and 48 (34 diatoms and 14 dinoflagellates) micro-phytoplankton species, respectively. Like sea surface, among the PGSs, ElliP and Cyl were the most dominant compared to other prominent PGSs like PoP, Elli, B, 2C, and Elli2CCyl (Supplementary Table 3). However, the species responsible for corresponding PGSs differed with SCML depths in different bioregions (Supplementary Table 3). All these PGSs cumulatively contribute up to 96 %, 93 %, and 94 % in shallow, intermediate, and deep SCML of total abundance, respectively.

3.5. S:V and GALD of PGSs in varying depths of SCML

The variability in S:V and GALD of PGSs showed distinct variability for SCML depths. For instance, S:V of Cyl showed a significant increase, ElliP and Elli showed a minor increase, and PoP and B showed a significant decrease with increasing depth of SCML. The GALD of Cyl and ElliP significantly decreased, PoP showed a minor decline, B showed a minor increase, and Elli showed no trend with increasing SCML depth. The average S:V and GALD for individual PGSs recorded for shallow, intermediate, and deep SCML are provided in Supplementary Table 4 for reference. The regression analysis between S:V and GALD revealed (i) shallow SCML: a significant negative for Cyl, ElliP, and Elli2CCyl, a significant positive for PoP and no significant negative correlation for B, (ii) intermediate SCML: a significant negative for Cyl, ElliP, PoP, B, and 2C, no significant negative and positive correlation for Elli and Elli2CCyl respectively, and (iii) deep SCML: significant negative for Cyl, ElliP, Elli, and 2C, not significant positive for PoP and not significant negative correlation for B and Elli2CCyl. Interestingly, the scaling exponent 'b' showed a decreasing trend from shallow to deep SCML for Cyl (−0.45, −0.33, and − 0.22), an increasing trend from shallow to deep SCML for B (−0.13, −0.27 and − 0.52), Elli (−0.22 and − 0.27) and 2C (−1.94 and − 3.55), decreasing from shallow to intermediate and again increasing in deep SCML for ElliP (−0.30, −0.24, and − 0.56) and no trend for PoP and Elli2CCyl (Figs. 3 and 4).

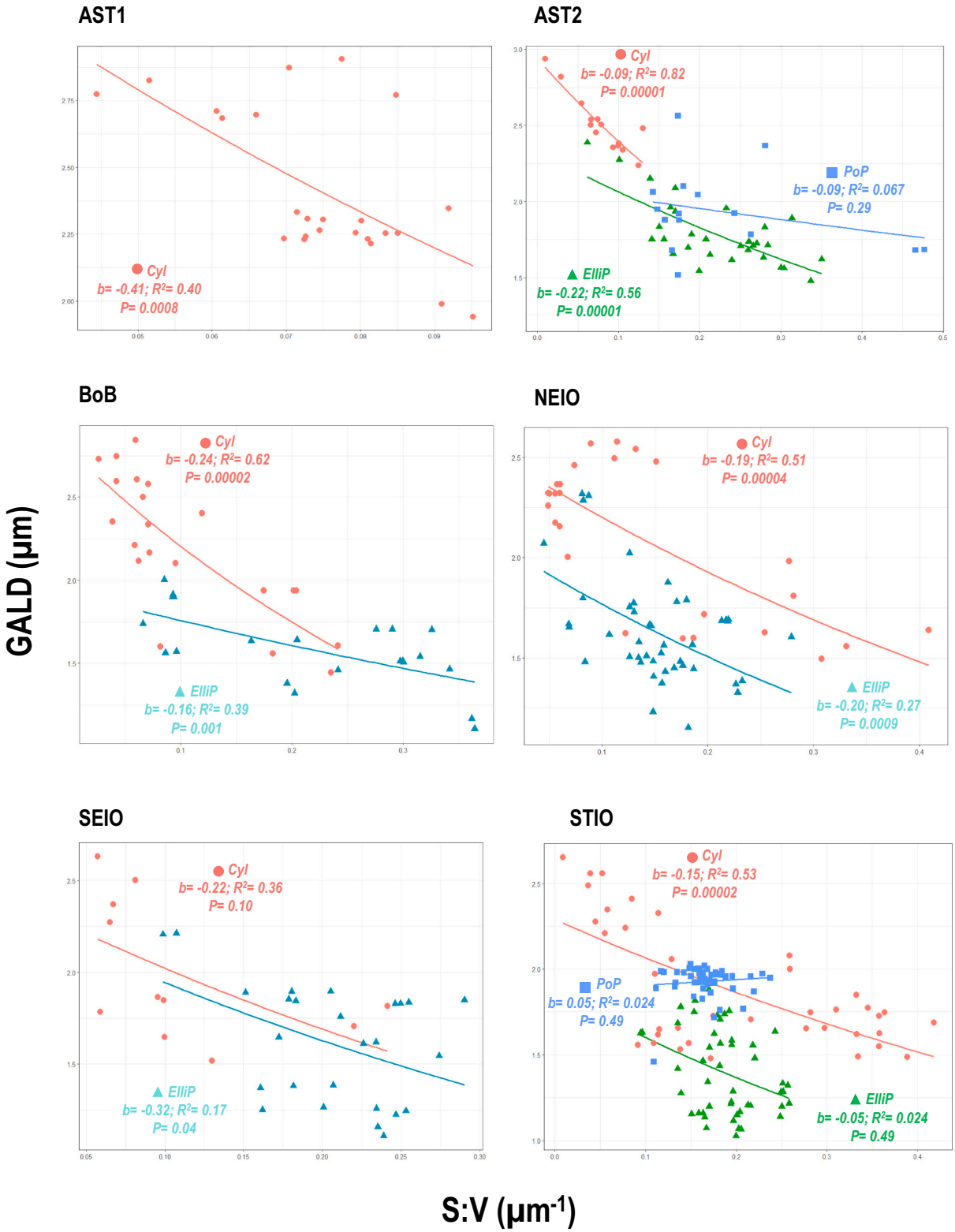


Fig. 2. Non-linear regression of dominant PGS in sea surface waters of the IO. AST1: Arabian Sea transect 1, AST2: Arabian Sea transect 2, BoB: Bay of Bengal, NEIO: North equatorial Indian Ocean, SEIO: South equatorial Indian Ocean, STIO: South tropical Indian Ocean, S:V: surface-to-volume ratio and GALD: greatest-axial-linear-dimension. ElliP: elliptic prism, Cyl: cylinder and PoP: prism on parallelogram.

3.6. Comparative results between the sea surface and SCML

The SCML recorded more PGSs (17 PGSs) than the corresponding surface waters (13 PGSs). In shallow, 12 (8 simple and 4 complex) and 15 (10 simple and 5 complex) PGSs belonging to 34 and 50 species of micro-phytoplankton were recorded in surface and SCML, respectively. Simple PGSs contributed 87 % and 96 %, whereas complex PGSs contributed 13 % and 4 % in shallow regions of the sea surface and SCML. Three simple (Cyl, ElliP, and PoP) and two complex (2C and Elli2CCyl) PGSs were common. Among simple PGSs, Cyl contributed 32

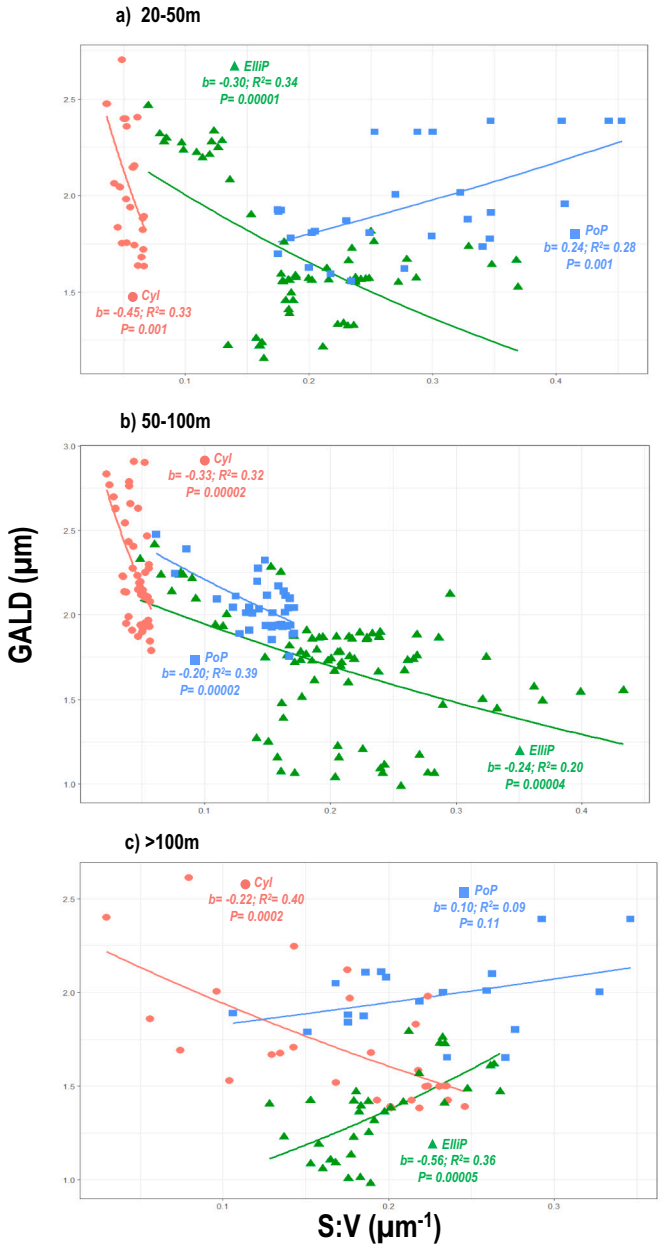


Fig. 3. Non-linear regression of dominant PGS in varying depths of SCML in the IO. S:V: surface-to-volume ratio, GALD: greatest-axial-linear-dimension, ElliP: elliptic prism, Cyl: cylinder and PoP: prism on parallelogram.

%, co-dominated by *Rhizosolenia styliformis*, *Bacteriastrum* sp., and *Probosica alata* on the surface, and 30 %, co-dominated by *Bacteriastrum* sp., *Dactyliosolen* sp., and *Thalassiosira* sp. in SCML. ElliP contributed 25 %, co-dominated by *Navicula* sp. and *Chaetoceros peruvianus* on the surface, and 41 %, dominated by various *Chaetoceros* species (e.g., *C. messanensis,* and *C. curvisetus*) in SCML. PoP contributed 17 % and 15 % in surface and SCML, respectively, dominated by *Pseudonitzschia* sp. Regarding complex PGSs, 2C contributed 5 %, dominated by *Protoperidinium* sp. in surface waters, whereas Elli2CCyl contributed 3 % and 2 % in surface and SCML, respectively dominated by *Tripos* species (e.g., *T. tripos*, *T. deflexus*, and *T. pentagonus*). Simple PGSs like Cyl showed no change in S:V and a significant decrease in GALD, PoP showed a significant increase in S:V and GALD, and ElliP showed a significant decrease in S:V and GALD (Fig. 5), whereas complex PGSs, 2C showed no change in S:V and a significant decrease in GALD between the sea surface and SCML.

In the intermediate region, 13 (8 simple and 5 complex) PGSs in surface and SCML belonging to 96 and 113 micro-phytoplankton species were recorded. Simple PGSs contributed 78 % and 95 %, whereas complex 12 % and 5 % in the intermediate region of the sea surface and SCML. Four simple (Cyl, ElliP, Elli, and PoP) and three complex (2C, ElliP4C, and Cyl2Hs) PGSs were common. Among simple PGSs, Cyl contributed 32 %, co-dominated by *Coscinodiscus* sp., *Leptocylindrus* sp., *Thalassiosira* sp., *Bacteriastrum* sp., and *Guinardia cylindrus* in surface and 26 % in SCML, co-dominated by *Bacteriastrum* sp., *Coscinodiscus* sp., and *Thalassiosira* sp. ElliP contributed 27 %, co-dominated by *Navicula* sp., *Chaetoceros* sp., and *Hemiaulus sinensis* in the sea surface, and 31 % in SCML, dominated by various *Chaetoceros* species (e.g., *C. messanensis,* and *C. lasiniosus*). Elli contributed 9 % in the sea surface water, dominated by *Prorocentrum* sp., and PoP contributed 26 % in SCML, dominated by *Pseudonitzschia* sp. Regarding complex PGSs, 2C contributed 7 % and 2 % in the sea surface and SCML, both dominated by *Protoperidinium* sp. and *Gonyaulax* sp. ElliP4C contributed 6 % in the sea surface, dominated by *Climacodium frauenfeldianum* and Cyl2Hs contributed 2 % in SCML, dominated by *Corethron* sp. Simple PGSs like Cyl and ElliP showed a significant increase in S:V and a decrease in GALD, PoP showed a significant increase in both S:V and GALD (Fig. 5) whereas, in complex PGSs, 2C showed no change in S:V and a significant decrease in GALD between surface and SCML.

In the deep region, 8 (5 simple and 3 complex) and 11 (8 simple and 3 complex) PGSs in the sea surface and SCML belonging to 25 and 48 micro-phytoplankton species were recorded. Simple PGSs contributed 83 % and 88 %, whereas complex 17 % and 12 % in deep regions of the sea surface and SCML. Three simple (Cyl, ElliP, and PoP) and three complex (2C, Elli2CCyl, and Cyl2Hs) PGSs were common. Among simple PGSs, Cyl contributed 12 % in the sea surface, co-dominated by *Asteromphalus* sp., *Rhizosolenia clevei*, and *Rhizosolenia hebetata*, and 24 % in SCML, co-dominated by *Bacteriastrum* sp. and *Coscinodiscus* sp. ElliP contributed 48 % in the sea surface, co-dominated by *Navicula* sp. and *Chaetoceros dadayi,* and 36 % in SCML, dominated by *Chaetoceros simplex*. PoP contributed 20 % in the sea surface, dominated by *Nitzschia* sp., and 13 % in SCML, dominated by *Pseudonitzschia* sp. Regarding complex PGSs, Cyl2Hs contributed 8 % in the sea surface, dominated by *Corethron* sp., 2C 6 % and 7 % in the sea surface and SCML, respectively, dominated by *Protoperidinium* sp., and Elli2CCyl contributed 3 % in SCML, co-dominated by *Tripos teres* and *Tripos horridius*. Simple PGSs like Cyl showed a significant increase in S:V and a decrease in GALD, PoP showed a significant increase in S:V and GALD, and ElliP showed no significant change in S:V and a decrease in GALD (Fig. 5), whereas, in complex PGSs, 2C showed no change in S:V and GALD between the sea surface and SCML.

The sea surface waters of shallow, intermediate, and deep regions recorded lower micro-phytoplankton and PGSs than SCML, all dominated by simple PGSs. The simple (Cyl, ElliP, and PoP) and complex (2C, Elli2CCyl, and Cyl2Hs) PGSs were common in all the layers, irrespective of the regions. However, Cyl dominated the sea surface and ElliP in the SCML of both shallow and intermediate regions, respectively. ElliP was dominant in the deep region (sea surface and SCML). The S:V in Cyl showed no change in shallow, increase in intermediate and deep regions, ElliP showed a decrease in shallow, increase in intermediate and no change in deep, PoP showed an increase, and 2C showed no change in all the regions between the sea surface and SCML. The GALD showed a decrease in Cyl, ElliP, 2C and an increase in PoP for all the areas except 2C, which showed no change only in the deep region.

4. Discussion

The existence of permanent SCML in IO (AS, BoB, equatorial IO, and STIO) has been well documented (Shulenberger and Reid, 1981) primarily focused on the formation and maintenance of SCML using satellite (Shah et al., 2020) or argo-float data (Jayaram et al., 2021). Fu et al. (2018) emphasized that the phytoplankton community structure defines the understanding of SCML characteristics. The phytoplankton

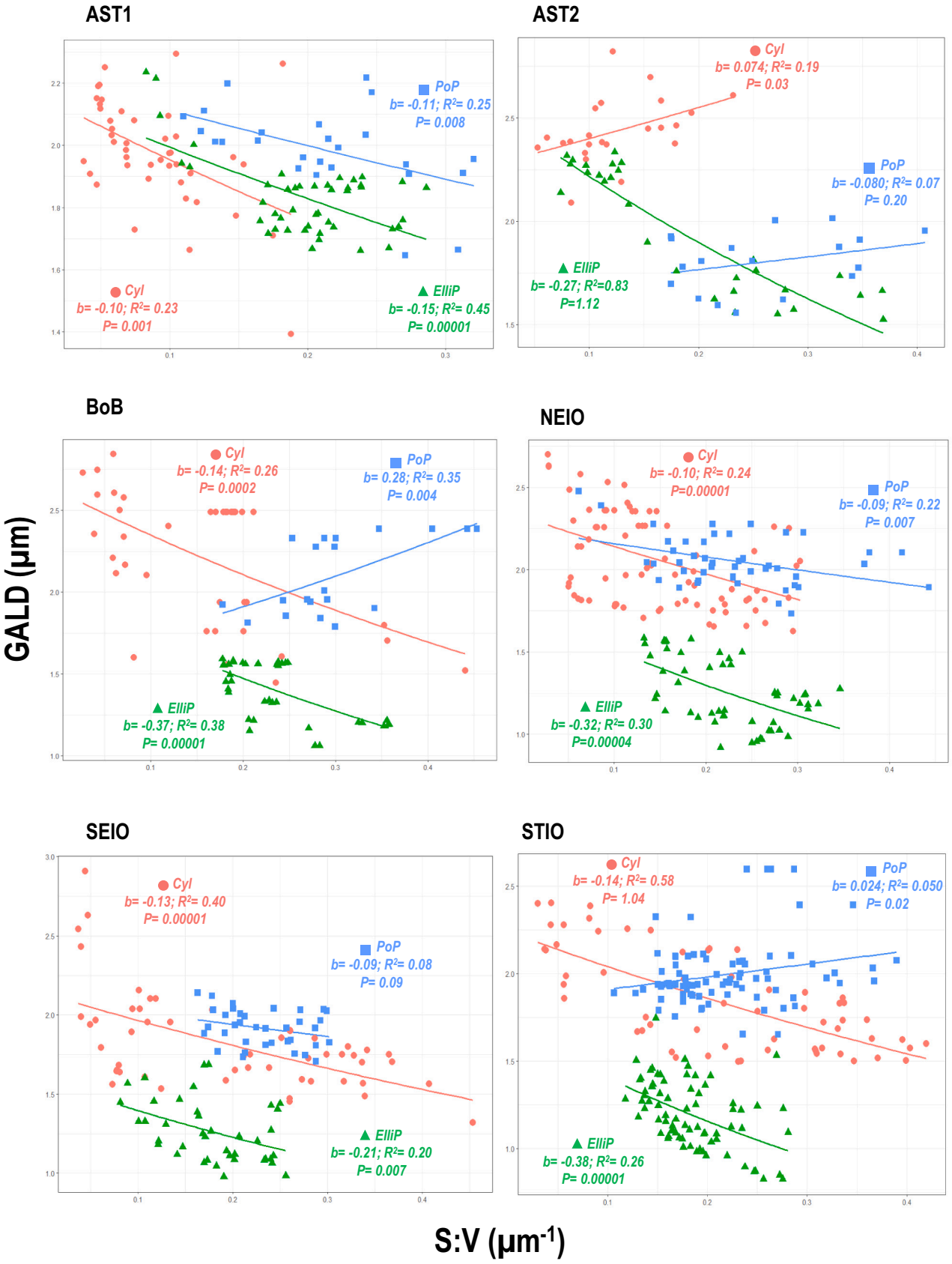


Fig. 4. Non-linear regression of dominant PGS in sub-surface chlorophyll maximum layer (SCML) of the IO. AST1: Arabian Sea transect 1, AST2: Arabian Sea transect 2, BoB: Bay of Bengal, NEIO: North equatorial Indian Ocean, SEIO: South equatorial Indian Ocean, STIO: South tropical Indian Ocean, S:V: surface-to-volume ratio, GALD: greatest-axial-linear-dimension, ElliP: elliptic prism, Cyl: cylinder and PoP: prism on parallelogram.

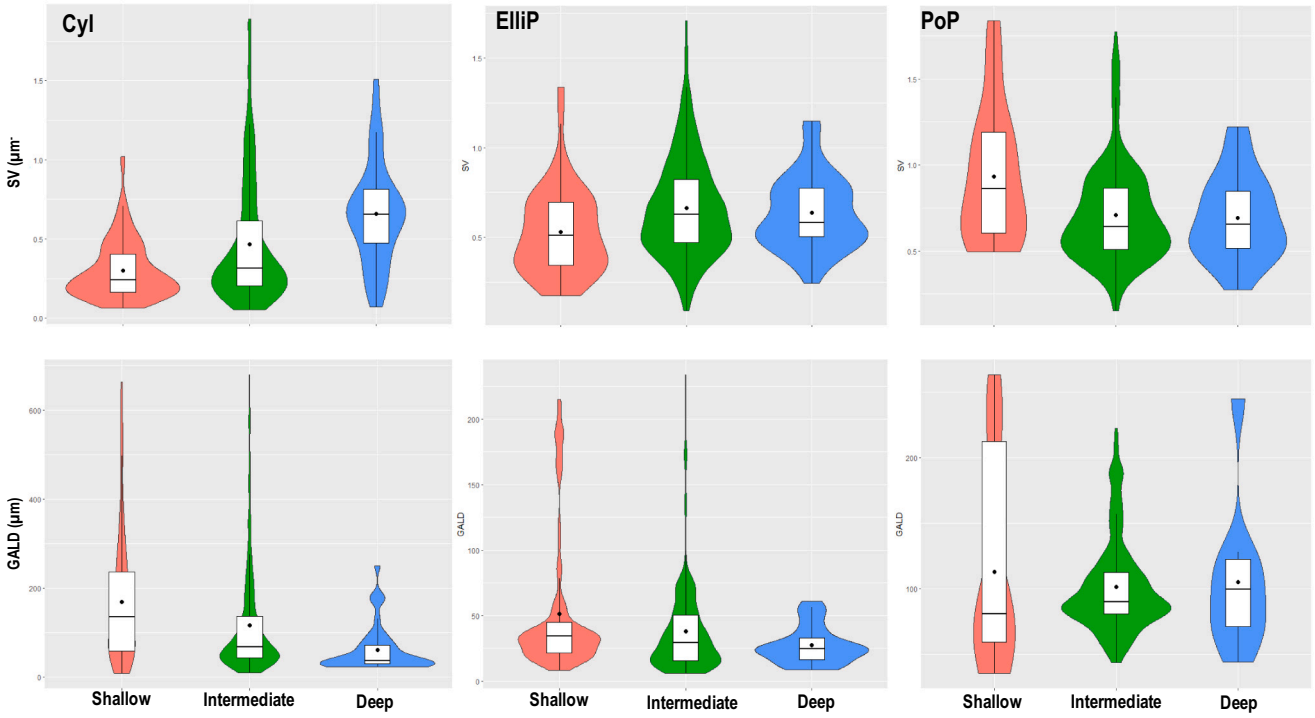


Fig. 5. Violin plot of morphological attributes (S:V and GALD) in dominant PGS from varying SCML depths. S:V: surface-to-volume ratio, GALD: greatest-axial-linear-dimension, SCML: sub-surface chlorophyll maximum layer, Cyl: cylinder, ElliP: elliptic prism, and PoP: prism on parallelogram.

species show high morphological plasticity, optimizing their performance in response to environmental variabilities. Therefore, morphological analysis could be used to estimate the ecological variability within which a species can persist. Moreover, in the past two decades, analyzing spatial and temporal patterns of phytoplankton assemblages using trait-based methods has become popular (see Naselli-Flores and Padisak, 2023 and references therein). Hence, it is crucial to establish an understanding of the morphological trait variability and community structure between the sea surface and SCML as various taxa play a pivotal role in biogeochemical processes, like carbon transfer to depth or higher trophic level, in new primary production (Revelante and Gilmartin, 1995; Goldman and McGillicuddy, 2003) and could help in predictions of ecosystem response to future climate changes (Barnett et al., 2019).

This study recorded 108 and 134 species representing only 45 % and 55 % of the PGSs (14 and 17 out of 31 described PGSs in Sun and Liu (2003)) described for phytoplankton in literature in the sea surface and SCML, respectively. The unrecorded 14 PGSs are represented mainly by the freshwater species or phytobenthos in the sunlit zone or belong to groups (e.g., flagellates, Euglenophyceae, Chlorophyceae) that were not recorded due to known technical limitations (e.g., preservatives and sample collection above 20 µm) through the microscopic approach. Despite methodological limitations, this study revealed that SCML harbors most of the described PGSs and species, showing dissimilar spatial distribution patterns concerning abundance, composition, and diversity. A better understanding of the SCML micro-phytoplankton community, key taxa, and morphological adaptations will be necessary to assess climate warming impact across IO effectively. The pelagic ecosystem trophic pathways could be modified if any variation in biomass, species composition, and size structure of the phytoplankton community within the SCML takes place (Legendre and Rassoulzadegan, 1996). Therefore, to better anticipate the community shifts and the functional implications for the ecosystem in changing global climate scenarios, it is of utmost importance to understand the relationship and variability of morphometric traits and taxonomy. This study discusses the variability in distribution patterns between bioregions and variable depths of SCML in the IO, having distinct hydrographic conditions in the subsequent sections.

4.1. Variability of diversity and morphological traits of PGSs in the sea surface

Simple elongated PGSs (e.g., Cyl, ElliP, and PoP) followed by complex shapes dominated in IO. ElliP and Cyl were the most prevalent PGSs in the sea surface waters but showed an opposite trend in distribution. For instance, Cyl showed a clear dominance in the northern (NIO, i.e., AS, BoB, and NEIO) than the southern IO (SIO, i.e., SEIO and STIO) and vice versa for ElliP. Interestingly, Cyl displayed taxonomic gradation where chain-forming taxa with or without setae dominated the NIO and solitary bigger taxa in SIO. While ElliP showed no such taxonomic variability (dominated by various species of *Chaetoceros*). Whereas in complex PGSs, the distribution was sporadic, and they are primarily present in the oligotrophic AST1, NEIO, SEIO, and STIO. The complex PGSs (Elli, 2C, and ElliP4C), which are dominated mainly by various pennate and dinoflagellate species, are known for their adaptive capabilities (presence of flagella and capability to survive in low nutrient conditions) in oligotrophic sea surface conditions (see Table 2). Since oligotrophic conditions are widespread in marine pelagic systems, PGS variability will also be similar. On the other hand, the morphological traits (S:V and GALD), which encode even the smallest environmental changes in their adaptive measures, are well reflected, i.e., low S:V (0.42 $\pm$ 0.18 µm^{-1}) and high GALD (219 $\pm$ 89 µm) values under mesotrophic conditions (i.e., in NIO) and high S:V (0.51 $\pm$ 0.07 µm^{-1}) and low GALD (102 $\pm$ 6 µm) under oligotrophic conditions (i.e., in SIO) (Fig. 6). The nutrient flow across the cell boundary might not increase with a meager increase of S:V as it also depends on the cell shape (nutrient flow declines as cell curvature decreases, i.e., cell radius increases; Kiorboe, 2008); therefore, elongated prolate cells can provide large nutrient flow compared to oblate cells with same surface area and volume (Karp-Boss and Boss, 2016). Hence, the richness of elongated shapes is generally greater than that of oblate shapes (Ryabov et al., 2021).

Interestingly, individual PGSs show distinct patterns in their

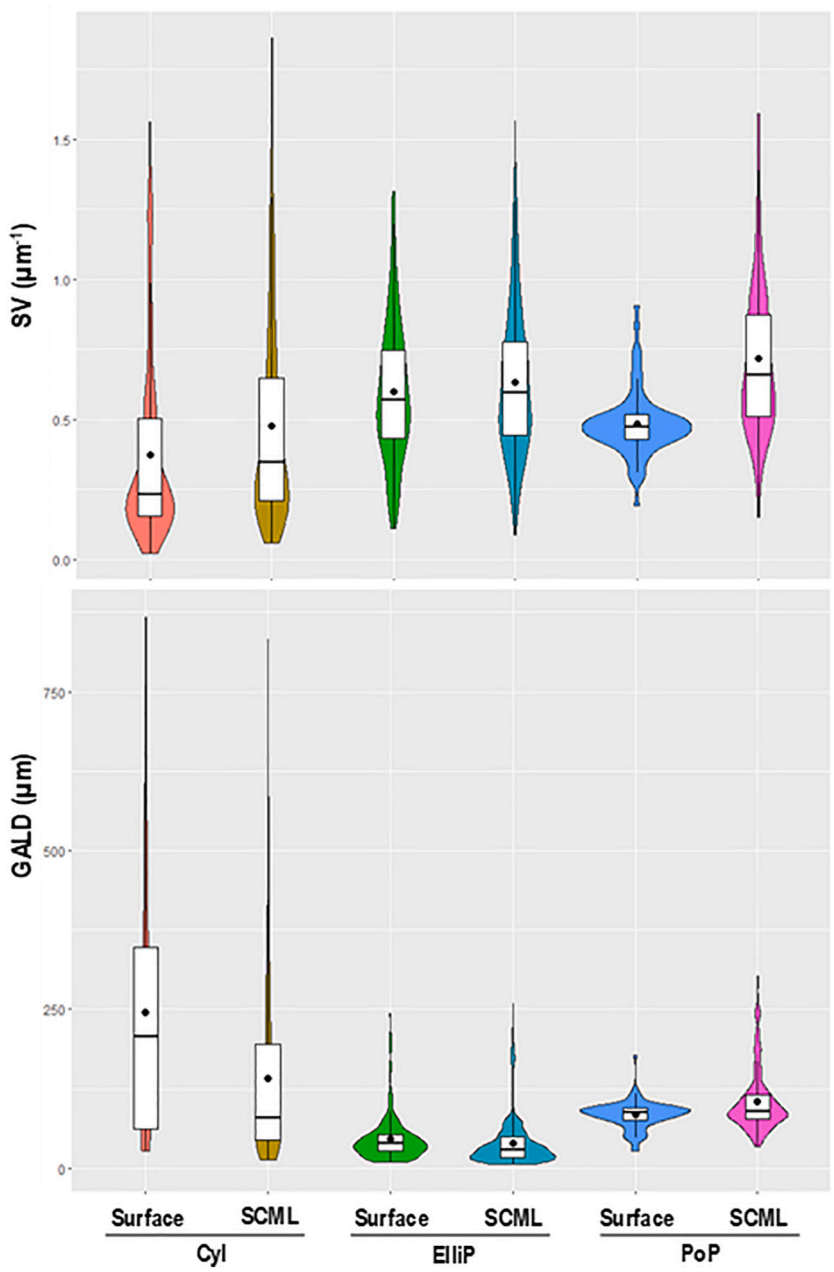


Fig. 6. Violin plot of morphological attributes (S:V and GALD) in dominant PGS from sea surface and SCML waters. S:V: surface-to-volume ratio, GALD: greatest-axial-linear-dimension, SCML: sub-surface chlorophyll maximum layer, Cyl: cylinder, ElliP: elliptic prism, and PoP: prism on parallelogram.

morphometric traits. For instance, the S:V of Cyl significantly increased from northern to southern IO, showing maximum values for STIO, whereas ElliP showed no such pattern (Fig. 7). The trends observed in Cyl could have been caused by environmental gradients (the trophic conditions and stratification). The water column becomes more stratified and oligotrophic towards equatorial regions. It is known that environmental conditions like nutrients, light, and temperature influence the shape and size distribution of phytoplankton (Naselli-Flores et al., 2007; Stanca et al., 2013), making size and shape a crucial determinants of fitness. Kruk and Segura (2012) also concluded that environmental factors select specific phytoplankton morphological groups. However, this study shows that such patterns are PGS-specific and majorly determined by the dominant taxa. For example, non-setae-bearing taxa like *Rhizosolenia*, *Pseudosolenia*, *Coscinodiscus*, and *Probosica* or taxa with short (*Bacteriastrum* in Cyl) and long setae (*Chaetoceros* in ElliP). Former ones seldom form chains and depend more on their morphological attributes for survival, whereas later chain lengths are independent of morphological attributes and, therefore, show no specific patterns or trends. Since the S:V decreases with cell volume, it has been assumed that natural selection should favor elongated PGSs (Lewis, 1976; Niklas, 2000). Hence, morphological attributes reflect the environmental variability more robustly in simple PGSs (like Cyl, ElliP, and PoP) than other PGSs and can act as a potential ecological proxy for the pelagic ocean.

4.2. Variability of diversity and morphological traits of PGS in varying depths of SCML

Like sea surface, PGSs are dominated by simple elongated shapes (e.g., Cyl, ElliP, and PoP) irrespective of the SCML depths and bioregions (Supplementary Figs. 2 and 4). ElliP, Cyl, and PoP were the most prevalent PGSs in shallow, intermediate, and deep SCML. The

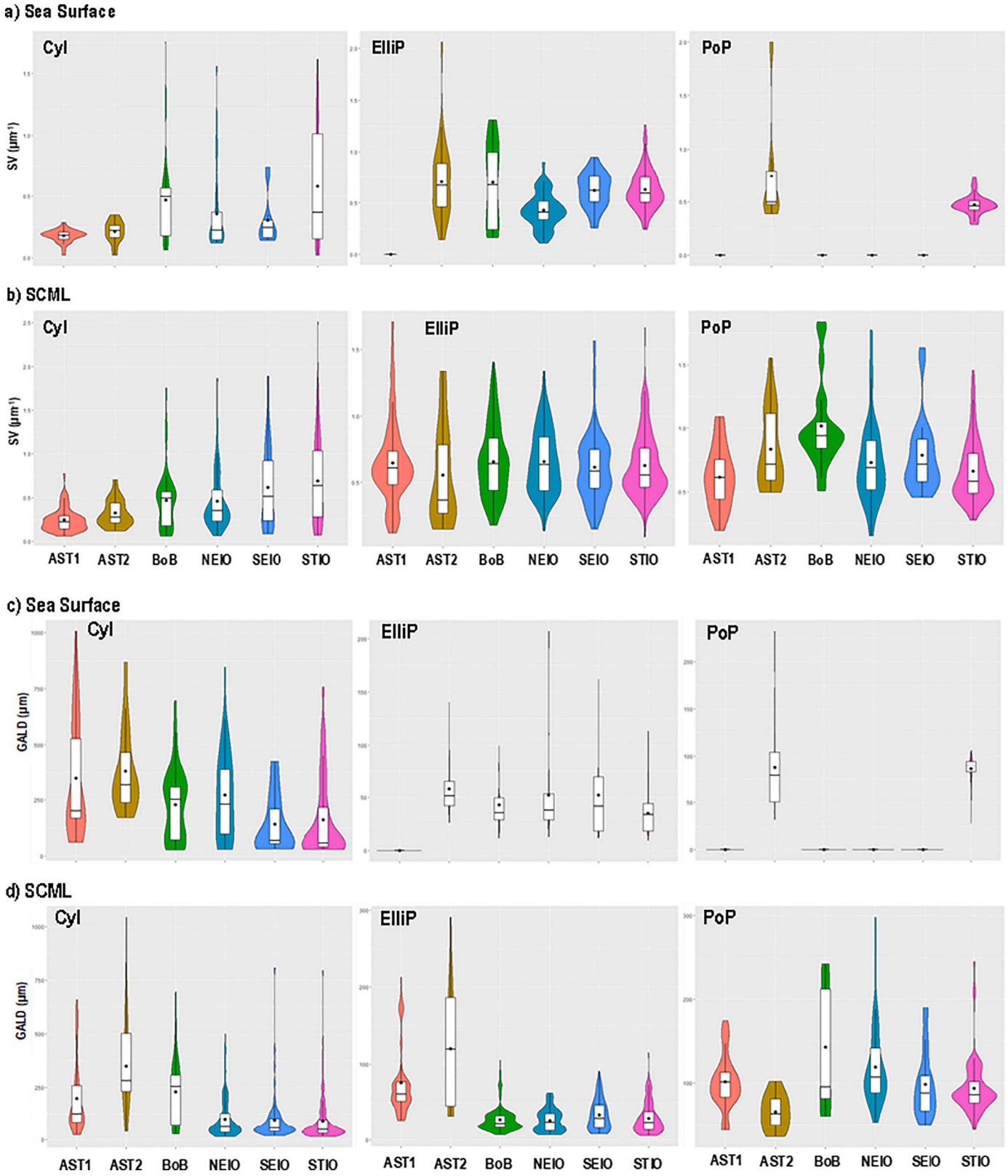


Fig. 7. Violin plot of morphological attributes (S:V and GALD) in dominant PGSs from sea surface and SCML of different regions in the Indian Ocean. AST1: Arabian Sea transect 1, AST2: Arabian Sea transect 2, BoB: Bay of Bengal, NEIO: North equatorial Indian Ocean, SEIO: South equatorial Indian Ocean, STIO: South tropical Indian Ocean, S:V: surface-to-volume ratio, GALD: greatest-axial-linear-dimension, Cyl: cylinder, ElliP: elliptic prism, and PoP: prism on parallelogram.

intermediate SCML harbored the maximum PGSs and taxa compared to shallow and deep. Though the dominance remained constant, the percentage contribution of simple PGSs (ElliP, Cyl, PoP, and B) gradually decreased except for Elli, which showed an opposite trend. In contrast, the contribution of complex PGSs (2C and Elli2CCyl) gradually increased with the increasing depth of SCML. However, the taxa in various SCML depths showed significant similarity between shallow and intermediate and dissimilarity to deep SCMLs. This similarity can be explained by the nutrient availability (N:P), which was relatively higher in shallow and intermediate but less in deep SCML. These two layers (shallow and intermediate) were dominated by *Pseudonitzschia* spp., which is well adapted to grow in varying light conditions (Bates, 1998; Houliez et al., 2023). Whereas the deep SCML was dominated by a heterotrophic dinoflagellate (*Protoperidinium* spp.), well known as a key contributor to the SCML community (Durham and Stocker, 2012; Cullen, 2015). Few microscopic observations have also reported increased dinoflagellate abundance in the SCML (Estrada et al., 2016; Barnett et al., 2019; Decembrini et al., 2020). The motility of dinoflagellates (response to resource gradients) can act as an essential trait in compensating for physiological disadvantages compared to diatoms (Ross and Sharples, 2007). *Protoperidinium* spp. is also known to be species-specific feeders and prefers to feed on diatoms majorly (Buskey, 1997). Some of the *Protoperidinium* species (*P. depressum*) have also shown survival for extended periods (up to 71 days) in conditions of starvation (Jakobsen and Hansen, 1997; Menden-Deuer et al., 2005). However, the capability to endure extended starvation is a useful strategy, especially for a species-specific feeder; their presence might not indicate optimal growth conditions (Gribble et al., 2007). *Chaetoceros simplex* was also found abundantly in deeper SCML. The presence of *Chaetoceros simplex* in low light and nutrient-poor conditions is also reported from the deeper waters of the western Pacific Ocean (Mou et al., 2022). On the other hand, ElliP and PoP were the most prevalent PGSs in SCML and were dominated by spore-forming (e.g., *Chaetoceros* spp., *Bacteriastrum* spp.; Bosak et al., 2015) and low-light-adapted taxa (e.g., *Pseudonitzschia* spp.).

The relation between morphological traits (S:V vs GALD) differed between SCML depths, suggesting different adaptive strategies to cope with prevailing conditions. The PGSs in shallow SCML showed low S:V and high GALD, while in intermediate and deep SCML, PGSs showed high S:V and low GALD (Fig. 4). For instance, high S:V and low GALD observed in deep and intermediate SCML could be due to low nutrient and light conditions (O'Farrell et al., 2007; Morabito et al., 2007) and vice versa for shallow SCML. Kruk et al. (2015) reported from subtropical estuary that the S:V ratio increased with the vertical attenuation coefficient and, supposedly, the extent of light limitation. Cell elongation gives micro-phytoplankton a competitive advantage by diminishing sinking velocity (Padisak et al., 2003), better nutrient absorption without affecting S:V ratio (Kleparski et al., 2022), enhancing light capture (Naselli-Flores and Barone, 2011) and can also be an adaptation to grazing (Petrucciani et al., 2022). The morphometric traits of the dominant PGSs between SCML depths show specific morphometric adaptation (like the ability to maintain an optimum S:V and GALD). For example, in shallow SCML, all dominant species in their respective PGSs maintained a low S:V (0.15–0.67 μm^{-1}) and high GALD (40–158 μm), whereas, in deep SCML, high S:V (0.37–0.90 μm^{-1}) and low GALD (27–72 μm) strategy was prevalent. The intermediate SCML S:V (0.20–0.92 μm^{-1}) and GALD (28–111 μm) values were higher than shallow but lower than deep SCML. Such trait variability could be due to nutrient limitation as light availability is the same at all SCML depths (i.e., 1–2 %). Though many studies have shown a strong effect of light (O'Farrell et al., 2007; Kruk et al., 2015) and nutrients (Naselli-Flores and Barone, 2011) on the phytoplankton morphology but under constant low light conditions, nutrients act as a strong controlling factor (Morabito et al., 2007; Charalampous et al., 2018). Moreover, the spectral quality of light (within the range of photosynthetic active radiation; PAR, 400–700 nm) other than the intensity plays a significant role for phytoplankton (Hintz et al., 2021). The spectral range of light shifts from a full spectrum at the sea surface to a limited (predominantly blue spectrum) in deeper layers (Kirk, 1994; Holtrop et al., 2021). Therefore, the spectral quality of light in shallow, intermediate, and deep SCML might be subjected to such spectral shifts, which may also be an additional factor influencing morphometric traits.

Additionally, variability in S:V was also observed for different PGSs between SCML depths, similar to that observed for the sea surface waters. For instance, S:V of Cyl increased significantly, and ElliP and Elli showed a minor increase, whereas PoP and B decreased significantly with increasing depth of SCML. The shallow and intermediate SCMLs were less stratified and nutrient-depleted than the deep SCMLs. Such environmental differences in SCMLs are strongly reflected in a similar pattern in the morphological attributes of Cyl, ElliP, and Elli, whereas PoP and B show opposite trends. Ryabov et al. (2021) considered PGSs like Cyl and ElliP elongated and PoP and B oblate shapes. They have argued that the rate of nutrient diffusion declines as cell curvature decreases; therefore, an elongated cell can provide a larger nutrient flow than oblate cells. They also observed that the maximum surface extension for oblate shapes are smaller than the elongated ones. Moreover, the opposite trends observed in PoP and B might also be because of the pennate diatom taxa (e.g., *Pseudonitzschia*, *Thalassiothirx,* and *Thalassionema*) that dominate these PGSs. These taxa are either known to be well adapted to thrive in low light conditions or form chains to overcome their geometric constraints. Hence, the elongated PGSs are more prevalent with robust morphological attributes responding to environmental conditions than the oblate PGSs. The observations suggest that light (both quantity and quality) and nutrients have a robust limiting influence on the morphological attributes of micro-phytoplankton in the oligotrophic pelagic system of IO.

4.3. Sea surface vs SCML

The sea surface and SCML taxa also differed and were governed by the prevailing environmental conditions in both layers. The trophic conditions are different across IO, like eutrophic conditions (Northeastern AS), mesotrophic conditions (central and southeastern AS, and BoB), and oligotrophic conditions (equatorial and STIO); therefore, the taxa are expected to be different (Sarma et al., 2021). The micro-phytoplankton assemblages between the surface and SCML reveal that the SCML community is well adapted to the subsurface environments by showing distinct assemblages from the surface. Few studies have reported that assemblage might be similar if SCML is formed due to growing cell accumulation near the sea surface. However, if SCML is formed due to active growth, the species assemblage may differ from the upper layer (Furuya and Marumo, 1983). In this study, except for AST2, all the SCML have formed below MLD, suggesting major environmental constraints governing community differences.

Additionally, morphometric traits (S:V and GALD) showed interesting results. For instance, S:V of dominant PGSs (e.g., Cyl, ElliP, and PoP) showed no specific pattern or trends between shallow SCML and the corresponding sea surface. Probably, environmental conditions showed similarity to shallow SCML within MLD. In contrast, the PGSs of intermediate and deep SCML showed distinct patterns with the corresponding sea surface due to differences in environmental conditions. For instance, dominant PGSs showed an increasing and decreasing trend in their S:V and GALD values, respectively. However, no such changes or patterns were noticed in complex PGSs like 2C, which correspond to dinoflagellates that can overcome any vertical environmental gradient by using their flagella for migration. An increase in S:V helps improve nutrient uptake in general (Raven, 1999; Kruk et al., 2015); therefore, the observed patterns in S:V and GALD might be in response to nutrient availability. The allometric scaling analysis of dominant PGSs in which the functional relationship between two measured quantities (S:V and GALD in this study), where a relative change in one quantity results in a relative proportional change in the other, in surface and SCML revealed

interesting information. For all dominant PGSs, any change in GALD was associated with very minimal change (decrease) in S:V (Figs. 2–4), suggesting the adaptation by dominant PGSs to conserve S:V. The degree of change in S:V was even less for SCML than the surface. Similar strategies have been reported previously from the north and southeastern Arabian Sea (Paul et al., 2023), the Mediterranean micro-tidal lagoon (Aubry et al., 2017), and the coast of the Salento peninsula (Stanca et al., 2013). However, in AS, nutrient availability and the prevailing hydrographic conditions determined the adaptive strategies adopted by dominant PGSs. The variations in allometric patterns are not evolutionary but result from random variations or local adaptive differences among populations (Neustupa, 2016). These variations have been identified as essential factors in morphological evolutions as individual allometric trajectories may act as constraints canalizing evolutionary change of morphology (Klingenberg, 2010; Wilson, 2013; Pelabon et al., 2014). Reynold has implicitly recognized morphological traits as "master traits" because physiological and ecological features are strongly regulated by shape and size (Reynolds, 2006; Weithof and Beisner, 2019) and represent organisms' response to environmental changes affecting ecosystem functioning (Kruk et al., 2021). The morphological attributes and their variability help species to increase their fitness to varying environmental factors. This morphological variability is known as "phenotypic plasticity" and can be produced by a single genotype (West-Eberhard, 1989). The realized niches can be made unstable by a species using phenotypic plasticity over space and time (Marrone et al., 2023). Therefore, given the above arguments, this study argues that S:V and GALD can act as robust morphological traits in the pelagic regions of IO. PGSs like Cyl and PoP respond very strongly, and ElliP sporadically to environmental factors aided by their morphological traits, making them proxies to map the phenotypic plasticity in large pelagic systems, which is predicted to change due to global warming.

Several modelling-based studies suggest climate warming will increase ocean stratification, reducing nutrient exchange between the deep ocean and the upper mixed layer (Bopp et al., 2001; Sarmiento et al., 2004). The stratification in the upper 200 m has increased by 5.3 % in the global ocean (in recent decades, i.e., 1960–2018), caused mainly by temperature changes (Li et al., 2020). According to Dutkiewicz et al. (2005), ocean stratification will deepen the nitracline, reducing nutrient supply to the euphotic layer by the end of this century and oceanic primary productivity by 14 %. Nonetheless, predicting the impact of such changes on marine ecosystems is elusive. Cermeño et al. (2008) indicated that enhanced nutrient limitation would reduce the competitive advantages of diatoms. As revealed in our study, the SCML formed at depths coincided with 1–2 % PAR and nitracline depth (within 10 m depth above or below).

Besides global warming and climate change, the increased nutrient influx (both natural and anthropogenic activity-driven) is one of the major issues affecting ecosystems' ecological status (e.g., Krishna et al., 2016; Thiagarajan et al., 2024), particularly primary producers (including their morphology and size). The northern Indian Ocean (i.e., AS and BoB), in addition to natural processes (e.g., upwelling, convective mixing, freshwater influx), receive higher river discharges and anthropogenic aerosols than the southern Indian Ocean (EIO and STIO) (e.g., Rasch et al., 2001; Zhang and Reid, 2010; Panda et al., 2024), which can be linked to rapid industrialization and other activities (e.g., Sridevi et al., 2023). Such nutrient inputs are generally limited to the sea surface layers, which mostly influence the surface phytoplankton community and morphometric traits. In this study, the morphometric traits (S:V and GALD), which showed a north-south gradient (i.e., the S:V gradually increased and GALD decreased), were positively correlated with nutrients, i.e., micro-phytoplankton size (i.e., elongated forms) increase with increasing nutrients. A higher S:V aids in higher nutrient uptake, more light exposure, and improves resistance against sinking (Naselli-Flores et al., 2007). However, any increase in the S:V could also risk a phytoplankton cell to photoinhibition or damage caused by higher PAR exposure at the sea surface (Kirk, 1994), leaving a shape-specific response of the morphometric traits, as evident in this study. Our findings align with Naselli-Flores and Barone (2007), who recorded more elongated phytoplankton shapes in a eutrophic waterbody with less light availability. The elongated micro-phytoplankton forms can have a competitive upper hand under turbulent and eutrophic environments, which can help non-flagellated forms (like *Skeletonema*, *Talassiosira*, and *Chaetoceros*) to out-compete other non-elongated phytoplankton forms (Hardikar et al., 2024).

In the case of SCML depths, a tight coupling for deep SCML PGSs (including S:V and GALD) with nutrients and light (PAR) was observed. Further, N:P values at different SCML depths varied according to nitracline, i.e., higher in shallow (2.21 ± 1.12) and intermediate (2.50 ± 4.32) than in deep (1.38 ± 0.33) SCML. The N:P value at deep SCML was low because it formed above the nitracline depth, and the gap between them was also greater. Further, the temperature negatively correlated with GALD and PGSs, suggesting relatively higher temperatures favored smaller phytoplankton cells. Therefore, under the predicted global warming scenario, deepening of nitracline might affect the different size and shape primary producers in the following ways: (i) smaller spherical phytoplankton (e.g., picoplankton, coccolithophores): these have less nutrient requirements and might be relatively less affected as they are well adapted to low light and low nutrient condition (known to have low Reynolds numbers with high S:V and low GALD, making nutrient uptake much easier; Fogg, 1991), (ii) bigger flagellated phytoplankton with complex PGS (like dinoflagellates) with high S:V and GALD: these cells might be moderately affected as they are equipped with various nutrition modes (e.g., autotrophy, heterotrophy, and mixotrophy) and can also evade low nutrient conditions using flagella for motility, and (iii) bigger simple PGS phytoplankton (without flagella; e.g., diatoms) with low to moderate S:V and GALD: these forms are dominant (80–90 %), possess distinct phenotypic plasticity, have higher nutrient requirements and might be severely affected by light and nutrient limitation. Therefore, their morphometric traits can offer a potential ecological proxy in predicted oceanic climate change scenarios (deeper nitracline with very low light and a relatively shallow SCML with low nutrients). Under such conditions, the morphological traits (S:V and GALD) can be useful tracers to delineate the adaptive strategies by different PGSs, i.e., PGS with high morphometric plasticity (like cylinder and prism on parallelogram) will have the upper hand over other PGS (like an elliptic prism) with limited plasticity. Nonetheless, further studies unraveling the dynamics of S:V and GALD of PGS with nitracline depth and PAR under the predicted future scenarios will provide more insights into the resilience or vulnerability of micro-phytoplankton (both at sea surface and SCML), biological pump efficiency per se, to the global change predictions.

5. Conclusion

This study concludes that the simple elongated PGSs (e.g., Cyl, ElliP, and PoP) were cosmopolitan, having similar dominance (with varying percentage contribution) patterns in the sea surface, SCML, and between the deep SCML and corresponding sea surface. However, they showed latitudinal gradients at the sea surface, i.e., north-south and south-north gradients for Cylindrical and Elliptic-prism PGS, respectively. In contrast, the complex PGS showed sporadic distribution. Further, the similarity between the PGSs (community and morphological trait) of SCML and the corresponding sea surface is based on the location of the former concerning MLD. Among SCMLs, the occurrence depth determined PGS dominance and its morphological attributes. Simple and complex PGS contribution gradually decreases and increases, respectively, with increasing SCML depth. Also, PGS in shallow SCML showed low S:V and high GALD, while in intermediate and deep SCML, high S:V and low GALD, indicating adaptive strategy, i.e., phenotypic plasticity behavior by dominant PGSs to capture light. Between the SCML depths, only simple PGS (Cylinder followed by Elliptic-prism and Prism on parallelogram) showed profound variability in morphological traits

showcasing strong phenotypic plasticity behavior. Further, a positive correlation between the morphometric traits (S:V and GALD) and nutrients was observed for surface and SCML depths. This study highlights the applicability of S:V and GALD as a potential ecological proxy to assess the ecological impact of physical processes (e.g., convective mixing, upwelling, eddies) and anthropogenic-driven activity (e.g., coastal eutrophication, aerosol deposition) linked to nutrient and light availability in oceanic systems. Since micro-phytoplankton are significant contributors to SCML, this study facilitates a better understanding of SCML ecology and biogeochemistry per se in predicted ocean change scenarios.

CRediT authorship contribution statement

Pranoy Paul: Writing – review & editing, Writing – original draft, Validation, Methodology, Investigation, Formal analysis, Data curation. **Jagadish S. Patil:** Writing – review & editing, Supervision, Resources, Project administration, Funding acquisition, Data curation, Conceptualization.

Declaration of competing interest

The authors declare that they have no known competing financial interests or personal relationships that could have appeared to influence the work reported in this paper.

Data availability

All data concerning the study are included in this manuscript, and some are provided as supplementary. However, it does not apply to material availability.

Acknowledgments

The authors are grateful to the Director, CSIR-National Institute of Oceanography, Goa, India for his support and encouragement. This work is part of the CSIR TraceBioMe project (MLP2018). The authors thank Drs. Samir Damare, Dr. Belle Shenoy, Mr. Anthony DeSouza, Mr. Milind Naik, Mr. Kallathin M, Mr. Kuldeep Kumar, Mr. Sheldon Rebello, Mr. Ramesh T, and the RV Sindhu Sadhana crew (SSD069 and 079) for their help in sampling. The first author also acknowledges UGC for fellowship. The authors are grateful to anonymous reviewers for their constructive suggestions. This is the NIO contribution number 7294.

Appendix A. Supplementary data

Supplementary data to this article can be found online at https://doi.org/10.1016/j.marpolbul.2024.116952.

References

Aubry, B.F., Pugnetti, A., Roselli, L., Stanca, E., Acri, F., Finotto, S., Basset, A., 2017. Phytoplankton morphological traits in a nutrient-enriched, turbulent Mediterranean microtidal lagoon. J. Plankton Res. 39 (3), 564–576. https://doi.org/10.1093/plankt/fbx008.

Baldry, K., Strutton, P.G., Hill, N.A., Boyd, P.W., 2020. Subsurface chlorophyll-a maxima in the southern ocean. Front. Mar. Sci. 7, 671. https://doi.org/10.3389/fmars.2020.00671.

Barnett, M.L., Kemp, A.E.S., Hickman, A.E., Purdie, D.A., 2019. Shelf Sea subsurface chlorophyll maximum thin layers have a distinct phytoplankton community structure. Cont. Shelf Res. 174, 140–157. https://doi.org/10.1016/j.csr.2018.12.007.

Barton, A.D., Pershing, A.J., Litchman, E., Record, N.R., Edwards, K.F., Finkel, Z.V., Kiørboe, T., Ward, B.A., 2013. The biogeography of marine plankton traits. Ecol. Lett. 16 (4), 522–534. https://doi.org/10.1111/ele.12063.

Bates, S.S., 1998. Ecophysiology and metabolism of ASP toxin production. In: Anderson, D.M., Cembella, A.D., Hallegraeff, G.M. (Eds.), Physiological Ecology of Harmful Algal Blooms. Springer-Verlag, pp. 405–426.

Behrenfield, M.J., Falkowski, P.G., 1997. Photosynthetic rates derived from satellite-based chlorophyll concentration. Limnol. Oceanogr. 42, 1–10. https://doi.org/10.4319/lo.1997.42.1.0001.

Bopp, L., Monfray, P., Aumont, O., Dufresne, J.L., Le Treut, H., Madec, G., Terray, L., Orr, J.C., 2001. Potential impact of climate change on marine export production. Global Biogeochem. Cycles 15 (1), 81–99.

Bosak, S., Šupraha, L., Nanjappa, D., Kooistra, W.H., Sarno, D., 2015. Morphology and phylogeny of four species from the genus Bacteriastrum (Bacillariophyta). Phycol 54 (2), 130–148. https://doi.org/10.2216/14-62.

Buskey, E.J., 1997. Behavioral components of feeding selectivity of the heterotrophic dinoflagellate Protoperidinium pellucidum. Mar. Ecol. Prog. Ser. 153, 77–89. https://doi.org/10.3354/meps153077.

Butts, T.J., Moody, E.K., Wilkinson, G.M., 2022. Contribution of zooplankton nutrient recycling and effects on phytoplankton size structure in a hypereutrophic reservoir. J. Plankton Res. 44 (6), 839–853. https://doi.org/10.1093/plankt/fbac045.

Cermeño, P., Dutkiewicz, S., Harris, R.P., Follows, M., Schofield, O., Falkowski, P.G., 2008. The role of nutricline depth in regulating the ocean carbon cycle. Proc. Natl. Acad. Sci. 105 (51), 20344–20349.

Charalampous, E., Matthiessen, B., Sommer, U., 2018. Light effects on phytoplankton morphometric traits influence nutrient utilization ability. J. Plankton Res. 40 (5), 568–579. https://doi.org/10.1093/plankt/fby037.

Clarke, K.R., Gorley, R.N., 2006. PRIMERv6: User Manual/Tutorial. PRIMER-E, Plymouth.

Clarke, K.R., Warwick, R.M., 2001. Change in Marine Communities: An Approach to Statistical Analysis and Interpretation. PRIMER-E, Plymouth.

Cullen, J.J., 1982. The deep chlorophyll maximum - comparing vertical profiles of chlorophyll-a. Can. J. Fish. Aquat. Sci. 39, 791–803. https://doi.org/10.1139/f82-108.

Cullen, J.J., 2015. Subsurface chlorophyll maximum layers: enduring enigma or mystery solved? Ann. Rev. Mar. Sci. 7, 207–239. https://doi.org/10.1146/annurev-marine-010213-135111.

de Boyer Montegut, C., Madec, G., Fischer, A.S., Lazar, A., Iudicone, D., 2004. Mixed layer depth over the global ocean: an examination of profile data and a profile-based climatology. J. Geophy. Res.: Oceans, 109(C12). doi:https://doi.org/10.1029/2004JC002378.

Decembrini, F., Caroppo, C., Bergamasco, A., 2020. Influence of lateral advection on phytoplankton size-structure and composition in a Mediterranean coastal area. Continent. Shelf Res. 209, 104216. https://doi.org/10.1016/j.csr.2020.104216.

Dugdale, R.C., Goering, J.J., 1967. Uptake of new and regenerated forms of nitrogen in primary productivity. Limnol. Oceanogr. 12, 196–206. https://doi.org/10.4319/lo.1967.12.2.0196.

Durante, G., Basset, A., Stanca, E., Roselli, L., 2019. Allometric scaling and morphological variation in sinking rate of phytoplankton. J. Phycol. 55, 1386–1393. https://doi.org/10.1111/jpy.12916.

Durham, W.M., Stocker, R., 2012. Thin phytoplankton layers: characteristics, mechanisms, and consequences. Ann. Rev. Mar. Sci. 4, 177–207. https://doi.org/10.1146/annurev-marine-120710-100957.

Dutkiewicz, S., Sokolov, A., Stone, P., Scott, J., 2005. Joint Program of the Science and Policy of Global Change Report, 122. Massachusetts Institute of Technology, Cambridge, MA.

Estrada, M., Delgado, M., Blasco, D., Latasa, M., Cabello, A.M., Benítez-Barrios, V., Vidal, M., 2016. Phytoplankton across tropical and subtropical regions of the Atlantic. Indian and Pacific oceans. PLoS One 11 (3), e0151699. https://doi.org/10.1371/journal.pone.0151699.

Finkel, Z.V., Beardall, J., Flynn, K.J., Quigg, A., Rees, T.A.V., Raven, J.A., 2010. Phytoplankton in a changing world: cell size and elemental stoichiometry. J. Plankton Res. 32 (1), 119–137. https://doi.org/10.1093/plankt/fbp098.

Fogg, G.E., 1991. The phytoplanktonic ways of life. New Phytol. 118 (2), 191–232.

Fu, M., Sun, P., Wang, Z., Wei, Q., Qu, P., Zhang, X., Li, Y., 2018. Structure, characteristics and possible formation mechanisms of the subsurface chlorophyll maximum in the Yellow Sea cold water mass. Cont. Shelf Res. 165, 93–105. https://doi.org/10.1016/j.csr.2018.07.007.

Furuya, K., Marumo, R., 1983. The structure of the phytoplankton community in the subsurface chlorophyll maxima in the western North Pacific Ocean. J. Plankton Res. 5, 393–406. https://doi.org/10.1093/plankt/5.3.393.

Garg, S., Gauns, M., Pratihary, A.K., 2024. Response of oceanic subsurface chlorophyll maxima to environmental drivers in the northern Indian Ocean. Environ. Res. 240, 117528. https://doi.org/10.1016/j.envres.2023.117528.

Goldman, J.C., McGillicuddy, D.J., 2003. Effect of large marine diatoms growing at low light on episodic new production. Limnol. Oceanogr. 48, 1176–1182. https://doi.org/10.4319/lo.2003.48.3.1176.

Grasshoff, K., Ehrhardt, M., Kremling, K. (Eds.), 1992. Methods of Seawater Analysis, 634Pp., Verl. Chem. Weinheim, Germany. https://doi.org/10.1002/9783527613984.

Gribble, K.E., Nolan, G., Anderson, D.M., 2007. Biodiversity, biogeography and potential trophic impact of *Protoperidinium* spp. (Dinophyceae) off the southwestern coast of Ireland. J. Plankton Res. 29 (11), 931–947. https://doi.org/10.1093/plankt/fbm070.

Grover, J.P., 1989. Influence of cell shape and size on algal competitive ability. J. Phycol. 25, 402–405. https://doi.org/10.1111/j.1529-8817.1989.tb00138.x.

Hanson, C.E., Pesant, S., Waite, A.M., Pattiaratchi, C.B., 2007. Assessing the magnitude and significance of deep chlorophyll maxima of the coastal eastern Indian Ocean. Deep Sea Res. Part II: Topical Studies in Oceanography 54 (8–10), 884–901. https://doi.org/10.1016/j.dsr2.2006.08.021.

Hardikar, R., Haridevi, C.K., Deshbhratar, S., 2024. Trait-based classification and environmental drivers of phytoplankton functional structure from anthropogenically

altered tropical creek. Thane Creek India. Mar. Poll. Bull. 198, 115767. https://doi.org/10.1016/j.marpolbul.2023.115767.
Herbland, A., Voituriez, B., 1979. Hydrological structure analysis for estimating the primary production in the tropical Atlantic Ocean. J. Mar. Res. 37, 10–87. https://elischolar.library.yale.edu/journal_of_marine_research/1461.
Hillebrand, H., Durselen, C.D., Kirschtel, D., Pollingher, U., Zohary, T., 1999. Biovolume calculation for pelagic and benthic microalgae. J. Phycol. 35, 403–424. https://doi.org/10.1046/j.1529-8817.1999.3520403.x.
Hintz, N.H., Zeising, M., Striebel, M., 2021. Changes in spectral quality of underwater light alter phytoplankton community composition. Limnol. Oceanogra. 66 (9), 3327–3337. https://doi.org/10.1002/lno.11882.
Holtrop, T., Huisman, J., Stomp, M., Biersteker, L., Aerts, J., Grébert, T., Partensky, F., Garczarek, L., Woerd, H.J., 2021. Vibrational modes of water predict spectral niches for photosynthesis in lakes and oceans. Nat. Ecol. Evol. 5, 55–66. https://doi.org/10.1038/s41559-020-01330-x.
Houliez, E., Schmitt, F.G., Breton, E., Skouroliakou, D.I., Christaki, U., 2023. On the conditions promoting *pseudo-nitzschia* spp. blooms in the eastern English Channel and southern North Sea. Harmful Algae 102424. https://doi.org/10.1016/j.hal.2023.102424.
Irwin, A.J., Finkel, Z.V., Schofield, O.M., Falkowski, P.G., 2006. Scaling-up from nutrient physiology to the size-structure of phytoplankton communities. J. Plankton Res. 28 (5), 459–471. https://doi.org/10.1093/plankt/fbi148.
Jakobsen H.H., Hansen P.J., 1997. Prey size selection, grazing and growth response of the small heterotrophic dinoflagellate *Gymnodinium* sp. and the ciliate *Balanion comatum*—a comparative study, Mar. Ecol. Prog. Ser., vol. 158, pg.75-86.doi:https://doi.org/10.3354/meps158075.
Jayaram, C., Udaya Bhaskar, T.V.S., Chacko, N., Prakash, S, Rao K.H., 2021. Spatio-temporal variability of chlorophyll in the northern Indian Ocean: a biogeochemical Argo data perspective. Deep–Sea Res. II., 183, 104928.doi:https://doi.org/10.1016/j.dsr2.2021.104928.
Kagami, M., de Bruin, A., Ibelings, B.W., Van Donk, E., 2007. Parasitic chytrids: their effects on phytoplankton communities and food-web dynamics. Hydrobiol 578, 113–129. https://doi.org/10.1007/s10750-006-0438-z.
Karp-Boss, L., Boss, E., 2016. The elongated, the squat and the spherical: Selective pressures for phytoplankton shape. In: Glibert, P.M., Kana, T.M. (Eds.), Aquatic Microbial Ecology and Biogeochemistry: A Dual Perspective. Springer International Publication, Geneva, Switzerland, pp. 25–34.
Kiorboe, T., 2008. A Mechanistic Approach to Plankton Ecology. Princeton University Press.
Kirk, J.T.O., 1994. Light and Photosynthesis in Aquatic Ecosystems, second ed. Cambridge University Press, Cambridge, 509pp.
Kleparski, L., Beaugrand, G., Edwards, M., Schmitt, F.G., Kirby, R.R., Breton, E., Gevaert, F., Maniez, E., 2022. Morphological traits, niche-environment interaction and temporal changes in diatoms. Prog. Oceanogra. 201, 102747. https://doi.org/10.1016/j.pocean.2022.102747.
Klingenberg, C.P., 2010. There's something afoot in the evolution of ontogenies. BMC Evol. Biol. 10, 221.
Krishna, M.S., Prasad, M.H.K., Rao, D.B., Viswanadham, R., Sarma, V.V.S.S., Reddy, N.P. C., 2016. Export of dissolved inorganic nutrients to the northern Indian Ocean from the Indian monsoonal rivers during discharge period. Geochim. Cosmochim. Acta 172, 430–443. https://doi.org/10.1016/j.gca.2015.10.013.
Kruk, C., Segura, A.M., 2012. The habitat template of phytoplankton morphology-based functional groups. Hydrobiol 698, 191–202. https://doi.org/10.1007/s10750-012-1072-6.
Kruk, C., Huszar, V.L., Peeters, E.T., Bonilla, S., Costa, L., Lürling, M., Reynolds, C.S., Schefer, M., 2010. A morphological classification capturing functional variation in phytoplankton. Fresh. Biol. 55 (3), 614–627. https://doi.org/10.1111/j.1365-2427.2009.02298.x.
Kruk, C., Martínez, A., Nogueira, L., Alonso, C., Calliari, D., 2015. Morphological traits variability reflects light limitation of phytoplankton production in a highly productive subtropical estuary (Río de la Plata, South America). Mar. Biol. 162, 331–341. https://doi.org/10.1007/s00227-014-2568-6.
Kruk, C., Devercelli, M., Huszar, V.L., 2021. Reynolds functional groups: a trait-based pathway from patterns to predictions. Hydrobiol 848, 113–129. https://doi.org/10.1007/s10750-020-04340-9.
Legendre, L., Rassoulzadegan, F., 1996. Food-web mediated export of biogenic carbon in oceans: environmental control. Mar. Ecol. Prog. Ser. 145, 179–193. https://doi.org/10.3354/meps145179.
Leonilde, R., Elena, L., Elena, S., Francesco, C., Alberto, B., 2017. Individual trait variation in phytoplankton communities across multiple spatial scales. J. Plankton Res. 39 (3), 577–588. https://doi.org/10.1093/plankt/fbx001.
Lepš, J., Šmilauer, P., 2003. Multivariate Analysis of Ecological Data Using CANOCO. Cambridge university press.
Lewis, W.M., 1976. Surface/volume ratio: implication for phytoplankton morphology. Science 192, 885–887. https://doi.org/10.1126/science.192.4242.885.
Li, G., Cheng, L., Zhu, J., Trenberth, K.E., Mann, M.E., Abraham, J.P., 2020. Increasing ocean stratification over the past half-century. Nat. Clim. Chang. 10 (12), 1116–1123. https://doi.org/10.1038/s41558-020-00918-2.
Litchman, E., Klausmeier, C.A., 2008. Trait-based community ecology of phytoplankton. The Annu. Rev. Ecol. Evol. Syst. 39, 615–639. https://doi.org/10.1146/annurev.ecolsys.39.110707.173549.
Litchman, E., Klausmeier, C.A., Schofeld, O.M., Falkowski, P.G., 2007. The role of functional traits and trade-offs in structuring phytoplankton communities: scaling from cellular to ecosystem level. Ecol. Lett. 10 (12), 1170–1181. https://doi.org/10.1111/j.1461-0248.2007.01117.x.
Litchman, E., de Tezanos Pinto, P., Edwards, K.F., Klausmeier, C.A., Kremer, C.T., Thomas, M.K., 2015. Global biogeochemical impacts of phytoplankton: a trait-based perspective. J. Ecol. 103(6). https://doi.org/10.1111/1365-2745.12438.
Margalef, R., 1978. Life-forms of phytoplankton as survival alternatives in an unstable environment. Oceanol. Acta 1, 493–509.
Marrone, F., Fontaneto, D., Naselli-Flores, L., 2023. Cryptic diversity, niche displacement, and our poor understanding of taxonomy and ecology of aquatic microorganisms. Hydrobiol 850 (6), 1221–1236. https://doi.org/10.1007/s10750-022-04904-x.
McLaughlin, F.A., Carmack, E.C., 2010. Deepening of the nutricline and chlorophyll maximum in the Canada Basin interior, 2003–2009. Geophys. Res. Lett. 37 (24). https://doi.org/10.1029/2010GL045459.
Menden-Deuer, S., Lessard, E.J., Satterberg, J., Grünbaum, D., 2005. Growth rates and starvation survival of three species of the pallium-feeding, thecate dinoflagellate genus *Protoperidinium*. Aquat. Microb. Ecol. 41 (2), 145–152. https://doi.org/10.3354/ame041145.
Mignot, A., Claustre, H., Uitz, J., Poteau, A., d'Ortenzio, F., Xing, X., 2014. Understanding the seasonal dynamics of phytoplankton biomass and the deep chlorophyll maximum in oligotrophic environments: a bio-Argo float investigation. Global Biogeochem. Cycles 28 (8), 856–876. https://doi.org/10.1002/2013GB004781.
Morabito, G., Oggioni, A., Caravati, E., Panzani, P., 2007. Seasonal morphological plasticity of phytoplankton in Lago Maggiore (N. Italy). Hydrobiol 578, 47–57. https://doi.org/10.1007/s10750-006-0432-5.
Mou, S., Zhang, Z., Zhao, H., Nair, S., Li, Y., Xu, K., Zhang, Y., 2022. A dark-tolerant diatom (*Chaetoceros*) cultured from the deep sea. J. Phycol. 58 (2), 208–218. https://doi.org/10.1111/jpy.13240.
Naselli-Flores, L., Barone, R., 2007. Pluriannual morphological variability of phytoplankton in a highly productive Mediterranean reservoir (Lake Arancio, southwestern Sicily). Hydrobiol 578, 87–95. https://doi.org/10.1007/s10750-006-0436-1.
Naselli-Flores, L., Barone, R., 2011. Invited review - fight on plankton! Or, phytoplankton shape and size as adaptive tools to get ahead in the struggle for life. Cryptogam. Algol. 32, 157–204. https://doi.org/10.7872/crya.v32.iss2.2011.157.
Naselli-Flores, L., Padisak, J., 2023. Analysis of morphological traits as a tool to identify the realized niche of phytoplankton populations: what do the shape of planktic microalgae, Anna Karenina and Vincent van Gogh have in common? Hydrobiol 1-17. https://doi.org/10.1007/s10750-023-05195-6.
Naselli-Flores, L., Padisak, J., Albay, M., 2007. Shape and size in phytoplankton ecology: do they matter? Hydrobiol 578, 157–161. https://doi.org/10.1007/s10750-006-2815-z.
Neustupa, J., 2016. Static allometry of unicellular green algae: scaling of cellular surface area and volume in the genus Micrasterias (Desmidiales). J. Evol. Biol. 29, 292–305. https://doi.org/10.1111/jeb.12781.
Niklas, K.J., 2000. The evolution of plant body plans—a biomechanical perspective. Ann. Bot. 85 (4), 411–438. https://doi.org/10.1006/anbo.1999.1100.
O'Farrell, I., de Tezanos Pinto, P., Izaguirre, I., 2007. Phytoplankton morphological response to the underwater light conditions in a vegetated wetland. Hydrobiol 578, 65–77. https://doi.org/10.1007/s10750-006-0434-3.
Padisak, J., Soroczki-Pinter, E., Rezner, Z., 2003. Sinking properties of some phytoplankton shapes and the relation of form resistance to morphological diversity of plankton—An experimental study. In Aquatic Biodiversity (ed. Martens, K.). Kluwer Academic Publishers, Dordecht, Netherlands, pp. 243–257.doi:https://doi.org/10.1007/978-94-007-1084-9_18.
Padisak, J., Crossetti, L.O., Naselli-Flores, L., 2009. Use and misuse in the application of the phytoplankton functional classification: a critical review with updates. Hydrobiol 621, 1–19. https://doi.org/10.1007/s10750-008-9645-0.
Pancic, M., Kiørboe, T., 2018. Phytoplankton defence mechanisms: traits and trade-offs: defensive traits and trade-offs. Biol. Rev. 93, 1269–1303. https://doi.org/10.1111/brv.12395.
Panda, P.P., Shukla, G., Kumar, A., Aswini, M.A., Kaushik, A., Nayak, G., Matta, V.M., 2024. Atmospheric deposition of mineral dust and associated nutrients over the equatorial Indian Ocean. Sci. Tot. Environ. 915, 169779. https://doi.org/10.1016/j.scitotenv.2023.169779.
Paul, P., Patil, J.S., Anil, A.C., 2021. Phytoplankton communities in marine intertidal rock-pools: effect of location, geometric shapes and allelopathy. J. Ear. Syst. Sci. 130 (3), 128. https://doi.org/10.1007/s12040-021-01591-5.
Paul, P., Patil, J.S., Anil, A.C., 2023. Variability in phytoplankton shape dominance in marine pelagic systems: prevalence of different adaptive strategies in the eastern Arabian Sea during the winter monsoon. Environ. Monit. Assess. 195 (4), 528. https://doi.org/10.1007/s10661-023-11062-7.
Pelabon, C., Firmat, C., Bolstad, G.H., Voje, K.L., Houle, D., Cassara, J., Rouzic, A.L., Hansen, T.F., 2014. Evolution of morphological allometry. Annu. N. Y. Acad. Sci. 1320, 58–75. https://doi.org/10.1111/nyas.12470.
Petrucciani, A., Chaerle, P., Norici, A., 2022. Diatoms versus copepods: could frustule traits have a role in avoiding predation? Front. Mar. Sci. 8, 804960. https://doi.org/10.3389/fmars.2021.804960.
Rasch, P.J., Collins, W.D., Eaton, B.E., 2001. Understanding the Indian Ocean experiment (INDOEX) aerosol distributions with an aerosol assimilation. J. Geophys. Res.: Atmospheres 106 (D7), 7337–7355. https://doi.org/10.1029/2000JD900508.
Raven, J.A., 1999. Picophytoplankton. Prog. Phycol. Res. 13, 33–106.
Regaudie-de-Gioux, A., Lasternas, S., Agustí, S., Duarte, C.M., 2014. Comparing marine primary production estimates through different methods and development of conversion equations. Front. Mar. Sci. 1, 19. https://doi.org/10.3389/fmars.2014.00019.

Revelante, N., Gilmartin, M., 1995. The relative increase of large phytoplankton in subsurface chlorophyll maximum of the northern Adriatic Sea. J. Plankton Res. 17 (17), 1535–1562. https://doi.org/10.1093/plankt/17.7.1535.
Reynolds, C.S., 1988. Functional morphology and the adaptive strategies of freshwater phytoplankton. Growth and reproductive strategies of freshwater phytoplankton 388–433.
Reynolds, C.S., 2006. The Ecology of Phytoplankton. Cambridge University Press, Cambridge, p. 535.
Reynolds, C.S., 2007. Variability in the provision and function of mucilage in phytoplankton: facultative responses to the environment. Hydrobiol 578 (1), 37–45. https://doi.org/10.1007/s10750-006-0431-6.
Reynolds, C.S., Huszar, V., Kruk, C., Naselli-Flores, L., Melo, S., 2002. Towards a functional classification of the freshwater phytoplankton. J. Plankton Res. 24 (5), 417–428. https://doi.org/10.1093/plankt/24.5.417.
Ross, O.N., Sharples, J., 2007. Phytoplankton motility and the competition for nutrients in the thermocline. Mar. Ecol. Prog. Ser. 347, 21–38. https://doi.org/10.3354/meps06999.
Ryabov, A., Kerimoglu, O., Litchman, E., Olenina, I., Roselli, L., Basset, A., Stanca, E., Blasius, B., 2021. Shape matters: the relationship between cell geometry and diversity in phytoplankton. Ecol. Lett. 24, 847–861. https://doi.org/10.1111/ele.13680.
Salmaso, N., Naselli-Flores, L., Padisak, J., 2015. Functional classifications and their application in phytoplankton ecology. Freshw. Biol. 60 (4), 603–619. https://doi.org/10.1111/fwb.12520.
Salmaso, N., Padisak, J., 2007. Morpho-functional groups and phytoplankton development in two deep lakes (Lake Garda, Italy and Lake Stechlin, Germany). Hydrobiol 578, 97–112. https://doi.org/10.1007/s10750-006-0437-0.
Sarma, V.V., Aswanikumar, V., 1991. Subsurface chlorophyll maxima in the north-western bay of Bengal. J. Plankton Res. 13 (2), 339–352. https://doi.org/10.1093/plankt/13.2.339.
Sarma, V.V.S.S., Prasad, M.H.K., Dalabehera, H.B., 2021. Influence of phytoplankton pigment composition and primary production on pCO2 levels in the Indian Ocean. J. Earth Syst. Sci. 130, 85. https://doi.org/10.1007/s12040-021-01598-y.
Sarmiento, J.L., Slater, R., Barber, R., Bopp, L., Doney, S.C., Hirst, A.C., Kleypas, J., Matear, R., Mikolajewicz, U., Monfray, P., Soldatov, V., 2004. Response of ocean ecosystems to climate warming. Global Biogeochem. Cycles 18 (3). https://doi.org/10.1029/2003GB002134.
Schott, F.A., McCreary Jr., J.P., 2001. The monsoon circulation of the Indian Ocean. Prog. Oceanogr. 51 (1), 1–123. https://doi.org/10.1016/S0079-6611(01)00083-0.
Shah, H.M., Smitha, B.R., Mohammad Hatha, A.A., Sudhakar, M., 2020. Subsurface chlorophyll maxima in the north eastern Arabian Sea: simulation on impact of warming. Ecol. Indic. 110, 105858. https://doi.org/10.1016/j.ecolind.2019.105858.
Shulenberger, E., Reid, J.L., 1981. The Pacific shallow oxygen maximum, deep chlorophyll maximum, and primary productivity, reconsidered. Deep-Sea Res. Part A: Oceanographic Research Papers 28 (9), 901–919. https://doi.org/10.1016/0198-0149(81)90009-1.
Simberlof, D., Dayan, T., 1991. The guild concept and the structure of ecological communities. Annu. Rev. Ecol. Syst. 22, 115–143. https://doi.org/10.1146/annurev.es.22.110191.000555.
Smayda, T.J., 1970. The suspension and sinking of phytoplankton in the sea. Oceanography and marine biology. An Annu. Rev. 8, 353–414.
Sridevi, B., Sabira, S., Sarma, V.V.S.S., 2023. Impact of ocean warming on net primary production in the northern Indian Ocean: role of aerosols and freshening of surface ocean. Environ. Sci. Pollut. Res. 30 (18), 53616–53634. https://doi.org/10.1007/s11356-023-26001-9.
Stanca, E., Cellamare, M., Basset, A., 2013. Geometric shape as a trait to study phytoplankton distributions in aquatic ecosystems. Hydrobiol 701, 99–116. https://doi.org/10.1007/s10750-012-1262-2.
Sun, J., Liu, D., 2003. Geometric models for calculating cell biovolume and surface area for phytoplankton. J. Plankton Res. 25 (11), 1331–1334. https://doi.org/10.1093/plankt/fbg096.
Sunda, W.G., Hardison, D.R., 2010. Evolutionary tradeoffs among nutrient acquisition, cell size, and grazing defense in marine phytoplankton promote ecosystem stability. Mar. Ecol. Prog. Ser. 401, 63–76. https://doi.org/10.3354/meps08390.
Taylor, F.J.R., 1973. General features of dinoflagellate material collected by the "Anton Bruun". In: During the International Indian Ocean Expedition. The Biology of the Indian Ocean. Springer, pp. 155–169.
Ter Braak, C.J., Smilauer, P., 2002. CANOCO reference manual and CanoDraw for Windows user's guide: software for canonical community ordination (version 4.5). www.canoco.com.
Thiagarajan, V., Nah, T., Xin, X., 2024. Impacts of atmospheric particulate matter deposition on phytoplankton: a review. Sci. Tot. Environ. 175280. https://doi.org/10.1016/j.scitotenv.2024.175280.
Tilman, D., Kilham, S.S., Kilham, P., 1982. Phytoplankton community ecology: the role of limiting nutrients. Annu. Rev. Ecol. Syst. 13 (1), 349–372. https://doi.org/10.1146/annurev.es.13.110182.002025.
Tomas, C.R. (Ed.), 1997. Identifying Marine Phytoplankton. Academic Press.
Weithof, G., Beisner, B.E., 2019. Measures and approaches in trait-based phytoplankton community ecology–from freshwater to marine ecosystems. Front. Mar. Sci. 6, 40. https://doi.org/10.3389/fmars.2019.00040.
Weithoff, G., 2003. The concepts of 'plant functional types' and 'functional diversity' in lake phytoplankton – a new understanding of phytoplankton ecology? Freshwat. Biol. 48, 1669–1675. https://doi.org/10.1046/j.1365-2427.2003. 01116.x.
West-Eberhard, M.J., 1989. Phenotypic plasticity and the origins of diversity. Annu. Rev. Ecol. Syst. 20, 249–278. https://doi.org/10.1146/annurev.es.20. 110189.001341.
Wilson, L.A.B., 2013. Allometric disparity in rodent evolution. Ecol. Evol. 3, 971–984. https://doi.org/10.1002/ece3.521.
Wirtz, K.W., 2011. Non-uniform scaling in phytoplankton growth rate due to intracellular light and CO2 decline. J. Plankton Res. 33, 1325–1341. https://doi.org/10.1093/plankt/fbr021.
Xiao, L.J., Wang, T., Hu, R., Han, B.P., Wang, S., Qian, X., Padisák, J., 2011. Succession of phytoplankton functional groups regulated by monsoonal hydrology in a large canyon-shaped reservoir. Water Res. 45 (16), 5099–5109. https://doi.org/10.1016/j.watres.2011.07.012.
Yasunaka, S., Ono, T., Sasaoka, K., Sato, K., 2022. Global distribution and variability of subsurface chlorophyll a concentrations. Ocean Sci. 18 (1), 255–268. https://doi.org/10.5194/os-18-255-2022.
Zhang, J., Reid, J.S., 2010. A decadal regional and global trend analysis of the aerosol optical depth using a data-assimilation grade over-water MODIS and Level 2 MISR aerosol products. Atmos. Chem. Phys., 10(22), 10949–10963. doi:https://doi.org/10.5194/acp-10-10949-2010, 2010.
Zhuang, Y., Jin, H., Chen, J., Ren, J., Zhang, Y., Lan, M., Zhang, T., He, J., Tian, J., 2020. Phytoplankton community structure at subsurface chlorophyll maxima on the western Arctic shelf: patterns, causes, and ecological importance. J. Geophy. Res.: Biogeosciences, 125(6), e2019JG005570. doi:https://doi.org/10.1029/2019JG005570.
Zohary, T., Padisák, J., Naselli-Flores, L., 2010. Phytoplankton in the physical environment: beyond nutrients, at the end, there is some light. Hydrobiol 639, 261–269. https://doi.org/10.1007/s10750-009-0032-2.

Environmental Science and Pollution Research
https://doi.org/10.1007/s11356-024-34913-3

RESEARCH ARTICLE

Geographic distribution of modern dinoflagellate cysts in surface sediments of the Arabian Sea: significance of taxa and morphometry as potential ecological indicators

Pranoy Paul[1,2] **· Jagadish Siddalingappa Patil**[1]

Received: 13 November 2023 / Accepted: 31 August 2024
© The Author(s), under exclusive licence to Springer-Verlag GmbH Germany, part of Springer Nature 2024

Abstract
Studies on dinoflagellate cysts in the Arabian Sea (AS) are limited to the coastal waters, but no information from the deeper depths. The dinoflagellate cyst assemblages in surface sediment samples (0–2 cm) from the deeper depths (up to ~ 4500 m) of central (oxygen minimum zone (OMZ)) and southeastern (oligotrophic) AS revealed that the relatively good numbers of cyst concentrations reach deeper depths of OMZ (3505 m) and oligotrophic (4368 m) regions, but the former harbored more cyst concentrations than the latter. The cyst concentration and species count (including HAB species) recorded here are lower compared to the eastern (EAS) and western (WAS) AS, but the autotrophic cyst dominance (74–83%) at deeper depths is in contrast with the heterotrophic dominance in coastal AS. Of the recorded 41 cyst species (belonging to 18 genera), four species (cyst of *Cladopyxis* sp., *Operculodinium janduchenei*, *Stelladinium bifurcatum*, and *Protoperidinium monospinum*) from the deepest part of oligotrophic AS form the first report. In contrast, *Spiniferites* and *Lingulodinium* cysts were common occurrences. Taxonomic comparison with literature revealed (i) the prevalence of more cosmopolitan species (32 species) which could be due to the prevalence of large and small-scale lateral transport of cysts in oligotrophic regions followed by OMZ and coastal regions, respectively, and (ii) very few region-specific species, i.e., cyst of *Protoperidinium latissimum*, *Lejeunecysta sabrina*, cyst of *Protoperidinium denticulatum* in EAS and *Impagidinium patulum*, and *I. strialatum*, in WAS. Interestingly, variability in the morphometry was evident between the coastal and open oceans in some cosmopolitan cysts, e.g., *Operculodinium centrocarpum* and *Lingulodinium machaerophorum*. These findings from the less studied pelagic regions will contribute to the growing knowledge of dinoflagellate cyst distribution patterns and highlight the significance of cyst taxa and morphology as potential ecological indicators for AS.

Keywords Dinoflagellate cysts · Arabian Sea · OMZ · Oligotrophic region · Coastal region · Deep sea

Introduction

Dinoflagellates are a diverse phytoplankton group and one of the important primary producers in marine ecosystems (Rodrigues and Patil 2021). Dinoflagellates (only 12–13%) are known to produce organic-walled and calcareous cysts as part of their life cycles (Head 1996), but in some cases, adverse environmental conditions (like changes in temperature, salinity, and nutrient flux) can also induce cyst production. Many of these resting organic-walled cysts are known to be resistant to physical, chemical, and biological degradation (Dale 1996) and settle at the bottom of the ocean floor. These cysts help dinoflagellates to form seed banks for blooms (including harmful algal blooms), produce toxins (e.g., *Alexandrium* and *Gymnodinium* species), and help in unwanted marine bio-invasion as they remain viable for many years (Matsuoka and Fukuyo 2000; Lundholm et al. 2011; Delebecq et al. 2020). Dinoflagellate cysts are also used as proxies for climate reconstruction and pollution (e.g., Pospelova et al. 2005; Hallegraeff and Gollasch 2006; Marret et al. 2009; Mertens et al. 2009a), as indicators for past environmental conditions (Pospelova et al. 2002; Marret and Zonneveld 2003), qualitative and quantitative

Responsible Editor: V.V.S.S. Sarma

✉ Jagadish Siddalingappa Patil
patilj@nio.res.in

[1] CSIR-National Institute of Oceanography, Dona Paula 403004, Goa, India

[2] School of Earth, Ocean and Atmospheric Sciences, Goa University, Taleigao Plateau 403 206, Goa, India

Published online: 12 September 2024

reconstructions of sea surface temperature (SST), sea surface salinity (SSS), sea-ice cover duration, or primary productivity (e.g., Mudie et al. 2002; Marret and Zonneveld 2003; Pospelova et al. 2006, 2015; Radi and de Vernal 2008; Zonneveld et al. 2008; de Vernal et al. 2013). However, to reconstruct past environmental conditions, one should understand the relationship between individual dinoflagellate cyst species and specific environmental parameters, which requires a region-specific understanding of the spatial distribution of cysts in relation to environmental conditions (e.g., Dale 1976, 2009; Pospelova et al. 2004, 2005).

The Arabian Sea (AS) is one of the interesting ocean basins as it is strongly influenced by the Asian Monsoon system, which regulates its biological productivity (Banse 1987) and also the presence of an intense oxygen minimum zone (OMZ) in the thermocline depths (~ 100 to 1000 m) (Morrison et al. 1998). The OMZ region and the southeastern AS are known to be relatively productive and oligotrophic, respectively (Vijayan et al. 2021). Dinoflagellate cysts are reported to be susceptible to oxidative degradation (Zonneveld et al. 1997) similar to organic matters, and therefore, cysts sensitive to oxidative degradations (e.g., cysts of *Protoperidinium* species) preserve well in the OMZ sediment (Narale et al. 2015). Though dinoflagellate cysts from the Arabian Sea (AS) have received ample attention, studies from OMZ and southeastern oligotrophic regions have received less attention than those from the productive coastal regions of the AS.

Most of the work on the dinoflagellate cyst from the coastal and oceanic regions of the western Arabian Sea (WAS) is studied and compiled by Zonneveld et al. (1997, 2003, and 2013) and Marret and Zonneveld (2003). The coastal regions in the WAS are known to be productive and driven by intensive upwelling (Marret and Zonneveld 2003; Sprangers et al. 2004; Holzwarth et al. 2007). Therefore, the reported high concentration of dinoflagellate cysts (139 to 75 000 cysts g^{-1}) in the coastal regions in the WAS can be linked to productivity. On the other hand, most of the work on dinoflagellate cysts from the coastal regions and port areas of the EAS are studied by various authors (Godhe et al. 2000; D'costa et al. 2008; D'silva et al. 2011, 2012; Narale et al. 2015; Rodrigues et al. 2019, 2022) focusing only on cyst assemblage. Interestingly, these studies have reported the dominance of heterotrophic dinoflagellate cysts, which are generally linked to the indicators for eutrophic environments and high productivity (Dale et al. 1999; Matsuoka 1999; Radi and Vernal 2004; Dale 2009; Price et al. 2018). However, a recent study by Rodrigues et al. (2022) from different levels of eutrophicated marine ports (Mangalore & Cochin port) located on the west coast of India showed the dominance of autotrophic dinoflagellate cysts (except Kandla port). Despite the coastal regions of the eastern Arabian Sea (EAS) being productive (driven by coastal upwelling), the concentration of dinoflagellate cysts is not as high compared to the WAS (Narale et al. 2013). Overall, these studies give us a general picture of dinoflagellate cyst distributions in the coastal regions, but the information from deeper depths (beyond 2000 m) is scarce. Generally, dinoflagellate cyst morphology, which is species-specific, makes them potential proxies for environmental factors (e.g., temperature, salinity). However, the information on the variability of cyst morphology from field samples representing different ecosystems is limited. A recent study documented variability in the morphometry of common cysts (with and without process) and correlated salinity values between the marine and estuarine ecosystems on the Indian coast (Rodrigues and Patil 2021), highlighting more measurements to provide better insights. Global datasets of dinoflagellate cysts distributed in surface sediments provide detailed information for a better understanding of the environmental drivers of cyst species at a larger basin scale (de Vernal et al. 2001; Marret and Zonneveld 2003; Zonneveld et al. 2013; de Vernal et al. 2020; Marret et al. 2020). Over the years, dinoflagellate studies (including cysts) in coastal settings received more attention than oceans because of major economic and health threats due to the increasing HAB events (Zonneveld et al. 2022). A recent study by Marret et al. (2020) on the distribution of dinoflagellate cysts across the world oceans highlighted the gap in the pelagic regions of the Indian Oceans. Therefore, a study of dinoflagellate cysts from the deep-sea sediments in the pelagic region of the AS will fill the gap in the current datasets and add to the biogeography of dinoflagellate cysts in the deepest parts of the AS. Through this study, the following was documented: (a) cyst assemblage from the deep-sea sediments (> 200 m water column depths); (b) differences in cyst assemblage between coastal, OMZ, and oligotrophic regions; (c) new records, if any; and (d) variations in morphometry of selected cosmopolitan dinoflagellate cysts. Further, by combining cyst datasets of the current study with that of the literature, major distributional patterns of dinoflagellate cysts are documented for the AS to identify the cosmopolitan and region-specific cyst taxa as well as morphometric differences of selected cosmopolitan taxa from the perspective of potential ecological indicators for the AS.

Materials and methods

Sample collection and hydrographic conditions

The study was conducted under the interdisciplinary program launched by the Council of Scientific and Industrial Research-National Institute of Oceanography (CSIR-NIO) called TraceBioMe. Under this program, the sampling and observations were made in the southeastern Arabian Sea from 12 January to 12 February 2020

onboard R/V *Sindhu Sadhana* (SSD069). Sediment cores were collected at eight stations (Fig. 1 and Table 1) representing coastal (station 1), oligotrophic (stations 2 to 5), and OMZ (stations 6 to 8) regions using the Maxi Multiple Corer (60 cm length × 100 mm diameter), which is the standard Bowers and Connelly corer currently used worldwide, (Ocean Scientific International Ltd). The sediment grain size (sand, > 63 μm; silt, 4–63 μm; and clay, < 4 μm) was measured by dry sieving and pipette analysis (Folk et al. 1970; Folk 1974). The sediment collected is silty (except in stations 1, 2, and 7). The sediment was sandy in station 1, while the sediment was silty clay in stations 2 and 7 (Table 1). The hydrographic details of the stations are published elsewhere (Singh et al. 2023). The sampling stations 6, 7, and 8 lie inside the denitrification zone, particularly in the thermocline depths (100–1000 m) of the AS (Naqvi, 1991), and the same was evident from dissolved oxygen (DO) profiles during the sampling period (Singh et al. 2023). Further, a relative increase in DO was also observed in the deeper waters (> 2000 m; Singh et al. 2023). Salinity data revealed the influence of Persian Gulf and Red Sea

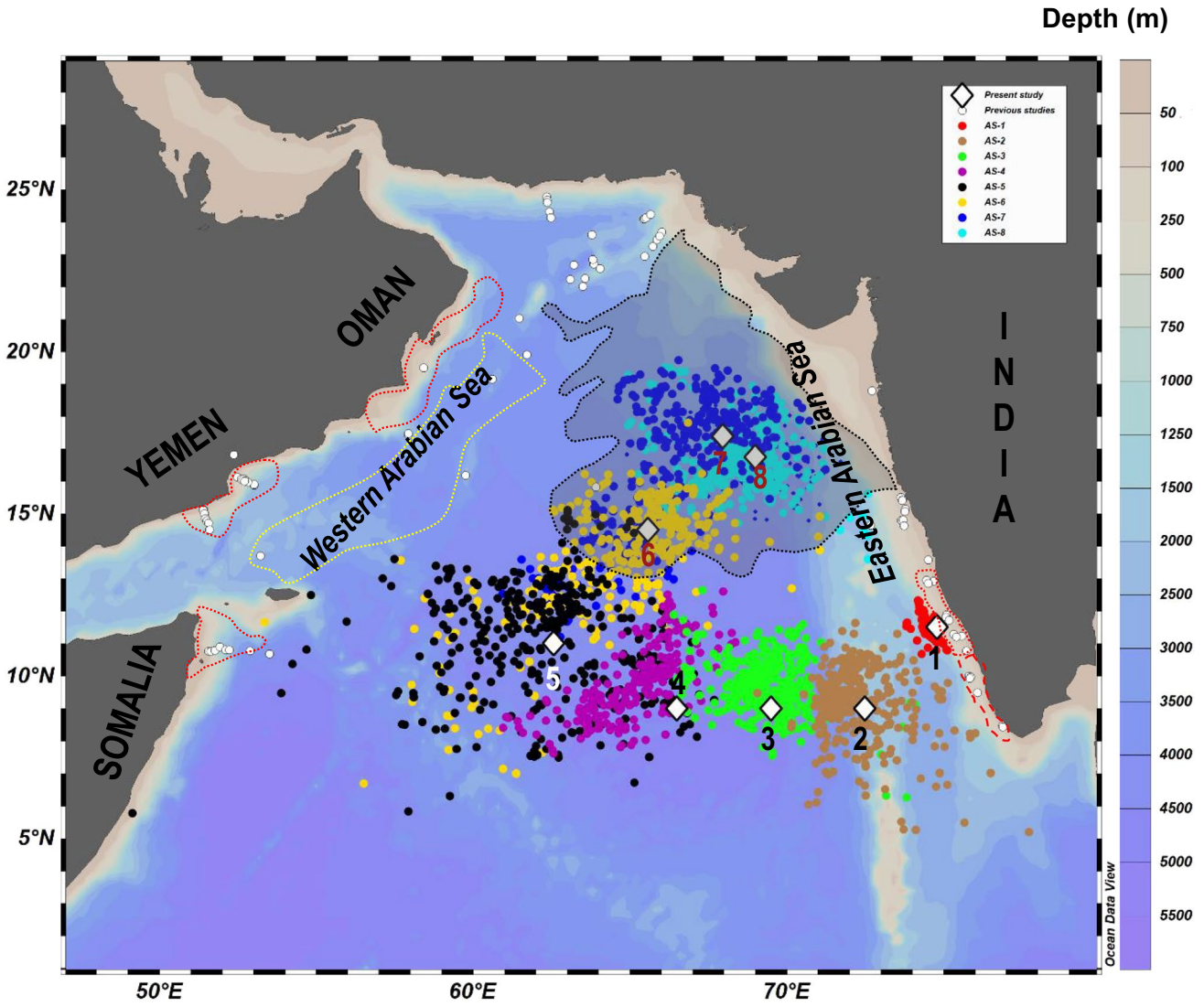


Fig. 1 The map shows sample locations plotted on a bathymetric map of the Arabian Sea and the possible surface origin locations of cysts in the surface sediment samples. The data points (indicating surface origin locations) showed in ODV plots are generated from the planktondrift simulation tool by selecting 11 m/day sinking speed scenario. The sampling stations are numbered and depicted in white-bordered diamond shapes. The colorful dots represent the cyst origin locations in the upper water column. The red and yellow dotted line shows coastal and oceanic upwelling zones (Marret and Zonneveld 2003; Banse 1968); the eastern AS experiences both weaker (bold red dash lines) and stronger (small red dot lines) coastal upwelling zone (Smitha et al., 2008); the shaded region with black dotted lines shows the denitrification zone (Naqvi, 1991). White circles indicate the locations from previous studies (e.g., Marret et al. 2020; Godhe et al. 2000; D'costa et al., 2008; Dsilva et al., 2011, 2012; Narale et al. 2015)

Table 1 Sampling locations, water depths, species count, number of cyst counted in 5 g wet sediment, heterotrophic to autotrophic ratio (H/A), and sediment type for each station. *AS* Arabian Sea, *OMZ* oxygen minimum zone, *m* meters, *N* dinoflagellate cyst count, *W* weight of wet sediment, *WC* water content

Regions of the Arabian Sea and sampling stations		Longitude (E)	Latitude (N)	Water depth (m)	Species count	Dinoflagellate cyst counted (5 g/wet weight; *N*)	Wet weight of sediment taken for count (g; *W*)	Proportion of sediment content (1 – WC)	Cyst concentration (cysts g^{-1} dry sediment = $N/(W \times (1 - WC))$)	Heterotrophic to autotrophic ratio (H/A)	Sediment type
Coastal AS	**1**	74.7	11.5	113	19	715	5	0.62	231	0.20	Sandy
Oligotrophic AS	**2**	72.5	9	2105	24	119	5	0.52	46	0.82	Silty clay
	3	69.5	9	4607	15	272	5	0.59	92	0.05	Silty
	4	66.5	9	4520	16	116	5	0.34	68	0.12	Silty
	5	62.5	11	4368	22	240	5	0.31	155	0.46	Silty
OMZ AS	**6**	65.5	14.5	3911	21	308	5	0.57	108	0.19	Silty
	7	67.9	17.3	3505	20	376	5	0.61	123	0.58	Silty clay
	8	69.0	16.7	3643	22	343	5	0.49	140	0.33	Silty

waters in thermocline depths of OMZ regions, and the influence of low saline Bay of Bengal (BOB) waters at the coastal station (Supplementary Fig. 1) and Arabian Sea high saline water (over a depth range of 75 to 100 m) was apparent during the sampling period (Singh et al. 2023). Surface chlorophyll was higher (0.2 to 1.14 mg m^{-3}) in the OMZ region, followed by coastal (0.26 mg m^{-3}) and oligotrophic region (0.06 mg m^{-3}).

Sample processing

The top 2 cm of each sediment core (0–2 cm) was processed following the palynological method (Matsuoka and Fukuyo 2000). A known weight (2–5 g) of wet sediment was sonicated for 1 min with distilled water (DW) and sieved through with 100 and 10 µm mesh repeatedly to remove salts and debris. Subsequently, the acid-free slurry was sieved through a tier of two different meshes (100 and 10 µm) to remove coarse and fine material. The retained residue on the 10 µm mesh was treated with 10% hydrochloric acid (HCl) for 24 h to remove calcium carbonate and later washed thoroughly with DW and then with 30% hydrofluoric acid (HF) to dissolve silicate materials. All the acid-treated samples were washed thoroughly with DW 4–5 times to remove acid. The acid-free residue was sieved again through 10 µm mesh and re-suspended carefully to 10 mL DW in a vial, and the entire 10 mL was analyzed microscopically (e.g., Cho and Matsuoka 2001; Matsuoka et al. 2003; Wang et al. 2004; Baula et al. 2011) using an inverted microscope (Olympus IX73) equipped with a digital camera (Qimaging MicroPublisher 5.0 RTV) at × 100–400 magnification for identification and quantification of dinoflagellate cysts. A total of 100–300 dinoflagellate cysts per sample were counted. In this study, dinoflagellate cyst abundances are represented by cyst concentrations and were calculated as the number of cysts per gram of dry sediment (cysts g^{-1}) using the formula $N/(W \times (1 - WC))$, where N is the total number of cysts, W is the wet sediment weight taken for analysis, and WC is the water content (Cho and Matsuoka 2001; Matsuoka et al. 2003). To estimate the water content, an extra sample from the top 0–2 cm of each core was taken, and a known weight (0.5–1 g) of the wet sample was dried at 70 °C for 24 h, and the weight difference between the wet and dried samples is the water content (Matsuoka et al. 2003). Further, Price et al. (2016), based on tracer experiments, documented an average loss of 8.2% of Lycopodium spores during processing, with the greatest loss occurring through the fine sieve and resulting in only a 4.8% overestimation of the cyst concentration. This suggests that, in our study, the loss is mainly during the sieving process as we have analyzed the entire residue sample (except station 1, i.e., coastal station) rather than just a portion. Additionally, the acids used in sediment processing are known to cause the dissolution of calcareous cysts (e.g.,

Scrippsiella) and the cysts lacking distinctive ornamentation (e.g., *Alexandrium*; Bravo et al. 2006). Considering their distribution restricted to shallow depths in coastal regions (Zonneveld et al., 2005; Wendler et al. 2002; Rodrigues et al. 2019 & 2022; Narale et al. 2015) and absence at 4035 m depth (Zonneveld et al., 2005), it is assumed that the methodology employed has not influenced the data generated in this study. Millero et al. (1998) reported that the water in the north-eastern AS is under-saturated in [CO_3^{2-}] below 3400 m; hence, the calcium carbonate dissolution might be more. Wendler et al. (2002) reported 81–96% and 50–84% decrease in calcareous cyst flux between the trap and the surface sediments from the north-eastern and south-western AS, respectively. These processes further confirm the absence of the calcareous dinoflagellate cysts in the AS's deeper depths (< 3500 m). Also, in stations, 1 (113 m) and 2 (2105 m), *Scrippsiella* and *Alexandrium* cysts' absence was confirmed by scanning the aliquots of untreated, distilled water cleaned, and sieved sediment samples. Taking these and Price et al. (2016) findings, it is assumed that the cyst loss in our study may not be significant, and the cyst concentration presented will represent near real concentrations with negligible impact on the variability in cyst assemblage, dominance pattern, and distribution trends presented in this study.

The identification of dinoflagellate cysts was based on various published literature (Wall and Dale 1968; Sonneman and Hill 1997; Matsuoka and Fukuyo 2000; liu et al. 2012; Radi et al. 2013; Rigel et al. 2022; Li et al. 2020; online version: https://www.marum.de/en/Modern_dinoflagellate_cyst_determination_key.html). Cysts with clear morphologies were identified at their species level; however, a few cysts that could not be identified at their species level were represented by the genus "spp." The light microscope micrographs of some dinoflagellate cysts recorded are also presented (Fig. 2). Further, the analyzed dinoflagellate cyst assemblage is categorized into autotrophic, mixotrophic, and heterotrophic following Marret et al. (2020). Moreover, some dinoflagellate cyst species like *Spiniferites ramosus* and *S. bulloideus*, which show minor interspecific morphological variations (e.g., size and process thickness), were grouped as *S. ramosus* (Li et al. 2023). Similarly, *S. mirabilis* and *S. hyperacanthus* are grouped as cysts of *Gonyaulax spinifera* complex (or *S. mirabilis/hyperacanthus* in this study) (de Vernal et al. 2020, 2018; Rochon et al. 2009), whereas other *Spiniferites* which could not be identified to the species level are included in *Spiniferites* spp. Along with the counts, the morphometric (body size and process length) measurements of the following predominant dinoflagellate cysts, which occurred in coastal, OMZ, and oligotrophic regions, were also recorded and presented: *Spiniferites ramosus* ($n = 9$–30), *Lingulodinium machaerophorum* ($n = 5$–8), and *Operculodinium centrocarpum* ($n = 5$–25).

Diversity indices

Community indices such as species count (number of species), Shannon–Wiener's diversity index (H'), Pielous evenness, and Margalef's species richness of dinoflagellate cysts for each station were determined using PRIMER—version 6 (PRIMER–E Ltd. Plymouth, UK). Species count for each station is presented in Table 2. Additionally, the community indices for oligotrophic and OMZ regions were also determined by averaging the data for each station in the respective regions, i.e., the average of stations 2 to 5 and 6 to 8 for oligotrophic and OMZ, respectively (supplementary Fig. 2).

Planktondrift simulation

Planktondrift simulation is applied to trace the potential dinoflagellate cyst sources. Planktondrift (https://planktondrift.science.uu.nl) is an online particle trace simulation tool developed to simulate the trajectories and dispersal patterns of virtual particles representing plankton in the ocean (Nooteboom et al. 2019, 2020). The planktondrift simulation utilizes climate models like the Ocean General Circulation Model for the Earth Simulator (OFES), Nucleus for European Modelling of the Ocean (NEMO), or the Parallel Ocean Program (POP). These climate models provide a 3D flow field of the ocean currents in which particles are released every 3 days for 6 years at the bottom of the ocean and tracked back in time along the flow field. These sinking particles are assumed to be heavier than water; therefore, a vertical sinking velocity is added to the velocity along the transport. This study used the OFES model of the planktondrift simulation tool to trace the possible surface origin locations for all sampling stations, which incorporates more sinking scenarios than other models for locations falling below 75° North and South (https://planktondrift.science.uu.nl). The typical sinking speed for dinoflagellate cysts is 11 m/day (Anderson et al. 1985), and the same was selected to run the simulations.

Results

Dinoflagellate cyst diversity and distribution

Overall, a total of 41 cyst species belonging to 18 genera, of which 17 autotrophic, 3 mixotrophic, and 21 heterotrophic species were found in the present study (Fig. 2 and Table 1). The total cyst concentration was maximum in coastal (231 cysts g^{-1}), followed by OMZ (124 cysts g^{-1}) and oligotrophic regions (90 cysts g^{-1}) (Fig. 3a). The lowest cyst concentration was recorded in oligotrophic station 2 (46 cysts g^{-1}). Univariate measures revealed the following: (i) the cyst species count was higher in OMZ (Fig. 3b), (ii) diversity was

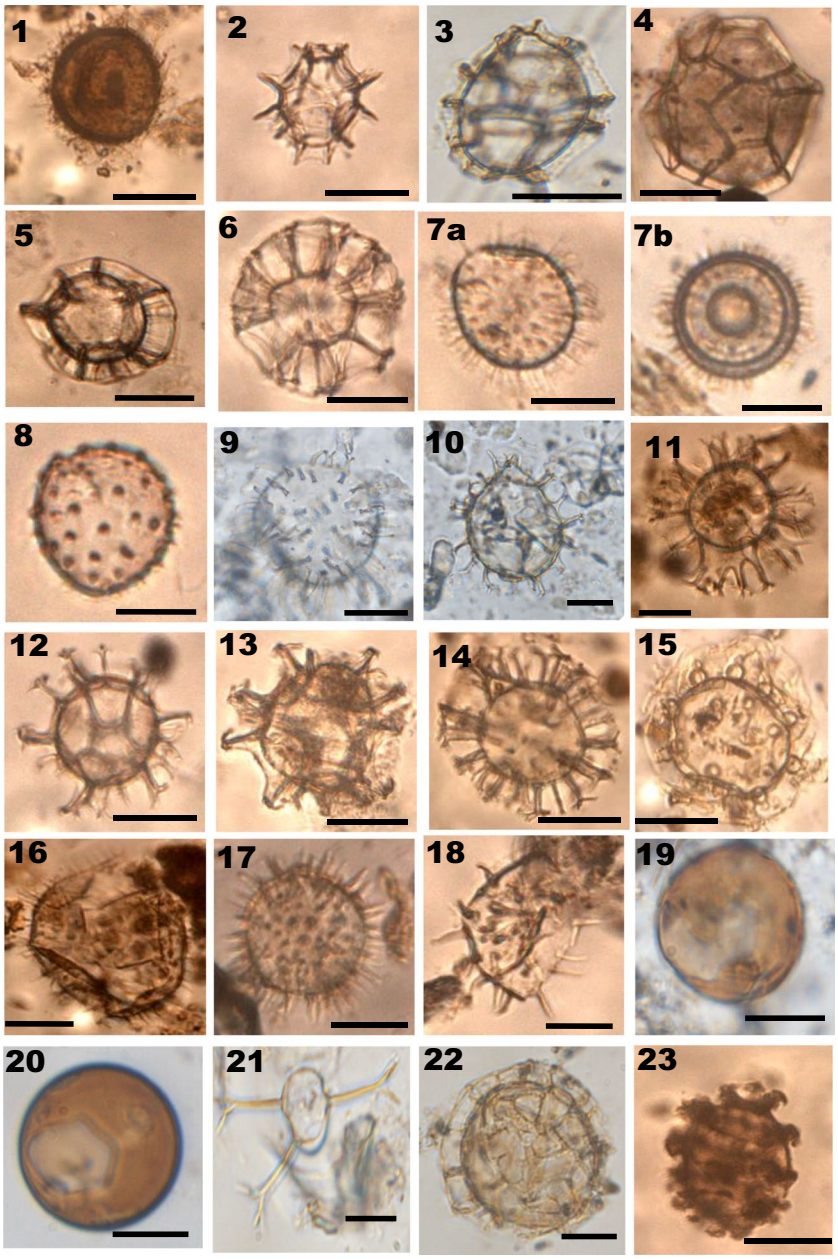


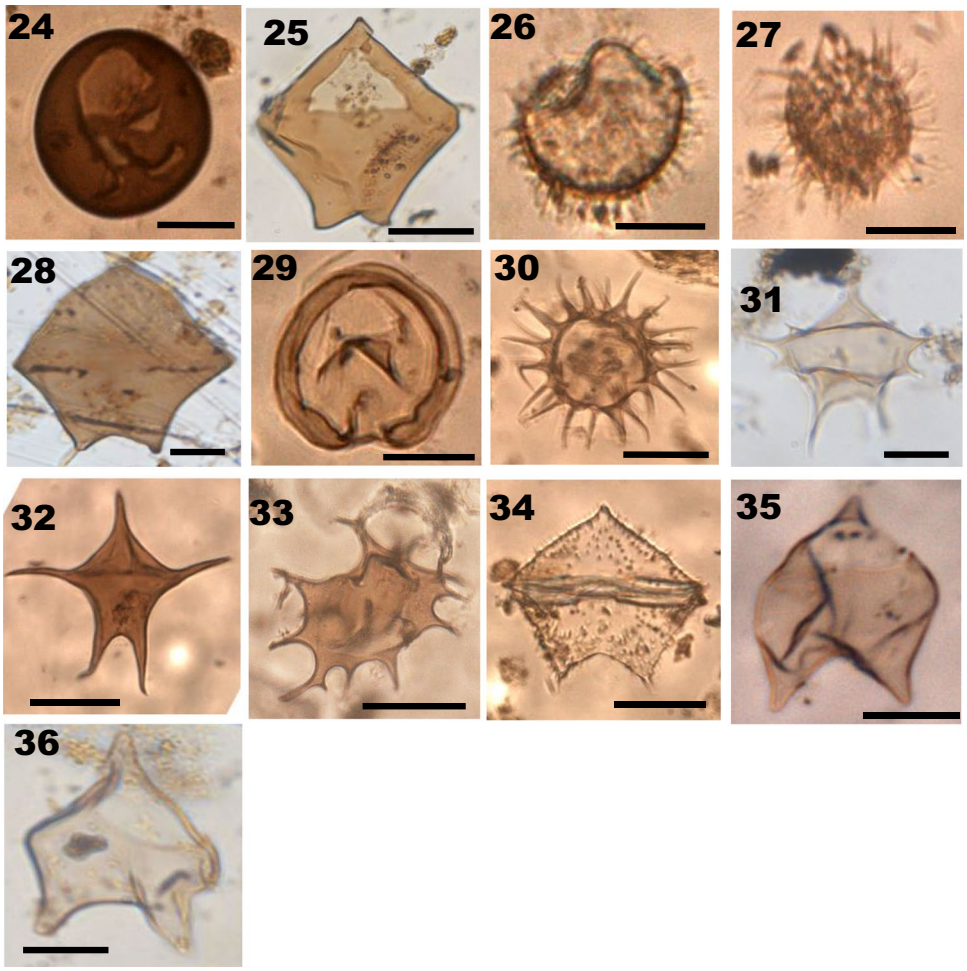
Fig. 2 Micrograph of autotrophic (1–15), mixotrophic (16–18), and heterotrophic (19–36) dinoflagellate cysts. Autotrophic: **1** *Bitectatodinium spongium*, **2** *Impagidinium aculeatum*, **3** *Impagidinium paradoxum*, **4** *Impagidinium patulum*, **5** *Impagidinium strialatum*, **6** *Nematosphaeropsis labyrinthus*, **7a**, **7b** *Operculodinium centrocarpum*, **8** *Operculodinium janduchenei*, **9** *Polysphaeridium zoharyi*, **10** *Spiniferites bentorii*, **11** *Spiniferites mirabilis*, **12** *Spiniferites ramosus*, **13** *Spiniferites* sp., **14** *Gonyaulax spiniferites* complex, and **15** *Tuberculodinium vancampoae*; mixotrophic: **16** cyst of *Polykrikos hartmannii*, **17** *Lingulodinium machaerophorum*, and **18** *Lingulodinium* sp.; and heterotrophic: **19** *Brigantedinium* sp., **20** *Brigantedinium simplex*, **21** cyst of *Cladopyxis* sp., **22** cyst of *Polykrikos kofoidii*, **23** cyst of *Polykrikos schwartzii*, **24** cyst of *Protoperidinium denticulatum*, **25** cyst of *Protoperidinium latissimum*, **26** cyst of *Protoperidinium monospinum*, **27** *Echinidinium* sp., **28** *Lejeunecysta sabrina* **29** *Selenopemphix nephroides*, **30** *Selenopemphix quanta*, **31** *Stelladinium bifurcatum*, **32** *Stelladinium reidii*, **33** *Stelladinium stellatum*, **34** *Trinovantedinium applanatum*, **35** *Votadinium calvum*, and **36** *Votadinium* sp. (all scale bar 20 micron)

relatively similar in the region (Fig. 3c), (iii) richness was higher in the oligotrophic region (Fig. 3d), and (iv) species evenness was higher in the oligotrophic region followed by OMZ and coastal regions of the AS (Fig. 3e).

In the oligotrophic region, maximum species count (24 species) and diversity index H' (2.7) were recorded in stations 2 and 5 (Supplementary Fig. 2), respectively. The other three stations in oligotrophic regions, where the depth varied from 2000 to 4600 m, recorded 15–22 species, 68–155 cysts g^{-1}, and 1.6–2.0 diversity index H' of dinoflagellate cysts. The deepest station 4 (depth 4607 m) recorded a relatively lower species count (only 16) and concentration (68 cysts g^{-1}). In the OMZ region, the species count was higher in station 8 (i.e., 22 taxa) followed by stations 6 and 7 (recorded 21 and 20 taxa, respectively) (supplementary Fig. 2). Station 8 recorded the maximum cyst concentration (140 cysts g^{-1}), followed by stations 7 (123 cysts g^{-1}) and 6 (108 cysts g^{-1}).

The cysts of autotrophic taxa dominated the assemblages than heterotrophic taxa in all the regions. Cysts produced by autotrophic taxa contribute 83%, 77%, and 74% to the total dinoflagellate cysts in the coastal, oligotrophic, and OMZ regions, respectively (Fig. 3f). The heterotrophic to autotrophic ratio (H/A) showed a slightly higher value in the OMZ (0.37) than in the oligotrophic (0.36) and coastal (0.20) regions (Fig. 4).

Fig. 2 (continued)



In the coastal and oligotrophic region, cyst assemblage was mostly dominated by autotrophic species like *Spiniferites* spp., cysts of *Gonyaulax Spinifera* complex, *S. ramosus*, and *S. mirabilis*, and mixotrophic species like *Lingulodinium* sp. representing 56% of the total dinoflagellate cyst assemblage. In the present study, potential HAB species cysts of three autotrophic and two mixotrophic cysts (cysts of *Gonyaulax Spinifera* complex, *Operculodinium centrocarpum*, *Polysphaeridium zoharyi*, cyst of *Polykrikos hartmannii*, and *Lingulodinium machaerophorum*) were recorded of which four were present in the deeper stations (i.e., stations 2–5) except cyst of *Polykrikos hartmannii* and four in the coastal station (i.e., station 1) except *Polysphaeridium zoharyi*.

On the contrary, in the OMZ region, the species count was higher in station 8 (i.e., 22 taxa) followed by stations 6 and 7 (recorded 21 and 20 taxa, respectively) (supplementary Fig. 2). Station 8 recorded the maximum cyst concentration (140 cysts g^{-1}), followed by stations 7 (123 cysts g^{-1}) and 6 (108 cysts g^{-1}). The OMZ region cyst assemblage was mostly dominated by autotrophic species like *Spiniferites* spp., *Spiniferites ramosus*, *Lingulodinium* sp., *Echinidinium* sp., *Nematosphaeropsis* sp., and *Impagidinium paradoxum* which represent 75% of the total dinoflagellate cyst assemblage. Among the five HAB species, three species in both station 6 (*Operculodinium centrocarpum*, *Gonyaulax Spinifera* complex and cyst of *Polykrikos hartmannii*) and station 7 (*Operculodinium centrocarpum*, *Gonyaulax Spinifera* complex and *Lingulodinium machaerophorum*) and all in station 8 were recorded. The comparison of cyst assemblage data revealed that the species count and abundance recorded in this study were low compared to the EAS and WAS (Fig. 5).

Morphometry of dinoflagellate cysts

The morphometric measurements of *Spiniferites ramosus* in the coastal ($l = 38 \pm 5$ µm, $w = 35 \pm 4$ µm, and PL = 11 ± 2 µm), oligotrophic ($l = 40 \pm 6$ µm, $w = 34 \pm 5$ µm, and PL = 10 ± 2 µm), and OMZ ($l = 38 \pm 4$ µm, $w = 34 \pm 3$ µm, and PL = 10 ± 2 µm) regions of the AS did not show any significant variation and fall within the reported size ranges ($l = 30$–46 µm, $w = 17$–43 µm, and PL = 1.2–12 µm) in the literature. The morphometric measurements of *Lingulodinium machaerophorum* in the coastal ($d = 35$ µm and PL = 6 µm), oligotrophic ($d = 49 \pm 5$ µm and PL = 13 ± 1 µm),

Table 2 Dinoflagellate cysts abundance (cysts g^{-1} dry weight) in all the stations of the Arabian Sea. *A* autotrophs, *M* mixotrophs, *H* heterotrophs. Trophic status is given following Marret et al. (2020). The motile affinity is based on Li et al. (2023), Marret et al. (2020), Ramírez-Valencia et al. (2021), and Rigel et al. (2022). Indet = indeterminate, + means previously reported, * means first report

	Trophic status	Motile affinity	Paleontological name	Coastal	Oligotrophic (OAS)				OMZ			OAS	OMZ	EAS	WAS
				St1	St2	St3	St4	St5	St6	St7	St8				
1	A	Unknown	*Bitectatodinium spongium*[4,5&6]	9.7	0.4	0.0	0.0	0.0	0.0	0.0	0.0	0.1	0.0	+	+
2	A	*Gonyaulax* sp. Indet	*Impagidinium aculeatum*[4&6]	0.0	0.8	1.9	5.3	11.3	10.2	0.0	0.2	4.8	3.5	+	+
3	A	*Gonyaulax* sp. Indet	*Impagidinium paradoxum*[4&6]	0.0	0.0	1.2	28.8	17.7	21.6	1.1	0.6	11.9	7.8	+	+
4	A	*Gonyaulax* sp. Indet	*Impagidinium patulum*[6]	0.0	1.0	0.5	2.9	4.8	1.1	0.3	0.0	2.3	0.5		+
5	A	*Gonyaulax* sp. Indet	*Impagidinium* sp.	0.0	1.0	0.0	3.8	0.6	0.0	0.0	0.0	1.4	0.0	+	+
6	A	*Gonyaulax* sp. Indet	*Impagidinium strialatum*[6]	1.6	0.0	0.0	2.4	1.0	10.5	3.3	0.2	0.8	4.7		+
7	A	*Gonyaulax spiniferites* complex	*Nematosphaeropsis labyrinthus*[4&6]	0.0	0.0	0.8	3.8	21.9	8.2	2.5	1.6	6.7	4.1	+	+
8	A	Unknown	*Nematosphaeropsis* sp.	0.0	0.0	0.0	0.0	0.0	8.8	8.2	4.1	0.0	7.0	+	+
9	A	*Protoperidinium reticulatum*	*Operculodinium centrocarpum*[1–6]	2.4	1.3	4.6	1.5	11.0	7.7	1.8	2.4	4.6	4.0	+	+
10	A	Unknown	*Operculodinium janduchenei**	0.0	0.2	0.0	3.8	1.9	5.8	3.3	0.0	1.5	3.0		
11	A	Unknown	*Operculodinium* sp.	0.0	0.0	1.5	0.0	0.0	0.7	0.2	0.0	0.4	0.3	+	+
12	A	*Pyrodinium bahamense*	*Polysphaeridium zoharyi*[3,5&6]	0.0	0.0	2.9	0.0	0.0	0.0	0.0	0.4	0.7	0.1	+	+
13	A	*Gonyaulax nezaniae*	*Spiniferites bentorii*[4&6]	0.0	0.0	0.5	0.0	0.0	0.0	0.0	0.0	0.1	0.0	+	+
14	A	*Gonyaulax whaseongensis*	*Spiniferites hyperacanthus*[4]	17.3	0.6	0.7	0.3	1.3	2.3	0.2	0.4	0.7	1.0	+	+
15	A	*Gonyaulax spiniferites* complex	*Spiniferites mirabilis*[1,3,4&6]	49.7	1.3	3.1	1.2	5.2	3.9	0.8	1.8	2.7	2.2	+	+
16	A	*Gonyaulax spiniferites* complex	*Spiniferites ramosus*[1,3,4&6]	70.2	9.8	49.8	2.6	3.5	0.5	38.7	28.2	16.5	22.5	+	+
17	A	*Gonyaulax spiniferites* complex	*Spiniferites* sp.	39.5	8.5	20.0	4.4	15.2	9.1	17.4	65.3	12.0	30.6	+	+
18	A	*Pyrophacus steinii*	*Tuberculodinium vancampoae*[2,3,5&6]	1.6	0.6	0.0	0.0	10.3	0.0	0.0	0.0	2.7	0.0	+	+
19	M	*Polykrikos hartmannii*	Cyst of *Polykrikos hartmannii*[1–3,5&6]	2.4	0.0	0.0	0.0	0.0	0.2	0.0	0.2	0.0	0.1	+	+
20	M	*Lingulodinium polyedrum*	*Lingulodinium machaerophorum*[1–6]	1.6	1.2	0.3	0.0	3.9	0.0	0.7	0.4	1.3	0.4	+	+
21	M	*Lingulodinium* sp.	*Lingulodinium* sp.	9.7	3.8	1.7	0.3	6.5	5.3	8.2	14.3	3.1	9.2	+	+
22	H	*Protoperidinium* sp.	*Brigantedinium simplex*[5&6]	0.0	1.0	0.0	0.0	0.0	0.0	0.0	0.0	0.2	0.0	+	+
23	H	*Protoperidinium conicoides*	*Brigantedinium* sp.[2,5&6]	0.0	0.0	0.0	0.0	0.0	0.0	0.0	0.2	0.0	0.1	+	+
24	H	*Cladopyxis* sp.	Cyst of *Cladopyxis* sp.*	0.0	0.0	0.0	0.0	0.3	0.0	0.0	0.0	0.1	0.0		
25	H	*Polykrikos kofoidii*	Cyst of *Polykrikos kofoidii*[2–5]	0.0	0.6	0.0	0.0	0.0	0.0	0.0	0.0	0.1	0.0	+	+
26	H	*Polykrikos schwartzii*	Cyst of *Polykrikos schwartzii*[1–3,5&6]	3.2	0.0	0.0	0.0	0.0	0.0	0.0	0.0	0.0	0.0	+	+
27	H	*Protoperidinium denticatum*	Cyst of *Protoperidinium denticatum*[3&5]	1.6	0.0	0.0	0.0	0.0	0.0	0.0	0.0	0.0	0.0	+	
28	H	*Protoperidinium latissimum*	Cyst of *Protoperidinium latissimum*[1,3&5]	0.0	0.4	0.0	0.0	0.6	0.0	0.0	0.0	0.3	0.0	+	
29	H	*Protoperidinium monospinum*	Cyst of *Protoperidinium monospinum**	0.0	0.0	0.0	0.0	3.2	0.0	0.0	0.0	0.8	0.0		
30	H	*Protoperidinium* sp.	Cyst of *Protoperidinium* sp.	2.4	2.5	0.0	0.9	3.5	2.5	3.6	6.5	1.7	4.2	+	+
31	H	Diplopsalid or Protoperidinioid group	*Echinidinium* sp.[4&6]	4.8	3.8	2.5	5.6	17.4	1.8	28.2	5.5	7.3	11.8	+	+
32	H	*Protoperidinium leonis*	*Lejeunecysta sabrina*[5]	0.8	0.0	0.0	0.0	0.0	0.0	0.0	0.0	0.0	0.0	+	
33	H	*Protoperidinium subinerme*	*Selenopemphix nephroides*[1–6]	0.0	4.8	0.0	0.0	7.1	5.3	2.3	2.0	3.0	3.2	+	+

Table 2 (continued)

	Trophic status	Motile affinity	Paleontological name	Coastal	Oligotrophic (OAS)				OMZ			OAS	OMZ	EAS	WAS
				St1	St2	St3	St4	St5	St6	St7	St8				
34	H		*Protoperidinium conicum*	8.9	0.0	0.0	0.0	0.0	0.0	0.2	0.2	0.0	0.1	+	+
35	H		Unknown	0.0	0.0	0.0	0.0	0.0	0.0	1.6	0.0	0.0	0.5	+	+
36	H		Unknown	0.0	0.2	0.0	0.0	0.0	0.2	0.0	0.0	0.0	0.1		
37	H		*Protoperidinium* spp.	0.0	0.8	0.0	0.3	6.5	1.8	0.0	0.0	1.9	0.6	+	+
38	H		*Protoperidinium compressum*	0.0	0.6	0.0	0.0	0.0	0.7	0.7	2.9	0.1	1.4	+	+
39	H		*Protoperidinium pentagonum*	1.6	0.0	0.0	0.0	0.0	0.0	0.0	0.2	0.0	0.1	+	+
40	H		*Protoperidinium oblongum*	1.6	0.8	0.0	0.0	0.0	0.0	0.0	2.2	0.2	0.7	+	+
41	H		*Protoperidinium steidingerae*	0.0	0.4	0.0	0.0	0.0	0.0	0.0	0.0	0.1	0.0	+	
			Sum	231	46	92	68	155	108	123	140	90	124		

Superscript numbers indicate species previously reported in those references, i.e., (1) Godhe et al. (2000), (2) D'costa et al. (2008), (3) D'silva et al. (2011), (4) Narale et al. (2015), (5) Rodrigues et al. (2022), and (6) Zonneveld et al. 2013

and OMZ ($d = 46 \pm 13$ µm and PL = 12 ± 4 µm) regions of the AS showed significant variation both in the body size and process length. However, they fall within the reported size ranges ($d = 31$–54 µm and PL = 2–21 µm) in the literature. The morphometric measurements of *Operculodinium centrocarpum* in the coastal ($d = 36$ µm and PL = 2 µm), oligotrophic ($d = 33 \pm 4$ µm and PL = 7 ± 2 µm), and OMZ ($d = 31 \pm 4$ µm and PL = 6 ± 1 µm) regions of the AS showed significant variation in process length but not in the body size. However, they fall within the reported size ranges ($d = 33$–48 µm and PL = 7–14 µm) in the literature (Fig. 6 and supplementary Table 2).

Planktondrift simulations to track the origin of dinoflagellate cysts

The drift simulations of dinoflagellate cysts revealed different transport patterns for the stations located in coastal, oligotrophic, and OMZ regions, suggesting different origins. For instance, the lateral transport of the dinoflagellate cysts in all the stations shows overlapping (except coastal station 1 and station 2), whereas station 5 has the maximum lateral transport even from the WAS and OMZ region. However, in OMZ stations (6, 7, and 8), the lateral transport of the dinoflagellate cysts was also relatively large but mainly confined to the OMZ region to a larger extent (Fig. 1).

Discussion

Factors influencing dinoflagellate cyst diversity and distribution

The present study on the dinoflagellate cyst community from the deepest part of the central (OMZ) and southeastern (oligotrophic) Arabian Sea revealed 41 species. The highest number of cysts was recorded at 113 m (station 1) and the lowest at a depth of 2105 m (station 2) in the coastal and oligotrophic regions of the AS, respectively. However, despite being one of the deepest locations in the oligotrophic region, station 5 (4368 m) recorded relatively higher cyst concentrations (i.e., 155 cysts g^{-1}) due to its proximity to productive OMZ and upwelling regions of the WAS and the same is evident from the planktondrift simulation (Fig. 1). The stations in the OMZ region also recorded relatively higher cyst concentrations (108–140 cysts g^{-1}). Dinoflagellate cysts are susceptible to oxidative degradation like organic matter (Zonneveld et al. 1997); however, an intense OMZ region might help in better preservation of cysts in the OMZ sediment supporting the highest cyst abundance in this region (Wendler et al. 2002). In addition, the OMZ region is considered relatively more productive due to the prevalence of high chlorophyll (i.e., 0.2 to 1.14 mg m^{-3}) than the SEAS,

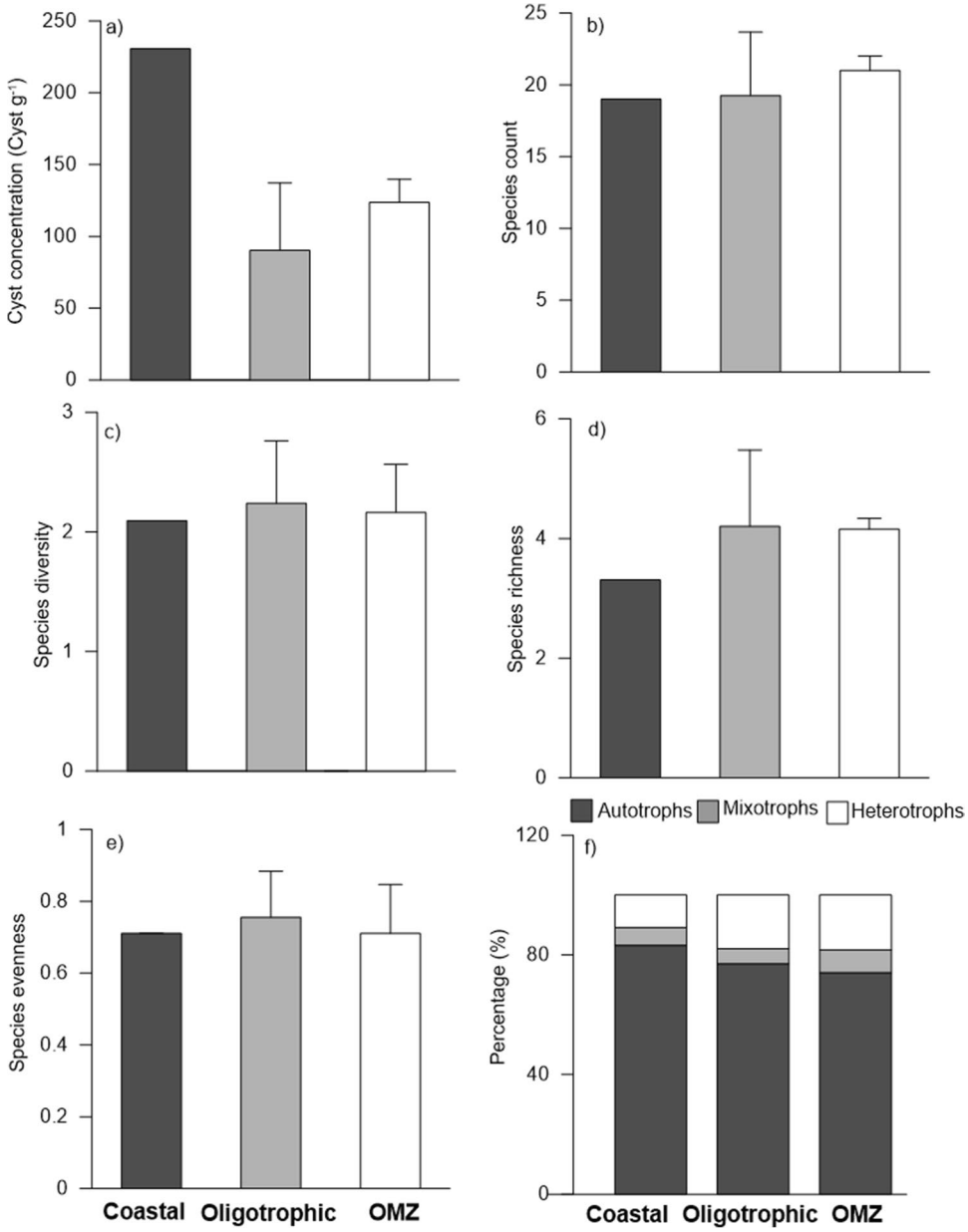


Fig. 3 Variations in dinoflagellate cyst **a** concentration, **b** species count, **c** species diversity, **d** species richness, **e** species evenness, and **f** autotrophic, mixotrophic, and heterotrophic contributions (%) in coastal and oligotrophic regions and oxygen minimum zone (OMZ)

which is oligotrophic, i.e., 0.06 to 0.26 mg m^{-3}. Moreover, the decay function within OMZ is less than the oxic portions of the ocean (Jensen et al. 2011; Roullier et al. 2014; Van Mooy et al., 2002). That implies that the relative proportion of organic matter that passes through OMZ is proportionally higher than that for oxic waters (Keil et al. 2016). Sarma et al. (2007) reported that the sinking flux of the particulate organic carbon (POC) to the deep sea (> 2500 m) is maximum in the AS (i.e., 13.3 mg C m^{-2} day^{-1}). Therefore, fewer and more concentrations of dinoflagellate cysts in the oligotrophic sediment of SEAS and OMZ sediment, respectively, are apparent. Interestingly, high cyst concentrations and similar composition in the coastal station and the OMZ region suggest both to be productive systems compared to oligotrophic regions. The distribution of dinoflagellate cysts in the sediments is determined by many factors, including the ecology of dinoflagellates, transport processes, and preservation conditions (Dale 1996; Zonneveld and Brummer 2000; Zonneveld et al., 2013). Further, in HAB monitoring, cyst documentation of harmful dinoflagellates from the field is one of the monitoring strategies (Anderson et al. 2012; Ribeiro et al. 2012), as any viable cyst can serve as the precursor for blooms. Given this, the present study lists five potential HAB species from both oligotrophic and OMZ regions of the AS. Four potential HAB species were found in the coastal station except *Polysphaeridium zoharyi*, and four (except the cyst of *Polykrikos hartmannii*) were found in the deepest parts of the AS. Most of these HAB species are

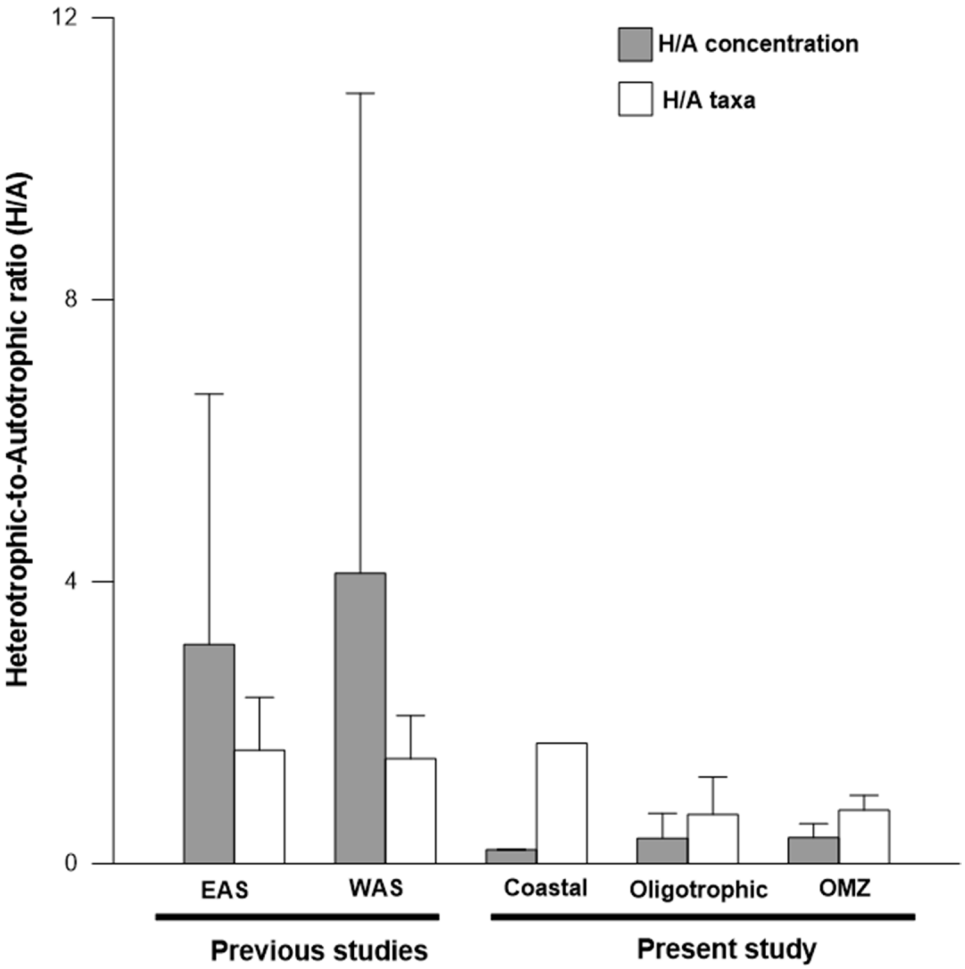


Fig. 4 The plot shows the comparison of heterotrophic to autotrophic ratio (H/A) among the regions of the Arabian Sea. EAS, eastern Arabian Sea; WAS, western Arabian Sea; OMZ, oxygen minimum zone. Data to calculate H/A for the western Arabian Sea are taken from Marret et al. (2020) and for the eastern Arabian Sea from various studies (e.g., D'costa et al., 2008; Dsilva et al., 2011, 2012; Narale et al. 2015 and Rodrigues et al. 2022). H/A concentration and H/A taxa are calculated using cyst concentration and species count data, respectively

known to produce various toxins like saxitoxin and yessotoxins. The cysts of HAB species might be a greater concern for the coastal station than the deeper stations. However, the presence of the cysts of HAB species in the deepest part of the AS might suggest the reach of coastal HAB events. Although an unbiased and complete inventory is essential for establishing general indicators of large-scale systems, adapting to updated procedures, such as combining metabarcoding high throughput sequencing and single-cyst morpho-molecular identification, is the way ahead. Nevertheless, the present study will serve as a benchmark for future studies.

Comparison of dinoflagellate cyst assemblage with previous studies in the AS

The concentration and diversity of dinoflagellate cysts in the EAS coastal regions were highly variable, depending on geographic location and season (Fig. 5). For instance, port areas followed by the strong (west coast of India) and weak (southern tip of the Indian peninsula) upwelling-influenced coastal stations harbor cyst concentrations in decreasing order (Fig. 1). Additionally, the sediment texture (silty/clayey sediment harbors more cyst concentration than sandy sediment), nutrient loading (e.g., eutrophication in port areas, nutrient-rich upwelled coastal water), and salinity variations (precipitation and riverine discharges during monsoon) are major drivers determining cyst concentration and community according to the geographic location (Smitha et al., 2008; D'costa et al. 2008; Dsilva et al. 2011; Rodrigues et al. 2019, 2022). Along the EAS coastal region (west coast of India), autotrophs and heterotrophs dominated in the highly productive southern and relatively less productive northern eutrophicated ports, respectively. The present coastal station, located near the southwest coast of India, falls under an intense upwelling-influenced area, and compared to previous studies, the cyst community differed, but the concentration was almost in the same range. This study observed autotrophic dominance, while the previous study reported autotrophic and heterotrophic in port (Rodrigues et al. 2019) and coastal (D'silva et al. 2011) regions, respectively. Generally, autotrophic and heterotrophic dominance are related to their higher planktonic production (Dale 1983; Anderson et al. 1995; Joyce et al. 2005) and eutrophic environments (Dale et al. 1999; Matsuoka 1999; Radi and Vernal 2004; Dale 2009; Price et al. 2018). Several

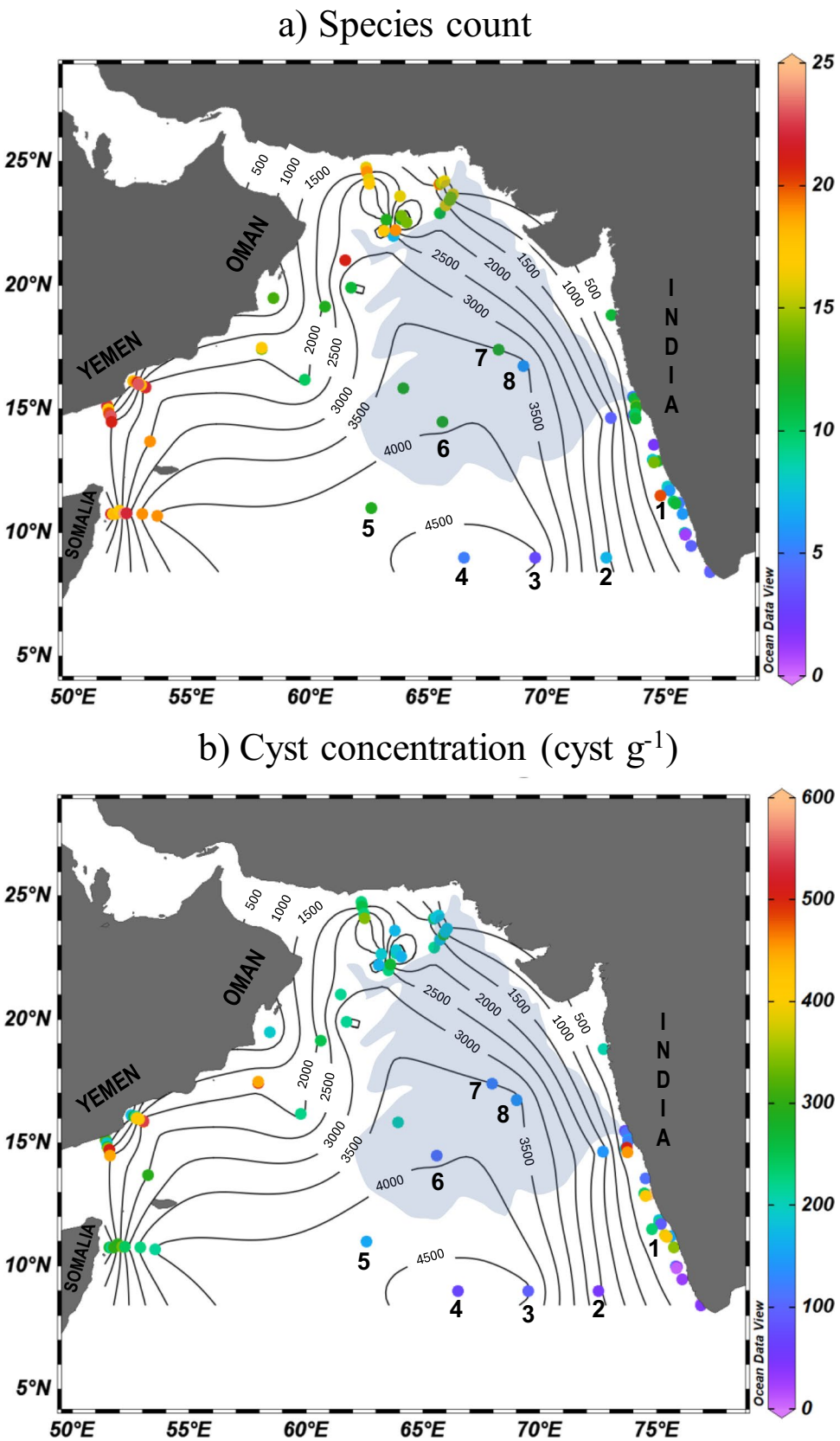


Fig. 5 Plots showing comparative data for dinoflagellate cysts **a** species count (number of species) and **b** dinoflagellate cyst concentration. Present study locations are represented using numbers. The shaded area represents the oxygen minimum zone (OMZ). Data for species count and concentration for comparison are taken from Zonneveld et al. (2013), D'Silva et al. (2011), Narale et al. (2015), Dcosta et al. (2008), and Rodrigues et al. (2022)

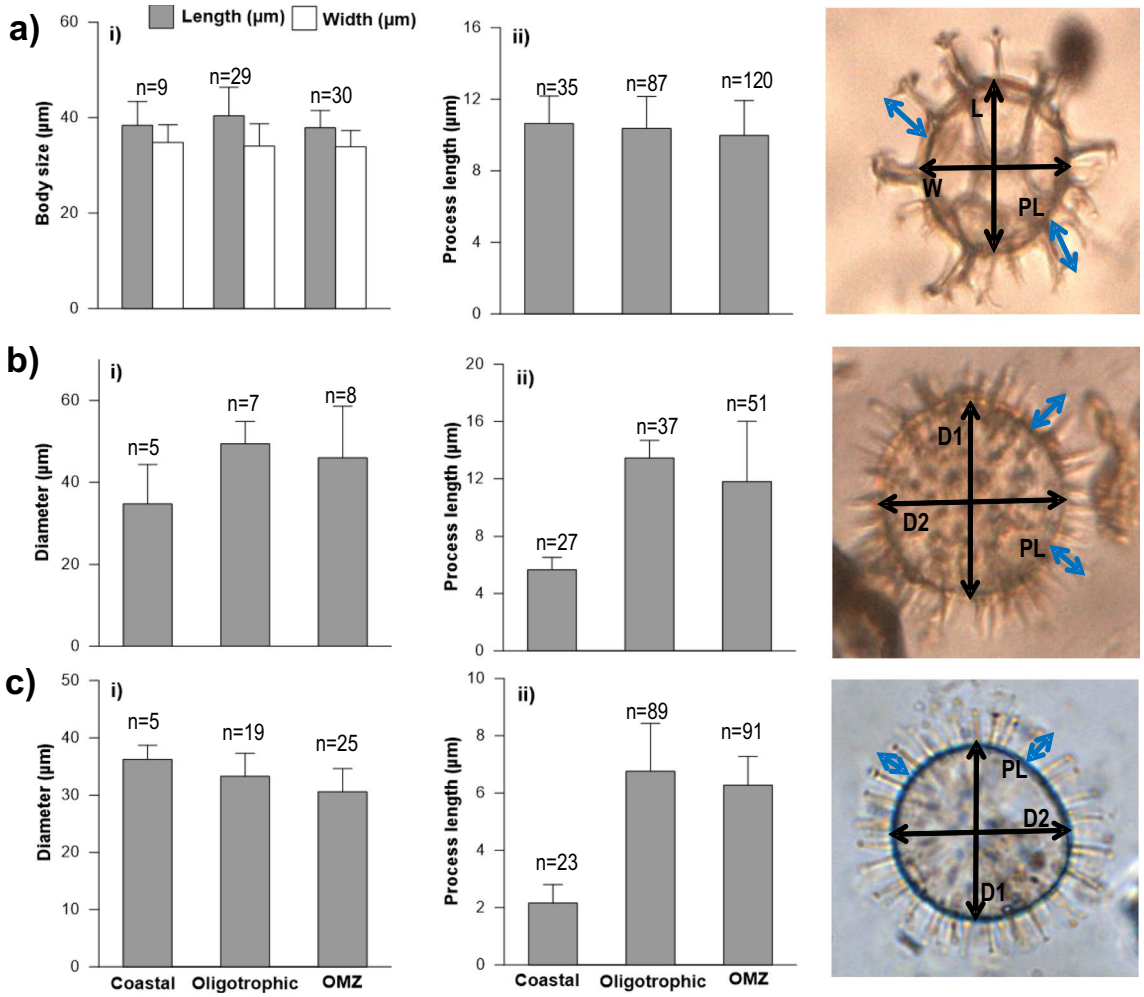


Fig. 6 The plot shows morphometric measurements of selected cosmopolitan dinoflagellate cysts body (L = length, W = width, and D = diameter) and process length (PL) in coastal, oligotrophic, and OMZ regions of the Arabian Sea. **a** *Spiniferites ramosus* (i) body size (length and width) and (ii) process length, **b** *Lingulodinium machaerophorum* (i) body size (diameter) and (ii) process length, and **c** *Operculodinium centrocarpum* (i) body size (diameter) and (ii) process length

studies documented that the dinoflagellate cysts, particularly heterotrophic to autotrophic (H/A) ratios, are good ecological indicators (Lewis et al. 1990; Radi and de Vernal 2004; Sangiorgi and Donders 2004; Verleye and Louwye 2010; Zonneveld et al. 2010; Hardy et al. 2016). However, such ratios are to be applied with caution in this region due to the seasonal variation in H/A ratios (Rodrigues et al. 2019). In the present study, the concentration and diversity of autotrophic dinoflagellate cysts were dominant irrespective of the regions, and the H/A concentration ratios are very low, i.e., concentration ratio < 1 in all the stations. The H/A concentration ratios of coastal (0.20) oligotrophic (0.36 ± 0.35) and OMZ (0.37 ± 0.20) are much lower than the average ratios reported for productive EAS (3.1 ± 3.5) and WAS (4.1 ± 6.8) despite large variations in the dominance of heterotrophic and autotrophic cysts (Fig. 4). However, the present study's taxa H/A ratio of coastal AS (except for the oligotrophic and OMZ regions, which were lower) showed a similar value to previously reported ratios from EAS and WAS. The prevalence of low productive oligotrophic and OMZ compared to coastal EAS and WAS could be the primary reason for the observed low H/A ratio in the former. Nevertheless, these findings suggested that the production of heterotrophic dinoflagellate cysts is less in the coastal, oligotrophic, and OMZ than the previous reports in the coastal AS.

Through the present study, we propose that of the recorded 41 species, 32 showed a cosmopolitan distribution in the AS basin (Table 2). Among them, 27 species recorded in this study were documented from the WAS and EAS, indicating their widespread occurrence in the region. Also, seven (cyst of *Cladopyxis* sp., cyst of *Protoperidinium latissimum*, *Lejeunecysta sabrina*, *Operculodinium janduchenei*, cyst of *Protoperidinium denticulatum*, *Protoperidinium monospinum*, and *Stelladinium bifurcatum*) and six (cyst

of *Cladopyxis* sp., *Impagidinium patulum*, *Impagidinium strialatum*, *Operculodinium janduchenei*, *Protoperidinium monospinum*, and *Stelladinium bifurcatum*) species recorded in this study were not reported from WAS and EAS, respectively. Further, four species (cyst of *Cladopyxis* sp., *Operculodinium janduchenei*, *Stelladinium bifurcatum*, and *Protoperidinium monospinum*) are found to be reported for the first time from the AS (Table 2). Such distinct demarcation in the distribution of certain dinoflagellate species could be related to variable productivity patterns as biological productivity in AS is tightly coupled to the physical forcing (e.g., monsoon reversals, currents, upwelling, fronts) mediated through nutrient availability. Cysts are thought to behave like silt particles in the water column as their size is within the silt range (Dale 1976, 1996; Mudie and Harland 1996) and, therefore, can be transported by ocean currents as they sink through the water column or be re-suspended by bottom currents after deposition (e.g., Dale 1976; Zonneveld and Brummer 2000). Various surfaces and associated undercurrents are well described in Schott and McCreary Jr. (2001) for the AS, which could play a role in large-scale dinoflagellate cyst transport. During the southwest monsoon season, strong upwelling in coastal Oman and Somalia is generally observed (Banse 1987). This phenomenon brings cool, nutrient-rich deep water to the surface, making the region very productive (Barber et al. 2001). This nutrient-rich water reaches 500–700 km offshore into the central AS (Morrison et al. 1998) and could also displace dinoflagellate cysts. The planktondrift simulations by Nooteboom et al. (2019) reported that the dinoflagellate cysts could be displaced up to 1570 km under the influence of currents from their origin location at the surface before they reach the ocean floor. The similar simulations used in this study also revealed large and small-scale lateral transport of the dinoflagellate cysts in oligotrophic regions followed by OMZ and coastal regions, respectively (Fig. 1). However, the lateral transport was more confined to coastal than OMZ regions. For instance, in the oligotrophic station 5, the lateral transport was from the productive upwelling region of the WAS, whereas in coastal station 1 and oligotrophic station 2, transport is confined to a smaller region. Interestingly, in stations 6, 7, and 8, the lateral transport was mostly restricted to the OMZ region. Hence, it is presumed that the prevalence of (i) large-scale lateral transport is a possible reason for the existence of more cosmopolitan dinoflagellate cyst species and (ii) the region-specific dinoflagellate cyst population can be linked to restricted lateral transport patterns. However, this aspect needs further investigation.

Furthermore, four dinoflagellate cyst species cysts of *Cladopyxis* sp., *Operculodinium janduchenei*, *Stelladinium bifurcatum*, and cyst of *Protoperidinium monospinum* were recorded in the deepest station (station 5) of the oligotrophic region and *Operculodinium janduchenei* and *Stelladinium bifurcatum* in both oligotrophic and OMZ regions. The available literature suggests that (i) cyst of *Cladopyxis* sp. has also previously been reported from the Pacific (central and tropical), tropical Atlantic, Sargasso Sea (Dale and Dale 1992) in deep-sea sediment traps, and on the shelf and slope of the South China Sea (Kawamura 2002); (ii) cyst of *P. monospinum* is recorded from the Mediterranean Sea; it is characteristically documented in tropical to equatorial regions of NW Africa and is generally found in high numbers in upwelling regions or when upwelled water is passed across oligotrophic waters (Zonneveld et al. 2013). Since monsoonal upwelling is a well-known phenomenon in the AS particularly WAS (Fig. 1), it is presumed that the influence of WAS upwelled water might be reaching up to station 5 and was also evident in the simulation plot (Fig. 1). However, more surveys in and around upwelling regions are warranted to relate cyst of *P. monospinum* distribution with the upwelling phenomenon in AS. (iii) *O. janduchenei* is reported from both temperate and equatorial regions, and the highest abundance is recorded from the eastern Indian Ocean off Indonesia (Zonneveld et al. 2013). (iv) *S. bifurcatum* has been reported from the eastern Pacific and east equatorial Atlantic oceans (Head et al. 2020), the western Bay of Bengal as *Stelladinium reidii* (in Uddandam et al. 2017), and in sediment traps from the South China Sea as *Stelladinium*-Type A (in Li et al. 2018). *S. bifurcatum* is mainly associated with warmer waters and highly productive conditions (Head et al. 2020).

Generally, dinoflagellate cyst morphology is species-specific, but their variability due to environmental factors such as temperature and salinity is well documented from both laboratory and field studies (e.g., Ellegaard et al. 2002; Mertens et al. 2009a, 2009b, 2010 and 2012; Rodrigues and Patil 2021). The variability in the morphology of some cosmopolitan cysts was also evident between coastal and open ocean types (Fig. 6). However, the variability varied with cyst types. For instance, larger and smaller cyst sizes for coastal and open oceans, respectively, and vice versa. *Bitectatodinium spongium* (coastal, $d = 52$ µm; open oceans, $d = 46$ µm) and *Operculodinium centrocarpum* (coastal, $d = 36$ µm; open oceans, $d = 31$ µm; Fig. 6c) belonged to the former types, while *Lingulodinium machaerophorum* (coastal, $d = 35$ µm; open oceans, $d = 49$ µm; Fig. 6b) and *Tuberculodinium vancampoae* (coastal, $l \times w = 92 \times 85$ µm; open oceans, $l \times w = 106 \times 87$ µm) belonged to the latter types. However, *Spiniferites ramosus* did not show any significant variation (Fig. 6a), and the dimensions are as per the literature. Hence, it is assumed that there could be variability in the cyst morphology of the recorded cosmopolitan cysts. Generally, the morphology of dinoflagellate cysts is species-specific, but their variability, particularly in cyst size and process length, due to environmental factors (temperature and salinity) makes them potential proxies for such factors (Rodrigues and Patil 2021). For instance, process

length in cyst of *Protoceratium reticulatum* (*O. centrocarpum*) and some *Spiniferites* species are linked to salinity conditions (Verleye et al. 2012; Ellegaard et al. 1998 and 2002) and the influence of changing temperatures on the morphology of *L. machaerophorum* and *Gonyaulax baltica* cysts (Hallett 1999; Mertens et al. 2012; Ellegaard et al. 2002). Given this, it is assumed that the cysts, which are cosmopolitan, will encode signatures that can be used as potential proxies, and this was evident in this study. The process length in *L. machaerophorum* and *O. centrocarpum* cysts that were encountered on the coast was relatively smaller than that of the ocean (Fig. 6b & c), suggesting the influence of low saline waters coming from monsoonal discharges and BOB (Hareeshkumar 2014). Though the average dimensions for most of the cysts are as per the literature values, the recorded ranges indicated the presence of cysts with smaller or larger dimensions (Supplementary Table 2). For instance, *Bitectatodinium spongium*, *Operculodinium centrocarpum*, *Impagidinium aculeatum*, *Nematosphaeropsis labyrinthus*, and cysts of *Polykrikos hartmannii* (from ocean) were smaller while cyst of *Polykrikos hartmannii* (from coastal) and *Impagidinium paradoxum* were relatively larger compared to those reported in the literature (Supplementary Table 2). Since these inferences are from a small sample population, more measurements from field samples representing different bioregions of the oceans are desirable to facilitate their robustness as potential environmental indicators. Nevertheless, this study will add information to a growing body of knowledge on dinoflagellate cyst distribution patterns (Marret and Zonneveld 2003; Zonneveld et al., 2013) from the less studied pelagic region of the AS.

Conclusion

This study provides the first account of dinoflagellate cyst distribution and diversity from oligotrophic and OMZ regions of the Arabian Sea. The cyst concentration was maximum in the coastal, followed by the OMZ, and least in the oligotrophic region (with an exception of station 5, located close to OMZ and the upwelling zone). However, the diversity and richness were higher in the oligotrophic and OMZ and least in the coastal regions of the AS. Cysts of autotrophic dinoflagellates were dominant irrespective of the regions. The taxonomic comparison revealed that most cysts are cosmopolitan (~56%) irrespective of water column depths, and the remaining were region-specific. This could be due to the prevalence of large-scale and restricted lateral transport patterns in the oligotrophic followed by OMZ and coastal regions, respectively. Further, taxa of *Cladopyxis* sp., *Operculodinium janduchenei*, *Stelladinium bifurcatum*, and cyst of *Protoperidinium monospinum* associated with different environmental conditions from the deepest part of oligotrophic AS form the first report. Also, variability in the morphology of the cosmopolitan cysts *Operculodinium centrocarpum* and *Lingulodinium machaerophorum* was evident between the coastal and open oceans. These findings from the less studied pelagic region will contribute to the growing body of knowledge on dinoflagellate cyst distribution patterns and highlight the significance of cyst taxa and morphology as potential ecological indicators for AS.

Supplementary Information The online version contains supplementary material available at https://doi.org/10.1007/s11356-024-34913-3.

Acknowledgements The authors are grateful to the Director of CSIR-National Institute of Oceanography (Goa, India) for his support and encouragement. The authors thank Dr. Samir Damare, Mr. Anthony D'Souza, Mr. Sheldon Rebello, Mr. Ramesh T, and the RV *Sindhu Sadhana* crew (SSD069) for their help in sampling. We are thankful to two anonymous reviewers for their constructive suggestions. This paper is NIO contribution number 7291.

Author contribution PP: sample collection, sample analysis, data analysis and interpretation, and manuscript writing; JSP: original concept, sample collection, data interpretation, and manuscript elaboration.

Funding This study was funded by TraceBioMe project (MLP2018).

Data availability All data concerning the study are included in this manuscript, and some are also provided as supplementary. However, it is not applicable for material availability.

Declarations

Ethical approval No animal testing was performed during this study.

Consent to participate Not applicable.

Consent for publication Not applicable.

Competing interests The authors declare no competing interests.

References

Anderson DM, Butman B, Fong D, Franks PJS, Geyer WR, Keafer BA, Loder T, Signeil ELP (1995) Sources, transport, and nutrient environment of toxic red tide populations in the Western Gulf of Maine. In: Gulf of Maine News. Regional Association for Research on the Gulf of Maine, pp. 6–9

Anderson DM, Lively JJ, Reardon EM, Price CA (1985) Sinking characteristics of dinoflagellate cysts. Limnol and Oceanogra 30(5):1000–1009. https://doi.org/10.4319/lo.1985.30.5.1000

Anderson DM, Cembella AD, Hallegraeff GM (2012) Progress in understanding harmful algal blooms: paradigm shifts and new technologies for research, monitoring, and management. Ann Rev of Mar Sci 4:143–176. https://doi.org/10.1146/annurev-marine-120308-081121

Banse K (1968) Hydrography of the Arabian Sea shelf of India and Pakistan and effects on demersal fishes. In Deep-Sea Res and Oceanogr Abstr 15(1):45–79. https://doi.org/10.1016/0011-7471(68)90028-4

Banse K (1987) Seasonality of phytoplankton chlorophyll in the central and northern Arabian Sea. Deep-Sea Res I 34:713–723. https://doi.org/10.1016/0198-0149(87)90032-X

Baula IU, Azanza RV, Fukuyo Y, Siringan FP (2011) Dinoflagellate cyst composition, abundance and horizontal distribution

in Bolinao, Pangasinan, Northern Philippines. Harmful Algae 11:33–44. https://doi.org/10.1016/j.hal.2011.07.002

Barber RT, Marra J, Bidigare RC, Codispoti LA, Halpern D, Johnson Z, Latasa M, Goericke R, Smith SL (2001) Primary productivity and its regulation in the Arabian Sea during 1995. Deep Sea Res Part II 48(6–7):1127–1172. https://doi.org/10.1016/S0967-0645(00)00134-X

Bravo I, Garcés E, Diogène J, Fraga S, Sampedro N, Figueroa RI (2006) Resting cysts of the toxigenic dinoflagellate genus Alexandrium in recent sediments from the Western Mediterranean coast, including the first description of cysts of A kutnerae and A peruvianum. Eur J Phycol 41(3):293–302. https://doi.org/10.1080/09670260600810360

Cho HJ, Matsuoka K (2001) Distribution of dinoflagellate cysts in surface sediments from the Yellow Sea and East China Sea. Mar Micropaleontol 42(3–4):103–123. https://doi.org/10.1016/S0377-8398(01)00016-0

Dale B (1976) Cyst formation, sedimentation, and preservation: factors affecting dinoflagellate assemblages in recent sediments from Trondheim fjord, Norway. Rev Palaeobot Palynol 22:39–60. https://doi.org/10.1016/0034-6667(76)90010-5

Dale B (1983) Dinoflagellate resting cysts: "benthic plankton". In Survival strategies of the algae 69–136

Dale B (1996) Dinoflagellate cyst ecology: modeling and geological applications. In: Jansonius, J., McGregor, D.C. (Eds.), Palynology: Principles and Applications. AASP Foundation 1249–1275

Dale B (2009) Eutrophication signals in the sedimentary record of dinoflagellate cysts in coastal waters. J Sea Res 61:103–113. https://doi.org/10.1016/j.seares.2008.06.007

Dale B, Dale AL (1992) Dinoflagellate contributions to the open ocean sediment flux. In Dinoflagellate contributions to the deep sea (Vol. 5, pp. 45–73). Woods Hole Oceanographic Institution Woods Hole

Dale B, Thorsen TA, Fjellsa A (1999) Dinoflagellate cysts as indicators of cultural eutrophication in the Oslofjord Norway. Estuar Coast Shelf Sci 48(3):371–382. https://doi.org/10.1006/ecss.1999.0427

D'Costa PM, Anil AC, Patil JS, Hegde S, D'Silva MS, Chourasia M (2008) Dinoflagellates in a mesotrophic tropical environment influenced by monsoon. Estuar Coast Shelf Sci 77:77–90. https://doi.org/10.1016/j.ecss.2007.09.002

de Vernal A, Henry M, Matthiessen J, Mudie PJ, Rochon A, Boessenkool KP, Eynaud F, Grosfjeld K, Guiot J, Hamel D, Harland R, Head MJ, Kunz-Pirrung M, Levac E, Loucheur V, Peyron O, Pospelova V, Radi T, Turon JL, Voronina E (2001) Dinoflagellate cyst assemblages as tracers of sea-surface conditions in the northern North Atlantic, Arctic and sub-Arctic seas: the new 'n=677' data base and its application for quantitative palaeoceanographic reconstruction. J Quat Sci 16:681–698. https://doi.org/10.1002/jqs.659

de Vernal A, Eynaud F, Henry M, Limoges A, Londeix L, Matthiessen J, Marret F, Pospelova V, Radi T, Rochon A, Van Nieuwenhove N (2018) Distribution and (palaeo) ecological affinities of the main Spiniferites taxa in the mid-high latitudes of the Northern Hemisphere. Palynology 42(sup1):182–202. https://doi.org/10.1080/01916122.2018.1465730

de Vernal A, Hillaire-Marcel C, Rochon A, Frechette B, Henry M, Solignac S, Bonnet S (2013) Dinocyst-based reconstructions of sea ice cover concentration during the Holocene in the Arctic Ocean, the northern North Atlantic Ocean and its adjacent seas. Quat Sci Rev 79:111–121. https://doi.org/10.1016/j.quascirev.2013.07.006

de Vernal A, Radi T, Zaragosi S, Van Nieuwenhove N, Rochon A, Allan E, De Schepper S, Eynaud F, Head MJ, Limoges A, Londeix L, Marret F, Matthiessen J, Penaud A, Pospelova V, Price A, Richerol T (2020) Distribution of common modern dinoflagellate cyst taxa in surface sediments of the Northern Hemisphere in relation to environmental parameters: the new n = 1968 database. Mar Micropaleontol 159:101796. https://doi.org/10.1016/j.marmicro.2019.101796

Delebecq G, Schmidt S, Ehrhold A, Latimier M, Siano R (2020) Revival of ancient marine dinoflagellates using molecular biostimulation. J Phycol 56(4):1077–1089. https://doi.org/10.1111/jpy.13010

D'Silva MS, Anil AC, Borole DV, Nath BN, Singhal RK (2012) Tracking the history of dinoflagellate cyst assemblages in sediments from the west coast of India. J Sea Res 73:86–100. https://doi.org/10.1016/j.seares.2012.06.013

D'Silva MS, Anil AC, D'Costa PM (2011) An overview of dinoflagellate cysts in recent sediments along the west coast of India. Indian J Geo-Mar Sci 40:697–709

Ellegaard M, Kulis DM, Anderson DM (1998) Cysts of Danish Gymnodinium nolleri Ellegaard et Moestrup sp. ined. (Dinophyceae): studies on encystment, excystment and toxicity. J Plankton Res 20:1743–1755. https://doi.org/10.1093/plankt/20.9.1743

Ellegaard M, Lewis J, Harding I (2002) Cyst–theca relationship, life cycle, and effects of temperature and salinity on the cyst morphology of Gonyaulax baltica sp. nov. (Dinophyceae) from the Baltic Sea Area. J Phycol 38:775–789. https://doi.org/10.1046/j.1529-8817.2002.01062.x

Folk RL (1974) The petrology of sedimentary rocks. Hemphill Publishing Co., Austin, Texas, p 182

Folk RL, Andrews PB, Lewis DW (1970) Detrital sedimentary rock classification and nomenclature for use in New Zealand. NZ J Geol Geophys 13(4):937–968

Godhe A, Karunasagar I, Karlson B (2000) Dinoflagellate cysts in recent marine sediments from SW India. Bot Mar 43:39–48. https://doi.org/10.1515/BOT.2000.004

Hallegraeff G, Gollasch S (2006) Anthropogenic introductions of microalgae. In: Graneli E, Turner JT (eds) Ecology of Harmful Algae. Springer, Berlin, Heidelberg, pp 379–390

Hallett RI (1999) Consequences of environmental change on the growth and morphology of Lingulodinium polyedrum (Dinophyceae) in culture. Doctoral Dissertation. University of Westminster

Hardy W, Penaud A, Marret F, Bayon G, Marsset T, Droz L (2016) Dinocyst assemblage constrains on oceanographic and atmospheric process in the Eastern Equatorial Atlantic over the last 44 Ka. Biogeosci 13(16):4823–4841. https://doi.org/10.5194/bg-13-4823-2016

Hareeshkumar PV (2014) Salinity variation in the southeastern Arabian Sea: a revisit. Ind J Mar Sci 44:1650–1658

Head MJ (1996) Modern dinoflagellate cysts and their biological affinities. InMcGregor, D. C. and Jansonius, J. (eds), *Palynology, Principles and Applications: Applications*. American Association of Stratigraphic Palynologists Foundation, United States 3:1197–1248

Head MJ, Pospelova V, Radi T, Marret F (2020) Stelladinium bifurcatum n sp, a distinctive extant thermophilic heterotrophic dinoflagellate cyst from the late Quaternary of the eastern Pacific and east equatorial Atlantic oceans. Marine Micropaleontol 159:101754. https://doi.org/10.1016/j.marmicro.2019.101754

Holzwarth U, Esper O, Zonneveld K (2007) Distribution of organic-walled dinoflagellate cysts in shelf surface sediments of the Benguela upwelling system in relationship to environmental conditions. Mar Micropaleontol 64(1–2):91–119. https://doi.org/10.1016/j.marmicro.2007.04.001

Jensen MM, Lam P, Revsbech NP, Nagel B, Gaye B, Jetten MSM, Kuypers MMM (2011) Intensive nitrogen loss over the Omani Shelf due to anammox coupled with dissimilatory nitrite reduction to ammonium. Isme J 5:1660–1670. https://doi.org/10.1038/ismej.2011.44

Joyce LB, Pitcher GC, du Randt A, Monteiro PMS (2005) Dinoflagellate cysts from surface sediments of Saldanha Bay, South Africa: an

indication of the potential risk of harmful algal blooms. Harmful Algae 4(2):309–318. https://doi.org/10.1016/j.hal.2004.08.001

Kawamura H (2002) Marine palynological records in the southern South China Sea over the last 44 kyr (Doctoral dissertation).

Keil RG, Neibauer JA, Biladeau C, Van Der Elst K, Devol AH (2016) A multiproxy approach to understanding the "enhanced" flux of organic matter through the oxygen-deficient waters of the Arabian Sea. Biogeosciences 13(7):2077–2092. https://doi.org/10.5194/bg-13-2077-2016

Lewis J, Dodge D, Powell AJ (1990) Quaternary dinoflagellate cysts from the upwelling system offshore Peru, hole 686, ODP Leg 112. Chapter 18. In: Proc Ocean Drill Program. Sci Results 112:323–328

Li Z, Pospelova V, Mertens KN, Liu L, Wu Y, Li C, Gu H (2023) Evaluation of organic-walled dinoflagellate cyst distributions in coastal surface sediments of the China Seas in relation with hydrographic conditions for paleoceanographic reconstruction. Quat Internat 661:60–75. https://doi.org/10.1016/j.quaint.2023.03.007

Li Z, Pospelova V, Kawamura H, Luo C, Mertens KN, Hernández-Almeida I, Yin K, Wu Y, Wu H, Xiang R (2020) Dinoflagellate cyst distribution in surface sediments from the South China Sea in relation to hydrographic conditions and primary productivity. Mar Micropaleontol 159:101815. https://doi.org/10.1016/j.marmicro.2019.101815

Li Z, Pospelova V, Lin H, Liu L, Song B, Gong W (2018) Seasonal dinoflagellate cyst production and terrestrial palynomorph deposition in the East Asian Monsoon influenced South China Sea: a sediment trap study from the Southwest Taiwan waters. Rev Palaeobot Palynol 257:117–139. https://doi.org/10.1016/j.revpalbo.2018.07.007

Liu D, Shi Y, Di B, Sun Q, Wang Y, Dong Z, Shao H (2012) The impact of different pollution sources on modern dinoflagellate cysts in Sishili Bay, Yellow Sea, China. Marine Micropaleontol 84:1–13. https://doi.org/10.1016/j.marmicro.2011.11.001

Lundholm N, Ribeiro S, Andersen TJ, Koch T, Godhe A, Ekelund F, Ellegaard M (2011) Buried alive -germination of up to a century-old marine protist resting stages. Phycologia 50(6):629–640. https://doi.org/10.2216/11-16.1

Marret F, Bradley L, de Vernal A, Hardy W, Kim SY, Mudie P, Penaud A, Pospelova V, Price AM, Radi T, Rochon A (2020) From bi-polar to regional distribution of modern dinoflagellate cysts, an overview of their biogeography. Mar Micropaleontol 159:101753. https://doi.org/10.1016/j.marmicro.2019.101753

Marret F, Mudie P, Aksu A, Hiscott RN (2009) A Holocene dinocyst record of a two-step transformation of the Neoeuxinian brackish water lake into the Black Sea. Quat Int 197:72–86. https://doi.org/10.1016/j.quaint.2007.01.010

Marret F, Zonneveld KAF (2003) Atlas of modern organic-walled dinoflagellate cyst distribution. Rev Palaeobot Palynol 125:1–200. https://doi.org/10.1016/S0034-6667(02)00229-4

Marret F, de Vernal A, Benderra F, Harland R (2001) Late Quaternary sea-surface conditions at DSDP Hole 594 in the southwest Pacific Ocean based on dinoflagellate cyst assemblages. J Quarter Sci. Published for the Quaternary Research Association 16(7):739–751

Matsuoka K (1999) Eutrophication process recorded in dinoflagellate cyst assemblages - a case of Yokohama Port, Tokyo Bay. Japan Sci Total Environ 231(1):17–35. https://doi.org/10.1016/S0048-9697(99)00087-X

Matsuoka K, Fukuyo Y (2000) Technical guide for modern dinoflagellate cyst study WESTPAC-HAB/WESTPAC/IOC. Japan Society for the Promotion of Science, 29 pp

Matsuoka K, Joyce LB, Kotani Y, Matsuyama Y (2003) Modern dinoflagellate cysts in hypertrophic coastal waters of Tokyo Bay Japan. J Plankton Res 25(12):1461–1470

Mertens KN, Bradley LR, Takano Y, Mudie PJ, Marret F, Aksu AE, Hiscott RN, Verleye TJ, Mousing EA, Smyrnova LL, Bagheri S (2012) Quantitative estimation of Holocene surface salinity variation in the Black Sea using dinoflagellate cyst process length. Quat Sci Rev 39:45–59. https://doi.org/10.1016/j.quascirev.2012.01.026

Mertens KN, Dale B, Ellegaard M, Jansson IM, Godhe A, Kremp A, Louwye S (2010) Process length variation in cysts of the dinoflagellate *Protoceratium reticulatum* from surface sediments of the Baltic-Kattegat-Skagerrak estuarine system: a regional salinity proxy. Boreas 40:242–255. https://doi.org/10.1111/j.1502-3885.2010.00193.x

Mertens KN, Gonzalez C, Delusina I, Louwye S (2009a) 30000 years of productivity and salinity variations in the late quaternary Cariaco Basin revealed by dinoflagellate cysts. Boreas 38:647–662. https://doi.org/10.1111/j.1502-3885.2009.00095.x

Mertens KN, Ribeiro S, Bouimetarhan I, Caner H, Combourieu Nebout N, Dale B, De Vernal A, Ellegaard M, Filipova M, Godhe A, Goubert E (2009b) Process length variation in cysts of a dinoflagellate *Lingulodinium machaerophorum* in surface sediments: investigating its potential as salinity proxy. Mar Micropaleontol 70:54–69. https://doi.org/10.1016/j.marmicro.2008.10.004

Millero FJ, Lee K, Roche M (1998) Distribution of alkalinity in the surface waters of the major oceans. Mar Chem 60(1–2):111–130. https://doi.org/10.1016/S0304-4203(97)00084-4

Morrison JM, Codispoti L, Gaurin S, Jones B, Manghnani V, Zheng Z (1998) Seasonal variation of hydrographic and nutrient fields during the US JGOFS Arabian Sea process study. Deep-Sea Res Part II: Topical Stud Oceanogr 45(10–11):2053–2101. https://doi.org/10.1016/S0967-0645(98)00063-0

Mudie PJ, Harland R (1996) Aquatic quaternary. In: Jansonius, J., McGregor, D.C. (Eds.), Palynology: Principles and Applications Vol. 2. AASP Foundation, Salt Lake City, pp. 843–877

Mudie PJ, Rochon A, Levac E (2002) Palynological records of red tide-producing species in Canada: past trends and implications for the future. Palaeogeogr Palaeoclimatol Palaeoecol 180:159–186. https://doi.org/10.1016/S0031-0182(01)00427-8

Naqvi WA (1991) Geographical extent of denitrification in the Arabian Sea in relation to some physical processes. Oceanologica Acta 14(3): 281–290.https://archimer.ifremer.fr/doc/00101/21257/

Narale DD, Naidu PD, Anil AC, Godad SP (2015) Evolution of productivity and monsoonal dynamics in the eastern Arabian Sea during the past 68ka using dinoflagellate cyst records. Palaeogeogr Palaeoclimatol Palaeoecol 435:193–202. https://doi.org/10.1016/j.palaeo.2015.06.006

Narale DD, Patil JS, Anil AC (2013) Dinoflagellate cyst distribution in recent sediments along the south-east coast of India. Oceanologia 55(4):979–1003. https://doi.org/10.5697/oc.55-4.979

Nooteboom PD, Bijl PK, Van Sebille E, Von Der Heydt AS, Dijkstra HA (2019) Transport bias by ocean currents in sedimentary microplankton assemblages: implications for paleoceanographic reconstructions. Paleoceanogr and Paleoclimatol 34(7):1178–1194. https://doi.org/10.1029/2019PA003606

Nooteboom PD, Delandmeter P, Van Sebille E, Bijl PK, Dijkstra HA, Von Der Heydt AS (2020) Resolution dependency of sinking Lagrangian particles in ocean general circulation models. PLoS ONE 15(9):e0238650. https://doi.org/10.1371/journal.pone.0238650

Pospelova V, Chmura GL, Boothman WS, Latimer JS (2002) Dinoflagellate cyst records and human disturbance in two neighboring estuaries New Bedford harbour and Apponagansett Bay Massachusetts (USA). Sci Total Environ 298(1):81–102. https://doi.org/10.1016/S0048-9697(02)00195-X

Pospelova V, Chmura GL, Boothman WS, Latimer JS (2005) Spatial distribution of modern dinoflagellate cysts in polluted estuarine sediments from Buzzards Bay (Massachusetts, USA)

embayments. Mar Ecol Prog Ser 292:23–40. https://doi.org/10.3354/meps292023
Pospelova V, Chmura GL, Walker HA (2004) Environmental factors influencing the spatial distribution of dinoflagellate cyst assemblages in shallow lagoons of southern New England (USA). Rev Palaeobot Palynol 128:7–34. https://doi.org/10.1016/S0034-6667(03)00110-6
Pospelova V, Pedersen TF, de Vernal A (2006) Dinoflagellate cysts as indicators of climatic and oceanographic changes during the past 40 kyr in the Santa Barbara Basin, southern California. Paleoceanogr 21:1–16. https://doi.org/10.1029/2005PA001251
Pospelova V, Price AM, Pedersen TF (2015) Palynological evidence for late quaternary climate and marine primary productivity changes along the California margin. Paleoceanogr 30:877–894. https://doi.org/10.1002/2014PA002728
Price AM, Gurdebeke PR, Mertens KN, Pospelova V (2016) Determining the absolute abundance of dinoflagellate cysts in recent marine sediments III: identifying the source of Lycopodium loss during palynological processing and further testing of the Lycopodium marker-grain method. Rev of Palaeobot and Palynology 226:78–90. https://doi.org/10.1016/j.revpalbo.2015.12.009
Price AM, Baustian MM, Turner RE, Rabalais NN, Chmura GL (2018) Dinoflagellate cysts track eutrophication in the Northern Gulf of Mexico. Estuar Coast 41(5):1322–1336. https://doi.org/10.1007/s12237-017-0351-x
Radi T, Bonnet S, Cormier MA, de Vernal A, Durantou L, Faubert E, Head MJ, Henry M, Pospelova V, Rochon A (2013) Operational taxonomy and (paleo-) autecology of round, brown, spiny dinoflagellate cysts from the Quaternary of high northern latitudes. Mar Micropaleontol 98:41–57. https://doi.org/10.1016/j.marmicro.2012.11.001
Radi T, de Vernal A (2004) Dinocyst distribution in surface sediments from the northeastern Pacific margin (40–60◦ N) in relation to hydrographic conditions, productivity and upwelling. Rev Palaeobot Palynol 128:169–193. https://doi.org/10.1016/S0034-6667(03)00118-0
Radi T, de Vernal A (2008) Last glacial maximum (LGM) primary productivity in the northern North Atlantic Ocean. Can J Earth Sci 45:1299–1316. https://doi.org/10.1139/E08-059
Ramírez-Valencia V, Paez-Reyes M, Salgado J, Sangiorgi F, Zúñiga-González AC, Amézquita A, Ibarra-Ávila H, González-Arango C (2021) Distribution of organic-walled dinoflagellate cysts in surface sediments of the southern Caribbean and the eastern tropical Pacific and its environmental implications. Mar Micropaleontol 167, 102000. https://doi.org/10.1016/j.marmicro.2021.102000
Ribeiro S, Amorim A, Andersen TJ, Abrantes F, Ellegaard M (2012) Reconstructing the history of an invasion: the toxic phytoplankton species Gymnodinium catenatum in the Northeast Atlantic. Biol Invasions 5:969–985. https://doi.org/10.1007/s10530-011-0132-6
Rigel CQ, Javier H, Ernesto GM, Rafael RM (2022) Assemblages of dinoflagellate resistance cysts and copepod eggs in superficial sediments at the upper Gulf of California. Conti Shelf Res 235:104648. https://doi.org/10.1016/j.csr.2022.104648
Rochon A, Lewis J, Ellegaard M, Harding IC (2009) The Gonyaulax spinifera (Dinophyceae) "complex": perpetuating the paradox? Rev of Palaeobot Palynol 155(1–2):52–60. https://doi.org/10.1016/j.revpalbo.2008.12.017
Rodrigues RV, Patil JS (2021) Salinity changes may influence dinoflagellate cyst morphometry: data from monsoon-influenced tropical coastal ecosystems. J Plankton Res 43(6):853–864. https://doi.org/10.1093/plankt/fbab072
Rodrigues RV, Patil JS, Anil AC (2022) Dinoflagellates cyst assemblage concerning trophic index for eutrophication from major ports along the west coast of India. Mar Pollut Bull 176:113423. https://doi.org/10.1016/j.marpolbul.2022.113423
Rodrigues RV, Patil JS, Sathish K, Anil AC (2019) Dinoflagellate planktonic-motile-stage and benthic-cyst assemblages from a monsoon-influenced tropical harbour: elucidating the role of environmental conditions. Estuar Coast Shelf Sci 226:106253. https://doi.org/10.1016/j.ecss.2019.106253
Roullier F, Berline L, Guidi L, Durrieu De Madron X, Picheral M, Sciandra A, Pesant S, Stemmann L (2014) Particle size distribution and estimated carbon flux across the Arabian Sea oxygen minimum zone. Biogeosciences 11:4541–4557. https://doi.org/10.5194/bg-11-4541-2014
Sangiorgi F, Donders TH (2004) Reconstructing 150 years of eutrophication in the North-Western Adriatic Sea (Italy) using dinoflagellate cysts, pollen and spores. Estuar Coast Shelf Sci 60:69–79. https://doi.org/10.1016/j.ecss.2003.12.001
Sarma VVSS, Dileep Kumar M, Saino T (2007) Impact of sinking carbon flux on accumulation of deep-ocean carbon in the Northern Indian Ocean. Biogeochemistry 82:89–100. https://doi.org/10.1007/s10533-006-9055-1
Schott FA, McCreary JP Jr (2001) The monsoon circulation of the Indian Ocean. Prog Oceanogr 51(1):1–123. https://doi.org/10.1016/S0079-6611(01)00083-0
Singh ND, Singh SK, Malla N, Chinni V (2023) Biogeochemical cycling of dissolved manganese in the Arabian Sea. Geochim Cosmochim Acta 343:396–415. https://doi.org/10.1016/j.gca.2022.12.030
Smitha BR, Sanjeevan VN, Vimalkumar KG, Revichandran C (2008) On the upwelling off the southern tip and along the west coast of India. J Coastal Res 24:95–102. https://doi.org/10.2112/06-0779.1
Sonneman JA, Hill DRA (1997) A taxonomic survey of cyst-producing dinoflagellates from recent sediments of Victorian coastal waters Australia. Bot Mar 40(1–6):149–178. https://doi.org/10.1515/botm.1997.40.1-6.149
Sprangers M, Dammers N, Brinkhuis H, Van Weering TC, Lotter AF (2004) Modern organic-walled dinoflagellate cyst distribution offshore NW Iberia; tracing the upwelling system. Rev Palaeobot Palynol 128(1–2):97–106. https://doi.org/10.1016/S0034-6667(03)00114-3
Uddandam PR, Prasad V, Rai J (2017) Dinoflagellate cyst distribution in sediments of western Bay of Bengal: role of sea surface conditions. Palaeogeogr Palaeoclimatol Palaeoecol 483:31–48. https://doi.org/10.1016/j.palaeo.2017.01.013
Van Mooy BAS, Keil RG (2002) Devol AH (2002) Impact of suboxia on sinking particulate organic carbon: enhanced carbon flux and preferential degradation of amino acids via denitrification. Geochim Cosmochim Acta 66:457–465. https://doi.org/10.1016/S0016-7037(01)00787-6
Verleye TJ, Mertens KN, Young MD, Dale B, McMinn A, Scott L, Zonneveld KA, Louwye S (2012) Average process length variation of the marine dinoflagellate cyst Operculodinium centrocarpum in the tropical and Southern Hemisphere Oceans: assessing its potential as a palaeosalinity proxy. Mar Micropal 86:45–58. https://doi.org/10.1016/j.marmicro.2012.02.001
Verleye TJ, Louwye S (2010) Recent geographical distribution of organic-walled dinoflagellate cysts in the Southeast Pacific (25–53 S) and their relation to the prevailing hydrographical conditions. Palaeogeogr Palaeoclimatol Palaeoecol 298:319–340. https://doi.org/10.1016/j.palaeo.2010.10.006
Vijayan AK, Reddy BB, Sudheesh V, Marathe PH, Nampoothiri VN, Harikrishnachari NV, Kavya P, Gupta GVM, Ramanamurthy MV (2021) Phytoplankton community structure in a contrasting physicochemical regime along the eastern Arabian Sea during the winter monsoon. J Mar Syst 215:103501. https://doi.org/10.1016/j.jmarsys.2020.103501
Wang Z, Matsuoka K, Qi Y, Chen J, Lu S (2004) Dinoflagellate cyst records in recent sediments from Daya Bay South China. Sea

Phycol Res 52(4):396–407. https://doi.org/10.1111/j.1440-183.2004.00357.x

Wall D, Dale B (1968) Modern dinoflagellate cysts and evolution of the peridiniales. Micropaleontol 14(3):265–304

Wendler I, Zonneveld KAF, Willems H (2002) Oxygen availability effects on early diagenetic calcite dissolution in the Arabian Sea as inferred from calcareous dinoflagellate cysts. Global Planet Change 34:219–239. https://doi.org/10.1016/S0921-8181(02)00117-0

Zhang Z, Ma W, Chai F (2022) Role of ocean circulation and settling of particulate organic matter in the decoupling between the oxygen minimum zone and the phytoplankton productive zone in the Arabian Sea: a modeling study. Front Mar Sci 9:927921. https://doi.org/10.3389/fmars.2022.927921

Zonneveld KAF (1997) Dinoflagellate cyst distribution in surface sediments from the Arabian Sea (northwestern Indian Ocean) in relation to temperature and salinity gradients in the upper water column. Deep-Sea Res II 44:1411–1443. https://doi.org/10.1016/S0967-0645(97)00007-6

Zonneveld KAF, Brummer GJA (2000) (Palaeo-)ecological significance, transport and preservation of organic-walled dinoflagellate cysts in the Somali Basin, NW Arabian Sea. Deep-Sea Res II 47:2229–2256. https://doi.org/10.1016/S0967-0645(00)00023-0

Zonneveld KAF, Susek E, Fischer G (2010) Seasonal variability of the organic-walled dinoflagellate cyst production in the coastal upwelling region off Cape Blanc (Mauritania): a five-year survey. J Phycol 46:202–215. https://doi.org/10.1111/j.1529-8817.2009.00799.x

Zonneveld KAF, Versteegh G, Kodrans-Nsiah M (2008) Preservation and organic chemistry of Late Cenozoic organic-walled dinoflagellate cysts: a review. Mar Micropaleontol 68(1–2):179–197. https://doi.org/10.1016/j.marmicro.2008.01.015

Zonneveld KAF, Versteegh GJ, de Lange GJ (1997) Preservation of organic-walled dinoflagellate cysts in different oxygen regimes: a 10,000 year natural experiment. Mar Micropaleontol 29(3–4):393–405. https://doi.org/10.1016/S0377-8398(96)00032-1

Zonneveld KAF, Grotheer H, Versteegh GJM (2022) Dinoflagellate cysts production, excystment and transport in the upwelling off Cape Blanc (NW Africa). Front Mar Sci 9:915755. https://doi.org/10.3389/fmars.2022.915755

Zonneveld KAF, Marret F, Versteegh GJM, Bogus K, Bonnet S, Bouimetarhan I, Crouch E, de Vernal A, Elshanawany R, Edwards L, Esper O, Forke S, Grøsfjeld K, Henry M, Holzwarth U, Kielt J, Kim S, Ladouceur S, Ledu D, Chen L, Limoges A, Londeix L, Lu S, Mahmoud MS, Marino G, Matsouka K, Matthiessen J, Mildenhal DC, Mudie P, Neil HL, Pospelova V, Qi Y, Radi T, Richerol T, Rochon A, Sangiorgi F, Solignac S, Turon J, Verleye T, Wang Y, Wang Z, Young M (2013) Atlas of modern dinoflagellate cyst distribution based on 2405 data points. Rev Palaeobot Palynol 191:1–197. https://doi.org/10.1016/j.revpalbo.2012.08.003

Zonneveld KAF, Sebastian Meier KJ, Esper O, Siggelkow D, Wendler I, Willems H (2005) The (palaeo) environmental significance of modern calcareous dinoflagellate cysts: a review. Paläontologische Zeitschrift 79:61–77. https://doi.org/10.1007/BF03021754

Publisher's Note Springer Nature remains neutral with regard to jurisdictional claims in published maps and institutional affiliations.

Springer Nature or its licensor (e.g. a society or other partner) holds exclusive rights to this article under a publishing agreement with the author(s) or other rightsholder(s); author self-archiving of the accepted manuscript version of this article is solely governed by the terms of such publishing agreement and applicable law.

Environ Monit Assess (2023) 195:528
https://doi.org/10.1007/s10661-023-11062-7

Variability in phytoplankton shape dominance in marine pelagic systems: prevalence of different adaptive strategies in the eastern Arabian Sea during the winter monsoon

Pranoy Paul · Jagadish S. Patil · Arga Chandrashekar Anil

Received: 29 November 2022 / Accepted: 27 February 2023
© The Author(s), under exclusive licence to Springer Nature Switzerland AG 2023

Abstract Phytoplankton communities from pelagic systems were assessed to explore the potential of using commonly used traits (such as cell geometry and taxa) as ecological function indicators from the data generated during the winter monsoon in the eastern Arabian Sea (AS). Altogether, data from two oceanic, i.e., convective mixing influenced non-oligotrophic northeastern-AS (NEAS-O) and Rossby wave-influenced oligotrophic southeastern-AS (SEAS-O) and one coastal (NEAS-C) cruises were utilized to decipher the ecological inferences. Overall phytoplankton shapes showed a high level of redundancy by selecting only a few dominant shapes (5 of 22 shapes), though taxonomic diversity was rich (164 species). The taxonomic and morphological approach adopted revealed high species and shape diversity in NEAS-O than in high-abundance NEAS-C and low-abundance SEAS-O. Also, the shape diversity and dominant shapes (cylinder, elliptic-prism, and prism-on-parallelogram) remained the same in oceans than NEAS-C where combined (cylinder + 2 half-sphere) and simple (elliptic-prism) shapes dominated. Additionally, the Rossby-wave front and its reminiscence in SEAS-O and sea-surface-temperature fronts in NEAS-C favored simple and combine shaped phytoplankton, respectively. The morphological properties assessment revealed that the dominant shapes adapted the strategy to conserve the optimal surface-to-volume ratio (S:V) irrespective of changes in greatest-axial-linear-dimension (GALD) in NEAS-O and SEAS-O but not in NEAS-C. However, the dominant shapes in the NEAS-O and SEAS-O opted for high S:V with low GALD and low S:V with high GALD, respectively, while high S:V with no relation with GALD in NEAS-C suggests the prevalence of different adaptive strategies to cope with the respective hydrographic conditions, particularly nutrient availability.

Keywords Phytoplankton · Taxonomy · Cell geometry · Northeastern Arabian Sea · Southeastern Arabian Sea · Winter monsoon

Introduction

Phytoplankton, which are vital in ecosystem functioning, food-web dynamics, fisheries, and biogeochemical cycling of essential micro and macronutrients, are not only taxonomically diverse but also show amazing intra- and inter-specific morphological diversity with organisms ranging greatly in the magnitude of size (Finkel et al., 2010) and a wide range of shapes (Hillebrand et al., 1999; Sun & Liu, 2003). Traditionally, the morphological

Supplementary Information The online version contains supplementary material available at https://doi.org/10.1007/s10661-023-11062-7.

P. Paul · J. S. Patil (✉) · A. C. Anil
CSIR-National Institute of Oceanography, Dona Paula 403004, Goa, India
e-mail: patilj@nio.org

P. Paul
School of Earth, Ocean, and Atmospheric Sciences, Goa University, Taleigao Plateau, Taleigao 403 206 Goa, India

Published online: 31 March 2023

attributes are being used only for taxonomic studies but it does not reflect the ecological functions (Naselli-Flores et al., 2007; Salmaso & Padisak, 2007). Lewis (1976) first noted the ecological value of morphological descriptors in phytoplankton resource acquisition (light and nutrient uptake) under the pressure of natural selection and competition. The adaptive value of the morphological variability and differences in morphology adopted for diverse ecological strategies by phytoplankton was studied by Margalef (1978) and later explored by Reynolds (1997). Few shapes are best adapted to certain environmental conditions than others so the phytoplankton with such shapes should have better fitness and diversity (Ryabov et al., 2021). The aquatic ecosystem's ecological state can be assessed by understanding the adaptive value of different phytoplankton morphologies; therefore, morphological diversity can be considered a key factor allowing a particular ecological group to withstand the various environmental conditions experienced in the ecosystem (Naselli-Flores, 2014).

The trait-based approaches in phytoplankton ecology have become common and such approaches have the potential to increase our insight into the organization of ecological communities and predict their reorganization under any environmental change (Litchman & Klausmeier, 2008). This is because phytoplankton are relatively simple and have well-defined traits that determine their ecological niche (Litchman & Klausmeier, 2008). The well-defined commonly used traits in phytoplankton can be classified into three categories (Litchman & Klausmeier, 2008; Weithoff & Beisner, 2019): (i) morphological — size, shape, greatest axial linear dimension (GALD), biovolume, mucilage presence/absence, and biological form (unicellular/colonial/filament/chains); (ii) physiological — presence/absence of silica demand, heterocysts (N_2-fixation), mixotrophy, toxin production, resting stages, dominant pigment type, nutrient, and/or light uptake parameters; and (iii) behavioral — presence/absence of flagella and aerotypes. Among all the above-mentioned traits, morphometric traits like size and shape are considered master traits (Weithoff & Beisner, 2019) which affect nutrient acquisition, sinking, and grazer susceptibility (Grover, 1989; Smayda, 1970; Thingstad et al., 2005). Size and shape are also plastic in nature and depend on many environmental variables, such as light levels, nutrient concentrations, and grazing pressure (Chisholm, 1992; Duarte et al., 1990).

Furthermore, in trait-based studies, species sharing similar adaptive traits are grouped even if they are taxonomically distinct (Simberloff & Dayan, 1991). From the phytoplankton viewpoint, the pelagic habitat and its main representative phyla and their ecology are relatively similar across both marine and freshwater ecosystems (Weithoff & Beisner, 2019). Despite such similarity, the focus of research differed between systems, i.e., the majority of research in the marine considered how traits and trait distribution derive processes that determine the environmental conditions (like biogeochemistry) but it is the opposite in the freshwater where the focus is on how communities respond to the environment and which environmental factors drive the trait-based community assembly (Weithoff & Beisner, 2019). For instance, the increasing uses of trait-based studies to explain and understand phytoplankton community is limited to distribution (Kruk et al., 2010), seasonal dynamics (Salmaso & Padisak, 2007), diversity, and community structure (Litchman & Klausmeier, 2008) in freshwater, whereas in the marine ecosystem, the studies are limited to spatiotemporal variation (Stanca et al., 2013), biogeographic trait patterns (Barton et al., 2013), biogeochemical processes such as primary production and nitrogen fixation (Breton et al., 2017), oceanic biogeochemistry (Litchman et al., 2007, 2015; Finkel et al., 2010), and phytoplankton dynamics (Alexander et al., 2015). Many morphological traits might be strategic and help in explaining phytoplankton differences and patterns under contrasting hydrodynamic conditions (Fraisse et al., 2013). Thus, morphological traits play a pivotal role in the determination of phytoplankton ecological niches (Aubry et al., 2017). The morphological adaptive strategy that results in response to environmental changes helps differently sized phytoplankton organisms to coexist making it like a geometric concurrence (Roselli & Basset, 2015; Segura et al., 2013). However, to our knowledge, the information on the variations in phytoplankton shapes concerning different hydrographic settings in the marine pelagic systems is not available and was addressed in the present study by selecting the eastern Arabian Sea in the Northern India Ocean, a well-studied system, as a reference. A similar approach was attempted to study the rock-pool micro-phytoplankton community from the intertidal zone (Paul et al., 2021) but studies from the open ocean are limited even though there exist few datasets on cell volumes (Chitari & Anil, 2017).

The Arabian Sea (AS) is considered one of the unique oceanic basins owing to its high productive

periods in winter (WM) and summer monsoon (SM) caused by the seasonal reversal of wind direction and associated drastic changes in the surface currents (Banse, 1987) and the data presented here corresponds to winter monsoon from eastern AS (EAS). The physical change in the water column associated with the reversal of monsoonal winds governs the productivity of the Arabian Sea (Wiggert et al., 2005). During WM, the hydrographic conditions in the northern and southern regions of EAS are significantly different, i.e., currents bring in high nutrients through convective mixing in the NEAS which supports phytoplankton production (including bloom; Banse, 1987; Sarma et al., 2019) and was also noticed in this study, i.e., higher in NEAS (both open and coastal) than SEAS-O (Supplementary Tables 1 and 2). The convective mixing in NEAS is triggered by the cold-dry north-easterly continental wind blowing over the surface waters causing evaporation (Madhupratap, et al., 1996; Weller et al., 2002). The convective mixing during winter monsoons deepens the mixed layer depth and enhances nutrient availability (Sawant & Madhupratap, 1996). Whereas in SEAS, WM is defined by the existence of seasonal down-welling Rossby waves (Shankar et al., 2002) which, along with its associated currents, brings the nutrient-enriched low saline water mass from the western boundary of the Bay of Bengal (Shenoi et al., 2002) and triggers primary producers (Kumar et al., 2004, Amol, 2018) in the otherwise warmer oligotrophic waters (Vijayan et al., 2021). Additionally, the mesoscale features such as sea surface temperature (SST) fronts supporting rich phytoplankton biomass than the adjoining non-fronts are also prevalent in AS. However, more SST fronts are reported in NEAS than in SEAS (Kurian et al., 2020). Therefore, in the present study, an attempt has been made to understand the distribution of phytoplankton shapes and species composition between contrasting hydrographic settings such as (a) nutrient-rich coastal and open ocean systems, (b) oligotrophic and non-oligotrophic ocean systems, and (c) SST fronts and non-fronts from both coastal and ocean ecosystems. Through this study, an attempt is made to explore the possibility of using phytoplankton shapes (>5 microns) as ecological function indicators in marine pelagic systems.

Methodology

Study area and sampling strategies

The present study was carried out in the north (NEAS) and the south (SEAS) EAS during the winter monsoon of 2015–2016. In the NEAS, two cruises, *R/V Sindhu Sankalp* (11–22 February 2015) in the open ocean (NEAS-O) and *R/V Sindhu Sadhana* (18 November- 2 December 2016) in the coastal (NEAS-C), were taken during late winter monsoon and early winter monsoon, respectively, and another cruise, *R/V Sindhu Sadhana* (6–17 November 2016), was taken in the open ocean of SEAS (SEAS-O) during early winter monsoon (Fig. 1 and Supplementary Fig. 1). The water samples from NEAS-O (20 stations), NEAS-C (38 stations), and SEAS-O (31 stations) were collected at discrete depths (surface to 100 m) with 10 L Niskin bottles attached to 32 Carousel Water Sampler (Sea-bird Electronics Inc.; SBE) which is operated with the SBE 911 plus CTD for real-time data acquisition. The hydrographic data revealed that in NEAS, the surface and sub-surface waters are more saline and are relatively cooler and warmer, respectively, than SEAS (Fig. 2). Also, the fluorescence and nutrient concentrations are relatively higher in NEAS than in SEAS. Additionally, differences in frontal and non-frontal regions were also observed. Most of the hydro-graphic data are published in detail elsewhere (see Bemal et al., 2018 and Sarma et al., 2019 for more details) and here, only a summary of the same is presented in Supplementary Tables 1 and 2.

Phytoplankton sample collection and analysis

A fixed volume (1L) of the water sample was preserved with 4% Lugol's iodine and used for further analysis. An aliquot (2–5 ml) of the sample volume in duplicate was analyzed from the concentrated (by sedimentation (48 h) and siphoning technique) 100 ml using an inverted microscope (IX-73 Olympus Make) to access the phytoplankton composition and abundance. The taxonomic identification of phytoplankton was carried out based on standard identification keys (Taylor, 1973; Tomas, 1997).

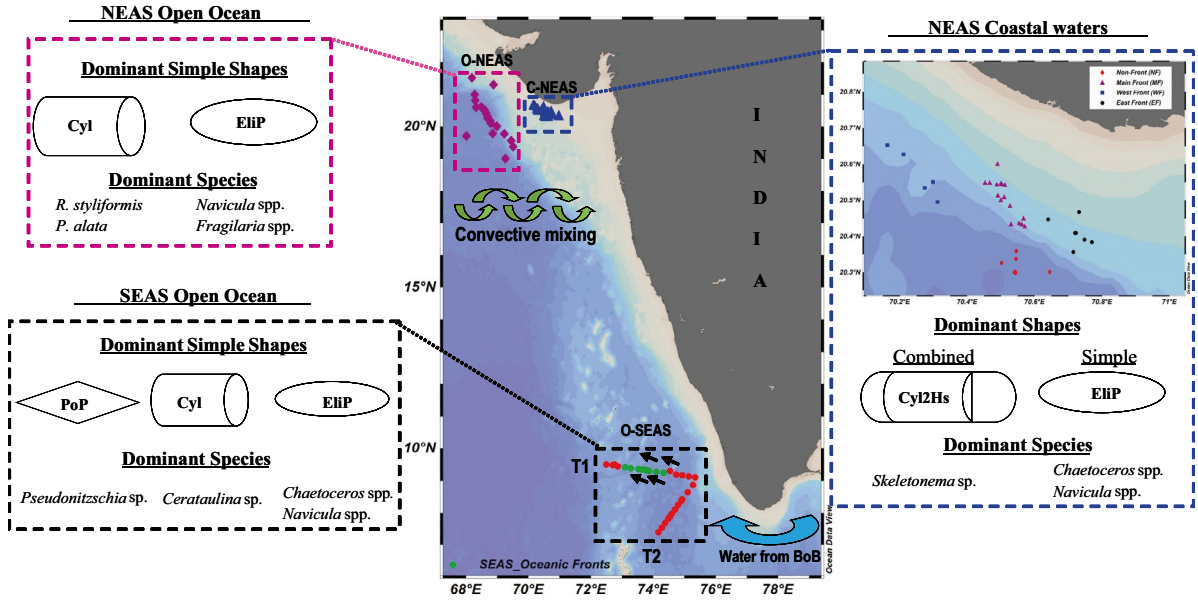


Fig. 1 Schematic showing location of the stations in the northeasternstern Arabian Sea - NEAS (both ocean and coastal) and southeastern Arabian Sea - SEAS (only ocean) along with the dominant taxa and shape and the prevailing hydrographic conditions. Green, blue, and black arrow indicate convective mixing, inflow of water from BOB, and Rossby wave. Note: Cyl, cylinder; ElliP, elliptic prism; PoP, prism on parallelogram; Cyl2Hs, cylinder+2 half sphere. T1 and T2 correspond to transects 1 and 2 in SEAS-O

The morphological measurements (length, width, breadth, area, volume, and maximum linear dimension) for each phytoplankton cell or colony were performed using a factory-calibrated FlowCAM (Fluid Imaging Technologies) at 4× magnification (flowcell 300 µm) and a microscope digital camera adapter system (QimagingMicroPublisher 5.0 RTV) attached to the inverted microscope at 200–600× magnification (Olympus IX73), respectively. These measurements were then used for the calculation of volume (V; μm^3) and surface area (S; μm^2) following Hillebrand et al. (1999) and Sun and Liu (2003). In algal ecology and physiology, shape and size variability play a key role (Capblancq & Catalan, 1994) wherein the surface/volume ratios of a biomass unit need to be maintained within physiologically necessary bounds in a given environment (Lewis, 1976). Given this, the surface-to-volume ratio (S:V) of the phytoplankton was calculated according to Lewis (1976) and Aubry et al. (2017). For chain-forming cells like *Chaetoceros* and *Skeletonema*, each cell in the chain was considered and the morphological measurements were taken in higher magnifications (400× or 600×). The greatest axial linear dimension (GALD; µm) or maximum linear dimension (Weithoff & Beisner, 2019) is measured directly from the linear dimensions like diameter, height, total length, and apical axis length of a given cell based on the geometric approximation given by Hillebrand et al. (1999) and Sun et al. (2003). Here, in this study, the GALD of a cell is measured according to its cell geometry as described by Ryabov et al. (2021). For instance, in the simple shapes, the maximum cell linear dimension (e.g., diameter in the sphere, height in ellipsoid and cylinder, apical axis length in prism on parallelogram) was considered GALD, whereas for combined shapes (Box+2 Cylinders, Cylinder+2 Half spheres, Ellipsoid+2 Cones+Cylinder, etc.,) consisting of few segments measured separately (e.g., cylinder with 2 half spheres), the sum of the linear dimensions of these parts or the total height or length was considered.

Overall, a total of 22 shapes were identified among which 11 shapes were simple (Box-B, Cone-C, Cylinder-Cyl, Cymbelloid-Cym, Ellipsoid-Elli, Elliptic prism-ElliP, Half sphere-Hs, Prism on parallelogram-PoP and Prism on triangle-PoT, Prolate spheroid-Ps, and Sphere-S) and 8 were combined (Box+2 Cylinders-B2Cyl, Box+Elliptic prism-BElliP, Cone+Half sphere-CHs, Cylinder+2 Half spheres-Cyl2Hs, Ellipsoid+2 Cones+Cylinder-Elli2CCyl), Elliptic

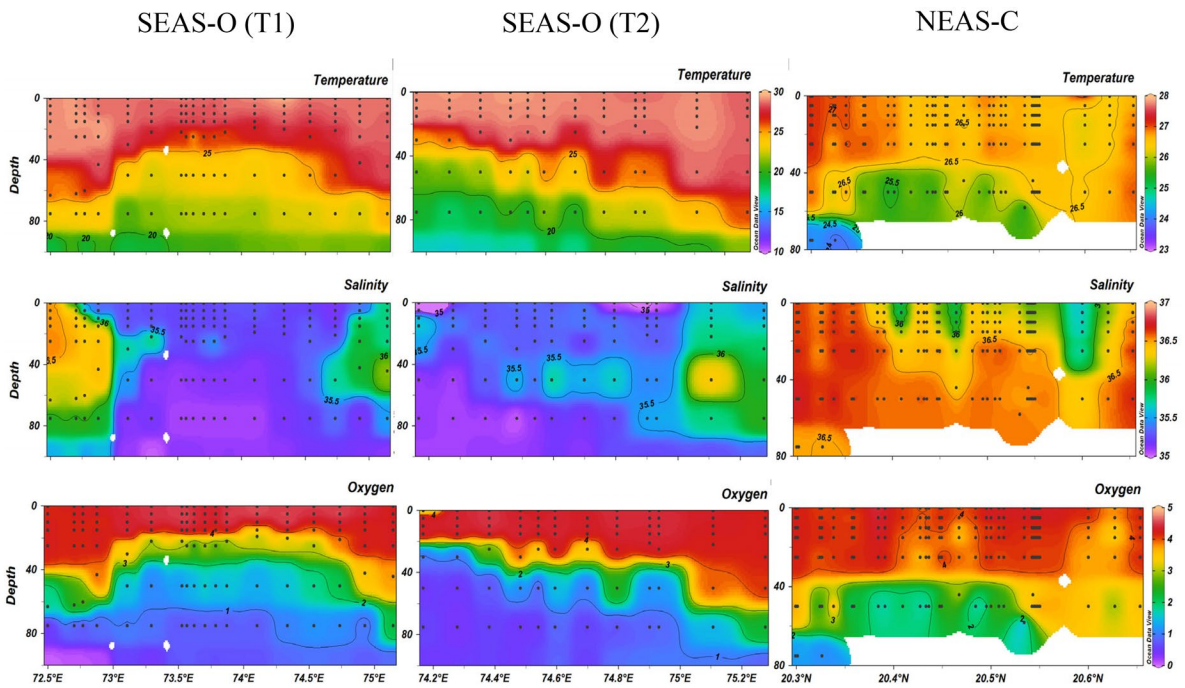


Fig. 2 The vertical distribution of temperature (°C), salinity (psu), and oxygen concentration (mL L^{-1}) in northeastern Arabian Sea coastal (NEAS-C) and southeastern Arabian Sea ocean (SEAS-O)

prism+4 Cones-ElliP4C, Prolate spheroid+2 Cylinders-Ps2Cyl, and 2 Cones-2C). Among them, the 3 shapes with their girdle view (e.g., Cyl, PoP, PoT) are considered equivalent to their original shape as the geometric formula was the approximation of the original shape.

Data analysis

Univariate measures such as species count, abundance, Shannon–Wiener's diversity, species richness, and evenness were performed on log-transformed species and shape data. The clustering of frontal and non-frontal phytoplankton was performed through the Bray–Curtis similarity and group average methods. For the analysis, log (x+1) transformed species and shape data were used, and the grouping was done at a 50% level to find the significant similarities. Furthermore, the log-transformed taxa and shape data were subjected to a two-way analysis of variance (ANOVA) to evaluate the variation between regions as well as between the frontal and non-frontal regions. The relationship between the greatest axial linear dimension (GALD) and S:V was determined by using linear regression on log(x+1) transformed data. The significance level was set at $p<0.05$ and the determination coefficient (R^2) was considered the proportion of variation in S:V which can attribute to GALD, whereas the slope (b) showed the degree to which the S:V would vary as GALD increases. If the slope (b) value is very low, for instance, $b=-0.06$ for PoP, that means a decrease in S:V of 0.06 μm^{-1} for each μm increase in GALD. The negative correlation between GALD and S:V in general means that as the GALD increases the S:V decreases, and vice versa. Univariate measures calculation and clustering analysis were performed using statistical software PRIMER 6, ANOVA was performed using Statistica software (release 8), linear regression analysis and box plots were plotted using R program (R core Team, 2020), and ODV plots were plotted using Ocean Data View 4 (Schlitzer, 2015).

Results

Taxonomic and shape diversity of the north-eastern Arabian Sea (NEAS)

A total of 133 (belonging to 63 genera) and 83 (belonging to 48 genera) species were recorded in the open ocean (NEAS-O) and coastal (NEAS-C) regions, respectively (Supplementary Table 3). In NEAS-O diatoms (81%) comprising 54 species (36 centric and 18 pennate species) followed by dinoflagellates (19%) comprising 89 species dominated the community, whereas in NEAS-C, diatoms (94%) comprising 44 species (30 centric and 14 pennate species) followed by dinoflagellates (6%) comprising 39 species dominated the phytoplankton community. Despite diatom dominance, the contribution to the total community was higher in the open ocean (82–98%) than in the coastal (77%) (Fig. 3). ANOVA revealed significant differences in phytoplankton community structure and species dominance between the open ocean and coastal region ($p = 0.003$). The diversity analysis reveals that the species count, richness, evenness, and diversity were higher in the NEAS-O than in NEAS-C except for the abundance which showed an opposite trend for both taxonomy and shape (Fig. 4a–j).

In the NEAS-O, centric diatoms *Rhizosolenia styliformis* and *Probosica alata* of Cyl shape followed by pennate diatoms *Lioloma* sp. of B shape and *Navicula* spp. of ElliP shape and dinoflagellate species *Protoperidinium* spp of 2C shape were the major contributors. Whereas in NEAS-C, centric diatom *Skeletonema* sp. of Cyl2Hs shape and *Leptocylindrus* sp. of Cyl shape followed by pennate diatom *Pseudonitzschia* spp. of PoP shape and *Thalassionema nitzschoides* of B shape and dinoflagellate species *Protoperidinium* spp. of 2C shape dominated the community. It is notably interesting that despite the overall phytoplankton community was diatom dominated, the community structure was quite different within diatoms except for the dinoflagellates.

All the recorded phytoplankton species are categorized into a total of 19 (11 simple and 8 combined) and 16 (11 simple and 5 combined) morphometric shapes from NEAS-O and NEAS-C, respectively. Simple-shaped (88%) phytoplankton dominated in NEAS-O, whereas combined-shaped (55%) in NEAS-C. Among the simple shapes, Cyl (54%) was the dominant shape followed by ElliP (9%), B (9%), Elli (6%), and ElliP4Cs

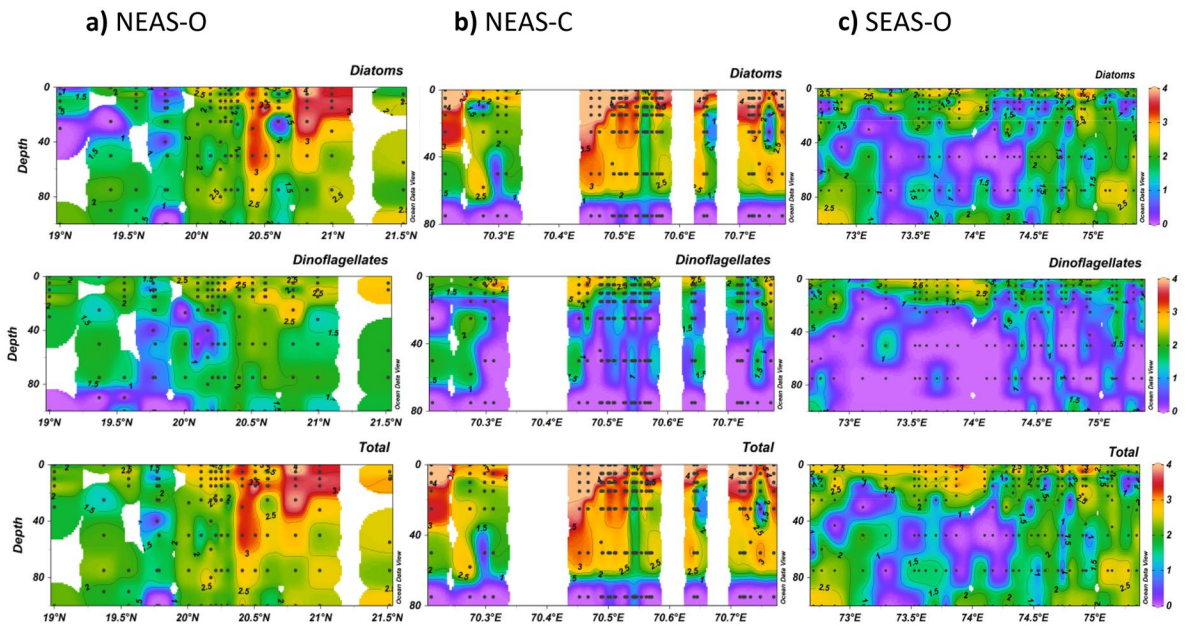


Fig. 3 Groupwise distribution of phytoplankton in the water column of NEAS and SEAS. NEAS-O, north-eastern Arabian Sea open ocean; NEAS-C, north-eastern Arabian Sea coastal region; and SEAS-O, south-eastern Arabian Sea open ocean

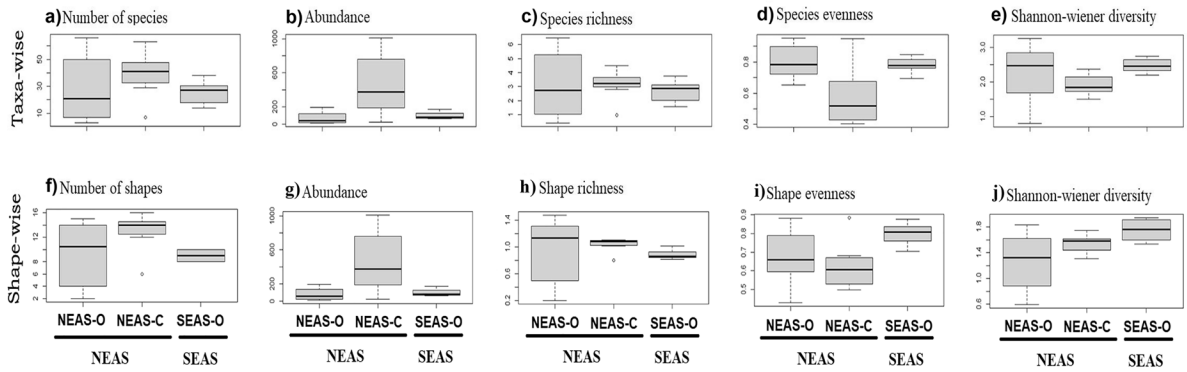


Fig. 4 Univariate measures of phytoplankton (both taxonomy and shape-wise) from NEAS (both coastal - NEAS-C and open ocean-NEAS-O) and SEAS (open ocean; SEAS-O). Station data are pooled and presented here

(5%) in NEAS-O. Maximum species diversity was observed in Elli2CCyl representing 36 phytoplankton species (all dinoflagellates) followed by Cyl with 27 species (22 centric diatoms and 5 dinoflagellates), Elli with 20 species (all dinoflagellate), and ElliP with 16 species (11 centric and 5 pennate diatoms). Among the combined shaped phytoplankton, Cyl2Hs (53%) was dominant followed by PoP (12%), ElliP (12%), and Cyl (12%) in NEAS-C. The maximum species diversity was observed in Cyl with 17 species (all centric diatoms) followed by ElliP with 14 species (11 centric and 3 pennate diatoms) and Elli with 14 species (all dinoflagellates).

The linear regression analysis of dominant phytoplankton shapes (abundance $\geq 60\%$) from NEAS-O revealed a significant negative correlation between GALD and S:V ($p < 0.05$), whereas no significant correlation was observed for NEAS-C (Fig. 8). In the NEAS-O, the determination of coefficient (R^2) for dominant shapes showed low values. However, in the present study, the dominant shapes (Cyl, ElliP, and PoP) of both coastal and open ocean ecosystems in NEAS adopted high S:V with a low GALD strategy. The results point out that all the dominant shapes in NEAS-O are attenuated (Cyl, ElliP, and PoP) and have adapted the strategy to conserve the optimal S:V which changes very minimally as the GALD increases (Fig. 8).

Additionally, the sampling at 38 stations in the NEAS-C region encompasses both frontal and non-frontal regions and is categorized and presented accordingly as follows: (a) east front (EF) comprising 7 stations, (b) west front (WF) comprising 5 stations, (c) main front (MF) comprising 18 stations, and (d) non-front (NF) comprising of 8 stations (Fig. S1). It is evident from the comparative community and diversity analysis that the frontal waters showed high abundance and species composition compared to the non-frontal waters (Fig. 5a–e). Among all the stations, MF recorded the maximum number of phytoplankton species followed by EF, NF, and WF waters. The phytoplankton abundance was higher in all the frontal stations compared to NF. Interestingly, species richness, evenness, and diversity were higher in the NF stations compared to all the frontal stations (MF, EF, and WF) (Fig. 5c–f). A total of 67 phytoplankton species (39 diatoms (26 centric and 13 pennate) and 28 dinoflagellate species) representing 44 genera were recorded in the MF followed by EF with 52 species (32 diatoms (20 centric and 12 pennate) and 20 dinoflagellate species) from 38 genera, NF 50 species (27 diatom (18 centric and 9 pennate) and 23 dinoflagellate species) from 34 genera, and WF 49 species (31 diatom (19 centric and 12 pennate) and 18 dinoflagellate species) from 36 genera. Diatoms in the frontal waters contributing 90–98% of the total abundance dominated the entire phytoplankton community, whereas dinoflagellates contributed only 2–10%. The non-frontal waters were also diatom-dominated contributing 81% of the total abundance and the remaining 19% were contributed by dinoflagellates.

The shape-based morphometric analysis from the frontal and non-frontal regions of NEAS-C reveals that simple shapes dominated the WF (56%) and NF (69%), whereas combined shapes dominated the EF (57%) and MF (55%). The dominant shapes

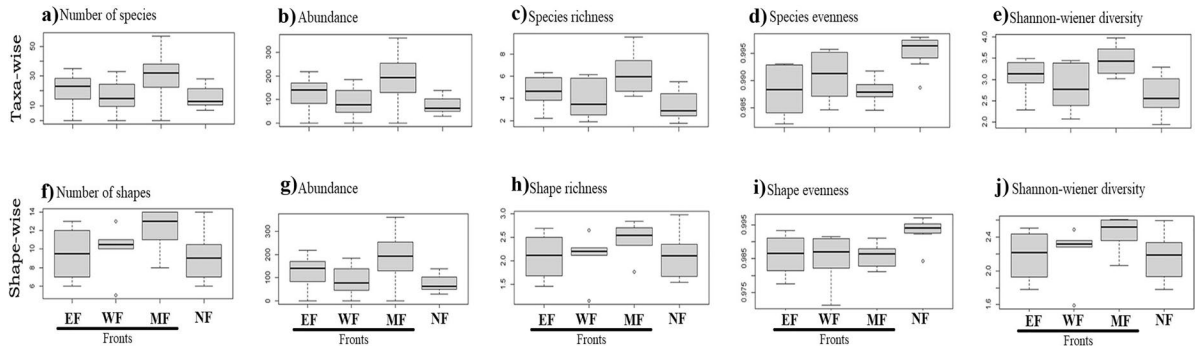


Fig. 5 Univariate measures of phytoplankton (both taxonomy and shape-wise) from frontal and non-frontal in coastal region of northeastern Arabian Sea (NEAS). EF, east front; WF, west front; MF, main front and NF, non-front. Station data frontal and non-frontal region are pooled and presented here

in all the frontal regions (except NF) were Cyl2Hs (43–56%) followed by PoP (11–15%), ElliP (11–12%), and Cyl (11–15%). The dominant shape in the NF region was Cyl (23%) followed by Cyl2Hs (22%), PoP (17%), and ElliP (15%). The maximum shape diversity in all the frontal (11–14 species) and non-frontal (13 species) regions was observed in the Cyl shape. However, the univariate measurement reveals that the shape richness, evenness, and diversity were higher in the non-frontal regions than in the frontal regions except for the abundance (N) which was higher in the frontal region (Fig. 5f–j).

The dominant shapes such as Cyl2Hs (centric diatom *Skeletonema* sp.), PoP (*Pseudonitzschia* spp.), ElliP (*Chaetoceros* spp. and *Navicula* spp), and Cyl (*Thalassiosira* spp. and *Leptrocylindrus* spp.) in the frontal region are represented by diatoms. In the non-frontal region, Cyl was the dominant shape and is majorly represented by *Leptocylindrus* spp. and *Thalassiosira* spp. Taxonomically, the centric diatom community was dominated by *Skeletonema* sp. and *Leptocylindrus* spp., whereas the pennate community was dominated by *Pseudonitzschia* spp. and *Navicula* spp. The dinoflagellate communities in both frontal and non-frontal waters were dominated by *Protoperidinium* spp. The cluster analysis for both taxonomy and shape shows two distinct clusters in which all the frontal stations (MF, EF, and WF) showed significant taxonomic similarity and formed one single cluster and NF as another cluster (Supplementary Fig. 4); however, the number of shapes was insignificant between the frontal and non-frontal regions. ANOVA also revealed significant ($p = 0.0001$) taxonomic differences between MF and NF regions but significant shape dissimilarity between frontal and non-frontal regions was not found ($p > 0.05$).

Taxonomic and shape diversity of the south-eastern Arabian Sea (SEAS)

A total of 74 phytoplankton species belonging to 35 genera were recorded from two transects (T1 and T2) in SEAS-O. Of the 74 species, 30 and 44 species were represented by diatoms (21 centric and 9 pennate species) and dinoflagellates, respectively, despite the high number of dinoflagellate species, the phytoplankton community was dominated by diatoms (77%). Unlike NEAS-O, the percentage contribution revealed the maximum contribution by pennate diatoms (48%) followed by centric diatoms (29%) and dinoflagellates (23%). The centric diatom community was dominated by *Cerataulina* sp. and *Chaetoceros* spp., whereas *Pseudonitzschia* spp. and *Thalassiothrix* sp. dominated the pennate diatom community. The dinoflagellate community was dominated by *Gyrodinium* sp., *Protoperidinium* spp., and *Scrippsiella* sp. Between the transects, transect 1 (T1) comprising 19 stations showed a slightly higher abundance compared to transect 2 (T2) comprising 12 stations. A total of 68 species belonging to 35 genera and 42 species belonging to 28 genera were recorded from T1 and T2 respectively. Of the 68 species in T1, 28 and 40 species were represented by diatoms (19 centric and 9 pennate species) and dinoflagellate, respectively. Whereas in T2, they were represented by an equal number of species, i.e., 21 species of diatom

(13 centric and 8 pennate species) and dinoflagellates. In both the transect, diatoms (76% in T1 and 84% in T2) dominated the community followed by dinoflagellates (24% in T1 and 16% in T2). Among the diatoms, the pennate contribution was higher than centric diatoms. Also, the community in both transects is represented by the same dominant species. For instance, in T1, the centric diatom community was dominated by *Cerataulina* sp., *Chaetoceros* spp., and *Thalassiosira* sp., whereas *Pseudonitzschia* spp. and *Navicula* sp. dominated among pennate diatoms. The dinoflagellate community was dominated by *Protoperidinum* sp., *Gyrodinium* sp., and *Scrippsiella* sp. In T2, *Chaetoceros* spp. and *Thalassiosira* sp. were the dominant centric diatoms whereas; *Pseudonitzschia* sp. and *Thalasiothrix* sp. dominated the pennate diatom community. *Gyrodinium* spp. and *Protoperidinium* spp. dominated the dinoflagellate community. Univariate measures revealed that T1 showed higher species number, abundance, richness, diversity, and evenness than T2 (Supplementary Fig. 2a–e).

All the recorded 74 phytoplankton species which are categorized into 12 morphometric shapes (9 simple and 3 combined) were recorded in the SEAS-O. Simple shapes showed maximum contribution (93–97%) compared to the combined shapes (3–7%). Considering the T1 and T2 transect, Cyl (23%) followed by PoP (19%), ElliP (18%), Elli, and B (14% each) dominated the phytoplankton community. Both the T1 and T2 recorded a similar number of shapes but Cyl (29%) dominated the former and PoP (32%) in the latter. ElliP2CCyl and Cyl showed maximum diversity representing 16 species each in T1 and Cyl (9 species) and Elli (7 species) in T2 showed the maximum diversity. The most dominant shape (Cyl) in T1 was represented by centric diatoms *Cerataulina* spp. and *Thalassiosira* spp. and the dominant shape PoP in T2 was represented by pennate diatom *Pseudonitzschia* spp. The diversity analysis of T1 and T2 revealed that shape abundance, evenness, and diversity were higher in T1 except for richness (d) which was higher in T2 (Supplementary Fig. 2f–j). Similar to NEAS-O, the linear regression analysis of dominant phytoplankton shapes (abundance $\geq 60\%$) revealed a significant negative correlation between GALD and S:V ($p < 0.05$) (Fig. 8) with the highest determination of coefficient (R^2) was recorded for PoP followed by Cyl. The dominant shapes (Cyl, ElliP, and PoP) of SEAS-O adopted low S:V with a high GALD strategy. The results point out that all the dominant shapes in SEAS-O are attenuated (Cyl, ElliP, and PoP) and have adapted the strategy to conserve the optimal S:V which changes very minimally as the GALD increases (Fig. 8).

Additionally, T1 in SEAS-O encompasses 19 stations in both frontal (F) and non-frontal (NF) regions and the results are presented accordingly. Of the 19 stations, 10 stations were frontal (F) and 9 stations were non-frontal (NF). Furthermore, the NF region was again divided into two zones NF-west (NFW) and NF-east (NFE). The diversity analysis shows that the species count, richness, evenness, and diversity are higher in the frontal region than in the NF regions except for the abundance which is higher in the NFE (Fig. 6a–e). A total of 45 species belonging to 24 genera and 38 belonging to 27 (in NFW) and 26 (in NFE)

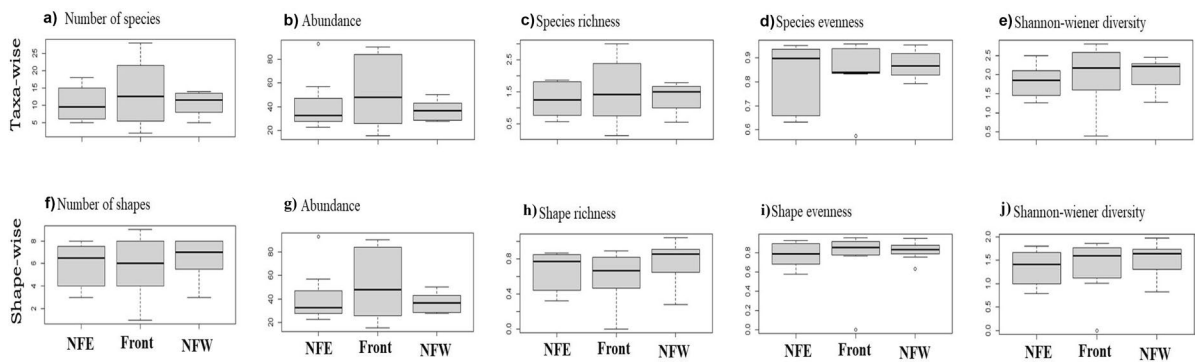
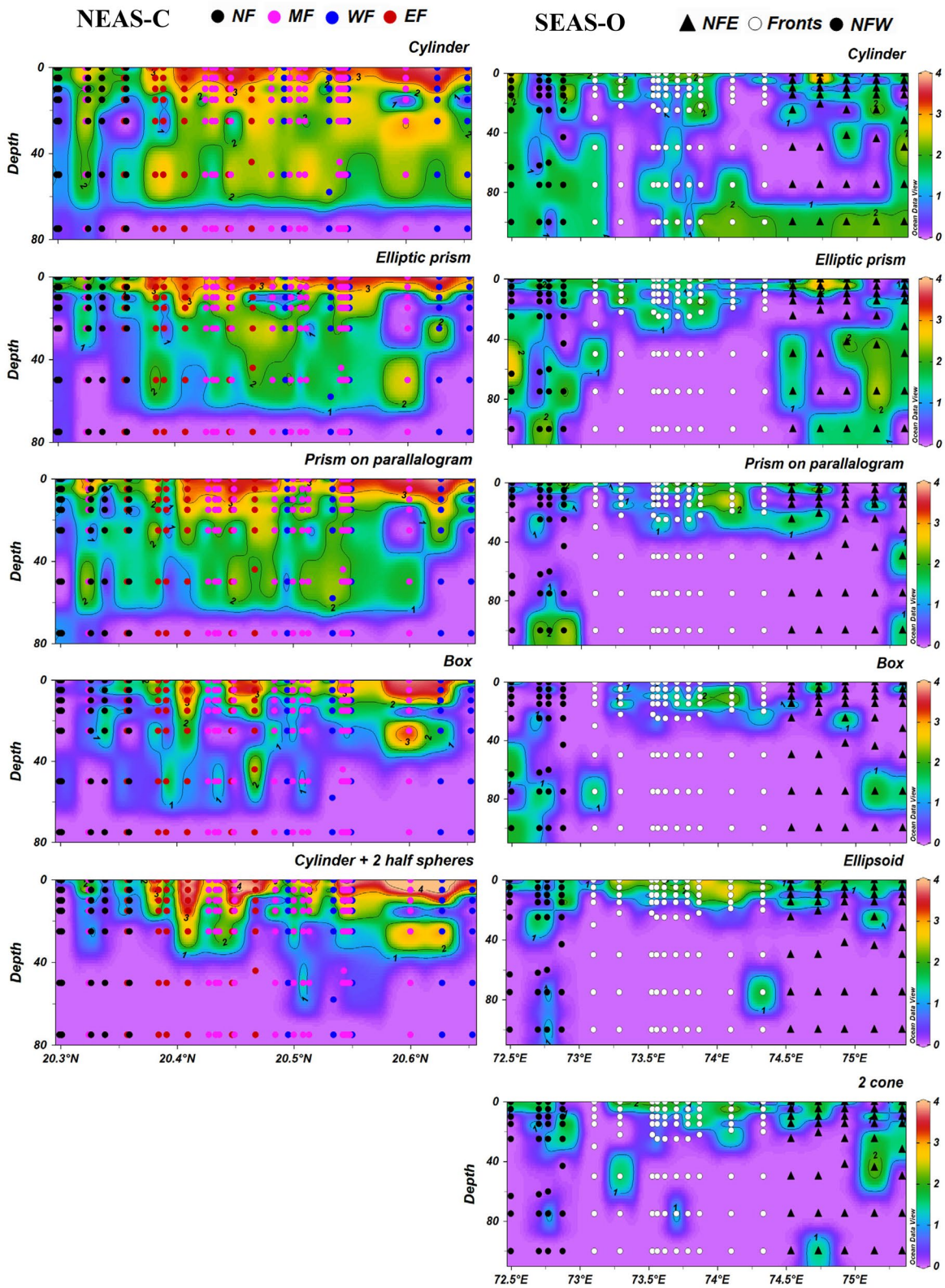


Fig. 6 Univariate measures of phytoplankton (both taxonomy and shape-wise) from frontal and non-frontal in oceanic region of southeastern Arabian Sea (SEAS). NFW, non-front west; F, frontal region; and NFE, non-front east. Station data frontal and non-frontal region are pooled and presented here


NEAS-C
NF MF WF EF
SEAS-O
NFE Fronts NFW
Cylinder
Elliptic prism
Prism on parallalogram
Box
Cylinder + 2 half spheres
Ellipsoid
2 cone
Depth
0
40
80
20.3°N
20.4°N
20.5°N
20.6°N
72.5°E
73°E
73.5°E
74°E
74.5°E
75°E
Ocean Data View

◂**Fig. 7** Distribution of dominant phytoplankton shape in the frontal and non-frontal water column of NEAS and SEAS. NEAS-C, coastal north-eastern Arabian Sea; SEAS-O, open ocean south-eastern Arabian Sea; NF, non-front; MF, main front; WF, west front; EF, east front; NFE, non-front east; and NFW, non-front west

genera were recorded in F and NF, respectively. Of the 45, 18 and 27 species correspond to diatoms (13 centric and 5 pennate species) and dinoflagellates, respectively, in F, whereas in NF, 20 diatoms (12 centric and 8 pennate species) plus 18 dinoflagellates and 16 diatoms (10 centric and 6 pennate species) plus 22 dinoflagellates were recorded from NFW and NFE, respectively. In all the regions, diatoms dominated the phytoplankton community, i.e., 70%, 79%, and 77% in frontal, NFW, and NFE, respectively. In the frontal region, pennate diatom (*Pseudonitzschia* spp.) dominated, whereas centric diatoms (*Chaetoceros* spp. and *Corataulina* sp.) dominated the NF (NFE and NFW) regions. The dinoflagellate community was dominated by *Gyrodinium* sp. and *Protoperidinium* spp. in both frontal and NF regions. The cluster analysis shows that frontal and NFE are significantly similar and form a single cluster in the dendrogram (Supplementary Fig. 3).

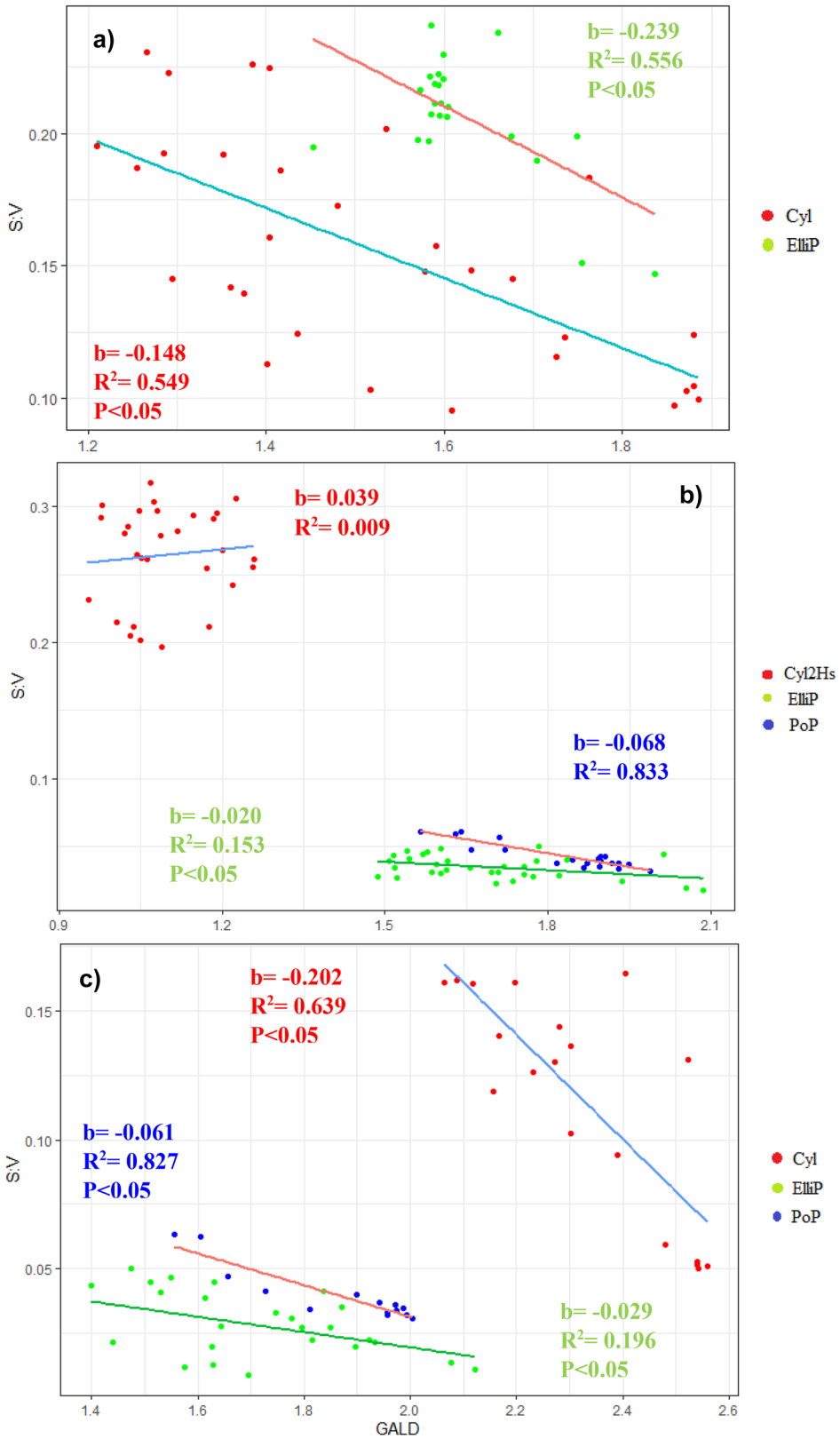
Between non-frontal (both NFW and NFE) and frontal, a total of 11 and 10 morphometric shapes were recorded in the former and later, respectively. Simple-shaped phytoplankton dominated (92–95%) both the frontal and non-frontal regions, whereas combined shape contributed only 5–8%. Among the simple shapes, Cyl-shaped phytoplankton dominated (28–41%) the non-frontal regions, whereas frontal regions were co-dominated by Elli (26%) and Cyl (21%) shape (Fig. 7). Interestingly, the species structure was different despite Cyl-shape was most dominant in both the frontal and non-frontal regions. In NFW, Cyl-shape was represented by *P. alata* and *Cerataulina* spp. and NFE was dominated only by *Cerataulina* spp. The Elli-shape was mostly represented by dinoflagellates (*Gyrodinium* spp. and *Scrippsiella* spp.) in the frontal regions. Maximum diversity among shapes in the frontal regions was observed with Cyl, Elli, and ElliP2CCyl, which were represented by 11 species each, whereas maximum species diversity among the non-frontal regions was observed with Cyl (7–10 species) and Elli (7–9 species) shapes. The diversity analysis reveals that NFE and NFW have a similar number of shapes and richness is relatively higher than in the frontal regions (Fig. 6f and d). NFE showed the maximum abundance followed by front and NFW. The cluster analysis showed that the non-frontal regions are similar to each other but dissimilar to the frontal regions but ANOVA does not show any significant dissimilarity ($p > 0.05$) (Supplementary Fig. 3).

Taxonomic and shape diversity comparison between NEAS-O and SEAS-O

The chain-forming centric diatoms (e.g., *P. alata* and *R. styliformis*; 62%) dominated the NEAS-O, whereas pennate diatoms (*Pseudonitzschia* spp.; 48%) dominated in the SEAS-O. The percentage contributions of diatom and dinoflagellates were different in the NEAS-O and SEAS-O where dinoflagellates contributed less (2%) in the former than the latter (23%). The dinoflagellate community was dominated by a single genus (*Protoperidinium* spp.) in NEAS-O, whereas *Gyrodinium* spp., *Protoperidinium* spp., and *Scrippsiella* spp. co-dominated the community in the SEAS-O. The abundance, species richness, evenness, and diversity were higher in the NEAS-O than in SEAS-O (Fig. 4a–e). The cluster analysis based on Bray–Curtis similarity shows that the NEAS-O and SEAS-O are significantly dissimilar (Supplementary Fig. 5). The shape richness was higher in NEAS-O (19 shapes) than in SEAS-O (12 shapes) (Fig. 4f–j). The most dominant shape was Cyl comprising 27 phytoplankton species (22 centric diatoms and 5 dinoflagellate species) and PoP comprising 3 pennate diatom species in NEAS-O and SEAS-O, respectively (Supplementary Fig. 6). The most species diverse shape Elli2CCyl comprised 36 and 16 dinoflagellate species in NEAS-O and SEAS-O, respectively. The univariate analysis revealed that the number of shapes, abundance, and shape richness was higher in NEAS-O compared to SEAS-O but shape evenness and diversity showed an opposite trend (Fig. 4f–j).

Discussion

This study recorded 164 species and represents most (accounting for up to 71%) of the geometric shapes (22 out of 31 described shapes of Sun and Liu (2003)) described for phytoplankton in literature (Supplementary Table 3). The remaining unrecorded 9 shapes are mostly represented by the freshwater


a)
b= -0.239
R²= 0.556
P<0.05
b= -0.148
R²= 0.549
P<0.05
S:V
Cyl
ElliP
b)
b= 0.039
R²= 0.009
b= -0.068
R²= 0.833
b= -0.020
R²= 0.153
P<0.05
Cyl2Hs
ElliP
PoP
c)
b= -0.202
R²= 0.639
P<0.05
b= -0.061
R²= 0.827
P<0.05
b= -0.029
R²= 0.196
P<0.05
GALD

◂**Fig. 8** Relationship between GALD and S:V for the 8 dominant shapes recorded in north-eastern (open and coastal) and south-eastern Arabian Sea during the study period. **a** NEAS-O, north-eastern Arabian Sea open-ocean; **b** NEAS-C, north-eastern Arabian Sea coastal waters; and **c** SEAS-O, south-eastern Arabian Sea open ocean; Cyl, cylinder; ElliP, elliptic prism; Cyl2Hs, cylinder + 2 half sphere; PoP, prism on parallelogram

species or the phytobenthos in the sunlit zone or belong to groups (e.g., flagellates, Euglenophyceae, Chlorophyceae) that were not recorded due to known technical limitations (e.g., preservatives) through microscopy approach. Among them, the latter may be of significance as the present study is dealing with species from marine pelagic systems but not from freshwater or benthic habitat. The phytoplankton marker pigment data for the eastern Arabian Sea, including from the presented NEAS-O transect (Sarma et al., 2018) and available literature (Bemal et al., 2019; Chandrasekhararao et al., 2018; Roy et al., 2015), indicated the presence of groups such as non-thecate dinoflagellates (peridinin), Chrysophyceae (19′-butanoyloxyfucoxanthin), haptophytes (19′-hexanoyloxyfucoxanthin), cyanobacteria (zeaxanthin), *Prochlorococcus* (divinyl chlorophyll a and b), chlorophytes (chl b), and prasinophytes (prasinoxanthin). Since the present study is based on microscopic analysis, only the dominant groups (> 5 µm) like diatoms and thecate dinoflagellates are possible to consider but not the above-mentioned groups (except picophytoplankton) due to methodological limitations (Lugols-Iodine and Formalin; Williams et al., 2016). Also, picophytoplankton are not considered and *Trichodesmium* though preserved well with the fixative but was not found in this study. Considering methodological limitations in the microscopic method, the phytoplankton shape data are generally underestimated, and even then, they are successfully used and tested to understand the phytoplankton dynamics in both freshwater (mostly community-related) and marine systems (process-related) (e.g., Aubry et al., 2017; Stanca et al., 2013). Despite methodological limitations, this study also revealed that EAS harbors most of the described phytoplankton shapes and species showing dissimilar spatial distribution patterns concerning abundance, composition, and diversity. In this study, the variability in distribution patterns between bioregions having distinct hydrographic conditions is discussed in the subsequent sections.

Variability between coastal and open ocean ecosystems

The contrast in the oceanographic conditions is well reflected in both taxa and morphology for the NEAS-C and NEAS-O phytoplankton communities. The diatom dominance (also reported in previous studies, e.g., by Vijayan et al., 2021 and references therein) is represented by different species and morphotypes but NEAS-O harbored rich species and shape diversity compared to the NEAS-C. Such high variability in geometric shape is not a coincidence but a morphological adaptation to environmental conditions. Similar findings are also reported from the coastal waters of the Salento Peninsula (Italy) where the phytoplankton shapes were dependent on environmental conditions and strongly varied with the season (Stanca et al., 2013). The winter convective mixing and advection induced the availability of high nitrate and phosphate concentration (Bemal et al., 2018; Sarma et al., 2018) favored high species and shape variability in the NEAS. Furthermore, the Rhizosolenoid diatom devoid of nitrogen-fixing endosymbionts (*Richelia*) also signifies nitrate availability (Padmakumar et al., 2010a, b). Among the recorded phytoplankton morphotypes, species with Cyl and Cyl2Hs dominated the NEAS-O and co-dominated the NEAS-C, where the chain-forming (*Skeletonema* sp. and *Leptocylindrus* spp.) and non-chain forming (*Rhizosolenoid*) centric diatoms dominated in NEAS-C and NEAS-O, respectively, showing spatial variations. In NEAS-C, the Cyl2Hs-shape (solely represented by *Skeletonema*) contributed more than half (53%) of the shape diversity. However, its distribution was restricted only to the upper water column (<40 m) (Supplementary Fig. 6) suggesting that Cyl2Hs-shape is the best fit only in the shallow waters or might have had a very strong mechanism to remain afloat in the sunlit zone to exploit the available resources (Durante et al., 2019; Smayda & Boleyn, 1966). For instance, in *Skeletonema*, a high S:V ratio (0.8; Smayda & Boleyn, 1966) and large colony formation are the key features to reducing the sinking rate. In general, the sinking rate is lower in elongated shapes (like Cyl, Cyl2Hs) than in spherical shapes (Durante et al., 2019). Whereas in the open ocean, the presence of apical process in Cyl-shape, i.e., *Rhizosolenia* sp. (as also shown in *Rhizosolenia setiger* by Smayda & Boleyn, 1966) might have

helped in reducing the sinking rate. Another experimental study also demonstrates that the spine aid in reducing the sinking rate (Padisak et al., 2003). The dominant (48%) Cyl-shaped diatom in NEAS-O was found to be evenly distributed throughout the water column (Supplementary Fig. 6), making it a successful and best-adapted shape among all the 19 shapes reported. The success of Cyl-shaped phytoplankton can also be inferred by its morphometric traits and adaptive strategies like conserving optimum S:V and high S:V with low GALD, respectively. The regression analysis revealed that the Cyl-shape showed a negative correlation between GALD and S:V with a very low slope ($b=0.131$) value. This means a decrease in S:V of 0.131 μm^{-1} for each µm increase in GALD, pointing out that the dominant shape in the NEAS-O ecosystem was attenuated and has adapted the strategy to conserve the optimal S:V which changes very minimally as the GALD increases.

Variability in contrasting oceanographic settings

Our study finds that both the taxonomic and shape diversity of phytoplankton were higher in the productive non-oligotrophic NEAS-O compared to the non-productive oligotrophic SEAS-O. Cyl-shaped centric diatoms dominated and co-dominated in NEAS-O and SEAS-O, respectively. However, the species representing Cyl-shape are different but were mostly dominated by centric diatoms. In NEAS-O, Rhizosolenoid (like *P. alata* and *R. styliformis*) diatoms dominated, whereas in SEAS-O *Cerataulina* sp., *P. alata*, and *Thalassiosira* sp. co-dominated with elliptic prism-shaped (*Chaetoceros* spp.) diatoms. *Cerataulina* spp. representing the Cyl-shape is well known for its bloom formation in nutrient-depleted turbulent waters (Ault et al., 2000; Lauria et al., 1999). Such spatial variability in morphotype dominance can be attributable to the prevalence of different hydrographic conditions in NEAS-O (biochemical changes driven by winter convective mixing) and SEAS-O (oligotrophic conditions). The oligotrophic conditions in the SEAS-O have resulted in the low abundance and chain-forming small pennate diatoms, which are known to have advantages over large phytoplankton cells under nutrient-limited conditions making them dominant (Finkel, 2007; Grover, 1989). The oligotrophic condition of SEAS-O is also revealed by the increased percentage contribution of dinoflagellate species (23%) known to be better adapted in nutrient-limited conditions and use their flagella in exploiting a stratified water column. Among the 12 shapes, simple and attenuated shapes like Cyl (23%), PoP (19%), and ElliP (18%) dominated the phytoplankton communities. The less shape diversity reflects the prevailing environmental conditions (oligotrophic waters), which could not afford to support the variety of other shapes, and only the best-adapted shapes flourished. However, it is interesting to note that even if the NEAS-O and SEAS-O showed very different hydrographical conditions and diversity, the shape dominance remained the same: simple attenuated shapes like Cyl or ElliP dominated across this vast gradient. All the dominant shapes have adopted the strategy of conserving their optimum S:V by showing negative correlation and minimal variations as the linear dimension changes (Fig. 8). Moreover, the adaptive strategies opted by the dominant shapes (Cyl, ElliP, and PoP) in NEAS-O and SEAS-O varied. In the NEAS-O, the dominant shapes (Cyl, ElliP, and PoP) opted for high S:V with low GALD, but the dominant shapes in SEAS-O opted for the opposite. Such consistency in morphological traits composition compared to species composition is also reported in various studies (Naselli-Flores & Barone, 2007; Weithoff & Gaedke, 2017; Salmaso & Padisak, 2007), pointing out the importance of trait-based studies. Therefore, it can be said that the phytoplankton cell geometry or shape in the eastern Arabian Sea (NEAS-O and SEAS-O) showed a high level of redundancy. Redundancy, in this case, means that even if the taxonomic diversity was high, only a small number of shapes dominated. The trait-based studies allow the quantitative assessment of community or ecosystem resistance or resilience to changes through functional redundancy (Lavorel & Garnier, 2002; McGill et al., 2006) which in turn can increase the predictability of future ecosystem function projections than the species-centered taxonomic approaches (Levine, 2016; Martini et al., 2021). Furthermore, the eastern Arabian Sea (NEAS-O and SEAS-O) is well known for the occurrence of large-scale phytoplankton blooms (D'Silva et al., 2012), and the species causing blooms are generally characterized by simple shapes. For example, spherical-shape *Noctiluca* bloom (Gomes et al., 2008; Sarma et al., 2019) and Cyl-shape *Trichodesmium* (Padmakumar et al., 2010b; Prabhu et al., 1965; Ramanamurthy et al., 1972). Therefore,

it can be assumed that because of such bloom events, the shape diversity could be heavily influenced and skewed towards the bloom-forming dominant shape in the study area (NEAS-O and SEAS-O). Even considering such events, the eastern AS (NEAS-O and SEAS-O) is dominated by simple shape phytoplankton, particularly the Cyl-shape, suggesting it is the most adapted shape irrespective of the oceanographic regions and hydrographic conditions. The Cyl-shape has a wide morphological variability associated with wide taxonomic variability and is also considered a more attenuated shape capable of conserving optimum S:V ratio very efficiently, therefore, making it the best fit with the prevailing environmental conditions (Aubry et al., 2017).

Variability in frontal and non-frontal regions

The mesoscale features (fronts or filaments), which are used to generate potential fisheries zone (PFZ) advisories, are considered hotspots for phytoplankton bloom (Franks, 1992; Hesse et al., 1989) and its formation both in coastal (Sarma et al., 2018; Vipin et al., 2015) and open ocean (Amol, 2018; Roy et al., 2015) regions of EAS is well documented. The phytoplankton community studies on frontal regions of the EAS are mostly based on marker pigments (Bemal et al., 2019; Kurian et al., 2020; Roy et al., 2015). However, detailed taxa and morphometry-based studies of the phytoplankton community variability in coastal and open ocean frontal regions are lacking and an attempt is made to delineate frontal influence on the phytoplankton shape dominance in EAS.

The phytoplankton shapes in EAS showed significant morphometric variability between NEAS-C and SEAS-O frontal regions. The frontal regions in NEAS-C were dominated by Cyl2Hs (43–56% and are solely represented by *Skeletonema*) and its dominance can be explained by the background condition or pre-existing phytoplankton community theory (Sarma et al., 2018). This suggests that Cyl2Hs-shaped phytoplankton was best adapted to exploit the frontal hydrographic conditions. The morphometric adaptations like high S:V (0.8) associated with low GALD in Cyl2Hs might have a major role. The dominance of chain-forming diatoms in the coastal frontal regions is also reported in the South China Sea (Liu et al., 2021) and EAS (Sarma et al., 2018). However, the non-frontal (NF) regions were equally dominated by Cyl (*Leptocylindrus* being the dominant one), Cyl2Hs (23–22%, PoP (17%), and ElliP (15%) shapes. This suggests that the NF regions have a higher competition among the species for the limited resources where all the major shapes flourished similarly to their potential, whereas Cyl2Hs shape competes with others in frontal conditions. However, it should be noted that the phytoplankton response to the frontal conditions is subjected to the prevailing background conditions and community (Kurian et al., 2020; Sarma et al., 2018). The background phytoplankton community is dominated by chain-forming centric diatoms but the percentage contribution and abundance were relatively less. Also, the species composition (particularly diatoms) was slightly different in the non-front regions compared to the frontal regions. Such morphological shift towards a more attenuated shape (like long chain-forming *Skeletonema*) is a type of adaptation, which show minimal variations in the S:V ratio to maximize chloroplast exposition to light, i.e., opting for the most elongated shape by maintaining the shortest diameter (Naselli-Flores & Barone, 2011).

In contrast to NEAS-C fronts, the shape dominance in the oligotrophic SEAS-O front is different despite both T1 and T2 transects showing the least shape diversity (only 12 shapes) with the former transect cutting across the frontal waters but not in the latter, i.e., T2 transect without fronts (Bemal et al., 2019). SEAS is seldom enriched by Rossby wave-associated fronts bringing in changes in hydrographic conditions but is less favorable to phytoplankton growth compared to the NEAS (Supplementary Table 2). Nevertheless, this study points out the influence of Rossby fronts on phytoplankton shape dominance and biological productivity per se. The frontal stations in SEAS-O showed a slight increase in abundance and diversity compared to those of non-frontal stations located on the western side (NFW) but not those on the eastern side (NFE). The availability of relatively higher inorganic nitrogen in frontal (2.06 μM) and NFE (1.54 μM) than NFW (1.02 μM) could be the reason for the differences in phytoplankton abundance. In NFE, the increased abundance can also be due to the reminiscence of frontal signature (Amol, 2018; Bemal et al., 2019; Vipin et al., 2015) along the path as the sampled front was associated with a strong current that was drifting at 40–50 cm s^{-1} westward (Bemal et al., 2019). The Rossby waves were drifting westward towards the offshore, which means that the NFE

should have the reminiscence of the Rossby front, and NFW (yet to be influenced by the Rossby front) is the true non-frontal region which is also evident from the salinity profile of water mass as explained in Bemal et al. (2019) in details. The reminiscence effect of the westward propagating Rossby front is also well reflected in the morphological and species diversity of the associated phytoplankton community. The dominance of the Cyl (41%) shape in the NFE and also the existence of the Elli-shape (7% though in less abundance) set the necessary background for the phytoplankton community, which took advantage of the Rossby front and co-dominated the frontal region. The frontal regions of SEAS-O were co-dominated by Elli (26%) and Cyl (21%) shapes representing dinoflagellate and centric diatoms, respectively. Even though dinoflagellates are considered poor competitors for inorganic nutrients (Litchman & Klausmeier, 2008), they are generally predominant in low-nutrient waters as observed in this study. For instance, the ability of *Gyrodinium* spp., Elli-shaped mixotrophic dinoflagellate, to rapidly increase almost three times and respond to the abrupt resource enrichment associated with the Rossby front proves that Elli-shaped phytoplankton has the required adaptive strategies (flagella and mixotrophy) to flourish in the given environmental conditions.

Conclusion

This study concludes that the phytoplankton cell shape in the eastern Arabian Sea showed a high level of redundancy by choosing only a few dominant shapes associated with high taxonomic diversity. The integrated approach (taxonomy and morphology) adopted in the present study revealed higher taxonomic and shape diversity in the convective mixing influenced non-oligotrophic NEAS-O than adjoining NEAS-C and oligotrophic SEAS-O. Interestingly, the shape diversity and dominance (Cyl, ElliP, and PoP) remained the same between NEAS-O and SEAS-O, and among the fronts, the combined and simple shaped phytoplankton out-competed in NEAS-C and SEAS-O. The assessment of morphological properties based on S:V and its relationship with GALD suggested the prevalence of different adaptive strategies to cope with respective hydrographic conditions in the open ocean (NEAS-O and SEAS-O) and coastal (NEAS-C) by conserving S:V despite the increase in GALD in the former and no change in the later.

Acknowledgements The authors are grateful to the Director of CSIR-National Institute of Oceanography for his support and encouragement. The authors also acknowledge the participants from the NIO-ship cell, the captain, and crew members of the cruises for helping us onboard. The support of Dr. V.V.S.S Sarma, Dr. D. V. Desai, and Dr. M. S. Krishna is gratefully acknowledged. We thank the two anonymous reviewers for their valuable suggestions for improving the manuscript. The first author also acknowledges UGC for fellowship. This is an NIO contribution no. 7038.

Author contribution Pranoy Paul: sample collection, samples analysis, data analysis and interpretation, and manuscript writing. Jagadish S. Patil: original concept, sample collection, data interpretation, and manuscript elaboration. AC Anil: manuscript elaboration and also co-supervised all works.

Funding This work is supported by the CSIR-National Institute of Oceanography Ocean Finder project (PSC0105).

Availability of data and materials All data concerning the study are included in this manuscript and some are also provided as supplementary. However, it does not apply to material availability.

Declarations

Ethics approval All authors have read, understood, and have complied as applicable with the statement on "Ethical responsibilities of Authors" as found in the Instructions for Authors and are aware that with minor exceptions, no changes can be made to authorship once the paper is submitted.

Competing interests The authors declare no competing interests.

References

Alexander, H., Rouco, M., Haley, S. T., Wilson, S. T., Karl, D. M., & Dyhrman, S. T. (2015). Functional group-specific traits drive phytoplankton dynamics in the oligotrophic ocean. *Proceedings of the National Academy of Sciences, 112*(44), E5972–E5979.

Amol, P. (2018). Impact of Rossby waves on chlorophyll variability in the southeastern Arabian Sea. *Remote Sensing Letters, 9*(12), 1214–1223.

Aubry, B. F., Pugnetti, A., Roselli, L., Stanca, E., Acri, F., Finotto, S., & Basset, A. (2017). Phytoplankton morphological traits in a nutrient-enriched, turbulent Mediterranean microtidal lagoon. *Journal of Plankton Research, 39*(3), 564–576.

Ault, T., Velzeboer, R., & Zammit, R. (2000). Influence of nutrient availability on phytoplankton growth and community structure in the Port Adelaide River, Australia:

Bioassay assessment of potential nutrient limitation. *Hydrobiologia, 429*, 89–103.

Banse, K. (1987). Seasonality of phytoplankton chlorophyll in the central and northern Arabian Sea. *Deep-Sea Research, 34*(5–6), 713–723.

Barton, A. D., Pershing, A. J., Litchman, E., Record, N. R., Edwards, K. F., Finkel, Z. V., Kiørboe, T., & Ward, B. A. (2013). The biogeography of marine plankton traits. *Ecology Letters, 16*(4), 522–534.

Bemal, S., Anil, A. C., & Amol, P. (2019). Picophytoplankton variability: Influence of Rossby wave propagation in the southeastern Arabian Sea. *Journal of Marine Systems, 199*, 103–221.

Bemal, S., Anil, A. C., Shankar, D., Remya, R., & Roy, R. (2018). Picophytoplankton variability: Influence of winter convective mixing and advection in the northeastern Arabian Sea. *Journal of Marine Systems, 180*, 37–48.

Breton, E., Christaki, U., Bonato, S., Didry, M., & Artigas, L. F. (2017). Functional trait variation and nitrogen use efficiency in temperate coastal phytoplankton. *Marine Ecology Progress Series, 563*, 35–49.

Capblancq, J., & Catalan, J. (1994). Phytoplankton: Which, and how much? In R. Margalef (Ed.), *Limnology Now: A Paradigm of Planetary Problems* (pp. 9–36). Elsevier Science B.V.

Chandrasekhararao, A. V., Kurian, S., Vidya, P. J., Gauns, M., Shenoy, D. M., Mulla, A., Naik, H., Reddy, T. V., & Naqvi, S. W. A. (2018). Phytoplankton response to the contrasting physical regimes in the eastern Arabian Sea during northeast monsoon. *Journal of Marine Systems, 182*, 56–66.

Chisholm, S. W. (1992). Phytoplankton size. *Primary productivity and biogeochemical cycles in the sea*, Plenum Press, New York, G.P. Falkowski, A.D. Woodhead (Eds.) 213–237.

Chitari, R. R., & Anil, A. C. (2017). Estimation of diatom and dinoflagellate cell volumes from surface water of the Northern Indian Ocean. *Oceanologia, 59*, 389–395.

D'Silva, M. S., Anil, A. C., Naik, R. K., & D'Costa, P. M. (2012). Algal blooms: A perspective from the coasts of India. *Natural Hazards, 63*, 1225–1253.

Duarte, C. M., Agusti, S., & Canfield, D. E., Jr. (1990). Size plasticity of freshwater phytoplankton: Implications for community structure. *Limnology and Oceanography, 35*(8), 1846–1851.

Durante, G., Basset, A., Stanca, E., & Roselli, L. (2019). Allometric scaling and morphological variation in sinking rate of phytoplankton. *Journal of Phycology, 55*, 1386–1393.

Finkel, Z. V., Beardall, J., Flynn, K. J., Quigg, A., Rees, T. A. V., & Raven, J. A. (2010). Phytoplankton in a changing world: Cell size and elemental stoichiometry. *Journal of Plankton Research, 32*(1), 119–137.

Finkel, Z. V. (2007). Does phytoplankton cell size matter? The evolution of modern marine food webs. *Evolution of Primary Producers in the Sea, 1*, 333–350.

Fraisse, S., Bormans, M., & Lagadeuc, Y. (2013). Morpho-functional traits reflect differences in phytoplankton community between rivers of contrasting flow regime. *Aquatic Ecology, 47*(3), 315–327.

Franks, P. J. (1992). Phytoplankton blooms at fronts: Patterns, scales, and physical forcing mechanisms. *Reviews in Aquatic Sciences, 6*, 121–137.

Gomes, H. R., Goes, J. I., Matondkar, S. G. P., Parab, S. G., Al-Azri, A. R. N., & Thoppil, P. G. (2008). Blooms of *Noctiluca miliaris* in the Arabian Sea—An in situ and satellite study. *Deep-Sea Research-I, 55*, 751–765.

Grover, J. P. (1989). Influence of cell shape and size on algal competitive ability. *Journal of Phycology, 25*, 402–405.

Hesse, K. J., Liu, Z. L., & Schaumann, K. (1989). Phytoplankton and fronts in the German Bight. *Scientia Marina, 53*, 187–196.

Hillebrand, H., Durselen, C. D., Kirschtel, D., Pollingher, U., & Zohary, T. (1999). Biovolume calculation for pelagic and benthic microalgae. *Journal of Phycology, 35*, 403–424.

Kruk, C., Huszar, V. L., Peeters, E. T., Bonilla, S., Costa, L., Lürling, M., Reynolds, C. S., & Scheffer, M. (2010). A morphological classification capturing functional variation in phytoplankton. *Freshwater Biology, 55*(3), 614–627.

Kumar, P. S., Narvekar, J., Kumar, A., Shaji, C., Anand, P., Sabu, P., Rijomon, G., Josia, J., Jayaraj, K., & Radhika, A. (2004). Intrusion of the Bay of Bengal water into the Arabian Sea during winter monsoon and associated chemical and biological response. *Geophysical Research Letters, 31*, 15.

Kurian, S., Chndrasekhararao, A. V., Vidya, P. J., Shenoy, D. M., Gauns, M., Uskaikar, H., & Aparna, S. G. (2020). Role of oceanic fronts in enhancing phytoplankton biomass in the eastern Arabian Sea during an oligotrophic period. *Marine Environmental Research, 160*, 105023.

Lauria, M. L., Purdie, D. A., & Sharples, J. (1999). Contrasting phytoplankton distribution controlled by tidal turbulence in an estuary. *Journal of Marine Systems, 21*, 189–197.

Lavorel, S., & Garnier, E. (2002). Predicting changes in community composition and ecosystem functioning from plant traits: Revisiting the Holy Grail. *Functional Ecology, 16*, 545–556.

Levine, J. M. (2016). A trail map for trait-based studies. *Nature, 529*, 163–164.

Lewis, W. M. (1976). Surface/volume ratio: Implication for phytoplankton morphology. *Science, 192*, 885–887.

Litchman, E., & Klausmeier, C. A. (2008). Trait-based community ecology of phytoplankton. *The Annual Review of Ecology, Evolution, and Systematics, 39*, 615–639.

Litchman, E., de Tezanos Pinto, P., Edwards, K. F., Klausmeier, C. A., Kremer, C. T., & Thomas, M. K. (2015). Global biogeochemical impacts of phytoplankton: a trait based perspective. *Journal of Ecology*, *103*(6), 1384–1396.

Litchman, E., Klausmeier, C. A., Schofield, O. M., & Falkowski, P. G. (2007). The role of functional traits and trade-offs in structuring phytoplankton communities: Scaling from cellular to ecosystem level. *Ecology Letters, 10*(12), 1170–1181.

Liu, Z., Li, Q. P., Ge, Z., & Shuai, Y. (2021). Variability of plankton size distribution and controlling factors across a coastal frontal zone. *Progress in Oceanography, 197*, 102665.

Madhupratap, M., Kumar, S. P., Bhattathiri, P. M. A., Kumar, M. D., Raghukumar, S., Nair, K. K. C., & Ramaiah, N. (1996). Mechanism of the biological response to winter cooling in the northeastern Arabian Sea. *Nature, 384*(6609), 549–552.

Margalef, R. (1978). Life-forms of phytoplankton as survival alternatives in an unstable environment. *Oceanologica Acta, 1*, 493–509.

Martini, S., Larras, F., Boyé, A., Faure, E., Aberle, N., Archambault, P., Bacouillard, L., Beisner, B. E., Bittner, L., Castella, E., &

Danger, M. (2021). Functional trait-based approaches as a common framework for aquatic ecologists. *Limnology and Oceanography, 66*(3), 965–994.

McGill, B. J., Enquist, B. J., Weiher, E., & Westoby, M. (2006). Rebuilding community ecology from functional traits. *Trends in Ecology & Evolution, 21*, 178–185.

Naselli-Flores, L., Padisak, J., & Albay, M. (2007). Shape and size in phytoplankton ecology: Do they matter? *Hydrobiologia, 578*, 157–161.

Naselli-Flores, L., & Barone, R. (2011). Fight on plankton! or, phytoplankton shape and size as adaptive tools to get ahead in the struggle for life. *Cryptogamie, Algologie, 32*(2), 157–204.

Naselli-Flores, L. (2014). Morphological analysis of phytoplankton as a tool to assess ecological state of aquatic ecosystems: The case of Lake Arancio, Sicily. *Italy. Inland Waters, 4*(1), 15–26.

Naselli-Flores, L., & Barone, R. (2007). Pluriannual morphological variability of phytoplankton in a highly productive Mediterranean reservoir (Lake Arancio, Southwestern Sicily). *Hydrobiologia, 578*, 87–95.

Padisak, J., Soroczki-Pinter, E., & Rezner, Z. (2003). Sinking properties of some phytoplankton shapes and the relation of form resistance to morphological diversity of plankton – An experimental study. *Hydrobiologia, 500*, 243–257.

Padmakumar, K. B., Menon, N. R., & Sanjeevan, V. N. (2010a). Occurrence of endosymbiont *Richelia intracellularis* (Cyanophyta) within the diatom *Rhizosolenia hebetata*in Northern Arabian Sea. *International Journal of Biodiversity and Conservation, 2*(4), 70–74.

Padmakumar, K. B., Smitha, B. R., Thomas, L. C., Fanimol, C. L., SreeRenjimma, G., Menon, N. R., & Sanjeevan, V. N. (2010b). Blooms of *Trichodesmium erythraeum* in the South Eastern Arabian Sea during the onset of 2009 Summer Monsoon. *Ocean Science Journal, 45*(3), 151–157.

Paul, P., Patil, J. S., & Anil, A. C. (2021). Phytoplankton communities in marine intertidal rock-pools: Effect of location, geometric shapes and allelopathy. *Journal of Earth System Science, 130*(3), 1–17.

Prabhu, M. S., Ramamurthy, S., Kuthalingam, M. D. K., & Dhulkhed, M. H. (1965). On an unusual swarming of the planktonic blue-green algae *Trichodesmium* spp., off Mangalore. *Current Science*, 34(3), 95–95.

R core Team. (2020). R: A language and environment for statistical computing. R foundation for statistical computing, Vienna, Austria. https://www.R-project.org/

Ramanamurthy, V. D., Selvakumar, R. A., & Bhargava, R. M. S. (1972). Studies on the blooms of *Trichodesmium erythraeum* (Ehr.) in the waters of the central west coast of India. *Current Science, 41*, 803–804.

Reynolds, C. S. (1997). Vegetation processes in the pelagic: A model for ecosystem theory. Ecology Institute, Oldendorf Luhe, Germany, 371.

Roselli, L., & Basset, A. (2015). Decoding size distribution patterns in marine and transitional water phytoplankton: From community to species level. *PLoS ONE, 10*(5), e0127193.

Roy, R., Chitari, R., Kulkarni, V., Krishna, M. S., Sarma, V. V. S. S., & Anil, A. C. (2015). CHEMTAX-derived phytoplankton community structure associated with temperature fronts in the northeastern Arabian Sea. *Journal of Marine Systems, 144*, 81–91.

Ryabov, A., Kerimoglu, O., Litchman, E., Olenina, I., Roselli, L., Basset, A., Stanca, E., & Blasius, B. (2021). Shape matters: The relationship between cell geometry and diversity in phytoplankton. *Ecology Letters, 24*(4), 847–861.

Salmaso, N., & Padisak, J. (2007). Morpho-functional groups and phytoplankton development in two deep lakes (Lake Garda, Italy and Lake Stechlin, Germany). *Hydrobiologia, 578*, 97–112.

Sarma, V. V. S. S., Desai, D. V., Patil, J. S., Khandeparker, L., Aparna, S. G., Shankar, D., D'Souza, S., Dalabehera, H. B., Mukherjee, J., Sudharani, P., & Anil, A. C. (2018). Ecosystem response in temperature fronts in the northeastern Arabian Sea. *Progress in Oceanography, 165*, 317–331.

Sarma, V. V. S. S., Patil, J. S., Shankar, D., & Anil, A. C. (2019). Shallow convective mixing promotes massive *Noctiluca scintillans* bloom in the northeastern Arabian Sea. *Marine Pollution Bulletin, 138*, 428–436.

Sawant, S., & Madhupratap, M. (1996). Seasonality and composition of phytoplankton in the Arabian Sea. *Current Science, 71*, 11.

Schlitzer, R. (2015). Ocean Data View. http://odv.awi.de

Segura, A. M., Kruk, C., Calliari, D., & Fort, H. (2013). Use of a morphology-based functional approach to model phytoplankton community succession in a shallow subtropical lake. *Freshwater Biology, 58*(3), 504–512.

Shankar, D., Vinayachandran, P., & Unnikrishnan, A. (2002). The monsoon currents in the north Indian Ocean. *Progress in Oceanography, 52*, 63–120.

Shenoi, S., Shankar, D., & Shetye, S. (2002). Differences in heat budgets of the near-surface Arabian Sea and Bay of Bengal: Implications for the summer monsoon. *Journal of Geophysical Research: Oceans, 107*, 1–14.

Simberloff, D., & Dayan, T. (1991). The guild concept and the structure of ecological communities. *Annual Review of Ecology and Systematics, 22*, 115–143.

Smayda, T. J. (1970). The suspension and sinking of phytoplankton in the sea. *Oceanography Marine Biology Annual Revision, 8*, 353–414.

Smayda, T. J., & Boleyn, B. J. (1966). Experimental observations on the flotation of marine diatoms. II. *Skeletonema costatum* and *Rhizosolenia setigera*. *Limnology and Oceanography*, *11*(1), 18–34.

Stanca, E., Cellamare, M., & Basset, A. (2013). Geometric shape as a trait to study phytoplankton distributions in aquatic ecosystems. *Hydrobiologia, 701*(1), 99–116.

Sun, J., & Liu, D. (2003). Geometric models for calculating cell biovolume and surface area for phytoplankton. *Journal of Plankton Research, 25*(11), 1331–1346.

Taylor, F. J. R. (1973). General features of dinoflagellate material collected by the "Anton Bruun" during the International Indian Ocean Expedition. *The biology of the Indian Ocean* (pp. 155–169). Springer.

Thingstad, T. F., Krom, M. D., Mantoura, R. F. C., Flaten, G. F., Groom, S., Herut, B., Kress, N., Law, C. S., Pasternak, A., Pitta, P., & Psarra, S. (2005). Nature of phosphorus limitation in the ultraoligotrophic eastern Mediterranean. *Science, 309*(5737), 1068–1071.

Tomas, C. R. (Ed.). (1997). *Identifying marine phytoplankton*. Academic Press.

Vijayan, A. K., Reddy, B. B., Sudheesh, V., Marathe, P. H., Nampoothiri, V. N., Harikrishnachari, N. V., Kavya, P.,

Gupta, G. V. M., & Ramanamurthy, M. V. (2021). Phytoplankton community structure in a contrasting physico-chemical regime along the eastern Arabian Sea during the winter monsoon. *Journal of Marine Systems, 215*, 103501.

Vipin, P., Sarkar, K., Aparna, S. G., Shankar, D., Sarma, V. V. S. S., Gracias, D. G., Krishna, M. S., Srikanth, G., Mandal, R., Rama Rao, E. P., & Rao, S. N. (2015). Evolution and subsurface characteristics of a sea-surface temperature filament and front in the northeastern Arabian Sea during November–December 2012. *Journal of Marine Systems, 150*, 1–11.

Weithoff, G., & Gaedke, U. (2017). Mean functional traits of lake phytoplankton reflect seasonal and inter-annual changes in nutrients, climate and herbivory. *Journal of Plankton Research, 39*, 509–517.

Weithoff, G., & Beisner, B. E. (2019). Measures and approaches in trait-based phytoplankton community ecology–From freshwater to marine ecosystems. *Frontiers in Marine Science, 6*, 40.

Weller, R. A., Fischer, A. S., Rudnick, D. L., Eriksen, C. C., Dickey, T. D., Marra, J., Fox, C., & Leben, R. (2002). Moored observations of upper-ocean response to the monsoons in the Arabian Sea during 1994–1995. *Deep Sea Research Part II: Topical Studies in Oceanography, 49*(12), 2195–2230.

Wiggert, J. D., Hood, R. R., Banse, K., & Kindle, J. C. (2005). Monsoon-driven biogeochemical processes in the Arabian Sea. *Progress in Oceanography, 65*(2–4), 176–213.

Williams, O. J., Beckett, R. E., & Maxwell, D. L. (2016). Marine phytoplankton preservation with Lugol's: A comparison of solutions. *Journal of Applied Phycology, 28*(3), 1705–1712.

Publisher's Note Springer Nature remains neutral with regard to jurisdictional claims in published maps and institutional affiliations.

Springer Nature or its licensor (e.g. a society or other partner) holds exclusive rights to this article under a publishing agreement with the author(s) or other rightsholder(s); author self-archiving of the accepted manuscript version of this article is solely governed by the terms of such publishing agreement and applicable law.

J. Earth Syst. Sci. (2021)130 128
https://doi.org/10.1007/s12040-021-01591-5

© Indian Academy of Sciences



Phytoplankton communities in marine intertidal rock-pools: Effect of location, geometric shapes and allelopathy

P Paul[1,2], J S Patil[1,*] and A C Anil[1]

[1] *CSIR-National Institute of Oceanography, Dona Paula 403 004, Goa, India.*
[2] *School of Earth, Ocean and Atmospheric Sciences, Goa University, Taleigao Plateau 403 206, Goa, India.*
**Corresponding author. e-mail: patilj@nio.org*

MS received 15 August 2020; revised 15 January 2021; accepted 26 January 2021

Biologically rich rock-pools (RPs) are prominent component of rocky intertidal habitat and this study elucidates the factors affecting the phytoplankton distribution from high-tide (HT), mid-tide (MT) and low-tide (LT) RPs (Anjuna rocky shores, Goa, India), during the summer season. Results revealed that the RP location determines the nature of phytoplankton assemblage. MT-RPs and LT-RPs supported rich microalgal diversity (species number/morphological shapes) than HT-RPs. However, the cell abundance was higher in latter than former RPs. In frequently flushed MT-RPs and LT-RPs, pennate diatoms (*Pseudonitzschia*, *Nitzschia*, *Thalasionema*, *Navicula*, and *Licmophora*) representing elongated shapes dominated, whereas in stagnant HT-RPs spherical/combined shaped dinoflagellates (*Amphidinium carterae sensu stricto* and *Bysmatrum gregarium*) dominated. Interestingly, even though the taxonomic assemblages changed temporally the shape dominance remained consistent suggesting shape as a robust morphological trait. Additionally, the study also revealed the existence of species-specific allelopathy on other microalgae by *Amphidinium* (potential harmful algae) indicating a type of adaptive strategy, in addition to eurytolerant capabilities, for its predominance in HT-RPs, which experiences varying environmental (light, temperature, and salinity) conditions.

Keywords. Rock-pools; microalgae; taxonomy; morphological traits; *Amphidinium*; allelopathy.

1. Introduction

Rock-pools (RPs) are a prominent component of any rocky intertidal habitat and are extensively studied for their diverse invertebrate fauna. The microalgal community assemblage, dynamics, and structure on a temporal and spatial scale, various biotic (grazing and interactions with different rock pool inhabitants) and abiotic (nutrient, light, temperature, salinity, tidal influence, pool size, and dimensions) factors influencing the assemblages and succession (Huggett and Griffiths 1986; Metaxas and Scheibling 1993, 1994, 1996a, b; Underwood and Skilleter 1996; Norberg 1998; Therriault and Kolasa 2001; Martins *et al.* 2007; Anusa *et al.* 2012; Soininen and Meier 2014; Häggqvist and Lindholm 2015, 2016; Rishworth *et al.* 2017; DaSilva *et al.* 2020) of rock-pools have been extensively studied throughout the world in fresh, brackish and marine ecosystems but not in

This article is part of the topical collection: Advances in Coastal Research.
Published online: 24 June 2021

the Indian sub-continent. The small size with well-defined boundaries, rock-pools can serve as perfect mesocosms to study the phytoplankton community dynamics (Metaxas and Scheibling 1994, 1996a). Microalgae from the adjacent waters are introduced into the rock-pools because of the tidal action and remain isolated from the adjacent seawater depending on the tidal amplitude and location of the rock-pools on the shore (Metaxas and Scheibling 1994). The importance of the tidal cycle in deciding the biotic and abiotic components of the rock-pools is greatly acknowledged (Metaxas and Scheibling 1993). Even though the Indian coastline has a significant amount of rocky shores (600 km approx.) abundant with rock-pools, it has not received the attention for microalgal research. Rock-pools play a very important role in the intertidal ecosystem and can serve as a seed bank (Baig *et al.* 2006; Patil *et al.* 2017) or even can cause a bloom of toxic algae causing fish-kill (Murray *et al.* 2015). Since RP microalgae experience/tolerate various order of environmental variability (like temperature, salinity, light, and anthropogenic disturbances) in a very short temporal scale, they are referred to as eurythermal, euryhaline, and euryphotic (Patil *et al.* 2017). Therefore to cope with such extreme conditions RP microalgae constantly compete through various physiological, morphological, and biochemical adaptations, like change in morphology and shape, producing specific enzymes/pigments/compounds, different nutrient acquisition strategies (like mixotrophy) and vertical migration (Legrand *et al.* 2003). Among them, the prevalence of physiological adaptation (photoprotection and photoinhibition) in RP microalgae was reported in a separate study (Patil *et al.* 2017). However, the present study characterizes the phytoplankton community based on the species composition and the morphological traits from the RPs located at different tidal levels. Also, the role of the allelopathic effect of dominant microalgae on the selected planktonic and benthic microalgae was elucidated. To understand the functional role of a particular organism in a given ecosystem various functional traits are being used (Padisak *et al.* 2003; Litchman and Klausmeier 2008). Phytoplankton assemblages under variable environmental conditions can perhaps be shaped by size and form selection in natural environments (Morabito *et al.* 2007). A variety of geometric shapes of microalgae co-existing together in an ecosystem is a form of adaptive strategy responding to the fluctuating environment (Margalef 1978; Reynolds 2006; Naselli-Flores *et al.* 2007). The functional classification approach has already been applied to understand the rock-pool microalgal assemblage and proved to be useful (Häggqvist and Lindholm 2015). Shape being the simplest morphological attribute carries ecological information as the environmental forcing influences it significantly (Grover 1989; Sommer 1998; Padisak *et al.* 2003; Naselli-Flores *et al.* 2007; Karp-Boss and Boss 2016). Using microalgae shape cannot only make it easier to understand the rock-pool assemblage, but can help in predictive studies. Although geometric shapes (morphological traits) have also been used to decipher the ecological understanding in marine waters (Stanca *et al.* 2013), never been used before to understand the community dynamics, particularly in a rock-pool ecosystem.

Knowing the fact that the west coast of India is rich in rocky shores and a dearth of study concerning the microalgal community of rock-pools exist, this study explored: (1) how the tidal levels and variations affect the rock-pool microalgal assemblages? (2) whether the geometric shape serves as a morphological trait to understand the distribution of rock-pool microalgal community?. Further, the microscopic observation of unpreserved samples during the sampling period indicated blooms of *Amphidinium carterae sensu stricto* (a potential harmful dinoflagellate) and *Bysmatrum gregarium* (Patil *et al.* 2017). Literature search revealed that the toxicity and allelopathy of *Amphidinium carterae* are studied and reported around the world, but not all the strains are found to be toxic (Jeong *et al.* 2001; Baig *et al.* 2006; Mandal *et al.* 2011; Murray *et al.* 2015). In view of this, experiments were also performed to confirm whether the bloom formations of *Amphidinium carterae* in RPs have any toxic or allelopathic effect on the dominant microalgal groups in the adjacent waters.

2. Materials and methods

2.1 *Study location and sampling strategy*

The rocky shores of Anjuna, Goa (15°34′34.986″N; 73°44′23.895″E) which is rich in rock-pools (RPs) and located on the western coast of India facing the Arabian Sea was selected for this study (figure 1). The study location is very unique owing to its various sized rock pools with flourishing

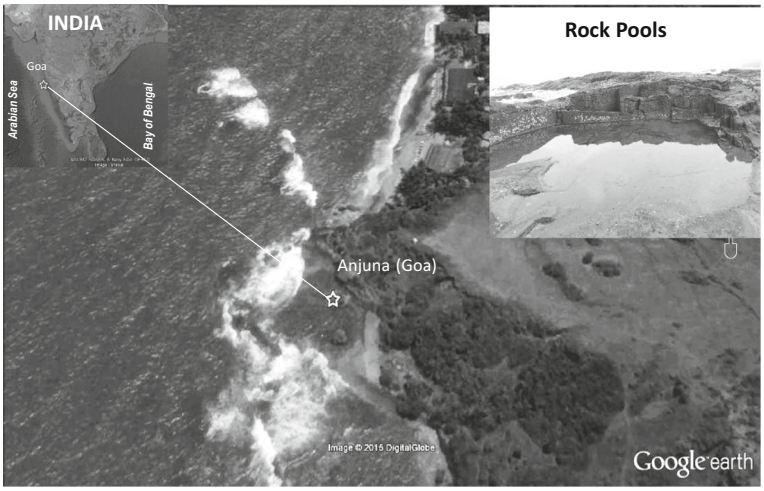


Figure 1. Location of the study site.

biodiversity, no intrusion or influence of freshwater source and relatively a tourist popular site makes it an ideal study area for rock pool research (Patil *et al.* 2017).

A total of nine RPs located at various tidal levels (three at each low tide (LT), mid-tide (MT), and high tide (HT)) were selected for water sampling. The sampling was carried out in the summer season of two different years (May 2014 and April 2015) during the LT every day for 15 days. The rationale for sampling during the summer season is as follows: (1) RPs experience maximum solar radiation resulting in increased water temperature, light penetration and salinity (due to evaporation), (2) Two summer seasons to confirm consistency in trends, (3) Feasibility for sampling keeping in mind the semi-diurnal nature of the tide in the region. The sampling days were designed in such a way so that the variation in both 'Flushed (F)' (when the RP water is replaced by the adjacent water with tidal action) and 'Non-flushed (NF)' (when the RP water is not replaced for several days particularly for HT-RPs) scenario can be apprehended. The first and last five days of the sampling where the tidal amplitude of the highest high tide was >1.8 all the RPs got flushed, whereas when the high tide amplitude was <1.8, only LT and MT-RPs got flushed except the HT-RP. The small quantity of undisturbed HT-RP water during the NF time was exposed to direct sunlight which made the environmental extremes inevitable. Environmental parameters (like temperature and salinity) were collected from the selected RPs of different tidal levels. During the sampling period, water temperature and salinity in HT-RPs ranged between 27–37°C and 28–49.5 PSU, respectively, whereas, water temperature and salinity in LT and MT-RPs ranged between 26–37°C and 35–38 PSU, respectively (Patil *et al.* 2017). The lowering of salinity during 2014 sampling was due to the occurrence of precipitation (up to 2.6 mm; MICD, NIO) during the latter half part of sampling. Even a small amount of precipitation is sufficient to lower salinity in RPs harbouring smaller volume of water. However, no precipitation occurred during 2015 sampling.

2.2 *Sample analysis*

A known volume (1 L) of the water samples collected from all the RPs were preserved with 4% Lugol's iodine at the site and then transported immediately (within 2 h) to the laboratory in dark condition for the analysis of microalgal composition and abundance (in triplicates) using an inverted microscope (IX-73 Olympus Make). The identification of microalgae was carried out manually based on the standard identification guides (Tomas 1997). Further, all the recorded species were assigned to their known geometric shapes as described in Hillebrand *et al.* (1999) and Sun and Liu (2003) to find out if shapes can be used as a functional trait. A total of 12 shapes were identified among which eight shapes were simple (Box (B), Cylinder (Cyl), Cymbelloid (Cym), Ellipsoid (Elli), Elliptic prism (ElliP), Gamphonemoid (Gam), Prism on parallelogram (PoP) and Prism on triangle (PoT)) and 4 were combined (Cylinder + 2 half spheres (Cyl2Hs), Ellipsoid + 2 cones + cylinder (Elli2CoCy), Prolate spheroid + 2 cylinders (Ps2Cy) and 2 cones (2C)).

2.3 *Experimental design to elucidate allelopathic effect of A. carterae on other microalgae*

The observation of unpreserved samples during the sampling period from the HT-RP waters under the microscope revealed a very high abundance of dinoflagellates, which prompted us to further isolate the microalgae and culture for detailed identification and experiments. The dinoflagellates were identified as *Amphidinium carterae sensu stricto* (potential harmful dinoflagellate) and *Bysmatrum gregarium*, formerly known as *B. caponii* (for identification details, refer Patil *et al.* 2017) and maintained in f/2 media (Guillard and Ryther 1962). The abundance data suggested their high number in HT-RPs whereas, other microalgae were less abundant and literature also advocated some of the *A. carterae* strain to be toxic (Murray *et al.* 2015). Given this, an experiment was designed to confirm the allelopathic effect of *A. carterae* on the various microalgae found in either the same HT-RP or adjacent waters. A diatom (*Skeletonema costatum*), green algae (*Dunaliella tertiolecta*), and a dinoflagellate (*Bysmatrum gregarium*) were selected as test organisms for the allelopathic effect of *A. carterae* cell-free filtrate. The culture of *A. carterae*, *S. costatum*, *D. tertiolecta* and *B. gregarium* were maintained at 27 ± 1°C under a light photocycle of 12:12 h light: dark in their exponential growth phase by weekly re-inoculation of fresh culture media.

2.4 *Amphidinium carterae culturing for cell-free filtrate and allelopathy evaluation*

In order to obtain large quantities of cell-free filtrate during stationary phase, *A. carterae* was cultured in four one litre sterile flasks containing 800 ml of f/2 media at 35 PSU salinity. The culture conditions are the same as mentioned above. The growth of *A. carterae* was monitored every day by cell counts (using haemocytometer and upright microscope (Olympus; 10× objective) until the culture reached its stationary phase so that it can be harvested to obtain a cell-free filtrate. The culture of *A. carterae* was harvested on 10th day to obtain cell-free filtrate and it was carried out by first passing through 10-µ mesh followed by filtering on 0.22-µ Millipore filter paper under very low pressure. The obtained cell-filtrate (designated as 100% strength) was then used for allelopathic experiments.

For the experiments, the different strength of cell free filtrate (100%, 75%, 50%, 25%, 10%) was evaluated for allelopathic effect against *S. costatum*, *D. tertiolecta* and *B. gregarium*. Additionally, all the cultures were grown in f/2 media and are treated as control (0%). The different strength of the cell-free filtrate was prepared using sterile 0.22 µ filtered seawater. The experiments were performed in triplicates in 150 ml polycarbonate bottles (Nalgene make) containing different strength cell-free filtrates enriched with f/2 media. A known number of the cell of *S. costatum* (1068 cells mL^{-1}), *D. tertiolecta* (2437 cells mL^{-1}) and *B. gregarium* (10 cells mL^{-1}) were inoculated in triplicates and incubated for 4 days at 27 ± 1°C under a light photocycle of 12:12 h light: dark. To evaluate the effect of allelopathy counting and morphological changes were observed every day for the period of 4 days. Counting was performed in the same way as mentioned above for *A. carterae* using haemocytometer and upright microscope (Olympus; 10× objective) and the abundance was expressed as cells/ml.

2.5 *Data analysis*

Univariate measures such as species count (S), Shannon–Wiener's index (H'), species richness (d), and evenness (J') were performed on log-transformed data for both species-wise and shape-wise data. Further, these data as well as abundance data (log-transformed data) were subjected to two-way analysis of variance (ANOVA) to evaluate the variation between the location of RPs as well as the periods of flushing and non-flushing. The clustering of RP microalgae was performed through the Bray–Curtis similarity and group average methods. For the analysis, long (x+1) transformed were used and the grouping was done at a 50% level to find the significant similarities with respect to shape-wise as well between the flushing/non-flushing period. For the allelopathy experiment, ANOVA followed by a post-hoc test was performed on the data which is normalized to day 0 values to find the significant differences among the treatments. Univariate measures calculation and clustering analysis were performed using statistical software PRIMER version 6 and ANOVA was performed using Statistica software (release 8).

3. Results

3.1 *Distribution of microalgae based on taxonomic nomenclature*

Altogether 79 microalgal species comprising 68 diatoms and 11 dinoflagellate species were recorded. However, the RP microalgal community exhibited distinct variations between (i) the years of sampling (i.e., 2014 and 2015), (ii) the location of the rock pools at different tidal level (LT, MT, and HT-RPs), and (iii) with the occurrence of tidal flushing in LT, MT, and HT-RPs with the adjacent water during sampling period (table 1; figure 2). More microalgal species number and abundance were recorded during 2015 compared to 2014 (table 1; figure 2) and probably the lower salinity due to the precipitation (pre-monsoon showers) could be the reason. Interestingly, during both the years, HT-RPs harboured high microalgal abundance compared to LT and MT-RPs. In contrast, univariate measures such as the number of species, diversity index, and the species richness revealed lower values for HT-RPs than MT and LT-RPs, and this trend was observed in both the years (figure 3). ANOVA for total abundance, number of species, species richness, and diversity revealed significant variations ($p < 0.001$) for inter-annual, location of pools, and periods of flushing and non-flushing. The microalgae composition of LT-RPs (74% and 61% in 2014 and 2015, respectively) and MT-RPs (50% and 64% in 2014 and 2015, respectively) were dominated by diatoms (of which pennate diatoms contribution was highest, i.e., 23–59% in both the years) followed by dinoflagellates (i.e., 26–36%) of which thecate dinoflagellates were the maximum contributors (9–65%). However, the composition was completely different in HT-RPs, wherein the community was dominated by dinoflagellates (83–96%) in both the years (figure 2). The pennate diatom community, in LT and MT-RPs, was mostly represented by *Pseudo-nitzschia* spp., *Nitzschia* spp., *Thalassionema* spp. and *Licmophora* sp., whereas the dinoflagellate community of HT-RPs was dominated by high abundance of *A. carterae* and *B. gregarium* (refer Patil *et al.* 2017 for details on identification).

It was further observed that in each pool, during both the years, the phytoplankton abundance and composition showed significant temporal variations (particularly during the flushing (F) and non-flushing (NF) periods and was mainly due to the variations in the intensity of the tidal flushing. The NF period recorded the least number of species in all the RPs compared to the F period in which 2014 showed the least compared to 2015 between both the years (figure 3). The species richness index shows higher species richness in F period in all the RPs than NF period in which LT-RPs show the highest value followed by MT and HT-RPs for both the years (figure 3). The Pielou's evenness (J′) index values revealed that the population in MT and LT-RPs are evenly distributed (J′ close to 1) compared to HT-RP's (negligible J′ value) and it was consistent during F and NF periods (figure 5c). The uneven distribution in HT-RPs was mainly due to the high abundance of *Bysmatrum* (during 2014) and *A. carterae* (during 2015) (table 1; figure 2). The cluster analysis at 50% Bray–Curtis similarity level using taxonomic data revealed two groups one is represented by LT and MT-RPs and the other by HT-RP (not shown).

3.2 *Microalgal composition and distribution based on geometric shape as trait*

The diversity indices for shapes show that the total number of shapes was more in 2015 (i.e., all the 12 shapes recorded) compared to 2014, wherein only nine shapes were recorded (figure 4). In 2014, LT-RPs were dominated by Gam (37–59%) shape followed by B (12–25%) and MT-RPs were dominated by Gam (up to 36%), Elli (up to 64%) and B (up to 47%) (figure 4). In both the RPs, 6–8 shape types were recorded during flushing (Fa and Fb) and non-flushing periods. In contrast, HT-RPs were dominated by Elli (99%) shape during both the F (six shape types in Fa and seven shape types in Fb) and NF (2 shape types) periods (figure 5). ANOVA revealed insignificant variations for shape diversity and richness for flushing and non-flushing periods. However, in the year 2015, LT-RPs were dominated by Ps2Cy (up to 26%), Gam (up to 17%), Elli (27–38%), and Gam (up to 18%), whereas MT-RPs were dominated by Ps2Cy (up to 40%), Cyl2Hs (up to 18%), Cyl2Hs (20%), Gam (20%), Elli (up to 33%) and 2C (up to 25%). Interestingly, similar to 2014, the HT-RPs were dominated by Elli (97%) during flushing and non-flushing periods. Similar to 2014, ANOVA revealed insignificant variations for shape diversity and richness for flushing and non-flushing periods. During 2015 sampling, the number of shapes

Table 1. *Phytoplankton abundance (cells L^{-1}) in low (LT), mid (MT) and high (HT) tide rock pools during non-flushing (NF) and flushing (Fa: before NF; and Fb: after NF) periods in summer month of both the years (2014 and 2015).*

	2014 (cells L^{-1})									2015 (cells L^{-1})								
	Fa			NF			Fb			Fa			NF			Fb		
Microalgae species	LT	MT	HT	LT	MT	HT	LT	MT	HT	LT	MT	HT	LT	MT	HT	LT	MT	HT
Pennate Diatoms																		
Achnanthes longipes	0	0	0	0	0	0	0	0	0	223	153	32	490	140	77	550	248	62
Amphiprora alata	0	0	0	0	0	0	0	0	0	10	15	0	0	0	0	0	15	0
Amphora sp.	0	0	0	0	0	0	1	1	0	7	18	0	0	10	27	7	10	5
Asterionellopsis sp.	5	0	0	0	0	0	0	0	0	0	0	0	0	0	0	0	0	0
Baccilaria sp.	0	0	0	0	0	0	0	0	0	23	35	52	0	0	0	0	0	0
Biddulphia sp.	0	0	0	0	0	0	0	0	0	7	0	0	3	0	0	0	3	0
Climacosphenia sp.	0	0	1	0	0	0	0	0	0	0	0	0	0	0	0	0	0	0
Cylindrotheca closterium	0	0	0	0	0	0	0	0	0	270	357	42	97	55	32	98	17	15
Cymbella sp.	0	0	0	0	0	0	0	0	0	0	0	0	12	8	0	0	15	5
Diatoma sp.	0	0	0	0	0	0	0	0	0	0	0	0	23	0	0	0	0	0
Diploneis sp.	1	0	0	0	1	0	0	0	2	27	27	0	17	13	5	10	0	3
Fragillariopsis sp.	0	0	0	0	0	0	0	0	0	13	0	0	42	25	417	62	13	103
Grammatophora marina	0	0	0	0	0	0	0	0	0	13	0	0	0	0	0	0	0	0
Gyrosigma sp.	0	0	0	0	0	0	0	0	0	0	3	0	25	0	0	0	5	0
Hantzschia sp.	0	0	0	0	0	0	0	0	0	0	0	0	0	0	0	5	0	0
Licmophora abbreviata	0	0	0	0	0	0	0	0	0	672	245	47	490	128	32	968	225	80
L. flabellata	0	0	0	0	0	0	0	0	0	8	0	0	0	0	0	168	50	48
L. gracilis	0	0	0	0	0	0	0	0	0	32	32	0	43	7	0	3	5	20
Licmophora sp.	8	3	0	5	1	0	11	0	0	0	32	0	0	0	0	0	0	0
Navicula sp1	5	2	4	1	2	3	4	4	14	0	0	0	0	0	0	0	0	0
Navicula sp2	1	0	1	1	3	0	0	0	11	45	0	127	20	5	3542	152	40	113
Navicula sp3	0	0	0	0	0	0	0	0	0	0	0	0	0	0	0	0	0	0
Navicula sp4	2	1	0	0	0	0	0	0	0	0	0	0	13	0	0	0	0	0
Navicula transitans f. delicatula	0	0	0	0	0	0	0	0	0	700	313	107	457	288	88	650	357	210
Nitzschia acicularis	0	0	0	0	0	0	0	0	0	85	40	3	18	0	18	18	3	0
N. longissima	0	0	0	0	0	0	0	1	0	0	77	7	37	10	7	8	35	8
N. sigma var intercedens	0	0	0	1	1	0	0	0	0	0	0	0	0	0	0	0	0	0
N. panduriformes	0	0	0	0	0	0	0	0	0	0	5	0	3	3	0	3	0	0
N. sigmoidea	0	1	0	0	1	0	0	0	0	0	0	0	0	0	27	0	0	15
Nitzschia sp.	0	2	0	2	0	0	0	5	0	0	27	38	0	0	0	0	0	0
Pinnularia sp.	0	0	0	0	0	0	0	0	0	103	47	82	178	42	195	163	150	25
P. virdis	0	0	0	0	0	0	0	0	0	0	0	3	0	0	0	0	0	0
Pleurosigma elongatum	0	0	0	0	0	0	0	0	0	0	0	0	0	0	0	0	0	0

Table 1. *(Continued.)*

	2014 (cells L^{-1})									2015 (cells L^{-1})								
	Fa			NF			Fb			Fa			NF			Fb		
Microalgae species	LT	MT	HT	LT	MT	HT	LT	MT	HT	LT	MT	HT	LT	MT	HT	LT	MT	HT
P. nomanii	1	2	1	0	1	0	1	1	0	45	15	7	0	3	0	25	12	7
Pleurosigma sp1	3	3	0	1	2	0	0	2	0	35	90	7	58	18	12	52	52	25
Pleurosigma sp2	0	0	0	0	0	0	0	0	0	0	0	0	12	0	0	0	0	0
Pseudonitzschia delicatissima	0	0	0	0	0	0	0	0	0	0	5	0	0	0	0	360	292	0
Pseudonitzschia sp.	0	0	0	0	0	0	6	1	3	7	22	20	12	0	22	142	115	95
P. striata	2	1	1	4	4	0	2	0	23	0	0	8	0	0	0	0	72	60
Striatella sp.	0	3	5	0	0	0	0	0	9	0	0	0	0	0	0	0	0	0
Surirella sp.	0	0	0	0	0	0	0	0	0	0	3	0	0	0	0	0	0	0
Synedra sp.	0	0	0	0	0	0	0	0	0	183	68	92	187	77	267	103	0	375
S. ulna	0	0	0	0	0	0	0	0	0	0	0	23	37	15	423	0	0	0
Tabellaria sp.	0	0	0	0	0	0	0	0	0	0	0	0	0	0	0	45	0	0
Thalassionema nitzschoides	10	3	0	8	9	0	7	2	0	173	128	5	165	27	268	260	148	58
Thalassiothrix sp.	1	2	2	2	1	0	0	0	14	0	12	17	0	0	97	27	13	43
Centric Diatoms																		
Asteriomphalus cleveanus	0	0	0	0	0	0	0	0	0	0	2	0	0	0	0	0	0	0
Campylodiscus sp.	0	0	0	0	0	0	0	0	0	0	0	0	0	0	0	0	0	950
Chaetoceros affinis	0	0	0	0	0	0	0	0	0	13	23	0	0	0	0	0	0	0
C. curviatus	0	0	0	0	0	0	0	0	0	30	0	0	0	0	0	0	0	0
C. debilis	0	0	0	0	0	0	0	0	0	12	67	0	0	0	0	2570	207	0
C. decipiens	0	0	0	0	0	0	0	0	0	0	22	0	0	0	0	68	32	0
C. lorenzianus	0	0	0	0	0	0	0	0	0	7	0	0	0	0	0	0	0	0
Cocconies sp.	0	0	0	0	0	0	0	0	0	0	0	0	7	0	0	13	13	0
Coscinodiscus sp.	0	0	0	1	1	0	0	0	0	17	10	0	3	13	0	8	8	0
Guinardia sp.	0	0	0	0	0	0	0	0	0	0	0	13	0	0	0	0	0	0
Hemidiscus sp.	0	0	0	0	0	0	0	1	0	0	0	0	0	0	0	2	0	0
Leptocylindrus danicus	0	0	0	0	0	0	1	0	0	45	0	0	23	0	0	0	0	0
Melosira moniliformis	1	0	0	0	0	0	2	0	0	310	67	0	67	0	0	70	0	20
Odontella senensis	0	0	0	0	0	0	0	0	0	3	0	0	0	0	0	0	0	0
Odontella sp.	0	0	0	0	0	0	0	0	0	0	0	0	0	0	0	10	0	0
Rhizosolenia hebeata	0	0	0	0	0	0	0	0	0	0	5	0	0	0	0	0	0	0
R. imbricata	0	0	0	0	0	0	1	0	0	0	0	0	0	0	0	0	0	0
R. setigera	0	0	0	0	0	0	0	0	0	183	620	100	0	0	0	12	17	0
R. setigera f. pungens	0	0	0	0	0	0	0	0	0	330	0	0	0	0	0	0	0	0
Skeletonema tropicum	0	0	0	0	0	0	0	0	0	150	157	67	15	0	0	190	70	57
Thalassiosira sp.	2	2	0	2	1	0	4	3	0	160	180	40	57	23	17	58	23	42
Triceratium sp.	0	0	0	0	0	0	0	0	0	3	8	0	0	0	0	15	3	0

Table 1. *(Continued.)*

Microalgae species	2014 (cells L^{-1})									2015 (cells L^{-1})								
	Fa			NF			Fb			Fa			NF			Fb		
	LT	MT	HT	LT	MT	HT	LT	MT	HT	LT	MT	HT	LT	MT	HT	LT	MT	HT
Dinoflagellates																		
Amphidinium cartarae	0	5	3928	0	0	419	0	0	3360	8	0	2142	0	0	10742	45	0	7
Dinophysis sp.	0	0	0	0	0	0	0	0	0	0	3	0	0	0	0	0	0	5
Prorocentrum gracile	0	0	0	0	0	0	0	0	0	28	0	0	73	3	0	48	18	3
P. micans	1	0	0	1	0	0	0	0	0	73	38	0	210	13	0	322	38	8
P. minimum	0	0	0	0	0	0	0	0	0	0	0	0	0	0	0	0	0	0
P. rostratum	0	0	0	0	0	0	1	0	0	0	0	0	0	0	0	0	0	0
Bysmatrum gregarium	4	5	177	19	4	1226	10	39	1559	813	613	37403	660	368	62578	3292	30	30090
Tripos furca	0	0	0	1	0	0	0	0	0	0	0	0	3	0	0	0	3	0
Gymnodinium sp.	0	0	0	0	0	0	0	0	0	28	17	8	32	278	0	158	15	743
Protoperidinium sp.	0	0	0	0	0	0	0	0	0	20	3	3	43	87	5	70	27	18
Scrippsiella sp.	0	0	0	0	0	0	0	0	0	287	22	658	167	120	827	402	38	485

recorded was relatively less in HT-RPs (9–10 shapes) compared to LT-RPs (11 shapes) and MT-RPs (12 shapes) (figure 5).

Thus, the shape diversity gradually decreased from LT-RPs to HT-RPs. The HT-RP was consistently dominated by Elli shape which is majorly represented by dinoflagellates (*A. carterae* and *B. gregarium*) in both the years (figure 5). The Gam shape was chiefly represented by *Licmophora* spp. in both the years. Shape PoP (representing *Nitzscia* spp., *Pseudonitzschia* spp. and *Pleurosigma* spp., i.e., mostly pennate diatoms) is the most diverse geometric shape comprising 10 species and 3 genera followed by EliP (9 species and 6 genera), Elli (7 species and 5 genera) and Cyl (5 species and 5 genera) in 2014. The most diverse shape in 2015 EliP (represented by a mixed group of pennate and centric diatoms) comprises of 23 species and 14 genera followed by PoP (14 species and 4 genera), Elli (11 species and 7 genera), Cyl (11 species and 8 genera) and B (9 species and 7 genera). Hence, the simple shapes dominated in terms of taxa richness in both years.

The shape-wise clustering of the RP microalgae population for the year 2014 at 50% Bray–Curtis similarity level revealed only one group showing Cyl, B, ElliP, and PoP to be significantly similar (figure 6). However, shape-wise clustering of RP microalgae for the year 2015 at 50% Bray–Curtis similarity level revealed five major groups in which group I (B and ElliP), group II (Gam and Ps2Cy), group III (2C and PoP), group IV (Cyl and Cyl2Hs) showed significant similarities, but group V (Elli) formed a single group in the cluster (figure 6). Similar to taxonomic data, the cluster analysis using shape data at 50% Bray–Curtis similarity level also revealed two groups wherein one is represented by LT and MT-RPs and the other by HT-RP figure 7).

3.3 *Effect of A. carterae cell-free filtrate on other microalgae*

The allelopathic effect of *A. carterae* cell-free filtrate was evaluated against the three microalgal cultures (i.e., *S. costatum, B. gregarium* and *D. tertiolecta*) and the results revealed that the allelopathy effect was species-specific. In the case of *S. costatum*, the maximum growth was observed in control (i.e., 0%) as compared to those grown in cell filtrates. Inhibition of *Skeletonema* growth increased with an increase in the strength of the

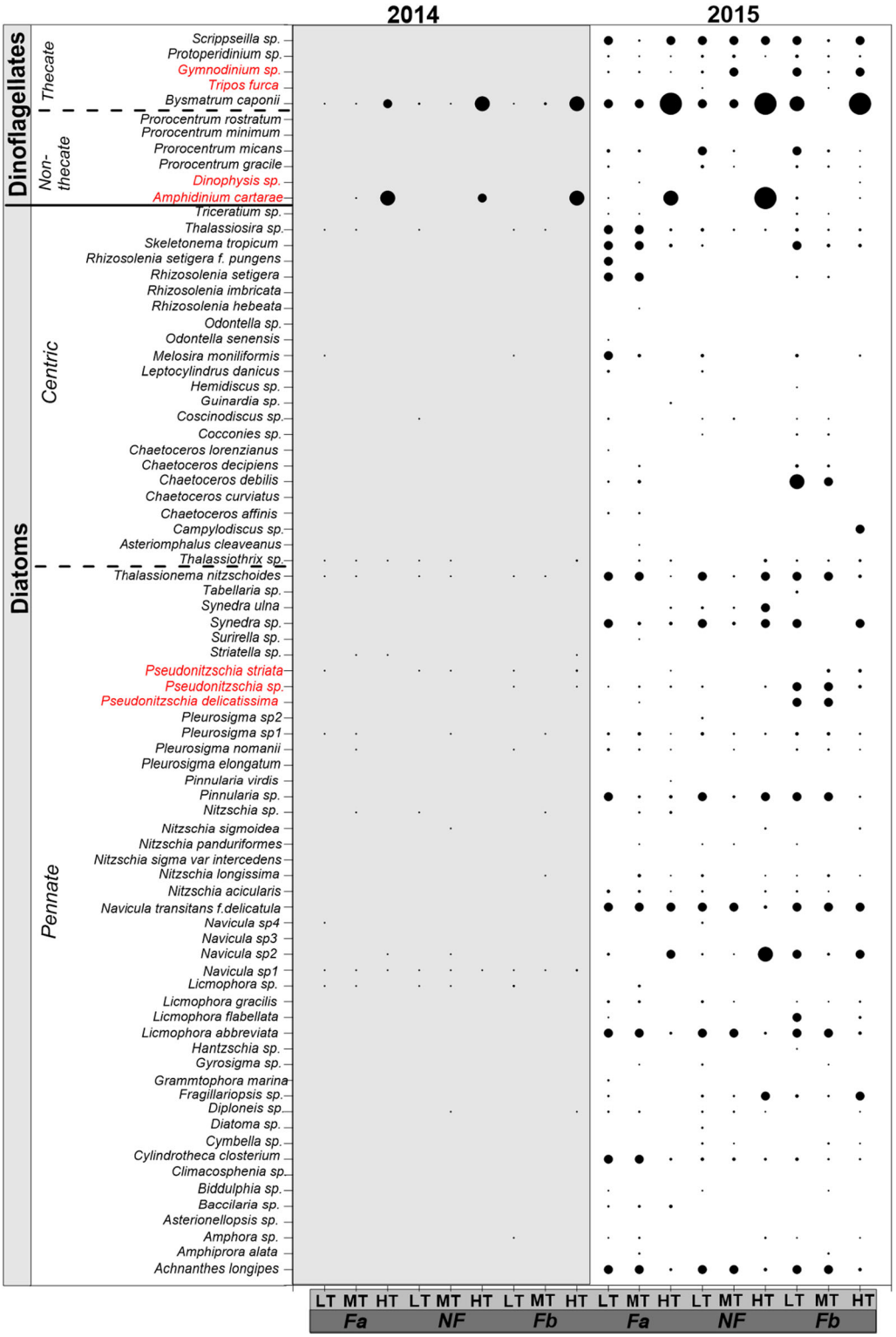


Figure 2. Bubble plot showing the temporal (2014 and 2015) and spatial (among low-tide (LT), mid-tide (MT), and high-tide (HT) rock pools) variation of the total rock pool phytoplankton abundance. The maximum symbol diameter corresponds to 70×10^3 cells L^{-1}. Fa: flushing during the first five days, NF: non-flushing, and Fb: flushing during the last five days of the 15 days sampling. Species highlighted in red are known to be toxic or harmful species.

cell-free filtrates (figure 8). Additionally, the morphological changes were also evident, for example the larger chains containing 16–17 cells were seen only in control, and those with reduced filtrate strength, the chain length was shorter containing 4–5 cells. Similar to *S. costatum*, growth inhibition

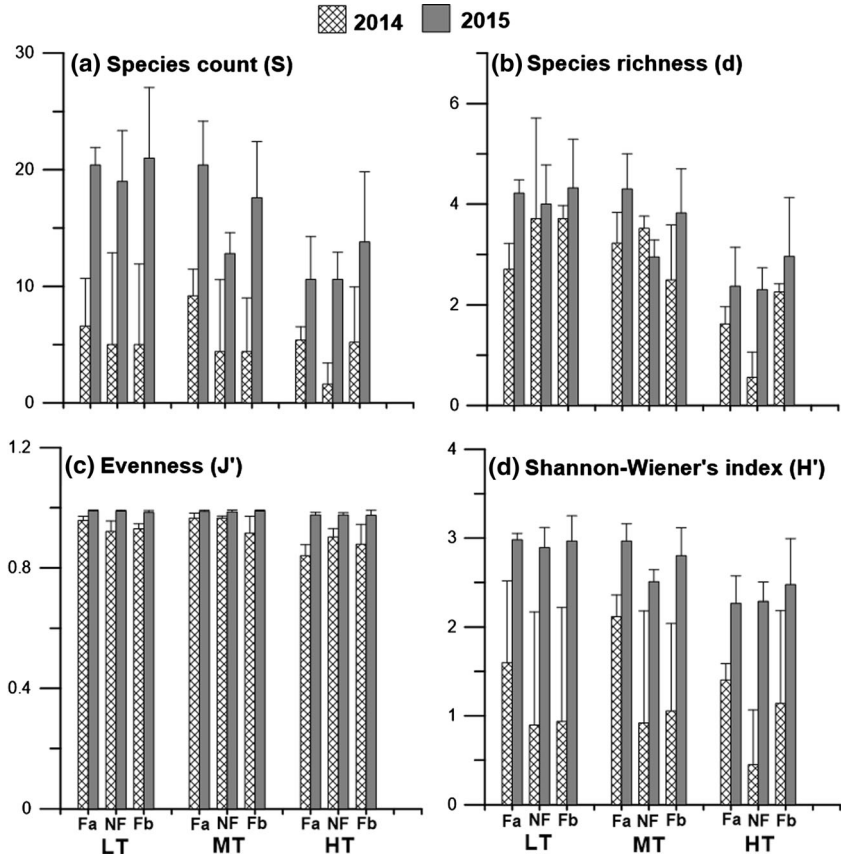


Figure 3. Taxonomy-wise diversity indices of RP microalgae. S: species count, d: species richness, J′: evenness, H′: Shannon–Weiner's index, Fa and Fb: flushing period, NF: non-flushing period, LT: low-tide, MT: mid-tide and HT: high-tide.

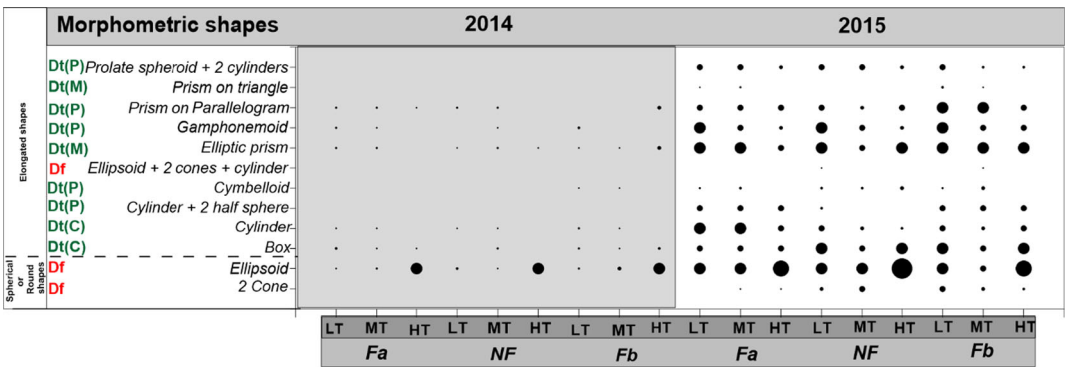


Figure 4. Bubble plot showing the temporal (2014 and 2015) and spatial (among low-tide (LT), mid-tide (MT), and high-tide (HT) rock pools) variation of the total rock pool phytoplankton abundance based on shapes. The maximum symbol diameter corresponds up to 80×10^3 cells L^{-1}. Fa: flushing during the first five days, NF: non-flushing, and Fb: flushing during the last five days of the 15 days sampling. Df: dinoflagellates; Dt(P): pennate diatoms; Dt(C): centric diatoms; Dt(M): both pennate and centric diatoms. Metaxas A and Lewis A G 1992 Diatom communities in tidepools: The effect of Intertidal height.

(up to 76%) in *B. gregarium* was also observed at higher concentrations (100% and 75%) of cell-free filtrate compared to control (figure 8). The number of cells in 100% filtrate strength was 6.5 cells/ml, whereas, in control, density was 26 cells/ml, on the 4th day. This suggests that, despite the slow growth of *B. gregarium*, the growth in the control was four times more than that observed in 100% filtrate concentration. Moreover, *B. gregarium* cells also showed some distinct morphological changes at higher concentrations (100%, 75%, and 50%) wherein the cells formed a dormant structure and remained non-motile but in control, the cell morphology and motility remained intact. ANOVA

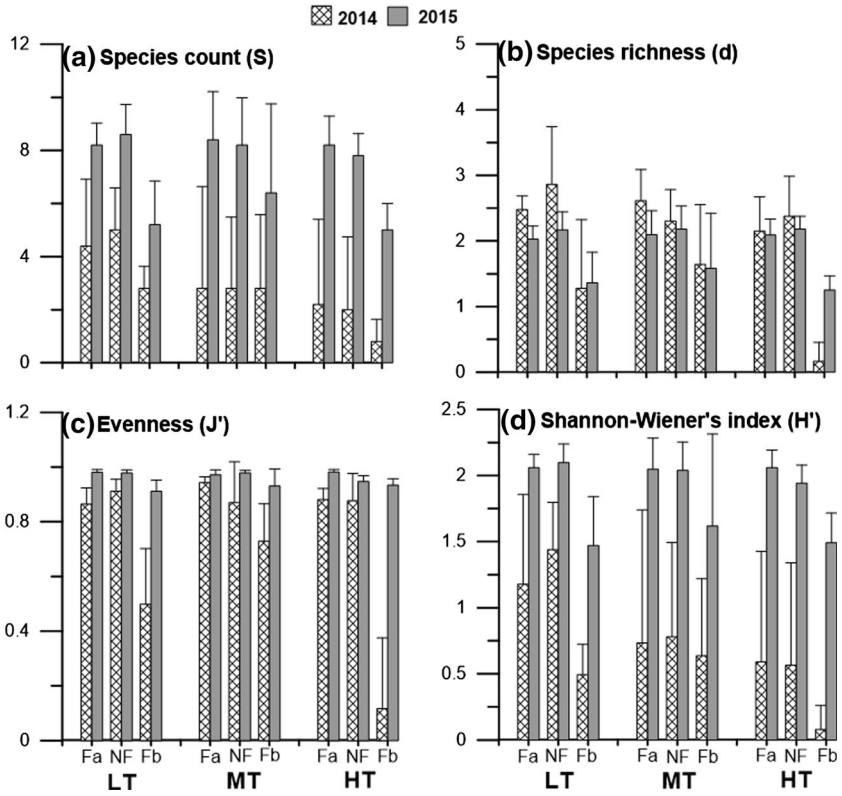


Figure 5. Diversity indices of RP microalgae based on shapes. S: species count, d: species richness, J′: evenness, H′: Shannon–Weiner's index, Fa and Fb: flushing period, NF: non-flushing period, LT: low-tide, MT: mid-tide and HT: high-tide.

revealed that, in the case of *S. costatum* and *B. gregarium*, significant inhibition with respect to filtrate strength ($p < 0.01$) and the highest was observed at 100% followed by 75% filtrate strength. Unlike *S. costatum* and *B. gregarium*, *D. tertiolecta* showed no growth inhibition or morphological changes even at the highest concentration. ANOVA also revealed an insignificant variation between the cell filtrate strength and control. Surprisingly the maximum growth was observed in 100% cell-free filtrate and the growth in 100% cell-free filtrate was ∼30% more compared to control on the 4th day suggesting a stimulatory effect (figure 8).

4. Discussion

4.1 *Influence of rock-pool location on the microalgal community based on taxonomic nomenclature*

The rock-pool microalgal community fluctuated greatly among the tidal locations and with the tidal flushing and non-flushing. Microalgae are introduced in the rock-pools by the tidal action from the adjacent seawater and the assemblages change consequently depending on the period of non-flushing of the pools. Tidal flushing based on the location of the rock-pools is one of the significant factors (Underwood and Skilleter 1996) in shaping and controlling the microalgal community on a very short temporal scale (Metaxas and Scheibling 1994). However, several factors do influence assemblage during such short timescale (Metaxas and Scheibling 1994). Tidal flushing not only brings the organisms from the adjacent sea but also adds fresh nutrients to the LT and MT-RPs which support rich phytoplankton assemblage compared to the HT-RPs (Soininen and Meier 2014). In our study, during both the years, diatoms with higher species diversity were dominant in the LT and MT-RPs and dinoflagellates, with lesser species diversity, in the HT-RPs (table 1; figure 2). The diatom dominance in LT and MT-RPs has also been reported in other studied RPs (Anusa *et al.* 2012; Soininen and Meier 2014; Rishworth *et al.* 2017). Among the diatoms, pennate species dominated LT and MT-RPs and they were mostly represented by elongated, chain-forming or branching types such as *Licmophora* spp., *Pseudonitzschia* spp., *Synedra* spp., *Navicula* spp., *Thalassionema* spp. and *Thalassiothix* spp. Since LT and MT-RPs are the most

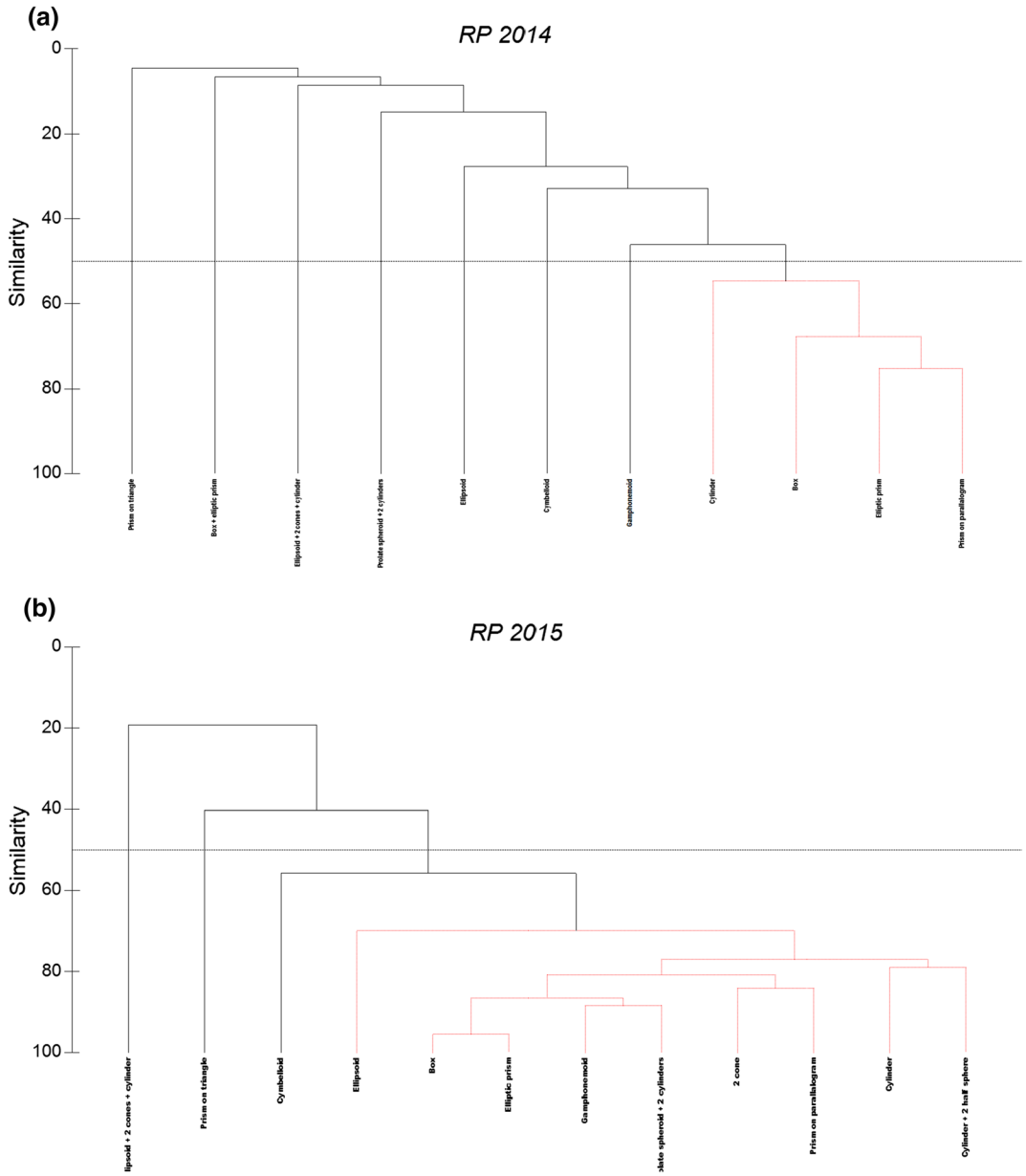


Figure 6. Cluster dendrogram based on geometric shapes for the year 2014 **(a)** and 2015 **(b)** using the Bray–Curtis similarity coefficient and group average method: grouping done at 50% similarity (data is log transformed; LT: low-tide, MT: mid-tide, HT: high-tide, Fa and Fb: flushing period and NF: non-flushing period).

turbulent and frequently flushed pools, the dominance of pennate forms (Padisak *et al.* 2003) with benthic lineage are not unusual (Metaxas and Lewis 1992; Metaxas and Scheibling 1996a, b). Whereas, the dominance of dinoflagellates in HT-RPs was mainly due to the blooms of *A. carterae* and *B. gregarium* (Patil *et al.* 2017). The HT-RPs selected in this study are relatively smaller compared to the LT and MT-RPs and therefore will experience higher environmental stress (temperature up to 40°C and salinity up to 67 PSU) and less frequent tidal flushing which in turn will influence the microalgal assemblage in the HT-RPs (Patil *et al.* 2017). The dinoflagellates *A. carterae* and *B. gregarium* (both are newly reported from Indian waters) are typically HT-RPs inhabitants even though present in the LT and MT-RPs in fewer numbers, which were found to be euryhaline, eurythermal and euryphotic (Patil *et al.* 2017). The photoprotection mechanism of these HT-RP dinoflagellates detailed in Patil *et al.* (2017) points out their adaptive capabilities to a varying light regime. The dinoflagellate blooms exhibited typical characteristics of S-strategists, i.e., species utilizing nutrients efficiently under resource-limited conditions (Reynolds 2006) and was the case in HT-RPs

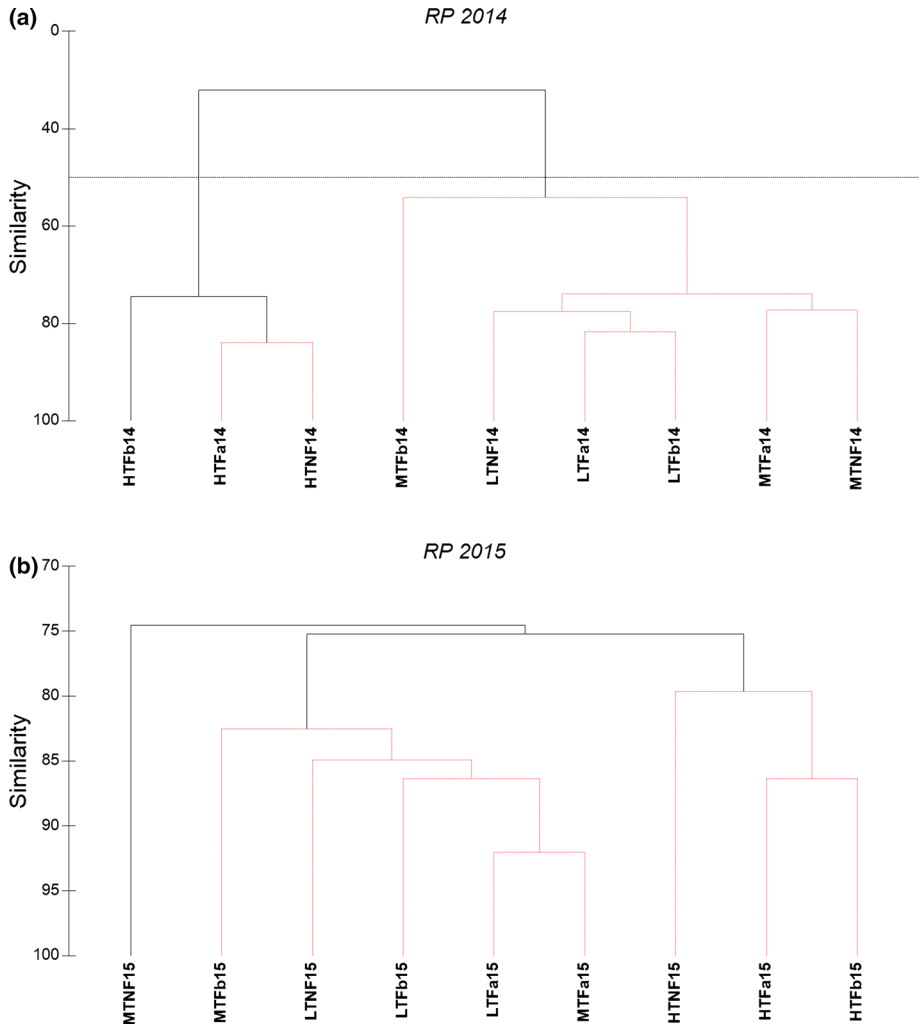


Figure 7. Cluster dendrogram based on geometric shapes with respect to flushing (Fa and Fb) and non-flushing (NF) period for the year **(a)** 2014 and **(b)** 2015 using the Bray–Curtis similarity co-efficient and group average method: grouping done at 50% similarity (data is log transformed; LT: low-tide, MT: mid-tide, HT: high-tide, Fa and Fb: flushing period and NF: non-flushing period).

due to non-flushing for considerable time. These findings are also consistent with Margalef's proposal (1978) which states that centric and pennate diatoms should dominate in high turbulence and flagellates should dominate under low turbulence conditions (Kiorboe 1993).

4.2 *Influence of rock-pool location on the microalgal community based on geometric shapes*

The present study is the first attempt to use the geometric shape as a trait to determine phytoplankton dynamics in the rock-pool ecosystem. Our results show that the RPs of the rocky shores of Anjuna, Goa are characterized by high morphological diversity in terms of shape. The LT and MT-RPs are relatively more diverse in terms of shape compared to HT-RPs (figures 4 and 5). All the recorded microalgae taxa were classified into 12 geometric shapes (Hillebrand *et al.* 1999; Sun and Liu 2003) and the morphological differences have a functional meaning which is well reflected in phytoplankton adaptive strategies (Lewis 1976; Margalef 1978; Naselli-Flores *et al.* 2007). Even though there is no specific literature suggesting a particular shape to be either spherical or elongated, many of the pre-defined shapes have been categorized based on the various published literature (Stanca *et al.* 2013; Karp-Boss and Boss 2016) to fall in either of the following categories spherical/round and elongated shape. Therefore, in the present study, it is assumed that shapes like 2-cones and ellipsoid can be classified as spherical or near-spherical shapes, whereas the rest of the shapes as elongated shapes. Any deviation from a perfect

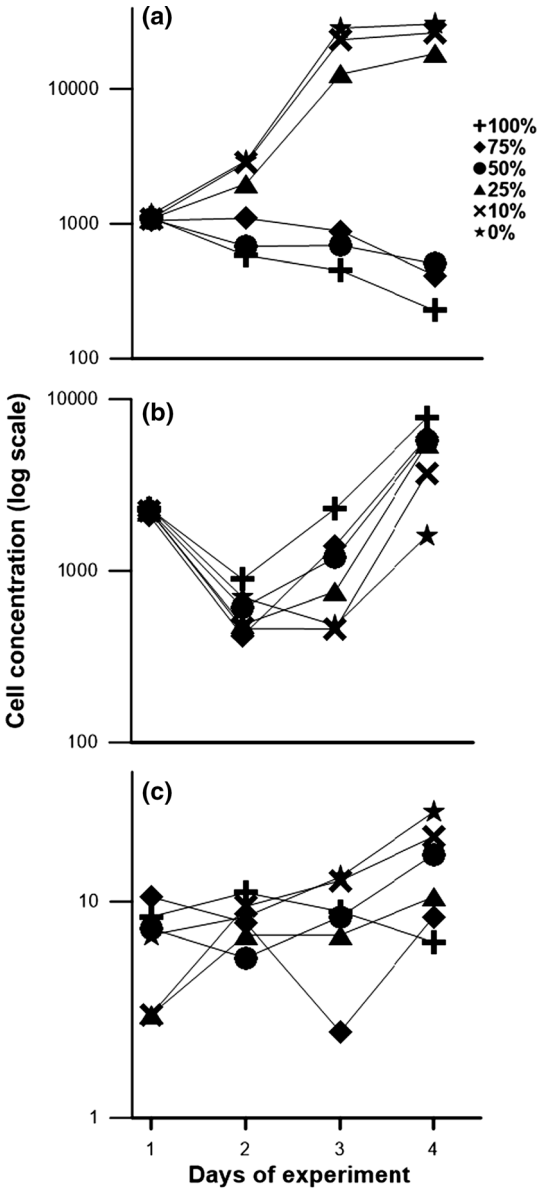


Figure 8. Effect of *A. carterae* cell-free filtrate on the growth of (**a**) *Skeletonema costatum,* (**b**) *Dunaliella tertiolecta,* and (**c**) *Bysmatrum gregarium* in different filtrate concentrations.

sphere is considered as an advantage for resource acquisition. The sphere represents the smallest boundary area occupying a given space, therefore, distortion from the spherical shape can increase the area of the surface which might represent a competitive adaptation to conserve an optimum surface to volume ratio, i.e., S:V (Lewis 1976; Reynolds 2006; Karp-Boss and Boss 2016). For instance, distortion of spherical shape diatoms to achieve an optimum S:V can allow them to sink more slowly than spheres of equivalent size and can also help to out-compete smaller ones for resource acquisition (Grover 1989; Padisak *et al.* 2003). It has also been reported that shapes such as elongated and round or combined shapes are prevalent in flushed and stagnant nutrient-limited RPs, respectively (Sommer 1998; Morabito *et al.* 2007) and is also evident in this study. For instance, the dominance of elongated and non-spherical shapes like Gam, PoP, and B in the frequently flushed LT and MT-RPs proves the success of these shapes in exploiting the abrupt nutrient input as well as surviving the frequent turbulence caused by tidal action (Naselli-Flores *et al.* 2007; Naselli-Flores and Barone 2007). In HT-RPs, dominance of Elli shape suggests the prevalence of a more stable, stratified, and nutrient-deprived water. This means that under such conditions, the elongated shapes will be replaced with round or combined shapes mostly represented by flagellates (dinoflagellate *A. carterae* and *B. gregarium* in this study), which competes poorly for inorganic nutrients (Litchman and Klausmeier 2008; Stanca *et al.* 2013). Another interesting finding of this study is that even though the taxonomic assemblage changed temporally (from 2014 to 2015), the shape dominance remained more or less consistent, i.e., ElliP and PoP were the most taxa-rich shapes, indicating the importance of shape as a robust morphological trait in microalgal studies enabling easy, less complicated non-taxonomic approach for better understanding of community dynamics. This also suggests that these particular morphological traits are selected by environmental pressure and must have some selective advantages compared to other shapes such as spherical shapes (Karp-Boss and Boss 2016). Periodic measurements of morphological trait succession can provide information on the health of the ecosystem (e.g., underwater light climate; Naselli-Flores and Barone 2007), essential functional processes (e.g., community assemblage; Salmaso and Padisak 2007), ecological characteristics of phytoplankton organisms (Naselli-Flores *et al.* 2007) and act as a useful monitoring tool without any mind-boggling taxonomic skills (Stanca *et al.* 2013).

4.3 *Allelopathy of bloom forming rock-pool dinoflagellate Amphidinium against other microalgae*

Various *Amphidinium* strains have shown toxic effects on other microalgae, nauplii larvae, and even fish (Baig *et al.* 2006; Murray *et al.* 2015) and the production of toxin is also considered as a type of physiological trait to deter predators (Litchman

and Klausmeier 2008). Literature revealed that the toxicity and allelopathy of *A. carterae* are studied and reported around the world (Jeong *et al.* 2001; Baig *et al.* 2006; Mandal *et al.* 2011; Murray *et al.* 2015). It has also been reported that *A. carterae*, which released substances or allelochemicals into the culture medium or environment inhibited or altered the growth of the co-cultured or co-existing microalgae (Xiaoqing *et al.* 2012). Further, the prevalence of high level of cryptic diversity within the *Amphidinium sensu stricto* (Murray *et al.* 2012) and variability in toxicity in some of them (Baig *et al.* 2006) is also well documented. Given this, the present study was conducted to confirm whether blooming of *A. carterae* (local strain) resulted suppression in the growth of other microalgae present in the HT-RPs by producing some sort of antagonistic allelopathic chemical. This is the first attempt to find out the allelopathic effect of cell-free filtrate of local strain *A. carterae* on various commonly occurring phytoplankton species in RPs and the adjacent waters. This study confirms that the cell-free filtrate of *A. carterae* does produce some allelochemicals, which have species-specific effect. The species specificity of the toxic effect of allelochemical is reported in a few studies elsewhere (Baig *et al.* 2006; Poulson *et al.* 2010). The maximum inhibition of growth by cell-free filtrate of *A. carterae* was noticed in *Skeletonema* cells followed by *Bysmatrum* (figure 8). However, results showed a stimulatory effect of cell-free filtrate of *A. carterae* on the green algae *Dunaliella* (figure 8). The stimulatory effect of allelochemical from other algae and cyanobacteria are also reported (Rice 1984; Suikkanen *et al.* 2005; Poulson *et al.* 2010). The allelopathy is often used as a tool to get an upper hand to compete for limited resources and also helps in the bloom formation of the organism (Granéli and Hansen 2006; Pavaux *et al.* 2020). Hence, it is assumed that the *A. carterae* might have used allelopathy as a physiological trait to suppress competitors in the HT-RPs, in addition to its eurytolerant adaptive capability against extreme temperature, salinity, and light (Patil *et al.* 2017). Such strategy might have enabled to compete against the limited resources to form blooms as evident from the composition data. These findings suggest that such a physiological trait (allelopathy) can also be related to 'competitor's suppression' in addition to 'predator's avoidance' as proposed by Litchman and Klausmeier (2008). It was also observed that *Skeletomena* being the most sensitive to the allelochemical followed by *Bysmatrum*. However, the inhibition in growth was observed only at higher strength of *A. carterae* filtrate suggesting that the tidal action (through dilution) could play a great role in the effectiveness of allelopathy as a competitive strategy in HT-RPs.

The morphological changes observed in *Bysmatrum* like temporary cyst-like structures induced by the cell-free filtrate of *A. carterae* might explain the coping mechanism of *Bysmatrum gregarium* which also co-existed with *A. carterae* in the HT-RPs. Temporary cyst formation which is used as a defense mechanism to resist allelochemicals is also reported in *Scrippsiella* (which is almost identical to *Bysmatrum*; Jeong *et al.* 2012) as well (Fistarol *et al.* 2004). A separate study also showed a weaker allelopathy effect by *A. carterae* filtrate on *Amphora coffeaeformis*, a biraphid benthic pennate, and biofilm-forming diatom (Patil and Jaskreet unpublished data). Nevertheless, the present study indicated that *Amphidinium* blooms in rock-pools will have a varying effect on planktonic and biofilm microalgae. However, further studies with mixed microalgal assemblage and the faunal component will lead to a better understanding of the impact on the microalgal community. Since *Amphidinium* experiences extreme environment in the rock-pools (Patil *et al.* 2017) elucidating the role of environmental parameters (e.g., temperature and salinity) on the allelochemical production and their effects need further attention.

5. Conclusion

This study highlight that the location of RPs determines the nature of phytoplankton assemblage. Less microalgal diversity (including shapes) and number of species were recorded in HT-RPs than MT and LT RPs. In frequently flushed RPs (MT and LT), pennate diatoms (*Pseudonitzschia*, *Nitzschia*, *Thalasionema*, *Navicula,* and *Licmophora*) representing elongated types dominated, whereas in stagnant HT-RPs spherical/combined shaped dinoflagellates (*Amphidinium sensu stricto* and *Bysmatrum gregarium*) dominated. Generally, elongate shapes are more successful in turbulent, well-mixed waters whereas spherical shapes in nutrient-limited, stratified, stagnant waters of the RPs. Interestingly, even though the taxonomic assemblage changed temporally, the shape dominance remained consistent suggesting the latter a robust morphological trait. The existence of

species-specific allelopathy on other microalgae by *Amphidinium* (known harmful algae of concern and dominant in HT-RPs) highlights a type of physiological trait to suppress competitors and might be one of the reasons for its predominance in HT-RPs experiencing varying environmental (light, temperature, and salinity) conditions.

Acknowledgements

The authors are grateful to the Director of CSIR-National Institute of Oceanography for his support and encouragement. We thank Drs N L Thakur and D Desai for co-ordinating intertidal rock pool experiments under the Ocean Finder project (PSC0105) and the project staff, who were involved in the experiments, for their help during sampling. We are also thankful to the two anonymous reviewers for their suggestions in improving the manuscript. First author also acknowledges UGC for fellowship. This is an NIO Contribution No. 6695.

Author statement

Paul P: Performed field sampling, laboratory experiments, samples analysis, data analysis and interpretation; J S Patil: Original concept, field and experiment planning, field sampling, data interpretation and manuscript elaboration; A C Anil: Manuscript elaboration and also co-supervised all works.

References

Anusa A, Ndagurwa H G T and Magadza C H D 2012 The influence of pool size on species diversity and water chemistry in temporary rock pools on Domboshawa Mountain, northern Zimbabwe; *Afr. J. Aqua. Sci.* **37(1)** 89–99.

Baig H S, Saifullah S M and Dar A 2006 Occurrence and toxicity of *Amphidinium carterae* Hulburt in the North Arabian Sea; *Harmful Algae* **5(2)** 133–140.

Da Silva K D P, Simões N R, De Oliveira D L, Silva F S and Barbosa L G 2020 Phytoplankton communities in freshwater rock pools: Structural and spatial dynamics in Brazilian drylands; *Limnetica* **39(1)** 487–498.

Fistarol G O, Legrand C, Rengefors K and Granéli E 2004 Temporary cyst formation in phytoplankton: A response to allelopathic competitors?; *Environ. Microbiol.* **6(8)** 791–798.

Granéli E and Hansen P J 2006 Allelopathy in Harmful Algae: A mechanism to compete for resources?; In: *Ecology of Harmful Algae. Ecological Studies Series* (eds) Granéli E and Turner J T, vol. **189**, Springer-Verlag, Berlin, pp. 189–201.

Grover J P 1989 Influence of cell shape and size on algal competitive ability; *J. Phycol.* **25** 402–405.

Häggqvist K and Lindholm T 2015 Phytoplankton communities in rock pools on the Åland Islands, SW Finland – environmental variables, functional groups and strategies; *Biodivers.* **16(1)** 15–26.

Häggqvist K and Lindholm T 2016 Phytoplankton, physical and chemical microscale variations in three brackish rock pools; *Phycol. Res.* **64** 241–250.

Hillebrand H, Durselen C D, Kirschel D, Pollingher D and Zohary T 1999 Biovolume calculation for pelagic and benthic microalgae; *J. Phycol.* **35** 403–424.

Huggett J and Griffiths C L 1986 Some relationships between elevation, physico-chemical variables and biota of intertidal rock pools; *Mar. Ecol. Prog. Ser.* **29** 189–197.

Jeong H J, Kang H, Shim J H, Park J K, Kim J S, Song J Y and Choi H J 2001 Interactions among the toxic dinoflagellate *Amphidinium carterae*, the heterotrophic dinoflagellate *Oxyrrhis marina*, and the calanoid copepods *Acartia* spp; *Mar. Ecol. Prog. Ser.* **218** 77–86.

Jeong H J, Jang S H, Kang N S, Yoo Y D, Kim M J, Lee K H, Yoon E Y, Potvin E, Hwang Y J, Kim J I and Seong K A 2012 Molecular characterization and morphology of the photosynthetic dinoflagellate *Bysmatrum caponii* from two solar Saltons in Western Korea; *Ocean Sci. J.* **47(1)** 1–18.

Karp-Boss L and Boss E 2016 The elongated, the squat and the spherical: Selective pressures for phytoplankton shape; In: *Aquatic microbial ecology and biogeochemistry: A dual perspective* (eds) Glibert P and Kana T M, Springer, Berlin, pp. 25–34.

Kiorboe T 1993 Turbulence, phytoplankton cell size, and the structure of pelagic food webs; *Adv. Mar. Biol.* **29** 1–72.

Legrand C, Rengefors K, Fistarol G O and Graneli E 2003 Allelopathy in phytoplankton–biochemical, ecological and evolutionary aspects; *Phycologia* **42(4)** 406–419.

Lewis W M 1976 Surface/volume ratio: Implication for phytoplankton morphology; *Science* **192** 885–887.

Litchman E and Klausmeier C A 2008 Trait-based community ecology of phytoplankton; *Ann. Rev. Ecol. Evol. Syst.* **39** 615–639.

Mandal S K, Singh R P and Patel V 2011 Isolation and characterization of exopolysaccharide secreted by a toxic dinoflagellate, *Amphidinium carterae* Hulburt 1957 and its probable role in harmful algal blooms (HABs); *Microb. Ecol.* **62** 518–527.

Margalef R 1978 Life-forms of phytoplankton as survival alternatives in an unstable environment; *Oceanol. Acta* **1** 493–509.

Martins G M, Hawkins S J, Thompson R C and Jenkins S R 2007 Community structure and functioning in intertidal rock pools: Effects of pool size and shore height at different successional stages; *Mar. Ecol. Prog. Ser.* **329** 43–55.

Metaxas A and Lewis A G 1992 Diatom communities in tidepools: The effect of Intertidal height; *Botanica Marina* **35** 1–10.

Metaxas A and Scheibling R E 1993 Community structure and organization of tidepools; *Mar. Ecol. Prog. Ser.* **98** 187–198.

Metaxas A and Scheibling R E 1994 Changes in phytoplankton abundance in tidepools over the period of tidal isolation; *Botanica Marina* **37** 301–314.

Metaxas A and Scheibling R E 1996a Spatial heterogeneity of phytoplankton assemblages in tidepools: Effects of abiotic and biotic factors; *Mar. Ecol. Prog. Ser.* **130** 179–199.

Metaxas A and Scheibling R E 1996b Top-down and bottom-up regulation of phytoplankton assemblages in tidepools; *Mar. Ecol. Prog. Ser.* **145** 161–177.

Morabito G, Oggioni A, Caravati E and Panzani P 2007 Seasonal morphological plasticity of phytoplankton in Lago Maggiore (N. Italy); *Hydrobiol.* **578** 47–57.

Murray S A, Kohli G S, Farrell H, Spiers Z B, Place A R, Dorantes-Aranda J J and Ruszczy K J 2015 A fish kill associated with a bloom of *Amphidinium carterae* in a coastal lagoon in Sydney, Australia; *Harmful Algae* **49** 19–28.

Murray S A, Garby T, Hoppenrath M and Neilan B A 2012 Genetic diversity, morphological uniformity and polyketide production in Dinoflagellates (*Amphidinium*, Dinoflagellata); *PLoS ONE* **7(6)** e38253, https://doi.org/10.1371/journal.pone.0038253.

Naselli-Flores L and Barone R 2007 Pluriannual morphological variability of phytoplankton in a highly productive Mediterranean reservoir (Lake Arancio, Southwestern Sicily); *Hydrobiologia* **578** 87–95.

Naselli-Flores L, Padisak J and Albay M 2007 Shape and size in phytoplankton ecology: Do they matter?; *Hydrobiologia* **578** 157–161.

Norberg J 1998 Effects of temperature and light on the composition of brackish-water rock pool ecosystem; *Aqua. Ecol.* **32** 323–334.

Padisak J, Soroczki-Pinter E and Rezner Z 2003 Sinking properties of some phytoplankton shapes and the relation of form resistance to morphological diversity of plankton – an experimental study; *Hydrobiologia* **500** 243–257.

Patil J S, Rodrigues R V, Paul P, Satish K, Rafi M and Anil A C 2017 Benthic dinoflagellate blooms in topical intertidal rock pools: Elucidation of photoprotection mechanisms; *Mar. Biol.* **164** 89–91.

Pavaux A-S, Berdalet E and Lemée R 2020 Chemical Ecology of the Benthic Dinoflagellate Genus Ostreopsis: Review of Progress and Future Directions; *Front. Mar. Sci.* **7** 498.

Poulson K L, Sieg R D, Prince E K and Kubanek J 2010 Allelopathic compounds of a red tide dinoflagellate have species-specific and context-dependent Impacts on phytoplankton; *Mar. Ecol. Prog. Ser.* **416** 69–78.

Reynolds C S 2006 *Ecology of Phytoplankton*; Cambridge University Press, Cambridge.

Rice E L 1984 *Allelopathy*; Academic Press, Orlando.

Rishworth G M, Perissinotto R, Miranda N A F, Bornman T G and Steyn P P 2017 Phytoplankton community dynamics within peritidal pools associated with living Stromatolites at the freshwater–marine interface; *Aquat. Sci.* **79** 357–370.

Salmaso N and Padisak J 2007 Morpho-Functional Groups and phytoplankton development in two deep lakes (Lake Garda, Italy and Lake Stechlin, Germany); *Hydrobiologia* **578** 97–112.

Soininen J and Meier S 2014 Phytoplankton richness is related to nutrient availability, not to pool size, in a subarctic rock pool system; *Hydrobiologia* **70** 137–145.

Sommer U 1998 Silicate and the functional geometry of marine phytoplankton; *J. Plank. Res.* **20** 1853–1859.

Stanca E, Cellamare M and Basset A 2013 Geometric shape as a trait to study phytoplankton distributions in aquatic ecosystems; *Hydrobiologia* **701** 99–116.

Suikkanen S, Fistaro G O and Granéli E 2005 Effects of cyanobacterial allelochemicals on a natural plankton community; *Mar. Ecol. Prog. Ser.* **287** 1–9.

Sun J and Liu D 2003 Geometric models for calculating cell biovolume and surface area for phytoplankton; *J. Plan. Res.* **25** 1331–1346.

Therriault T W and Kolasa J 2001 Desiccation frequency reduces species diversity and predictability of community structure in coastal rock pools; *Israel J. Zoo.* **47(4)** 477–489.

Tomas C R 1997 *Identifying marine phytoplankton*; Academic Press, New York, 858p.

Underwood A J and Skilleter G A 1996 Effects of patch size on the structure of assemblages in rock pools; *J. Exp. Mar. Biol. Ecol.* **197** 63–90.

Xiaoqing J I, Xiaotian H, Baijuan Y and Zhiming Y 2012 Analysis on allelochemicals in the cell-free Filtrates of *Amphidinium carterae*; *Acta Ecologica Sinica* **32(6)** 1745–1754.

Corresponding editor: N V Chalapathi Rao